

AD-A274 831



93410

# IONOSPHERIC EXPOSURE FACILITY SPACELABORATORY HANDBOOK

Science Applications International Corporation

2215 North Loop East  
Austin, Texas 78706

October 1993

Final Report

APPROVED FOR PUBLIC RELEASE; DISTRIBUTION IS UNLIMITED



PHILLIPS LABORATORY

Space and Missiles Technology

AIR FORCE MATERIEL

WRIGHT-PATTERSON AIR FORCE BASE

DAYTON, OHIO 45433-6150

DEC 24 1993

Directorate  
MAND

This final report was prepared by Science Applications International Corporation, Albuquerque, New Mexico, under Contract F29601-91-C-0071, Job Order IR2NTBAA with the Phillips Laboratory, Kirtland Air Force Base, New Mexico. The Laboratory Project Officer-in-Charge was Mr. William T. Kemp (VTET).

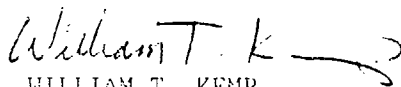
When Government drawings, specifications, or other data are used for any purpose other than in connection with a definitely Government-related procurement, the United States Government incurs no responsibility or any obligation whatsoever. The fact that the Government may have formulated or in any way supplied the said drawings, specifications, or other data, is not to be regarded by implication, or otherwise in any manner construed, as licensing the holder, or any other person or corporation; or as conveying any rights or permission to manufacture, use, or sell any patented invention that may in any way be related thereto.

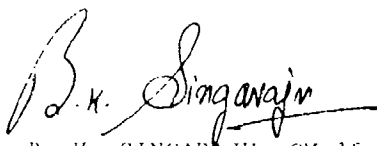
This report has been authored by a contractor and employees of the United States Government. Accordingly, the United States Government retains a nonexclusive royalty-free license to publish or reproduce the material contained herein, or allow others to do so, for the United States Government purposes.

This report has been reviewed by the Public Affairs Office and is releasable to the National Technical Information Service (NTIS). At NTIS, it will be available to the general public, including foreign nationals.

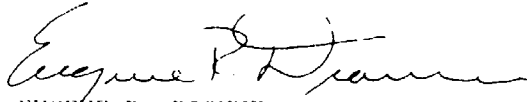
If your address has changed, if you wish to be removed from the mailing list, or if your organization no longer employs the addressee, please notify PL/VTET, Kirtland AFB, NM 87117-5776 to help maintain a current mailing list.

This report has been reviewed and is approved for publication.

  
WILLIAM T. KEMP  
Project Officer

  
B. K. SINGARAJU, GM-15  
Chief, Electronics and Software  
Division

FOR THE COMMANDER

  
EUGENE R. DIONNE  
Colonel, USAF  
Director, Space and Missiles  
Technology

DO NOT RETURN COPIES OF THIS REPORT UNLESS CONTRACTUAL OBLIGATIONS OR NOTICE ON A SPECIFIC DOCUMENT REQUIRES THAT IT BE RETURNED.

# DISCLAIMER NOTICE



THIS DOCUMENT IS BEST  
QUALITY AVAILABLE. THE COPY  
FURNISHED TO DTIC CONTAINED  
A SIGNIFICANT NUMBER OF  
COLOR PAGES WHICH DO NOT  
REPRODUCE LEGIBLY ON BLACK  
AND WHITE MICROFICHE.

REPORT DOCUMENTATION PAGE			Form Approved OMB No 0704-0188	
Public reporting burden for this collection of information is estimated to average 1 hour per response, including the time for reviewing instructions, searching existing data sources, gathering and maintaining the data needed, and completing and reviewing the collection of information. Send comments regarding this burden estimate or any other aspect of this collection of information, including suggestions for reducing this burden, to Washington Headquarters Services, Directorate for Information Operations and Reports, 1215 Jefferson Davis Highway, Suite 1204, Arlington, VA 22202-4302 and to the Office of Management and Budget, Paperwork Reduction Project (0704-0188), Washington, DC 20503.				
1. AGENCY USE ONLY (Leave blank)	2. REPORT DATE September 1993	3. REPORT TYPE AND DATES COVERED Final 6 Jan 92 - 31 Aug 93		
4. TITLE AND SUBTITLE  LONG DURATION EXPOSURE FACILITY SPACE OPTICS HANDBOOK		5. FUNDING NUMBERS  C: F29601-91-C-0071 PE: 61101F PR: IR2N TA: TB WU: AA		
6. AUTHOR(S)  William T. Kemp*, Edward Taylor*, Carl Bloemker, Frank White, Gary Rensner, and Alan Watts**		8. PERFORMING ORGANIZATION REPORT NUMBER		
7. PERFORMING ORGANIZATION NAME(S) AND ADDRESS(ES)  Science Applications International Corporation 2109 Air Park Road, SE Albuquerque, NM 87106		10. SPONSORING/MONITORING AGENCY REPORT NUMBER  PL-TN--93-1067		
9. SPONSORING/MONITORING AGENCY NAME(S) AND ADDRESS(ES)  Phillips Laboratory Kirtland AFB, NM 87117-5776		11. SUPPLEMENTARY NOTES  *Phillips Laboratory, Kirtland AFB, New Mexico **POD Associates, Incorporated, Albuquerque, New Mexico		
12a. DISTRIBUTION/AVAILABILITY STATEMENT  Approved for public release; distribution is unlimited.		12b. DISTRIBUTION CODE		
13. ABSTRACT (Maximum 200 words)  This handbook provides a user a space optics design guide to materials based on the Long Duration Exposure Facility (LDEF) Space Optics Experiments. The materials covered are refractive optics, coatings, filters, mirrors, second surface mirrors, quartz microbalances, and fiber optics. The guide presents the data and the experience learned from the LDEF Space Optics Experiments in one volume in a user-friendly fashion. The data reported in the handbook are a compilation of the data published by the individual experimenters. Natural space environment data with an emphasis on the microparticle environment are also presented.				
14. SUBJECT TERMS  LDEF, Natural Space Environments, Optical Materials, Optical Systems			15. NUMBER OF PAGES  416	
			16. PRICE CODE	
17. SECURITY CLASSIFICATION OF REPORT  Unclassified	18. SECURITY CLASSIFICATION OF THIS PAGE  Unclassified	19. SECURITY CLASSIFICATION OF ABSTRACT  Unclassified	20. LIMITATION OF ABSTRACT  SAR	



## GENERAL INSTRUCTIONS FOR COMPLETING SF 298

The Report Documentation Page (RDP) is used in announcing and cataloging reports. It is important that this information be consistent with the rest of the report, particularly the cover and title page. Instructions for filling in each block of the form follow. It is important to *stay within the lines* to meet optical scanning requirements.

**Block 1. Agency Use Only (Leave blank).**

**Block 2. Report Date.** Full publication date including day, month, and year, if available (e.g. 1 Jan 88). Must cite at least the year.

**Block 3. Type of Report and Dates Covered.** State whether report is interim, final, etc. If applicable, enter inclusive report dates (e.g. 10 Jun 87 - 30 Jun 88).

**Block 4. Title and Subtitle.** A title is taken from the part of the report that provides the most meaningful and complete information. When a report is prepared in more than one volume, repeat the primary title, add volume number, and include subtitle for the specific volume. On classified documents enter the title classification in parentheses.

**Block 5. Funding Numbers.** To include contract and grant numbers; may include program element number(s), project number(s), task number(s), and work unit number(s). Use the following labels:

C - Contract	PR - Project
G - Grant	TA - Task
PE - Program Element	WU - Work Unit Accession No.

**Block 6. Author(s).** Name(s) of person(s) responsible for writing the report, performing the research, or credited with the content of the report. If editor or compiler, this should follow the name(s).

**Block 7. Performing Organization Name(s) and Address(es).** Self-explanatory.

**Block 8. Performing Organization Report Number.** Enter the unique alphanumeric report number(s) assigned by the organization performing the report.

**Block 9. Sponsoring/Monitoring Agency Name(s) and Address(es).** Self-explanatory.

**Block 10. Sponsoring/Monitoring Agency Report Number. (If known)**

**Block 11. Supplementary Notes.** Enter information not included elsewhere such as: Prepared in cooperation with...; Trans. of...; To be published in... When a report is revised, include a statement whether the new report supersedes or supplements the older report.

**Block 12a. Distribution/Availability Statement.** Denotes public availability or limitations. Cite any availability to the public. Enter additional limitations or special markings in all capitals (e.g. NOFORN, REL, ITAR).

**DOD** - See DoDD 5230.24, "Distribution Statements on Technical Documents."

**DOE** - See authorities.

**NASA** - See Handbook NHB 2200.2.

**NTIS** - Leave blank.

**Block 12b. Distribution Code.**

**DOD** - Leave blank.

**DOE** - Enter DOE distribution categories from the Standard Distribution for Unclassified Scientific and Technical Reports.

**NASA** - Leave blank.

**NTIS** - Leave blank.

**Block 13. Abstract.** Include a brief (*Maximum 200 words*) factual summary of the most significant information contained in the report.

**Block 14. Subject Terms.** Keywords or phrases identifying major subjects in the report.

**Block 15. Number of Pages.** Enter the total number of pages.

**Block 16. Price Code.** Enter appropriate price code (*NTIS only*)

**Blocks 17. - 19. Security Classifications.** Self-explanatory. Enter U.S. Security Classification in accordance with U.S. Security Regulations (i.e., UNCLASSIFIED). If form contains classified information, stamp classification on the top and bottom of the page.

**Block 20. Limitation of Abstract.** This block must be completed to assign a limitation to the abstract. Enter either UL (unlimited) or SAR (same as report). An entry in this block is necessary if the abstract is to be limited. If blank, the abstract is assumed to be unlimited.

## PREFACE

While the goal of compiling a handbook for optical material that flew on LDEF was clear from the beginning, the process of contacting all the LDEF experimenters and gathering the test data was a challenging task. The task of putting this information in a usable format that would not confuse the user, let alone the authors, was also very challenging. The final document is the result of the assistance and support of numerous people. At this time the authors would like to give a special thanks to Jill Price and Heidi Raybould, at SAIC, for keeping the authors on track and assembling the final document.

In order to assure that the handbook was in a usable format and had technical merit, several colleagues were asked to review the handbook. The authors wish to thank James Mason, NASA/Goddard Space Flight Center; Howard Herzig, NASA/Goddard Space Flight Center; Joel Edelman, LDEF Corporation; Julian Reinheimer, Aerospace Corporation; Wayne Stuckey, Aerospace Corporation; Sandra Gyetvay, Aerospace Corporation; Michael Meshishnek, Aerospace Corporation; Linda DeHainaut, Phillips Laboratory; and Dale Atkinson, POD Associates, Inc. These reviewers had only a very short time to absorb, analyze, and comment on this extensive document. Thank you once again for taking time out of your busy schedule to assist in reviewing this document.

The cover picture is used with the permission of the National Aeronautics and Space Administration (NASA). The picture is of the Long Duration Exposure Facility (LDEF) satellite, deployed on 7 April 1984. LDEF is backdropped against Florida, the Bahama Bank, the Gulf of Mexico and Atlantic ocean. The picture was taken by the crew aboard the Challenger, Flight 41-C.

1984-12-13 10:00:00

A-1  
93-30199



93 12 13 047 iii/iv

## TABLE OF CONTENTS

<u>Chapter</u>	<u>Page</u>
1 EXECUTIVE SUMMARY .....	1-1
2 INTRODUCTION .....	2-1
3 SPACE ENVIRONMENTS .....	3-1
3.0 OVERVIEW .....	3-1
3.1 GENERAL SPACE ENVIRONMENT SPECIFICATIONS .....	3-1
3.2 INDIVIDUAL SPACE ENVIRONMENT SPECIFICATIONS .....	3-4
3.2.1 Atomic Oxygen .....	3-4
3.2.2 Trapped Radiation .....	3-5
3.2.3 Meteoroids and Man-Made Debris .....	3-10
3.2.3.1 Meteoroids .....	3-11
3.2.3.2 Man-Made Debris .....	3-15
3.2.4 Ultraviolet (UV) Radiation/Solar Exposure .....	3-21
3.2.5 Vacuum .....	3-22
3.2.6 Microgravity/Accelerations .....	3-24
4 LDEF OBSERVATIONS .....	4-1
4.1 SUMMARY OF LDEF OPTICAL MATERIALS/EXPERIMENTS .....	4-1
4.2 OPTICAL SYSTEM DESIGN PARAMETERS .....	4-2
4.3 REFRACTIVE OPTICS FOR UV/VISIBLE SYSTEMS .....	4-6
4.3.1 Uncoated UV/Visible Refractive Optics .....	4-6
4.3.1.1 Impact Effects .....	4-6
4.3.1.2 Atomic Oxygen .....	4-12
4.3.1.3 Scatter .....	4-12
4.3.1.4 Absorption/Transmission/Reflectance .....	4-13
4.3.1.5 Darkening .....	4-15
4.3.1.6 Stress .....	4-16
4.3.1.7 Contamination/Deterioration .....	4-19
4.3.2 Coated UV/Visible Refractive Optics .....	4-20
4.3.2.1 Impact Effects .....	4-20
4.3.2.2 Atomic Oxygen .....	4-21
4.3.2.3 Scatter .....	4-21
4.3.2.4 Absorption/Transmission/Reflectance .....	4-21
4.3.2.5 Darkening .....	4-24
4.3.2.6 Stress .....	4-24
4.3.2.7 Contamination/Deterioration .....	4-25
4.4 REFRACTIVE OPTICS FOR IR SYSTEMS .....	4-27
4.4.1 Uncoated IR Refractive Optics .....	4-29
4.4.1.1 Impact Effects .....	4-29
4.4.1.2 Atomic Oxygen .....	4-31

## TABLE OF CONTENTS (Continued)

<u>Chapter</u>		<u>Page</u>
	4.4.1.3 Scatter . . . . .	4-32
	4.4.1.4 Absorption/Transmission/Reflectance . . . . .	4-36
	4.4.1.5 Darkening . . . . .	4-38
	4.4.1.6 Stress . . . . .	4-38
	4.4.1.7 Contamination/Deterioration . . . . .	4-39
4.4.2	Coated IR Refractive Optics . . . . .	4-40
	4.4.2.1 Impact Effects . . . . .	4-40
	4.4.2.2 Atomic Oxygen . . . . .	4-41
	4.4.2.3 Scatter . . . . .	4-41
	4.4.2.4 Absorption/Transmission/Reflectance . . . . .	4-42
	4.4.2.5 Darkening . . . . .	4-43
	4.4.2.6 Stress . . . . .	4-43
	4.4.2.7 Contamination/Deterioration . . . . .	4-43
4.5	COATINGS FOR UV/VISIBLE SYSTEMS . . . . .	4-45
	4.5.1 Coated UV/Visible Optics . . . . .	4-48
	4.5.1.1 Impacts . . . . .	4-48
	4.5.1.2 Atomic Oxygen . . . . .	4-49
	4.5.1.3 Scatter . . . . .	4-50
	4.5.1.4 Absorption/Transmission/Reflectance . . . . .	4-50
	4.5.1.5 Darkening . . . . .	4-52
	4.5.1.6 Stress . . . . .	4-53
	4.5.1.7 Contamination/Deterioration . . . . .	4-53
4.6	COATINGS FOR IR SYSTEMS . . . . .	4-55
	4.6.1 Coated IR Optics . . . . .	4-56
	4.6.1.1 Impacts . . . . .	4-56
	4.6.1.2 Atomic Oxygen . . . . .	4-61
	4.6.1.3 Scatter . . . . .	4-61
	4.6.1.4 Absorption/Transmission/Reflectance . . . . .	4-61
	4.6.1.5 Darkening . . . . .	4-63
	4.6.1.6 Stress . . . . .	4-63
	4.6.1.7 Contamination/Deterioration . . . . .	4-63
4.7	OPTICAL FILTERS FOR UV/VISIBLE SYSTEMS . . . . .	4-66
	4.7.1 Covered UV/Visible Optical Filters . . . . .	4-68
	4.7.1.1 Impacts . . . . .	4-68
	4.7.1.2 Atomic Oxygen . . . . .	4-69
	4.7.1.3 Scatter . . . . .	4-69
	4.7.1.4 Absorption/Transmission/Reflectance . . . . .	4-69
	4.7.1.5 Darkening . . . . .	4-70
	4.7.1.6 Stress . . . . .	4-70
	4.7.1.7 Contamination/Deterioration . . . . .	4-70

## TABLE OF CONTENTS (Continued)

<u>Chapter</u>		<u>Page</u>
	4.7.2 Exposed UV/Visible Optical Filters . . . . .	4-71
	4.7.2.1 Impacts . . . . .	4-71
	4.7.2.2 Atomic Oxygen . . . . .	4-71
	4.7.2.3 Scatter . . . . .	4-71
	4.7.2.4 Absorption/Transmission/Reflectance . . . . .	4-71
	4.7.2.5 Darkening . . . . .	4-74
	4.7.2.6 Stress . . . . .	4-74
	4.7.2.7 Contamination/Deterioration . . . . .	4-74
4.8	OPTICAL FILTERS FOR IR SYSTEMS . . . . .	4-75
	4.8.1 IR Optical Filters . . . . .	4-76
	4.8.1.1 Impacts . . . . .	4-76
	4.8.1.2 Atomic Oxygen . . . . .	4-77
	4.8.1.3 Scatter . . . . .	4-77
	4.8.1.4 Absorption/Transmission/Reflectance . . . . .	4-77
	4.8.1.5 Darkening . . . . .	4-80
	4.8.1.6 Stress . . . . .	4-80
	4.8.1.7 Contamination/Deterioration . . . . .	4-80
4.9	MIRRORS . . . . .	4-81
	4.9.1 Mirrors . . . . .	4-81
	4.9.1.1 Impacts . . . . .	4-81
	4.9.1.2 Atomic Oxygen . . . . .	4-84
	4.9.1.3 Scatter . . . . .	4-85
	4.9.1.4 Absorption/Transmission/Reflectance . . . . .	4-86
	4.9.1.5 Darkening . . . . .	4-88
	4.9.1.6 Stress . . . . .	4-88
	4.9.1.7 Contamination/Deterioration . . . . .	4-89
4.10	SECOND SURFACE MIRRORS . . . . .	4-90
	4.10.1 Second Surface Mirrors . . . . .	4-92
	4.10.1.1 Impacts . . . . .	4-92
	4.10.1.2 Atomic Oxygen . . . . .	4-92
	4.10.1.3 Scatter . . . . .	4-92
	4.10.1.4 Absorption/Transmission/Reflectance . . . . .	4-92
	4.10.1.5 Darkening . . . . .	4-93
	4.10.1.6 Stress . . . . .	4-93
	4.10.1.7 Contamination/Deterioration . . . . .	4-93
4.11	QUARTZ CRYSTAL MICROBALANCES . . . . .	4-94
	4.11.1 Quartz Crystal Microbalances . . . . .	4-94
	4.11.1.1 Impacts . . . . .	4-94
	4.11.1.2 Atomic Oxygen . . . . .	4-95
	4.11.1.3 Scatter . . . . .	4-95
	4.11.1.4 Absorption/Transmission/Reflectance . . . . .	4-95
	4.11.1.5 Darkening . . . . .	4-98

## TABLE OF CONTENTS (Continued)

<u>Chapter</u>	<u>Page</u>
4.11.1.6 Stress	4-99
4.11.1.7 Contamination/Deterioration	4-99
4.12 RELATED MATERIALS EXPERIMENTS	4-101
4.12.1 Related Space Optical Materials	4-102
4.12.1.1 Impacts	4-102
4.12.1.2 Atomic Oxygen	4-104
4.12.1.3 Scatter	4-106
4.12.1.4 Absorption/Transmission/Reflectance	4-106
4.12.1.5 Darkening	4-106
4.12.1.6 Stress	4-107
4.12.1.7 Contamination/Deterioration	4-107
5 OPTICAL DESIGN CONSIDERATIONS: IMPACT OF LDEF RESULTS AND ANALYSES	5-1
5.1 INTRODUCTION	5-1
5.2 CRITICAL INTERACTIONS FOR OPTICAL SYSTEMS	5-2
5.3 PREFERRED OPTICAL COMPONENTS	5-8
5.3.1 Benign Environment	5-8
5.3.2 Minimum-Exposure Environment	5-8
5.3.3 Maximum-Exposure Environment	5-10
5.4 GENERAL OPTICAL DESIGN CONSIDERATIONS	5-11
5.4.1 Contamination Control	5-11
5.4.2 Micrometeoroid Damage	5-12
5.4.3 Ionizing Radiation Damage	5-14
5.4.4 Atomic Oxygen	5-15
5.5 RECOMMENDATIONS FOR ADDITIONAL PROCESSING OF LDEF DATA	5-15
6 THE EFFECTS OF MICROMETEOROIDS AND DEBRIS (M&D)	6-1
6.1 SPACECRAFT MICROPARTICLE IMPACT FLUX DEFINITION	6-1
6.1.1 Introduction	6-1
6.1.2 Man-made Debris	6-2
6.1.3 Micrometeoroids	6-4
6.1.4 Impact Effects	6-7
6.1.5 Predictions and LDEF Comparisons	6-9
6.1.6 Caveats on the Microparticle Models	6-10
6.1.7 Elliptical Orbits	6-12
6.2 ANALYSIS OF CRATER EFFECTS ON OPTICS	6-14
6.2.1 Fractional Area Damage	6-14
6.2.2 Optical BRDF Scatter Calculations	6-16
6.2.2.1 Equivalent Contamination Approach	6-17
6.2.2.2 Alternative Analytic Approach	6-19
6.2.2.3 Mie Scatter Calculations	6-21

## TABLE OF CONTENTS (Concluded)

<u>Chapter</u>	<u>Page</u>
6.2.2.4 Total Intergated Scatter versus BRDF .....	6-21
6.2.2.5 General Comments on Scattering Predictions/Measurements .....	6-23
6.2.3 Parametric Scatter Calculations .....	6-24
6.3 CONCLUSIONS FOR M&D IMPACT EFFECTS ON OPTICS .....	6-27
7 SPACE EFFECTS ON FIBER OPTIC SYSTEMS AND COMPONENTS ORBITED ON THE LDEF .....	7-1
7.1 EXPERIMENTAL CONFIGURATIONS AND FIBER OPTIC SYSTEMS AND COMPONENT EXPOSURES TO THE SPACE ENVIRONMENT .....	7-3
7.1.1 PL Experiment #701 (M0004) - Space Environment Effects on Fiber Optic Systems .....	7-3
7.1.1.1 Optical Transmission Measurements .....	7-4
7.1.1.2 In Orbit Temperature Cycling Measurements .....	7-5
7.1.1.3 Brief Analysis of On-Orbit Recorded Optical Fiber Transmission Data .....	7-7
7.1.1.4 On-Orbit Radiation Dosimeter Measurements .....	7-7
7.1.1.5 On-Orbit Micro-Meteorite and Debris Impacts .....	7-10
7.1.2 Experiment S0109 - Space Exposure of Fiber Optic Cables .....	7-12
7.1.3 M0003-8 Fiber Optic Experiment .....	7-13
7.1.4 Experiment S0050 - Optical System Components .....	7-13
7.1.5 Experiment M0006 - Space Orbitied Fiber Optic Bundle .....	7-14
7.2 CONCLUSIONS .....	7-15
APPENDICES	
A LDEF EXPERIMENT LOCATIONS, ENVIRONMENTS & MATERIALS	A-1
B EXPERIMENT DESCRIPTIONS .....	B-1
C LIST OF REFERENCES .....	C-1
D LIST OF ACRONYMS .....	D-1
E LDEF PHOTOGRAPHS AND DATA REFERENCES .....	E-1

## CHAPTER 1

### EXECUTIVE SUMMARY

Experiments from Long Duration Exposure Facility (LDEF) have provided and will continue to provide valuable information about the performance of space optical materials and optical sensor design in the space environment. LDEF provided valuable data on the effects meteoroids and debris, atomic oxygen (AO), contamination, ionizing radiation, vacuum, thermal cycling, and solar irradiation have on space optical experiments.

The principal investigators have not completed testing. One of the main impediments in completing the reduction is the contamination of the samples. The contamination was a result of the outgassing and decomposition of materials on the LDEF spacecraft. To completely understand and make final conclusions about the impact the space environment had on LDEF optical samples, it will be necessary to make additional measurements after the LDEF samples have been cleaned.

Despite the contamination, valuable information has already been obtained. This information is summarized below:

- Contamination can be a major problem in space for optical systems. On the LDEF spacecraft contamination resulted in the complete loss of transmission for some optical samples. The use of materials which outgas or decompose should be avoided in the vicinity of optical components.
- Atomic oxygen degraded the optical materials that are physically soft, such as KRS-5 and KRS-6, as well as uncoated copper and silver metallic reflectors. Caution should be exercised when using these materials in orbits below 800 km where atomic oxygen dominates.
- Uncoated materials were found to be quite resistant to the space environment.
- Dielectric and metallic-coated optics exhibited delamination. The probable cause of this is thermal cycling. The use of these materials in an "athermal" system will reduce this problem.
- Certain materials, such as ZnS, degrade in space.



- Hard-coated infrared (IR) multilayer coatings performed well in the space environment.
- Contaminated IR components which were properly cleaned showed little or no degradation in optical properties.

This information is used to develop a set of design considerations for optical systems. The design considerations are based on grouping the optical elements according to the environments they will see. The three groups are benign, minimal exposure, and maximum exposure. Based on the LDEF results and analyses to date, materials have been identified which are appropriate for each exposure level.

## CHAPTER 2 INTRODUCTION

The purpose of this handbook is to provide the user a space optics design guide based on the LDEF space optics experiments. The guide presents the data and experience learned from the LDEF space optics experiments in one volume and in a user-friendly fashion.

LDEF was a passive satellite with no telemetry of data to the earth during the mission. LDEF contained 57 different experiments mounted in 86 individual out-facing trays and also on the interior of the structure. LDEF was placed in a 478-km altitude, 28.5°-inclination orbit. The LDEF mission was originally scheduled to last between 10 months to a year. However, LDEF was not retrieved until after almost 5.75 years in space. During this time the original orbit decayed from 482 km down to 320 km.

The 57 LDEF experiments were divided by NASA into five categories: heat pipes and thermal, materials and coatings, science, power and propulsion, and electronics and optics. The optic experiments, the focus of this design guide, can be divided into the following areas: refractive optics (both coated and uncoated); filters; metal films; fiber optics; and quartz microbalances. LDEF experiments other than the optics experiments, such as the power experiments, provided valuable related data, especially for coating materials and thin films. The data reduction for the optical experiments is being done by the individual experimenters. As of the writing of this handbook, the data reduction effort was ongoing; provisions have been made in the formatting of the handbook to allow periodic updates.

The data reported in the handbook are a compilation of the data published by the individual experimenters. The handbook is divided into seven chapters and five appendices. The first two chapters are the executive summary and the introduction.

Chapter 3 of the handbook is an environments summary chapter. This information is provided for two specific reasons: (1) to understand any environmental effects that

contributed to the results observed so as to interpret the LDEF experimental results properly and (2) to understand the environments and their effects so as to apply LDEF results properly to spacecraft design for other orbits and missions.

Chapter 4 is a compilation of the data that have been reduced and reported to date for the LDEF optics experiments. The data are categorized by material according to the observed effects.

Chapter 5 provides an insight into the impact the LDEF experiments, results, and analysis have with regard to the design of space optical systems. These design guidelines are not based on the complete data set contained in Chapter 4. A large portion of Chapter 4 data is what happened and the complete analysis of what caused the effect on the individual components has not been completed. In developing a list of preferred "working" components, the biggest driver is the spacecraft self-contamination of the samples. Since this contamination limits understanding of the real performance of the components, only optical components which were cleaned were considered in developing this chapter.

Chapter 6 provides a more detailed discussion of the low-Earth-orbit (LEO) microparticle environment than was given in Chapter 3, since the microparticle environment is becoming increasingly important in the design of space subsystems. The material in Chapter 6 describes in more detail the impact flux of microparticles, the models used to predict cratering effects on optics, and gives a brief description of the effects these craters have on optical performance.

Chapter 7 provides a detailed discussion of space effects on fiber optics. With the rapid development of photonics technology devices during the past few decades and with a large number of light-wave systems emerging, it was deemed appropriate to provide a detailed description of the active and passive systems and components flown on LDEF that was separate from Chapter 4 to provide an easy reference for the users of this guide.

Appendix A provides a description of the LDEF experiment locations and correlates these locations to specific environments experienced. The total micrometeoroid/debris impacts per square meter, the cumulative equivalent sun hours for each LDEF tray row, and the atomic oxygen fluence are shown and correlated to specific LDEF locations.

Appendix B provides a list of the experimenters and an experiment description.

Appendix C provides a list of published references.

Appendix D provides a glossary to define acronyms and other terms used in the report.

Appendix E is associated with Chapter 4 and contains the data graphs and photographs published by the various LDEF experimenters to date and cited in Chapter 4 to illustrate the observed damage from the space environments.



## **CHAPTER 3 SPACE ENVIRONMENTS**

### **3.0 OVERVIEW**

During its flight, LDEF was exposed to a number of natural space environments that depend on the LDEF orbit and lifetime. It is important to understand these environments for two reasons. First, it is important to understand any environmental effects that contributed to the results observed so as to interpret the LDEF experimental results properly. Second, it is important to understand the environments and effects so as to apply LDEF results properly to spacecraft design for other orbits and missions. Because of the need to interpret the data properly and to apply these data to spacecraft design properly, the following sections are provided. Specific effects of these environments on optical materials will be discussed in Chapter 4.

### **3.1 GENERAL SPACE ENVIRONMENT SPECIFICATIONS**

Because a number of the space environments depend on the LDEF orbit, it is important to identify the orbit of LDEF as precisely as possible. The LDEF was launched into Earth orbit in April 1984. While in space, it flew in a circular orbit having an inclination of 28.5°. The orbital altitude was initially approximately 478 km (257 nmi). When the LDEF was retrieved, the orbit had decayed to an altitude of approximately 320 km (179 nmi). Table 3.1-1 (extracted from Ref. 1) shows the orbital altitude history of LDEF.

The natural space environment has many components. Table 3.1-2 shows current references for these environmental specifications. For the LDEF orbit, the environments of most interest to the LDEF principal investigators are atomic oxygen, ionizing radiation, natural meteoroids, man-made debris, ultraviolet (UV) radiation, vacuum, and microgravity. These environments are relevant to understanding the observations in LDEF experiments and

to extrapolating LDEF results to spacecraft designs for other orbits. Each of these environments is discussed briefly below.

**Table 3.1-1. LDEF Orbit Mission History**

LDEF MISSION DAY	LDEF ALTITUDE (km)
0	478.7
300	475.8
1000	469.1
1300	466.2
1500	461.5
1700	449.5
1800	433.6
1900	412.8
2000	388.8
2050	368.0
2105	319.4

Some of the environments experienced by the LDEF experiments are particularly sensitive to the LDEF tray locations. Of particular interest are the atomic oxygen, sun hours, and micrometeoroid/debris environments. A more detailed description of these particular environments is provided in Appendix A to augment the more general discussions that follow.

**Table 3.1-2. Natural Space Environment Specifications**

ENVIRONMENT	ENVIRONMENTAL SPECIFICATION
Solar Radiation	MIL-STD-1809, Paragraph 5.7
Lunar Radiation	Handbook of Geophysics and Space Environment, Paragraph 25.2.1.2
Earth Shine	Handbook of Geophysics and Space Environment, Paragraph 13.1.1
Earthlimb	Handbook of Geophysics and Space Environment, Paragraph 13.4
Aurora	Handbook of Geophysics and Space Environment, Paragraph 12.2
Zodiacal Light	Handbook of Geophysics and Space Environment, Figures 25-3, -4, -5
Galactic Optical Background	Handbook of Geophysics and Space Environment, Chapter 25
Stellar Optical Background	Handbook of Geophysics and Space Environment, Table 25-10
Atomic Oxygen	Handbook of Geophysics and Space Environment, Paragraph 21.2.5
Trapped Radiation	MIL-STD-1809, Paragraph 5.1.2
Solar Flare	MIL-STD-1809, Paragraph 5.1.3
Other Nuclear Fluence	MIL-STD-1809, Paragraph 5.1.3.3
Galactic Cosmic Radiation	Handbook of Geophysics and Space Environment, Paragraph 6.2.1.1, Figure 6-2
Meteoroids	NASA SP-8013
Man-Made Orbital Debris	NASA Technical Memorandum 100471
Neutral Atmosphere	MIL-STD-1809, Paragraph 5.3
Plasma Environment	MIL-STD-1809, Paragraph 5.2
Geomagnetic Field	MIL-STD-1809, Paragraph 5.5



## 3.2 INDIVIDUAL SPACE ENVIRONMENT SPECIFICATIONS

### 3.2.1 Atomic Oxygen

The LDEF was launched into Earth orbit at a time of near-minimum activity in the Sun's 11-year solar cycle and was retrieved almost 6 years later at a time of near-maximum solar activity. The mean profiles for atomic oxygen number densities at solar minimum and at solar maximum are shown in Figure 3.2-1 (extracted from Ref. 9). The upper and lower bounds of the LDEF altitude are shown.

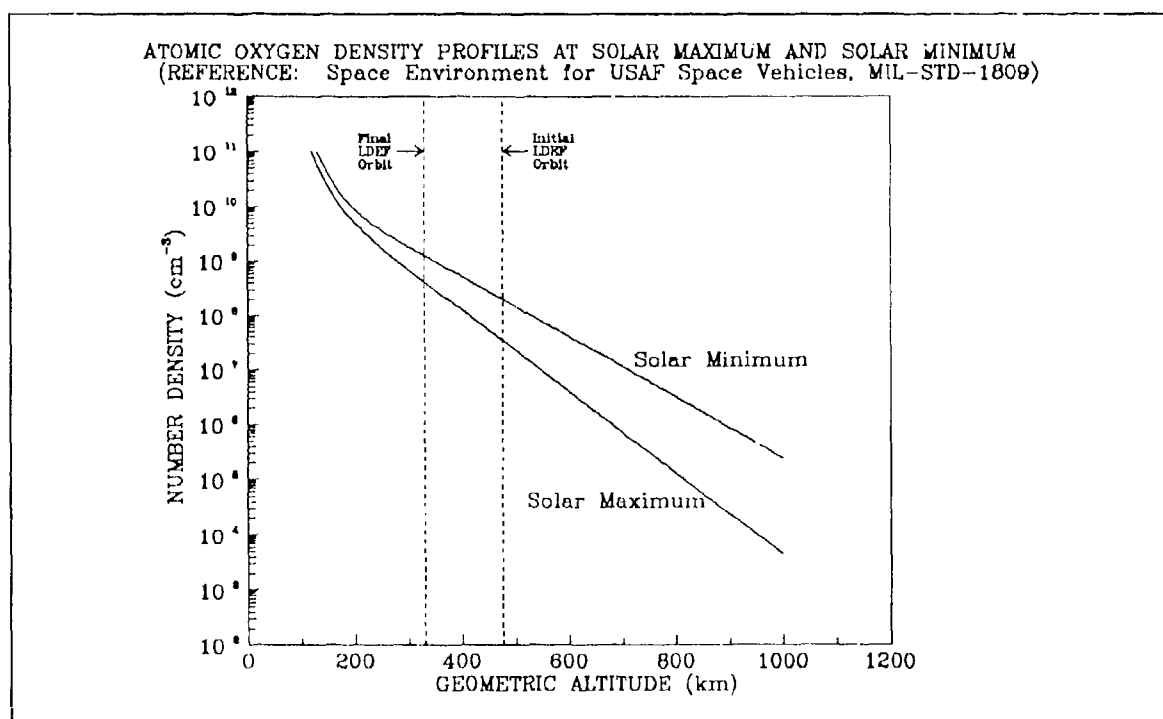


Figure 3.2-1. Atomic Oxygen Number Densities at Solar Minimum and Solar Maximum

The day-to-night number density ratio for atomic oxygen is approximately 25 above 500 km and decreases to one at the turbopause (approximately 100 km). The diurnal variation is less than a factor of four at all altitudes and latitudes near equinox. Variations

are small at low latitudes throughout the year. (During magnetic storms, the atomic oxygen density shows only small variation at all latitudes.)

To understand the materials effects for LDEF experiments, the total atomic oxygen fluence is of interest. The altitude of the flight, the orientation of the surfaces with respect to the ram direction, and the extent of solar activity determine the atomic oxygen fluence. This fluence is given as flux (atoms/cm<sup>2</sup>/sec)  $\times$  exposure period (seconds), with flux defined as number density of atomic oxygen (atoms/cm<sup>3</sup>)  $\times$  orbital velocity (cm/s).

From Reference 1, the history of the atomic oxygen flux striking the leading surfaces of the LDEF during the mission is presented in Figure 3.2-2. This flux history was calculated using current upper atmospheric models, the history of the tracked LDEF altitude, and the monitored  $F_{10.7}$  solar radiation and magnetic indexes. As can be seen, the flux during the latter months of the mission was almost two orders of magnitude greater than the flux encountered early in the mission.

Utilizing this flux history, the total atomic oxygen fluence on the leading LDEF surfaces in the ram direction was determined to be  $9.09 \times 10^{21}$  atoms/cm<sup>2</sup>. (The total atomic oxygen fluence as a function of LDEF tray position is presented in Appendix A.)

#### **3.2.2 Trapped Radiation**

In order to function in space, satellites must contend with the effects of trapped radiation. As a result of early satellite experiments, the existence of geomagnetically-trapped particles encircling the Earth was discovered. When electrons, protons, and other charged particles encounter the Earth's magnetic field, the field traps many of them. They oscillate back and forth along the lines of force, and since the magnetic field encircles the Earth, the trapped particles completely encircle the Earth.

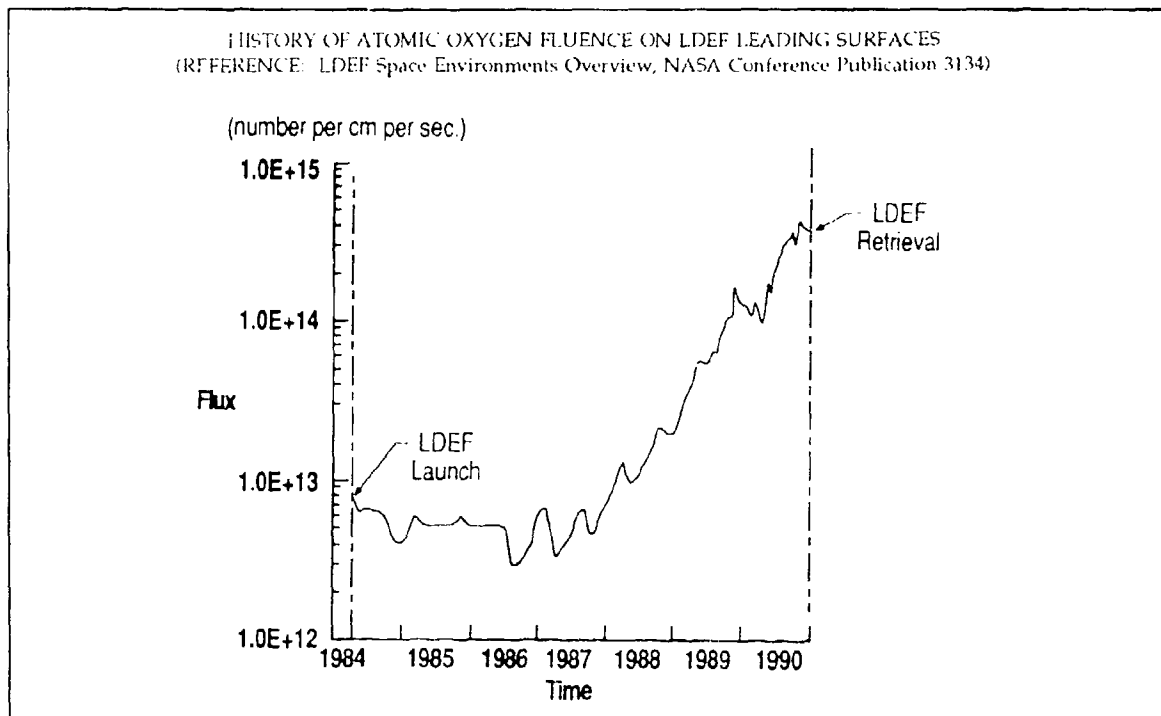


Figure 3.2-2. History Of Atomic Oxygen Fluence On LDEF Leading Surfaces

The so-called Van Allen belt has inner and outer portions. Both protons and electrons permeate the toroidal-shaped volume occupied by the Van Allen radiation belts. The protons are most intense at approximately 4000 km (2200 miles). The electron flux peaks at approximately 19,000 km (9900 miles). The volume of low-particle density separating the inner and outer portions of the belt is often called the "slot." Experience has shown that space vehicles in low circular orbit, roughly 230 km to 650 km (125-350 miles) receive an insignificant amount of radiation from the Van Allen zones. NASA has done an extensive amount of modeling (based on flight test data) to represent the radiation environments and their variation with altitude and inclination. The most current models are the AP-8 proton model (Ref. 2) and the AE-8 electron model (Ref. 4). Figures 3.2-3 and 3.2-4 (extracted from Refs. 2 and 4) illustrate the omnidirectional fluxes of electrons and protons over various altitudes and inclinations. As seen, at altitudes below 500 km, electron fluxes are about  $10^8$  to  $10^{10}$  electrons/cm<sup>2</sup>/day and proton fluxes are about  $10^5$  to  $10^6$  protons/cm<sup>2</sup>/day.

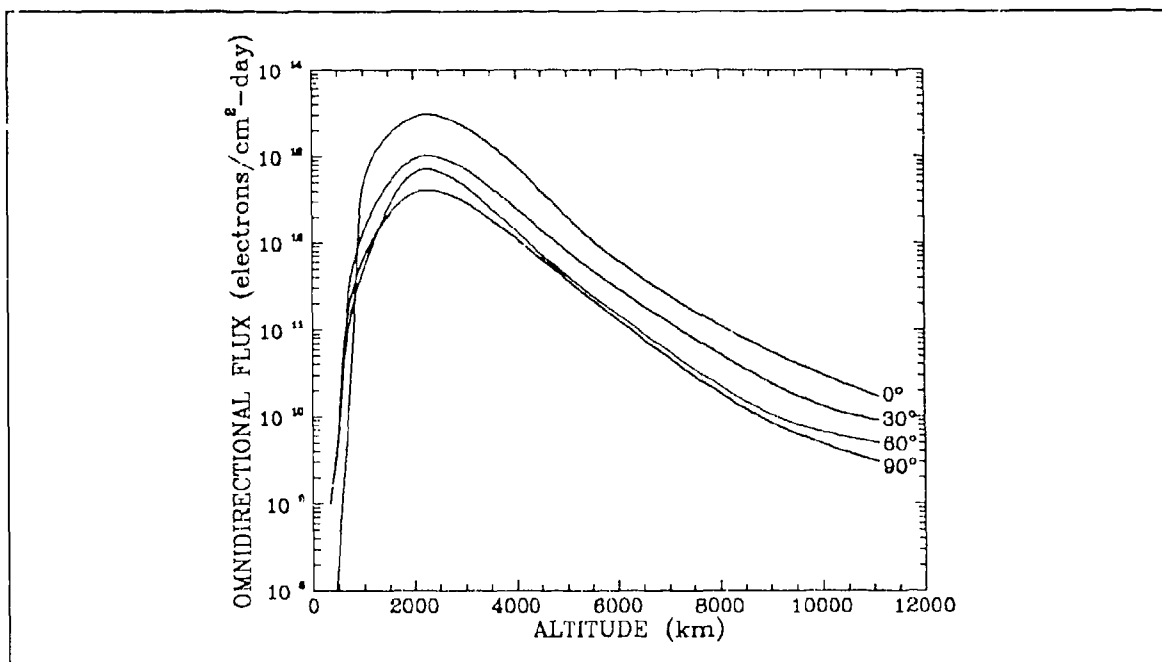


Figure 3.2-3. Circular Orbit Integration Electron Flux For Energies Above 0.5 MeV

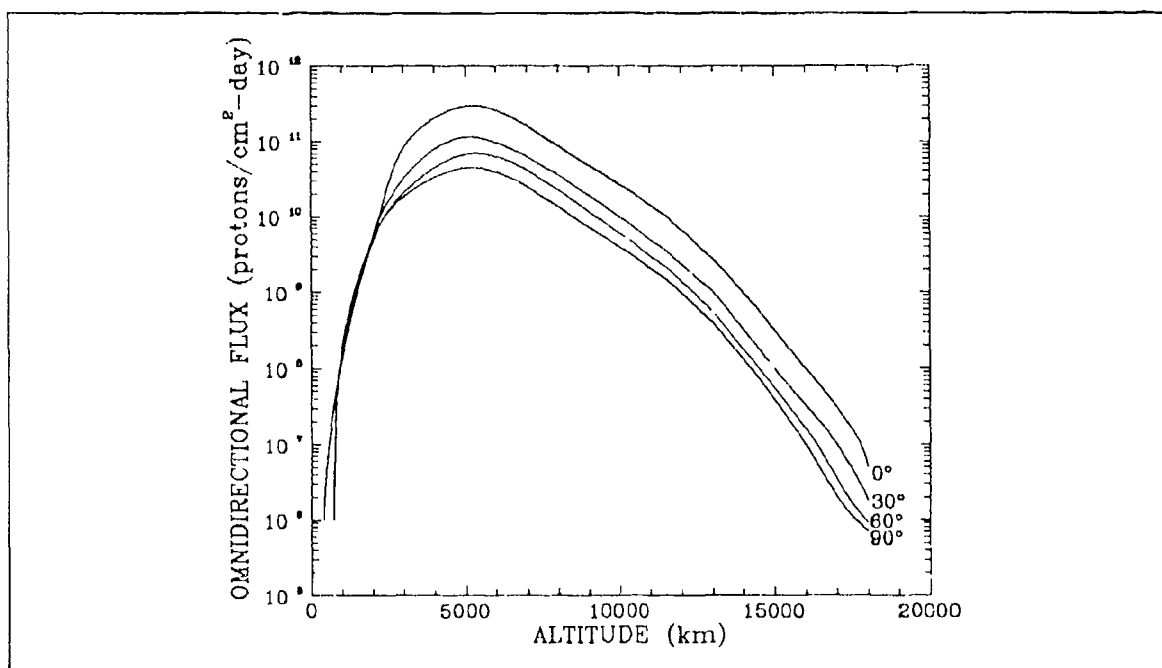


Figure 3.2-4. Circular Orbit Integration Proton Flux For Energies Above 4 MeV

### 3.2, Individual Space Environment Specifications

The radiation belts are approximately azimuthally-symmetric, except near what is termed the South Atlantic Anomaly. The magnetic field strength is lower than normal over the South Atlantic because of the dipole field geometry. Therefore, the radiation belts reach their lowest altitudes in this area. The LDEF orbit was well below the Earth's Van Allen radiation belts, except at the South Atlantic Anomaly.

The predicted integral fluence of the trapped electrons on the LDEF is shown in Figure 3.2-5 (Ref. 1). The predicted trapped proton integral fluence for LDEF is shown in Figure 3.2-6 (Ref. 1).

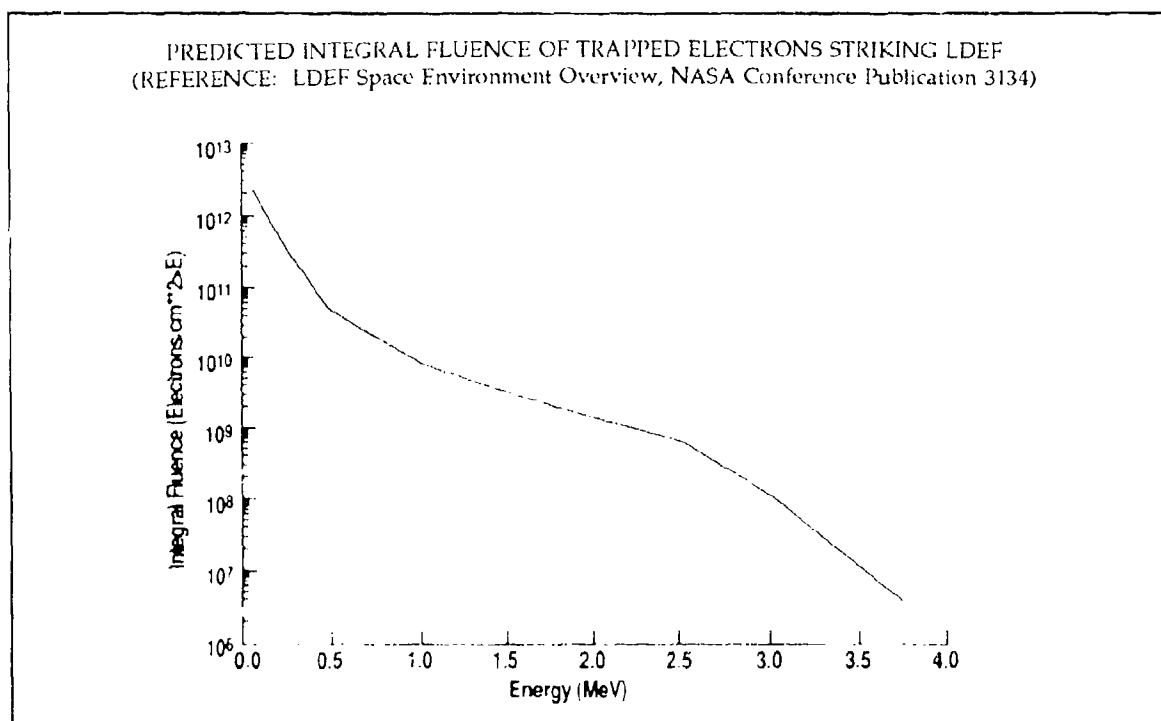


Figure 3.2-5. Predicted Integral Fluence Of Trapped Electrons Striking the LDEF

The primary components that contribute most to the penetrating charged particle radiation encountered are galactic cosmic rays and the geomagnetically-trapped Van Allen protons. Where shielding is less than 1.0 g/cm², geomagnetically-trapped electrons also make

### 3.2. Individual Space Environment Specifications

a significant contribution. For the above figures (3.2-3 through 3.2-6), the standard Vette models (Refs. 2-4) were used (together with the associated magnetic field models and the solar conditions). The geomagnetically-trapped electrons dominated the LDEF surface absorbed radiation dose.

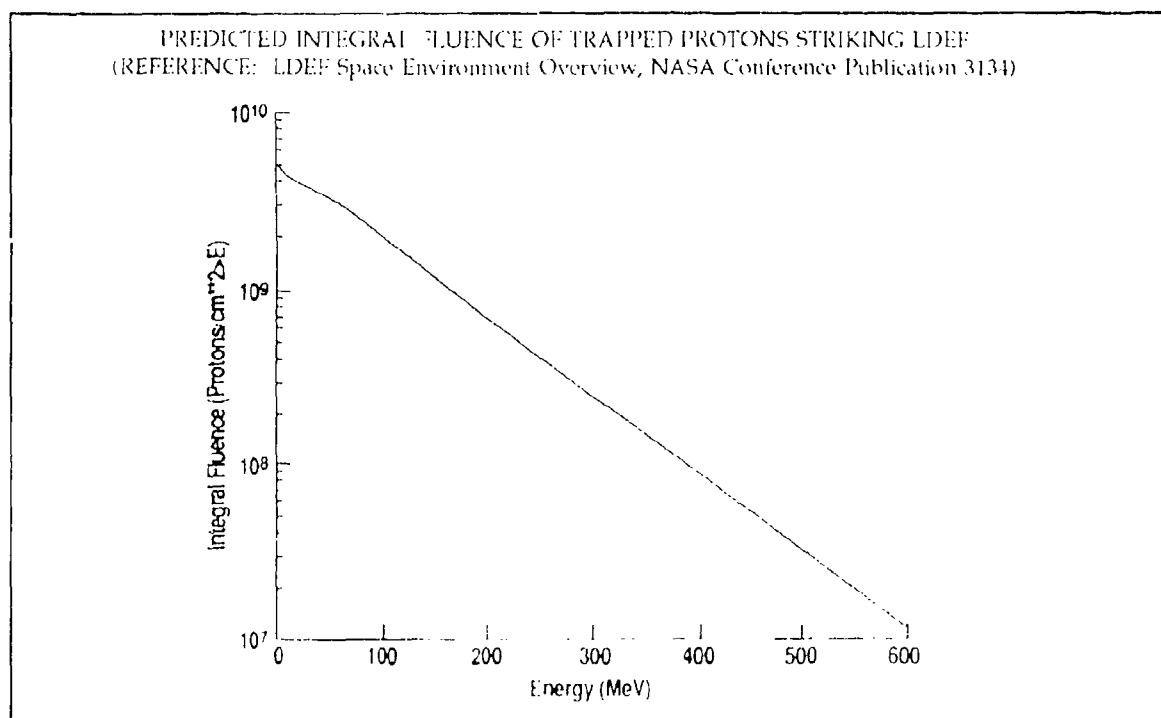


Figure 3.2-6. Predicted Integral Fluence Of Trapped Protons Striking the LDEF

Based on observed radiation doses from various thermoluminescent dosimeter (TLD) experiments, model improvements have been suggested for predicting the trapped proton angular distribution including both the pitch angle and east-west effects (Refs. 5-8). As a result of these experiments, predictions of the LDEF mission's trapped proton exposure have been made using the currently accepted models with improved resolution near mission end and better modeling of solar cycle effects. Mission fluences were reduced by 20 percent from pre-flight predictions. Calculations using directionally-dependent trapped proton spectra

predicted smaller doses than those measured, being 50 percent of measured values at the trailing and earth end and about 80 percent near the leading edge (Ref. 8)<sup>1</sup>.

#### **3.2.3 Meteoroids and Man-Made Debris**

The current models which are used most frequently to predict natural meteoroid and man-made debris impacts on spacecraft are shown in Figure 3.2-7 (Ref. 1). Based on these models, the largest man-made debris particles or the largest natural meteoroid particles one should expect to have impacted on the LDEF would be approximately 0.5 mm in diameter. An impact of a particle of this size is consistent with the size of the largest crater observed on the retrieved LDEF (Ref. 1). These models also indicate that in the particle size range from approximately 0.02 mm to 0.2 mm more of the impact particles would have been natural meteoroids rather than man-made debris. In the size range less than 0.02 mm in diameter, the models indicate that man-made debris particles should have dominated the impacts.

The man-made debris model includes an assumption that the small debris particles are in orbits similar to the orbits observed for the large trackable Earth orbiting debris objects. The assumption means that debris particles would have impacted primarily on the leading surfaces of the LDEF and that no debris impacts should be expected on the trailing LDEF surfaces (craters with man-made debris residue in them have been found on the trailing LDEF surfaces) (Ref.1). The model for the natural meteoroids assumes that they approach the Earth randomly from all directions with a distribution of velocities that average about 20 km/sec. This assumption means that the leading surface of the LDEF would also have been impacted

---

<sup>1</sup> Thermoluminescent dosimeter (TLD) measurements in four LDEF experiments have yielded absorbed dose as a function of shielding thickness near the leading and trailing edges and at the Earth side of the LDEF vehicle. A consistent set of dose values is produced which defines much of the LDEF radiation environment and provides comparisons for dose calculations using advanced trapped proton predictions and transport codes. Dose rates up to 3.14 mGy/d (0.48 g/cm<sup>2</sup> shielding) and down to 1.26 mGy/d (15.4 g/cm<sup>2</sup> shielding) were found near the trailing edge. The dose rate range near the leading edge was 0.99-1.22 mGy/d (2.90-1.37 g/cm<sup>2</sup> shielding) and at the Earth end it was 1.14-1.86 mGy/d (10.0-1.76 g/cm<sup>2</sup> shielding). (Ref. 8)

### 3.2, Individual Space Environment Specifications

more frequently by meteoroids than the trailing LDEF surfaces. The meteoroid models, unlike the debris models, indicate that a substantial number of meteoroid particles will strike the trailing surfaces of the LDEF. (This is generally consistent with the distribution of the craters found on the LDEF.) Specifics concerning each of these environments follow.

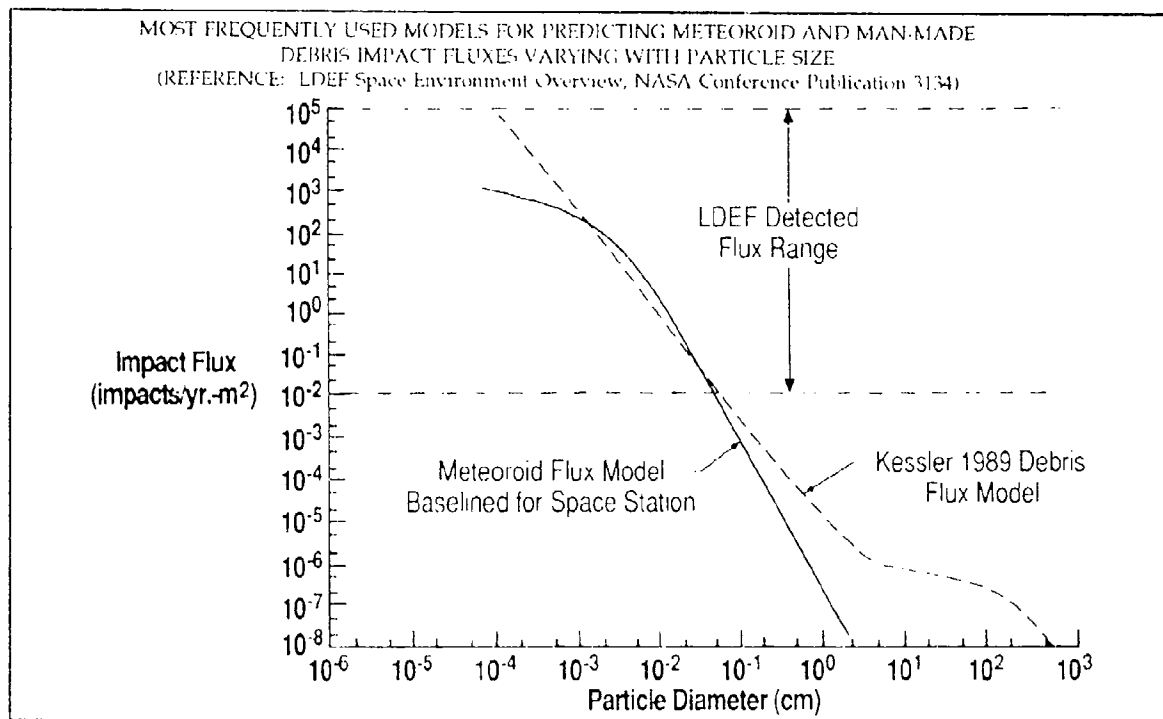


Figure 3.2-7. Most Frequently Used Models For Predicting Meteoroid and Man-Made Debris Impact Fluxes Varying With Particle Size

#### 3.2.3.1 Meteoroids

Meteoroids are solid particles moving in interplanetary space and originate from both cometary and asteroidal sources. Because of their velocity, density, and mass, meteoroids can cause damage to vehicles operating in space. The type and extent of the damage depend on vehicle size, vehicle structural configuration, and exposure time in space, as well as on meteoroid characteristics.



**3.2.3.1.1 Meteoroid Flux and Density.** Figure 3.2-8 (Ref. 11) shows a curve depicting the meteoroid flux. The data presented are used to determine the number of expected collisions per year between a space vehicle of a given cross-sectional area (in the ram direction) and meteoroids of a given diameter. The meteoroid flux curve is roughly approximated by the following equation, assuming a meteoroid density<sup>2</sup> of 0.5 g/cm<sup>3</sup> (see Refs. 9 and 10):

$$\log_{10}(F) = -14.37 - 1.213 \log_{10}(m)$$

where,

F = cumulative meteoroid flux (particles/m<sup>2</sup>/sec)

m = mass in grams (valid for 10<sup>-6</sup> ≤ m ≤ 1)

Reference 10 cites a flux component for micrometeoroids (defined as having diameters < 50 μm). The micrometeoroid density is generally assumed to be 2 g/cm<sup>3</sup> for these particles. The meteoroid flux for these smaller particles is given by (see Ref. 10):

$$\log_{10}(F) = -14.339 - 1.584 \log_{10}(m) - 0.063 [\log_{10}(m)]^2$$

where,

F = cumulative meteoroid flux (particles/m<sup>2</sup>/sec)

m = mass in grams (valid for 10<sup>-12</sup> ≤ m ≤ 10<sup>-6</sup>)

---

<sup>2</sup> The density of meteoroids is open to serious uncertainty as it has not been a measured quantity. Although meteorites have been examined, they are generally considered to have been meteoroids of asteroidal origin. The meteoroid density of interest is for particles which result from the break-up of cometary material. The cometary meteoroid has been described as a conglomerate of dust particles bound together by frozen gases. The flux-mass relationship assumed a mass density less than 1 g/cm<sup>3</sup>. Values of density calculated from photographic and radar observations have ranged from 0.16 g/cm<sup>3</sup> to 4 g/cm<sup>3</sup>. In assessing the available density data, related assumptions, and calculation procedures, the opinion is that the lower densities obtained from radar observed meteor data were not reliable and that the higher densities were not typical of cometary debris (Ref. 11). From the assessment, 0.5 g/cm<sup>3</sup> was chosen as the value for the mass density of meteoroids (both sporadic and stream) of cometary origin.

---

**3.2.3.1.2 Meteoroid Velocity.** Meteoroids can approach earth from both prograde and retrograde directions. The geocentric velocity of meteoroids is expected to range from 11 to 72 km/sec on the basis of celestial mechanics (see Ref. 11). Analyses of photographic and radar observations of meteors entering the Earth's atmosphere have confirmed this range. Based on the velocity information available, primarily from photographic meteor measurements, and on the basis of the assumption of independence of mass and velocity, an average atmospheric entry velocity of 20 km/sec has been adopted as the average velocity of sporadic meteoroids. The probability distribution for this average velocity is given in Figure 3.2-9 (Ref. 11).

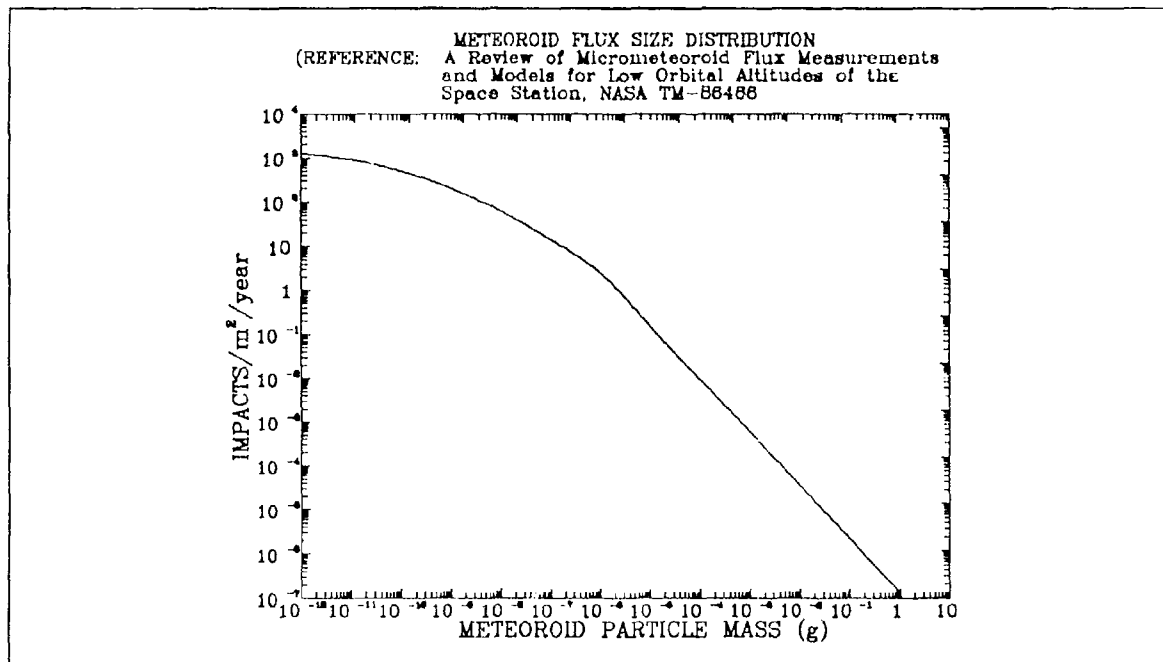


Figure 3.2-8. Meteoroid Flux Size Distribution

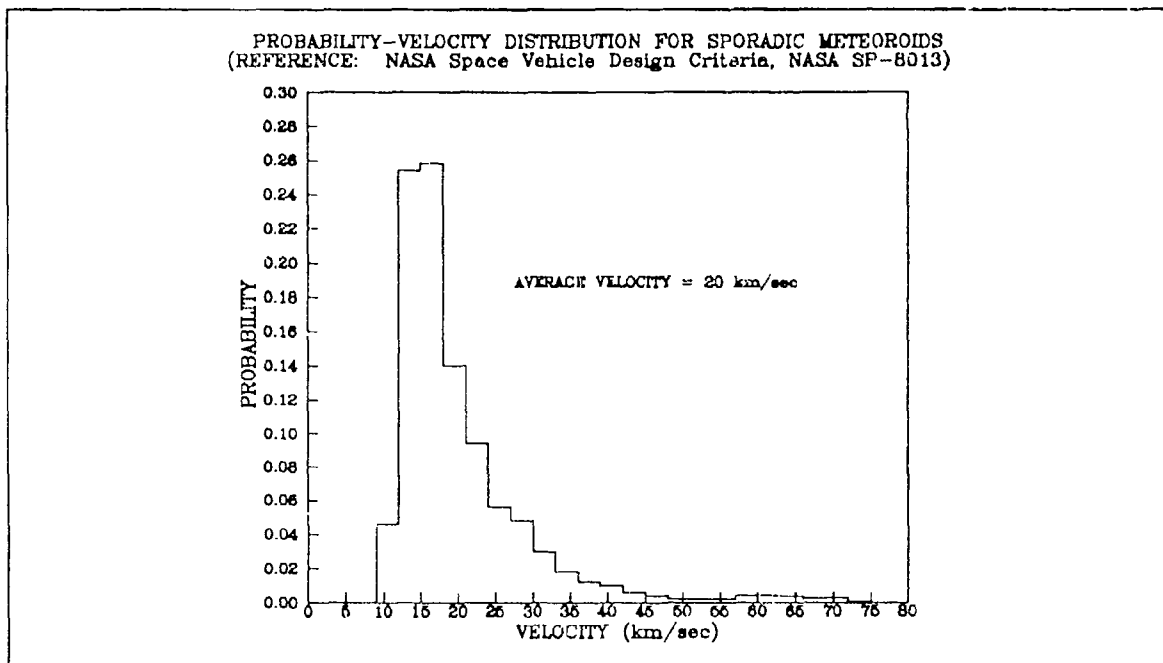


Figure 3.2-9. Velocity Probability Distribution For Sporadic Meteoroids

**3.2.3.1.3 Gravitational Defocusing Factor.** There are two phenomena which influence the actual flux encountered by spacecraft in near-Earth orbits. These phenomena are the gravitational and shielding effects of the Earth and the Moon. The actual number of meteoroid impacts encountered by a spacecraft, obtained from Earth-based observational techniques and orbital direct measurements, is found to have been enhanced by Earth's gravity; i.e., the sporadic flux model is gravitationally-focused. To correct for the Earth's gravitational enhancement at a given distance above the Earth, the average sporadic or total meteoroid flux must be multiplied by the defocusing factor. The factor, as a function of distance above the center of the Earth in Earth radii is given in Figure 3.2-10 (Ref. 10).

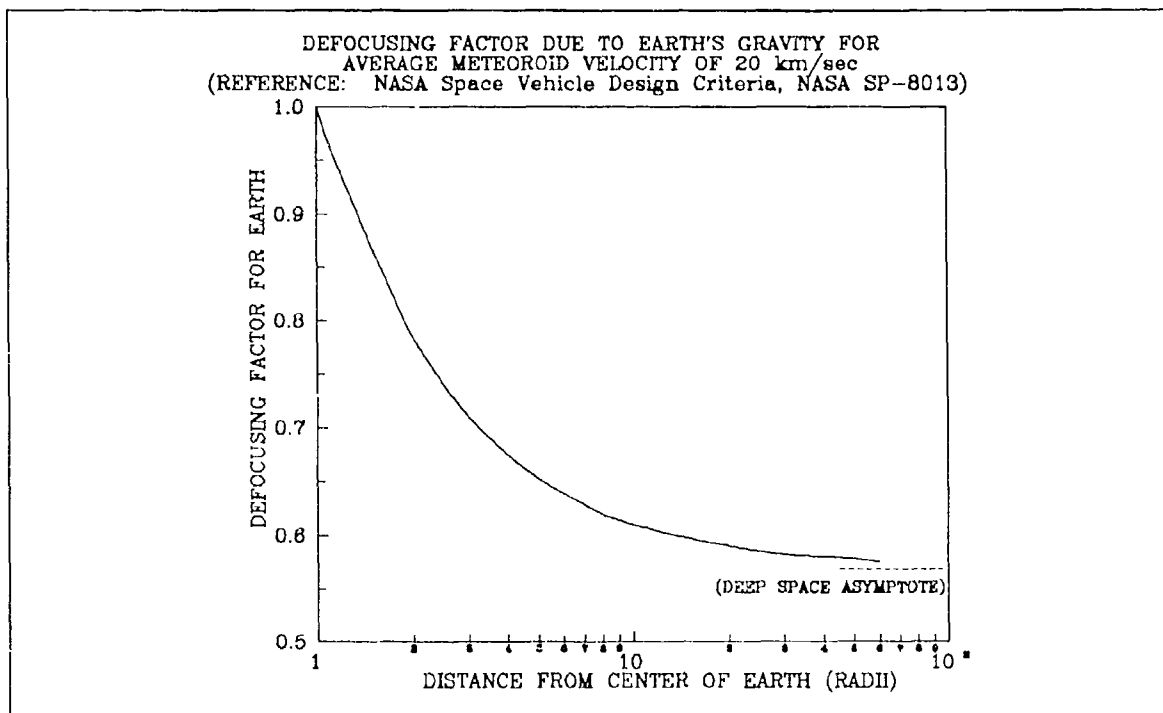


Figure 3.2-10. Defocusing Factor Due To Earth's Gravity For Average Meteoroid Velocity of 20 km/sec.

### 3.2.3.2 Man-Made Debris

Within about 2000 km above the Earth's surface there is an estimated 3,000,000 kg of man-made orbiting objects. These objects are in mostly high inclination orbits and sweep past one another at an average speed of 10 km/sec. Most of this mass is concentrated in approximately 3000 spent rocket stages, inactive payloads, and a few active payloads. A smaller amount of mass, approximately 40,000 kg, is in the remaining 4000 objects currently being tracked by U.S. Space Command radars. Most of these objects are the result of more than 90 on-orbit satellite fragmentations. Recent ground telescope measurements of orbiting debris combined with analysis of hypervelocity impacts on the returned surfaces of the Solar Maximum Mission satellite indicate a total mass of approximately 1000 kg for orbital debris sizes of 1 cm or smaller, and approximately 300 kg for orbital debris smaller than 1 mm.

### 3.2, Individual Space Environment Specifications

---

This distribution of mass and relative velocity is sufficient to cause the orbital debris environment to be more hazardous than the meteoroid environment to most spacecraft operating in Earth orbit below 2000 km.

Mathematical modeling of this distribution of orbital debris predicts that collisional fragmentation will cause the amount of mass in the 1 cm and smaller size range to grow at twice the rate as the accumulation of total mass in Earth orbit. Over the past 10 years, this accumulation has increased at an average rate of 5 percent per year, indicating that the small sizes should be expected to increase at 10 percent per year.

**3.2.3.2.1 Debris Flux and Density.** The cumulative flux of orbital debris of size  $d$  and larger on spacecraft orbiting at altitude  $h$ , inclination  $i$ , in the year  $t$ , when the solar activity for the previous year is  $S$ , is given by the following equation (Ref. 12):

$$F(d,h,i,t,S) = k \cdot \Phi(h,S) \cdot \Psi(i) \cdot [F_1(d) \cdot g_1(t) + F_2(d) \cdot g_2(t)]$$

where

- $F$  = flux impacts per square meter of surface area per year
- $k$  = 1 for randomly tumbling surface; must be calculated for a directional surface
- $d$  = orbital debris diameter in centimeters
- $t$  = time expressed in years
- $h$  = altitude in kilometers ( $h \leq 2000$  km)
- $S$  = 13-month smoothed 10.7 cm-wavelength solar flux expressed in  $10^4$  Jy; retarded by 1 year from  $t$
- $i$  = inclination in degrees

and

$$\Phi(h,S) = \frac{\Phi_1(h,S)}{\Phi_1(h,S) + 1}$$

$$\Phi_1(h,S) = 10^{(h/200 - S/140 - 1.5)}$$

### 3.2, Individual Space Environment Specifications

---

$$F_1(d) = 1.05 \times 10^{-5} \cdot d^{-2.5}$$

$$F_2(d) = 7.0 \times 10^{10} \cdot (d + 700)^{-6}$$

$p$  = assumed annual growth rate of mass in orbit

$$g_1(t) = (1 + 2 \cdot p)^{(t - 1985)}$$

$$g_2(t) = (1 + p)^{(t - 1985)}$$

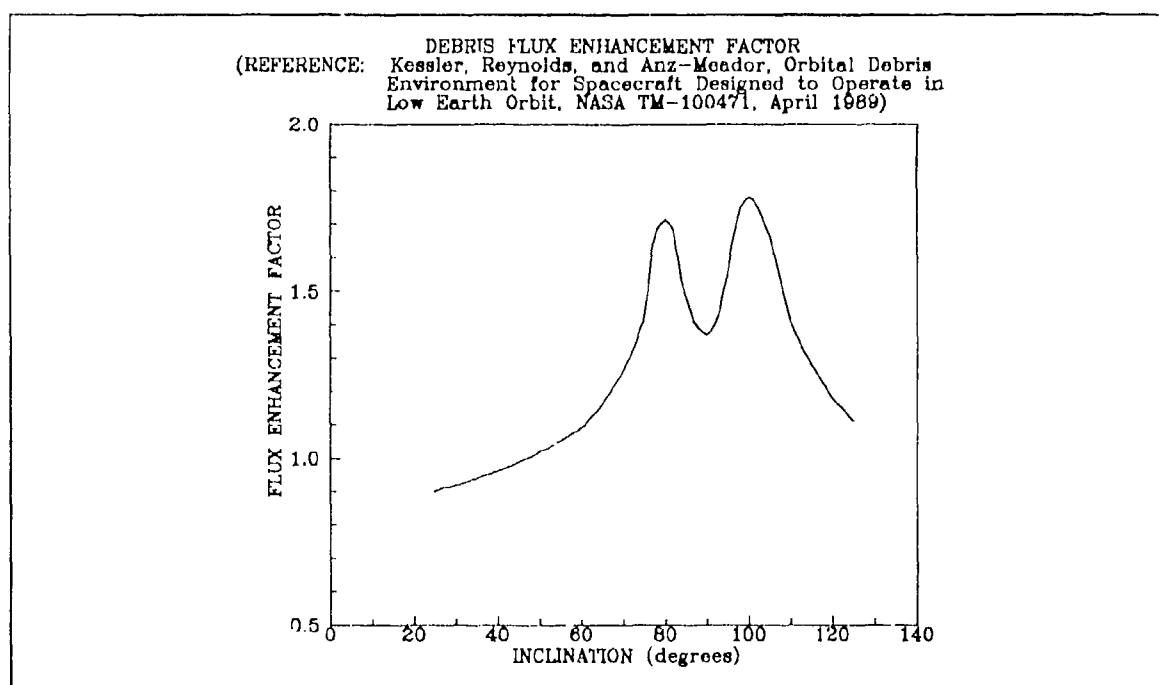
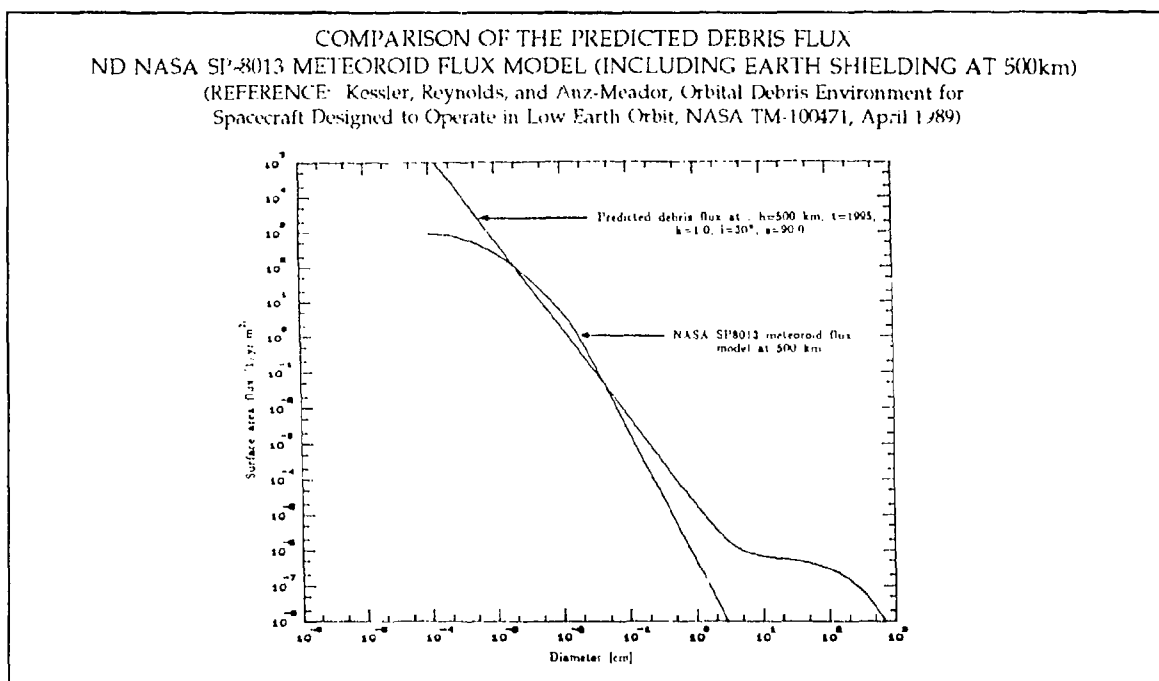
An average 11-year solar cycle has values of  $S$  which range from 70 at solar minimum to 150 at solar maximum.

To illustrate the application of this model, Figure 3.2-11 (Ref. 12) shows an example orbital debris flux (compared to the meteoroid flux from Ref. 11) for a 500 km, 30° orbit with  $t = 1995$ ,  $k = 1.0$ , and  $S = 90.0$ .

The average mass density for debris objects 1 cm in diameter and smaller is 2.8 g/cm<sup>3</sup>. The average mass density for debris larger than 1 cm is based on observed breakups, area-to-mass calculations derived from observed atmospheric drag, ground fragmentation tests, and known intact satellite characteristics. This density has been found to fit the following relationship:

$$\rho_{g/cm^3} = 2.8 \cdot d^{-0.74}$$

The inclination-dependent function  $\psi$  is a ratio of the flux on a spacecraft in an orbit of inclination  $i$  to that flux incident on a spacecraft in the current population's average inclination of approximately 60°. The flux enhancement factor,  $\psi$ , is shown in Figure 3.2-12 (Ref. 12).



**3.2.3.2.2 Orbital Debris Velocity and Direction Distribution.** Averaged over all altitudes, the unnormalized collision velocity distribution, i.e., the number of impacts with velocities between  $v$  and  $v + dv$ , relative to a spacecraft with orbital inclination  $i$  is given by the following equations:

$$f(v) = (2 \cdot v \cdot v_o - v^2) \cdot (G \cdot e^{-((v - A \cdot v_o)/(B \cdot v_o))^2}) + (F \cdot e^{-((v - D \cdot v_o)/(E \cdot v_o))^2}) + H \cdot C \cdot (4 \cdot v \cdot v_o - v^2)$$

where  $v$  is the collision velocity in kilometers per second,  $A$  is a constant, and  $B, C, D, E, F, G, H$ , and  $v_o$  are functions of the orbital inclinations of the spacecraft. The values of these constants and parameters are as follows:

$A =$	2.5	
$B =$	0.5	$i < 60$
	$0.5 - 0.01 (i - 60)$	$60 < i < 80$
	0.3	$i > 80$
$C =$	0.0125	$i < 100$
	$0.0125 + 0.00125 (i - 100)$	$i > 100$
$D =$	$1.3 - 0.01 (i - 30)$	
$E =$	$0.55 + 0.005 (i - 30)$	
$F =$	$0.3 + 0.0008 (i - 50)^2$	$i < 50$
	$0.3 - 0.01 (i - 50)$	$50 < i < 80$
	0.0	$i > 80$
$G =$	18.7	$i < 60$
	$18.7 + 0.0289 (i - 60)^3$	$60 < i < 80$
	250.0	$i > 80$
$H =$	$1.0 - 0.0000757 (i - 60)^2$	
$v_o =$	$7.25 + 0.015 (i - 30)$	$i < 60$
	7.7	$i > 60$

---



### 3.2, Individual Space Environment Specifications

When  $f(v)$  is less than zero, the function is to be reset equal to zero. An example for the unnormalized collision velocity distribution for an inclination at  $30^\circ$  is shown in Figure 3.2-13 (Ref. 12).

There are other methods which have produced larger values for the average relative velocity between a satellite and a piece of space debris in LEO. By using the tracked debris population provided by radar observations, the average relative velocity may be calculated through numerical simulation of possible encounters or through direct averaging (Ref. 13). Both of these methods derive an average collision velocity of 10 km/s. Figure 3.2-14 (extracted from Ref. 13) shows the range of relative velocities from various altitudes and orbital inclinations.

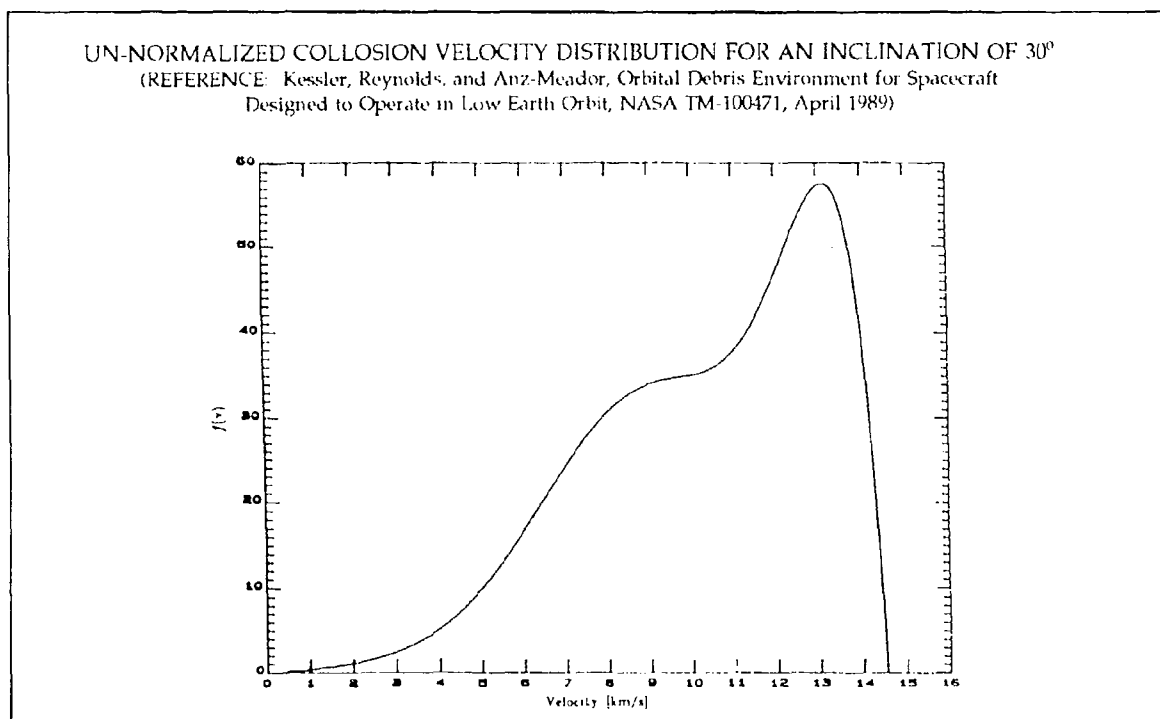


Figure 3.2-13. Un-normalized Collision Velocity Distribution for an Inclination of  $30^\circ$

Calculations have been done recently supporting near-term strategic programs for the number of impacts per square meter by particles of various sizes. Figure 3.2-15 (Ref. 14) shows a typical set of results for the number of expected impacts as a function of altitude at 60° inclination for the environment expected in the 1996-2002 timeframe. A description of the relative impacts versus position of LDEF trays is presented in Appendix A. A more detailed description of the meteoroid and space debris environments and effects is contained in Chapter 6.

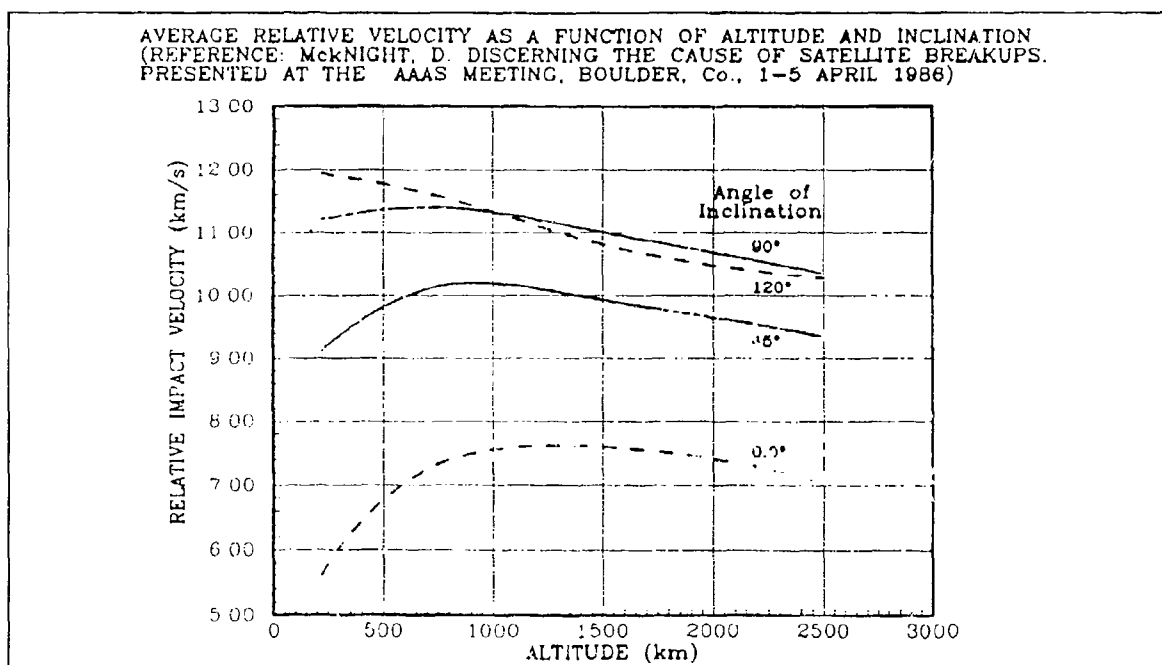


Figure 3.2-14. Average Relative Velocity Expected Between An Object and A Piece Of Space Debris As A Function of Altitude and Inclination.

#### 3.2.4 Ultraviolet (UV) Radiation/Solar Exposure

The Sun's extreme ultraviolet (EUV) and UV output varies in a pattern similar to sunspot number (SSN), and this variability translates into a variation of energy available to

### 3.2. Individual Space Environment Specifications

the thermosphere. The resulting variation of exospheric temperature, in turn, produces a solar cycle variation of atmospheric density. Since little EUV radiation reaches the ground, direct EUV flux observations have been made only rarely. However, we can infer the value based on solar radio flux measurements at 2800 MHz because EUV and 2800-MHz fluxes have shown a fairly good correlation. The 2800-MHz flux is better known as the 10.7-cm flux (or  $F_{10.7}$ ). Although the correlation is not exact (and varies from one sunspot cycle to the next), the patterns are similar enough to be useful. The  $F_{10.7}$ -flux history for the LDEF mission is shown in Figure 3.2-16 (Ref. 1). The widely varying levels of solar activity were monitored by the  $F_{10.7}$ -flux, but also by counts of solar flares and Sun spots and by measurements of the geomagnetic index.

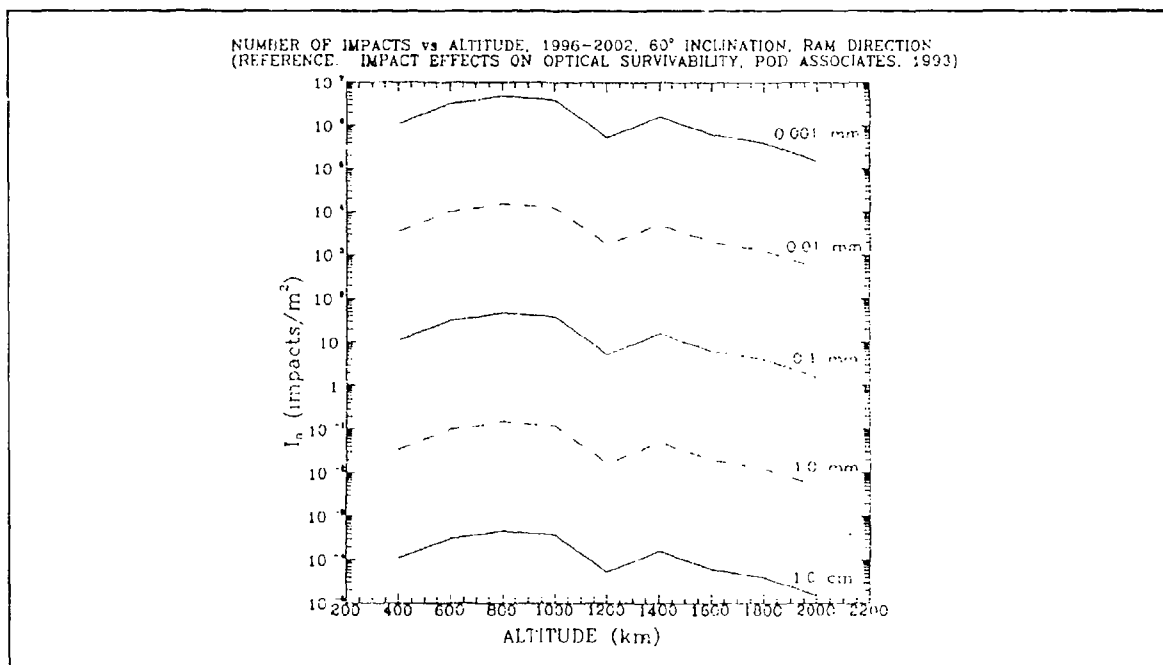


Figure 3.2-15. Number of Debris Impacts vs. Altitude, 1996-2002 Period, 60° Inclination From the Ram Direction

### 3.2, Individual Space Environment Specifications

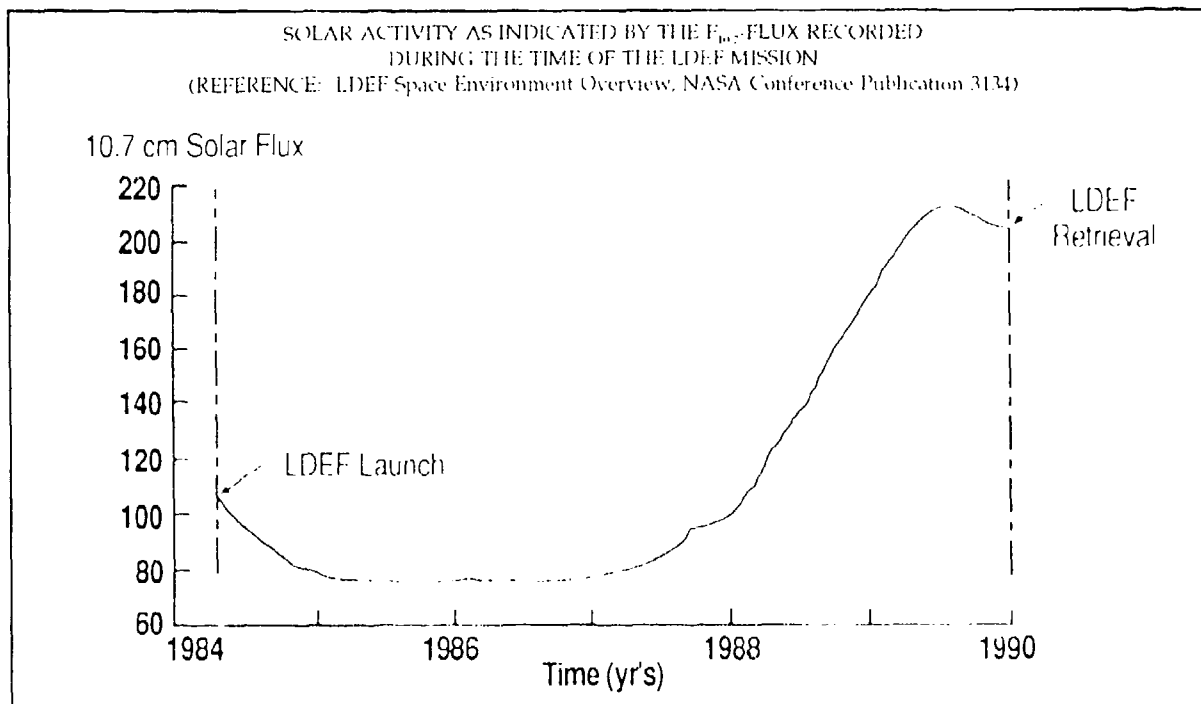


Figure 3.2-16. Solar activity as indicated by the  $F_{10.7}$ -Flux recorded during the time of the LDEF mission.

The number of sun hours to which LDEF experiments were exposed is a function of orbit (e.g., eclipse times, etc.) and sun  $\beta$ -angle. The calculated cumulative equivalent sun hours for each LDEF tray row is presented in detail in Appendix A.

#### 3.2.5 Vacuum

Neglecting the contribution from LDEF generated contamination, the molecular/atomic density adjacent to the individual LDEF surfaces at any given time was dependent on the LDEF orbital altitude, the solar activity<sup>4</sup>, and the orientation of the surface with respect to the LDEF velocity vector. The density increased as the altitude decreased and as the solar

<sup>4</sup> The LDEF was launched into Earth orbit at the time of near-minimum activity in the Sun's 11-year solar cycle and was retrieved almost 5.75 years later at a time of near maximum solar activity. This solar cycle is found to have near record highs for solar activity.

### *3.2, Individual Space Environment Specifications*

---

activity increased. The density also built up adjacent to leading surfaces as a result of ram effects, and it diminished adjacent to trailing surfaces as a result of wake shielding effects.

The ambient molecular/atomic density along the LDEF orbit was lowest early in the mission while the LDEF orbital altitude was above about 450 km; the solar activity was near minimum (approximately  $1.86 \times 10^7$  molecules/cm<sup>3</sup>). The predominant molecular/atomic species at that time were atomic oxygen (approximately  $1.56 \times 10^7$  molecules/cm<sup>3</sup>) (see Chapter 3.2.1), and nitrogen (second in abundance with a density several orders of magnitude lower than the atomic oxygen).

The ambient molecular/atomic density along the LDEF orbit was highest (approximately  $6.58 \times 10^8$  molecules/cm<sup>3</sup>) late in the mission when the orbital altitude had decayed to approximately 320 km; the solar activity had increased to near-record highs. The predominant molecular/atomic species at that time was still atomic oxygen (approximately  $5.42 \times 10^8$  molecules/cm<sup>3</sup>) and nitrogen was still second in abundance (approximately  $1.06 \times 10^8$  molecules/cm<sup>3</sup>).

The ram effects made the molecular/atomic density adjacent to surfaces on the leading side of the LDEF approximately an order of magnitude higher than the ambient density. The wake shielding effects reduced the molecular/atomic density adjacent to surfaces on the trailing side of the LDEF more than an order of magnitude. (The molecular/atomic densities presented above were extracted from Ref. 1).

#### **3.2.6 Microgravity/Accelerations**

The LDEF experiments were exposed to very low accelerations during the mission since the platform was passively stabilized and there were no systems on board to generate

### *3.2, Individual Space Environment Specifications*

---

vibrations or shocks. The acceleration level at the center of the LDEF remained less than  $10^{-7}$  g throughout the mission.



## **CHAPTER 4**

### **LDEF OBSERVATIONS**

On LDEF there were 57 different experiments in 86 trays which were divided, according to Boeing, into mechanical, electrical, thermal, and optical experiments. The purpose of this section is to identify and collate the published data from LDEF experiments relating to space optics. (Discussions on design implications of these data are deferred to Chapter 5.) At this time, the reduction and reporting of the on-orbit data by the LDEF experimenters are not complete. This section contains the data that have been reported to date by the experimenters. The structure of this handbook was designed to allow periodic updates as additional data reduction is reported by the LDEF experimenters.

#### **4.1 SUMMARY OF LDEF OPTICAL MATERIALS/EXPERIMENTS**

There are literally hundreds of optical materials from which a system designer can choose. These are catalogued in references such as the Handbook of Military Infrared Technology and individual glass manufacturer catalogs, among others. A representative set of current, state-of-the-art optical materials and designs were tested on LDEF. This experimental data set provides valuable insights into the space response of modern optical materials and designs.

The optics flown on LDEF can be divided according to a number of individual design features: refractive/reflective, substrates/windows, coatings/filters, UV/visible or infrared (IR) transmission, etc. To make this handbook as useful as possible, a number of groupings have been established to categorize LDEF materials. Table 4.1-1 shows the groupings followed within this handbook and identifies the LDEF materials within each group that are included in this section. Optical design parameters associated with the materials in Table 4.1-1 and tested on LDEF are discussed in the following section.



**Table 4.1-1. Optical Components Flown on LDEF**

OPTICAL COMPONENTS	LDEF MATERIALS
Optical Glasses and Crystals (Refractive and Reflective, UV/Visible and IR)	Aluminosilicate, borosilicate, lead silicate, potash borosilicate, SiO <sub>2</sub> , soda lime silica, soda potash lime, titanium silicate, black glass (low scatter), CaF <sub>2</sub> , CdTe, Ge, Si, KRS-5, KRS-6, ZnSe, BaF <sub>2</sub> , Al <sub>2</sub> O <sub>3</sub> , Corning 7940, Suprasil W, Ge (polycrystalline, high purity), and UV-transmissive windows (MgF <sub>2</sub> , sapphire [Al <sub>2</sub> O <sub>3</sub> ], CaF <sub>2</sub> , LiF, and SiO <sub>2</sub> )
Optical Filters (UV/Visible and IR)	CdSe, Ge, PbTe, PbF <sub>2</sub> , SiO, ZnS, Cryolite on SiO <sub>2</sub> , SiO on SiO <sub>2</sub> , ThF <sub>2</sub> on SiO <sub>2</sub> , Antirejection (AR) coating on MgF <sub>2</sub> , assorted optical bandpass filters between 0.3 and 1.1 $\mu$ m (Schott glasses), neutral density filters (Corion), narrow band (Corion), hot mirrors (Corion visible transmitting), Lyman alpha and 1600 Å UV filters, Al <sub>2</sub> O <sub>3</sub> on SiO <sub>2</sub> , MgF <sub>2</sub> on SiO <sub>2</sub> , assorted OCLI filters, and Ge on SiO <sub>2</sub>
Metal Films/Mirrors (Reflective, UV/Visible and IR)	Ag on SiO <sub>2</sub> , Al on SiO <sub>2</sub> , Au-plated Al [2024-T351], Au-plated Al [6003], Au on SiO <sub>2</sub> , Ir on SiO <sub>2</sub> , Nb on SiO <sub>2</sub> , Os on SiO <sub>2</sub> , Pt on SiO <sub>2</sub> , Cu on SiO <sub>2</sub> , Ag on C, Ag on SiO <sub>2</sub> , Ta on SiO <sub>2</sub> , W on SiO <sub>2</sub> , Sn on SiO <sub>2</sub> , Zn on SiO <sub>2</sub> , OSR mirrors [Au, Al, Ag], molybdenum mirror, and diamond turned copper mirror

## 4.2 OPTICAL SYSTEM DESIGN PARAMETERS

There are a number of parameters associated with the optics shown in Table 4.1-1 that are important parts of optical system design. The value of the LDEF data is in the characterization of the degradation of these parameters as the optical materials are exposed to the space environments.

From a system performance viewpoint, the degradation of each individual optical element can degrade system performance. For example, if transparent elements are degraded by the space environments, these degradations can change the element transmission, can increase the scatter and absorption, and can degrade the overall image resolution. For optical coatings, environment degradations can alter the wavelength-dependent transmission and reflection properties, can initiate other types of damage (such as deterioration), and can contaminate other nearby optical components. On LDEF, experiments were conducted to examine the degradation of transparent elements, optical coatings, and other materials (such as

diffuse paints). Degradation of these elements due to darkening, contamination, erosion, discoloration, impacts, pitting, or delamination caused by space environments was analyzed by the LDEF experimenters.

Table 4.2-1, Materials versus Effects, provides a guide to the parameters tested on LDEF for optical materials that have been published to date and are included in this chapter. The table divides the optical elements flown on LDEF (see Section 4.1) into refractive and reflective components, including substrates, coatings, filters, and mirrors as well as other components of interest like quartz crystal microbalances (QCMs). These elements are listed down the left-hand column of the matrix in Table 4.2-1. Across the top of the matrix, the parameter effects that are of concern to system optical performance are identified.

Within the cross-reference matrix are filled circles, hollow circles, and empty cells. Filled circles identify data sections where data are discussed that have been reduced and reported by the LDEF experimenters. The hollow circles identify data sections where reduced and reported data have been found and are generally applicable to materials discussed within that section, but are discussed elsewhere within this chapter. (Following the matrix column up or down from the hollow circles will show where sections contain the actual data discussions, as marked by a filled circle.) Empty cells within the matrix identify areas where data are not available. An empty cell does not necessarily mean that there was no experiment in this category on LDEF, but perhaps that the data have not been reduced and reported by the LDEF experimenters. As this handbook is updated, these cells will be filled as the new data are brought into the handbook.

The numbering index in the table also provides a convenient index of where the data are located in this section. For example, suppose one wishes to examine the data base on the effects of AO on uncoated refractive optics for a visible sensor system. The section number within which to find these data is found by combining the indices of succeeding levels of indenture from the table. The left-hand index on materials shows that uncoated refractive

## 4.2, Optical System Design Parameters

optics for visible systems are addressed in section .3.1 of Chapter 4 (4.3.1) and AO is addressed in section .2 of 4.3.1. Thus one would locate that data in Section 4.3.1.2 of this report.

**Table 4.2-1. Materials Versus Effects Matrix**

<div style="display: flex; align-items: center; justify-content: center;"> <div style="transform: rotate(-45deg); transform-origin: center;"> <div style="width: 100px; height: 100px; border: 1px solid black; position: relative;"> <div style="position: absolute; top: 0; right: 0; width: 50%; height: 50%; border: 1px solid black; transform: rotate(45deg);"></div> </div> </div> <div style="margin-left: 10px;"> <div style="text-align: center;">EFFECTS</div> <div style="text-align: center;">MATERIALS</div> </div> </div>			.1	.2	.3	.4	.5	.6	.7
			I M P A C T S	A O T X O Y M G I E C N	S C A T T E R	T R E A F F L E M I T S A N I T I O N /	D A R K E N I N G	S T R E S S	C O N T A M I N A T I O N
.3	Refractive Uv/Vis	.1 Uncoated	●	●	○	●	●	●	●
		.2 Coated	○	●	●	●	●	●	○
.4	Refractive Infrared	.1 Uncoated	●	○	●	○	○	○	●
		.2 Coated	○	○	○	○	○	○	○
.5	Coatings Visible	.1	○	○	○	●			○
.6	Coatings Infrared	.1	●	○	○	○	○	○	●
.7	Filters UV/Visible	.1				●			
.8	Filters Infrared	.1				●			
.9	Mirrors	.1	●	●	○	○		○	●
.10	Mirrors Second Surface	.1	●						●
.11	Quartz Crystal Micro Balances	.1				●			●
.12	Related Optical Experiments	.1	●	●	●	●	●	●	●

## *4.2. Optical System Design Parameters*

---

At the beginning of each of the following data sections is an "a" table which lists the materials addressed in that section, the experiment location (so that the environments may be determined from Appendix A), the tables and figures related to that material (which are in Appendix E), and comments which are applicable to each table or figure. Each table or figure in Appendix E identifies the reference from which it was obtained, the experiment on which it was flown, and any appropriate comments concerning the data and the results observed. A section may also include a "b" table. A "b" table lists data pertinent to the section, but the data are discussed in detail in another section. The section in which the data are discussed is referenced in the table.

In reporting on the LDEF observations for the material flown and for which the data have been reduced, it was often difficult to decide how to place optical material within the groupings/parameters as shown in Table 4.2-1. For example, when multilayer optical filters were flown, it also might be appropriate to include the flight data in the section covering coated refractive optics besides reporting the flight data in the filters section. However, in order to avoid needless duplication, it was decided that experimental data would be discussed only once.

Materials which are applicable to more than one optical category (e.g.,  $MgF_2$  is used for both UV and IR optical systems) are discussed just once in the most relevant section (see the "a" and "b" table discussion above). In addition, at the beginning of the major sections is a table that shows when effects for specific optical materials are cross referenced to other sections. This avoids needless text duplication and repetition. To make this handbook the most useful to optical designers, when it is appropriate to discuss LDEF results for optical materials from other sections, a summary table of those materials is provided and cross-references are given to direct the reader to appropriate sections containing the primary data discussion. (This table is identified with a "b" suffix indicating that the primary data discussion for these materials are in other sections and not in the current section. The data discussion section for these materials is identified in a footnote to the "b" table.)

### **4.3 REFRACTIVE OPTICS FOR UV/VISIBLE SYSTEMS**

A variety of refractive optics materials was flown on LDEF that transmit in the UV/visible wavelengths. The LDEF data currently available for UV/visible refractive optics are discussed below and are subdivided into uncoated and coated configurations. Table 4.3.a shows a summary of the experiments containing refractive UV/visible optics. Table 4.3.b is a cross-reference of the UV/visible refractive optics flown on LDEF cross-correlated with the kinds of effects studied on LDEF for these materials.

#### **4.3.1 Uncoated UV/Visible Refractive Optics**

##### **4.3.1.1 Impact Effects**

All LDEF UV/visible refractive optics samples suffered some impact damage due to either micrometeoroids or man-made debris. Impact damage consisted of various nicks and chips, or small quasi-hemispherical craters surrounded by spalls with conchoidal surfaces. Spalls extended out by a factor of 5 to 20 times the central crater size. Radial cracks generally extended two times the spall diameter beyond the spall region. In some cases stringers or fibers of molten material were observed.

The major effect of the impact damage is to produce an increase in optical scatter, but apparently, only negligible changes in overall reflectivity or transmission (see Sections 4.3.1.3 and 4.3.1.4 below). This is expected because of the overall low value of fractional area affected. Chapter 6 discusses the overall expectations for hypervelocity impacts on optics.

#### 4.3.1. Uncoated Refractive Optics for UV/Visible Systems

**Table 4.3.a. Experiment Summary for Refractive UV/Visible Optics**

EXPERIMENT	REFRACTIVE UV/VISIBLE OPTICAL MATERIALS
A0147	Uncoated fused silica and fused silica combinations
A0171	Coated fused silica
A0172	Uncoated fused silica, low iron soda-lime-silica glass, Pyrex 7740 glass, Vycor 7913 glass, BK-7 glass, and Zerodur glass ceramic
M0003-2	Uncoated fused silica (T22 Supersil-W1, Amersil) and coated fused silica (MgF <sub>2</sub> )
M0003-7	Al <sub>2</sub> O <sub>3</sub> on SiO <sub>2</sub> , Si on SiO <sub>2</sub> , NaF <sub>2</sub> on SiO <sub>2</sub>
S0014	Uncoated fused silica
S0050-1	CaF <sub>2</sub> , MgF <sub>2</sub> , LiF, Al <sub>2</sub> O <sub>3</sub> (synthetic sapphire) and uncoated fused silica
S0050-2	Uncoated fused silica, uncoated ULE™, ULE™/Ag coating, and coated fused silica (AR coatings, solar rejection coatings)

Table 4.3.1.1a summarizes and provides a guide to the materials contained in this section. Table 4.3.1.1b shows references to related materials/effects covered in other sections of this handbook.

In general, the impact damage to the fused silica consisted of various nicks and chips, or small quasi-hemispherical craters surrounded by surface spalls with conchoidal surfaces. The spalls produced the equivalent of wide shallow craters around the central craters proper, with the spall extending out by factors of 5 to 20 times the central crater size. In some cases radial cracks extended out beyond the spall region, generally by a factor of about two times the spall diameter, but occasionally by much larger factors. This effect tended to occur only for the larger impact craters. For most cases the impact damage was very localized to the immediate vicinity of the impact sites. In some cases some small residue from the impactor was observed, or "stringers/fibers" of molten fused silica were observed. The number and sizes of the craters were largest for the leading edge, as expected (Ref. 1).

Table 4.3.b. Refractive Optics for UV/Visible Systems Flown on LDEF

MATERIALS	EFFECTS						
	I M P A C T S	A T O M I C  O X Y G E N	A B S / T R A N / R E F L	D A R K E N I N G	S T R E S S	S C A T T E R	C O N T A M / D E T E R
<i>UNCOATED UV/VISIBLE REFRACTIVE OPTICS</i>							
Fused Silica (SiO <sub>2</sub> )	•	•	•	•	•	◦	•
Zerodur	•				•		
Pyrex	•				•		
BK-7	•				•		
Soda-Lime-Silica	•				•		
ULE™			•	•	•		
CaF <sub>2</sub>			•		•		•
MgF <sub>2</sub>			•				•
LiF			•				•
Al <sub>2</sub> O <sub>3</sub>			•				•
Vycor					•		

• Data contained in this section

◦ Data contained in other, cross referenced sections

Table 4.3.b. Refractive Optics for UV/Visible Systems Flown on LDEF (Cont.)

MATERIALS	EFFECTS						
	I M P A C T S	A T O M I C  O X Y G E N	A B S / T R A N / R E F L	D A R K E N I N G	S T R E S S	S C A T T E R	C O N T A M / D E I E R
COATED UV/VISIBLE REFRACTIVE OPTICS							
MgF <sub>2</sub> /Fused Silica	○					●	
MgF <sub>2</sub> ( $\lambda=1.06\mu$ )/2-thick on Fused Silica	○						
Fused Silica/Solar Rejection			●		●		●
ULE <sup>TM</sup> /Ag			●		●		●
Fused Silica/AR			●		●		●
NaF <sub>2</sub> /SiO <sub>2</sub>	○						
Al <sub>2</sub> O <sub>3</sub> /SiO <sub>2</sub>	○						
Si/SiO <sub>2</sub>							○

● Data contained in this section

○ Data contained in other, cross-referenced sections

Impacts on other optical glasses, including BK-7, Pyrex, ULE<sup>TM</sup>, and Zerodur tended to be similar to those in fused silica. This is expected, since the major differences in these glasses (for impact response) are mostly in melting temperatures, compressive yield strengths and/or fracture toughness. Lower melt temperatures, together with the possibility of



#### 4.3.1, Uncoated Refractive Optics for UV/Visible Systems

differential fractionation of the components, associated with BK-7, can be expected to allow bubbles to more readily form, and such were seen surrounding some impact craters.

Likewise, lower melt temperatures will promote more "stringer/fiber" production within the craters and a larger "melt zone" around the crater.

**Table 4.3.1.1a. Impact Effects Data Base for Uncoated Refractive UV/Visible Optics**

MATERIALS	FIGURES	LDEF LOCATION	COMMENTS
Fused Silica	E.1	E5	Localized impact damage.
	E.2	E5	Localized damage. Radial cracking does occur but does not propagate a great distance from impact site.
	E.3	D2	Molten glass jetting. Fibers 100 $\mu$ m long projecting from the fuse zone.
	E.9	D2	Characterization of impact site damage.
Zerodur	E.4	D2	Central pit surrounded by fragmented material with radial cracks. Debris captured in melt zone.
	E.5	D2	No melt. Similar damage to that shown in Figure E 4.0 except in central fusion zone.
	E.9	D2	Characterization of impact site damage.
Pyrex	E.6	D2	Damage area 5 times central pit radius.
	E.7	D2	Oblique impact produced strongly direction splash. Crater is circular.
	E.9	D2	Characterization of impact site damage.
BK-7	E.8	D2	Temperature and pressure for vaporization exceeded.
	E.9	D2	Characterization of impact site damage.
Soda-Lime-Silica	None	D2	Temperature and pressure for vaporization exceeded.
	E.9	D2	Characterization of impact site damage.

**Table 4.3.1.1b. Impact Effects Data Base for Uncoated Refractive IR Optics Applicable to Uncoated UV/Visible Optics**

MATERIALS	FIGURES	LDEF LOCATION	COMMENTS
Fused Silica <sup>1</sup>	E.34	D9	Exposed 69 months. Localized chipping and fracture extending many particle diameters.
	E.35	D9	Damage areas are potential high scatter, high absorption areas.
SiO <sub>2</sub> <sup>1</sup>	E.36	D4	No discernible changes except for debris.

<sup>1</sup> Data relevant to this material is discussed in Section 4.4.1.1

During impact, ejecta with the highest velocity is generated closest to the central pit. According to the model after Melosh (Ref. 2), a particle impacting at a velocity of 13 km/s produces ejecta with velocities up to 5 km/s. Presuming fibers were produced by the highest velocity ejecta, the time to pull fibers 100  $\mu$ m in length was about  $2 \times 10^{-8}$  seconds (Ref. 1). Damage surrounding the impacts extends to a radius about 5 times the central pit radius. Bubbles escaping the melt region of a BK-7 sample indicate temperatures and pressures at impact reached those needed for vaporization of the micrometeorite and/or glass. Evidence of vaporization was observed in BK-7 and soda lime-silica glasses which contain volatile components (Ref. 1). One of the three impacts observed in Zerodur shows no evidence of melting (Ref. 1). These two glasses are clearly the most volatile of those glasses examined in that they include relatively low boiling components, unlike the Pyrex or fused silica glasses which did not display evidence of bubble evolution. The major effect of the impact damage produced a significant increase in optical scatter, but apparently, only negligible changes in overall reflectivity or transmission. This is expected because of the overall low value of fractional area affected (Ref. 1). Chapter 6 discusses the overall expectations for hypervelocity impacts on optics.

Crater shape is relatively independent of impact angle for impacts at angles greater than 10° from the surface plane of the target. Projectile shape largely determines crater

#### 4.3.1, Uncoated Refractive Optics for UV/Visible Systems

---

shape, even for normal impact. Impact features believed to arise from micrometeorites incident at angles between 20° and 45° have been observed in lunar craters. The unsymmetric glass ejecta or debris field associated with the impact in the Pyrex sample is evidence that impact occurred at an oblique angle. The formation of frozen strands of glass develops in the early stages of impact. This would account for the extension of filaments in the direction of impact before excavation of the crater was complete. Also, radial cracks extending from the impact extrapolate to an origin off-center of the excavation in the direction of the splash. These observations indicate the projectile velocity had a large component in the direction of the debris field (Ref. 1). There are a number of ground-based experiments that support these observations (e.g., Ref. 3). The effects of oblique impacts have also been confirmed by CTH hydro-code modeling (e.g., Ref. 4).

##### 4.3.1.2 Atomic Oxygen

Fused silica flown on experiment S0050-2 was found to be resistant to the atomic oxygen (AO) environment, as expected for an oxide, and no significant erosion was observed. Table 4.3.1.2a summarizes and provides a guide to the materials contained in this section.

Table 4.3.1.2a. Atomic Oxygen Data Base for Uncoated Refractive UV/Visible Optics

MATERIALS	FIGURES	LDEF LOCATION	COMMENTS
Fused Silica	None	E5	No damage was discernible

##### 4.3.1.3 Scatter

Fused silica was found in general not to be resistant to the scatter effects as expected, though no discernible damage was observed except for metallic film fragments on the surface. Table 4.3.1.3b shows references to related materials/effects covered in other sections of this

---

#### 4.3.1, Uncoated Refractive Optics for UV/Visible Systems

---

handbook. The data shown are from experiment M0003-2, leading edge samples, and are typical of observed fused silica responses. This high scatter response is consistent with the susceptibility of leading edge samples to impact cratering (see Section 4.3.1.1) producing high scatter sites (Ref. 5).

**Table 4.3.1.3b. Scatter Effects Data Base for Uncoated Refractive IR Optics  
Applicable to Uncoated UV/Visible Optics**

MATERIALS	FIGURES	LDEF LOCATION	COMMENTS
Fused Silica <sup>1</sup>	E.36	D9	Impact sites produce areas of high scatter
	E.37	D9	70-month exposure. Scatter intensity from crater center five times that of background. Fracture lines are high scatter sites
	E.38	D9	Scatter varies by two orders of magnitude across the surface
	E.39	D9	Cleaning reduced scatter three orders of magnitude
	E.40	D9	70-month exposure similar to 9-month exposure

<sup>1</sup> Data relevant to this material are discussed in Section 4.4.1.3.

#### 4.3.1.4 Absorption/Transmission/Reflectance

Because of organic contamination, there was a significant decrease in the transmission of all samples from experiment S0050-2. After cleaning the fused silica and ULE™ samples transmission returned to nearly pre-flight values. No data are available on the effects of cleaning on the other samples.

Table 4.3.1.4a summarizes and provides a guide to the materials contained in this section.

#### 4.3.1, Uncoated Refractive Optics for UV/Visible Systems

**Table 4.3.1.4a. Transmission Data Base for Uncoated Refractive UV/Visible Optics**

MATERIALS	FIGURES	LDEF LOCATION	COMMENTS
Fused Silica	E.10	E5	Cleaning returned sample to pre-flight values
ULE™ Glass	E.11	E5	Cleaning returned sample to pre-flight values
CaF <sub>2</sub>	E.12	E5	Organic contaminant on both surfaces. Catastrophic loss in UV. Transmission ranges from 0 at 200nm to 50 percent at 380nm
MgF <sub>2</sub>	E.13	E5	Organic contamination. Catastrophic loss in UV. Better than CaF <sub>2</sub> and LiF because organic contamination is only on front surface.
	E.14	E5	Same as E.13.
LiF	E.15	E5	Similar to CaF <sub>2</sub>
	E.16	E5	Similar to E.15. Catastrophic loss in UV.
Al <sub>2</sub> O <sub>3</sub>	None	E5	Organic contamination. Substrate does not transmit below 150 nm
SiO <sub>2</sub>	None	E5	Organic contamination. Substrate does not transmit below 150 nm

In the S0050-1 experiment materials overall, the transmission of uncoated fused silica was observed to decrease by about 30 to 50 percent, mostly in the wavelength range of 200 nm to 700 nm. The major cause of this was contamination from other LDEF components, in particular silicon-rich deposits thought to be from outgassing of RTV silicones. After cleaning, the transmission generally returned to the pre-flight values within about 1 percent (Ref. 6).

Because of this organic contamination, there was also a significant decrease in the transmission of CaF<sub>2</sub>, MgF<sub>2</sub>, LiF, Al<sub>2</sub>O<sub>3</sub>, and SiO<sub>2</sub>. The ratio of the contaminated CaF<sub>2</sub> flight sample to the ground controlled sample showed the transmission monotonically increasing from zero at 200 nm to more than 50 percent at 380 nm (Ref. 6). The higher transmission measured for the MgF<sub>2</sub> window relative to the CaF<sub>2</sub> and LiF windows was probably due to the fact that there was no back film on the MgF<sub>2</sub> window (Ref. 6).

#### *4.3.1. Uncoated Refractive Optics for UV/Visible Systems*

---

As observed from the S0050-2 experiment, there was a significant decrease in transmission of the uncoated ULE™ glass (up to 45 percent) post-flight over the wavelength range of 350 to 1000 nm. However, this was due to contaminant, and the original transmission was recovered after cleaning (Ref. 7). Of interest is the fact that the density of the contaminant deposited on the sample varied between coatings and substrate materials. As an example, prior to cleaning, the transmission of the uncoated fused silica sample was reduced from 94 to 68 percent at 350 nm, while that of the uncoated ULE™ sample reduced from 94 to 45 percent (Ref. 7).

##### **4.3.1.5 Darkening**

No radiation darkening was observed in the fused silica, and changes in transmission were associated only with the surface contamination, or (slightly) with impact damage scattering. Also, no darkening was observed for ULE™, even though ULE™ is known to be particularly sensitive to radiation darkening (Ref. 8).

Table 4.3.1.5a summarizes and provides a guide to the materials contained in this section.

**Table 4.3.1.5a. Darkening Effects Data Base for Uncoated Refractive UV/Visible Optics**

MATERIALS	FIGURES	LDEF LOCATION	COMMENTS
Fused Silica	None	E5	No darkening evident
ULE™ Glass	None	E5	No darkening evident

These results are consistent with expectations for the electron, proton, and UV environment in the LDEF orbit where the radiation environments are fairly benign. For

higher orbital altitudes, it is anticipated that concerns about radiation darkening should be increased because of the increased severity of the radiation environments.

#### **4.3.1.6 Stress**

Stresses were measured in some LDEF samples. Both compression and tension stresses were observed, though the magnitudes were small. These small stresses were found to have negligible effect on optical performance, including the  $\text{CaF}_2$  sample even though a micrometeoroid impact forced cleaving in the sample.

Table 4.3.1.6a summarizes and provides a guide to the materials contained in this section.

Mechanical testing of glasses impacted by micrometeorites was performed using a diametral flexure test. The test subjects a centrally loaded disk, supported at three points, to dynamic loading in a controlled environment. This method of testing eliminates effects of flaws on the periphery of the sample (Ref. 1).

Mechanical stresses imposed on the tensile surface of the sample during mechanical testing are symmetric with respect to the loading points of the fixture. Impacts not occurring in the geometrical center of the sample are subjected to stresses less than the maximum applied stress. No micrometeorite or space debris impacts occurred in the geometrical center of the samples and no fracture was observed (except for  $\text{CaF}_2$ ) to initiate from surface flaws associated with micrometeorite or space debris impacts (Ref. 1).

Table 4.3.1.6a. Stress Effects Data Base for Uncoated Refractive UV/Visible Optics

MATERIALS	FIGURES	LDEF LOCATION	COMMENTS
Fused Silica	E.17	E5	Strength of exposed sample indistinguishable from control sample
	E.19	D2	
ULE™	E.17	E5	Strength of exposed sample indistinguishable from control sample
BK-7	E.19	D2	Strength of exposed sample indistinguishable from control sample
Soda-Lime-Silica	E.17	D2	Strength of exposed sample indistinguishable from control sample
Pyrex	E.17	D2	Strength of exposed sample indistinguishable from control sample
	E.19		
Vycor	E.17	D2	Strength of exposed sample indistinguishable from control sample
	E.19		
Zerodur	E.17	D2	Strength of exposed sample indistinguishable from control sample
	E.19		
CaF <sub>2</sub>	E.18	B8	Fractured sample

The highest stress at an impact site was 50 percent of the stress to produce failure. Thus it is deduced that the effect of micrometeorite or space debris impacts reduced the glass strength by less than 50 percent for the impacts experienced in these experiments. A part from the crater visible on the surface, damage to glass extends beneath the flaw a distance depending on propagation of the radial cracks. Though a micrometeoroid may not penetrate the glass, the resulting defect lowers the maximum stress the glass is capable of sustaining before fracture. Stress concentration developed by the presence of a surface impact degrades the strength with a square root dependence on flaw size. Fracture mechanics permit calculation of strength from flaw size and fracture toughness parameters. Assuming the damage field from a micrometeorite or space debris impact is hemispherical, the influence of impact damage penetrating to a depth of 100  $\mu\text{m}$  decreases the strength to 35 percent of the measured value. Based on these arguments, failure of the Zerodur sample should have



#### *4.3.1. Uncoated Refractive Optics for UV/Visible Systems*

---

initiated at the impact site with an applied load at the geometric center of the sample of less than 100MPa (1 kbar). This suggests the extent of damage below the impact is actually no greater than 1/4 the radius of the crater observed on the surface, thus a hemispherical damage zone surrounding the impact site is not true. This accords with the evidence that craters in glass are usually shallow relative to their diameters because of surface spalls (Ref. 1).

The S0050-2 samples were measured photoelastically for stress before and after flight using birefringence polarimetry. The control samples were also measured for comparison purposes. A summary of the observed S0050-2 results follows (Ref. 7):

- On the uncoated glass and high reflectance silver coated samples, the contaminant, on the average, induced a compressive stress of 42 psi. After cleaning, the stress levels closely matched those of the pre-flight measurements.
- On the fused silica antireflectance coated sample, the contaminant did not induce any measurable stress. A stress change could not be measured on the solar rejection coated samples due to the high level of stress in the coating, and the variation in stress between samples. A reduction in the stress levels in this coating was measured on both the flight and control samples. No significant stress change was measured between the flight samples after cleaning and the control samples.

The micrometeoroid/debris impact on the  $\text{CaF}_2$  sample from experiment A0056 occurred near the edge of the sample holder. The impact crater was about 1 mm in diameter with a spallation zone diameter of about 5.5 mm. The substrate cleaved in two directions outward from the crater site to the opposite sides of the sample, and at an angle of about 75°, breaking the sample into three pieces. This verifies the fragile and brittle nature of  $\text{CaF}_2$  as a substrate material, while remaining optically functional (Ref. 16).

#### 4.3.1. Uncoated Refractive Optics for UV/Visible Systems

##### 4.3.1.7 Contamination/Deterioration

A brown discoloration caused by a contaminating film was evident on most of the S0050-1 LDEF samples. The film appeared brittle. No discoloration of bulk optical material was noted.

Table 4.3.1.7a summarizes and provides a guide to the materials contained in this section.

**Table 4.3.1.7a. Contamination Data Base for Uncoated Refractive UV/Visible Optics**

MATERIALS	FIGURES	LDEF LOCATION	COMMENTS
MgF <sub>2</sub>	E.20	E5	Organic film appeared brittle
	E.21	E5	Decrease in transmittance due to contamination
LiF	E.22	E5	Organic film present on both surfaces
	E.23	E5	Organic film appeared sprayed on
Al <sub>2</sub> O <sub>3</sub>	E.24	E5	Organic film present on both surfaces
SiO <sub>2</sub>	E.25	E5	Little contamination. Showed substrate selectivity
CaF <sub>2</sub>	E.26	E5	Organic film present on both sides

A Fourier Transform Infrared (FTIR) spectrometer optimized for the 3.4  $\mu\text{m}$  spectral region was used to measure thin organic films on experiment S0050-1 samples. Strong narrow methyl and methylene absorption bands are in this (3.4  $\mu\text{m}$ ) spectral region. The 3.4  $\mu\text{m}$  contamination measurements on the MgF<sub>2</sub>, CaF<sub>2</sub>, and LiF windows were typical of many hydrocarbons. This probably is a result of nearby material outgassing. The absence of 3.4  $\mu\text{m}$  absorption on SiO<sub>2</sub> showed substrate selectivity (Ref. 6).

#### 4.3.1. Uncoated Refractive Optics for UV/Visible Systems

Photographs of the  $\text{MgF}_2$  window showed sharp edges of the adhering film indicating the film is brittle. Patterns on the film indicate the contaminant may be of low viscosity. LiF photographs indicate a sprayed texture to the film (Ref. 6).

#### 4.3.2 Coated UV/Visible Refractive Optics

##### 4.3.2.1 Impact Effects

A specific discussion of materials related to Uncoated Refractive UV/Visible Optics is presented in Section 4.6.1.1, Impacts Effects on IR Coatings. In general, all samples showed some impact effects. Those samples flown on experiment M0003-2 and on the leading edge (at locations D8 and D9) showed several microfractures; the trailing edge samples experienced crazing as the primary effect. The  $\text{NaF}_2$  on  $\text{SiO}_2$  sample flown on experiment M0003-7 showed delamination and damage (layer removal) by solar UV and AO. Table 4.3.2.1b shows references to related materials covered in other handbook chapters.

Table 4.3.2.1b. Impact Effects Data Base for UV/Visible Coatings Applicable to Coated Refractive UV/Visible Optics

MATERIALS/ SUBSTRATE	FIGURES	IDEF LOCATION	COMMENTS
$\text{MgF}_2$	E-47	D9	Damage is localized
$\text{NaF}_2$	E-48	D9	Damage layer removed from around impact due to UV or AO
$\text{Cr}/\text{Ag}/\text{ThF}_4$	E-49	D9	Overall damage area is several times crater size. Coating failure is observed.
$\text{Ag}(\text{Al}_2\text{O}_3/\text{Si})^1$ on Polished Silicon <sup>1</sup>	E-50	D8	Microfractured, corroded, cratered
$\text{Al}_2\text{O}_3$	E-51	D3	Microfractured, flaked
$\text{As}_2\text{Se}_3$	E-52	D3	Crazed, discolored
$\text{Au}^1$	E-53	D4	Unchanged

<sup>1</sup> Data relevant to this material are presented in Section 4.6.1.1

### 4.3.2. Coated Refractive UV/Visible Optics

---

#### 4.3.2.2 Atomic Oxygen

At the present time, no data have been found for this section.

#### 4.3.2.3 Scatter

For  $\text{MgF}_2$  coated silica, the induced scatter was found to be less for the leading edge than for the trailing one. This result was essentially the same for both 9-month and 69-month exposures (Refs. 5 and 9).

As shown in Figure E.28, there was over an order of magnitude change in the bidirectional reflectance distribution function (BRDF) above 5 degrees delta theta (Ref. 7).

Table 4.3.2.3a summarizes the materials and provides comments concerning the data contained in this section.

**Table 4.3.2.3a. Scatter Effects Data Base for Coated UV/Visible Refractive Optics**

MATERIALS	FIGURES	LDEF LOCATION	COMMENTS
$\text{MgF}_2$ /Fused Silica	E.27	D9 D4	Leading edge showed less scatter than trailing edge
Ag/UHF <sup>TM</sup>	E.28	E5	increase in scatter

#### 4.3.2.4 Absorption/Transmission/Reflectance

All of the substrates and coatings experienced a significant performance reduction after flight, but after cleaning with normal solvent drag means (except for the AR-coated samples

#### 4.3.2. Coated Refractive UV/Visible Optics

---

which could not be cleaned), the sample optical performance returned to the pre-flight measured values (Ref. 7).

Table 4.3.2.4a summarizes and provides a guide to the materials contained in this section.

**Table 4.3.2.4a. Absorption/Transmittance/Reflectance Data Base for Coated Refractive UV/Visible Optics**

MATERIALS/ COATINGS	FIGURES	LDEF LOCATION	COMMENTS
Fused silica/ Solar rejection	E.29	E5	Contamination reduced transmission. Cleaning returned sample to pre-flight value.
	E.30	E5	Contamination reduced transmission. Cleaning returned sample to pre-flight value.
ULE™/Ag	E.31	E5	Contamination reduced transmission. Cleaning returned sample to pre-flight value.
Fused Silica/ Anti-reflection	E.32	E5	Contamination reduced transmission. Normal cleaning methods not effective. Needed exposure to oxygen plasma to improve performance

Table 4.3.2.4b shows references to related materials/effects covered in other sections of this handbook.

The flight samples from experiment S0050-2 were measured for optical performance from 350 to 1200 nm. Of interest in the measurements is the fact that the optical density of the contaminant deposited on the sample varied between coatings and substrate materials. As an example, the transmission of the uncoated fused silica sample was reduced from 94 to 68 percent at 350 nm, while that of the uncoated ULE™ sample was reduced from 94 to 45 percent (Ref. 7).

#### 4.3.2. Coated Refractive UV/Visible Optics

**Table 4.3.2.4b. Absorption/Transmission/Reflectance Effects Data Base for UV/Visible Coatings Applicable to Coated Refractive UV/Visible Optics**

MATERIALS/ SUBSTRATE	FIGURES	LDEF LOCATION	COMMENTS
Al-MgF <sub>2</sub> / B1664 Glass <sup>1</sup>	E.41	B3	Outside/inside samples had significantly-reduced reflectance over all wavelengths.
ThF <sub>4</sub> -Ag/ B1664 Glass <sup>1</sup>	E.42	B3	Outside/inside samples showed little change in reflectance over all wavelengths.
Al <sub>2</sub> O <sub>3</sub> -Ag/ Kanigen <sup>1</sup>	E.43	B3	Outside/inside samples had significantly-reduced reflectance except at the blue end.
Al-MgF <sub>2</sub> / Kanigen <sup>1</sup>	E.44	B3	Inside sample had significant reduction in reflectance at upper end. Outside sample had significant reduction across the entire band.
MgO-MgF <sub>2</sub> / B1664 Glass <sup>1</sup>	E.45	B3	Inside sample showed slight shift in reflectance. Outside sample had little reduction at the blue end but a slight shift to the high end.
	E.46	B3	Inside sample showed a significant reduction in transmittance at the blue end. Outside sample had a significant reduction in transmission at the blue end and a slight reduction at the upper end.
Visible 1060 nm mirror/TiO <sub>2</sub> -SiO <sub>2</sub> on B1664 Glass <sup>1</sup>	None	B3	Remained optically efficient.

<sup>1</sup> Data relevant to this material are presented in Section 4.5.1.4

For the case of an antireflection (AR) coating (SiO<sub>2</sub>/TiO<sub>2</sub>)( $\lambda = 1.06 \mu\text{m}$  wavelength) the transmission decreased by up to 40 percent at 475 nm and 20 percent at 900 nm, but actually increased by 10 percent at 600 nm. These effects were due to a contamination layer. The contamination was not removable by normal solvent drag means. An attempt to remove the contamination using an oxygen plasma for 3 hours only partially restored the transmission, and the improvement was only about 10 percent and was limited to the wavelength range of 350 to 550 nm (Ref. 7).

#### *4.3.2. Coated Refractive UV/Visible Optics*

---

For a sample with a solar rejection coating, the post-flight transmission was almost identical to the pre-flight values, with a 3 percent decrease in the wavelength range of 1000 to 1150 nm (Ref. 7).

A high reflectance silver coated flight sample (with contaminant) and a control sample were measured for BRDF. A near order-of-magnitude increase in scattered light was measured above  $10^\circ$  delta theta on the flight sample versus that of the control sample (Ref. 7).

#### **4.3.2.5 Darkening**

No radiation darkening was evident on either the ULE™ or the fused silica glass substrates flown in experiment S0050-2. These results are consistent with expectations for the electron, proton, and UV environment in the LDEF orbit where the radiation environments are fairly benign. For higher orbital altitudes, it is anticipated that concerns about radiation darkening of ULE™ should be increased because of the increased severity of the radiation environments. Care should be taken in the use of ULE™ at these higher altitudes (Ref. 8).

#### **4.3.2.6 Stress**

For both AR coatings and solar rejection coatings tested in experiment S0050-2, very little change in stresses was observed for post flight versus pre flight (Ref. 7).

Table 4.3.2.6a summarizes and provides a guide to the materials contained in this section.

#### 4.3.2. Coated Refractive UV/Visible Optics

**Table 4.3.2.6a. Stress Data Base for Coated Refractive UV/Visible Optics**

MATERIALS/ COATING	FIGURES	IDEF LOCATION	COMMENTS
Fused Silica/AR	E.33	E5	Contaminant did not introduce measurable stress
Fused Silica/ AR/Uncoated side	E.33	E5	Contaminant did not introduce measurable stress
ULE <sup>TM</sup> /Ag	E.33	E5	After cleaning, pre- and post-flight measurements were very similar

The samples were measured photoelastically for stress before and after flight using birefringence polarimetry. The control samples were also measured for comparison purposes. A summary of the results follows (Ref. 7):

- On the uncoated glass and high reflectance silver coated samples, the contaminant, on the average, induced a compressive stress of 42 psi. After cleaning, the stress levels closely matched those of the pre-flight measurements.
- On the fused silica AR coated sample, the contaminant did not induce any measurable stress.
- A stress change could not be measured on the solar rejection coated samples due to the high level of stress in the coating, and the variation in stress between samples.
- No significant stress change was measured between the flight samples after cleaning and the control samples. The stresses also maintained their signs, with compressions remaining compressions, etc.

#### 4.3.2.7 Contamination/Deterioration

X-ray Photoelectron Spectroscopy (XPS) analysis of experiment S0050 2 samples showed the substrates and coatings to be covered with a thin layer of polymer which contained silicon. The contaminant, a light brown stain, was removed fairly easily with normal cleaning techniques (except for the AR coating) (Ref. 7).



#### 4.3.2, Coated Refractive UV/Visible Optics

Table 4.3.2.7b shows references to related materials/effects covered in other sections of this handbook.

**Table 4.3.2.7b. Contamination/Deterioration Effects Data Base for UV/Visible Coatings Applicable to Coated UV/Visible Optics**

MATERIALS/ SUBSTRATE	FIGURES	IDEF LOCATION	COMMENTS
Ge/ZnS/ThF <sub>4</sub> <sup>1</sup>	None	B.3	Peeling of coating due to vacuum or thermal cycling

<sup>1</sup> Data relevant to this material are presented in Section 4.5.1.7.

For most of the experiment S0050-2 samples the contaminant was silica-like in nature, but on the ULE<sup>TM</sup> substrate and the AR coating, the contaminant was visibly darker and appeared similar in structure to the silicone of the rubber gasket which was used to mount the optics. However, neither the relative atomic percentages or the relative sizes of the silicon and oxygen peaks from the XPS conclusively prove that the contaminant is a residue from the mounting rubber gasket. Other silicon sources must be considered as well (Ref. 1).

Depth sputtering through the AR coating clearly shows the SiO<sub>2</sub>/TiO<sub>2</sub> layers for both the control and flight samples. However the flight sample has a layer at the surface approximately 30 Å thick, rich in carbon and silicon. The carbon content rises as the contamination layer is sputtered away and disappears at the contamination-AR layer interface. The total time required to sputter to the bottom of the SiO<sub>2</sub>/TiO<sub>2</sub> layers was almost identical for both the flight and control samples. Since the hardness of the coating on both samples were assumed to be similar, the sputtering rates would have been equivalent, making the total coating thicknesses the same. This indicates that either the top surface of the flight coating has been removed and replaced with the silicon/carbon layer, or the silicon/carbon has fused into the SiO<sub>2</sub> layer (Ref. 7).

## 4.4 REFRACTIVE OPTICS FOR IR SYSTEMS

A variety of refractive optics materials was flown on LDEF that transmit in the IR wavelengths. The LDEF data currently available for refractive IR optics are discussed below and are subdivided into uncoated and coated configurations. Table 4.4.a shows a summary of the experiments containing refractive IR optics. Table 4.4.b is a cross-reference of the IR refractive optics flown on LDEF cross-correlated with the kinds of effects studied on LDEF for these materials.

**Table 4.4.a. Experiment Summary for Refractive IR Optics**

EXPERIMENT	REFRACTIVE IR OPTICAL MATERIALS
A0138-4	ZnSe, ZnSe/ZnS/ThF <sub>4</sub> on ZnSe
A0147	Uncoated fused silica
A0171	Coated fused silica
A0172	Uncoated fused silica, low iron soda-lime-silica glass, Pyrex 7740 glass, Vycor 7913 glass, BK-7 glass, and Zerodur glass ceramic
M0003-2	Uncoated fused silica (T22 Supersil-W1 Amersil) and coated fused silica (MgF <sub>2</sub> )
M0003-7	Al <sub>2</sub> O <sub>3</sub> on SiO <sub>2</sub> , Si on SiO <sub>2</sub> , NaF <sub>2</sub> on SiO <sub>2</sub>
S0014	Uncoated fused silica
S0050-1	CaF <sub>2</sub> , MgF <sub>2</sub> , LiF, Al <sub>2</sub> O <sub>3</sub> (synthetic sapphire) and uncoated fused silica
S0050-2	Uncoated fused silica, uncoated ULE™, ULE™/Ag coating, and coated fused silica (AR coatings, solar rejection coatings)

**Table 4.4.b. Refractive Optics for IR Systems Flown on LDEF**

MATERIALS	EFFECTS						
	I M P A C T S	A T O M I C  O X Y G E N	A B S / T R A N / R E F L	D A R K E N I N G	S T R E S S	S C A T T E R	C O N T A M / D E T E R
<i>UNCOATED IR REFRACTIVE OPTICS</i>							
Fused Silica (SiO <sub>2</sub> )	•	○	○	○	○	•	•
Zerodur	○				○		
Pyrex	○				○		
BK-7	○				○		
Soda-Lime-Silica	○				○		
ULE™ Glass			○		○		
CaF <sub>2</sub>			○		○		
MgF <sub>2</sub>			○				
LiF			○		○		
Al <sub>2</sub> O <sub>3</sub>			○				○
ZnSe			○				
Vycor					○		

- Data contained in this section
- Data contained in other, cross referenced sections

#### 4.4. Refractive Optics for IR Systems

Table 4.4.b. Refractive Optics for IR Systems Flown on LDEF (Cont.)

MATERIALS	EFFECTS						
	I M P A C T S	A T O M I C  O X Y G E N	A B S / T R A N / R E F L	D A R K E N I N G	S T R E S S	S C A T T E R	C O N T A M / D E T E R
<b>COATED IR REFRACTIVE OPTICS</b>							
MgF <sub>2</sub> /Fused Silica	○	○	○			○	○
MgF <sub>2</sub> (λ=1.06μ)/2-thick on Fused Silica	○					○	○
NaF <sub>2</sub> on SiO <sub>2</sub>	○						
AlO <sub>3</sub> /SiO <sub>2</sub>	○						○
ULE™/Ag			○		○		
Si <sub>3</sub> /SiO <sub>2</sub>							○
ZnSe/ZnS/ThF <sub>3</sub> on ZnSe			●				

• Data contained in this section

○ Data contained in other, cross referenced sections

#### 4.4.1 Uncoated IR Refractive Optics

##### 4.4.1.1 Impact Effects

All LDEF refractive IR optics samples suffered some impact damage due to either micrometeoroids or man-made debris. Impact damage consisted of various nicks and chips,

#### 4.4.1, Uncoated Refractive IR Optics

---

or small quasi-hemispherical craters surrounded by spalls with conchoidal surfaces similar to that seen for uncoated refractive UV/visible optics. The phenomenology discussion pertaining to Section 4.3.1.1 also applies to this section. Table 4.4.1.1a summarizes and provides a guide to the materials contained in this section. Table 4.4.1.1b shows references to related materials/effects covered in other sections of this handbook.

**Table 4.4.1.1a. Impact Effects Data Base for Uncoated Refractive IR Optics**

MATERIALS	FIGURES	LDEF LOCATION	COMMENTS
Fused Silica	E.34	D9	Exposed 70 months. Localized chipping and fracture extending many particle diameters.
	E.35	D9	Damage areas are potential high scatter, high absorption areas.
SiO <sub>2</sub>	E.36	D4	No discernible changes except for debris.

In general, fused silica seemed to be more susceptible to impact damage than was SiO<sub>2</sub> (Refs. 5 and 9). However, these samples were placed in different LDEF locations--D9 for fused silica versus D4 for SiO<sub>2</sub>. Location D9 is near the leading edge or "ram" direction; location D4 is near the trailing edge. This seems to imply that the ram direction may be a location where optical materials are more susceptible to impact damage (i.e., there is a directional dependence on the micrometeoroid/debris environment). Other data for uncoated SiO<sub>2</sub> samples flown in other experiments on LDEF near the leading edge were not found. Thus, it is difficult to provide a direct comparison between fused silica and SiO<sub>2</sub> concerning their relative susceptibilities to impact damage.

#### 4.4.1, Uncoated Refractive IR Optics

**Table 4.4.1.1b. Impact Effects Data Base for Uncoated Refractive UV/Visible Optics  
Applicable to Uncoated Refractive IR Optics**

MATERIALS	FIGURES	LDEF LOCATION	COMMENTS
Fused Silica <sup>1</sup>	E.1	E5	Localized impact damage.
	E.2	E5	Localized damage. Radial cracking does occur but does not propagate a great distance from impact site.
	E.3	D2	Molten glass jetting. Fibers 100 $\mu$ m long projecting from the fuse zone.
	E.9	D2	Characterization of impact site damage.
Zerodur <sup>1</sup>	E.4	D2	Central pit surrounded by fragmented material with radial cracks. Debris captured in melt zone.
	E.5	D2	No melt. Similar damage to that shown in Figure E.4 except in central fusion zone.
	E.9	D2	Characterization of impact site damage.
Pyrex <sup>1</sup>	E.6	D2	Damage area 5 times central pit radius.
	E.7	D2	Oblique impact produced strongly directional splash. Crater is circular.
	E.9	D2	Characterization of impact site damage.
BK-7 <sup>1</sup>	E.8	D2	Temperature and pressure for vaporization exceeded.
	E.9	D2	Characterization of impact site damage.
Soda-Lime-Silica <sup>1</sup>	None	D2	Temperature and pressure for vaporization exceeded.
	E.9	D2	Characterization of impact site damage.

<sup>1</sup> Data relevant to this material are presented in section 4.3.1.1.

#### 4.4.1.2 Atomic Oxygen

As with the data obtained for Section 4.3.1.2, the fused silica flown on experiment S0050-2 was found to be resistant to the AO environment, as expected for an oxide, and no

#### 4.4.1. Uncoated Refractive IR Optics

---

significant erosion was observed. Table 4.4.1.2b shows references to related materials/ effects covered in other chapters of this handbook.

**Table 4.4.1.2b. Atomic Oxygen Data Base for Uncoated Refractive UV/Visible Optics  
Applicable to Uncoated Refractive IR Optics**

MATERIALS	FIGURES	LDEF LOCATION	COMMENTS
Fused Silica <sup>1</sup>	None	E5	No damage was discernible

<sup>1</sup> Data relevant to this material are presented in Section 4.3.1.2.

#### 4.4.1.3 Scatter

The optical scatter increased significantly for many samples in experiment M0003-2. Much of this increase was due to surface contamination resulting from outgassing of various silicones and hydrocarbons on LDEF and partially due to particulate debris. Post-retrieval cleaning removed the contamination and reduced the scatter by up to three orders of magnitude. However, impact induced cratering and cracking still gave local scatter of up to five orders of magnitude above the background level. The data demonstrated that the leading edge suffered most, but there was also an indication that the scatter was increasing to some kind of limit or equilibrium because the increase in scattering in the 9-month exposures was similar to the increase in scattering in the 70 month exposure samples (Refs. 5 and 9). Table 4.4.1.3a summarizes and provides a guide to the materials contained in this section.

#### 4.4.1. Uncoated Refractive IR Optics

**Table 4.4.1.3a. Scatter Effects Data Base for Uncoated Refractive IR Optics**

MATERIALS	FIGURES	LDEF LOCATION	COMMENTS
Fused Silica	E.35	D9	Impact sites produce areas of high scatter
	E.37	D9	70-month exposure. Scatter intensity from crater center five orders of magnitude times that of background. Fracture lines are high scatter sites.
	E.38	D9	Scatter varies by two orders of magnitude across the surface
	E.39	D9	Cleaning reduced scatter three orders of magnitude
	E.40	D9	70-month exposure similar to 9 month exposure

For the M0003 2 samples, a three phase characterization plan was developed and is being implemented to determine sample optical performance degradations and to correlate measured degradation with space exposure. During Phase I, which is still ongoing as of this writing, the optical performance is being evaluated and correlated to sample flight position and exposure duration. Phase I measurements are nondestructive and include: (1) full surface photography, (2) high resolution microscopy and photography, (3) preparation of a detailed surface map, (4) absorption, (5) transmission and reflectance, (6) ellipsometry, (7) scatter (BRDF), and (8) an impact site count.

Phase II will investigate the fundamental reasons for performance degradation. Techniques will be used to determine surface morphology and chemistry, film depth profiles, atomic population density, erosion depth, and mass loss. Techniques designed to investigate the fundamental reasons for performance degradation are in many cases intrusive and cannot be undertaken until Phase I measurements are complete.

During Phase III, selected samples will be cleaned according to standard and/or innovative optical cleaning procedures. Selected Phase I tests will be repeated to determine if



#### 4.4.1. Uncoated Refractive IR Optics

---

the sample's performance can be restored to an acceptable level. A small number of samples will also be tested for laser damage.

The following paragraphs contain the most recent status of the Phase I results.

Full-Surface Photography: Full-surface photography has proven to be a valuable tool for surface mapping and is a simple technique in which the sample is placed in a dark room, illuminated by a high intensity light at a high angle of incidence, and photographed. The photograph shows surface irregularities as points of scattered light. All full surface photographs were taken in a Class-100-clean environment. Each sample surface (front and back) has been photographed twice, once with the sample fiducial mark at 0° to the direction of illumination and again at 90°. The photographs reveal that surface contamination and damage vary greatly from sample to sample (Refs. 5 and 9).

There are significantly more scatter sites on LDEF flown samples than the control sample, implying that the LDEF space environment significantly increased surface contamination and/or damage. The increase in contamination/damage becomes even more apparent in photographs of samples exposed for longer periods of time. The scatter sites shown in the full surface photographs are being investigated with differential interference contrast are being made for unusual contamination areas and impact sites. Optical measurements are being made on the highly blemished surface areas as well as on the cleaner areas (Refs. 5 and 9).

Microscopy: Initial microscopy on the optical samples was performed by The Aerospace Corporation (Los Angeles, California) at the time the samples were removed from the trays. Phillips Laboratory is performing a final microscopic evaluation on each sample. The full-surface photographs which have been taken of each surface are assisting in locating some sites requiring careful examination in Phase I and Phase II characterization. The extent of debris and micrometeoroid-caused damage varies. For example, a strike on MgF<sub>2</sub>-coated

#### 4.4.1, Uncoated Refractive IR Optics

---

fused silica is relatively constrained. In contrast, an impact on uncoated fused silica produced localized chipping and fracture zones extending many particle diameters. Optics with damaged areas such as these are potentially high-scatter and high-absorption optics (Refs. 5 and 9).

Scatter Measurements: BRDF measurements on the optical samples were made on a research grade scatterometer, High Resolution Scatter Mapping Instrument (HRSMI), operated in the Phillips Laboratory Optical Components Branch. The HRSMI is capable of high-resolution-scatter measurements and surface-scatter mapping. All scatter data reported to date were taken at 6328 Å. It is anticipated that samples flown on the leading edge and/or exposed for longer periods of time may be more highly scattering than samples flown on the trailing edge and/or exposed for shorter periods of time. The sample surface was exposed on the leading edge for 70 months; therefore it was anticipated that this surface would be highly scattering. The scatter map (shown in Appendix E) shows scatter varying two orders of magnitude across the sample surface (Refs. 5 and 9).

The effects of micrometeoroid damage are important for brittle materials. Investigators have found fracture lines extending 2 cm from impact sites. Scatter intensity from the center of the crater is five orders of magnitude greater than the sample background. Fracture lines extending from the crater are high scatter sites on the surface and are indicated in the mapping by rows of peaks. The intensity of the peaks is between one and three orders of magnitude greater than the surface background (Refs. 5 and 9).

Scattered intensity versus detector angle for various fused silica samples were evaluated. The data show the expected trend between trailing edge and leading edge samples; namely, that the ground control sample and the trailing edge, 3-month sample, are the lowest scattering of the four samples, while the leading edge are the most highly scattering (Ref. 9). The two leading edge data curves had the same shape implying that the contamination contributing to scatter is the same on both surfaces. Further, the measured scatter on both the

#### 4.4.1, Uncoated Refractive IR Optics

---

70-month and 9-month exposed samples is the same. Two possible explanations for this phenomenon are: (1) whatever is causing the scatter reached a limiting or equilibrium condition where scatter is no longer affected or (2) contamination on the 70-month sample was removed by AO, radiation, or some other type of scrubbing effect which lowered the scatter to a level comparable to the 9-month exposure sample (Refs. 5 and 9).

A preliminary attempt to determine the presence and magnitude of scattering from surface contamination was made. Scatter from the unexposed side of the leading edge, 70-month, uncoated fused silica sample was measured; the data shows the surface is highly scattering. The surface was then blown with an air brush in an attempt to remove contamination, and the scatter measurement was repeated. The data show that the surface scatter was not reduced. An alcohol drag was then performed twice on one-half of the surface, and the scatter was remeasured. The data show that cleaning the surface reduced the scatter three orders of magnitude. This is a significant reduction in scatter, indicating that there is considerable contamination on the sample surface and that blowing the surface with air is not effective in removing it (Refs. 5 and 9).

#### 4.4.1.4 Absorption/Transmission/Reflectance

Samples flown on experiment AO138-4 (LDEF location B3, leading edge) were tested for spectral performance. Post flight tests indicate no significant differences in ZnSe spectral performance (Ref. 10). Table 4.4.1.4a summarizes and provides a guide to the material contained in this section.

**Table 4.4.1.4a. Absorption/Transmission/Reflectance Data Base for  
Uncoated Refractive IR Optics**

MATERIAL	FIGURES	LDEF LOCATION	COMMENTS
ZnSe	None	B3	No significant difference in spectral performance.

#### 4.4.1, Uncoated Refractive IR Optics

Table 4.4.1.4b shows references to related materials/effects covered in other sections of this handbook.

**Table 4.4.1.4b. Absorption/Transmission/Reflectance Data Base for Uncoated Refractive UV/Visible Optics Applicable to Uncoated Refractive IR Optics**

MATERIALS	FIGURES	LDEF LOCATION	COMMENTS
Fused Silica <sup>1</sup>	E.10	E5	Cleaning returned sample to pre-flight values
ULE <sup>TM</sup> Glass <sup>1</sup>	E.11	E5	Cleaning returned sample to pre-flight values
CaF <sub>2</sub> <sup>1</sup>	E.12	E5	Organic contaminant on both surfaces. Catastrophic loss in UV. Transmission ranges from 0 at 200nm to 50 percent at 380nm
MgF <sub>2</sub> <sup>1</sup>	E.13	E5	Organic contamination. Catastrophic loss in UV. Better than CaF <sub>2</sub> because organic contamination is only on front surface (Contamination film inadvertently removed from back surface).
	E.14	E5	Same as E.13.
LiF <sup>1</sup>	E.15	E5	Similar to CaF <sub>2</sub>
	E.16	E5	Similar to E.15.
Al <sub>2</sub> O <sub>3</sub> <sup>1</sup>	None	E5	Organic contamination. Substrate does not transmit below 150 nm
SiO <sub>2</sub> <sup>1</sup>	None	E5	Organic contamination. Substrate does not transmit below 150 nm

<sup>1</sup> Data relevant to this material are presented in Section 4.3.1.4

Because of organic contamination, there was a significant decrease in the transmission of all samples. After cleaning, the fused silica and ULE<sup>TM</sup> samples transmission returned to nearly pre-flight values. No data are available on the effects of cleaning on the other samples. It should be noted that these data from Section 4.3.1.4 are for fused silica samples flown on LDEF near the trailing edge. The fused silica samples from experiment M0003-2 were flown near the leading edge. The exact correlation between leading edge and trailing edge effects are still to be resolved among the LDEF experimenters.

#### 4.4.1.5 Darkening

Specific discussions concerning materials of interest, such as uncoated fused silica, are covered in Section 4.3.1.5, Darkening Effects on Uncoated Refractive UV/Visible Optics. No radiation darkening was observed in the fused silica. The argument concerning differences in responses for trailing edge versus leading edge samples discussed in the previous section on transmission do not apply here for darkening. There is no assumed directional-dependence in the radiation environments.

Table 4.4.1.5b shows references to related materials/effects covered in other sections of this handbook.

**Table 4.4.1.5b. Darkening Effects Data Base for Uncoated Refractive UV/Visible Optics  
Applicable to Uncoated Refractive IR Optics**

MATERIALS	FIGURES	LDEF LOCATION	COMMENTS
Fused Silica <sup>1</sup>	None	E5	No darkening evident

<sup>1</sup> Data relevant to this material are presented in Section 4.3.1.5

#### 4.4.1.6 Stress

Specific discussions concerning materials of interest, such as uncoated fused silica, are covered in Section 4.3.1.6, Stress Effects on Uncoated Refractive UV/Visible Optics. In the UV/visible samples flown in experiment S0050-2, stresses were observed in the fused silica but were found to have a negligible effect on optical performance.

Table 4.4.1.6b shows references to related materials/effects covered in other sections of this handbook.

#### 4.4.1. Uncoated Refractive IR Optics

**Table 4.4.1.6b. Stress Effects Data Base for Uncoated Refractive UV/Visible Optics  
Applicable to Uncoated Refractive IR Optics**

MATERIALS	FIGURES	LDEF LOCATION	COMMENTS
Fused Silica <sup>1</sup>	E.17	E5	Strength of exposed sample indistinguishable from control sample
	E.19	D2	
ULE <sup>TM</sup>	E.17	E5	Strength of exposed sample indistinguishable from control sample
BK-7 <sup>1</sup>	E.19	D2	Strength of exposed sample indistinguishable from control sample
Soda-Lime-Silica <sup>1</sup>	E.17	D2	Strength of exposed sample indistinguishable from control sample
Pyrex <sup>1</sup>	E.17	D2	Strength of exposed sample indistinguishable from control sample
Vycor <sup>1</sup>	E.17	D2	Strength of exposed sample indistinguishable from control sample
Zerodur <sup>1</sup>	E.17	D2	Strength of exposed sample indistinguishable from control sample
CaF <sub>2</sub>	E.18	B8	Fractured sample

<sup>1</sup> Data relevant to this material are presented in Section 4.3.1.6.

As with preceding sections, the data from Section 4.3.1.6 are for the experiment S0050-2 fused silica samples flown on LDEF near the trailing edge. The fused silica samples from experiment M0003-2 were flown near the leading edge. The exact correlation between leading edge and trailing edge effects is still to be resolved among the LDEF experimenters.

#### 4.4.1.7 Contamination/Deterioration

A brown discoloration caused by a contaminating film was evident on most of the S0050-1 LDEF samples. The film appeared brittle. No discoloration of bulk optical material was noted.

#### 4.4.1. Uncoated Refractive IR Optics

---

Table 4.4.1.7b shows references to related materials/effects covered in other sections of this handbook.

**Table 4.4.1.7b. Contamination Data Base for Uncoated Refractive UV/Visible Optics  
Applicable to Uncoated Refractive IR Optics**

MATERIALS	FIGURES	LDEF LOCATION	COMMENTS
MgF <sub>2</sub> <sup>1</sup>	E.20	E5	Organic film appeared brittle
	E.21	E5	Organic film present on front surface
LiF <sup>1</sup>	E.22	E5	Organic film present on both surfaces
	E.23	E5	Organic film appeared sprayed on
Al <sub>2</sub> O <sub>3</sub> <sup>1</sup>	E.24	E5	Organic film present on both surfaces
SiO <sub>2</sub> <sup>1</sup>	E.25	E5	Showed substrate selectivity
CaF <sub>2</sub> <sup>1</sup>	E.26	E5	Organic film present on both sides

<sup>1</sup> Data relevant to this material are presented in Section 4.3.1.7.

#### 4.4.2 Coated IR Refractive Optics

##### 4.4.2.1 Impact Effects

A specific discussion of materials related to Uncoated Refractive IR Optics is presented in Section 4.6.1.1, Impacts Effects on IR Coatings. In general, all samples showed some impact effects. Particularly, those samples flown in leading edge locations showed several microfractures. Table 4.4.2.1b shows references to related materials/effects covered in other sections of this handbook.

#### 4.4.2. Coated Refractive IR Optics

**Table 4.4.2.1b. Impact Effects Data Base for IR Coatings Applicable to Coated Refractive IR Optics**

MATERIALS/ SUBSTRATE	FIGURES	LDEF LOCATION	COMMENTS
MgF <sub>2</sub> / Fused Silica <sup>1</sup>	E.47	D9	Damage is localized
NaF <sub>2</sub> <sup>1</sup>	E.48	D9	Damage layer removed from around impact layer due to UV or AO
TiF <sub>2</sub> /Ag/Cr/ Mo <sup>1</sup>	E.49	D9	Overall damage area is several times crater size Coating failure is observed
Ag+(Al <sub>2</sub> O <sub>3</sub> /Si) <sup>1</sup> Polished Silicon <sup>1</sup>	E.50	D8	Microfractured, corroded, cratered
Al <sub>2</sub> O <sub>3</sub> /SiO <sub>2</sub> <sup>1</sup>	E.51	D3	Microfractured, flaked
As <sub>2</sub> Se <sub>3</sub> / SiO <sub>2</sub> <sup>1</sup>	E.52	D3	Crazed, discolored
Au/ Ni/Al <sup>1</sup>	E.53	D4	Unchanged

<sup>1</sup> Data relevant to this material are presented in Section 4.6.1.1

#### 4.4.2.2 Atomic Oxygen

At the present time, no data have been found for this section.

#### 4.3 Scatter

As discussed in Section 4.3.2.3, for MgF<sub>2</sub>-coated fused silica on experiment M0003 2, the induced scatter was found to be less for the leading edge than for the trailing one. This result was essentially the same for both 9 month and 69-month exposures (Refs. 5 and 9).

Table 4.4.2.3b shows references to related materials/effects covered in other sections of this handbook



#### 4.4.2. Coated Refractive IR Optics

**Table 4.4.2.3b. Scatter Effects Data Base for Coated Refractive UV/Visible Optics  
Applicable to Coated Refractive IR Optics**

MATERIALS	FIGURES	LDEF LOCATION	COMMENTS
MgF <sub>2</sub> /Fused Silica <sup>1</sup>	E.27	D9 D3	Leading edge showed less scatter (coating may be removed by AO)
Ag/ULE <sup>TM</sup>	E.28	E5	Increase in scatter

<sup>1</sup> Data relevant to this material are presented in Section 4.3.2.3.

#### 4.4.2.4 Absorption/Transmission/Reflectance

All of the substrates and coatings flown on experiment S0050-2 experienced a significant performance reduction after flight, but after cleaning (except for the AR-coated samples which could not be cleaned), the sample optical performance returned to the pre-flight measured values (Ref. 7).

Table 4.4.2.4b shows references to related materials/effects covered in other sections of this handbook.

**Table 4.4.2.4b. Absorption/Transmission/Reflectance Effects Data Base for IR Coatings  
Applicable to Coated Refractive IR Optics**

MATERIALS/ SUBSTRATE	FIGURES	LDEF LOCATION	COMMENTS
ThF <sub>4</sub> /Ag/ B1664 Glass <sup>1</sup>	E.42	B3	Outside/inside samples showed little change in reflectance over all wavelengths.
Al <sub>2</sub> O <sub>3</sub> -Ag/Kanigen <sup>1</sup>	E.43	B3	Outside/inside samples had significantly-reduced reflectance except at the blue end.
ULE <sup>TM</sup> /Ag <sup>2</sup>	E.31	E5	Contamination reduced transmission. Cleaning returned sample to pre flight value.

<sup>1</sup> Data relevant to this material are presented in Section 4.5.1.4

<sup>2</sup> Data relevant to this material are presented in Section 4.3.2.4

#### 4.4.2, Coated Refractive IR Optics

---

##### 4.4.2.5 Darkening

At the present time, no data have been found for this section.

##### 4.4.2.6 Stress

For both AR coatings and solar rejection coatings tested in experiment S0050-2, very little change in stresses was observed for post-flight versus pre-flight comparisons (Ref. 7).

Table 4.4.2.6b shows references to related materials/effects covered in other sections of this handbook.

**Table 4.4.2.6b. Stress Data Base for Coated Refractive UV/Visible Optics  
Applicable to Coated Refractive IR Optics**

MATERIALS/ COATING	FIGURES	LDEF LOCATION	COMMENTS
Fused Silica/Ag <sup>1</sup>	E.33	E5	After cleaning, pre- and post flight measurements were very similar
ULTEM/Ag <sup>1</sup>	E.33	E5	After cleaning, pre- and post flight measurements were very similar

<sup>1</sup> Data relevant to this material are presented in Section 4.3.2.6

##### 4.4.2.7 Contamination/Deterioration

A number of optical materials flown on LDEF showed signs of contamination. Analysis of flight samples flown on experiment S0050-2 showed the substrates and coatings to be covered with a thin layer of polymer which contained silicon. The contaminant, a light brown stain, was removed fairly easily with normal cleaning techniques (except for the AR coating) (Ref. 7).

#### 4.4.2. Coated Refractive IR Optics

Table 4.4.2.7b shows references to related materials/effects covered in other sections of this handbook.

**Table 4.4.2.7b. Contamination/Deterioration Effects Data Base for IR Coatings  
Applicable to Coated Refractive IR Optics**

MATERIALS/ SUBSTRATE	FIGURES	UDEF LOCATION	COMMENTS
Ag+(Al <sub>2</sub> O <sub>3</sub> /ZnS) <sup>1</sup> / Polished Mo <sup>1</sup>	E.59	D8	Discolored and hazed.
Si/SiO <sub>2</sub> <sup>1</sup>	E.60	D3	Particle contamination.
PbF <sub>2</sub> /SiO <sub>2</sub> <sup>1</sup>	E.61	D3	Dark red contamination.
MgF <sub>2</sub> (λ=1.06μm)/ 2 thick on Fused Silica <sup>1</sup>	E.54	D4	Fibrous matter and film fragments. Blisters.
ZnS/SiO <sub>2</sub> <sup>1</sup>	E.55	D9	Showed surface cracking and flaking
Al <sub>2</sub> O <sub>3</sub> /SiO <sub>2</sub> <sup>1</sup>	E.56	D3	Randomly-distributed blisters and flaking
As <sub>2</sub> Se <sub>3</sub> <sup>1</sup>	E.52	D3	Slight crack at edge. Contaminated.
MgF <sub>2</sub> <sup>1</sup>	E.54	D4	Entire coating is crazed and blistered around debris spot.
	E.57	D4	Entire coating is crazed and blistered around debris spot.
	E.58	D4	Entire coating is crazed and blistered around debris spot.

<sup>1</sup> Data relevant to this material are presented in Section 4.6.1.7

## 4.5 COATINGS FOR UV/VISIBLE SYSTEMS

A number of coatings covered under IR systems are equally applicable to UV/visible systems. To avoid needless duplication, section citations within the IR section are given along with a descriptive table for these materials; the narrative material is not reproduced in this chapter. Table 4.5.a shows a summary of the experiments containing coatings for UV/visible systems. All UV/visible coatings in this experiment were flown near the trailing edge of the LDEF spacecraft.

**Table 4.5.a. Experiment Summary for UV/Visible Optics Coatings**

EXPERIMENT	UV/VISIBLE OPTICAL COATINGS
A0034	SiO <sub>2</sub> on Pyrex, Os/Al on Quartz, Ag/Al on Quartz, Au/Al on Quartz, and MgF <sub>2</sub> /Al on Quartz
A0138.4	MgF <sub>2</sub> /Al on B1664 glass, MgF <sub>2</sub> /Al on Kangened Al, MgO/MgF <sub>2</sub> on B1664 glass, LaF <sub>3</sub> /Chiolite/MgF <sub>2</sub> on B1664 glass, ThF <sub>4</sub> /Ag on B1664 glass, ThF <sub>4</sub> /Ag on Kangened Al, LiF/Al on B1664 glass, LiF/Al on Kangened Al, Al <sub>2</sub> O <sub>3</sub> /MgF <sub>2</sub> on Kangened Al, 250 nm dielectric on B1664 glass, 1060 nm dielectric/TiO <sub>2</sub> /SiO <sub>2</sub> on B1664 glass, and 10.6 μm mirror/Gc ZnS ThF <sub>4</sub> on B1664 glass.
A0138.5	Al on glass, Pt on glass

Table 4.5.b shows the UV/visible coatings and the effects addressed by the LDEF experimenters.

Table 4.5.b. Coatings for UV/Visible Systems

MATERIALS	EFFECTS						
	I M P A C T S	A T O M I C  O X Y G E N	A B S / T R A N / R E F L	D A R K E N I N G	S T R E S S	S C A T T E R	C O N T A M / D E T E R
MgF <sub>2</sub> /Fused Silica	○	○				○	○
Al-MgF <sub>2</sub> /B1664 Glass			•				
ThF <sub>4</sub> Ag/B1664 Glass			•				
Al <sub>2</sub> O <sub>3</sub> -MgF <sub>2</sub> /Kaugen			•				
Al-MgF <sub>2</sub> /Kaugen			•				
MgO-MgF <sub>2</sub> /B1664 Glass			•				
Visible 1060 nm mirror/TiO <sub>2</sub> , SiO <sub>2</sub> , on B1664 Glass			•				
10.6 μm mirror/Gc ZnS-ThF <sub>4</sub> on B1664 Glass			•				
Cr/Ag/ThF <sub>4</sub> /Mo	○						
Ag+(Al <sub>2</sub> O <sub>3</sub> /Si) <sup>+</sup> on Polished Si	○						
Al <sub>2</sub> O <sub>3</sub> /SiO <sub>2</sub>	○						○
NaF <sub>2</sub> on SiO <sub>2</sub>	○						

• Data contained in this section

○ Data contained in other, cross-referenced sections

Table 4.5.b. Coatings for UV/Visible Systems (Cont.)

MATERIALS	EFFECT						
	I M P A C T S	A T O M I C  O X Y G E N	A B S / T R A N / R E F L	D A R K E N I N G	S T R E S S	S C A T T E R	C O N T A M / D E T E R
As <sub>2</sub> Se <sub>3</sub> /SiO <sub>2</sub>	○						○
Au/Ni/Al	○						
AlO <sub>3</sub> /MgF <sub>2</sub> /MERK 11611 on B1664 Glass			●				
Fused Silica/Solar Rejection			○		○		
UHF <sup>1</sup> /Ag			○		○		
Fused Silica/Antireflectance			○		○		
LaF <sub>3</sub> /Chalcite/MgF <sub>2</sub>					○		
Ge/ZnS/11H <sub>2</sub>						●	
Ag+(Al <sub>2</sub> O <sub>3</sub> /ZnS) <sup>1</sup> on Polished Mo							○
Si/SiO <sub>2</sub>							○
PbF <sub>2</sub> /SiO <sub>2</sub>							○
MgF <sub>2</sub> (λ=1.06μ)/2 thick on Fused Silica							○
ZnS/SiO <sub>2</sub>							○

● Data contained in this section

○ Data contained in other, cross-referenced sections

Table 4.5.b. Coatings for UV/Visible Systems (Cont.)

MATERIALS	EFFECTS						
	I M P A C T S	A T O M I C  O X Y G E N	A B S / T R A N / R E F L	D A R K E N I N G	S T R E S S	S C A T T E R	C O N T A M / D E T E R
Al on Glass			○				
Pt on Glass			○				
SiO <sub>2</sub> /Al on Pyrex							•
Os/Al on Quartz							•
Ag/Al on Quartz							•
Au/Al on Quartz							•
MgF <sub>2</sub> /Al on Quartz							•

• Data contained in this section

○ Data contained in other, cross-referenced sections

#### 4.5.1 Coated UV/Visible Optics

##### 4.5.1.1 Impacts

All discussions of impact effects on IR coatings that are equally applicable to UV/visible coatings are covered in Section 4.6.1.1, Impacts Effects on IR Coatings. In general, all samples showed some impact effects. Those samples flown on experiment

#### 4.5. Coatings for UV/Visible Optics

M0003-2 and on the leading edge (at locations D8 and D9) showed several microfractures. The trailing edge samples were crazed, but so were the control samples leading the experimenters to the conclusion that crazing is related to coating manufacturing stresses, and not necessarily related to the space environment.

Table 4.5.1.1b shows references to related materials/effects covered in other sections of this handbook.

**Table 4.5.1.1b. Impact Effects Data Base for IR Coatings  
Applicable to UV/Visible Coatings**

MATERIALS/ SUBSTRATE	FIGURES	LDEF LOCATION	COMMENTS
MgF <sub>2</sub> / Fused Silica <sup>1</sup>	F-47	D9	Damage is localized
Cu/Ag/ThF <sub>4</sub> /Mo <sup>1</sup>	F-49	D9	Overall damage area is several times crater size Coating failure is observed
Ag+(AlO <sub>2</sub> /Si) <sup>1</sup> on Polished Silicon <sup>1</sup>	F-50	D8	Microfractured, corroded, cratered
AlO <sub>2</sub> /SiO <sub>2</sub> <sup>1</sup>	F-51	D3	Microfractured, flaked
As <sub>2</sub> Se <sub>3</sub> / SiO <sub>2</sub> <sup>1</sup>	F-52	D3	Crazed, discolored
Au/Ni/Al <sup>1</sup>	F-53	D4	Unchanged
MgF <sub>2</sub> (λ = 1.06μm)/ 2 thick on Fused Silica <sup>1</sup>	F-54	D4	Crazed, Contaminated
NaF <sub>2</sub> on SiO <sub>2</sub> <sup>1</sup>	F-48	D9	Damaged layer removed around impact due to UV or AO

<sup>1</sup> Data relevant to this material are presented in Section 4.6.1.1

#### 4.5.1.2 Atomic Oxygen

At the present time, no data have been found for this section.



#### 4.5.1.3 Scatter

All discussions of scatter effects on coated UV/visible refractive optics that are equally applicable to UV/visible coatings are covered in Section 4.3.2.3, Scatter Effects on Coated UV/Visible Refractive Optics. As discussed in Section 4.3.2.3, for  $\text{MgF}_2$  coated silica the induced scatter was found to be less for the leading edge than for the trailing one. This result was essentially the same for both 9-month and 69-month exposure (Refs. 5 and 9).

Table 4.5.1.3b shows references to related materials/effects covered in other sections of this handbook

**Table 4.5.1.3b. Scatter Effects Data Base for Coated UV/Visible Refractive Optics Applicable to UV/Visible Coatings**

MATERIALS	FIGURES	LDEF LOCATION	COMMENTS
$\text{MgF}_2/\text{Fused Silica}^1$	E.27	D9 D4	Leading edge showed less scatter (coating removal by AO)
$\text{Ag}/\text{ULF}^{\text{TM}}$	E.28	F-5	Increase in scatter

<sup>1</sup> Data relevant to this material are presented in Section 4.3.2.3

#### 4.5.1.4 Absorption/Transmission/Reflectance

In experiment AO138-4, the  $\text{Al}/\text{MgF}_2$  coating on B1664 glass substrate showed a relative reflectance loss of 16 percent and on a Kanigened Al substrate showed a 23-percent loss. Whether the samples were cleaned prior to post-flight examination is not reported by the experimenter. There was very little degradation in the  $\text{Au}$ ,  $\text{Al}_2\text{O}_3/\text{Ag}$ , and  $\text{ThF}_4/\text{Ag}$  coatings whether they are on B1664 glass or Kanigened Al substrates (Ref. 10).

#### 4.5. Coatings for UV/Visible Optics

Table 4.5.1.4a summarizes and provides a guide to the materials contained in this section.

**Table 4.5.1.4a. Absorption/Transmission/Reflectance Effects Data Base for UV/Visible Coatings**

MATERIALS/ SUBSTRATE	FIGURES	LOCATION	COMMENTS
Al-MgF <sub>2</sub> / B1664 Glass	E.41	B3	Outside/inside samples had significantly-reduced reflectance over all wavelengths.
TbF <sub>3</sub> -Ag/ B1664 Glass	E.42	B3	Outside/inside samples showed little change in reflectance over all wavelengths.
Al <sub>2</sub> O <sub>3</sub> -Ag/ Kanigen	E.43	B3	Outside/inside samples had significantly-reduced reflectance except at the blue end.
Al-MgF <sub>2</sub> / Kanigen	E.44	B3	Inside sample had significant reduction in reflectance at upper end. Outside sample had significant reduction across the entire band.
MgO-MgF <sub>2</sub> / B1664 Glass	E.45	B3	Inside sample showed slight shift in reflectance. Outside sample had little reduction at the blue end but a slight shift to the high end.
	E.46	B3	Inside sample showed a significant reduction in transmittance at the blue end. Outside sample had a significant reduction in transmission at the blue end and a slight reduction at the upper end.
Visible + 1060 nm mirror/TiO <sub>2</sub> -SiO <sub>2</sub> on B1664 Glass	None	B3	Remained optically efficient.
Al <sub>2</sub> O <sub>3</sub> /MgF <sub>2</sub> /MERK 11611 on B1664 Glass	None	B3	Slight reduction in transmittance at blue end of spectrum and slight increase in transmittance at high end.

Table 4.5.1.4b shows references to related materials/effects covered in other sections of this handbook.

#### 4.5. Coatings for UV/Visible Optics

**Table 4.5.1.4b. Transmittance Data Base for Coated Refractive UV/Visible Optics  
Applicable to UV/Visible Coatings**

MATERIALS/ COATINGS	FIGURES	LDEF LOCATION	COMMENTS
Fused Silica/Ag <sup>1</sup>	E 28	E5	Contamination reduced transmission. An increase in scatter was measured.
Fused silica/ Solar rejection <sup>1</sup>	E.29	E5	Contamination reduced transmission. Cleaning returned sample to pre-flight value
	E.30	E5	Contamination reduced transmission. Cleaning returned sample to pre-flight value
ULE™/Ag <sup>1</sup>	E 31	E5	Contamination reduced transmission. Cleaning returned sample to pre-flight value
Fused Silica/ Anti-reflection <sup>1</sup>	E.32	E5	Contamination reduced transmission. Normal cleaning methods not effective. Needed exposure to oxygen plasma to improve performance

<sup>1</sup> Data relevant to this material are presented in Section 4.3.2.1

In experiment A0138-4, the MgO/MgF<sub>2</sub> coating on B1664 glass showed a significant reduction in spectral width for each trailing edge flight sample (20 - 38 percent reduction). This is to be compared with the TiO<sub>2</sub>/SiO<sub>2</sub> coating on B1664 glass which remained optically efficient even though the flight sample showed some thin cracking. The Al<sub>2</sub>O<sub>3</sub>/MgF<sub>2</sub> AR coating showed a very slight (< 1 percent) reduction in average transmittance over a spectral range of 400 - 1000 nm (Ref. 10).

##### 4.5.1.5 Darkening

To date, no data have been identified for UV/visible coatings for this effect.

## 4.5. Coatings for UV/Visible Optics

---

### 4.5.1.6 Stress

All discussions of stress effects on IR coatings that are equally applicable to UV/visible coatings is covered in Section 4.3.2.6, Stress Effects on Coated IR Optics. For both AR coatings and solar rejection coatings tested in experiment S0050-2, very little change in stresses was observed for post-flight versus pre-flight.

Table 4.5.1.6b shows references to related materials/effects covered in other sections of this handbook.

**Table 4.5.1.6b. Stress Data Base for Coated Refractive UV/Visible Optics Applicable to UV/Visible Coatings**

MATERIALS/ COATING	FIGURES	LDEF LOCATION	COMMENTS
Fused Silica/AR <sup>1</sup>	E-33	I-5	Contaminant did not introduce measurable stress
Fused Silica/ AR/Uncoated side <sup>1</sup>	E-33	I-5	Contaminant did not introduce measurable stress
ULFIM/Ar <sup>1</sup>	E-33	I-5	After cleaning, pre- and post flight measurements were very similar

<sup>1</sup> Data relevant to this material are presented in Section 4.3.2.6

### 4.5.1.7 Contamination/Deterioration

Coatings including many high stressed layers (oxides and fluorides) show an evident risk of mechanical degradation due to thermal cycling.

Table 4.5.1.7a summarizes and provides a guide to the materials contained in this section.

**Table 4.5.1.7a. Contamination/Deterioration Effects Data Base for UV/Visible Coatings**

MATERIALS/ SUBSTRATE	FIGURES	LDEF LOCATION	COMMENTS
Ge/ZnS/ThF <sub>4</sub> on B1664 Glass	None	B3	Peeling of coating due to vacuum or thermal cycling
SiO/Al on Pyrex	None	C3 C9	Degradation in UV spectral reflectance due to contamination.
Os/Al on Quartz	None	C3 C9	Complete oxidation of the silver film and complete oxidation and evaporative removal of Os film on leading edge.
Ag/Al on Quartz	None	C3 C9	Complete oxidation of the silver film in both leading edge and trailing edge samples.
Au/Al on Quartz	None	C3 C9	Slight visual difference in leading edge samples. No obvious effect on trailing edge samples.
MgF <sub>2</sub> /Al on Quartz	None	C3 C9	No visible effect in leading edge or trailing edge samples

The Ge/ZnS/ThF<sub>4</sub> coating on B1664 glass was flown on experiment AO138-4 and tested at 10.6  $\mu\text{m}$  wavelength. No significant changes in reflectance were measured due to any contamination observed. It is not known whether the sample was cleaned prior to making the reflectance measurements (Ref. 10).

The contaminant collector mirrors (SiO/Al/Pyrex, Os/Al/Quartz, Ag/Al/Quartz, Au/Al/Quartz, and MgF<sub>2</sub>/Al/Quartz) were flown on experiment AO034. All samples were examined visually and reflectance measurements were made to determine the effect of the observed contaminants. For the SiO sample, contaminant coloration was observed on both leading and trailing edge samples resulting in degraded spectral reflectance. For the Cs and Ag samples, oxidation and surface removal was observed contaminating the surfaces. The leading and trailing edge samples of the Au and MgF<sub>2</sub> were found to have little or no effect (Ref. 11).

#### 4.5, Coatings for UV/Visible Optics

Table 4.5.1.7b shows references to related materials/effects covered in other sections of this handbook.

**Table 4.5.1.7b. Contamination/Deterioration Effects Data Base for IR Coatings  
Applicable to UV/Visible Coatings**

MATERIALS/ SUBSTRATE	FIGURES	LDEF LOCATION	COMMENTS
Ag+(Al <sub>2</sub> O <sub>3</sub> /ZnS) <sup>4</sup> / Polished Mo <sup>1</sup>	E.59	D8	Corroded and hazed.
Si/SiO <sub>2</sub> <sup>1</sup>	E.60	D3	Particle contamination.
PbF <sub>2</sub> /SiO <sub>2</sub> <sup>1</sup>	E.61	D3	Dark red contamination.
MgF <sub>2</sub> (λ=1.06μm)/ 2 thick on Fused Silica <sup>1</sup>	E.54	D4	Fibrous matter and film fragments.
ZnS/SiO <sub>2</sub> <sup>1</sup>	E.55	D9	Showed surface cracking and flaking
Al <sub>2</sub> O <sub>3</sub> /SiO <sub>2</sub> <sup>1</sup>	E.56	D3	Randomly-distributed blisters and flaking
As <sub>2</sub> Se <sub>3</sub> /SiO <sub>2</sub> <sup>1</sup>	E.52	D3	Slight crack at edge. Contaminated.
MgF <sub>2</sub> /Fused Silica <sup>1</sup>	E.54	D4	Entire coating is crazed and blistered around debris spot
	E.57	D4	Entire coating is crazed and blistered around debris spot
	E.58	D4	Entire coating is crazed and blistered around debris spot

<sup>1</sup> Data relevant to this material are presented in Section 4.6.1.7.

#### 4.6 COATINGS FOR IR SYSTEMS

All data contained in this section are from samples flown on experiment Stations AO138-4, M0003-2, -6, -7, and S0050-2. Table 4.6.a shows a summary of the experiments containing IR optical coatings.

Table 4.6.a. Experiment Summary for IR Optical Coatings

EXPERIMENT	IR OPTICAL COATINGS
AO183-4	LaF <sub>3</sub> /Chiolite/MgF <sub>2</sub> , Ge/ZnS/ThF <sub>4</sub> on B1664 Glass, ThF <sub>4</sub> /Ag on B1664 Glass, Al <sub>2</sub> O <sub>3</sub> /Ag on Kanigened Al, ZnS on Ge
M0003-2	MgF <sub>2</sub> /fused silica, ThF <sub>4</sub> /Ag/Cr on Mo, MgF <sub>2</sub> ( $\lambda = 1.06\mu\text{m}$ )-2-thick on fused silica
M0003-6	Au on Ni/Al
M0003-7	Ag+(Al <sub>2</sub> O <sub>3</sub> /Si) <sup>3</sup> on polished Si, Al <sub>2</sub> O <sub>3</sub> on SiO <sub>2</sub> , As <sub>2</sub> Se <sub>3</sub> on SiO <sub>2</sub> , ZnS on SiO <sub>2</sub> , Al+(Al <sub>2</sub> O <sub>3</sub> /ZnS) <sup>4</sup> on polished Mo, Si on SiO <sub>2</sub> , PbF <sub>2</sub> on SiO <sub>2</sub> , NaF <sub>2</sub> on SiO <sub>2</sub>
S0050-2	Ag on ULE™

Table 4.6.b is a cross-reference for the IR coatings and the effects addressed by the LDEF experimenters.

#### 4.6.1 Coated IR Optics

##### 4.6.1.1 Impacts

In general, all samples flown on M0003-2 showed some impact effects. Those samples flown on the leading edge (at locations D8 and D9) showed several microfractures.

Table 4.6.1.1a summarizes and provides a guide to the materials contained in this section.

Table 4.6.b. Coatings for IR Systems

MATERIALS	EFFECTS						
	I M P A C T S	A T O M I C  O X Y G E N	A B S / T R A N / R E F L	D A R K E N I N G	S T R E S S	S C A T T E R	C O N T A M / D E T E R
MgF <sub>2</sub> /Fused Silica	•	○	○			○	•
LaF <sub>3</sub> /Chiolite/MgF <sub>2</sub>					○		
Cr/Ag/ThF <sub>4</sub> /Mo	•						
Ag+(Al <sub>2</sub> O <sub>3</sub> /Si) <sup>3</sup> on Polished Si	•						•
Al <sub>2</sub> O <sub>3</sub> /SiO <sub>2</sub>	•						•
As <sub>2</sub> Se <sub>3</sub> /SiO <sub>2</sub>	•						•
Au/Ni/Al	•						
MgF <sub>2</sub> (λ=1.06μm)/2-thick on Fused Silica	•						•
ZnS/SiO <sub>2</sub>							•
Ag+(Al <sub>2</sub> O <sub>3</sub> /ZnS) <sup>4</sup> on Polished Mo							•
Si/SiO <sub>2</sub>							•
PbF <sub>3</sub> /SiO <sub>2</sub>							•
NaF <sub>2</sub>	•						

• Data contained in this section

○ Data contained in other, cross-referenced sections



Table 4.6.b. Coatings for IR Systems (Cont.)

MATERIALS	EFFECTS						
	I M P A C T S	A T O M I C  O X Y G E N	A B S / T R A N / R E F L	D A R K E N I N G	S T R E S S	S C A T T E R	C O N T A M / D E T E R
10.6 $\mu$ m Mirror/Ge-ZnS-ThF <sub>4</sub> on B1664 Glass			•				
ThF <sub>4</sub> /Ag on B1664 Glass			○				
Al <sub>2</sub> O <sub>3</sub> /Ag on Kanigened Al			○				
ULE™/Ag			○		○		
ZnS on Ge			•				
TiO <sub>2</sub> /SiO <sub>2</sub> on B1664 Glass			○				
ZnSe/ZnS/ThF <sub>4</sub> on ZnSe			○				

• Data contained in this section

○ Data contained in other, cross-referenced sections

Table 4.6.1.1a. Impact Effects Data Base for IR Coatings

MATERIALS/ SUBSTRATE	FIGURES	I,DEF LOCATION	COMMENTS
MgF <sub>2</sub> /Fused Silica	E.47	D9	Damage is localized
NaF <sub>2</sub> on SiO <sub>2</sub>	E.48	D9	Damage layer removed from around impact due to UV or AO
ThF <sub>4</sub> /Ag/Cr/Mo	E.49	D9	Overall damage area is several times crater size Coating failure is observed
Ag+(Al <sub>2</sub> O <sub>3</sub> /Si) <sup>3</sup> Polished Silicon	E.50	D8	Microfractured, corroded, cratered
Al <sub>2</sub> O <sub>3</sub> /SiO <sub>2</sub>	E.51	D3	Microfractured, flaked
As <sub>2</sub> Se <sub>3</sub> /SiO <sub>2</sub>	E.52	D3	Crazed, discolored
Au/Ni/Al	E.53	D4	Unchanged
MgF <sub>2</sub> (λ=1.06μm)/ 2 thick on Fused Silica	E.54	D4	Crazed, Contaminated

An MgF<sub>2</sub> coating was applied to fused silica and flown as part of experiment M0003-2. The impact damage tended to be less localized than for bare fused silica, with more extensive crazing and a larger tendency to involve long cracks originating at the impact site. Further, local delamination of the coating(s) occurred around the edge of the craters. The clearly-identified craters were much deeper than the coatings, and thus were mostly in the fused silica, and produced the same conchoidal surfaces as for bare silica. Synergistic effects were also observed (e.g., for NaF<sub>2</sub> coatings), such that coating material was sometimes removed around the impact site owing to the further interactions with either UV and/or AO. The extensive crazing was apparently not only caused by the impacts, however, since even ground controls of MgF<sub>2</sub> displayed similar effects, suggesting that the problem was associated with high in-situ stresses generated at manufacture. Further, there were no indications that the crazing itself significantly interacted with the cratering phenomena, or vice versa (Ref. 9).

M0003-2 coatings on Mo also showed damage areas many times the crater size leading to coating failure (Ref. 9).

From experiment M0003-7, observations show, for  $\text{Ag}+(\text{Al}_2\text{O}_3/\text{Si})^3$  on polished Si, three small impact craters, surrounded by localized cracking on the exposed coating surface. The coating was cracked in spirals at the perimeter of the exposure area. The coating appeared to be blistered in the vicinity of the spiral cracks; flaking in the cracked region revealed a corroded and discolored residual surface (Ref. 12).

For the  $\text{Al}_2\text{O}_3$  coating on  $\text{SiO}_2$ , fine fractures which intersect and terminate in defects in the coating were discernible in the exposed surface areas. There were some small areas where the coating had flaked away revealing the smooth surface of the substrate. A small number of individual blisters or bubbles were discernible in the coating. These features varied in size, were randomly distributed, and were present globally on the surface (Ref. 12).

These observations are to be contrasted with the  $\text{As}_2\text{Se}_3$  coating on  $\text{SiO}_2$  sample. After space exposure, the coating appeared nonuniform in color to the eye. At high magnification, it was apparent that the exposed surface was crazed and that the observed variation in color is due to the presence of contiguous green patches in the otherwise pink coating. There were no discernible morphological features associated with the green patches and they did not correspond to the crazed fragments in the coating (Ref. 12).

For the M0003-6 experiment, a sample of electroplated Au on Ni/Al, when examined, showed a small quantity of debris on the surface, but no other changes were discernible (Ref. 12).

A micrometeoroid impact site was found on one of the samples. The impact crater measured 0.3 mm in diameter by 0.03 mm deep. Multiple fractures occurred in the glass at the impact site (Ref. 7).

### 4.6.1.2 Atomic Oxygen

At the present time, no data have been found for this section

### 4.6.1.3 Scatter

Specific discussions of scatter effects on coated UV/visible refractive optics that are equally applicable to IR coatings (i.e.,  $\text{MgF}_2$ ) are covered in Section 4.3.2.3, Scatter Effects on Coated UV/Visible Refractive Optics. For  $\text{MgF}_2$ -coated silica, the induced scatter was found to be less for the leading edge than for the trailing one. This result was essentially the same for both 9-month and 69-month exposures (Refs. 5 and 9).

Table 4.6.1.3b shows references to related materials/effects covered in other sections of this handbook.

**Table 4.6.1.3b. Scatter Effects Data Base for Coated UV/Visible Refractive Optics Applicable to IR Coatings**

MATERIALS	FIGURES	LDEF LOCATION	COMMENTS
$\text{MgF}_2$ /Fused Silica <sup>1</sup>	E.27	D9 D4	Leading edge showed less scatter than trailing edge
Ag/ULE <sup>TM</sup>	E.28	E5	Increase in scatter

<sup>1</sup> Data relevant to this material are presented in Section 4.3.2.3.

### 4.6.1.4 Absorption/Transmission/Reflectance

Specific discussions of absorption/transmission/reflectance effects on UV/visible coatings that are equally applicable to IR coatings (i.e.,  $\text{MgF}_2$ ) are covered in Section 4.5.1.4, Absorption/Transmission/Reflectance Effects on Coatings for UV/Visible Optics. Within the

#### 4.6, Coatings for IR Optics

Section 4.5.1.4 data, the Al/MgF<sub>2</sub> coating on B1664 glass showed a relative reflectance loss of 16 percent and on Kanigen, 23 percent loss. Whether the samples were cleaned prior to post-flight examination is not reported by the experimenter. There was very little degradation in the Au, Al<sub>2</sub>O<sub>3</sub>/Ag, and ThF<sub>4</sub>/Ag coatings whether they are on B1664 glass or Kanigened Al.

Table 4.6.1.4a summarizes and provides a guide to the materials contained in this section.

**Table 4.6.1.4a. Absorption/Transmission/Reflectance Effects Data Base for Coatings**

MATERIALS/ SUBSTRATE	FIGURES	LDEF LOCATION	COMMENTS
Ge-ZnS-ThF <sub>4</sub> on B1664 Glass	None	B3	No significant change.

Table 4.6.1.4b shows references to related materials/effects covered in other sections of this handbook.

**Table 4.6.1.4b. Absorption/Transmission/Reflectance Effects Data Base for UV/Visible Coatings Applicable to IR Coatings**

MATERIALS/ SUBSTRATE	FIGURES	LDEF LOCATION	COMMENTS
ThF <sub>4</sub> -Ag/ B1664 Glass <sup>1</sup>	E.42	B3	Outside/inside samples showed little change in reflectance over all wavelengths.
Al <sub>2</sub> O <sub>3</sub> -Ag/Kanigened Al <sup>1</sup>	E.43	B3	Outside/inside samples had significantly-reduced reflectance except at the blue end.
ULE™/Ag <sup>2</sup>	E.31	E5	Contamination reduced transmission. Cleaning returned sample to pre-flight value.

<sup>1</sup> Data relevant to this material are presented in Section 4.5.1.4.

<sup>2</sup> Data relevant to this material are presented in Section 4.3.2.4.

### 4.6.1.5 Darkening

At the present time, no data have been found for this section.

### 4.6.1.6 Stress

LDEF contaminants did introduce some stress in IR coating materials. In general, however, the amount of stress was negligible and did not affect the coatings optical performance as seen in Table 4.6.1.6b for fused silica- and ULE<sup>TM</sup>-based optics. MgF<sub>2</sub>-based optics, however, did not survive the contamination-induced stress (see Table 4.6.1.6b).

Table 4.6.1.6b shows references to related materials/effects covered in other sections of this handbook.

**Table 4.6.1.6b. Stress Data Base for Coated Refractive IR Optics  
Applicable to IR Coatings**

MATERIALS/ COATING	FIGURES	LDEF LOCATION	COMMENTS
Fused Silica/Ag <sup>1</sup>	E.33	E5	After cleaning, pre- and post-flight measurements were very similar
ULE <sup>TM</sup> /Ag <sup>1</sup>	E.33	E5	After cleaning, pre- and post-flight measurements were very similar
LaF <sub>3</sub> /Chiolite/MgF <sub>2</sub> <sup>1</sup>	None	B3	Did not survive because of high stress levels

<sup>1</sup> Data relevant to this material are presented in Section 4.3.2.6.

### 4.6.1.7 Contamination/Deterioration

A number of materials flown on LDEF showed signs of contamination as well as flaking and blistering of the coatings. Table 4.6.1.7a summarizes and provides a guide to the materials contained in this section.

Table 4.6.1.7a. Contamination/Deterioration Effects Data Base for IR Coatings

MATERIALS/ SUBSTRATE	FIGURES	LDEF LOCATION	COMMENTS
Ag+(Al <sub>2</sub> O <sub>3</sub> /ZnS) <sup>4</sup> / Polished Mo	E.59	D8	Corroded and hazed.
Si/ SiO <sub>2</sub>	E.60	D3	Particle contamination.
PbF <sub>2</sub> / SiO <sub>2</sub>	E.61	D3	Dark red contamination.
MgF <sub>2</sub> (λ=1.06μm)/ 2 thick on Fused Silica	E.54	D4	Fibrous matter and film fragments.
ZnS/SiO <sub>2</sub>	E.55	D9	Showed surface cracking and flaking
Al <sub>2</sub> O <sub>3</sub> /SiO <sub>2</sub>	E.56	D3	Randomly distributed blisters and flaking
As <sub>2</sub> Se <sub>3</sub> /SiO <sub>2</sub>	E.52	D3	Slight crack at edge. Contaminated.
MgF <sub>2</sub> /SiO <sub>2</sub>	E.54	D4	Entire coating is crazed and blistered around debris spot
	E.57	D4	Entire coating is crazed and blistered around debris spot
	E.58	D4	Entire coating is crazed and blistered around debris spot

From experiments M0003-2 and -7, a number of IR coatings were seen to become contaminated and to deteriorate in the space environments. The Ag + (Al<sub>2</sub>O<sub>3</sub>/ZnS)<sup>4</sup> coating on Mo appeared hazy and discolored on the exposed surface. Multiple zones of discoloration were apparent. The variation in discoloration was presumed to be the result of varying degrees of dendritic growth. A high density of spots was apparent over the entire coating. Grain boundaries in the substrate were also apparent through the coating (Ref. 12).

For the Si/SiO<sub>2</sub> sample, a great deal of debris was on the coating surface, but the surface remained highly specular. The PbF<sub>2</sub>/SiO<sub>2</sub> sample had a large number of subsurface polishing scratches. Features, which may be bubbles, pinholes, or growth nodules in the coatings were seen to have formed preferentially along these scratches (Ref. 12).

The  $\text{MgF}_2$  coating on  $\text{SiO}_2$  was seen to be crazed on both the flight and control samples. A great deal of extraneous debris, including fibrous matter and metallic film fragments, was present on the surface. There were three large spots of debris on the spaceward side of the sample where the coating was crazed more extensively. There were also blisters around these debris spots (Ref. 12).

The  $\text{ZnS}$  coating on the  $\text{SiO}_2$  substrate was buckled in a regular pattern on two large areas of the surface. The entire coating was blistered. Large blisters, exhibiting many orders of interference fringes, were discernible on the surface of the sample at low magnification. In addition, a high density of very small blisters was apparent throughout the coating at magnifications of 200X and greater. The surface was, however, relatively clean of debris (Ref. 12).

For the  $\text{Al}_2\text{O}_3$  coating on  $\text{SiO}_2$ , fine fractures which intersect and terminate in defects in the coating were discernible in the exposed surface areas. There were some small areas where the coating had flaked away revealing the smooth surface of the substrate. A small number of individual blisters or bubbles were discernible in the coating. These features varied in size, were randomly distributed, and were present globally on the surface (Ref. 12).

These observations are to be contrasted with the  $\text{As}_2\text{Se}_3$  coating on  $\text{SiO}_2$  sample. After space exposure, the coating appeared non-uniform in color to the eye. At high magnification, it was apparent that the exposed surface was crazed and that the observed variation in color is due to the presence of contiguous green patches in the otherwise pink coating. There were no discernible morphological features associated with the green patches and they did not correspond to the crazed fragments in the coating (Ref. 12).



## 4.7 OPTICAL FILTERS FOR UV/VISIBLE SYSTEMS

There were many different filter systems flown on LDEF, including metal-dielectric blockers, metal-dielectric bandpassers, all-dielectric hot mirrors/detector trimmers, and all-dielectric bandpassers. The filters discussed in this chapter were flown in experiment Stations A0138-4, A0147, and S0050. Table 4.7.a shows a summary of the experiments containing UV/visible optical coatings.

**Table 4.7.a. Experiment Summary for UV/Visible Optical Coatings**

EXPERIMENT	UV/VISIBLE OPTICAL COATINGS
A0138-4	Al-MgF <sub>2</sub> on MgF <sub>2</sub> Substrate (1216 Å), Al-MgF <sub>2</sub> on MgF <sub>2</sub> Substrate (1270 Å), Al-MgF <sub>2</sub> on Quartz Substrate (2430 Å)
A0147	ZnS/Cryolite/Silver on Fused Silica (Cemented with Epon 328), ZnS/Cryolite/Silver on Fused Silica (Air-spaced, No Cement), ThF <sub>4</sub> /Cryolite/Al/ZrO <sub>2</sub> on Fused Silica (Air-spaced, No Cement), ZrO <sub>2</sub> /Cryolite/Silver on Fused Silica (Air-spaced, No Cement), ZnS/ThF <sub>4</sub> on Fused Silica (Air-spaced, No Cement), ThF <sub>4</sub> /Cryolite/Al on Fused Silica (Air-spaced, No Cement), PbF <sub>2</sub> /Cryolite on Fused Silica (Air-spaced, No Cement), ZnS/Cryolite/Silver on Fused Silica (Cemented with APCO R313)
S0050-1	Narrow-Band Corion <sup>1</sup> , Neutral Density Band Corion <sup>1</sup> , Broadband Corion <sup>1</sup>

<sup>1</sup> These filters were provided by Corion Corporation, Holliston, MA. Specific material stack-ups for the filter were not explicitly identified. The narrow-band filters were composed of quarter-wave thick stacks of dielectric materials. The neutral density filters did not use quarter-wave dielectric stacks but were composed of a single layer of Inconel coating which provides approximately uniform attenuation across the visible spectrum. The hot-mirror interference filters were deposited on glass with a ThF<sub>4</sub> layer at the surface. One of the wide-band hot-mirror filters was examined by SEM and was found to be composed of eleven layers of (ThF<sub>4</sub>/ZnS) pairs deposited on a glass substrate.

Table 4.7b shows the UV/visible optical filter materials and the effects addressed by the LDEF experimenters.

Table 4.7b. UV/Visible Optical Filters

MATERIALS	EFFECTS						
	I M P A C T S	A T O M I C  O X Y G E N	A B S / T R A N / R E F L	D A R K E N I N G	S T R E S S	S C A T T E R	C O N T A M / D E T E R
Narrow-Band Corion			•				
Neutral Density Band Corion			•				
Broadband Corion			•				
Al-MgF <sub>2</sub> on MgF <sub>2</sub> Substrate (1216 Å)			•				
Al-MgF <sub>2</sub> on MgF <sub>2</sub> Substrate (1270 Å)			•				
Al-MgF <sub>2</sub> on Quartz Substrate (2430 Å)			•				
ZnS/Cryolite/Silver on Fused Silica (Cemented with Epon 828)			•				
ZnS/Cryolite/Silver on Fused Silica (Air-spaced, No Cement)			•				
ThF <sub>4</sub> /Cryolite on Fused Silica (Air-spaced, No Cement)			•				
ZrO <sub>2</sub> /Cryolite/Silver on Fused Silica (Air-spaced, No Cement)			•				
ZnS/ThF <sub>4</sub> on Fused Silica (Air-spaced, No Cement)			•				

- Data contained in this section
- Data contained in other, cross-referenced sections

Table 4.7b. UV/Visible Optical Filters (Cont.)

MATERIALS	EFFECTS						
	I M P A C T S	A T O M I C  O X Y G E N	A B S / T R A N / R E F L	D A R K E N I N G	S T R E S S	S C A T T E R	C O N T A M / D E T E R
ThF <sub>4</sub> /Cryolite on Fused Silica (Air-spaced, No Cement)			•				
PbF <sub>2</sub> /Cryolite on Fused Silica (Air-spaced, No Cement)			•				
ZnS/Cryolite on Fused Silica (Cemented with APCO R313)			•				

• Data contained in this section

• Data contained in other, cross-referenced sections

#### 4.7.1 Covered UV/Visible Optical Filters

The UV/visible filters discussed in this section were flown on LDEF with an aluminum cover. (The remainder of the UV/visible filters flown on LDEF were exposed directly to the space environment. These filters are discussed in Section 4.7.2.)

##### 4.7.1.1 Impacts

At the present time, no data have been found for this section.

## 4.7, Optical Filters for UV/Visible Optics

### 4.7.1.2 Atomic Oxygen

At the present time, no data have been found for this section.

### 4.7.1.3 Scatter

At the present time, no data have been found for this section.

### 4.7.1.4 Absorption/Transmission/Reflectance

The most common responses for filters was slight to significant reduction in transmittance accompanied by shifts in center wavelength toward the blue. Table 4.7.1.4a summarizes and provides a guide to the materials contained in this section.

**Table 4.7.1.4a Transmittance Data Base For UV/Visible Optical Filters Exposed Indirectly To Space Environment**

MATERIALS	FIGURES	LDEF LOCATION	COMMENTS
Narrow-Band Corion <sup>1</sup>	E.62	E5	Reduced transmission
Neutral Density Band Corion <sup>1</sup>	E.63	E5	No change in transmittance
Broadband Corion <sup>1</sup>	E.64	E5	No change in transmittance
Al-MgF <sub>2</sub> on MgF <sub>2</sub> Substrate (1216 Å)	E.65	B3	Reduced transmittance and shift in center wavelength
Al-MgF <sub>2</sub> on MgF <sub>2</sub> Substrate (1270 Å)	E.66	B3	Reduced transmittance and shift in center wavelength
Al-MgF <sub>2</sub> on Quartz Substrate (2430 Å)	E.67	B3	Reduced transmittance and shift in center wavelength

<sup>1</sup> These filters were provided by Corion Corporation, Holliston, MA. Specific material stack-ups for the filter were not explicitly identified. The narrow-band filters were composed of quarter-wave thick stacks of dielectric materials. The neutral density filters did not use quarter-wave dielectric stacks but were composed of a single layer of Inconel coating which provides approximately uniform attenuation across the visible spectrum. The hot-mirror interference filters were deposited on glass with a ThF<sub>4</sub> layer at the surface. One of the wide-band hot-mirror filters was examined by SEM and was found to be composed of eleven layers of (ThF<sub>4</sub>/ZnS) pairs deposited on a glass substrate.

#### *4.7, Optical Filters for UV/Visible Optics*

---

From experiment S0050-1, the Corion narrow- and broad-band optical filters showed a small but significant reduction in transmission and is believed to be related to degradation of the cement used in the filter construction (Ref. 13). Neutral density filters (inconel films) show increased transmission, likely due to erosion of the deposited layer. Organic deposits are seen on the films. The deposits are greater in the center than along the rim where the samples were covered (Ref. 14).

The samples from AO138-4 (the 1216 Å, 1270 Å, and 2430 Å filters) all showed reduced transmittance and a shift in center wavelength toward the blue (Ref. 10).

##### **4.7.1.5 Darkening**

At the present time, no data have been found for this section.

##### **4.7.1.6 Stress**

At the present time, no data have been found for this section.

##### **4.7.1.7 Contamination/Deterioration**

A number of filter materials flown on LDEF were retrieved with contamination. A typical example is the set of samples from experiment S0050. On the LDEF tray, the green epoxy-fiberglass mounting strips were changed to a walnut brown where they were exposed to the space environment. Where covered, the original green color was maintained. The tray was covered with a light coating of brown stain which is believed by NASA to be the result of Z-306 thermal-control black paint outgassing in the space environment and becoming fixed

#### *4.7, Optical Filters for UV/Visible Optics*

---

in place by the effects of solar UV. The weight density of this material has been estimated to be 0.2 mg/cm<sup>2</sup> (Ref. 15). Analysis of this contamination is still underway as of this writing.

#### **4.7.2 Exposed UV/Visible Optical Filters**

The UV/visible filters discussed in this section were flown on LDEF exposed directly to the space environment.

##### **4.7.2.1 Impacts**

At the present time, no data have been found for this section.

##### **4.7.2.2 Atomic Oxygen**

At the present time, no data have been found for this section.

##### **4.7.2.3 Scatter**

At the present time, no data have been found for this section.

##### **4.7.2.4 Absorption/Transmission/Reflectance**

Narrow- and broad-band optical filters showed a small but significant reduction in transmission and is believed to be related to degradation of the cement used in the filter construction. Neutral density filters (inconel films) show increased transmission, likely due to erosion of the deposited layer (Refs. 13 and 14).

Table 4.7.2.4a summarizes and provides a guide to the materials contained in this section.

**Table 4.7.2.4a Absorption/Transmittance/Reflectance Data Base For UV/Visible Optical Filters Exposed Directly To Space Environment**

MATERIALS	FIGURES	LDEF LOCATION	COMMENTS
Narrow-Band Corion <sup>1</sup>	E.68	E5	Reduced transmission
	E.69	E5	Shift in center wavelength
	E.70	E5	Broadening of bandpass
Neutral Density Band Corion <sup>1</sup>	E.72	E5	Increased transmittance
Broadband Corion <sup>1</sup>	E.65	E5	Reduced transmittance
	E.66	E5	Deterioration of interference coatings
Al-MgF <sub>2</sub> on MgF <sub>2</sub> Substrate (1216 Å)	E.74	B3	Reduced transmittance and shift in center wavelength
Al-MgF <sub>2</sub> on MgF <sub>2</sub> Substrate (1270 Å)	E.75	B3	Reduced transmittance and shift in center wavelength
Al-MgF <sub>2</sub> on Quartz Substrate (2430 Å)	E.76	B3	Reduced transmittance and shift in center wavelength
ZnS/Cryolite/Silver on Fused Silica (Cemented with Epon 828)	E.77	B8	Reduced transmittance
ZnS/Cryolite/Silver on Fused Silica (Air-spaced, no cement)	E.78	B8	Slight reduction in transmittance with slight shift of center wavelength
ThF <sub>4</sub> /Cryolite on Fused Silica (Air-space, no cement)	E.79	B8	Increase in transmittance (due to pinholes in some of the metal-dielectric coatings)
ZrO <sub>2</sub> /Cryolite/Silver on Fused Silica (Air-spaced, no cement)	E.80	B8	Reduced transmittance
ZnS/ThF <sub>4</sub> on Fused Silica (Air-spaced, no cement)	E.81	B8	Slight decrease in transmittance near short wave cutoff. Slight increase in transmittance near bluer wavelengths (apparent reduction in extinction coefficient of ZnS)

**Table 4.7.2.4a Absorption/Transmittance/Reflectance Data Base For UV/Visible Optical Filters Exposed Directly To Space Environment (Cont.)**

MATERIALS	FIGURES	LDEF LOCATION	COMMENTS
ThF <sub>4</sub> /Cryolite on Fused Silica (Air-spaced, No Cement)	E.82	B8	Increase in transmission (due to pinholes in some of the metal-dielectric coatings)
PbF <sub>2</sub> /Cryolite on Fused Silica (Air-spaced, No Cement)	E.83 E.84	B8	Reduced transmittance (due to increase absorption in the lead compound)
ZnS/Cryolite/Silver on Fused Silica (Cemented with APCO R313)	E.85	B8	Slight reduction in transmittance

<sup>1</sup> These filters were provided by Corion Corporation, Holliston, MA. Specific material stack-ups for the filter were not explicitly identified. The narrow-band filters were composed of quarter-wave thick stacks of dielectric materials. The neutral density filters did not use quarter-wave dielectric stacks but were composed of a single layer of Inconel coating which provides approximately uniform attenuation across the visible spectrum. The hot-mirror interference filters were deposited on glass with a ThF<sub>4</sub> layer at the surface. One of the wide-band hot-mirror filters was examined by SEM and was found to be composed of eleven layers of (ThF<sub>4</sub>/ZnS) pairs deposited on a glass substrate.

From experiment S0050-1, the Corion narrow- and broad-band optical filters showed a small but significant reduction in transmission believed to be related to degradation of the cement used in the filter construction (Ref. 13). Neutral density filters (inconel films) show increased transmission, likely due to erosion of the deposited layer. Organic deposits are seen on the films. The deposits are greater in the center than along the rim where the samples were covered (Ref. 14).

The samples from AO138-4 (the 1216 Å, 1270 Å, and 2430 Å filters) all showed reduced transmittance and a shift in center wavelength toward the blue (Ref. 10).

For the AO147 filters, with the exception of the lead compounds, the filters survived very well. The Epon cement degraded somewhat at 500 nm (other wavelengths were masked by the filter). The failure mode (degradation) of the lead compounds was a wavelength-independent increase in absorption with no change in spectral characteristic. In an instrument, signal would be lost but spectral stability maintained. In the case of filters containing Al



layers, the transmission increases were attributed to the pinholes which developed during exposure. This form of failure would reduce signal to noise but would not influence spectral band position or width. The reason for the development of pinholes has not yet been established by the experimenters. One possibility identified is that defects or contamination in the coating caused local heating due to increased absorption which, in turn, caused coating removal (Ref. 24).

##### **4.7.2.5 Darkening**

At the present time, no data have been found for this section.

##### **4.7.2.6 Stress**

At the present time, no data have been found for this section.

##### **4.7.2.7 Contamination/Deterioration**

A number of filter materials flown on LDEF were retrieved with contamination. A typical example is the set of samples from experiment S0050. On the LDEF tray, the green epoxy-fiberglass mounting strips were changed to a walnut brown where they were exposed to the space environment. Where covered, the original green color was maintained. The tray was covered with a light coating of brown stain which is believed by NASA to be the result of Z-306 thermal-control black paint outgassing in the space environment and becoming fixed in place by the effects of solar UV. The weight density of this material has been estimated to be 0.2 mg/cm<sup>2</sup> (Ref. 15). For the exposed filter materials, organic deposits were seen on the films. The deposits were greater in the center than along the rim where the samples were covered. Analysis of this contamination is still underway as of this writing.

#### 4.8 OPTICAL FILTERS FOR IR SYSTEMS

There were two experiments that contained optical filter materials designed for use with IR optics. Table 4.8.a shows a summary of the experiments containing IR optical coatings.

**Table 4.8.a. Experiment Summary for IR Optical Filters**

EXPERIMENT	IR OPTICAL FILTERS
A0056	CaF <sub>2</sub> , Low Index Ratio Quarter-Wave Blocking ZnSe/ZnS/KRS-5 on KRS-6 Substrate, PbTe/ZnS on Ge Substrate 15 $\mu$ m 10 percent HBW L-Spacer THW Band-Pass Filter, PbTe/ZnS 8-12 $\mu$ m Tscheyshev Edge Band-Pass Filter (Antireflected) on Ge Substrate, PbTe/ZnS 14.5 $\mu$ m 0.7 percent HBW Split-Spacer Fabry-Perot Band-Pass Filter on Ge Substrate
A0138	ZnS/Chiolite on BK7G18 and RG780 Glasses (820 nm Interference Filter)

Table 4.8.b shows the IR optical filter materials and the effects addressed by the LDEF experimenters.

Table 4.8.b. Infrared Optical Filters

MATERIALS	EFFECTS						
	I M P A C T S	A T O M I C  O X Y G E N	A B S / T R A N / R E F L	D A R K E N I N G	S T R E S S	S C A T T E R	C O N T A M / D E T E R
CaF <sub>2</sub>	•						
Low Index Ratio Quarter-Wave Blocking ZnSe/ZnS/KRS-5 on KRS-6 Substrate			•				
PbTe/ZnS on Ge Substrate 15 $\mu$ m 10 percent HBW L-Spacer THW Band- Pass Filter			•				
PbTe/ZnS 8-12 $\mu$ m Tscheyshv Edge Band-Pass Filter (Antireflected) on Ge Substrate			•				
PbTe/ZnS 14.5 $\mu$ m 0.7 percent HBW Split-Spacer Fabry-Perot Band-Pass Filter on Ge Substrate			•				
ZnS/Chiolite on BK7G18 and RG780 Glasses (820 nm Interference Filter)			•				

• Data contained in this section

• Data contained in other, cross-referenced sections

#### 4.8.1 IR Optical Filters

##### 4.8.1.1 Impacts

From experiment A0056, it is seen that the micrometeoroid/debris impact on the CaF<sub>2</sub> sample occurred near the edge of the sample holder. The impact crater was about 1 mm in

diameter with a spallation zone diameter of about 5.5 mm. The substrate cleaved in two directions outward from the crater site to the opposite sides of the sample, and at an angle of about 75°, breaking the sample into three pieces. This verifies the fragile and brittle nature of  $\text{CaF}_2$  as a substrate material, while remaining optically-functional (Ref. 16).

Table 4.8.1.1a summarizes and provides a guide to the materials contained in this section.

**Table 4.8.1.1a. Impacts Effects Base For Infrared Optical Filters**

MATERIALS	FIGURES	LDEF LOCATION	COMMENTS
$\text{CaF}_2$	E.18	B8	$\approx 1$ mm diameter impact crater with spallation zone diameter of $\approx 5.5$ mm. Substrate cleaved in two directions outward from the crater site to the opposite sides of the sample, and at an angle of $\approx 75^\circ$ , breaking sample into three pieces

##### 4.8.1.2 Atomic Oxygen

At the present time, no data have been found for this section.

##### 4.8.1.3 Scatter

At the present time, no data have been found for this section.

##### 4.8.1.4 Absorption/Transmission/Reflectance

The primary experiment providing data in this area is experiment A0056. In general, the results of experiment A0056 show that the effects of space exposure on the

#### 4.8, Optical Filters for IR Optics

high-performance filters were negligible. No significant changes were found either in transmission or spectral position of any hard-coated II-VI/PbTe-based multilayers on Ge substrates. The softer materials were adversely affected in their physical and optical properties by the long exposure in space, from a reduced transmission to a complete opacity (Ref. 16).

Table 4.8.1.4a summarizes and provides a guide to the materials contained in this section.

**Table 4.8.1.4a. Absorption/Transmission/Reflectance Effects Base For Infrared Optical Filters**

MATERIALS	FIGURES	LDEF LOCATION	COMMENTS
Low Index Ratio Quarter-Wave Blocking ZnSe/ZnS/KRS-5 on KRS-6 Substrate <sup>1</sup>	E.86	G12	Reduced transmission
PbTe/ZnS on Ge Substrate 15 $\mu$ m 10 percent HBW L-Space THW Band-Pass Filter	E.87	G12	No significant changes in transmission or spectral position
PbTe/ZnS 8-12 $\mu$ m Tschebyshev Edge Band-Pass Filter (Antireflected) on Ge Substrate	E.88	B8	No significant changes in transmission or spectral position
PbTe/ZnS on Ge Substrate 14.5 $\mu$ m 0.7 percent HBW Split-Spacer Fabry-Perot Band-Pass Filter	E.89	B8	No significant changes in transmission or spectral position
ZnS/Chiolite on BK7G18 and RG780 Glasses (820 nm Interference Filter)	E.90	B8	Slight reduction in transmission

<sup>1</sup> KRS-6 substrate is Thallium-Chlorine-Bromine with a 33-layer ZnS/KRS-5 and ZnSe/KRS-5 coating. KRS 5 is Thallium-Bromine-Iodine.

The optical IR filters/materials in experiment A0056 are divided into three main categories: uncoated, soft-coated, or hard-coated. Soft-coated filter materials comprised principally KRS-5 (TlBrI)-based multilayers deposited on KRS-5 or KRS-6 (TlClBr) substrates. These materials were designed to utilize long-wavelength Reststrahl blocking properties by multilayer interference. Hard-coated filter materials comprised spectral filters from atmospheric-sensing, weather forecasting, research and planetary satellites (NIMBUS 4-7, ITOS, TIROS-N, PIONEER, and GALILEO) that were current at the time of the LDEF flight. The filter materials are primarily Pb-based on Ge substrates. A brief description of data (Ref. 16) for uncoated, soft-coated, and hard-coated materials follows:

Uncoated: Correlation of average transmittance was very high between pre- and post-flight measurements. A consistent loss in transmission (-0.765 percent) was indicated but this was sufficiently close to zero to infer no change within the transmission accuracy envelope permitted (Ref. 16).

Soft-coated: Comparison of pre- and post-flight average transmittance values was made from samples from both sites, and the correlation was very low (-0.168) indicating no correlation between pre- and post-flight sample spectra. This was also evident from visual inspections where gross physical degradation and delamination of the coatings and substrate materials was evident, having occurred as a result of space exposure and the effects of AO bombardment. Post-flight visual and spectral analysis of the soft materials showed that less degradation had occurred in the Earth-facing tray (G12) than in the leading edge tray (B8) (Ref. 16)

Hard-coated: Pre- and post-flight comparisons were well correlated. They showed a small and consistent loss in transmission for both, within the accuracy envelope. These samples are considered stable and show no degradation for the exposure. A PbTe/ZnS-based sample was cleaned in 1,1,1-Trichloroethane and 2-propanol and remeasured. The spectrum remained unchanged and it was deduced that the surface was not contaminated by exposure to

space; its loss of transmission therefore, according to the experimenter, must be ascribed to another mechanism (Ref. 16).

#### **4.8.1.5 Darkening**

At the present time, no data have been found for this section

#### **4.8.1.6 Stress**

At the present time, no data have been found for this section

#### **4.8.1.7 Contamination/Deterioration**

At the present time, no data have been found for this section

## 4.9 MIRRORS

All data contained in this section are from samples flown on experiment stations M0003-2, -7, and -11. Table 4.9.a shows a summary of the experiments containing mirror samples. Table 4.9.b shows the mirror materials and the effects addressed by the LDEF experimenters.

**Table 4.9.a. Experiment Summary for Mirrors**

EXPERIMENT	MIRRORS
AO034	SiO/Al on Pyrex, Os/Al on Quartz, Ag/Al on Quartz, Au/Al on Quartz, MgF <sub>2</sub> /Al on Quartz
AO114	Sputtered Cu on fused silica and OFHC copper
AO138-3	WRe/Si on Glass
AO138-4	LaF <sub>3</sub> /Chiolite/MgF <sub>2</sub> on B 1664 Glass, Al/MgF <sub>2</sub> on B1664 Glass, ThF <sub>4</sub> /Ag on B1664 Glass, Al <sub>2</sub> O <sub>3</sub> /Ag on Kanigened Al, MgO/MgF <sub>2</sub> on B1664 Glass, TiO <sub>2</sub> /SiO <sub>2</sub> on B1664 Glass, Ge/ZnS/ThF <sub>4</sub> on B1664 Glass, MgF <sub>2</sub> /Al on Kanigened Al
AO138-5	Al on Glass, Pt on Glass
M0003-2, -7, and -11	Bare Mo, Cu, Diamond-Turned Cu, Diamond-Turned Ni-plated Cu, ThF <sub>4</sub> /Ag/Cr on Mo, (Si/Al <sub>2</sub> O <sub>3</sub> ) <sup>3</sup> /Ag on Polished Si, (ZnS/Al <sub>2</sub> O <sub>3</sub> ) <sup>4</sup> /Ag on Polished Mo, and (ZnS/ThF <sub>4</sub> ) <sup>5</sup> /Ag on Polished Mo

### 4.9.1 Mirrors

#### 4.9.1.1 Impacts

LDEF mirror samples showed localized damage at the sites of impact. Table 4.9.1.1a summarizes materials and provides a guide to data contained in this section.



Table 4.9b. Mirrors

MATERIALS	EFFECTS						
	I M P A C T S	A T O M I C  O X Y G E N	A B S / T R A N / R E F L	D A R K E N I N G	S T R E S S	S C A T T E R	C O N T A M / D E T E R
Cu	•	•					
Ni-Cu	•	•					
Ni							•
Diamond-Turned Cu							•
LaF <sub>3</sub> /Chiolite/MgF <sub>2</sub> on B1664 Glass					○		
Al/MgF <sub>2</sub> on B1664 Glass			○				
ThF <sub>4</sub> /Ag on B1664 Glass			○				
Al <sub>2</sub> O <sub>3</sub> /Ag on Kanigened Al			○				
MgO/MgF <sub>2</sub> on B1664 Glass			○				
Visible + 1060-nm Mirror/TiO <sub>2</sub> -SiO <sub>2</sub> on B1664 Glass			○				
10.6-μm Mirror/Ge-ZnS-ThF <sub>4</sub> on B1664 Glass			○				
MgF <sub>2</sub> /Al on Kanigened Al			○				
Bare Mo						○	

- Data contained in this section
- Data contained in other, cross-referenced sections

Table 4.9.b. Mirrors (Cont.)

MATERIALS	EFFECTS						
	I M P A C T S	A T O M I C  O X Y G E N	A B S / T R A N / R E F L	D A R K E N I N G	S T R E S S	S C A T T E R	C O N T A M / D E T E R
SiO/Si on Pyrex							○
Os/Al on Quartz							○
Ag/Al on Quartz							○
Au/Al on Quartz							○
MgF <sub>2</sub> /Al on Quartz							○
WRe/Si on Glass			•				
Al on Glass			•				
Pt on Glass			•				
(ZnS/Al <sub>2</sub> O <sub>3</sub> ) <sup>4</sup> /Ag/Mo	•		•				○
(ZnS/TbF <sub>4</sub> ) <sup>5</sup> /Ag/Mo	•		•				
(Si/Al <sub>2</sub> O <sub>3</sub> ) <sup>3</sup> /Ag/Si	○		•				

• Data contained in this section

○ Data contained in other, cross-referenced sections

#### 4.9, Mirrors

**Table 4.9.1.1a. Impacts Effects Data Base on Mirrors**

MATERIALS	FIGURES	LDEF LOCATION	COMMENTS
Cu	E.91	D9	No damage to substrate beyond area of impact.
Ni-Cu	E.95	D9	Splatter of resolidified matter around craters. Damage is similar to that seen in uncoated Cu.
(ZnS/Al <sub>2</sub> O <sub>3</sub> ) <sup>4</sup> /Ag on Polished Mo	None	D8	Impacts revealed multilayer structure. Evidence of melting around impact sites.
(ZnS/ThF <sub>4</sub> ) <sup>5</sup> /Ag on Polished Mo	None	D4	Splatter of resolidified matter around craters.

Cu and Ni-Cu metal mirrors were evaluated for this effect and all of the LDEF samples showed localized damage at the site of impact. No damage to the mirror substrates was observed beyond the area of impact (Ref. 9). Impacts on a (ZnS/Al<sub>2</sub>O<sub>3</sub>)<sup>4</sup>/Ag/Mo mirror revealed the multilayer structure and also showed signs of melt (Ref. 17). On a (ZnS/ThF<sub>4</sub>)<sup>5</sup>/Ag/Mo sample, impacts did not reveal the multilayer structure but debris was splattered about the site (Ref. 17).

#### 4.9.1.2 Atomic Oxygen

Copper mirrors were flown on experiment A0114 on both the leading and trailing edge. The trailing edge showed little effect of AO. The samples on the leading edge received a total fluence of  $8.72 \times 10^{21}$  oxygen atoms/cm<sup>2</sup>. X-ray diffraction measurements and high resolution profilometry showed that the copper was converted stoichiometrically to Cu<sub>2</sub>O (Ref. 18).

Table 4.9.1.2a summarizes materials and provides a guide to data contained in this section.

#### 4.9, Mirrors

**Table 4.9.1.2a. Atomic Oxygen Effects Data Base on Mirrors**

MATERIALS	FIGURES	LDEF LOCATION	COMMENTS
Cu	None	C9	Copper was converted stoichiometrically to Cu <sub>2</sub> O.

#### 4.9.1.3 Scatter

The data reported in this section are from experiment M0003-2. Table 4.9.1.3a summarizes and provides a guide to the materials contained in this section.

**Table 4.9.1.3a. Scatter Effects Data Base on Mirrors**

MATERIALS	FIGURES	LDEF LOCATION	COMMENTS
Bare Mo	None	D4 D8 D9	Scatter data taken at 1.064 $\mu$ m. All samples highly scattering.

The bare Mo mirror sample was flown as part of the M0003-2 experiment. Samples were flown on the leading edge and the trailing edge of LDEF and received exposures of 3 months, 6 months, 9 months, and 69 months. Scatter data were taken at 1.064  $\mu$ m. All samples were highly scattering. Except for the leading edge, 69-month sample, a trend did not appear between samples exposed on the trailing edge and samples exposed on the leading edge. Even though all samples were highly scattering, the optic exposed for the full duration of the flight (the 69-month exposure) scatters more than one order of magnitude more light than do samples exposed for 9 months or less (Ref. 5).

## 4.9.1.4 Absorption/Transmission/Reflectance

A number of absorption/transmission/reflectance effects on UV/visible and IR mirrors were reported on by LDEF experimenters. The primary data discussions for these materials are covered in the UV/visible and IR coatings sections. The data reported on in this section are from experiments AO138-3, AO138-5 and M0003-7. Table 4.9.1.4a summarizes and provides a guide to the materials contained in this section. Table 4.9.1.4b shows references to related materials/effects covered in other sections of this handbook.

Table 4.9.1.4a. Absorption/Transmission/Reflectance Effects Data Base on Mirrors

MATERIALS	FIGURES	LDEF LOCATION	COMMENTS
WRe/Si on Glass	E.112	B3	Peak reflectivities are within 10 to 15 percent of pre-flight measurements
Al on Glass	E.110	B3	Loss of reflectance less than 10% over whole spectral range for samples internal to spacecraft. Loss of reflectance of up to 30% at 220 nm for space-facing samples
Pt on Glass	E.111	B3	Loss of reflectance around 10% at three specific test wavelengths (58.4 nm, 74.4 nm, and 121.6 nm) for samples internal to spacecraft. Loss of reflectance of up to 35% at 121.6 nm for space-facing samples
(Si/Al <sub>2</sub> O <sub>3</sub> ) <sup>3</sup> /Ag on Polished Si	None	D8	Minimal reduction in reflectance at the desired wavelength, 2.8 $\mu$ m, but with an indication of surface oxidation and reduction of reflectance at longer wavelengths (i.e., 2-4 $\mu$ m)
(ZnS/Al <sub>2</sub> O <sub>3</sub> ) <sup>4</sup> /Ag on Polished Mo	None	D8	Significant reduction in reflectance with apparent spectral shift of the reflectance maximum. Dendritic growth also apparent.
(ZnS/ThF <sub>4</sub> ) <sup>5</sup> /Ag on Polished Mo	None	D4	Significant reduction in reflectance with apparent spectral shift of the reflectance maximum. Dendritic growth also apparent.

**Table 4.9.1.4b. Absorption/Transmission/Reflectance Effects Data Base for Coatings Applicable to Mirrors**

MATERIALS/ SUBSTRATE	FIGURES	LDEF LOCATION	COMMENTS
Al-MgF <sub>2</sub> / B1664 Glass <sup>1</sup>	E.41	B3	Outside/inside samples had significantly-reduced reflectance over all wavelengths.
ThF <sub>4</sub> -Ag/ B1664 Glass <sup>1</sup>	E.42	B3	Outside/inside samples showed little change in reflectance over all wavelengths.
Al <sub>2</sub> O <sub>3</sub> -Ag/ Kanigen <sup>1</sup>	E.43	B3	Outside/inside samples had significantly-reduced reflectance except at the blue end.
Al-MgF <sub>2</sub> / Kanigen <sup>1</sup>	E.44	B3	Inside sample had significant reduction in reflectance at upper end. Outside sample had significant reduction across the entire band.
MgO-MgF <sub>2</sub> / B1664 Glass <sup>1</sup>	E.45	B3	Inside sample showed slight shift in reflectance. Outside sample had little reduction at the blue end but a slight shift to the high end.
	E.46	B3	Inside sample showed a significant reduction in transmittance at the blue end. Outside sample had a significant reduction in transmission at the blue end and a slight reduction at the upper end.
Visible 1060 nm mirror/TiO <sub>2</sub> -SiO <sub>2</sub> on B1664 Glass <sup>1</sup>	None	B3	Remained optically efficient.
10.6 μm mirror/Ge- ZnS-ThF <sub>4</sub> on B1664 Glass <sup>2</sup>	None	B3	No significant change

<sup>1</sup> Data relevant to this material are presented in Section 4.5.1.4.

<sup>2</sup> Data relevant to this material are presented in Section 4.6.1.4.

For the AO138-3 sample, the WRe/Si on glass mirror was evaluated using a classical reflectometer. The peak post-flight reflectivities of the mirror were found to be within 10 to 15 percent of the pre-flight measurements. This degradation was estimated to be due in part to the 3 nm contamination observed by the experimenters on the mirror surface (Ref. 25).

For the AO138-5 samples, the Al and Pt coatings on Glass were flown as witness mirrors for the ruled and holographic diffraction gratings portions of the experiment. There were two sets of space-borne samples: one set was space-facing and a second set was turned inward. For the inward facing sample set, both Al and Pt witness mirrors experienced some degradation in reflectance. The Al coating lost less than 10-% reflectivity over the whole spectral range while the Pt coating lost reflectivity of around 10-% for three discrete test wavelengths (58.4 nm, 74.4 nm, and 121.6 nm). For the space-facing sample set, both Al and Pt witness mirrors experienced degradations in reflectivity that were more pronounced than for the inward-facing samples. The Al coating lost up to 30-% reflectivity (at 220 nm) while the Pt coating lost up to 35-% reflectivity (at 121.6 nm) (Ref. 23).

For the M0003-7 samples, the  $(\text{Si}/\text{Al}_2\text{O}_3)^3/\text{Ag}$  on polished Si mirror showed a minimal reduction in reflectance at the desired wavelength of 2.8  $\mu\text{m}$ , but with an indication of surface oxidation and reduction in reflectance at longer wavelengths (i.e., 3-4  $\mu\text{m}$ ). Zinc-sulfide-based coating designs,  $(\text{ZnS}/\text{Al}_2\text{O}_3)^4/\text{Ag}$  on polished Mo and  $(\text{ZnS}/\text{ThF}_4)^5/\text{Ag}$  on polished Mo, showed significant reductions in reflectance at the desired wavelength with large spectral shifts of the reflectance maxima apparent. Dendritic formations were also seen. A combination of thermal cycling and irradiation effects probably provided energy for the dendrite formation process (Ref. 23).

### 4.9.1.5 Darkening

At the present time, no data have been found for this section.

### 4.9.1.6 Stress

Table 4.9.1.6b shows references to related materials/effects covered in other sections of this handbook.

**Table 4.9.1.6b. Stress Data Base for Coated Refractive Optics  
Applicable to Mirrors**

MATERIALS/ COATING	FIGURES	LDEF LOCATION	COMMENTS
LaF <sub>3</sub> /Chiolite/MgF <sub>2</sub> <sup>1</sup>	None	B3	Did not survive because of high stress levels

<sup>1</sup> Data relevant to this material are presented in Section 4.3.2.6.

#### 4.9.1.7 Contamination/Deterioration

All samples were hazed and discolored with corrosion spots on the surface. The Cu sample showed grain boundaries (Ref. 9). Table 4.9.1.7a summarizes and provides a guide to the materials contained in this section.

**Table 4.9.1.7a. Contamination/Deterioration Effects Data Base for Mirrors**

MATERIALS/ SUBSTRATE	FIGURES	LDEF LOCATION	COMMENTS
Ni	E.92	D9	Corroded and hazed surrounded by discoloration zone.
Diamond-Turned Cu	E.93	D4	Hazy, discolored surface with corrosion spots.
	E.94	D4	Hazy, discolored surface showing grain boundaries.

Table 4.9.1.7b shows references to related materials/effects covered in other sections of this handbook.



**Table 4.9.1.7b. Contamination/Deterioration Effects Data Base for IR Coatings  
Applicable to Mirrors**

MATERIALS/ SUBSTRATE	FIGURES	LDEF LOCATION	COMMENTS
(ZnS/Al <sub>2</sub> O <sub>3</sub> ) <sup>4</sup> /Ag Polished Mo <sup>1</sup>	E.59	D8	Corroded and hazed.
SiO/Si on Pyrex <sup>2</sup>	None	C3 C9	Degradation in UV spectral reflectance due to contamination.
Os/Al on Quartz <sup>2</sup>	None	C3 C9	Complete oxidation of the silver film and complete oxidation and evaporative removal of Os film on leading edge.
Ag/Al on Quartz <sup>2</sup>	None	C3 C9	Complete oxidation of the silver film in both leading edge and trailing edge samples.
Au/Al on Quartz <sup>2</sup>	None	C3 C9	Slight visual difference in leading edge samples. No obvious effect on trailing edge samples.
MgF <sub>2</sub> /Al on Quartz <sup>2</sup>	None	C3 C9	No visible effect in leading edge or trailing edge samples.

<sup>1</sup> Data relevant to this material are presented in Section 4.6.1.7.

<sup>2</sup> Data relevant to this material are presented in Section 4.5.1.7.

#### 4.10 SECOND SURFACE MIRRORS

Second surface mirror (SSM) materials were flown on LDEF experiments M0003-5, M0003-11, and S1002. Data obtained for this handbook were from experiment S1002. The SSM coatings were deposited in the configurations of the SSM/interference filter (IF) and SSM/IF/conductive layer (LS) and were characterized by analyzing the change in the coating's solar absorptivity ( $\alpha$ ) and emissivity ( $\epsilon$ ). All the space-exposed surfaces showed increases in solar absorptivity of varying magnitudes. The magnitude of the solar absorptivity change varied from sample to sample but spanned the values of negligible change to 0.14 dependent upon the amount of contamination deposited. The second surface mirrors discussed below were in experiment S1002 (Ref. 19).

Table 4.10.a shows a summary of the experiments containing SSMs.

**Table 4.10.a. Experiment Summary for Second Surface Mirrors**

EXPERIMENT	SECOND SURFACE MIRRORS
S1002	Quartz/Silver With Interference Filter, Quartz/Silver With Interference Filter and Conductive Layer

Table 4.10.b shows the SSM materials and the effects addressed by the LDEF experimenters.

**Table 4.10.b. Second Surface Mirrors**

MATERIALS	EFFECTS						
	I M P A C T S	A T O M I C  O X Y G E N	A B S / T R A N / R E F L	D A R K E N I N G	S T R E S S	S C A T T E R	C O N T A M / D E T E R
Quartz/Silver With Interference Filter	•						•
Quartz/Silver With Interference Filter and Conductive Layer	•						•

• Data contained in this section

• Data contained in other, cross-referenced sections

#### 4.10.1 Second Surface Mirrors

##### 4.10.1.1 Impacts

The quartz-silver mirrors did suffer some micrometeoroid/debris effects showing some cratering with adjacent conchoidal areas. No estimate of the effect of these craters on the mirror performance has been reported to date, however (Ref. 20).

Table 4.10.1.1a summarizes and provides a guide to the materials contained in this section.

**Table 4.10.1.1a. Impacts Effects Data Base For Second Surface Mirrors**

MATERIALS	FIGURES	LDEF LOCATION	COMMENTS
Quartz/Silver	E.96	E3	Micrometeoroid impact caused crater with several large conchoidal areas adjacent to impact site.

##### 4.10.1.2 Atomic Oxygen

At the present time, no data have been found for this section.

##### 4.10.1.3 Scatter

At the present time, no data have been found for this section.

##### 4.10.1.4 Absorption/Transmission/Reflectance

At the present time, no data have been found for this section.

#### 4.10, Second Surface Mirrors

---

##### 4.10.1.5 Darkening

At the present time, no data have been found for this section.

##### 4.10.1.6 Stress

At the present time, no data have been found for this section.

##### 4.10.1.7 Contamination/Deterioration

The mirror samples reported in the LDEF data base did show some of the contamination reported by other experimenters. However, there was no noticeable increase or only very slight increases in the solar absorptivity of the mirrors. No appreciable change in thermal emissivity was seen in either of the S1002 experiment samples (Ref. 19). Table 4.10.1.7a summarizes and provides a guide to the materials contained in this section.

**Table 4.10.1.7a. Contamination/Deterioration Effects Data Base For  
Second Surface Mirrors**

MATERIALS	FIGURES	LDEF LOCATION	COMMENTS
Quartz/Silver With Interference Filter <sup>1</sup>	None	E3	No noticeable increase of solar absorptivity ( $\alpha$ ) due to contamination ( $\Delta\alpha = 0$ ). No appreciable change in thermal emissivity ( $\epsilon$ ) ( $\Delta\epsilon = 0$ )
Quartz/Silver With Interference Filter and Conductive Layer <sup>2</sup>	None	E3	Very slight increase of solar absorptivity ( $\alpha$ ) due to contamination ( $\Delta\alpha = 0.02$ ). No appreciable change in thermal emissivity ( $\epsilon$ ) ( $\Delta\epsilon = 0$ )

<sup>1</sup> This configuration with interference filter had three quarter-wave layer pairs of ZnS/Al<sub>2</sub>O<sub>3</sub> followed by layers of ZnS and Al on the SSM. The SSM is formed by layers of Teflon, Al, Ag, Inconel, IX 93500, on Al.

<sup>2</sup> This configuration with interference filter and conductive layer had a layer of In<sub>2</sub>O<sub>3</sub>, followed by four quarter-wave layer pairs of ZnS and Al<sub>2</sub>O<sub>3</sub>, followed by layers of PMMA and Al on the SSM (same composition as above).

## 4.11 QUARTZ CRYSTAL MICROBALANCES

The Quartz Crystal Microbalances (QCMs) flown on LDEF were of interest as contamination monitors for companion optics. All data contained in this section are from samples flown on experiments M0003-14 and S1002. Table 4.11.a shows a summary of the experiment containing QCMs.

**Table 4.11.a. Experiment Summary for QCMs**

EXPERIMENT	QCM CONFIGURATIONS
M0003-14	(1) QCM crystals with 9000 Å of aluminum and aluminum oxide ( $\text{Al} + \text{Al}_2\text{O}_3$ ) and a top layer of 150 Å of $\text{In}_2\text{O}_3$ and (2) crystals with 9000 Å of ( $\text{Al} + \text{Al}_2\text{O}_3$ ) and a top layer of 150 Å of ZnS. Each of the QCMs consisted of a pair of crystals, one exposed to the environment and termed the "sense" crystal, and one that remained unexposed and, hence, termed the "reference" crystal.
S1002	(1) QCM crystals with 9000 Å of aluminum and aluminum oxide ( $\text{Al} + \text{Al}_2\text{O}_3$ ) and a top layer of 150 Å of $\text{In}_2\text{O}_3$ and (2) crystals with 9000 Å of ( $\text{Al} + \text{Al}_2\text{O}_3$ ) and a top layer of 150 Å of ZnS.

Table 4.11.b shows the QCM materials and the effects addressed by the LDEF experimenters.

### 4.11.1 Quartz Crystal Microbalances

#### 4.11.1.1 Impacts

At the present time, no data have been found for this section.

#### 4.11, Quartz Crystal Microbalances

Table 4.11.b. Quartz Crystal Microbalances

MATERIALS	EFFECTS						
	I M P A C T S	A T O M I C  O X Y G E N	A B S / T R A N / R E F L	D A R K E N I N G	S T R E S S	S C A T T E R	C O N T A M / D E T E R
In <sub>2</sub> O <sub>3</sub> /Al/Al <sub>2</sub> O <sub>3</sub> on Quartz			•				•
ZnS/Al/Al <sub>2</sub> O <sub>3</sub> on Quartz			•				•

• Data contained in this section

• Data contained in other, cross-referenced sections

##### 4.11.1.2 Atomic Oxygen

At the present time, no data have been found for this section.

##### 4.11.1.3 Scatter

At the present time, no data have been found for this section.

##### 4.11.1.4 Absorption/Transmission/Reflectance

Data for the Experiment M0003-14 samples were taken and analyzed by LDEF experimenters concerning absorption and reflectance. For all crystals, there was an increase

#### 4.11, Quartz Crystal Microbalances

in average reflectance with increasing wavelength. Positions of the wavelength maxima and minima in the interference patterns are shifted negligibly (Ref. 21).

Table 4.11.1.4a summarizes and provides a guide to the materials contained in this section.

**Table 4.11.1.4a. Transmission/Reflectance Effects Data Base For Quartz Crystal Microbalances**

MATERIALS	FIGURES	LDEF LOCATION	COMMENTS
In <sub>2</sub> O <sub>3</sub> /Al/Al <sub>2</sub> O <sub>3</sub> on Quartz	E.97 E.98	D3 D9	For all crystals, there is an increase in average reflectance with increasing wavelength. Positions of the wavelength maxima and minima in the interference patterns are shifted negligibly. Trailing edge material (D3, active) experienced amplitude modulation in uncorrected diffuse reflectance (probably due to thickness interference). Leading edge material (D9, active) showed nearly identical modulation amplitudes.
ZnS/Al/Al <sub>2</sub> O <sub>3</sub> on Quartz	E.99 E.100	D3 D9	For all crystals, there is an increase in average reflectance with increasing wavelength. Positions of the wavelength maxima and minima in the interference patterns are shifted negligibly. Trailing edge material (D3, passive) experienced amplitude modulation in uncorrected diffuse reflectance (probably due to thickness interference). Leading edge material (D9, passive) showed significant modulation amplitudes over entire wavelength band.

The data analysis was two-phased: an FTIR absorption analysis and an uncorrected diffuse reflectance analysis (Ref. 21). Each is discussed as follows:

FTIR: An absorption characteristic of the Si-O stretching vibration is observed on the leading edge sense crystals 1 and 3 at 1061 cm<sup>-1</sup>. The most noticeable observation about these spectra is the absence of absorption at 1061 cm<sup>-1</sup> on the leading edge reference crystals

#### *4.11, Quartz Crystal Microbalances*

---

2 and 4, as well as on all the trailing edge crystals 5 through 8. Since we know from the other measurements that Si is indeed present on the surface of the sense crystals on both the leading and trailing edges, results from the FTIR spectra must be interpreted as a measure of the relative concentrations of Si on the leading versus the trailing edges, as well as sense versus reference crystals, scaled by the sensitivity of this measurement. Other absorptions due to C-H, C=O, and C=C stretching vibrations and C-H deformations were observed in both leading and trailing edge crystals at approximately the same frequencies. All the crystals indicate the presence of C-H vibrations in the range 2900 to 2500  $\text{cm}^{-1}$ . In QC 3, there is strong absorption at 3339  $\text{cm}^{-1}$ , which is due to the O-H stretch from water or alcohols on the surface. A weak absorption at  $\sim 1640 \text{ cm}^{-1}$  seen in crystals 3, 4, 6, 7, and 8 is the C=C stretch from unsaturated hydrocarbons. An absorption at 955  $\text{cm}^{-1}$  appears fairly consistently at the same position in all crystals with the exception on sample 4 where this peak is shifted to 948  $\text{cm}^{-1}$ . Although the assignment of the absorption at 955  $\text{cm}^{-1}$  remains ambiguous at the present time, it is most likely due to C-H deformations from alkenes. Other likely causes for this absorption could be the symmetric and asymmetric bends from  $\text{SiH}_3$  or an Si-O-R (aromatic) stretching vibration. Shifts in the Si-O stretching vibrations, which generally occur in the range 1110 to 1000  $\text{cm}^{-1}$ , from either Si-O-R (aliphatic) or Si-O-Si, may be an alternative explanation. An absorption that generally appears in the range 760 to 740  $\text{cm}^{-1}$  in both the leading and trailing edge crystals is found to be always shifted to higher frequencies in the sense crystals compared to the corresponding reference crystals. The most likely assignment of this absorption is the Al-O stretch from the aluminum oxide layer present in all the crystals. C-H deformations due to alkanes could also be contributed to absorption at this frequency. Changes in local environment, especially on the sense crystals, could account for the shifts in the position of this peak (Ref. 21).

Reflectance: Uncorrected diffuse reflectance was measured as a function of wavelength for each pair of sense-reference crystals on the leading and trailing edges. For all the crystals, it can be seen that with increasing wavelength, there is an increase in the corresponding average reflectance. In addition, it is seen that all the crystals also displayed



thickness interference patterns in their reflectances. While the modulation amplitudes in crystals 1 and 2 (LDEF leading edge, active crystals) are nearly identical, differences in modulation between QCs 5 and 6 (LDEF trailing edge, active crystals), and QCs 7 and 8 (LDEF trailing edge, passive crystals) fall within a wide range of 2 to 20 percent in the wavelength range 2000 to 5000 Å. The most striking differences are observed with the QC pair 3 and 4 (LDEF leading edge, passive crystals), where it is seen that the modulation amplitude in crystal 3 is significantly lower (by 10 to 50 percent) over the entire wavelength range (2000 to 10,000 Å) than that of the reference crystal 4 (Ref. 21).

On observing the position of the wavelength maxima and minima in the interference patterns in each of the sense-reference crystal pairs, they appear to be shifted negligibly with respect to each other as well as with respect to the other crystal pairs, and are not large enough to result in significantly different values for the product ( $n \times d$ ), where  $n$  is the refractive index of the film and  $d$  is the film thickness (Ref. 21).

In addition, the range of wavelengths at which these interferences are observed (2000 to 12,000 Å) is so large that a 150 Å top layer either of  $\text{In}_2\text{O}_3$  or ZnS cannot be responsible for the interferences. Thus, it is postulated that these interferences are more likely due to the underlying  $\text{Al}/\text{Al}_2\text{O}_3$  layer. A likely explanation for the observed behavior is that surface roughness can cause an increased scattering, which in turn, can dampen the modulated amplitude of the reflected wave. In particular, analysis of the tilted samples reveals that QC 3 shows an overall thinning of the top ZnS layer and particularly shows a reduction in the concentration of zinc present on the surface. This could result in scattering by sulphur particles or other contaminants on the surface and an overall damping of the modulated amplitude (Ref. 21).

##### 4.11.1.5 Darkening

At the present time, no data have been found for this section.

#### *4.11, Quartz Crystal Microbalances*

---

##### **4.11.1.6 Stress**

At the present time, no data have been found for this section.

##### **4.11.1.7 Contamination/Deterioration**

In a portion of Experiment M0003-14, 150 Å of ZnS and In<sub>2</sub>O<sub>3</sub> were deposited on separate QCM prior to the flight, and by measuring the difference in QCM frequencies between the pre- and post-flight, it was determined that approximately 8 nm of contamination were deposited during the flight. Si (probably from silicone) is the key contaminant identified on the surface of all the crystals. The level of Si contamination is found to be higher on the leading edge than on the trailing edge. Other, lesser contaminants found on several of the crystals include Mg, Ca, K, Na, Ag, Cl, Sn, and Pb. Contamination source(s) are still to be resolved (Ref. 21).

Table 4.11.1.7a summarizes and provides a guide to the materials contained in this section.

SEM photographs of all the crystals were obtained at various magnifications. EDAX revealed (Ref. 21) that:

- Higher Si contamination on the sense crystal on the leading edge than on the sense crystal on the trailing edge, but a higher Si contamination on the reference crystal on the trailing edge than on the leading edge
- Comparing sense crystal 3 with reference crystal 4 on the leading edge and with crystals 7 and 8 on the trailing edge, it is observed that although the increase in the Zn and S concentrations on tilting are comparable, the ZnS coating appears to have thinned in sense crystal 3, as indicated by considerably lower percentages of both Zn and S in QC 3 relative to QCs 4, 7, and 8. While these measurements were not performed before flight, all samples were deposited such that the coatings should have been identical.

**Table 4.11.1.7a. Contamination/Deterioration Effects Data Base  
For Quartz Crystal Microbalances**

MATERIALS	FIGURES	LDEF LOCATION	COMMENTS
In <sub>2</sub> O <sub>3</sub> /Al/Al <sub>2</sub> O <sub>3</sub> on Quartz	None	D3 D9	Si (probably from silicone) is the key contaminant identified on the surface of all the crystals. Level of Si contamination is found to be higher on the leading edge than on the trailing edge. Other, lesser contaminants found on several of the crystals include Mg, Ca, K, Na, Ag, Cl, Sn, and Pb. Contamination source(s) still to be resolved.
ZnS/Al/Al <sub>2</sub> O <sub>3</sub> on Quartz	None	D3 D9	Si (probably from silicone) is the key contaminant identified on the surface of all the crystals. Level of Si contamination is found to be higher on the leading edge than on the trailing edge. Other, lesser contaminants found on several of the crystals include Mg, Ca, K, Na, Ag, Cl, Sn, and Pb. Contamination source(s) still to be resolved.
In <sub>2</sub> O <sub>3</sub> /Al <sub>2</sub> O <sub>3</sub> on Quartz	None	E3	Frequency increase by 33 Hz due to $\approx 1$ nm contamination layer. Contaminant not identified specifically.
ZnS/Al <sub>2</sub> O <sub>3</sub> on Quartz	None	E3	Frequency increase by 225 Hz due to $\approx 8$ nm contamination layer. Contaminant not identified specifically.

Using XPS, a comparison of leading edge crystals (1,2,3, and 4) versus trailing edge crystals (5,6,7, and 8) indicates that there is a higher percentage Si coverage on the leading edge. In addition, a comparison of the sense crystals versus the reference crystals indicates a higher percentage Si coverage on the sense crystals (Ref. 21).

The SIMS technique was used to gather more information on the Si contamination area coverage, and depth profiles. A thin film of carbon was first deposited on the surface of all the samples to minimize charging, and the analyses were performed by sputter etching through the carbon film. This technique worked well on the In<sub>2</sub>O<sub>3</sub>-coated crystals. It did not work as well on the ZnS-coated crystals. Depth profiles and elemental analyses were made

#### *4.11, Quartz Crystal Microbalances*

---

with an Applied Research Laboratories (ARL) ion microprobe mass analyzer (IMMA) using a 1 nA primary beam of oxygen ions accelerated to 4.5 kV and focused to approximately 15  $\mu\text{m}$  in diameter. The depth profiles were made following elements of each of the contaminants (Si, K, Mg), and the coating (In, Zn), and the substrate (Al) (Ref. 21).

A survey of the results shows that the Si<sup>+</sup> intensity is approximately 1 to 2 orders of magnitude higher on the sense crystals compared to the reference crystals, and appears to be approximately an order of magnitude higher on the leading edge sense crystals compared to the trailing edge sense crystals. Depth profiles showing the distribution of Si relative to In and Zn for the In<sub>2</sub>O<sub>3</sub>-coated crystals show that on the sense crystal 1, a layer of Si occurs above the In<sub>2</sub>O<sub>3</sub> layer. On the reference crystal 2, there is no distinct indication of Si coverage of the In<sub>2</sub>O<sub>3</sub> layer. The presence of a significantly smaller Si layer above the In<sub>2</sub>O<sub>3</sub> layer is detected on the sense crystal 5, while on the reference crystal 6, Si is not present on the surface. Similar results are obtained from the ZnS-coated crystals although interpretation is hindered by charging of the sample upon reaching the ZnS layer (Ref. 21).

With regard to the S1002 samples (flown in E3), QCM measurements and physical surface analyses done by the experimenter indicated between 1 and 8 nm contamination layers on all space-exposed surfaces. The QCM frequencies increased during the mission. The frequency of the QCM (ZnS) increased relatively strongly by 225 Hz and of the QCM (In<sub>2</sub>O<sub>3</sub>) by 33 Hz only (Ref. 19).

#### **4.12 RELATED MATERIALS EXPERIMENTS**

A variety of other materials was flown on LDEF from which data can be obtained that are relatable to space optical systems. The LDEF data available from selected adjunct experiments are discussed below. Table 4.12.a shows a summary of experiments related to

#### 4.12, Related Material Experiments

---

space optics. Table 4.12.b shows the related optical materials and the effects addressed by the LDEF experimenters.

**Table 4.12.a Experiment Summary for Related Space Optics Materials**

EXPERIMENT	RELATED SPACE OPTICS MATERIALS
AO034	Thermal control coatings on borosilicate or fused silica windows: Z-93 paint, A-276 paint, S-13G paint, S-13G/LO paint, Z-306 Chemglaze, and YB-71 ZOT paint
M0003-4	7940 coverglass/Mark III E, 7940 coverglass (bare), 7940 coverglass/Mark III D, 7940 coverglass with 350 nm coating, Ceria with 350 nm coating
M0003-8	P1700 Polysulfone/T300 Graphite, PMR-15 Polyimide/C600 Graphite, 934 Epoxy/T300 Graphite

#### 4.12.1 Related Space Optical Materials

##### 4.12.1.1 Impacts

Table 4.12.1.1a summarizes and provides a guide to the materials contained in this section. Experiment M0003-4 was a solar optics experiments which flew uncoated and coated fused silica cover glass. Fused silica is used for refractive optics and substrates for optical systems. Long, fine fractures emanated from impact craters. Coatings are microfractured and flaking at the edges. Blisters appear along fractures. Dendritic growths are apparent (Ref. 12). The solar cell covers showed similar impact damage as the refractive optics components.

Table 4.12.b. Related Space Optics Materials

MATERIALS	EFFECTS						
	I M P A C T S	A T O M I C  O X Y G E N	A B S / T R A N / R E F L	D A R K E N I N G	S T R E S S	S C A T T E R	C O N T A M / D E T E R
Thermal Control Paints (Z-93 paint, A-276 paint, S-13G paint, S-13G/LO paint, Z-306 Chemglaze, and YB-71 ZOT paint)							•
7940 Coverglass (bare)	•						
7940 Coverglass/Mark IID	•						
7940 Coverglass/Mark IIIE	•						
7940 Coverglass with 350 nm Coating							
Ceria with 350 nm Coating							
P1700 Polysulfone/T300 Graphite		•			•		
PMR-15 Polyimide/C600 Graphite		•			•		
934 Epoxy/T300 Graphite		•			•		

• Data contained in this section

• Data contained in other, cross-referenced sections

#### 4.12, Related Material Experiments

**Table 4.12.1.1.a Impact Effects On Related Optics Materials**

MATERIALS/ COATING	FIGURES	LDEF LOCATION	COMMENTS
7940 coverglass/ MARK IIIE	E.101	D9	Long fine fractures. Coating blistered and flaked
	E.102	D9	
7940 coverglass Bare	E.103	D9	Parallel fractures in cover glass
	E.104	D9	
	E.105	D9	
7940 coverglass/ MARK IIID	E.106	D9	Dendritic growths along fractures

#### 4.12.1.2 Atomic Oxygen

Data from two experiments, AO034 and M0003-8, were found for this section. Table 4.12.1.2a summarizes and provides a guide to the materials contained in this section.

**Table 4.12.1.2.a Atomic Oxygen Effects On Related Optics Materials**

MATERIALS	FIGURES	LDEF LOCATION	COMMENTS
Thermal Control Paints on Window Substrates	E.114	C9 C3	Material erosion as evidenced by induced changes in fluorescence
P1700 Polysulfone/T300 Graphite	E.107	D9	Material erosion
PMR-15 Polyimide/C600 Graphite	E.108	D9	Material Erosion
934 Epoxy/T300 Graphite	E.109	D9	Material Erosion

#### *4.12, Related Material Experiments*

---

Thermal control paints flown on experiment AO034 showed evidence of AO effects. Fluorescent emissions from the thermal control coatings under black-light illumination revealed patterns of material-dependent visible changes as a result of AO exposure (and solar UV). For the six types of thermal control coatings, the induced changes in fluorescence are similar in pattern for the three zinc oxide-based coatings (Z93, S13G, and S13G-LO) as well as for the two polyurethane-based coatings (A276 and Z306). The zinc orthotitanate (YB-71) coatings provided no detectable evidence of intrinsic or induced fluorescence. The intrinsic yellow glow of the three zinc oxide-based coatings under black-light illumination is suppressed as a result of exposure on the leading edge. Fluorescent emission of S13G and S13G-LO directly exposed on the trailing edge is shifted in color to longer wavelengths (orange), while the fluorescence of Z93 specimens directly exposed on the trailing edge is apparently suppressed to the same degree as Z93 specimens on the leading edge (Ref. 11).

Specimens of the two polyurethane-based coatings were included only in the leading edge unit. Distinct fluorescent emission under black-light illumination is seen for specimens of these coatings exposed under the UV-windows, excluding AO. This induced fluorescence is generally lost as a result of exposure to AO for specimens of these coatings on the leading edge, although the Z306 specimen directly exposed on the leading edge is faintly fluorescent when viewed under black-light at an angle approximately  $10^\circ$  off-normal (Ref. 11).

These material-dependent fluorescence changes induced in the coatings as a result of the space exposure were found to be governed primarily by AO (and solar UV) exposure. Detailed spectral measurements of fluorescent emission are being obtained by the experimenter to correlate with the flight specimen black-light observations. Laboratory AO (and UV) exposure testing of the specimens is still in progress by the experimenters to investigate the nature of these induced effects further (Ref. 11).

Experiment M0003-8 flew specimens of organic matrix/graphite fiber reinforced composites at both the leading and trailing edges of LDEF. Graphite/Epoxy materials are



#### *4.12, Related Material Experiments*

---

under consideration for use as sunshades for optical systems. The LDEF experiments provide insight to the performance of these materials in an AO environment. The leading edge of the exposed composites suffered AO erosion. Leading edges using these materials will require AO protection. Photomicrographic results showed that the leading edge of organic composites could experience recession with 3 to 7 mils of material loss (Ref. 22).

##### **4.12.1.3 Scatter**

To date, no data have been found for this section.

##### **4.12.1.4 Absorption/Transmission/Reflectance**

To date, no absorption/transmission/reflectance data have been found for this section.

##### **4.12.1.5 Darkening**

While no cryogenic optics were flown on LDEF, cryogenic optics are important for IR applications. A recently completed series of experiments under BMDO PMA 1501 has shown that cryo-optics which contain impurities will darken when subjected to low levels of radiation. This did not happen when care was taken in controlling impurity concentrations in the optics.

## 4.12, Related Material Experiments

---

### 4.12.1.6 Stress

Post-flight tensile moduli values compare favorably with preflight values for the epoxy and polysulfone system. Compression moduli data for the epoxy and polysulfone systems are questionable due to the severe end blooming (Ref. 22).

Table 4.12.1.6a summarizes and provides a guide to the materials contained in this section.

**Table 4.12.1.6a. Stress Effects On Related Optics Materials**

MATERIALS	FIGURES	LDEF LOCATION	COMMENTS
P1700 Polysulfone/T300 Graphite	E.113	D9	Favorable pre- and post-test tensile moduli comparable
PMR-15 Polyimide/C600 Graphite	E.113	D9	Favorable pre- and post-test tensile moduli comparable
934 Epoxy/T300 Graphite	E.113	D9	Favorable pre- and post-test tensile moduli comparable

The compression and tensile test results are based on a limited sample. Pre- and post-flight strength values are very similar but well below anticipated values (Ref. 22).

### 4.12.1.7 Contamination/Deterioration

Experiment AO034 was an AO outgassing experiment on which UV windows and mirrors were included adjacent to thermal coatings. This experiment showed that severe transmission/ reflectance losses could result for space optical materials if they are located too close to thermal control paints (Ref. 11). Experiment M0003-4 was an experiment examining space effects on solar power components. This experiment showed that coatings on glass can crack and flake when exposed to the space environment (Ref. 12).

#### 4.12, Related Material Experiments

Table 4.12.1.7a summarizes and provides a guide to the materials contained in this section.

**Table 4.12.1.7a Contamination/Deterioration Effects On Related Optics Materials**

MATERIALS/ COATINGS	FIGURES	LDEF LOCATION	COMMENTS
Thermal Control Paints on Window Substrates	E 114	C9 C3	Contamination from thermal paints severely degraded optical performance.
7940 Coverglass/ 350 nm coating	E.115	C9	Perimeter hazed. Coating cracked and flaked.
Ceria/ 350 nm coating	E.116	C9	Perimeter hazed. Coating cracked and flaked.

The AO034 thermal control coatings consisted of YB-71, Z-93, S13G, S13G-LO, A276, and Z-306 paints. Molecular contamination on the inner surface of the UV-grade quartz windows flown along with the coating samples provided one comparable measure of the optical degradation attributable to the various types of coatings. These contaminated films were yellow and red in color and bonded relatively strongly to the inner glass surfaces (Ref. 11).

The visible darkening of the AO034 flight windows and the measured degradation in UV transmittance were significantly greater for the leading edge samples than for the trailing edge samples. Since the inner surfaces of the sealed (teflon gasket) windows were not exposed to AO, one cause for the enhanced deposition on the leading edge windows identified by the experimenters may be thermal in origin, arising from different susceptibilities to deposition as a result of more rapid cooling during sun/shadow transitions for the LDEF row receiving more direct sun illumination in the early mission phase when outgassing should have been more prevalent. The transmission losses of these windows indicate the relative severity of contamination effects resulting from outgassing and solar UV-induced photochemical reaction for the various types of underlying thermal control coatings (Ref. 11).

#### 4.12, Related Material Experiments

---

The AO034 experimenters also noted some obvious discrepancies in the response to space exposure for a few of the coating specimens compared to the average response observed for specimens of a type. The experimenters believe that this indicates the existence of batch variations which must be considered in generalized predictions of response to space exposure (Ref. 11).

#### *4.0, References*

---

## **CHAPTER 5**

### **OPTICAL DESIGN CONSIDERATIONS: IMPACT OF LDEF RESULTS AND ANALYSES**

#### **5.1 INTRODUCTION**

This chapter presents the conclusions and inferences drawn from the LDEF data presented in Chapter 4. Because there was a variety of experiments, materials, LDEF locations, and environments experienced, the data set is multi-faceted. To capture this multi-faceted nature, the following material endeavors to categorize the LDEF results into groups useful to optical designers. As will be seen, these groups align with optical system design parameters.

The LDEF experimenters attempted to address the following optical system-related concerns:

- Degradation of transparent elements (darkening, impacts, contamination) which:
  - Reduces the throughput of available light for photometric, radiometric, and imaging systems
  - Degrades image resolution
  - Increases scattering which, in turn, increases background noise.
- Degradation of optical coatings (erosion, discoloration, delamination, pitting, contamination) which produces:
  - Holes in coating that may alter material wavelength-dependent transmission and reflection properties
  - Surface contamination on coatings that may decrease throughput of light
  - Increased scattering which, in turn, increases background noise.
- Degraded or damaged coatings which encourage other types of damage that lead to:

- Redeposition of contaminants, including damaged coating materials, on other system optics (leading to loss of resolution, reduced throughput, wavelength dependence)
- Permanent changes in multilayer-coating thicknesses due to thermal cycling at high temperatures
- Degradation of diffuse paints or diffuse metal coatings in optical systems (erosion, discoloration) which may cause:
  - Baffling efficiency to decrease due to increase in specular reflection or the baffling efficiency to increase due to an increase roughness of baffle surface topography
  - Redeposition on other materials
  - Contamination of system optics (leading to loss of resolution, reduced throughput, and/or altered wavelength dependence)
- Degradation of fiber optics (radiation darkening, impacts, contamination) that result in:
  - Reduced transmission
  - Complete loss of signal
  - Increased system bit error rate (digital)
  - Decreased signal-to-noise ratio (analog)

In the chapters that follow, the experimental results presented in Chapter 4 will be categorized in terms of the impact they have on the performance of optical systems. The emphasis is on sorting through the extensive, expanding LDEF database to find "what worked". It is expected that more items will be added to the "working" category as data continue to become available.

## 5.2 CRITICAL INTERACTIONS FOR OPTICAL SYSTEMS

Figure 5.1 shows, for a generic optical system, the design flow from the natural environments which can impact a system through the component response to the sensor response. As can be seen from the figure, in the design of an optical system for space, the

## 5.2, Critical Interactions for Optical Systems

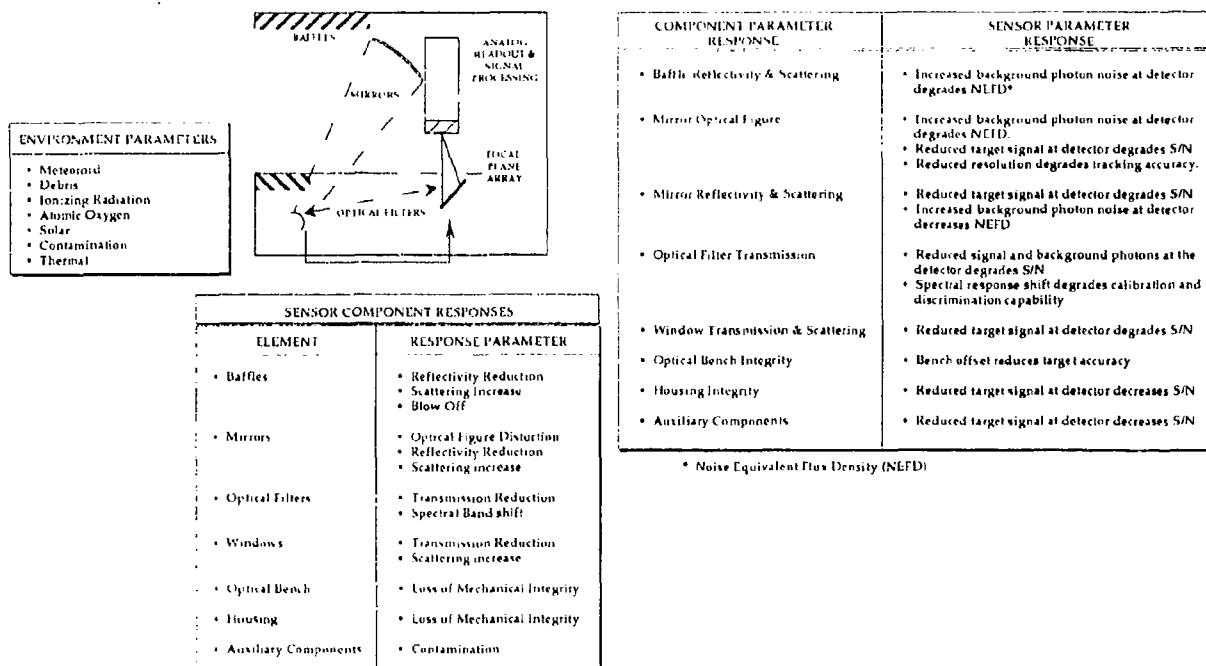


Figure 5.1. Critical Interactions for Assessment of Environmental Effects on Sensors



## *5.2, Critical Interactions for Optical Systems*

---

majority of the optical components will not experience the full range of hazards observed on LDEF. The following observations can be made:

- All of the components will experience the ionizing radiation environment.
- Depending upon the design, all the components can experience the thermal environment and be subjected to contamination.
- External components such as primary mirrors, windows, baffles, and the sun shade can experience the effects of solar radiation, AO, and micrometeoroids and debris.

Based on the operational environments to which the components might be subjected and based on the specific system design features, three groupings can be defined to classify the exposure for optical components in a space system: (1) benign exposure, (2) minimal exposure, and (3) maximum exposure. Each is discussed briefly in the context of space environment exposures in the following sections.

**The benign environment.** Unless the optical system is designed specifically to observe the sun, most optical elements will not be exposed to prolonged solar radiation. For long-range surveillance missions, internal temperatures will be controlled to at most a few degrees. Fluxes of AO and micrometeoroids will be negligible. The benign environment category best applies to components "buried" in a telescope assembly, for example, and also applies to experiments flown in the inside of the LDEF spacecraft cylinder. (Specific contamination effects are not considered representative, but must be considered in any optical design.)

**The minimal-exposure environment.** This category describes an optical component exposed to a minimum micrometeoroid and debris environment and also to the solar flux, but with a low level of AO exposure. This category best applies to "external" telescope components which are not looking in or near the ram direction; this category also applies to experiments on the trailing edge position on LDEF.

**The maximal-exposure environment.** This category describes an optical component exposed to micrometeoroids and debris and solar flux, with a high level of AO exposure. This category applies to "external" telescope components looking in or near the ram direction and to experiments on the leading edge position on LDEF.

In progressing from benign exposure to maximum exposure, each environment exposure can be characterized as more severe than the one preceding it. For this report, it was assumed that any optical component that "works" in the more-severe environment is deemed to also work in all less-severe environments. This is not axiomatic and any deviations found through future work will be reported as the handbook is updated.

In order to form a coherent assessment of the magnitude of effects for each of these three categories, it is necessary to describe the effects associated with specific LDEF experimental configurations (experimental location and environments exposures). As shown in Figure 5.2, the LDEF experiments were located on the surface of a cylindrical shape. The spacecraft was oriented so that its axis of symmetry was pointed at the earth, and so that its direction of travel was about normal ( $8.1^\circ$  off) to Row 9. LDEF Solar radiation, AO, and micrometeoroid and debris values, as a function of position, are given in Appendix A.

The solar-radiation-driven thermal cycle (once per orbit) consisted of 15 orbits per day for a total of about 34,000 orbits in the longest (70-month) LDEF exposure time. The nominal temperature cycle was from  $-23^\circ\text{C}$  to  $+66^\circ\text{C}$ , a  $160^\circ\text{F}$  swing. This average was suggested to have local variations, depending on the geometry and the local absorptance of the solar radiation. Interior locations had the potential for lower swings in temperature, since the time period for the thermal variation was about 1.6 hours. Space radiation (e.g., charged particles and gamma rays) characteristic of the LEO space environment were also present. Contamination of optics was observed to be very dependent on the particular experiment setting.

### LDEF Orbital Flight Orientation

Launch	April 6, 1984	
Deploy	April 8, 1984	260 NM @28.5°
Retrieval	January 12, 1990	178 NM
Landing	January 20, 1990	
32,420 Orbits	854,000,000 Miles	

- Gravity Graic  
Stabilized Attitude

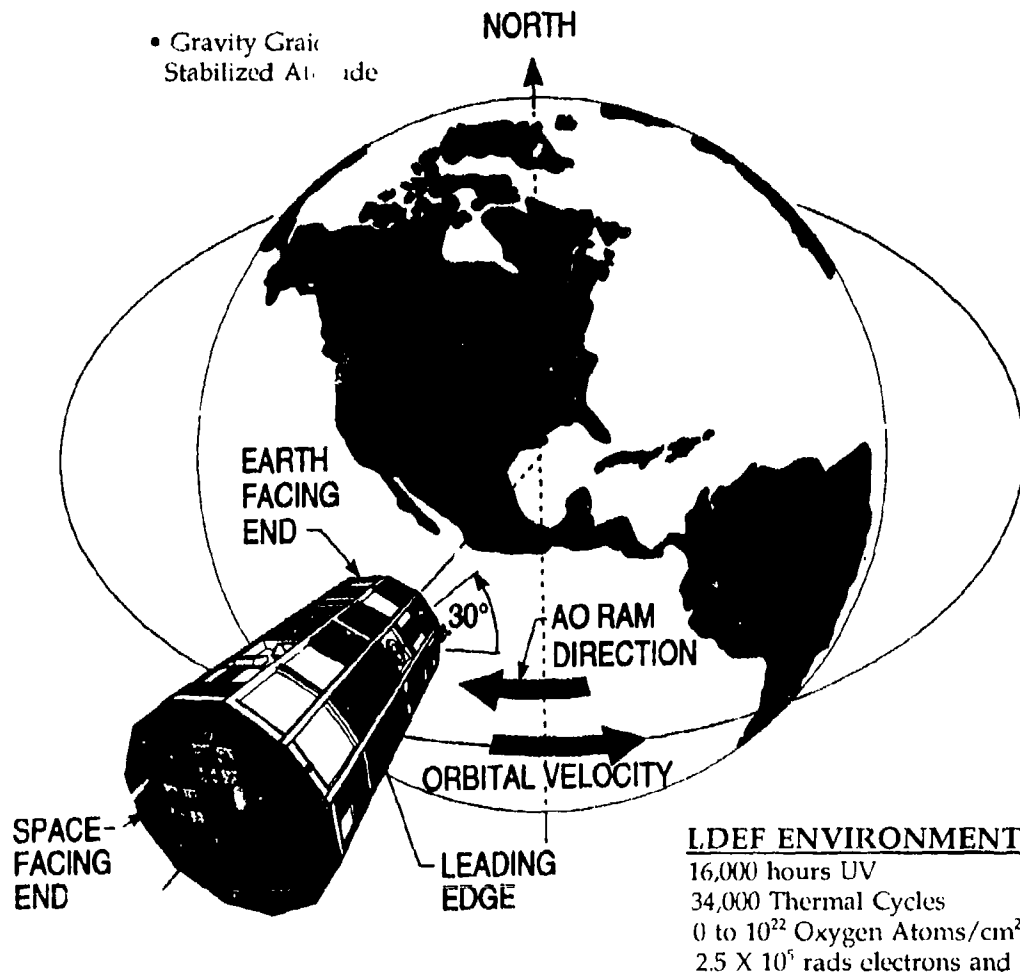


Figure 5.2. LDEF Orbital Flight Orientation

## *5.2, Critical Interactions for Optical Systems*

---

**Definition of "working" optics materials.** Demonstration of "working" in the context of this document means that no serious degradation was observed as a result of exposure to the space environments in the optical component response parameters of Figure 5.1. For example, for optical substrates and metal reflectors (with and without protective overcoatings), demonstration of working acceptably requires showing minimal physical damage, showing no overcoating or other visual degradation (such as darkening of substrates and coatings), and, for the metal reflectors, showing no debonding between the metal, its substrate, and the overcoat.

For reflective and refractive optics, a required test of a component working acceptably is demonstrating that the post-flight reflectivity versus wavelength (transmissivity for substrates) is comparable to that seen pre-flight. (Regrettably, this test is one that is not presently available for many of the LDEF optical samples because they have been contaminated, have not yet been cleaned, and, therefore, are not categorized as "working.") In developing the list of preferred "working" optical components, the biggest driver is the contamination of the samples. Because contamination skews and clouds the examination of the real behavior of the optical materials after space environment exposure, this limited consideration of optical components to only those elements which were cleaned. Measurements made on contaminated components, in most cases, showed a significant decrease in the measured parameter (e.g., either reflectivity or transmissivity for reflective or refractive optics, respectively) and it cannot be known whether the observed degradation is the result of the surface contamination or the result of poor optical material performance.

When contamination was not a factor (as when examining the samples for stress, darkening, or impacts degradation), a working optical component was identified when post-retrieval measurements were comparable to the pre-flight measurements and when the slight changes in the post-flight measurements did not degrade the optical element performance.

Working components are identified in the following sections. There are a number of components which are not included but which may be acceptable under other conditions than those experienced in the LDEF orbit. These materials are discussed in Section 5.4, General Optical Design Considerations.

### **5.3 PREFERRED OPTICAL COMPONENTS**

#### **5.3.1 Benign Environment**

The buried components, particularly optical filters and mirrors, are exposed to the benign environment. Based on the data from the LDEF experimenters, the components listed in Table 5.1 showed little degradation in the minimum exposure environment, therefore, they are acceptable for the benign environment. Although some of the components listed were not shielded from the environments, they are included for the simple reason that the LDEF data demonstrate that these components can withstand an even more severe space environment, thus qualifying them as working components in the benign environment.

#### **5.3.2 Minimum-Exposure Environment**

Space optical components which may be exposed to the minimum-exposure environment include optical windows/substrates, baffles, and the sunshade. In some instances, optical filters and/or mirrors may fall into this category. To avoid repetition, when filters or mirrors are expected to be exposed to a minimal level of the space environment, reference to Table 5.1 will provide the pertinent information concerning the appropriate working components. The optical materials, listed in Table 5.1, showed little degradation in the minimum-exposure environment.

Table 5.1. Optical Elements Acceptable to Minimum-Exposure Space Environment

ELEMENT	COMPONENT	EXPERIMENT
Mirrors/ Reflectors	Fused Silica/Ag	S0050-2
	ULE™/Ag	
	Al/LiF/Kanigen	A0138-4
	ZnZc/ZnS/ThF <sub>4</sub> on ZnSe	
	Ag/Al <sub>2</sub> O <sub>3</sub> /Kanigened Al	
	Ge/ZnS/ThF <sub>4</sub> /Glass	
	ThF <sub>4</sub> /Ag on B1664 Glass	
	Ag/ThF <sub>4</sub> /Kanigen	
	(Si/Al <sub>2</sub> O <sub>3</sub> ) <sup>1</sup> /Ag/Si	M0003-2
	Al <sub>2</sub> O <sub>3</sub> /CaF <sub>2</sub>	
	Visible 1060 nm Mirror/TiO <sub>2</sub> -SiO <sub>2</sub> on B1664 Glass	M0003-7
	10.6 μm Mirror/Ge-ZnS-ThF <sub>4</sub> on B1664 Glass	
	Au/Glass	A0138-3
	Pt/Glass	
Filters	PbTe/ZnS/ZnSe on Ge	A0056
	PbTe/ZnS on Ge	
	ZnS/Chiolite on BK7G18 and RG780 Glasses	
	Ge/SiO on Al <sub>2</sub> O <sub>3</sub>	
	PbF <sub>2</sub> on ZnSe	
	SiO on Si	
	ZnS/Cryolite/Ag on Fused Silica	A0147
	TiO <sub>2</sub> /ZrO <sub>2</sub> /SiO <sub>2</sub> /B1664 Glass	
	ThF <sub>4</sub> /Cryolite/Fused Silica	
	ZnS/ThF <sub>4</sub> on Fused Silica	
	PbS/Cryolite/Ag on Fused Silica	
	ThF <sub>4</sub> /Cryolite/Al/ZrO <sub>2</sub> on Fused Silica	

**Table 5.1. Optical Elements Acceptable to Minimum-Exposure Space Environment (Cont.)**

ELEMENT	COMPONENT	EXPERIMENT
Windows/ Substrates	Fused Silica	S0050-2
	Fused Silica/Solar Rejection	
	Fused Silica/Ag	
	ULE™ Glass	
	ULE™ Glass/Ag	
	SiO <sub>2</sub>	M0003-2
	Fused Silica	A0172
	ULE™	
	BK-7	
	Soda-Lime-Silica	
	Pyrex	
	Vycor	
	Zerodur	
	Ge	A0056
	Si	
	CdTe	
	Al <sub>2</sub> O <sub>3</sub>	
	Y-Cut Quartz	
	Z-Cut Quartz	
	Ge/ZnS/ThF <sub>4</sub> /Ge	A0138-4
	ZnS/Ge	

### 5.3.3 Maximum-Exposure Environment

Space optical components which may encounter the maximum-exposure environment include the same or similar materials to the minimum-exposure environment: windows,

### *5.3, Preferred Optical Components*

---

baffles and the sunshade. As before, in some instances optical filters and/or mirrors may also fall into this category. Within the LDEF data reported to date, all of the windows/baffles/sunshade materials have been flown on the LDEF trailing edge. Based on this position, the materials are viewed as working in the minimum-exposure environment, but not necessarily in the maximum-exposure environment. As such, no materials can be reported at this time as being acceptable, working optical materials in the maximum-exposure environment. This conclusion will be updated as more LDEF data are reported by the experimenters.

This leaves the optical designer in an uncomfortable position if placing optics in the maximum-exposure environment is unavoidable. Experiment M0003 has reported that the following optical components survived in this environment: Au on Al, Al on fused silica, and bare fused silica. These components have not been measured for reflectivity and/or transmissivity. However, based on results of the less-severe, minimally-exposed environment, a best-guess suggestion would be to use bare fused silica as a window, and aluminum on fused silica, with a fused silica protective overcoat, as a mirror.

## **5.4 GENERAL OPTICAL DESIGN CONSIDERATIONS**

### **5.4.1 Contamination Control**

Many of the substances on LDEF degraded in the environment of AO and solar radiation (especially UV). Outgassing from heated substances, followed by (possibly UV-accelerated) deposition on cooler optical surfaces was common. Graphite epoxies, which are being considered for use as sunshades, may outgas. Preservation of the performance of optical surfaces calls for strict control of potential contamination sources.



### 5.3, Preferred Optical Components

---

Two potential design approaches are temperature control and material selection. Temperature control is the maintaining of constant lower temperatures where possible. Although it is a good design approach to "athermalize" the optical system, *i.e.*, to design the system so that its optical performance is unchanged if the entire system changes in temperature together, it is still a good policy to contain potential temperature excursions.

Material selection involves not only the optical components but other spacecraft materials such as thermal control materials, adhesives, and optical mounting materials which can be potential contamination sources. Some of these substances degraded on LDEF and became contamination sources. Other materials had their thermal-control properties degraded. These results are summarized in Table 5.2. Even the acceptable items may not withstand the highest levels of AO. For example, D-111 black thermal-control (TC) paint was crazed and contaminated on the leading edge, with maximum AO flux, but was acceptably unchanged in the trailing edge position, with minimum AO flux. An interesting occurrence is that black coatings for baffles seem to age in the space environment and improve the performance of the baffles.

#### 5.4.2 Micrometeoroid Damage

The effects of micrometeoroid and debris damage is discussed in detail in Chapter 6. Here we will discuss the considerations to be given in an optical design.

Micrometeoroid damage causes cratering in optical surfaces; for brittle, crystalline materials such as  $\text{CaF}_2$ , the substrate can be cleaved. If the  $\text{CaF}_2$  is used as a window to hold off significant pressure, it is more likely to burst from the pressure. (When  $\text{CaF}_2$  windows are tested to failure to establish burst statistics, it was shown that their yield stresses get higher when the window surfaces are polished to a smoother figure.) With  $\text{CaF}_2$ , burst safety

### 5.3, Preferred Optical Components

factors must account for reductions due to cratering. If cratering leaves high residual stresses, thermal cycling following cratering has the potential to expand the region of damage further.

**Table 5.2. Thermal Control Materials, Adhesives, and Optical Mounting Materials**

<b>MATERIAL THAT GENERATED CONTAMINANTS OR DEBRIS</b>	<b>MATERIALS WHICH ARE ACCEPTABLE (FROM DEBRIS/CONTAMINATION POINT OF VIEW)</b>
Silver Teflon (Ag/FEP) film	ITO-coated Kapton
Aluminized and bare Kapton	
Aluminized Mylar	
Delrin	
Teflon	
Black RTV	
<b>MATERIALS THAT SHOWED LOSS OF THERMAL-CONTROL PROPERTIES</b>	<b>MATERIALS WHICH ARE ACCEPTABLE (FROM THERMAL-CONTROL PROPERTIES POINT OF VIEW)</b>
White TC paint with $\text{TiO}_2$ , $\text{Eu}_2\text{O}_3$ , $\text{Al}_2\text{O}_3$ , and ZnO pigments: Chemglaze A276, S13GLO	Z-93, YB-71, PCB-Z white TC paints
Black TC paint Chemglaze Z306	D-111 black TC paint
Black Anodized Al (bleached by UV)	Chromic Acid Anodized Aluminum

Cratering can be a local phenomenon, especially if the substrates are metals or glassy hard materials such as fused silica. When the cratering penetrates the coating, it exposes the underlying layers to the environment. If that environment includes AO, the AO can attack underlying layers, expanding out from the cratering site, even though there may be an outer protective coating. Thus, in an environment of micrometeoroid damage and AO, fused silica over aluminum on a fused silica substrate is preferred to the same coating with silver substituted for the aluminum.

A major impact of cratering (and contamination) is to increase the scattering at the damaged surface. For metal surfaces, this can appear as a small decrease in reflectivity. The

#### *5.4, General Optical Design Considerations*

---

roughened surface appears to "trap" a small portion of the light, reflecting it among "rough" regions on the surface until a portion is absorbed.

In general, the scattering surface diffracts the light into directions (spatial frequencies) which are not desirable. In considering the resolution of an optical system, light from the target is scattered (diffracted) from the desired low spatial frequencies into undesired high spatial frequencies, typically higher than the (spatial) frequency bandpass of the optical system. This transfer of energy from low to high spatial frequency is seen in a lowering of the peak in the system Modulation Transfer Function (MTF) curve, and can be treated acceptably as an optical element with its own MTF which limits the total system bandpass.

The scattering surface can scatter light not from the target into the target's image. As such, it becomes a noise source, which increases in power as the scattering gets worse. Typically, this implies an increase in noise from the target's background, with a modest decrease in signal-to-noise ratio (SNR). However, if the scatterer is illuminated brightly, e.g., by direct solar radiation or by an anti-satellite laser blinder, the SNR can undergo a major decrease. In designing for stray light control (baffles and shrouds), this should be considered.

##### **5.4.3 Ionizing Radiation Damage**

Optical materials flown on LDEF did not show damage due to ionizing radiation. Because of the low radiation environment to which these components were exposed due to the LDEF orbit, care must be exercised in picking components to be used in higher altitude LEO. At these higher altitudes, the radiation environment will become quite severe and could result in darkening of optical components, such as ULE™. While no cryogenic experiment was flown on LDEF, it has been shown that poor control over contaminants in cryogenic components will result in darkening due to the radiation environment.

### 5.4.4 Atomic Oxygen

While soft materials, such as KRS-5, suffered damage on LDEF, it was due to attack by AO. At altitudes above 800 km, AO is no longer considered a major design concern. Therefore, for higher-altitude LEO missions, these materials may be suitable for use.

## 5.5 RECOMMENDATIONS FOR ADDITIONAL PROCESSING OF LDEF DATA

A large number of samples in many experiments have yet to undergo measurements of (spectrally-dependent) transmission and reflection. A prioritization of samples for this process is recommended, as follows:

- Physically undamaged, "unchanged" multilayer dielectric coatings.
- Physically undamaged, "unchanged" coatings and substrates.
- Physically undamaged, "contaminated" coatings and substrates *which can be successfully cleaned*.
- Other coatings and substrates.

For multilayer dielectric coatings, measurements of (spectrally-dependent) reflection is critical to assure no degradation. As shown in the results for experiment S0050-2, certain surfaces can be cleaned of contaminants and restored to their pre-flight values (section 4.5.1.4). By prioritizing ongoing experimental assessments this way, a better understanding of what "worked" will soon be available.

#### *5.4, General Optical Design Considerations*

---

## **CHAPTER 6**

### **THE EFFECTS OF MICROMETEORIDS AND DEBRIS (M&D)**

A general introduction to the microparticle space environment for low Earth orbit (LEO) was given in Chapter 3. An in-depth description of the M&D environment, the models used, and its effect on optics is given in Ref. 1. This chapter provides a detailed summary of the material in Ref. 1.

#### **6.1 SPACECRAFT MICROPARTICLE IMPACT FLUX DEFINITION**

##### **6.1.1 Introduction**

The microparticle environment encountered by a spacecraft in low and medium Earth orbit (LEO and MEO, respectively) is defined by two sources: man-made debris from space activity since October 1957, and naturally occurring micrometeoroids. The two models used in these computations have reduced the raw data obtained so far into functions that characterize the microparticle fluxes. These flux data must then be transformed to the appropriate moving coordinate system of an orbiting satellite, and then integrated over the required mission life time. Due to the vector addition rules for impact velocity, the front end (RAM direction) of a satellite will experience more microparticle impacts than the rear end (the TRAIL end). The model predictions are in the form of number of cumulative impacts/m<sup>2</sup>/year versus a given impactor size distribution (i.e., for impactors greater than or equal to a given size) and also as functions of the crater sizes expected versus impactor sizes.

A computer program, SPENV (Space Environment) models the micrometeoroid and space debris environment encountered by a spacecraft in an orbit between 200 and 4000 km. The phenomenology numerically computed is provided by B.G. Cour-Palais (Ref. 2) for micrometeoroids and by D. Kessler (Ref. 3) and R.C. Reynolds for space debris. The models are outlined in NASA SP-8013 (Ref. 2), and NASA-TM-100471 (Ref. 3) with recent, 1990.

## *6.1, Spacecraft Microparticle Impact Flux Definition*

---

data, provided in a recent Phillips Laboratory briefing by Kessler (Ref. 4), respectively. The predicted results from the program are being compared with the data seen from the Interplanetary Dust Experiment (IDE), and other cratering and penetration data, from the LDEF satellite. The following is a brief discussion of the models, and the predictions obtained, and how these predictions compare with experimental data.

### **6.1.2 Man-made Debris**

The microparticle environment is described in terms of two separate models, one for the man-made debris, and the second one for the naturally occurring micrometeoroids. The existing Kessler debris model assumes that the particles are all in circular orbits and, therefore, have a common speed with that of any spacecraft which is also in a circular orbit at the same altitude. This logic immediately implies that hits can only be in the plane which is parallel to the Earth's surface. Therefore, only the RAM and SIDES can be hit and there will be no hits on either the SPACE end, the EARTH end, or the TRAIL end. The debris model predicts that the number of hits per area, per time are functions of altitude, the 11 year solar cycle, orbit inclination, particle size, and time. A growth model has been assumed which has two components--one component due to continued launches and a second component due to fragmentation resulting from explosions and collisions between the various pieces within orbit. An important point to note is that for debris altitudes greater than 700 km there is only a simple growth factor, since the influence of the atmosphere is negligible. However, as altitude decreases below 700 km the effect of the atmosphere becomes increasingly important and there is a cyclic component to the history which is due to the solar cycle behavior and the consequential atmospheric heating effect.

When bodies collide with each other, or fragment due to explosions, there is a fractal fragmentation log-log function describing the relative cumulative number of particles against the size of the particles. Ground based experiments, for example performed by Physical

### 6.1, Spacecraft Microparticle Impact Flux Definition

Sciences, Incorporated (Ref. 5), using hypervelocity impact tests, have confirmed that the general trend for this cumulative data as a function of the size of the resulting particles is very similar to that seen for the space debris and micrometeoroids, as shown in Figure 6-1. In all cases the cumulative particle data tend to scale inversely with the size of the particle to some power, where the index tends to be about at least 2.25 for debris and up to about 3.5 for micrometeoroids. For the smaller particles, below 1 micron, the micrometeoroid flux is observed to level off.

Knowing the velocity of collision it is possible to calculate the angle of impact relative to the normal to the RAM direction, as seen in Figures 6-2 through 6-4. This is given by a simple cosine relationship. Having determined the polar distribution (which is all within the plane parallel to the Earth's surface), it is possible to calculate the relative number of hits for a given surface orientation. This is obtained by using the polar diagram and calculating the local cosine directions of arrival versus the local normal to the surface. This methodology reveals that the relative number of collisions is a maximum on the RAM surface and gradually drops towards 0 as the surface is rotated towards the TRAIL end. Figures 6-2 through 6-4 illustrate these polar distributions. Note how they display "butterfly" shapes, with details dependent on the spacecraft orbit inclination. Clearly indicated is the fact that there is an exclusion angle for impacts near the RAM vector, demonstrating the dearth of direct head-on collisions.

With regard to the mean density of the debris, the present recommendation is that for particles smaller than 0.5 cm the mean density be set at  $4.0 \text{ g/cm}^3$ . This is based on the fact that most of such small particles consists of either small alumina particles (e.g., from propellants) or the debris from paint and pigments, which are usually comprised of such materials as titania and zinc oxide. For larger particles greater than 0.5 cm the density is initially about  $2.8 \text{ g/cm}^3$  (representing aluminum) but becomes a decreasing factor of the size of the particle (i.e.,  $\rho = 2.8/d^{0.74}$ ). The basic explanation for this is that the particles are not



### *6.1, Spacecraft Microparticle Impact Flux Definition*

---

solid bodies but rather portions of structures which, therefore, act as if partially hollow and pseudo-porous.

The data given by the Kessler model is one of hits versus impactor diameter. However, a large amount of the data base, such as seen on LDEF and on other spacecraft (e.g., Solar Max), is in the form of hits versus crater or perforation diameters. It is, therefore, necessary to relate one to the other. It is well known that for a given size particle the greater the density and the greater the impact speed the larger will be the size of the crater. To date, a simple scaling law has been applied to relate the size of the crater to the size of the particle causing it. This simple rule involves a cube-root law of ratio of density of incoming particle to the target material and makes use of a two-thirds power law for the collision velocity (i.e., the "energy scaling" rule). See Figure 6-5. The normalizer is based on known terrestrial Aluminum (Al) into Al impact data. The literature on impact dynamics is full of analytic "curve fits" of such cratering (at least 19 equations have been identified). Recent work (Ref. 6) has produced new scaling laws. These new laws will be applied to the analysis of LDEF in the future, however, the overall changes in interpretation are expected to be small (e.g., less than 20 percent). The impacts are a function of the local collision velocity relative to the surface normal, and the latter depends on the orientation of a given surface. Thus, it follows that the ratio of crater diameter to particle diameter is also orientation dependent. In particular, since the impact speed decreases going from RAM to TRAIL, the ratio (crater diameter/particle diameter) also decreases going from RAM to TRAIL. Note that this effect is in addition to the change in impact flux. Therefore, the cumulative "crater count" is doubly affected.

#### **6.1.3 Micrometeoroids**

For micrometeoroids, it should be noted that the Earth passes through many "tubes" of micrometeoroid orbits during its annual orbit. These orbits vary from those which are only

### 6.1, Spacecraft Microparticle Impact Flux Definition

---

slightly more elliptical than the Earth's to those with very large semi-major axes. This gives possible velocities up to 42 km/s for micrometeoroids at the Earth's orbital radius, while the Earth itself has an orbital speed of approximately 30 km/s. Since some of the micrometeoroid orbits are retrograde relative to the Earth (e.g., the Leonids) the potential head-on collisional speed can be up to 72 km/s. However, the vast majority of the micrometeoroid orbits are prograde and consequently the lower collisional speed is about 12 km/s relative to the Earth. The micrometeoroid orbits encompass a wide range of inclinations relative to the Earth's ecliptic plane. The orbital velocity of the spacecraft adds a further modulation to these values. The average of the collisional speeds for a spacecraft is about 19 km/s (ignoring local angles of arrival to a given surface).

For short mission times of less than 1 year, it would be necessary to correctly track exactly which of the micrometeoroid orbits have been intercepted by the Earth. However, for a multiyear mission, where collisions occur with a large number of micrometeoroid orbits, the assumption is that the micrometeoroids are coming in towards the Earth from all possible directions and, therefore, the system appears to be geocentric on average.

Zook (Ref. 7) has provided data (e.g., NASA SP-8013) which gives the relative velocity of the micrometeoroids as seen by a stationary spacecraft not rotating around the Earth and also as seen by a spacecraft with its orbital speed. The data base for these velocity distributions has been provided by Erickson (Ref. 8). They are in the form of weighted velocities, including the relative number of impacts as a function of velocity. Figure 6-6 illustrates the Erickson data showing the geocentric and spacecraft-centered relative velocities.

By inspecting all the possible combinations of collisional velocity and angle of arrival relative to the spacecraft RAM vector, it is possible to derive a matrix which can be read for each angle of arrival and given in the form of weighted numbers versus collisional speed. This allows a polar diagram to be established which is three dimensional and axially

### *6.1, Spacecraft Microparticle Impact Flux Definition*

---

symmetric around the RAM axis. A two-dimensional plot is shown in Figure 6-7. This plot gives the velocity for the mean number of impacts per kilometers per second. This would be a truly axially symmetric distribution if the spacecraft orbit was at a very high altitude such that Earth shielding could be ignored. However, for lower orbits, the Earth subtends an exclusion angle such that some particles cannot be seen from the side of the Earth. This shielding angle has no effect for impacts arriving on the SPACE end of the spacecraft. However, it does influence all the possible impacts on every other surface, including RAM, SIDES, TRAIL, and especially the EARTH facing side. For sufficiently low altitude, the EARTH face will suffer 0 impacts, while the RAM, TRAIL, and SIDES will see exactly one half the free-space values. In free space the RAM will experience the largest number of impacts, but at LEO the RAM count can be less than that for the SPACE end. The effect of Earth shielding is shown in Figure 6-8.

Unlike the case of man-made space debris, the micrometeoroid flux in LEO (less than 2000 km) is assumed to be essentially independent of the altitude since the particles are experiencing only a one-shot transfer through the atmosphere and, therefore, are not in orbit long enough to be significantly influenced by the atmosphere. Further, the gravitational focusing effect described in Chapter 2 changes very little for such altitudes (e.g., 10 percent at 2000 km). Likewise, because of the assumption of the geocentric distribution, there is no correlation with the spacecraft orbital inclination. Unlike the case of man-made space debris, NASA presently recommends that for the lower orbit micrometeoroid distribution the mean density is about  $0.5 \text{ g/cm}^3$ . This is primarily because most of the microparticles are from cometary ices. There are, additionally, some asteroidal sources which can include materials up to iron and nickel with densities up to  $7.8 \text{ g/cm}^3$ . However, these constitute only a very small fraction of the total number of micrometeoroids seen in LEO. As with the man-made space debris, it is necessary to convert from crater sizes due to impacts versus the impactor size itself. Thus, use must be made of the NASA recommended micrometeoroid density in order to update the ratio of crater size to particle size. This will again be a function of surface such that on the RAM surface, the overall ratio of cratering versus particle size would

be larger than for any other surface. Figure 6-9 displays the crater-to-particle ratio for the polar orientations for micrometeoroids impacting aluminum.

With regard to the LDEF orbit, the model presently predicts that the ratio of impacts for the SPACE-looking end versus the EARTH-looking end should be about 10.5. Figure 6-8 shows the relative number of hits per square meter, for the specific case of particle sizes greater than 1 $\mu$ m, as a function of altitude. It can be seen that the SPACE-looking end is essentially a constant (the observed slight increase, seen in the plot, is merely due to rounding errors in the computer routine which has not been optimized) while the RAM and SIDES start with noticeably lower impact numbers which gradually increase as the altitude increases. Ultimately, for very high altitudes the RAM surface will contain the largest number of hits. Also seen from the diagram is the fact that the EARTH-facing surface receives the minimum number of hits which reduce to 0 as the altitude collapses to 0.

### 6.1.4 Impact Effects

Regarding the effect of impacts on a body, for thick ductile targets relative to impactor sizes, craters will be formed. These craters have lips varying from plastic flow to molten splatter. Conversely, for foil targets much thinner than the particle diameter, perforations occur where the hole size is only slightly larger than the particle size. However, secondary damage can occur due to the punched-out section and the remnants of the incoming particle. For high velocity impacts both the impactor and portions of the target are vaporized. For lower velocities the impactor and target or foil remnants remain molten or solid and secondary damage is possible due to ricochets and/or impacts with material behind foils. A problem of concern is brittle materials, such as AO protection layers (usually oxides), glasses and ceramics. In addition to craters there are frequently observed conchoidal surface spalls around the crater and star cracks moving radially away from the crater. This situation is similar to the well-known stone penetrating a glass window. Also, when dealing with layered

targets with relatively weak adhesion between layers and quite significant differences in acoustic impedances of materials, it is common to observe delaminations in the neighborhood of the crater. Other synergies occur, such as interaction with UV, AO and thermal cycling. For example, plastics (e.g., Kapton, Mylar, Teflon) tend to embrittle under UV exposure, and the combined effects of impacts, AO and thermal cycling, can reduce thermal control paints to fine dust, thereby posing a contamination hazard.

Averaging over all behavior for both the space debris and micrometeoroids, cratering tends to give a ratio of crater size to particle size with a mean value of about 5. However, for local spalls the ratio of spall radius to particle radius is about 20. When brittle target star cracks are formed, the star crack pattern itself has been observed to extend outward for up to almost 100 times the original size of the particle, dependent on materials and impact velocity. These effects may have serious repercussions for the responses of optics which use brittle materials, particularly for the case of larger high velocity particles. The major problem is one of "sand-blasting" of surfaces by small particles. The much larger impactors have an exceedingly low probability of collision (except for very large area spacecraft, such as Space Station Freedom) but can produce catastrophic events by rupturing pressure vessels, etc.

The "sand blasting" can remove AO coatings, which worsens the synergistic AO erosion on materials, and can upset optics, associated telescope baffles, solar cells, star trackers, and thermal radiator surfaces. Existing data on space flown ductile metallic mirrors (Ref. 9) such as aluminum, steel or aluminum-coated steel, have indicated that there is only a relatively small change in actual reflectivity (e.g., less than 1 percent, determined by on-board measurements of absorptivity and emissivity) even for greater than 20 year lifetimes. However, this represents data since 1970, and the man-made debris has been escalating more rapidly in the recent past.

Unfortunately, there is, to date, limited existing data on any corresponding increases in the BRDF (units of  $\text{sr}^{-1}$ ) scattering. For optics which merely collect light these data suggest

minimal effects but for imaging optics, increases in associated scatter may be very important. Further, if AO-susceptible reflectors (e.g., silver) are employed it is necessary to use an AO overcoat. The ability of impactors to penetrate the AO layer implies serious potential problems. For example, an AO layer of thickness 400 Å can be penetrated by a particle of only 200 Å diameter, and the flux for such small particles is very high (but also very uncertain for these sizes). Thus, the silver layer could rapidly become subject to AO attack, particularly since the brittle AO layer will suffer from large star-cracks.

#### **6.1.5 Predictions and LDEF Comparisons**

Using the models described above predictions (Ref. 10) have been done for the LDEF satellite. Some selected results are shown in Figures 6-10 to 6-13. In general, it can be seen that the existing models fit the experimental data within a factor of about 2 to 3. Note that the true LDEF RAM surface was accidentally set at 8° to the intended orientation (toward the NORTH). This effect has been included by giving quotes at: 352, 322, 292,....., degrees, etc., rather than at 0, 30, 60,.....etc., for the 12 faces around the body.

These data are based primarily on crater counts, especially in the aluminum structure of LDEF (longerons and intercostals). It is observed that for the smallest particles the crater count asymptotes, whereas the Kessler debris model predicts a steady increase with decreasing particle size. This effect may be due to the anodized coating on the aluminum. This alumina coating is both tougher and of higher density than the metal. Consequently, the craters will be smaller than in the metal and may artificially cause the roll-off. Other data, available from the Interplanetary Dust Experiment (IDE) on LDEF, also provide information for the smaller particles. These data indicate a higher flux than the aluminum crater count. It should also be noted that the IDE data are for mean flux rates, whereas the actual time dependent IDE data show dynamic variations in flux rates ranging from 0 to 1000 times the mean flux rate. The IDE data also indicate that the many orbital particles are in elliptical orbits (again not

predicted in the models) and that these particles are in clouds, thus causing the dynamic flux rate variations.

### **6.1.6 Caveats on the Microparticle Models**

Many caveats should be applied to the existing models which define the microparticle space flux environment. The present assumption that all debris orbits are purely circular automatically forbids any collision on either the SPACE-end or the EARTH-end. In reality, many orbits must be slightly elliptical (due to random collisions and explosions) while others are strongly elliptical (due to rocket exhaust products and explosions in Hohmann transfer orbits) and, therefore, there will be a contribution to both SPACE-end and EARTH-end, and additional hits on the TRAIL.

For random debris orbits the self-collision rate per volume per time (causing yet more fragmentation) is proportional to the square of the particle density per volume, to the mean cross-sectional collisional area, and the mean collision speed. Thus, the small particle population should increase rapidly versus that for the larger sizes. Kessler is fully aware of the implications and indicates that beyond a critical particle density (per volume) a "runaway" situation occurs, with self-collisions causing the population to grow even without further space launches. Indeed, Kessler suggests that this situation may have already occurred for the debris at altitudes of about 1000 and 1500 km, where air drag effects are negligible.

With regard to the natural environment of micrometeoroids, the biggest caveat concerns the suggestion that the particles are apparently geocentric. In reality, this will only be approximately true for long lived missions; particularly those that include a large number of satellite orbits together with a large number of precessions of the spacecraft orbital plane. Furthermore, it should be noted that in attempting to correlate the observations on LDEF

### 6.1, Spacecraft Microparticle Impact Flux Definition

---

versus the model predictions for the environment, the answers are sensitive to assumptions with regard to crater sizes versus particle sizes.

Examination of the LDEF data reveals an interesting bias in the impact flux (Ref. 11): the peak flux is NOT symmetrically distributed about the RAM direction in the plane parallel to the Earth's surface (i.e., the two SIDES are not equal as expected). This effect cannot be readily explained for man-made debris since the interception of a circular spacecraft orbit with a circular debris orbit must necessarily involve two collisions per orbit (except for the rare condition of "kissing" orbits at apogee or perigee). These two states give symmetry about the RAM axis, thereby causing the RAM direction to experience the greatest number of hits.

One probable explanation lies with the micrometeoroids. In reality each interception of a micrometeoroid orbit "tube" with the Earth always results in the flux being "one-sided" with respect to the Earth's orbit. Either the flux is "inward bound" towards the sun, or it is "outward bound" from the sun. Further, the flux appears to be monodirectional at the instant of interception. Thus, the true "Earth-shielding" is really simple ecliptic geometric shadowing for LEO (i.e., NOT the subtended solid angle of the Earth seen by the spacecraft). Thus, a spacecraft in LEO could be shielded from the particles for almost a complete half orbit if the plane of its orbit is close to that of the orbit of the micrometeoroids. The result can be a bias such that one "half" of the spacecraft experiences the impacts while the other half sees none. The "half" will include surfaces ranging from the RAM through SPACE round to the TRAIL, with one SIDE receiving more impacts than the corresponding other SIDE, and the exact surfaces involved will depend on the local plane of the spacecraft orbit relative to that of the micrometeoroids. Note that the LDEF inclination of  $28.5^\circ$  together with the Earth's axial tilt of  $23.5^\circ$  meant that, with orbital precession, the plane of LDEF's orbit oscillated between  $5^\circ$  and  $52^\circ$  relative to the ecliptic. There were about 38 complete orbital precessions during LDEF's life-time (precession rate of about  $6.5^\circ$  per day) and about 32,000 complete orbits.



## *6.1, Spacecraft Microparticle Impact Flux Definition*

---

Elliptical debris orbits can also sometimes introduce impact asymmetries, especially for orbit planes which are at large angles to the target satellite orbit plane, where it is possible to have only one intersection point between the orbits.

### **6.1.7 Elliptical Orbits**

Efforts have begun looking at ways to update the Kessler model for debris to allow for inclusion of noncircular debris orbits. LDEF data demonstrates that such orbits exist since several impacts of debris have been unambiguously identified on the TRAIL surface (at least 15 percent of the total crater count). Kessler's (Refs. 12 and 13) preliminary analyses suggest that the most probable source of this debris are orbits from Hohmann transfers out to GEO and with small inclinations (i.e., less than 30°). Currently the impact options for an assumed group of debris orbits with small inclinations and with apogee at GEO and various perigee values down to 200 km are being analyzed. The various impact options on the LDEF satellite have been identified, and the analyses confirm that the major effect is to give TRAIL impacts, but also with a small contribution to the SPACE and EARTH surfaces, and a larger contribution to the SIDES.

The purpose of this analysis is to allow assessment of the effects of elliptical debris orbits on any other satellite orbit, since the present Kessler analysis does not allow such facts to be determined. In particular, if the satellite were in a retrograde orbit (e.g., launched out of Vandenberg to the north-west), then the elliptical orbit debris would add to the RAM impacts, which would be at very high collision speed. Such facts need quantifying.

Figures 6-14 through 6-18 give the impact conditions for LDEF. Figure 6-14 shows the coordinate system used. The RAM-TRAIL axis is Y, the SIDE-SIDE axis is X, while the SPACE-EARTH axis is Z. Figure 6-15 shows the absolute impact speeds. The minimum corresponds to the case of the elliptical debris orbit which just "kisses" the LDEF orbit (i.e.,

### *6.1, Spacecraft Microparticle Impact Flux Definition*

---

has a perigee equal to LDEF's orbit radius). The parabola indicates the hits for all other perigees down to 200 km. Figures 6-16 through 6-18 illustrate the components of the impact velocity which are along the normal to the TRAIL, SPACE/EARTH, and SIDES surfaces, respectively. Symmetry causes the two SIDE conditions to be identical. Likewise, the SPACE and EARTH conditions are equal.

The calculations indicate that for LDEF the absolute impact speeds were up to 5.0 km/s, while the normal components of impact velocity were up to about 1.8 km/s on the TRAIL surface. The SPACE/EARTH surfaces involved only small velocities (0.3 km/s) and the SIDE surfaces involved velocities up to 4.7 km/s. These numbers are consistent with recent quotes from Kessler (Fred Hörz, NASA JSC, private communication).

Figures 6-19 through 6-22 show the corresponding results for a satellite in a **different** orbit, namely an altitude of 1600 km and inclination of 60°. Note that these calculations give somewhat larger impact velocities (up to 8.5 km/s absolute). The implication is that such other satellite orbits will also suffer from debris impact damage on the TRAIL, SIDES, and SPACE and EARTH surfaces, but also on the RAM surface. One importance of these elliptical debris orbits is that they cause impacts on the EARTH surface. Such hits cannot occur with the "standard" Kessler circular debris orbit model. Thus, ordinarily only micrometeoroids can hit this surface (causing only a small increase in scatter due to the Earth-shielding effect). The elliptical debris orbits intersect the circular target orbits at small angles, namely up to 10.6° from the SPACE/EARTH surface plane for the LDEF altitude, and up to 22.6° for an altitude of 1600 km. Taking into account the vectors for velocities, this results in impacts on the SPACE/EARTH surfaces which are at 50.2° from the surface normal for the LDEF altitude, and at 21.6° from the surface normal for the 1600 km altitude. Thus, high-inclination, high-altitude orbits are most susceptible.

### *6.1, Spacecraft Microparticle Impact Flux Definition*

---

Note that the reference to "maximum angle of hits in circular orbit" is the included angle of the circular orbit of the target satellite where hits due to debris in elliptical orbits can occur.

Elliptical orbit analysis is continuing in order to re-estimate the possible concerns for EARTH-looking optics, which are frequently employed and ordinarily considered relatively "safe" from impacts. The actual data from LDEF has not yet been scrutinized in detail (e.g., via chemical analysis) for the EARTH surface, so no comments can yet be made concerning debris impacts on this surface.

## **6.2 ANALYSIS OF CRATER EFFECTS ON OPTICS**

Impacts on optics can cause simple pseudo-hemispherical craters (for ductile metals), or craters surrounded by conchoidal front-surface spalls and sometimes radial "star" cracks (brittle glasses and ceramics). For multilayer packages the impacts can also induce delamination of the various layers. Note that real craters are rarely hemispherical, and the ratio of depth to diameter usually lies in the range of 0.3 to 0.7. New hypervelocity impact scaling laws take these factors into account.

### **6.2.1 Fractional Area Damage**

The many calculations give predictions of cumulative impacts per area of surface versus particle size and crater size, for a range of altitudes, orbit inclinations, and satellite surface orientations. To estimate the fractional damage areas, the cumulative impact-versus-size function is first differentiated, then the function is multiplied by the corresponding areas of the craters, and finally reintegrated.

## 6.2, Analysis of Crater Effects on Optics

---

For example, if the cumulative number (CN) =  $A / D^n$  hits per area for particles greater than diameter  $D$ , with  $A$  a constant, and  $n$  the power index, then it can be shown that the corresponding fractional area damage is given by:

$$\text{Fractional area} = (\pi / 4) \times k^2 \times (n / (n - 2)) \times A / D^{n-2}$$

where  $k$  is the ratio of the crater diameter to the impactor diameter. For the case of small debris (less than 1 cm),  $n$  has the value of 2.5. The above equation can then be rewritten:

$$\text{Fractional area} = (\pi / 4) \times k^2 \times 5 \times \text{CN}_{(D_{\min})} \times D_{\min}^2$$

The value depends on  $D_{\min}$  since  $n$  is greater than 2. To consider a specific case, we calculate the fractional area of erosion for the RAM surface for the case of an altitude of 1000 km and inclination of 60°. The existing models predict that such an orbit is one of the worst in terms of combined micrometeoroid and debris impacts. For this case  $k \sim 7.0$ . Assuming that craters of size down to about 1  $\mu\text{m}$  are important (this is comparable to operating wavelengths, and the thicknesses of quarter-wave dielectric optical layers) we obtain:

$$\text{Fractional area} = 7.3 \times 10^{-4}, \text{ i.e., about 0.1 percent.}$$

This is a significant amount of erosion and can be expected to produce significant optical scatter, as discussed below. Note, however, that the LDEF data have indicated that the Kessler model is tending to overpredict the debris population at the smaller sizes. Consequently, the above estimate is probably too large, by perhaps a factor of three (the error would be much larger if an attempt was made to include submicron debris particles). However, the above calculation is only for man-made debris, and the micrometeoroids will also contribute, though to a smaller degree. Further, the above calculation applies only to simple cratering. If the damage zone includes surface spalling and/or radial cracks the effective area increases rapidly. LDEF itself

indicated areal erosions of about 1 percent on the thermal control materials facing into the RAM.

### **6.2.2 Optical BRDF Scatter Calculations**

The anticipated effects of impact damage on optics include: (a) a reduction in reflectivity (for mirrors), (b) a reduction in transmission (for lenses and/or windows), and (c) an increase in optical scatter (for both mirrors and lenses/windows). Experiments by Mirtich (Ref. 9), whereby metallic mirrors were impacted by small particles, demonstrated that reflectivity gradually decreased as the total surface impact energy density increased (i.e., ergs/cm<sup>2</sup> of the particle kinetic energy). Since the crater surfaces remain reflective, the decrease in reflectivity is probably related to the surface roughening which gradually produces the equivalent effect of producing a "light-trapping" baffle-like surface. However, calculations of the corresponding energy flux expected for the micrometeoroids and space debris for even 10 year missions in LEO suggest this effect to be small. Reports by Mirtich of data from space flown mirrors with missions up to 20 years (e.g., the SERT and OSO satellites) indicate very small reductions in reflectivity (less than 1 percent) in agreement with the predictions. (Note that these mirrors are non-recovered: the data are via telemetry and consist of emission/absorption in-situ measurements). Thus, changes in reflectivity (or transmission) are expected to be small. The major problem is increases in optical scatter.

Optical scatter produces three effects: (1) a reduction in light throughput, (2) a reduction in resolution, and (3) a reduction in signal to noise due to background "light-up". This can occur either due to light from bright sources (other than the required target) within the field of view, or can occur for bright sources nominally outside of the field of view if the light is redirected into the optical train path. Of these three effects item 3 is usually the one of greatest concern.

### 6.2.2.1 Equivalent Contamination Approach

The computations to date indicate the cumulative hit rate (per square meter) for an assumed mission time of 6 years, starting in 1996, and show hits versus impactor diameters for differing spacecraft surface orientations. These data are now augmented with information versus crater sizes. From the latter it is possible to establish first-order estimates of increases in optical scatter. This is done by determining the equivalent "contamination level" as defined in MIL-STD 1246A. Young (Ref. 14) has already performed both experiments and computations (using Mie optical scatter theory) to derive increases in BRDF as functions of contamination levels for small particles on mirror surfaces. Thus, by finding the "equivalent" conditions (assuming craters scatter in a similar manner to spheres on a mirror) it is possible to derive the BRDF as functions of wavelength and cratering for any chosen spacecraft surface.

Figure 6-23 illustrates the MIL-STD 1246A data plotted on the same scales as used for the cumulative impacts (per area) versus crater sizes. Note that each "level" plot curves over as the size decreases (rather like the behavior for micrometeoroids), and that this tendency to asymptote is most obvious for the lower "levels". For reference, note that the meaning of "level" is that the distribution is one for which there is one particle per square foot of surface area (equal to 10.76 per  $\text{m}^2$ ) of size "level" microns diameter (e.g., "200" means there is one particle/ $\text{ft}^2$  of diameter 200  $\mu\text{m}$ ). The data from Figure 6-23 are compared to each of the impact-versus-crater plots, and a mean estimate of equivalent contaminant level is obtained. Clearly, since the two groups of data do not have the same power index, there is no unique solution. However, optical scatter will be dominated by the larger craters, and so the "best" definition of equivalent "level" is found by matching the data at the larger sizes.

As an example, consider the data for the RAM for an altitude of 1000 km and inclination of 60°. The predictions for debris give about 10.76 impacts/ $\text{m}^2$  for craters of diameter about 0.1 cm (1000  $\mu\text{m}$ ), while for micrometeoroids the corresponding size is about 0.06 cm (600  $\mu\text{m}$ ). Thus, the equivalent MIL-STD levels are about "1000" and "600", respectively. However, the

## 6.2, Analysis of Crater Effects on Optics

---

predictions for cratering "slew" across the MIL-STD plots, such that for craters of size 10  $\mu\text{m}$  the corresponding "levels" are about "400" and "100", respectively. Reference to the work of Young allows peak BRDF (units of  $\text{sr}^{-1}$ ) values (near  $0^\circ$  off specular) to be estimated. For a working wavelength of 5  $\mu\text{m}$  these are:

For debris:

$$\text{BRDF} (\text{sr}^{-1}) = 10 \text{ ("level" 1000) to } 0.10 \text{ ("level" 400)}$$

For micrometeoroids:

$$\text{BRDF} (\text{sr}^{-1}) \approx 0.78 \text{ ("level" 600) to } 1.0 \times 10^{-4} \text{ ("level" 100)}$$

For the EARTH direction, however, the corresponding crater size is about 250  $\mu\text{m}$  (level "250") with a slew to level "50" for 10  $\mu\text{m}$  craters, and applies only to micrometeoroids (since Kessler's model does not allow impacts on the Earth-facing surface). At 5  $\mu\text{m}$  wavelength the corresponding scatter is:

For micrometeoroids:

$$\text{BRDF} = 9.8 \times 10^{-1} \text{ ("level" 250) to } 3.1 \times 10^{-6} \text{ ("level" 50)}$$

Clearly, the RAM surface suffers from far more scatter than does the EARTH surface.

Scrutiny of Young's data reveals that his results can be approximately fitted by:

$$\text{BRDF} = 2.5 \times 10^{-11} \times (\text{level})^5 / \lambda^2$$

## 6.2, Analysis of Crater Effects on Optics

---

for near-specular scatter, with the wavelength ( $\lambda$ ) in microns. Note the rapid escalation in the scatter as the "level" increases.

### 6.2.2.2 Alternative Analytic Approach

An alternative approach to estimating the scatter is as follows. The fundamental relationship for scatter from craters (assumed the same as from spheres) is:

$$\text{BRDF} = \pi^2 \times D^4 \times N / 16\lambda^2$$

where D is the crater diameter, N is the number of craters per unit area, and  $\lambda$  is the operating wavelength. By first differentiating the function describing the cumulative impact rate (per area), multiplying by  $D^4$ , and re-integrating, we obtain the BRDF for the overall distribution.

Since both the micrometeoroid and debris cumulative impacts obey the form, cumulative number =  $D^n$ , the result is:

$$\text{BRDF} = \pi^2 \times (n/(4-n)) \times k^4 \times \text{CN}_{D_{\max}} \times D_{\max}^4 / 16\lambda^2$$

where n is the power index describing the cumulative number of impacts versus particle size (in the neighborhood of the value of  $D_{\max}$ ), k is the ratio of crater diameter to particle diameter (D), CN is the predicted cumulative hit rate, and  $\lambda$  is the wavelength.

The above equation involves the quantity  $D_{\max}$ , which is the largest particle diameter to be used in the calculation. To determine the latter, the following logic is applied: if there is less than one (1) impact on the given optic, then there is no longer a meaningful definition of N, the areal impact density. Thus, knowing the area of the optic, the corresponding hits per square



## 6.2, Analysis of Crater Effects on Optics

---

meter are computed. Referring to the predicted cumulative impact data versus particle size, the value of  $D_{\max}$  is determined.

As an example, consider an optic of area  $100 \text{ cm}^2$ . For one crater, there is an areal density of 100 per  $\text{m}^2$  (or 0.01 per  $\text{cm}^2$ ), thus, this defines  $CN_{D_{\max}}$ . For debris,  $n = 2.5$  and  $k = 7.0$  (for the RAM surface). Reference to the particle plots of impacts on the RAM surface for the 1000 km,  $60^\circ$  orbit, gives the value  $D_{\max} = 70 \text{ }\mu\text{m}$  for debris. For micrometeoroids,  $n = 3.0$  and  $k = 3.8$ , leading to  $D_{\max} = 70 \text{ }\mu\text{m}$  also.

Substituting into the equation for scatter (at  $5 \text{ }\mu\text{m}$  wavelength), we obtain:

For debris:

$$\text{BRDF} = 0.24$$

For micrometeoroids:

$$\text{BRDF} = 0.037$$

For the EARTH looking surface, we have  $n = 2.7$ ,  $k = 3.25$ , and  $D_{\max} = 25 \text{ }\mu\text{m}$ , and only micrometeoroids apply. Thus, we obtain (for  $5 \text{ }\mu\text{m}$  wavelength):

$$\text{BRDF} = 2.2 \times 10^{-4}$$

Thus, once more, the scatter for the RAM surface is much greater than for the EARTH surface.

Although none of the above quotes for scatter can be considered precise, it is seen that both approaches yield similar values (especially if the larger "level" quotes are used), and both

calculational methods suggest the scatter for the RAM surface is enormous compared to that for the EARTH looking surface.

### 6.2.2.3 Mie Scatter Calculations

The most accurate procedure for calculating optical scatter is to use the Mie scatter theory. Mie scatter logic has been incorporated recently into the SPENV environmental code to automatically integrate over the impactor/crater size distributions. The detailed analysis makes use of studies done by Lowell David Lamb (Ref. 15) at the University of Arizona, whose Ph.D. thesis concerns IR scattering for small particles on substrates. The Mie calculations incorporate the optical constants for the material and, thus, can handle both highly reflective and poorly reflective conditions. The results of the calculations give values of BRDF versus off-specular angle, with peak BRDF values close to those estimated by the earlier methods for highly reflective surfaces. The BRDF data can be integrated over the  $2\pi$  solid angle to give the corresponding total integrated scatter (TIS).

### 6.2.2.4 Total Integrated Scatter versus BRDF

The Mie scatter data of Young gives BRDF as a function of off-specular angle. Inspection of these data reveals that the BRDF rapidly decreases over the range of 0 to  $10^\circ$ , and then follows a pseudo-exponential law for larger angles. To a reasonable approximation, the data for large angles ( $> 20^\circ$ ) are given by:

$$\text{BRDF} = 5.4 \times 10^{-5} \times (\text{level})^5 \times \exp(-8.91 \times 10^{-2} \times \text{degrees}) / \lambda^2$$

By integrating Young's data for BRDF versus off-specular angle over a  $2\pi$  solid angle, the TIS can be obtained. A simple graphical integration gives:

$$\text{TIS} = 2.2 \times 10^{-2} \times \text{BRDF}(0^\circ), \text{ or } \text{TIS} = 5.5 \times 10^{-15} \times (\text{level})^5 / \lambda^2$$

with  $\lambda$  in microns. Note that for  $\text{BRDF}(0^\circ) > 45.5$ , this implies that the total scatter is greater than the input, which is obviously nonsense. The conclusion is that for the larger degrees of scatter, the BRDF versus angle data must change its form, versus the lower cases (Young only presented data for contamination levels of 500 and below). Indeed, Mie scatter calculations show that as the craters (or particles) become larger, the scatter becomes ever-more forward scattered into small angles. Thus, the small-angle peak BRDF values increase faster than the "wings" of large angle scatter. Consequently, the TIS slowly asymptotes towards unity for very bad scatter, while the peak BRDF continuously increases. Thus, extrapolation of Young's data becomes suspect for large degrees of scatter. Clearly, the estimates of scatter for the RAM surface, quoted above, are within this uncertain region. Figures 6-24 and 6-25 illustrate the relationship between TIS and peak BRDF for both moderate and large cases of scatter, as obtained from Mie-SPENV code for space impacts. TIS is linear with BRDF, for the moderate case, but is nonlinear for large scatter. The proportionality is almost identical to that deduced from the data of Young (i.e.,  $\text{TIS} = 2.1 \times 10^{-2} \times \text{peak BRDF}$ ) for the small scatter case.

All of the above presupposes that the optic behaves as if a metallic mirror with simple hemispherical craters. In reality, many mirrors (or lenses) are made of dielectrics and employ multiple thin layers (quarter-wave optical phasing logic). These materials are usually brittle. Upon hypervelocity impact, the damage consists of irregular craters with conchoidal surfaces, surrounded by star-cracks which can extend up to about 100 times the size of the impacting particle. To assess the optical scatter for these conditions it will be necessary to invoke the theory of dielectric needles as done by Van de Hulst (Ref. 16). Present analysis indicates that the cracks represent only a small total area compared to the craters and surface spalls. Further, narrow cracks are inefficient scattering sites. Hence the preliminary conclusion is that the craters and surface spalls dominate the optical scatter.

### 6.2.2.5 General Comments on Scattering Predictions/Measurements

Thus far, all the analyses have presupposed that pseudo-hemispherical craters in an optical surface scatter light in a similar manner to that for spherical particles on the surface. While Mie scatter theory is exact for spherical particles it is very difficult to apply for nonspherical particles, because of the lack of symmetry in the boundary conditions. Specifically, the issue of "equivalence" between craters and particles has not been demonstrated and presently remains a first-order assumption. However, it is probably a reasonable assumption. Measurements of optical scatter are notorious for their lack of consistency. Measurements made using independent BRDF or TIS instruments rarely obtain identical results for a given sample measurement, and the disagreements can range from minor to significant. These variations can be a consequence of differences in the equipment optical beam diameters, differing detector sizes, beam power fluctuations, detector sensitivity, etc. Since even measurements of scatter can be inconsistent, it is most unlikely that predictions of scatter can ever be considered very accurate. Rather, all such predictions should be viewed as indicating probable trends.

The predictions of scatter from craters are in addition to any other scatter mechanism, whether due to actual contamination on the surface or due to surface morphology (e.g., rms roughness). Surface roughness and/or small particle contamination usually gives wide large-angle "wings" to the BRDF data, whereas the larger, fewer, craters tend to scatter mostly into smaller angles close to specular reflection. Further, although standard optical scatter theory assumes that BRDF is inversely proportional to the operational wavelength squared, it is known that some materials do not display this behavior, with beryllium mirrors being an example (the observed large-angle scatter reduces much slower than expected as the wavelength increases due to a complex, poorly understood, interaction of the anisotropic crystal surface morphology and the optical skin depth).

Lastly, it should be emphasized that the present scatter predictions do not accurately handle the case of cratering in thin-layer coated optics. The assumption at present is that for

craters much deeper than the layer stack thickness only the substrate properties should be included to predict scatter. This approach is incorrect for the many smaller craters with depths comparable to the stack thicknesses.

### 6.2.3 Parametric Scatter Calculations

A parametric series of peak BRDF optical scatter predictions have been done for a series of orbits ranging from 400 km to 2000 km altitude and with inclinations of 0, 30, and 60°. For all these cases the mission time periods are 1996 to 2002, and the assumed operational wavelength is 5.0  $\mu\text{m}$  (BRDF varies with the inverse square of the wavelength), and the optic is assumed to have an area of 100  $\text{cm}^2$ . In addition, BRDF has been computed for the specific case of LDEF. Figure 6-26 shows the results for LDEF. The data are given for the micrometeoroids and debris independently and are plotted as a function of the angular position from RAM (0°) in the plane parallel to the Earth's surface (i.e., RAM, SIDES, and TRAIL). On the left vertical axis are also plotted the scatter for the SPACE and EARTH facing surfaces. In all cases each surface was assumed to have a full  $2\pi$  view for impacts (i.e., no local telescope tube shielding).

For LDEF the predictions show that the micrometeoroids contribute the most to the overall scatter. The data also clearly indicate the very small degree of optical scatter for the EARTH looking surface. The scatter value for the SPACE looking surface is about  $4.2 \times 10^{-2}$  (per steradian). The data demonstrate that for angles greater than about  $\pm 35^\circ$  from RAM the scatter is always less than for the SPACE end, while for angles less than this the scatter is worse for the near-RAM surfaces and peaks on that surface with a value of about  $7.8 \times 10^{-2}$ .

Data were recently presented at the LDEF 2<sup>nd</sup> Symposium (San Diego, CA) by Linda Dehainaut (Ref. 17) of BRDF measurements on bare fused silica samples. The observed values ranged from  $2.45 \times 10^{-7}$  to about  $3.85 \times 10^{-2}$  (near the impact sites), with a mean value of about  $10^{-5}$ . These values are comparable to the peak ones computed for LDEF given here, if the low

reflectivity of fused silica is taken into account. The exact optical scatter behavior of craters in fused silica is not yet fully understood. The predictions essentially assume craters in a metallic reflector, whereas fused silica has only about 4 percent reflectivity, and the scatter should scale with the reflectivity, all other factors equal. For example, if the sample had a coefficient of refraction of 1.0 (i.e., it wasn't an optic) then scatter would be totally independent of surface morphology, and obviously also 0.

Figures 6-27 through 6-38 show the predictions as functions of altitude and inclination for nonshielded optics. As the altitude increases, the debris scatter increases rapidly up to the 800 -1000 km range (where debris dominates toward the RAM), and then gradually decreases for higher altitudes. However, there is a local peak in the debris at about 1500 km. The debris-induced scatter is always worse for the higher inclinations. The scatter due to micrometeoroids is independent of orbit inclination and slowly increases with altitude (below 2000 km). The SPACE surface suffers from a constant degree of scattering independent of both inclination and altitude. There is a very large range of predicted peak BRDF values, from a high of 0.56 (800 km, 60°, RAM) to a low of 0.072 (400 km, 0°, RAM).

Figures 6-39 through 6-41 show the predictions for some options which include telescope shrouds, for the cases of 30, 60 and 80° of "exclusion angle" for an orbit at 1600 km and 60° inclination. The "exclusion angle" is the angle measured from the surface of the optic which prevents direct impacts on the optic due to the telescope wall.

For a circular optic of 100 cm<sup>2</sup>, the diameter is 11.28 cm (4.44 inch). Thus, for exclusion angles of 30, 60, and 80° the telescope wall must have a length of 6.51, 19.54, and 64 cm, respectively.

Note the odd trend of the data as the exclusion angle increases. While the micrometeoroid-induced scatter merely decreases monotonically versus this angle, the debris-induced scatter is observed to drop rapidly for the RAM and to display a local peak at about 20°

off-RAM. The explanation for this behavior lies in the "butterfly" plots for the polar diagram of debris flux versus the spacecraft velocity vector. The Kessler model predicts that the debris approaches the RAM surface in the form of two off-RAM lobes. When the exclusion angle is small (i.e., we have  $2\pi$  viewing), the impacts on the surface involve an integral over both the lobes. However, when this angle is large (viewing angle small) the telescope effectively differentiates the lobes. Thus, the "hole" in the RAM direction reveals itself, and the peak scatter corresponds to the optic looking directly into one of the lobes.

As can be seen, the use of telescope shrouding can dramatically reduce the scatter predictions provided a sufficiently large exclusion angle is involved. For a  $30^\circ$  exclusion angle, the RAM BRDF is only reduced from 0.24 to 0.20; for a  $60^\circ$  exclusion angle the reduction is from 0.24 to 0.013; while for an  $80^\circ$  exclusion angle the reduction is from 0.24 to  $9 \times 10^{-5}$  (at  $20^\circ$  off-RAM), all for the same orbit of 600 km altitude and  $60^\circ$  inclination. However, the use of a large exclusion angle implies a reduced field of regard for the optic. Hence to overcome the latter it would be necessary to maneuver the entire telescope tube. Systems which rely on pan-tilt mirrors cannot use large exclusion angles, else the field of view would include looking "at" the telescope tube itself.

The use of "exclusion angles" in this manner addresses only the case of direct impacts on an optic. However, it is possible to have indirect hits. For example, an impactor could hit the inside of the telescope tube (including a baffle) and cause secondary ejecta to hit the optic. Likewise, for a thin-walled tube an impactor could completely perforate the wall and again generate ejecta. If the "target" material is one which produces copious secondary debris (e.g., Martin Black is notorious for this effect, releasing many micron-sized surface particles when subject to mechanical shock) then it is possible for this debris to again cause at least a contamination problem on the optic (this debris is mostly of low velocity and thus unlikely to cause much in the way of actual crater damage). However, most targets do not produce such debris: rather they merely throw off material in the "normal" manner of impact cratering. In the

## 6.2, Analysis of Crater Effects on Optics

---

latter case the resulting blow-off is usually of smaller sizes than the original impactor, although the total mass is larger than the impactor.

The previously used logic for optical scatter indicates that scatter increases with the fourth (4<sup>th</sup>) power of the particle diameter. Thus, for a given mass, the scatter will be low provided the mean particle size is much smaller than the original impactor. This follows immediately from:

$$\text{BRDF} = \text{constant} \times N \times D^4, \text{ and } M = \text{constant} \times N \times D^3$$

Thus,

$$\text{BRDF} = \text{constant} \times M^{4/3}/N^{1/3}$$

where M is the total mass and N is the number of particles. Hence for a given mass of blow-off the scatter decreases as the number of individual particles involved increases. Thus, under most circumstances, it is anticipated that secondary ejecta optical scattering is less important than that due to the (initial) direct impacts.

## 6.3 CONCLUSIONS FOR M&D IMPACT EFFECTS ON OPTIC

The present conclusions are that the major effect of M&D impacts on optics is to produce an increase in scatter, but only minor changes in reflectivity and/or transmission. The scatter increases as the impact crater sizes increase and as the areal density of impacts increases. The effect is nonlinear with the size of the optic. The larger the optic the more likely a large crater will occur resulting in more induced scatter for the large optic. Also the increase in scatter is nonlinear with mission time. As time increases, the probability of an impact by a larger particle also increases, which causes the optical scatter to increase in a supralinear manner. The scatter is dominated by crater formation rather than by crack generation. Soft targets (e.g., metals and



### *6.3, Conclusions for M&D Impact Effects on Optics*

---

plastics) will produce the largest craters. Hard targets (glasses and ceramics) produce smaller pure craters; however, these craters are frequently surrounded by larger surface spalls giving the effect of larger shallow craters. Multilayer optics can also suffer from delamination effects around the impact sites, which produce large local changes in reflectivity or transmission and scatter.

The degree of scatter depends on the orbit (altitude, inclination and time) and on the pointing direction. RAM is usually the worst direction to point while EARTH is usually the best (safest) direction.

The use of telescope shrouding can significantly reduce the scatter provided the angle for entry of particles is small. This is at the expense of the optical field of regard.

Experiments have been performed (Ref. 18) to compare impact damage in optics with the induced scatter. These data are being compared with both theory and the results from LDEF. The HYPER plasma-drag gun was used at Auburn University, Alabama, to throw particles at various optics. Optical scatter measurements also are being performed. Three types of samples (1 inch diameter) were used: aluminum (2000 Å) coated fused silica,  $\text{Si}_3\text{N}_4$  (600 Å) coated aluminum, and a 15-layer quarter-wave (tuned to 1.06  $\mu\text{m}$ ) stack of alternating  $\text{Si}_3\text{N}_4$  and  $\text{SiO}_2$  layers on a fused silica substrate. The impactors were olivine and alumina of sizes 50 - 100  $\mu\text{m}$  diameter, and the impact speeds were in the range of 8 - 12 km/s. On average, there were about 10 impacts per sample.

Control samples were placed in the HYPER facility, but without firing any particles, to check for overall background contamination. Pre- versus post-test measurements of TIS indicated no large contamination problems (e.g., at levels of  $\text{TIS} \leq 0.01$ ). For the impacted samples the increase in TIS was significant, increasing by factors of 10x to 100x. Post-test analysis of specific samples using the Mie-SPENV code for the known craters (numbers and sizes) gave predictions within factors of about 5 those measured. This work is ongoing and will be

### *6.3, Conclusions for M&D Impact Effects on Optics*

---

completed by the end of 1993. Comparisons with the LDEF data are still in progress, and will be completed as part of this work.

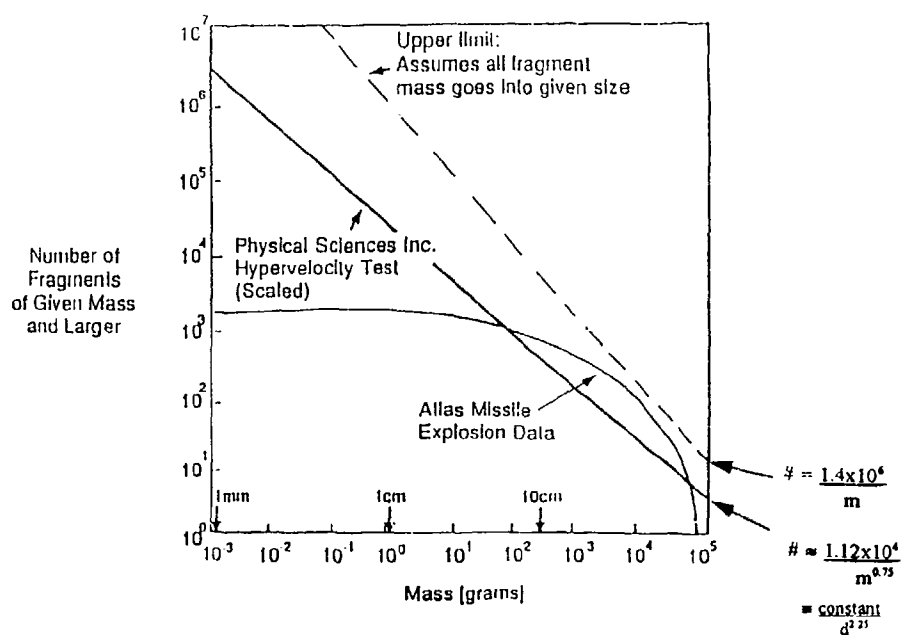


Figure 6-1: Expected Number of Fragments From the Breakup of a 1400kg satellite

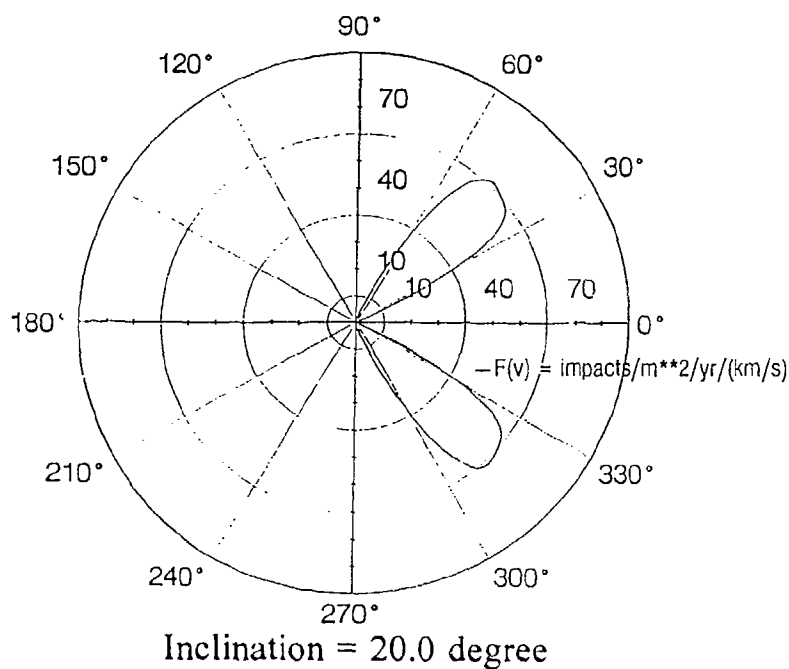


Figure 6-2: Kessler f(v) Function (20°)

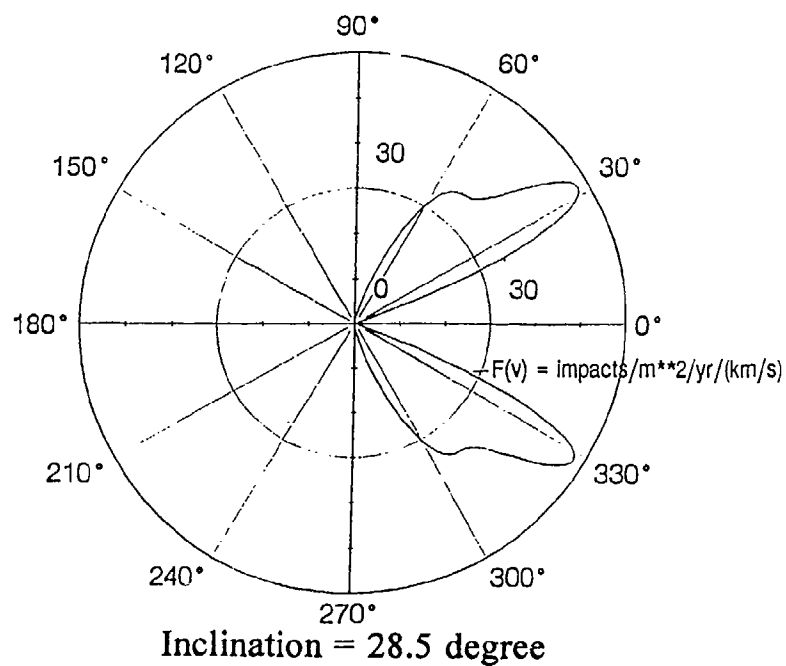


Figure 6-3: Kessler  $f(v)$  Function (28.5°)

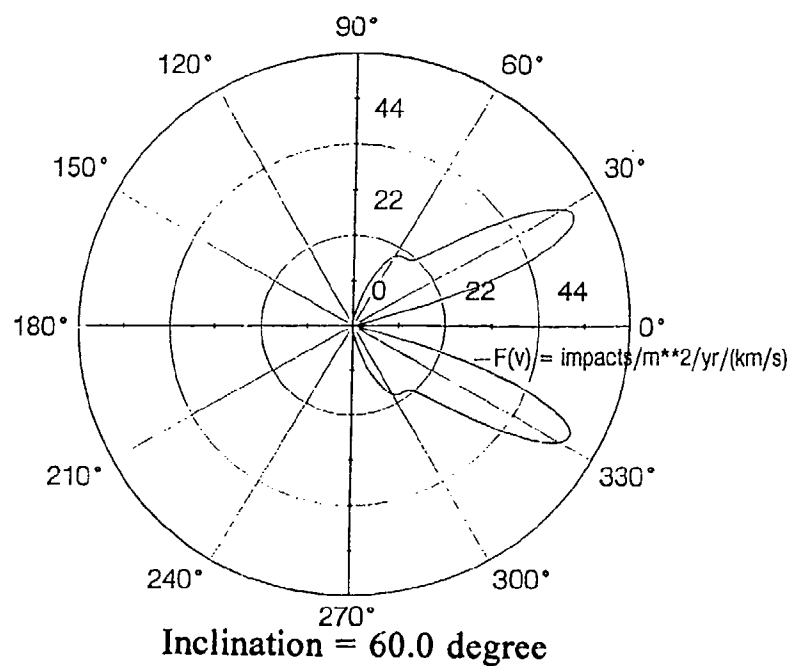


Figure 6-4: Kessler  $f(v)$  Function (60°)

## CRATERS VERSUS IMPACTS

- LDEF Data Mostly Craters or Perforations
- Data in Form of Cumulative Craters for  $\geq d_c$
- To Convert Craters to Impacts Need  $\frac{d_c}{d_p}$
- Simple Law Used  $\frac{d_c}{d_p} = k \left( \frac{\rho_p}{\rho_t} \right)^{1/3} v^{2/3}$

where  $\rho_p$  = particle density  
 $\rho_t$  = s/c target density  
 $v$  = collision speed  
 $k$  = normalized to Al/Al impacts

- $\frac{d_c}{d_p}$  is Orientation Dependent
- For Perforations  $\frac{d_c}{d_p} \sim 1$  for thin foils

Figure 6-5: Craters Versus Impacts

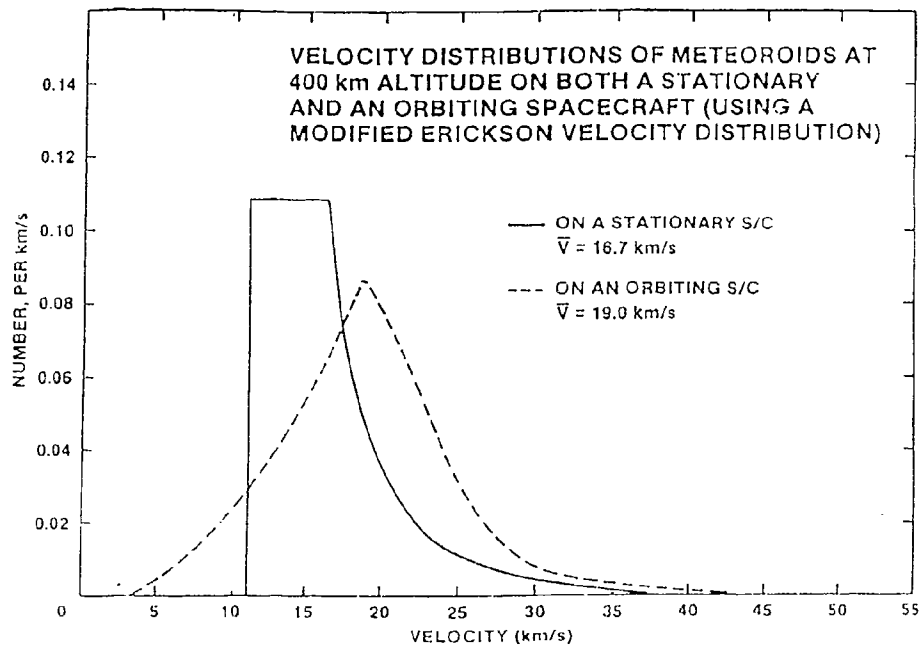


Figure 6-6: Velocity Distributions of Meteoroids

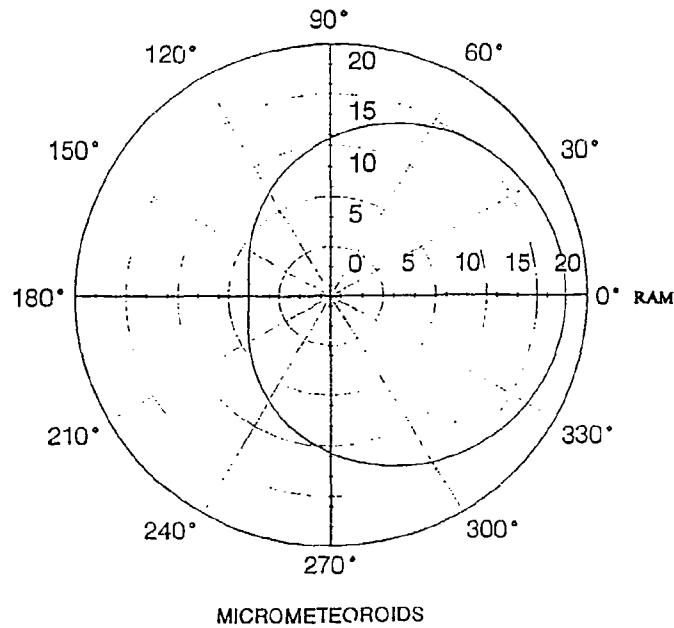


Figure 6-7: Average Velocity vs Polar Angle

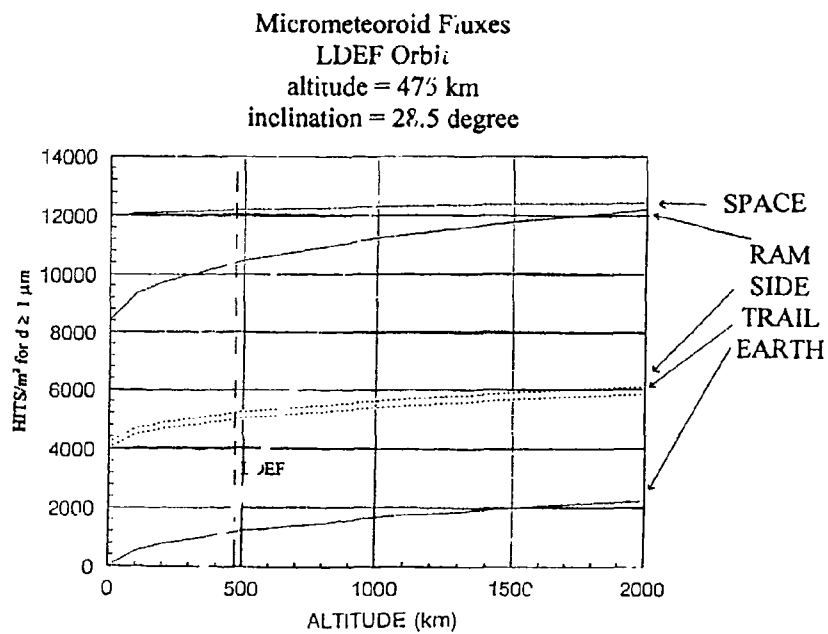


Figure 6-8: Micrometeoroid Fluxes

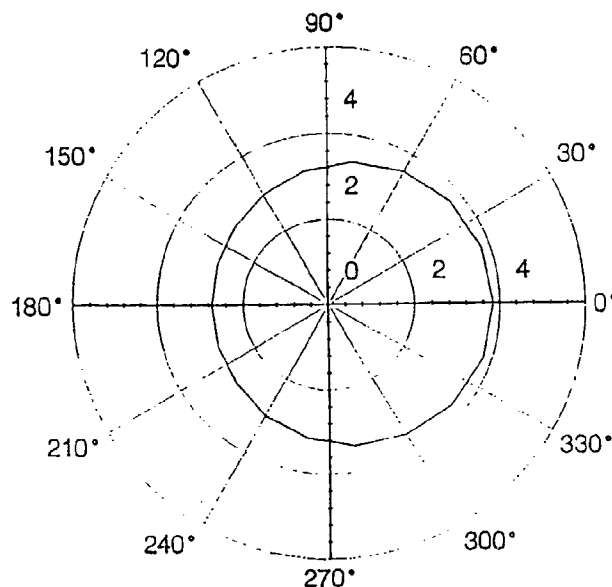


Figure 6-9: Ratio Crater/Particle Diameter vs Angle from RAM for Micrometeoroids

Comparison of LDEF Data to Model Predictions  
352 Degrees From Ram Direction: 5.75 Years Exposure  
Impacts On Aluminum Surface

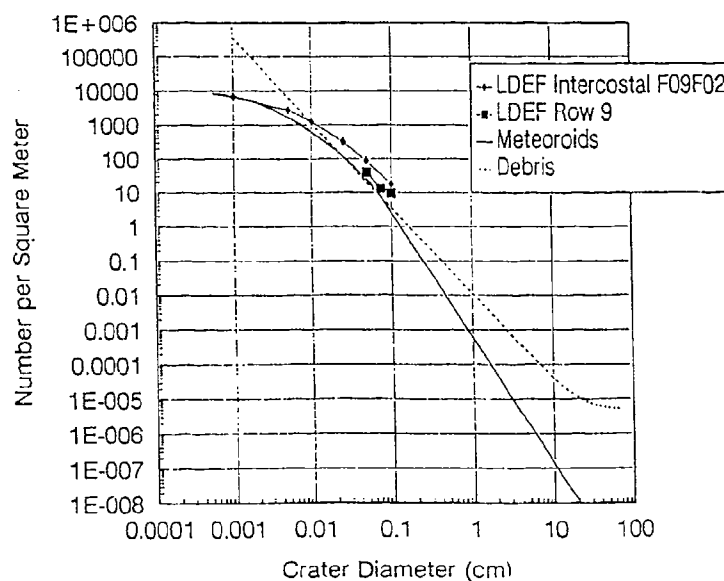


Figure 6-10: Comparison of crater diameters to number of craters per square meter.  
Data collected from the LDEF intercostals and rows. 352 Degrees from RAM Direction

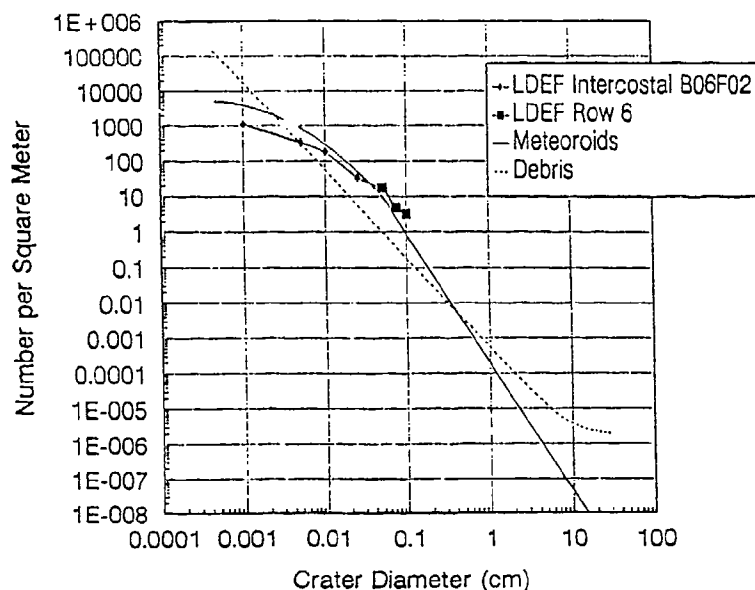


Figure 6-11: Comparison of crater diameters to number of craters per square meter. Data collected from the LDEF intercostals and rows. 262 Degrees from RAM Direction

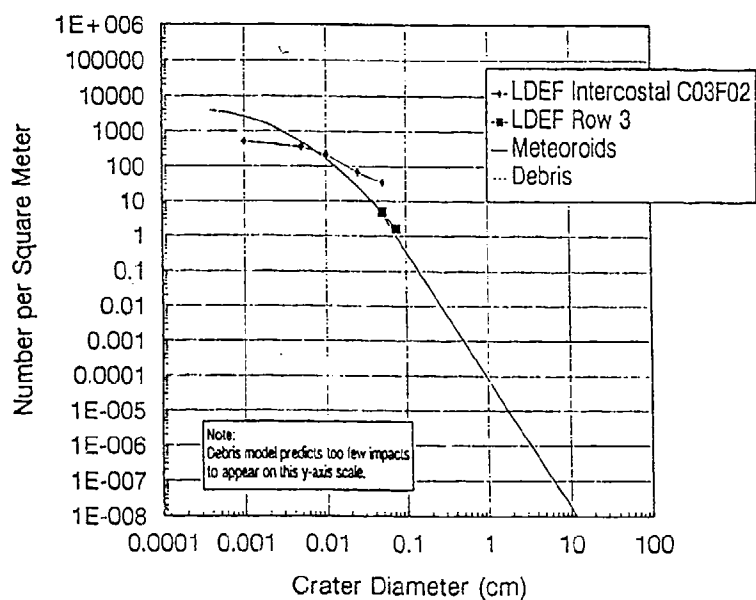


Figure 6-12: Comparison of crater diameters to number of craters per square meter. Data collected from the LDEF intercostals and rows. 172 Degrees from RAM Direction



Comparison of LDEF Data to Model Predictions  
82 Degrees From Ram Direction: 5.75 Years Exposure  
Impacts On Aluminum Surface

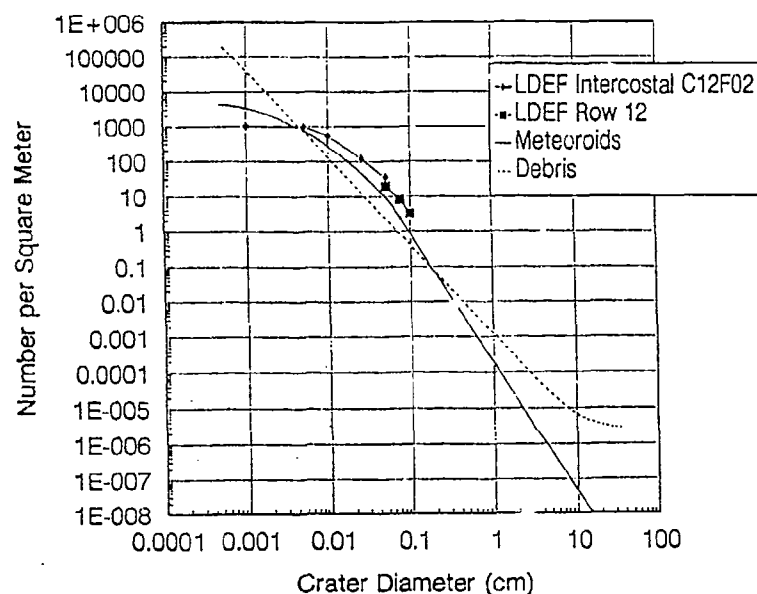


Figure 6-13: Comparison of crater diameters to number of craters per square meter. Data collected from the LDEF intercostals and rows. 82 Degrees from RAM Direction

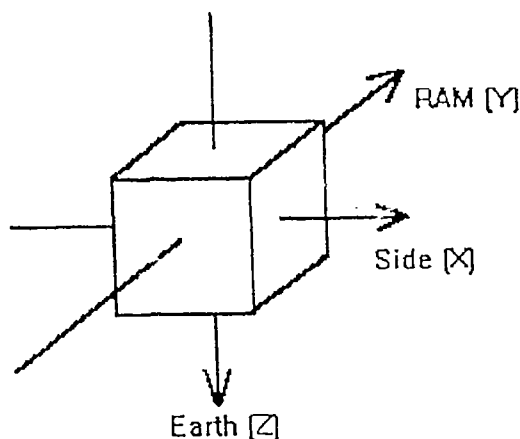


Figure 6-14: Coordinate system for standard satellite directions

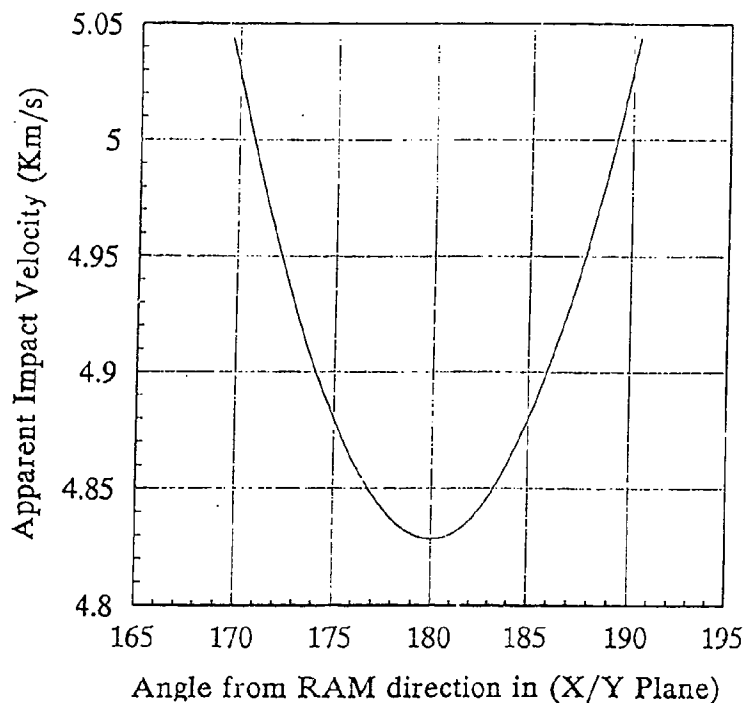


Figure 6-15: Apparent Impact Velocity of Elliptic orbits with a Circular orbit at 475 Km Inclined at  $28.5^\circ$  Maximum angle of hits in circular orbit:  $51.375^\circ$ .

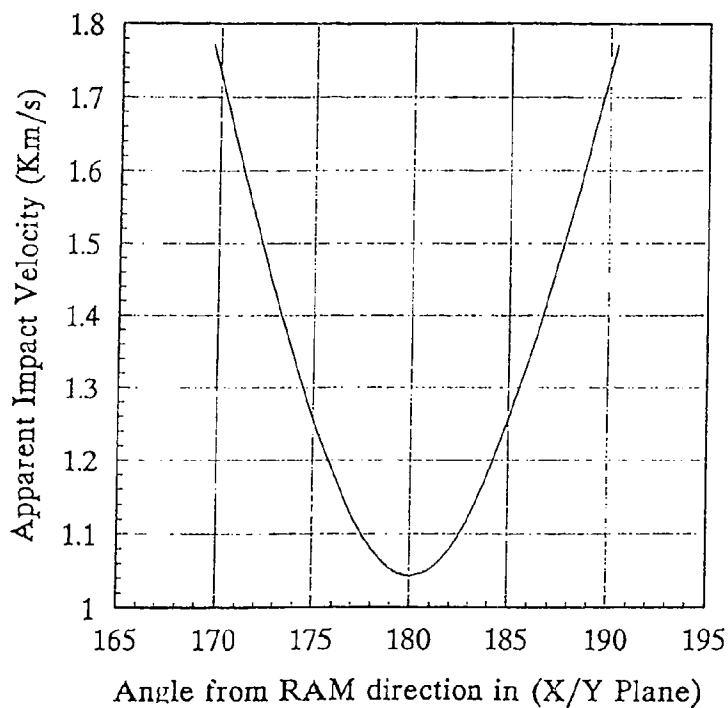


Figure 6-16: Y-Component of Impact Velocity of Elliptic orbits with a Circular orbit at 475 Km Inclined at  $28.5^\circ$  Maximum angle of hits in circular orbit:  $51.375^\circ$ .

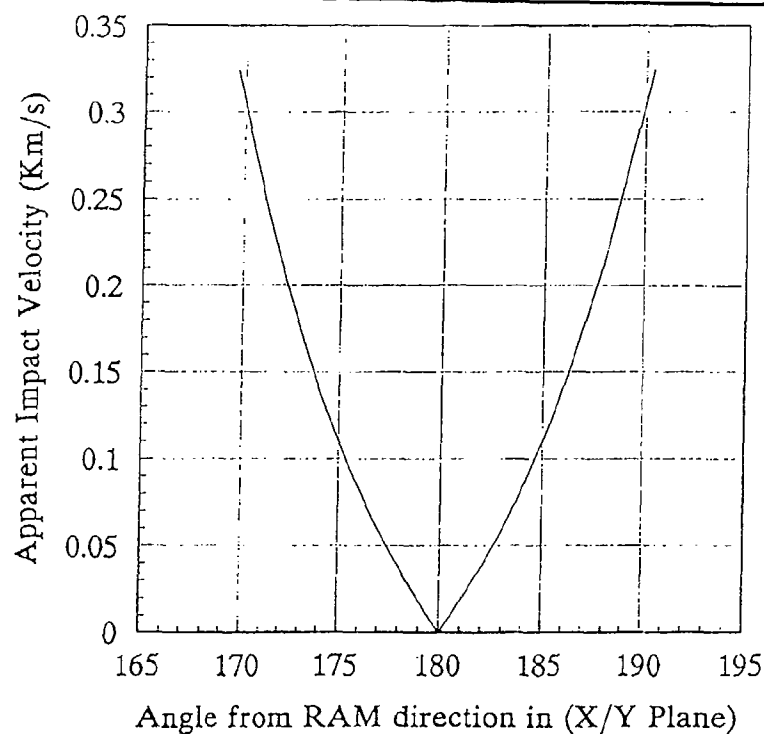


Figure 6-17: X-Component of Impact Velocity of Elliptic orbits with a Circular orbit at 475 Km Inclined at 28.5° Maximum angle of hits in circular orbit: 51.375.

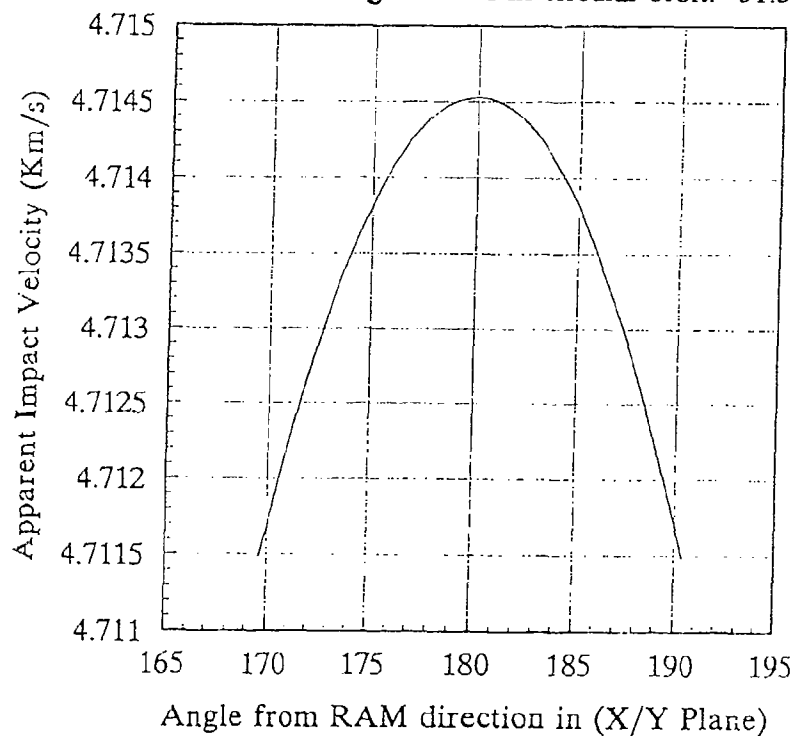


Figure 6-18: Z-Component of Impact Velocity of Elliptic orbits with a Circular orbit at 475 Km Inclined at 28.5° Maximum angle of hits in circular orbit: 51.375.

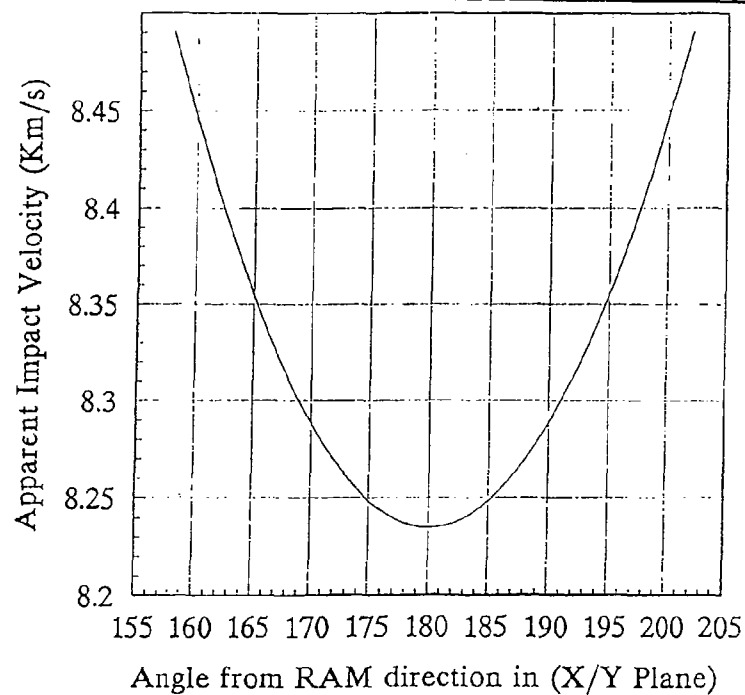


Figure 6-19: Apparent Impact Velocity of Elliptic orbits with a Circular orbit at 1600 Km Inclined at 60° Maximum angle of hits in circular orbit: 110.8.

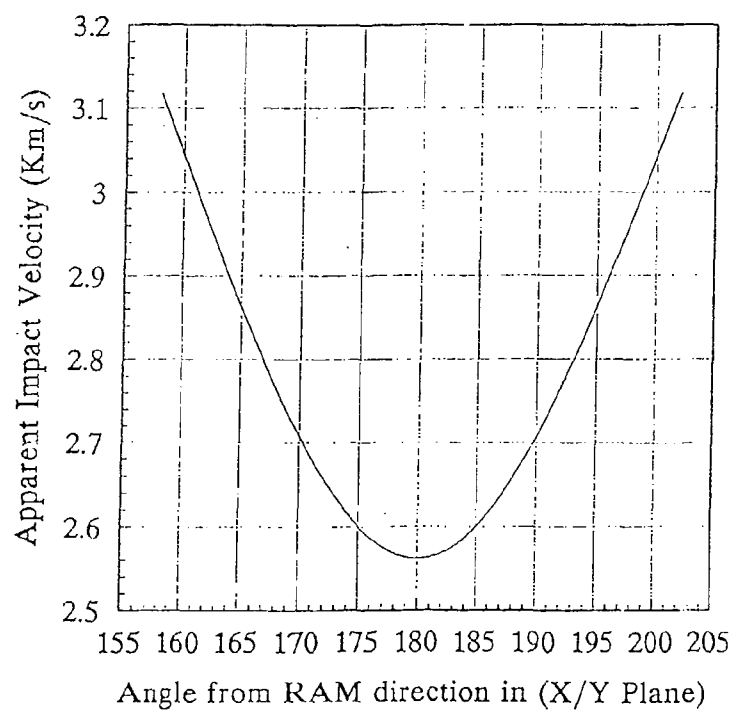


Figure 6-20: Y-Component of Impact Velocity of Elliptic orbits with a Circular orbit at 1600 Km Inclined at 60° Maximum angle of hits in circular orbit: 110.8.

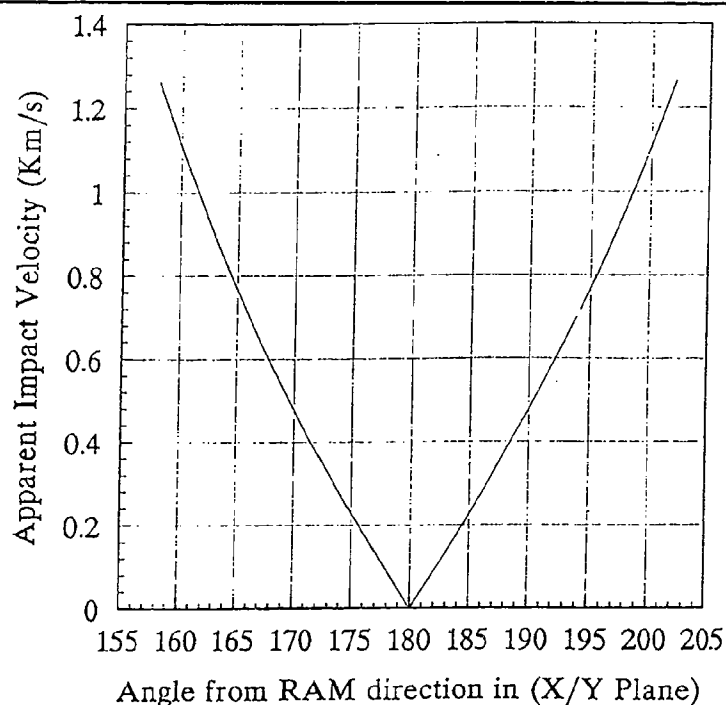


Figure 6-21: X-Component of Impact Velocity of Elliptic orbits with a Circular orbit at 1600 Km Inclined at 60° Maximum angle of hits in circular orbit: 110.8.

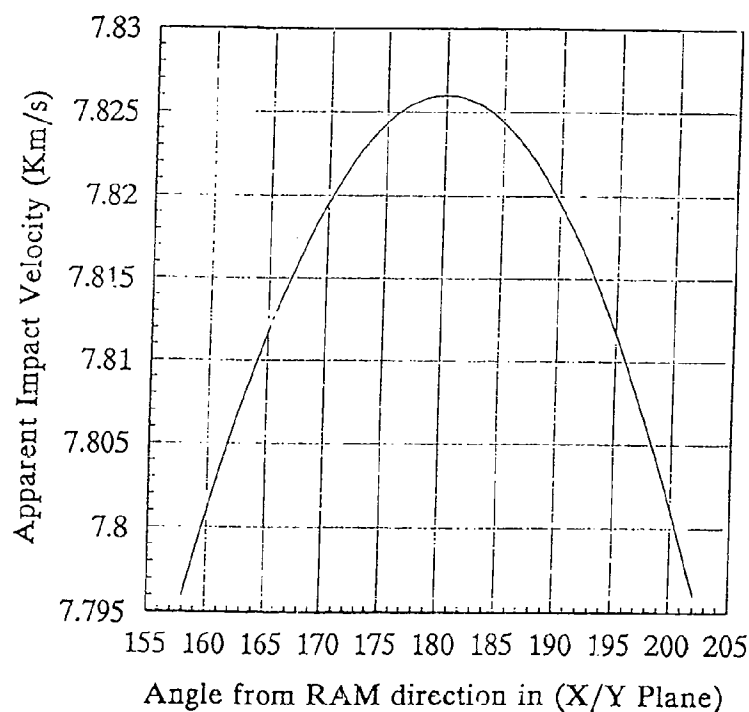


Figure 6-22: Z-Component of Impact Velocity of Elliptic orbits with a Circular orbit at 1600 Km Inclined at 60° Maximum angle of hits in circular orbit: 110.8.

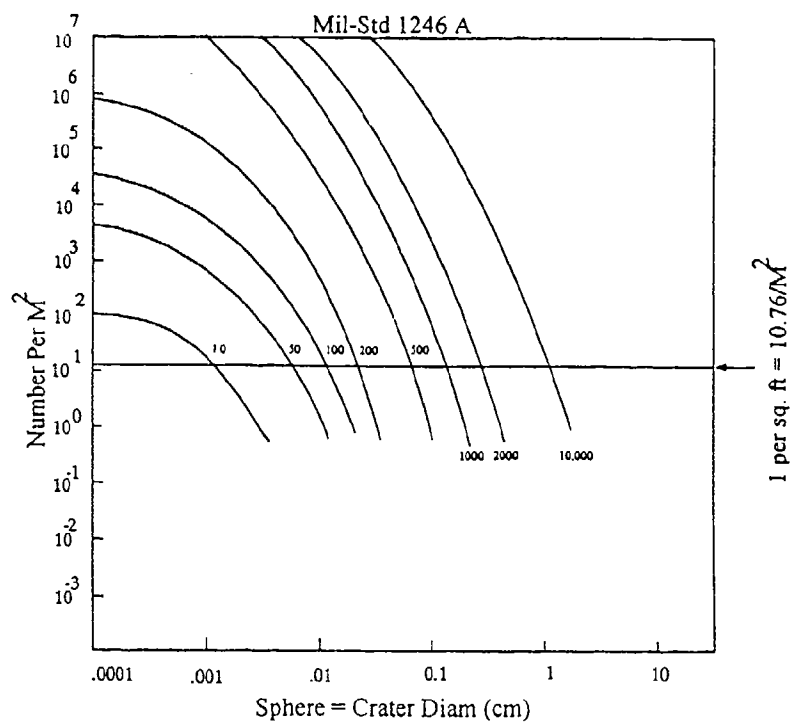


Figure 6-23: Definition of Mil-Std 1246A

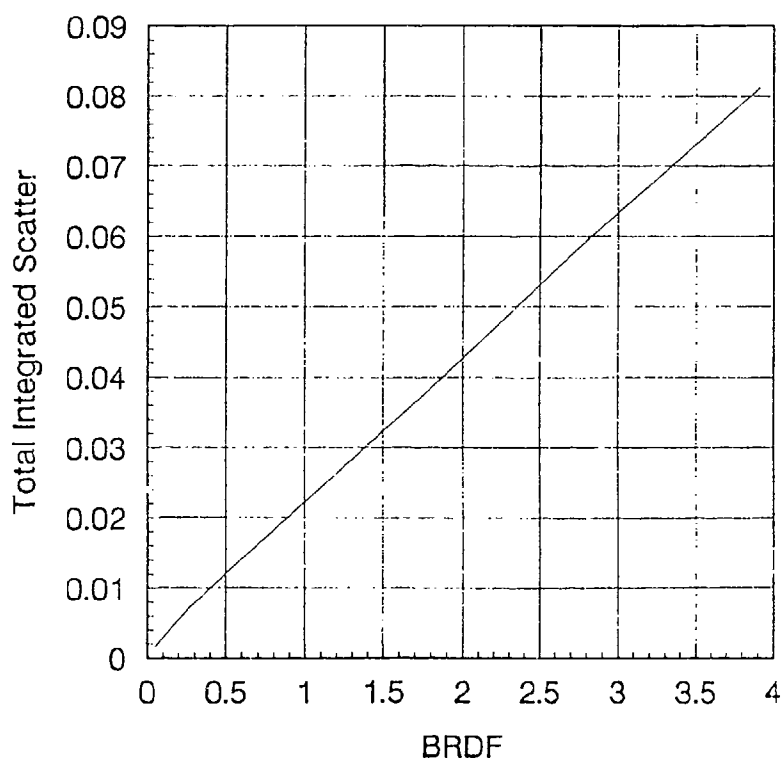


Figure 6-24: TIS vs BRDF

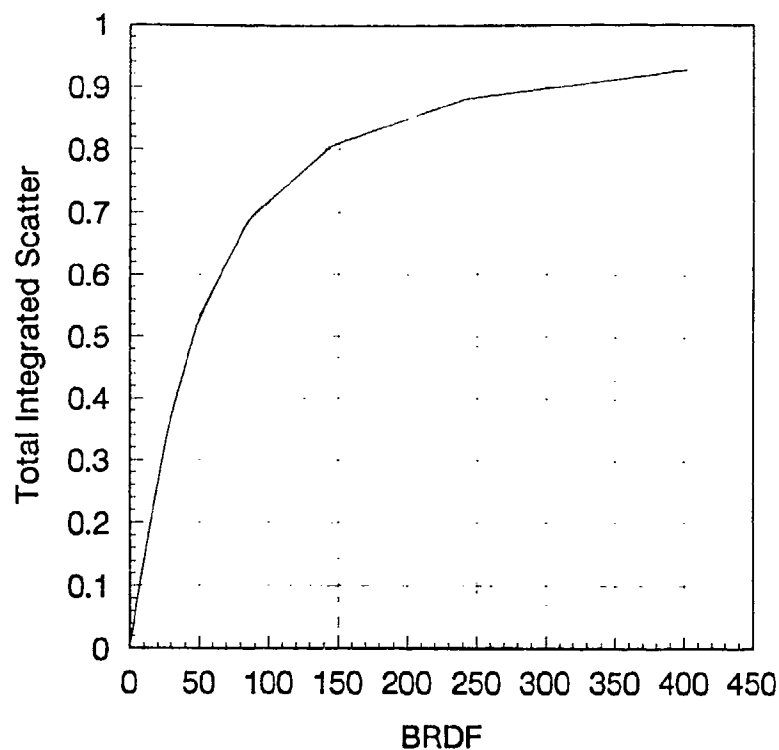


Figure 6-25: Total Integrated Scatter vs BRDF

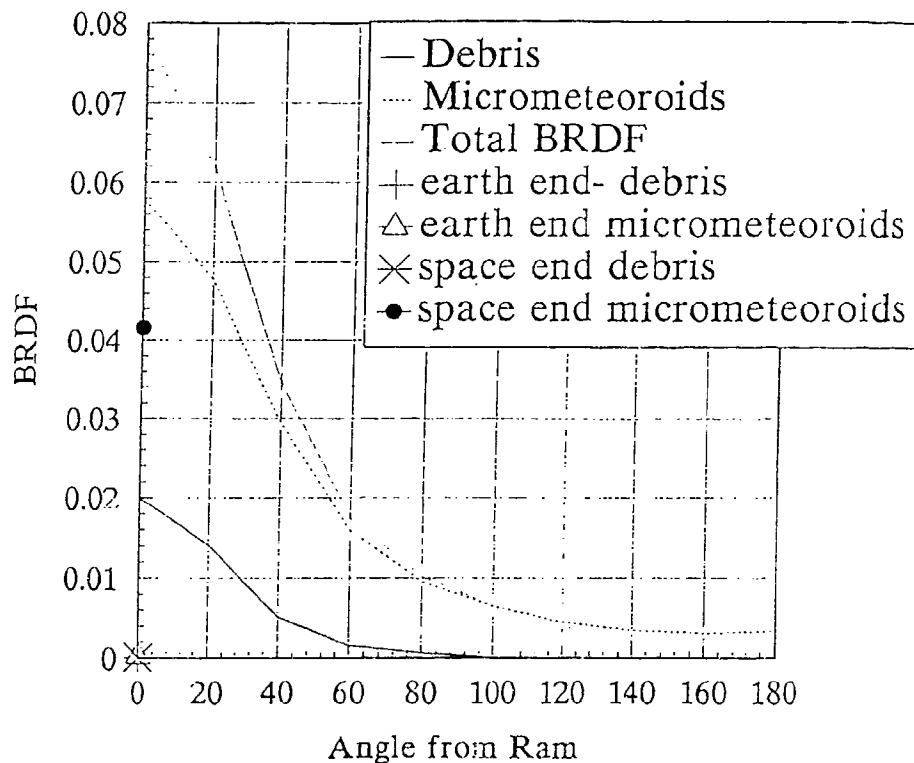


Figure 6-26: Variation in BRDF with Angle from RAM LDEF

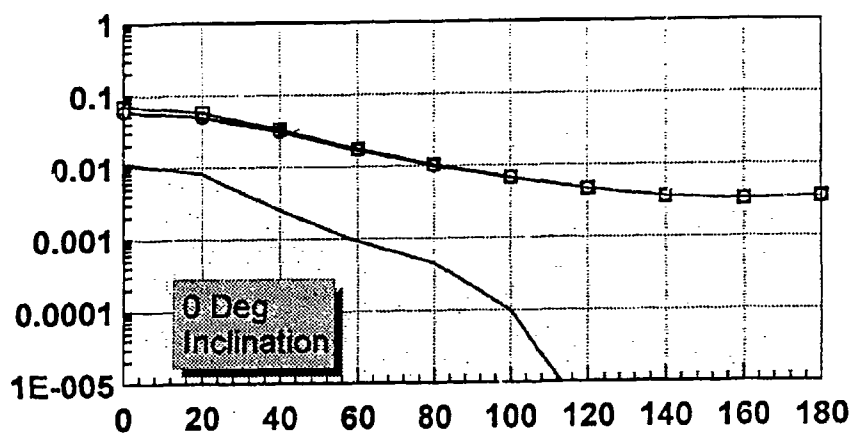


Figure 6-27: Variation in BRDF with Angle from RAM at 400km (0° - Inclination)

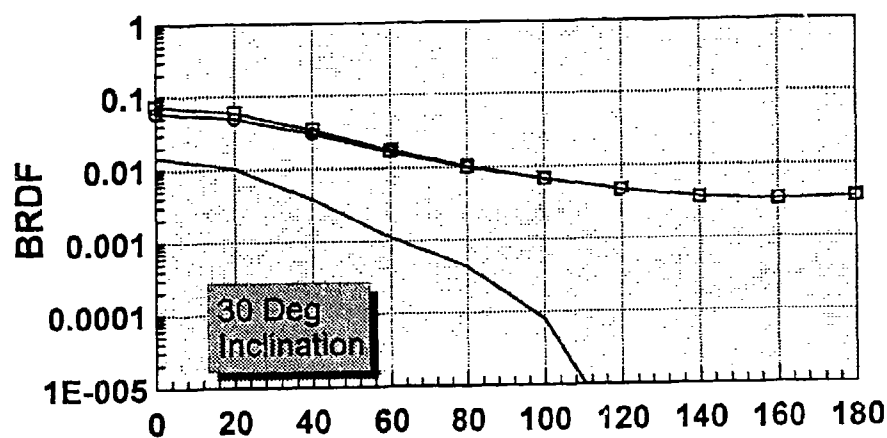


Figure 6-28: Variation in BRDF with Angle from RAM at 400km (30° - Inclination)

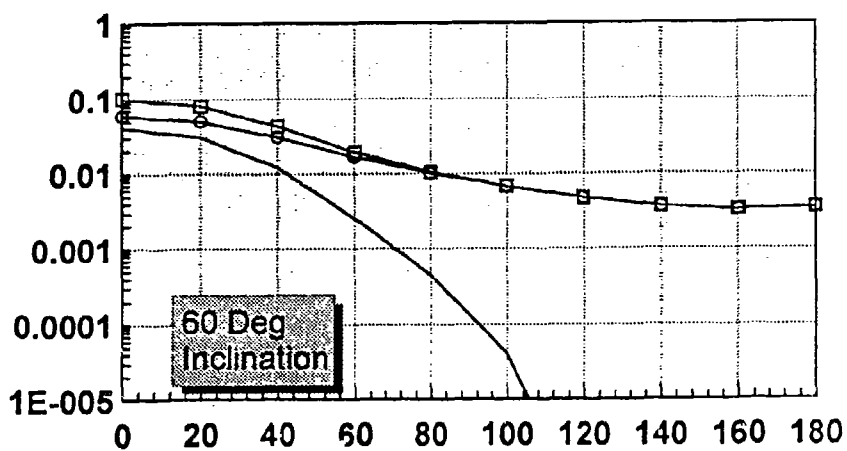


Figure 6-29: Variation in BRDF with Angle from RAM at 400km (60° - Inclination)



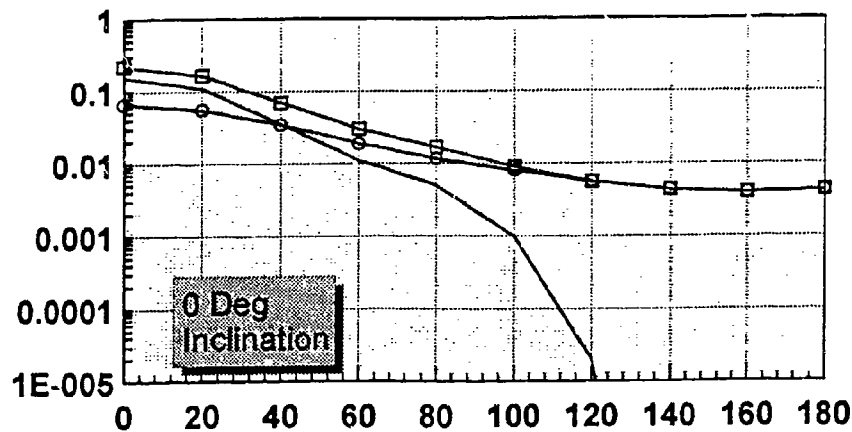


Figure 6-30: Variation in BRDF with Angle from RAM at 800km (0° - Inclination)

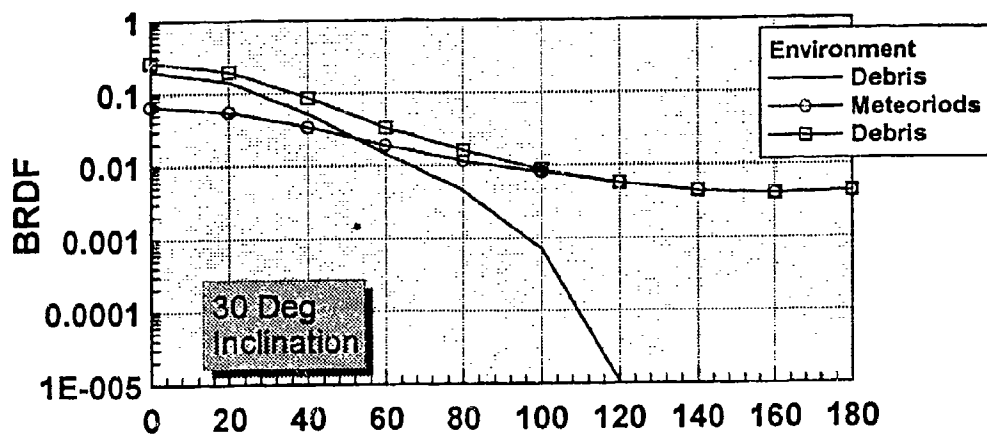


Figure 6-31: Variation in BRDF with Angle from RAM at 800km (30° - Inclination)

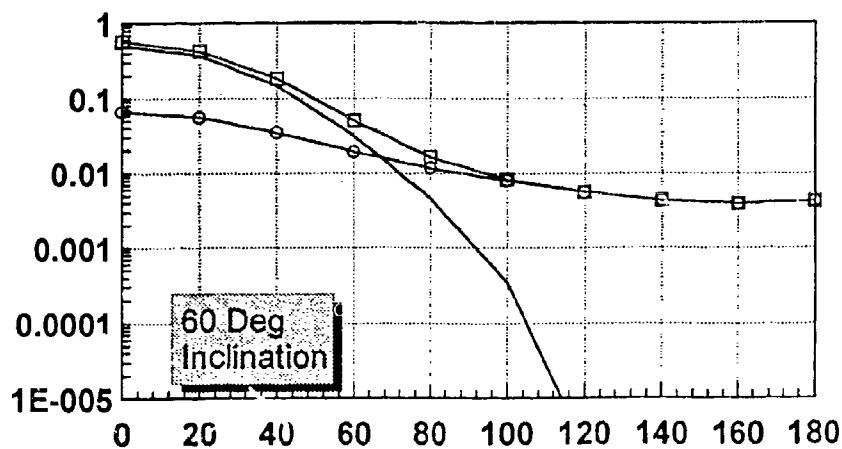


Figure 6-32: Variation in BRDF with Angle from RAM at 800km (60° - Inclination)

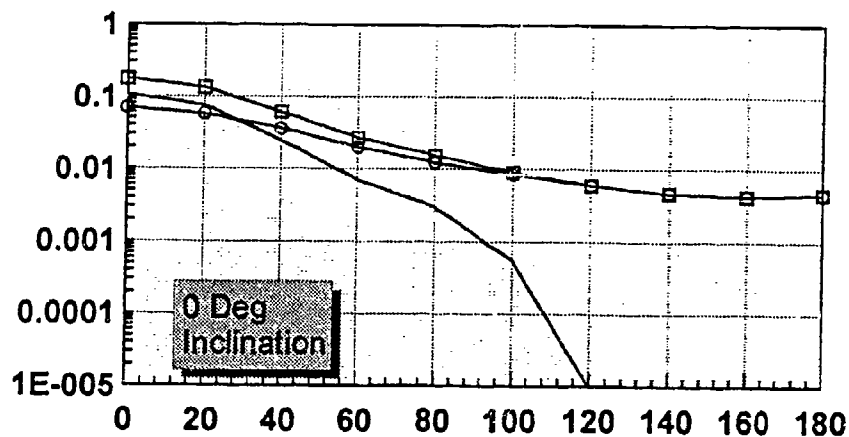


Figure 6-33: Variation in BRDF with Angle from RAM at 1000km (0° - Inclination)

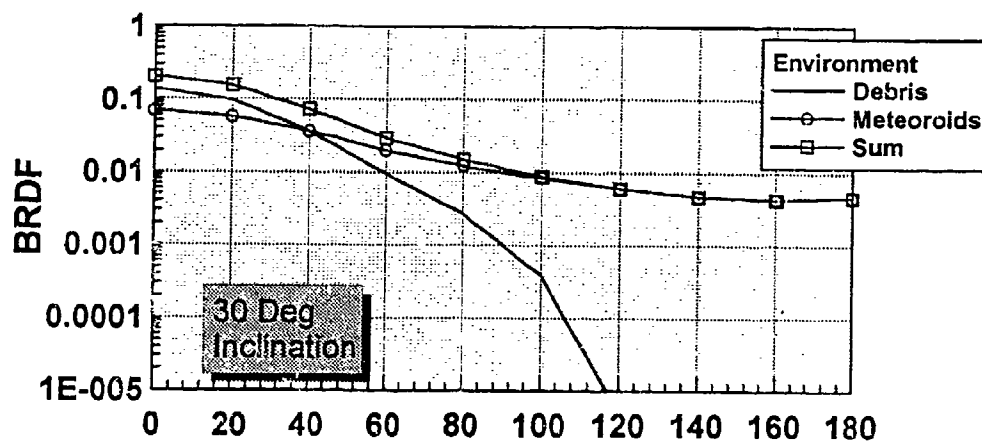


Figure 6-34: Variation in BRDF with Angle from RAM at 1000km (30° - Inclination)

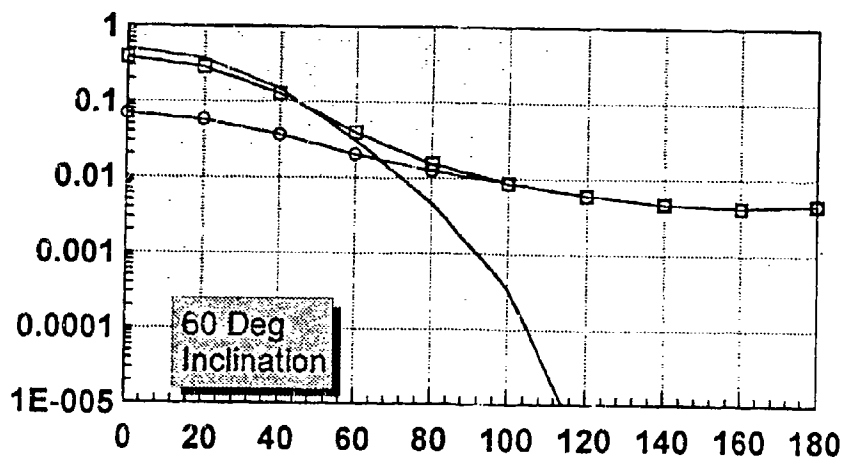


Figure 6-35: Variation in BRDF with Angle from RAM at 1000km (60° - Inclination)

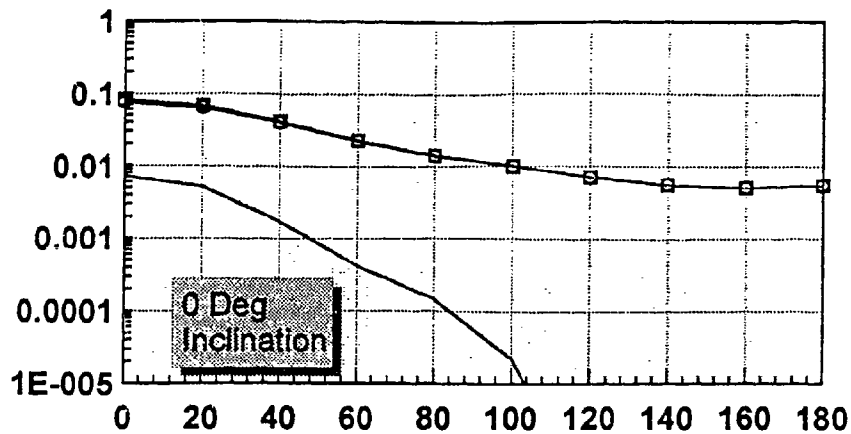


Figure 6-36: Variation in BRDF with Angle from RAM at 1600km (0° - Inclination)

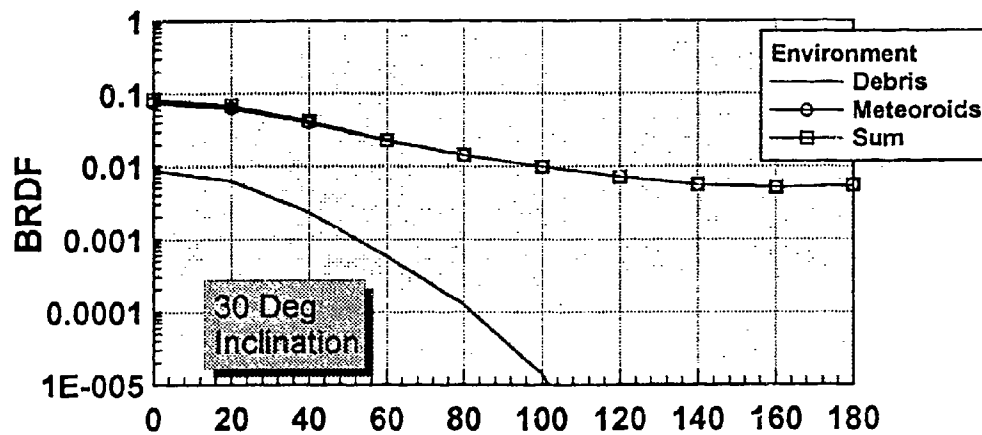


Figure 6-37: Variation in BRDF with Angle from RAM at 1600km (30° - Inclination)

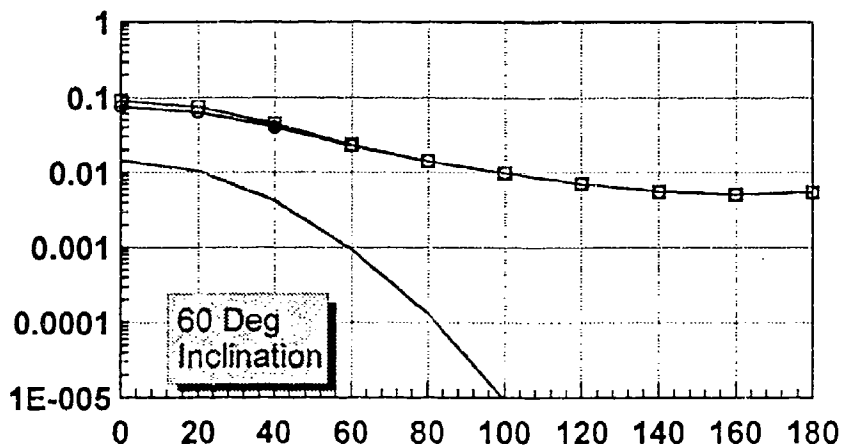


Figure 6-38: Variation in BRDF with Angle from RAM at 1600km (60° - Inclination)

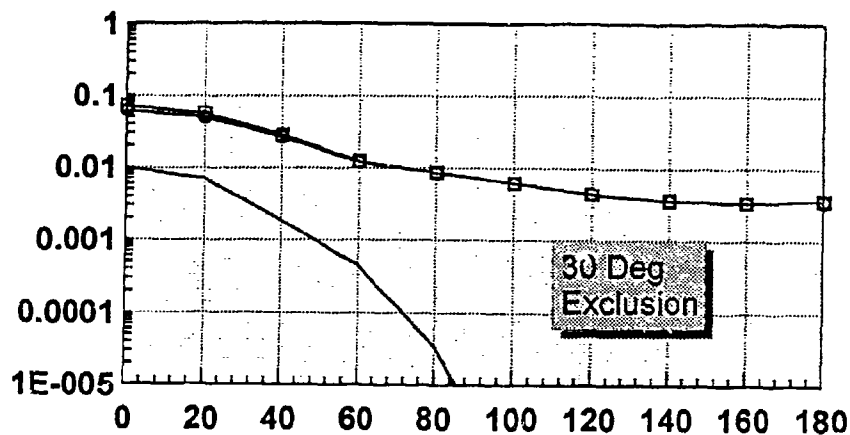


Figure 6-39: Variation in BRDF with Angle from RAM at 1600km and 60° Inclination (30° Telescope Exclusion Angle)

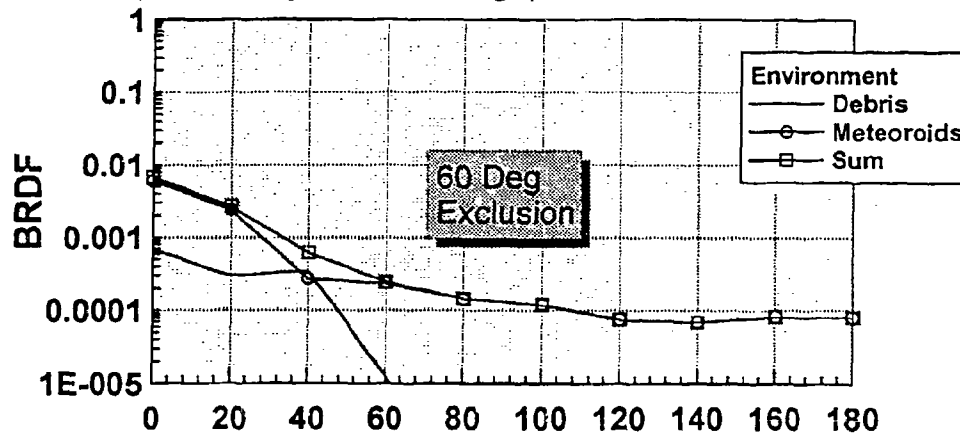


Figure 6-40: Variation in BRDF with Angle from RAM at 1600km and 60° Inclination (60° Telescope Exclusion Angle)

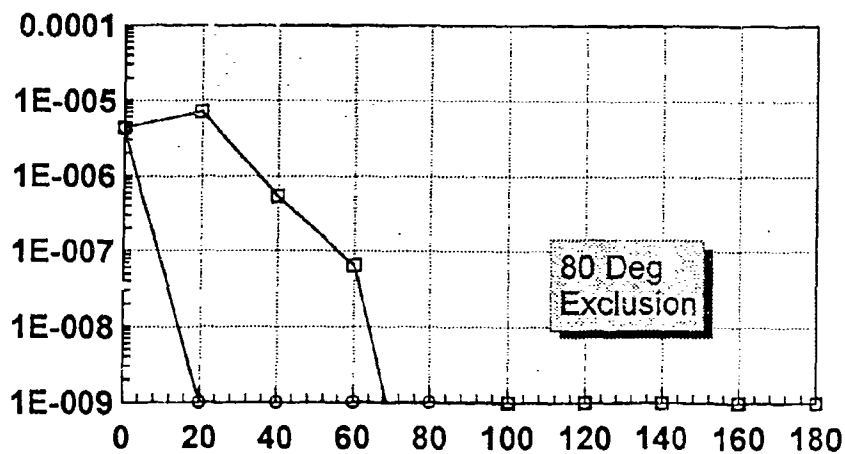


Figure 6-41: Variation in BRDF with Angle from RAM at 1600km and 60° Inclination (80° Telescope Exclusion Angle)



## CHAPTER 7

### SPACE EFFECTS ON FIBER OPTIC SYSTEMS AND COMPONENTS ORBITED ON THE LDEF

With the rapid development of photonics technology devices during the past few decades and a plethora of lightwave systems emerging, certain fundamental issues remain regarding the applicability of the technology to the rigors of the space environment. Some facets of photonic technologies have recently been successfully demonstrated in space. For example, the first demonstration of the capability of active FO systems to operate in a prolonged space orbit was achieved with the Phillips Laboratory Fiber Optics Space Demonstration, Experiment #701 "Space Environment Effects on Fiber Optic Systems." Deliberate and prolonged orbital exposure of the experiment's four operating fiber optic data transmission systems aboard NASA's Long Duration Exposure Facility (LDEF) proved conclusively that early 1980's era fiber optic systems could successfully withstand adverse space environmental effects. These effects included wide and frequent temperature cycling, AO scavenging, exposure to UV radiation, micrometeorite and debris impactors, and space radiation doses ranging to 25 krad (Si). Figure 7-10 shows the condition of the experiment shortly after LDEF recovery.

Recovered by the shuttle Columbia in December 1990, the optical fiber systems aboard PL Exp #701 continue to function to this date. Future space demonstrations of fiber and other photonic technologies will be concerned with incorporating much of the knowledge learned from this key experiment's active and passive fiber optic technologies. The content of this chapter will briefly summarize the lessons learned and data gathered from PL Exp #701 and other LDEF-orbited experiments conducted by: Georgia Tech Research Institute; Jet Propulsion Laboratory; the Boeing Co.; and other DoD organizations. Information regarding the results of analyses of Experiment A0138-7, "Optical Fibers and Components," has not been made available. For completeness, this experiment by CERT/ONERA-DERTS has been included in Table 7-1, but not discussed within this chapter.

Throughout this handbook, reference is made to the various space-induced adverse environments, including temperature and radiation effects. Valuable detail can be found in Chapters 3 through 5 regarding solar-induced effects, AO effects, and micrometeorite and debris impactor phenomena. The optical fiber systems and components aboard the LDEF experienced a wide variety of space environmental effects because of their different locations and shielding geometries. Table 7-1 briefly summarizes some of the measurements achieved in the FO experiments. While this table is rather brief, it illustrates that the early demonstration of fiber optic systems, subsystems, and components in prolonged LEO were divided into several categories regarding operational parameters and space exposure geometries. These included active systems (M0004 and M0003-8) and passive systems and components (M0004, S0109, S0050, M0006 and A0138-7). Not all of the experiments nor all of the experimental components were space exposed. For example, only the active cabled FO links were space-exposed on the M0004 Experiment, while the light emitting diodes (LEDs), PIN photo diodes (PINs), and connectors used to power the experiment were contained within the shielded tray volume. Similarly, Experiment S0109 contained no sources or detectors to actively drive the space exposed cabled optical fibers of this experiment. A second active experiment (M0003-8) by the Boeing Co. studied single and multi-contact connectors, but was not space-exposed since the experiment was shielded from the direct space environment. Only a few of the many passive components contained on Experiment S0050 were directly exposed to the space environment, while on Experiment M0006, a bundle of 1800 passive optical fibers was space-exposed over a period of approximately 11 months.

## **7.1 EXPERIMENTAL CONFIGURATIONS AND FIBER OPTIC SYSTEMS AND COMPONENT EXPOSURES TO THE SPACE ENVIRONMENT**

### **7.1.1 PL Experiment #701 (M0004) - Space Environmental Effects on Fiber Optic Systems**

The discussion of PL EXP #701's performance aboard the LDEF mission is perhaps the most complete knowledge to date of the space performance of several types of different optical fibers in an operational system configuration. As an example of the FO technologies studied aboard LDEF, the data resulting from this active experiment will be highlighted.

PL Exp #701 was designed as a feasibility demonstration for FO technology in space applications, and to study the performance of operating fiber systems exposed to space environmental factors such as galactic radiation and wide temperature cycling. Four active digital FO links were directly exposed to the space environment for a period of 2,114 days. The links were situated aboard the LDEF with the cabled, single fiber windings atop an experimental tray containing instrumentation for exercising the experiment while in orbit. Despite the unplanned and prolonged exposure to trapped and galactic radiation, wide temperature extremes, AO interactions, and micrometeorite and debris impacts, in most instances, the optical data links performed well within the experimental limits. Analysis of the recorded orbital data clearly indicates that fiber optic applications in space will meet with success. Tests and analysis of the experiment at the PL's Photonics Research Group are continuing. This is the first known and extensive database of active FO link performance during prolonged space exposure. PL Exp #701 is widely acknowledged as a benchmark accomplishment that clearly demonstrates, for the first time, that FO technology can be successfully used in a variety of space applications.



#### 7.1.1.1. Optical Transmission Measurements

Following orbital deployment by the shuttle *Challenger*, the experiment was activated and performed the first of its scheduled 76 optical data transmission measurements (Refs. 1, 2, and 3) for the planned year in orbit. Thirty measurements were performed in the first 6 months at intervals of 6 days, while the remaining 46 measurements were performed at 4-day intervals over the second half of the year. Shown in Figure 7-1 is a block diagram of measurement circuitry. Figure 7-2 illustrates a portion of the electronic/optoelectronic layout.

Two basic tests were conducted on each space exposed FO link by the circuitry as represented in Figure 7-1. The first of these tests was designed to measure the signal strength and, hence, Signal-to-Noise Ratio (SNR), of each digital FO link. This test is referred to as a "Burst Error Run." A 10-bit pseudo-random generator was used to generate a digital stream of "data" for the measurements. The receivers were AC coupled and the data were bipolar, non-return-to-zero (NRZ) format. The experiment used a model developed by Gilbert (Ref. 4) to examine the bit stream for errors.

In the SNR measurements, the voltage from the optical receivers was compared to a "threshold voltage." A high-speed comparator used this threshold voltage to decide if the signal from the optical receivers was a logical "1" or a logical "0." Initially, the error counters were cleared, the threshold was set to zero volts, and a "packet" of 130,944 bits was passed through the FO link. The data stream from the optical receivers were compared to a reference signal from the pseudo-random generator. If there were less than 128 independent (Type I in the Gilbert model) errors in the data passed through the FO link, the experiments incremented the threshold voltage by 1.25 mV. The error counters were subsequently reset to zero, and another packet of 130,944 bits was passed through the link, and error measurements were made again. This process continued until at least 128 independent errors were detected in a packet of 130,944 bits. At that point, the experiment recorded into RAM the values of the error counters and the number of times that the threshold voltage was incremented. The

### *7.1, Experimental Configurations and Fiber Optic Systems and Component Exposures to the Space Environment*

---

experiment then conducted the SNR measurements on the next link in the sequence, until all four links had been examined.

Following the SNR measurements, the experiment began the burst error runs. In this mode, the threshold voltage at the comparator was held constant at 0 volts. Since the receivers were AC coupled, 0 volts was the optimal threshold for the system. That is, for any given signal strength, 0 volts was a threshold and would have resulted in the fewest possible errors in the data stream. The error counters were reset to 0 at the beginning of the BER for each FO link, but they were not cleared between successive packets of 130,944 bits. With zero volts as the threshold, a packet of 130,944 bits was passed through the link. If less than 128 independent errors accumulated, the experiment passed another 130,944-bit packet through the FO link. The process continued until either 128 (or more) independent errors accumulated, or a total of  $10^9$  bits had been passed through the link. When either of these conditions was met, the experiment recorded into RAM the values of the error counters and the number of bit packets that had been passed through the link. The BER measurement was then conducted on the next FO link in the sequence, until all four links had been examined.

After the BER measurements, the experiment transferred the data stored in RAM to the Experiment Power and Data System (EPDS). The EPDS gave the data a "time stamp" and recorded the data to magnetic tape. Both the Data Processor Control Assembly (DPCA) and the Magnetic Tape Memory (MTM) units of the EPDS functioned properly during the entire mission and have continued to work in post-flight testing.

#### **7.1.1.2. In Orbit Temperature Cycling Measurements**

Prior to performing the SNR and BER measurements, the experiment controller directed the measurement of temperatures at eight thermistor locations within the experiment tray volume (Fig. 7-3). These temperatures were valuable in studying the optical fiber

### *7.1, Experimental Configurations and Fiber Optic Systems and Component Exposures to the Space Environment*

---

performance. However, it must be realized that the temperature measurements were made at the very beginning of the four FO link performance runs. Therefore, as much as 30 minutes could have elapsed between the temperature measurements and the last BER measurement.

The time stamp assigned to each experiment reflected the end of that data taking period. By examining the performance of each link, it was possible to determine the total time elapsed for completing the entire experiment run. If a link was greatly degraded in performance for a particular run, then the time required to evaluate the link was significantly reduced. The experiment controller would then proceed to examine the next link.

Therefore, under this scenario, the maximum time required to fully sequence each of the four links was less than 31 minutes, bringing the temperature measurements in time proximity with the link performance measurements. Thus, the temperature gradient, or change, was minimized for the special case where a link was highly degraded in performance and the data run was truncated.

Discerning the orbital beta-angle (Ref. 5) during the periods of experiment operation was very important, since the temperature variations can be accounted for and correlated to the on-board PL Exp #701 thermistor measurements. Since the LDEF orbital period was approximately 94 minutes, the actual tray temperature may have changed significantly during many of the data runs. For example, the experiment could have passed from the daytime space exposure condition to the daytime sun exposure condition, or vice-versa, or other variations, in the 30-minute sequencing interval, changing conditions under which the link measurements were performed.

Therefore, the results reported herein must be qualified due to these possible transient conditions. An accounting and correlation between LDEF thermal data (Refs. 5 and 6) and the PL Exp #701 thermistor measured data was performed and Figure 7-4 illustrates a partial

## ***7.1, Experimental Configurations and Fiber Optic Systems and Component Exposures to the Space Environment***

---

analysis of this situation, while Tables 7-2 and 7-3 give the typical temperatures and thermistor locations recorded for the inner tray volume.

### **7.1.1.3. Brief Analysis of On-Orbit Recorded Optical Fiber Transmission Data**

Shown in Figures 7-5, 7-6, 7-7, and 7-8 are the performance data for the four FO links described in Table 7-4. The data indicate that links #3 and #4 experienced approximately 1.0 Db and 0.2 Db deviation, respectively, in SNR measurements during the first year in orbit. The reduction of SNR data in links #1 and #2 is also shown.

An example of cabling influence resulting in these responses and on the ability of optical fibers to perform in space can be seen in Figures 7-6 and 7-7. Here, two identical plastic-coated silica fibers were cabled using different technologies that were available at the time that the experiment was designed. FO link #2 used a loose-tube configuration, which theoretically allowed a fiber encased by the loose tube to experience a greater degree of freedom than that of a tightly wrapped fiber, such as found in FO link #3. The intent in the loose-tube configuration was to lessen micro- and macro-bending losses induced by cabling restrictions or flexing. However, the data indicated the conformal fiber performance far exceeded that of the loose-tube configuration.

### **7.1.1.4. On-Orbit Radiation Dosimeter Measurements**

Another objective of PL Exp #701 involved the study of the trapped and galactic radiation effects on the four space exposed FO link performance. Several studies have been conducted on LDEF received doses (E. V. Benton, *Analysis of Dosimeters Aboard LDEF Exp M0004*, 26 Jun 90 and 29 Aug 90 - Unpublished reports). The selection of optical fibers over the period 1978-1982, for inclusion in the experiment, was based upon the best known

### *7.1, Experimental Configurations and Fiber Optic Systems and Component Exposures to the Space Environment*

---

technology at the time of the experiment fabrication, and on the results of radiation sensitivity experiments that were performed (Refs. 7-11) on a variety of candidate and PL Exp #701 optical fibers. Table 7-5 contains a listing of the space exposed fibers and a short description of their characteristics.

In order to measure the accumulated dose and spectrum of the space radiation environment, both thermo-luminescent dosimeters (TLDs) and plastic nuclear-track detectors (PNTDs) were located within the experimental tray volume. This inclusion of the detectors on PL Exp #701 constituted a cooperative arrangement between the University of San Francisco and the PL Exp #701 project office. Comparisons of the radiation dose received by PL Exp #701 and other experiment can be found elsewhere (Ref. 12).

The TLDs and PNTDs were enclosed in a sealed container and co-located within the EPDS shielded volume (Fig. 7-9). Each was mounted on a separate 45° wedge, with their inclined surfaces facing 90° with respect to each other. This orientation was chosen to optimize the various shielding directions experienced within, and exterior to, the tray volume. A complete description of the composition of the TLD and PNTD materials may be found elsewhere.

The results of an interim analysis based on a 1-D shielding model indicated that the space exposed optical fibers experienced a total dose varying from 238 rad(Si), to 25 Krad(Si), depending on shielding provided by the fiber cabling materials and hold down clamps. The analysis accounts for boundary conditions of lightly shielded fibers (typically 0.01 to 0.05 g/cm<sup>2</sup>) to substantial shielded portions of the fiber, particularly those portions under the hold-down clamps (1.06 g/cm<sup>2</sup>; Fig. 7-10). The fiber doses resulted primarily from geomagnetically-trapped electrons, since the galactic cosmic ray contribution was estimated to constitute (Ref. 12) approximately 1 to 3 percent of the trapped proton dose at typical shielding (greater than 1 g/cm<sup>2</sup>). Therefore, for a shielding of less than 1.0 g/cm<sup>2</sup>, trapped

### 7.1, Experimental Configurations and Fiber Optic Systems and Component Exposures to the Space Environment

---

electrons dominate the surface-absorbed dose (Ref. 12). Shown in Table 7-5 is an analysis performed for predicting ranges of doses experienced by the FO links.

While the optical fiber links were calculated to have received a substantial dose over the 2,114 days in orbit, no direct evidence of permanent induced radiation damage has been observed to date. As may be seen in Figure 7-4, the external tray temperature - extrapolated from the internal measurements and calibrations - ranged from approximately +57° C to -29° C. The fibers orbited in this experiment were known to possess good radiation annealing properties, enhanced by elevated temperatures. Optical power levels present in the fiber links during the first year in orbit (typically 30  $\mu$ W) would have significantly contributed to any photo-induced annealing (photo-bleaching). The one notable exception to this early prediction involves Fiber Link #1. However, while radiation induced damage is not ruled out, more probable causes for the observed losses include micro- and macro-bending effects, fiber pistoning, and/or connector caused misalignments. All of these effects can be explained by temperature dependence and are currently under investigation.

Thus, as a result of this early analysis, it is concluded that no permanent effects due to space-induced radiation occurred in the external FO links. The same rationale may be used to predict any expected radiation damage for the passive fibers within the tray volume, and also the light-emitting diode sources and the pin photodiode detectors (all currently under investigation). The doses received by these components are currently being correlated with the TLD and PNTD calibrations. For example, an interim analysis (E. V. Benton, *Analysis of Dosimeters Aboard LDEF Exp M0004*, 26 Jun 90 and 29 Aug 90, Unpublished Reports) determined that the experiment tray shielding (minimum of 2.4 g/cm<sup>2</sup>) resulted in a high LET data of 0.88 mrad(Si)/day (total dose of 1.86 rad(Si)) with measured integral flux of  $3.6 \times 10^4$  cm<sup>-2</sup> s<sup>-1</sup> sr<sup>-1</sup> (for LET Si  $\geq$  50 MeV cm<sup>2</sup> g<sup>-1</sup>). The TLD doses varied from 100 times to 125 times the LET dose, or 186 - 233 rad(Si). The FO components used in the experiment would not have been expected to be affected at these levels since they were pretested prior to launch

at 200 krad(Si) to 1 Mrad(Si) levels and showed little (approximately 0.6 Db) permanent damage.

#### **7.1.1.5. On-Orbit Micro-Meteorite and Debris Impacts**

Shown in Figure 7-11 is a photograph of one section of the experiments' surface. This surface, which provided shielding for the EPDS, measured 0.41 m x 0.91 m and was composed of a 1 mm thick aluminum alloy (6061-T6) and was painted with Chemglaze (A276). This coated protective sheet (PS) and a thermal fiberglass cover coated with aluminized Mylar provided additional protection to the shielded EPDS, MTM, DPCA, and dosimeters immediately below. As may be seen in Figure 7-12, the impactors on the EPDS protective cover were tallied and compared to impactors experienced by the Solar Max satellite during its 4-year stay in orbit (Ref. 13). While both satellites were in low-inclination orbits, they experienced different periods of solar activity (Solar Max: 1980 - 1985; LDEF: 1984 - 1990). This may account for the differences in flux values. A tally of the number of large craters (>300  $\mu$ m) and small craters (>100  $\mu$ m) yielded 29 large and 264 small. A more detailed accounting of analyses performed on impactor chemical composition, directionality of impacts, and other related effects can be found in recently published data (Ref. 14).

Figures 7-13 and 7-14 illustrate some typical impactor sites experienced by the space-exposed optical fiber cables and surrounding materials. Evident in Figure 7-15, is a classic impactor region on a fiber link faceplate. Protective materials between the exterior cabling and the single element optical fiber can be seen protruding from the outermost cabling in Figure 7-13. However, this optical fiber still continues to function correctly, since it was not severed by the impactor.

Figure 7-16 is a photographic close-up of the impactor site on Link #4. Notice there is no evidence of any optical fiber damage, although the cabling and protective jacketing

materials are damaged. Our analysis and testing of this particular link revealed that the single fiber within the cabling was indeed broken by an impactor. In order to detect the breakage, two investigative methods were used since normal microscopy and IR detection methods employed at KSC did not ascertain any breakage.

The first method consisted of passing continuous visible laser light ( $\lambda=6328 \text{ \AA}$ ) through the transmitter end of the fiber. This allowed a very small amount of scattered light to penetrate or scatter through the Kevlar strength members and Hytrel jacketing and be observed. Under normal link operating conditions, light of a wavelength of 830 nm is present for approximately 26 ms, making detection of any low-level short-duration scattered light difficult.

The second investigative scheme involved an optical time-domain reflectometer (OTDR) measurement. Figure 7-17 illustrates that the impactor caused breakage at a distance of 18.9 m from the optical transmitter end, or 27.4 m from the receiver end. The sum of these distances measured to the impactor site agreed within OTDR error to the link length, 48 m. It is estimated that this breakage occurred between day 365 and day 2,114 in orbit. Prior to the 365th day, this particular link performed in an excellent manner, as recorded in the orbital data tape, testifying to the applicability of fiber optics in space.

Thus, despite numerous micrometeorite and space debris impacts experienced by the cabled fibers and experiment surfaces, only a single optical fiber was observed to be severed over the 2,115 days in orbit. This event occurred after the scheduled data acquisition portion of the mission was completed.

Perhaps the most profound conclusion that may be drawn from the PL Exp #701 performance is that the 1978 - 1980 era FO technology orbited operated excellently, and that newer and improved FO technology should perform in a superior manner.



This experiment demonstrated for the first time, under deliberate space exposure and over an unscheduled extended time period, that well-designed FO systems can survive and perform in the space environment.

#### **7.1.2 Experiment S0109 - Space Exposure of Fiber Optic Cables**

This passive experiment contained 10 fiber optic cable samples, 4 of which were space-exposed with the remaining 6 within a shielded volume. The space exposed cabling surrounding the fibers experienced similar UV radiation or aging effects, as discussed earlier in detail for the M0004 Experiment. Early examination of the cabled fiber responses to temperature following the LDEF recovery first revealed that no measurable changes in performance were observed. In a later report up to 10 Db/km excess loss over the -55° to +70° C range was reported in the majority of cabled fibers tested following the orbit and was believed to be due to more than one mechanism, but not identified. Several techniques were employed in baselining any fiber intrinsic loss increases following the orbital exposure. Not all fibers were baselined using a common technique and it was reported that long-term damage - residual losses did exist. These data were later explored again, drawing comparisons between recently irradiated samples of the various fiber types and the orbited fibers. Other effects, such as contamination to unprotected fiber connectors located within the tray volume, have also been observed. There was no positive indication from direct measurements on these flight connectors that (any) significant loss can be attributed to contamination. A more-complete description of the post-orbit analyses of this passive experiment can be found elsewhere (Ref. 12).

### **7.1.3 M0003-8 Fiber Optic Experiment**

This experiment was an active experiment orbited on the LDEF. It was a sub-experiment of M0003, "Space Environment Effects on Spacecraft Materials." The purpose of the M0003-8 Experiment was to gather data on the stability of fiber optic multi-contact connectors (Hughes 20 contact C-21 series connectors, which accommodate size #16 fiber optic termini). As shown in Figure 7-18, the experiment was operated at a wavelength of 905 nm, and the data was recorded over approximately 111 2-hour periods with 32 recordings per period during the first 400-plus days of the flight (the data ran out of tape).

An extensive discussion of the data recorded aboard this LDEF experiment can be reviewed elsewhere (Refs. 14 and 15). However, post-orbit tests were compared to previously recorded pre-orbit measurements and resulted in the conclusion that the FO components and in particular, the connectors studied, experienced no degradation following the LDEF recovery. In essence, no fiber pistoning, or connector degradation due to radiation and other space environmental effects were noted. The lack of radiation effects on the optical fibers is easily explainable since the lengths used were very short (1/2 and 2 meters). The total system performance variation since the experiment was fabricated and tested in 1978 was measured to be a plus (+) 0.2 Db increase experienced during the LDEF orbit, following orbital recovery (Nov 1990). The experiment tested the same as it did in 1978. The principal investigator concluded that the experiment operated in a relatively benign environment and was designed to perform reliably, which it did, experiencing little or no degradation in the LDEF orbit.

### **7.1.4 Experiment S0050 - Optical System Components**

This passive experiment contained both shielded and exposed electro-optic and FO components. Individual components were mounted on aluminum subpanels which were

covered by a thin aluminum sunshade, with several components left unshielded. Table 7-6 lists the EO components orbited, while Table 7-7 presents data reported for an EO modulator. Figure 7-19 depicts the performance of a GaAsP LED orbited aboard the LDEF with that of a stored diode of the same type, showing that the diodes reproduced their original characteristics. Similarly, the EO modulator data shown in Table 7-7 showed no measurable changes in optical transmission. The half-wave voltage and roll-off frequency can be observed to be within experimental errors. Other non-fiber optic technology based components (optical filters, paints) were included in this experiment, and the reader is referred elsewhere. (Note: Data on other detectors, lasers, etc., as shown in Table 7-6 were not reported at the time of this writing.) The principal investigator concluded that the changes noted in the retested components (following the LDEF recovery) appear as much related to the passage of time as to the effects of the space environment, but that organic materials, multilayer optical interference filters, and extreme IR reflectivity of black paints have shown unexpected changes.

#### **7.1.5 Experiment M0006 - Space Orbited Fiber Optic Bundle**

This experiment was a subset of the M0006 "Space Environment Effects Experiment." The post-orbit analysis of the FO bundle (Table 7-8) included investigation of the attenuation of optical signal transmission, numerical aperture, and fiber spectral responses over a wide wavelength range. The measurements were performed in a sequenced manner or hierarchy in order to determine if the optical fibers experienced any space radiation-induced attenuation. The cable bundle contained 1800 individual fibers which were oriented 40° distant from the trailing edge of the LDEF. Exposure to the space environment occurred over the period 21 Apr 84 through 15 Mar 85. As shown in Table 7-9, attenuation measurements were in a sequenced manner or hierarchy in order to prevent the inadvertent annealing or photobleaching of any space-induced permanent attenuation in the fiber bundle. By performing measurements at longer wavelengths and relatively low optical powers, the

### *7.1, Experimental Configurations and Fiber Optic Systems and Component Exposures to the Space Environment*

---

activation of photobleaching is minimized or avoided. Figure 7-20 illustrates a typical spectrophotometric scan showing little deviation between the control and the space orbited bundle of fibers. The detailed results of this investigation can be found elsewhere (Refs. 12 and 14). It was concluded that photobleaching of suspected space-induced radiation color centers did not occur. Due to the extremely short length of the cabled bundle of fibers (61.7 cm), the accuracy of the attenuation measurements was determined to be  $\pm 0.14$  dB/m, a value far greater than any expected space-radiation induced losses. It was concluded that if any permanent attenuation was experienced by the bundle while in orbit, it was less than 0.14 dB/m. This was also supported by other measurements such as numerical aperture (N.A.). Far-field measurements were performed using a Fourier transforming and relay lens system to measure the N.A. The acceptance angles were determined to be  $62.8^\circ \pm 2.5^\circ$  for the control bundle, resulting in an N.A. of  $0.52 \pm 0.02$ . The orbited bundle measurements resulted in an acceptance angle of  $64.7^\circ \pm 2.5^\circ$  and an N.A. of  $0.54 \pm 0.02$ . These and other measurements covered in greater detail within the cited literature indicated that little, if any, adverse effects were experienced by cabled optical fiber bundle in LEO.

## **7.2 CONCLUSIONS**

The general conclusions that may be drawn from the summary of LDEF FO experiments presented in this chapter are as follows:

- FO technology is mature for space applications, providing a judicious choice of space worthy components is made.
- Very little radiation-induced permanent damage (if any) was observed to directly degrade the optical fibers and shielded optoelectronic components composing the FO systems aboard the LDEF in LEO.

## 7.2, Conclusions

---

- Temperature cycling and temperature extremes can degrade certain optical fibers. Care must be taken to choose temperature insensitive fibers for space applications.
- Other space environments factors such as UV radiation, space debris, micrometeorite impactors and AO can cause material damage to cabled fibers. Care must be taken to provide adequate protection, particularly for extended orbital periods.
- While the LDEF FO experiments were generally successful in their ability to perform or withstand the LEO environment, extrapolation of these results to other orbital conditions should be approached with caution (for example, the radiation environment experienced by the LDEF, while in LEO, was relatively benign compared to fluxes in other (higher) satellite orbits. Thus, there is no direct method based on in-situ data which exists for predicting performance in more adverse radiation environments.)

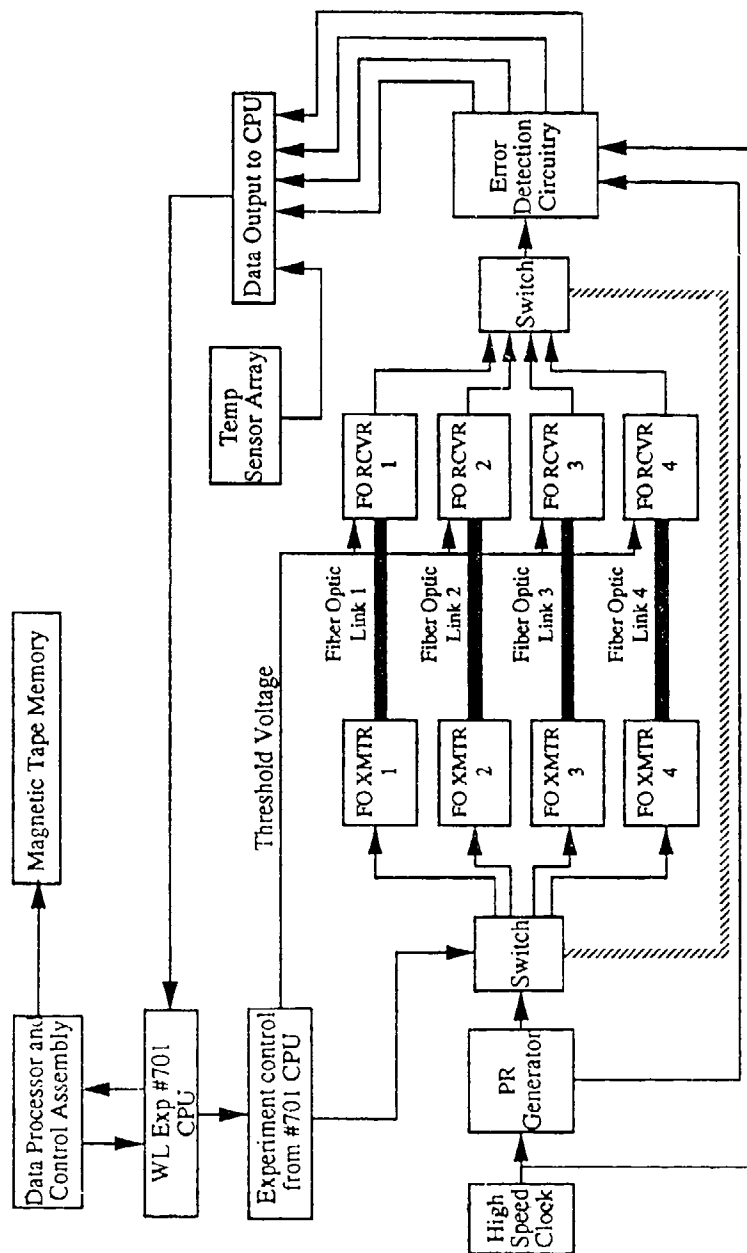


Figure 7-1. Configuration of Experiment hardware. This hardware was used to measure the performance of the four active FO links contained in PL Experiment #701 (M0004). The experiment measured the temperature at various locations within the tray volume and the performance of the FO links by measuring the SNR and BER of each link.

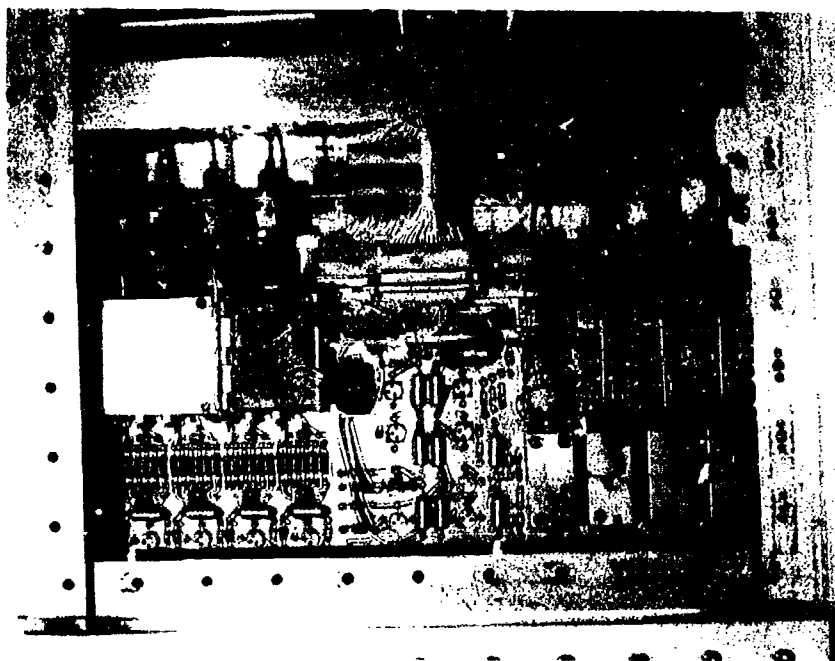
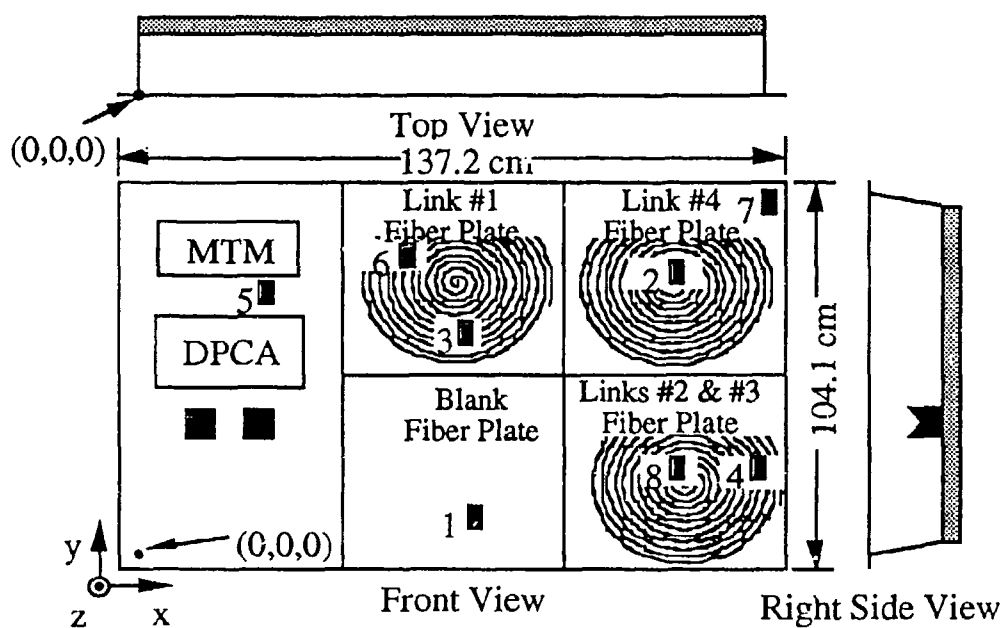


Figure 7-2. View of the Experimental Tray



Note: Intersection of tray flanges is the (0,0,0) point. Negative z values are into the interior volume of the experiment tray.

■ Thermistors    ■ Dosimeters

Figure 7-3. Thermistor, Optical Fiber, and Dosimeter Locations.



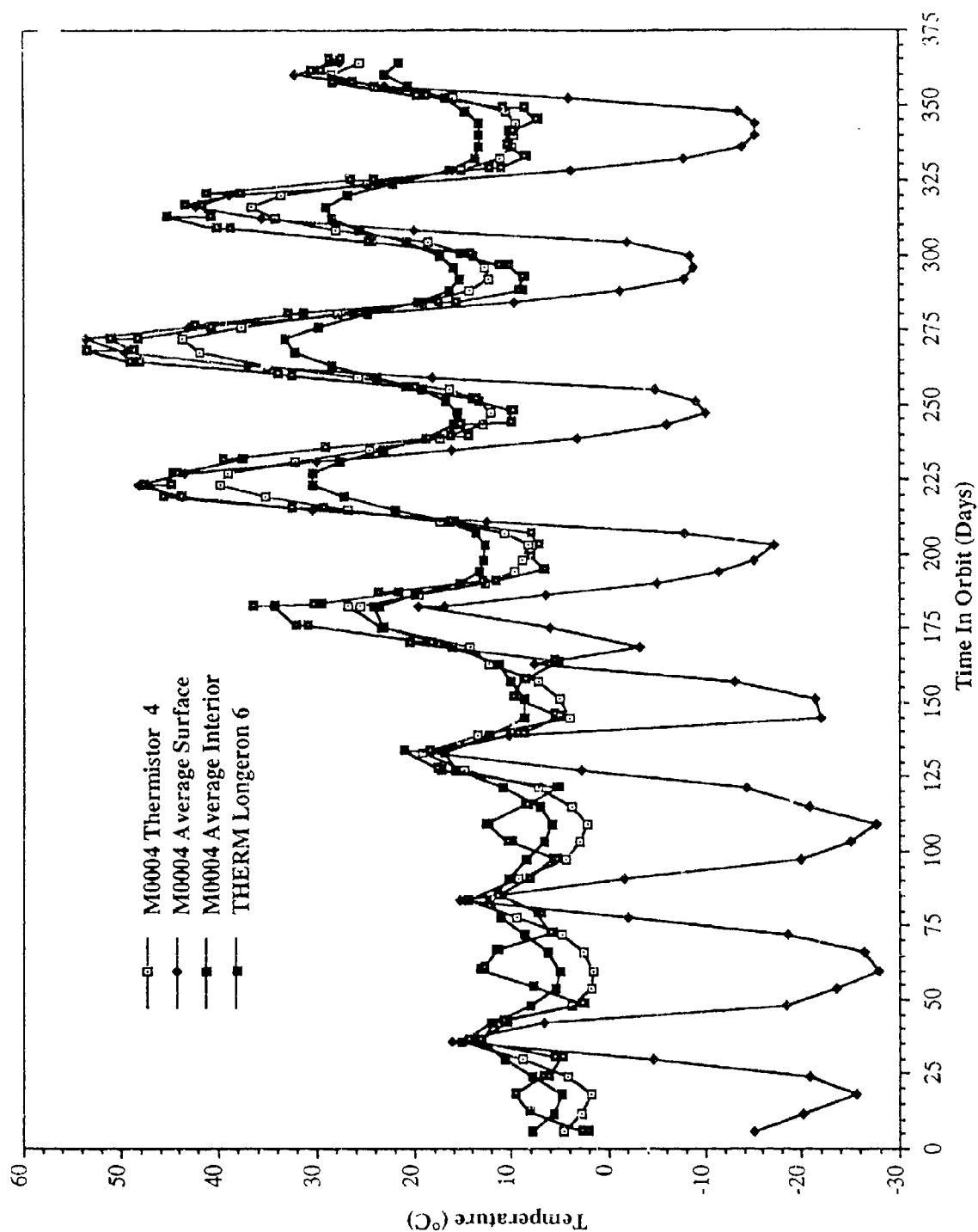


Figure 7-4. Comparison of PL Exp #701 Space Temperature Measurements and Therm Model Data.

PL Experiment #701 - M0004  
In-Flight Performance of Link #1

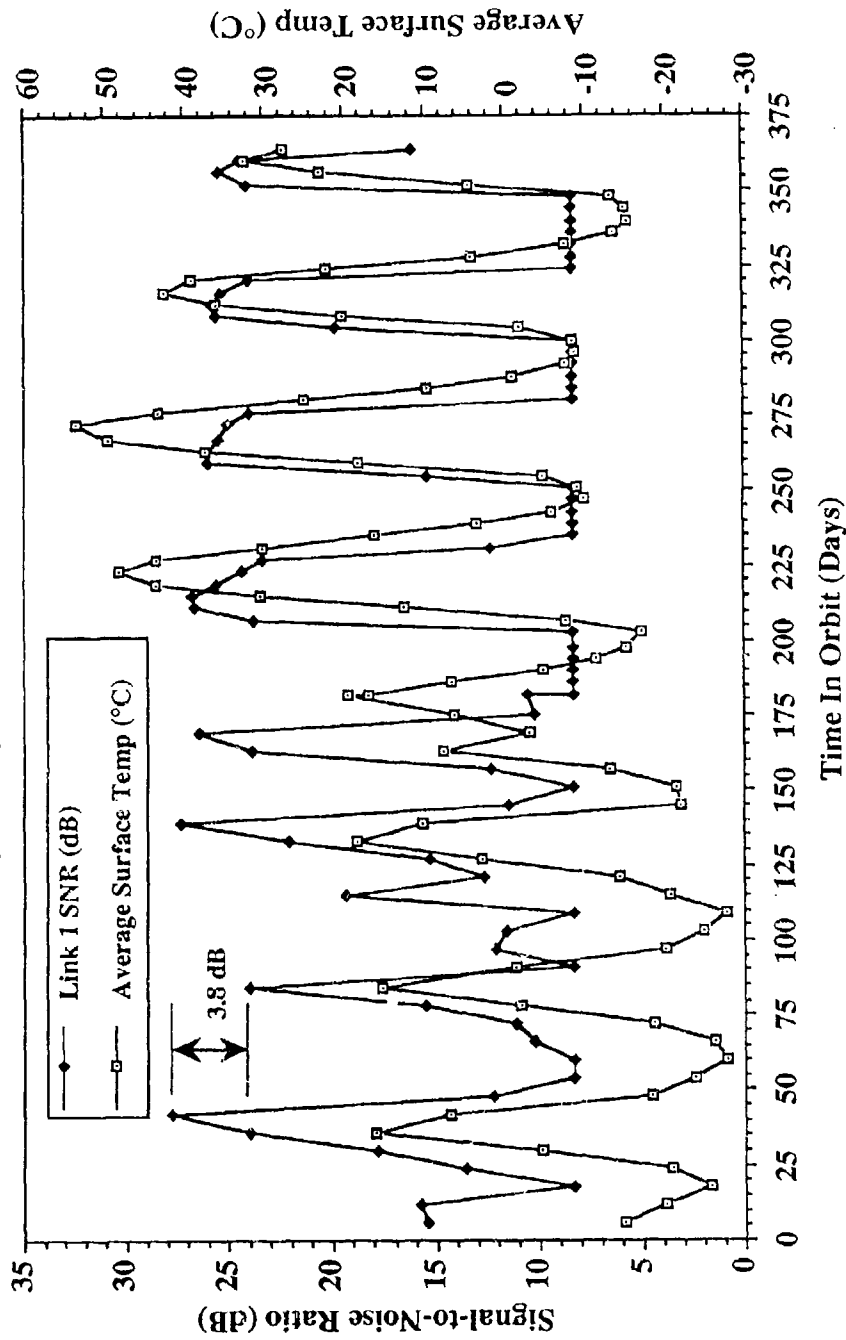


Figure 7-5. Space Orbit Performance of PL Exp #701 FO Link #1.

PL Experiment #701 - M0004  
In-Flight Performance of Link # 2

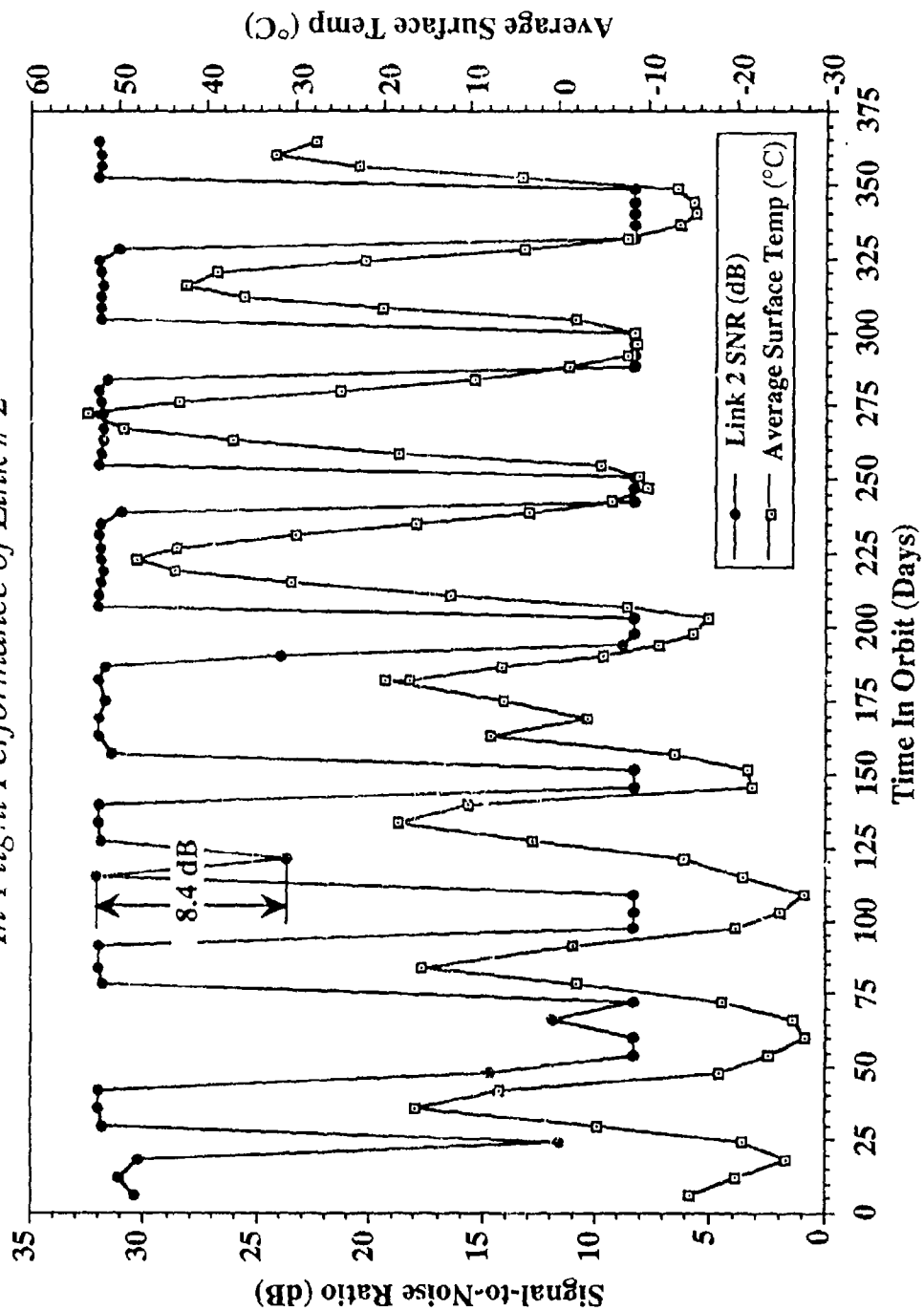


Figure 7-6. Space Orbit Performance of PL Exp #701 FO Link #2.

PL Experiment #701 - M0004  
*In-Flight Performance of Link #3*

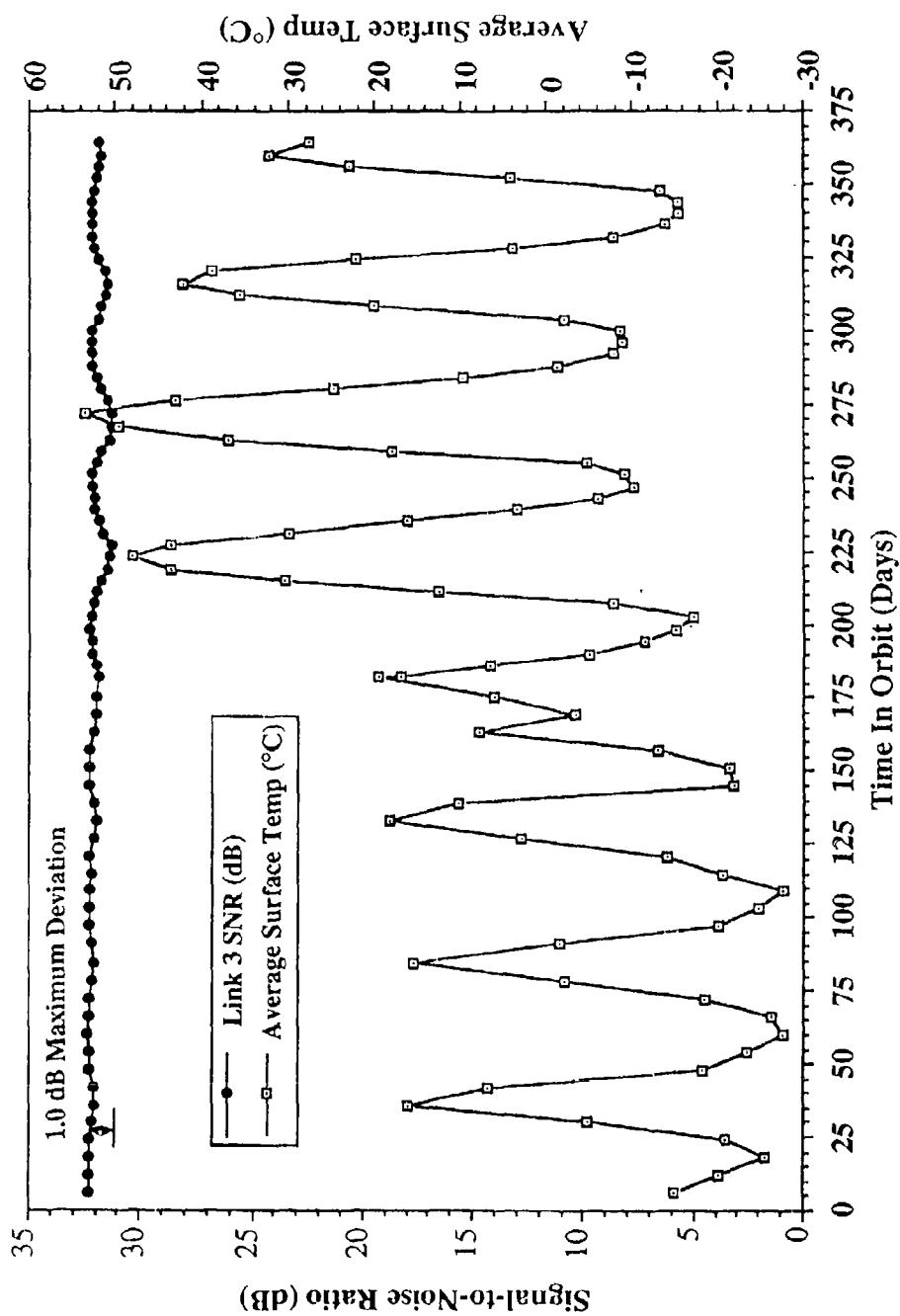


Figure 7-7. Space Orbit Performance of PL Exp #701 FO Link #3.

PL Experiment #701 - M0004  
In-Flight Performance of Link #4

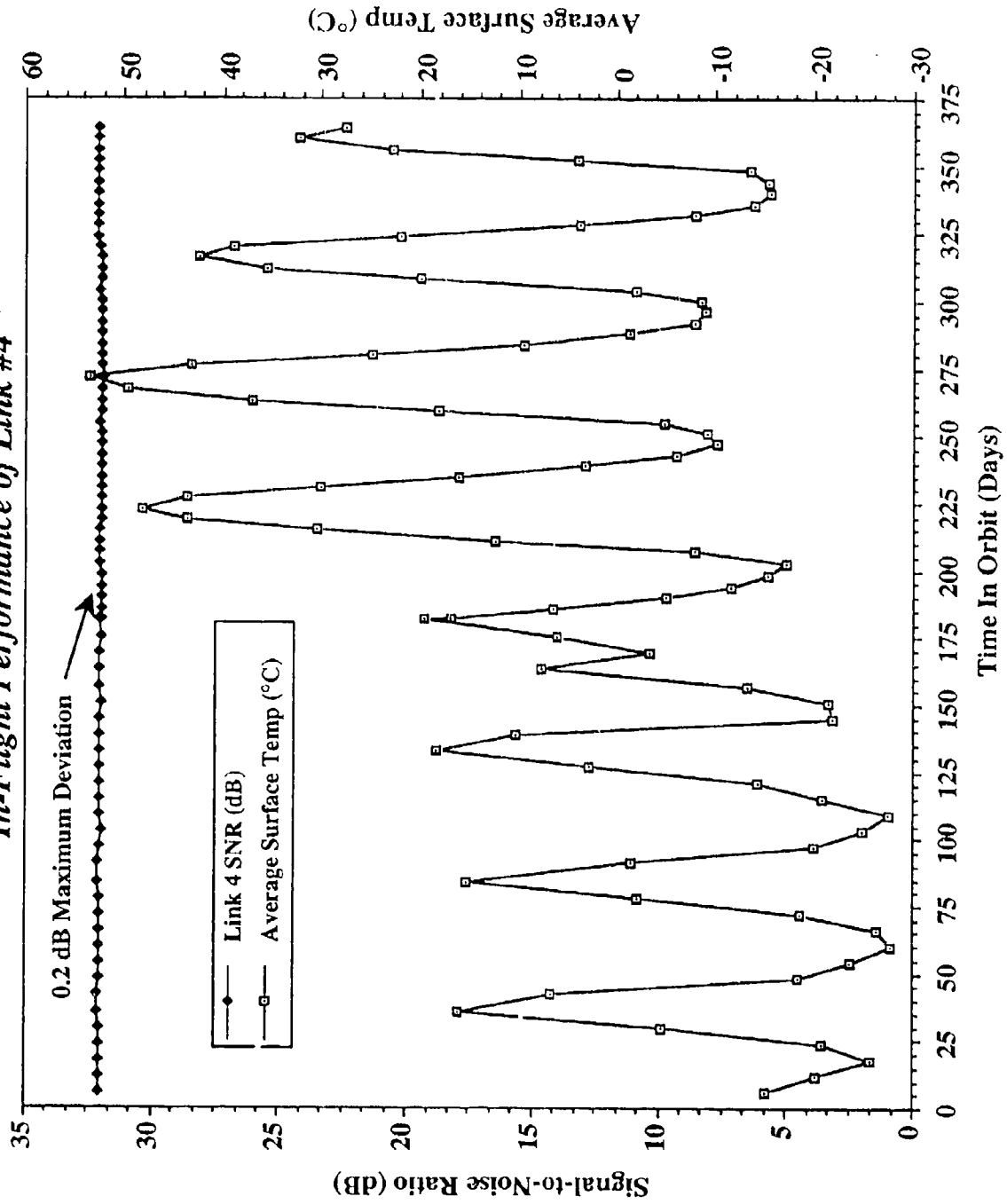


Figure 7-8. Space Orbit Performance of PL Exp #701 FO Link #4.

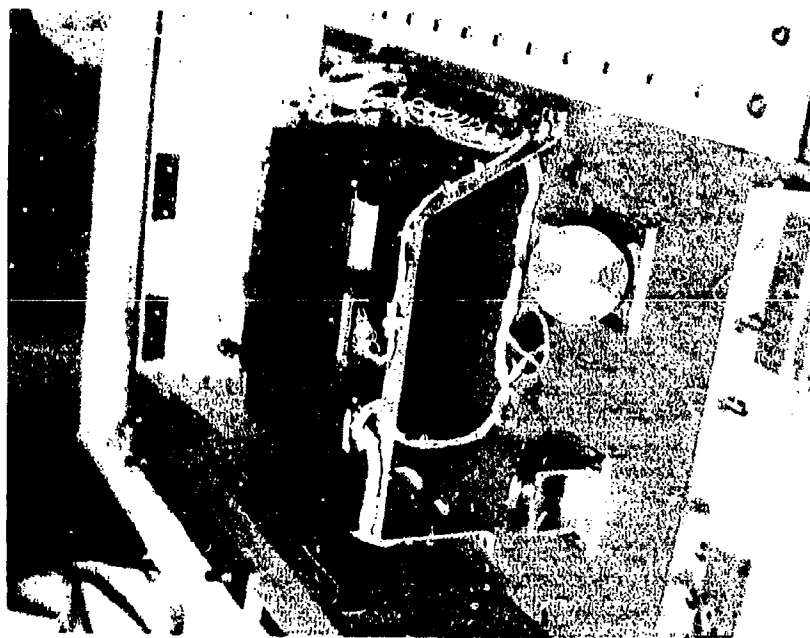


Figure 7-9. Location and Orientation of Dosimeters.

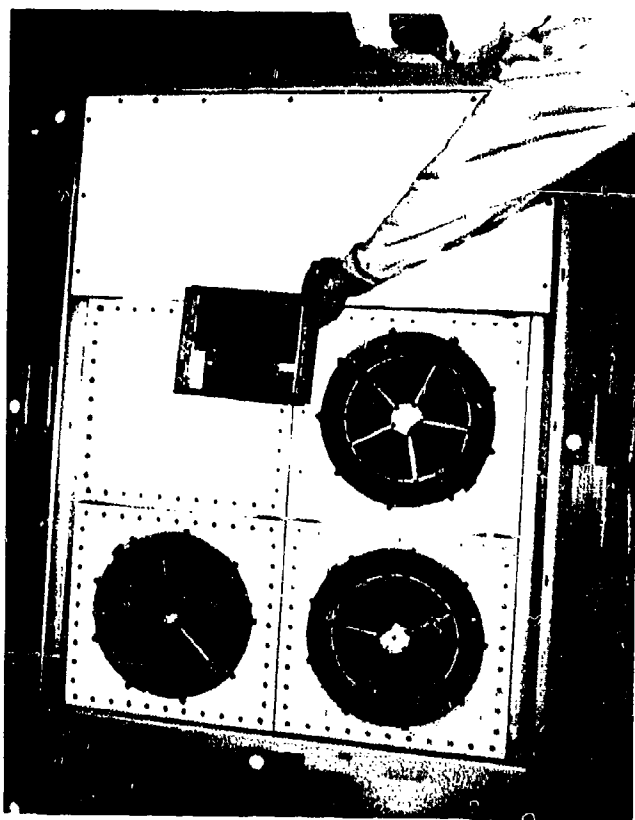


Figure 7-10. A Close-Up of PL Exp #701 at KSC.

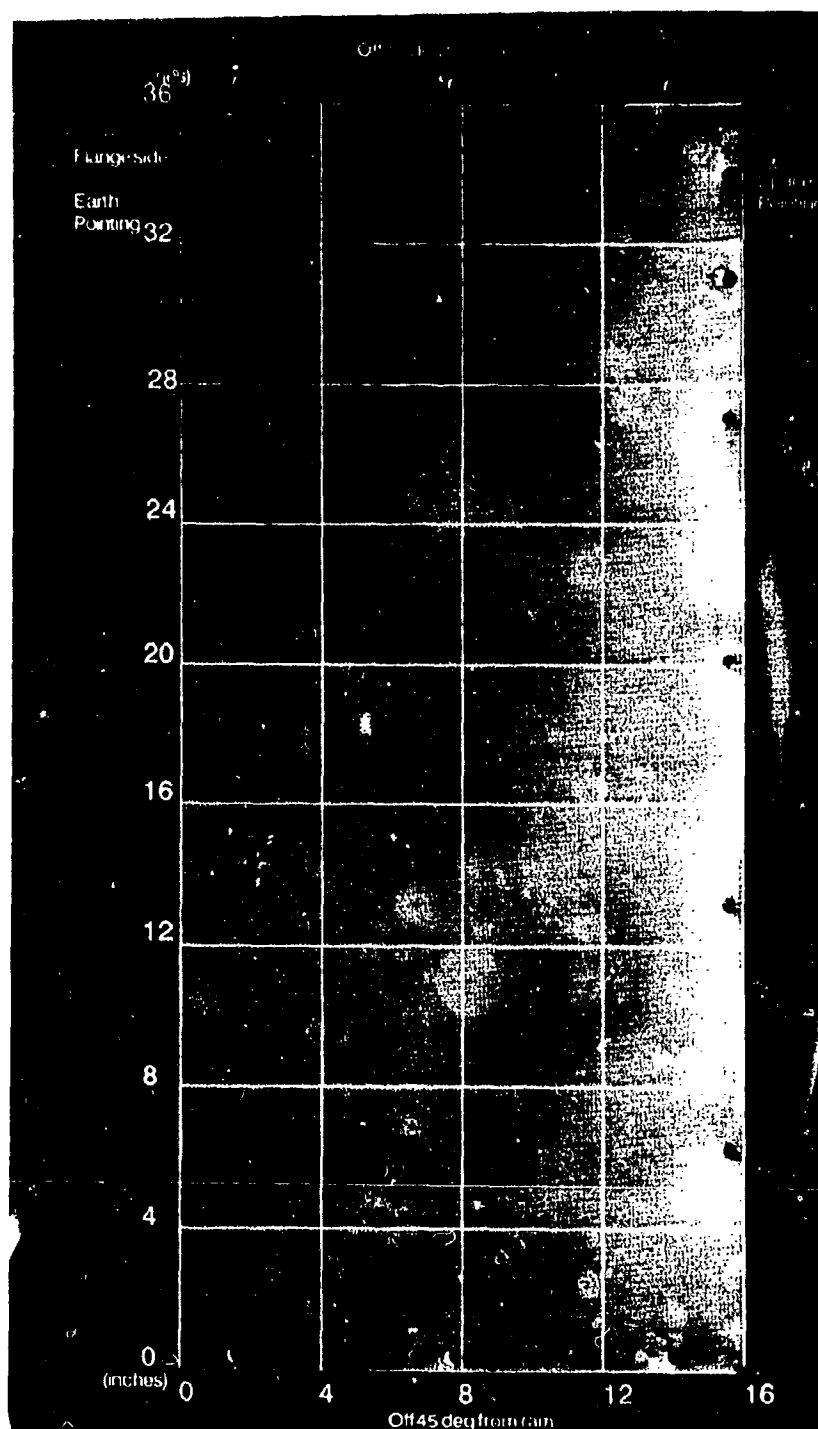


Figure 7-11. A Photograph of the EPDS Cover Plate with Coordinate Grid Superimposed.

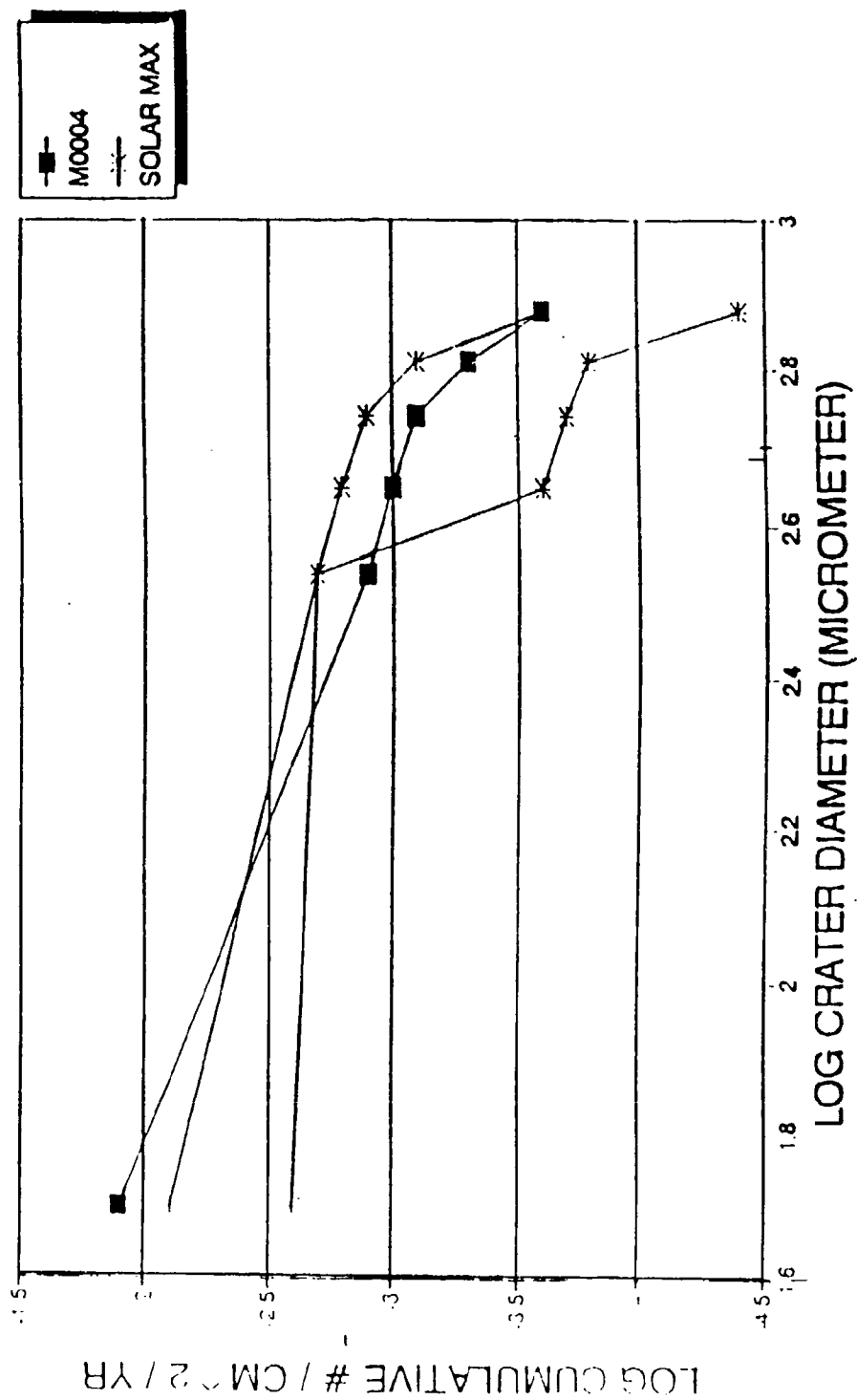


Figure 7-12. Comparison of PL Exp #701 and Solar Max Satellite Impactor Flux Data





Figure 7-13. Example of Impactor Site on PL #701 FO Link #2.



Figure 7-14. Example of Impactor Site on PL Exp #701 FO Link #4.



Figure 7-15. Close-up of PL Exp #701 Link #4 Impactor Region.

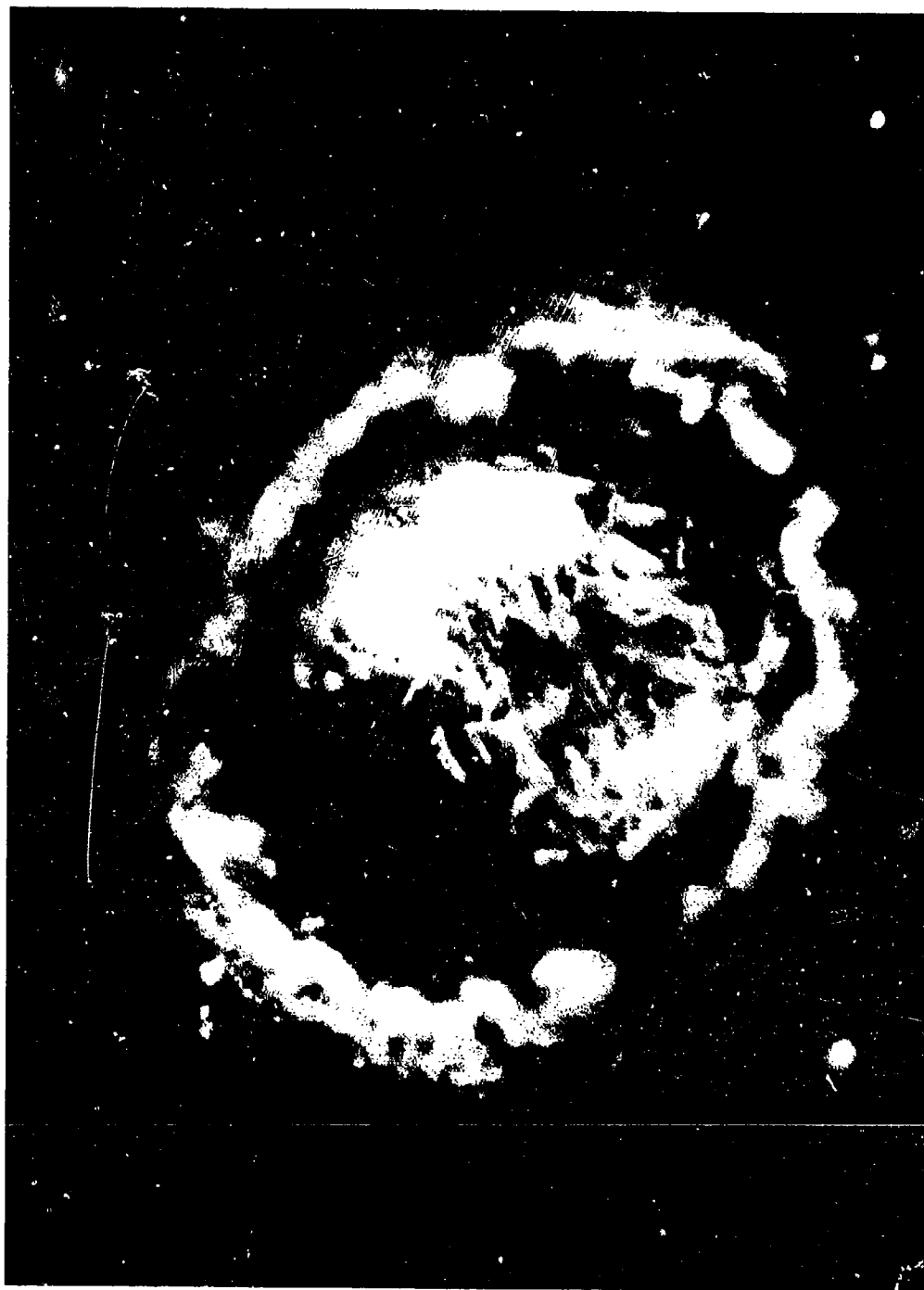


Figure 7-16. Close-up of Impactor Region on PL #701 FO Link #4.

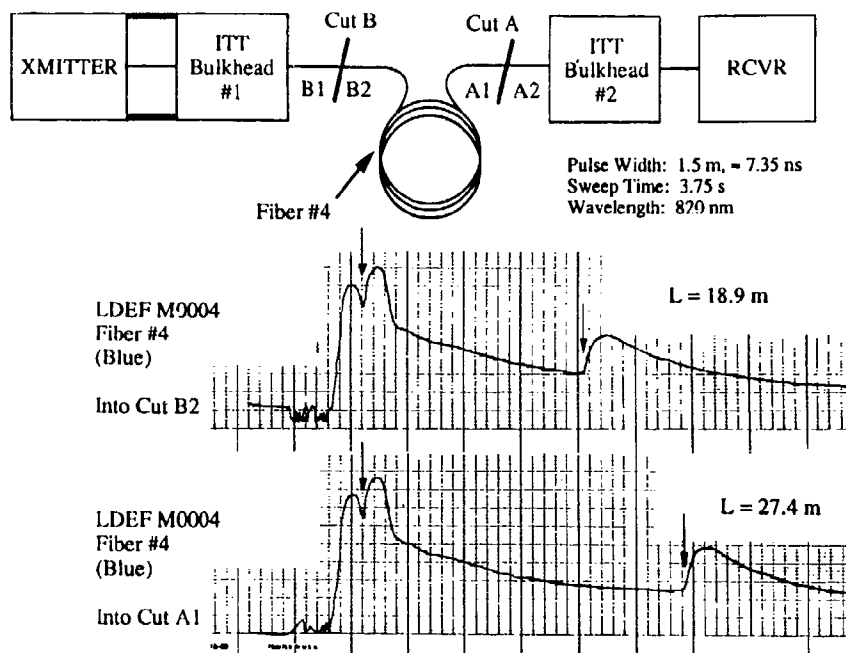


Fig. 11 OPTICAL TIME DOMAIN REFLECTOMETRY ANALYSIS OF IMPACTOR LOCATION ON WL EXP #701, FO LINK #4.

Figure 7-17. Optical Time Domain Reflectometry Analysis of Impactor Location on PL Exp #701 FO Link #4.

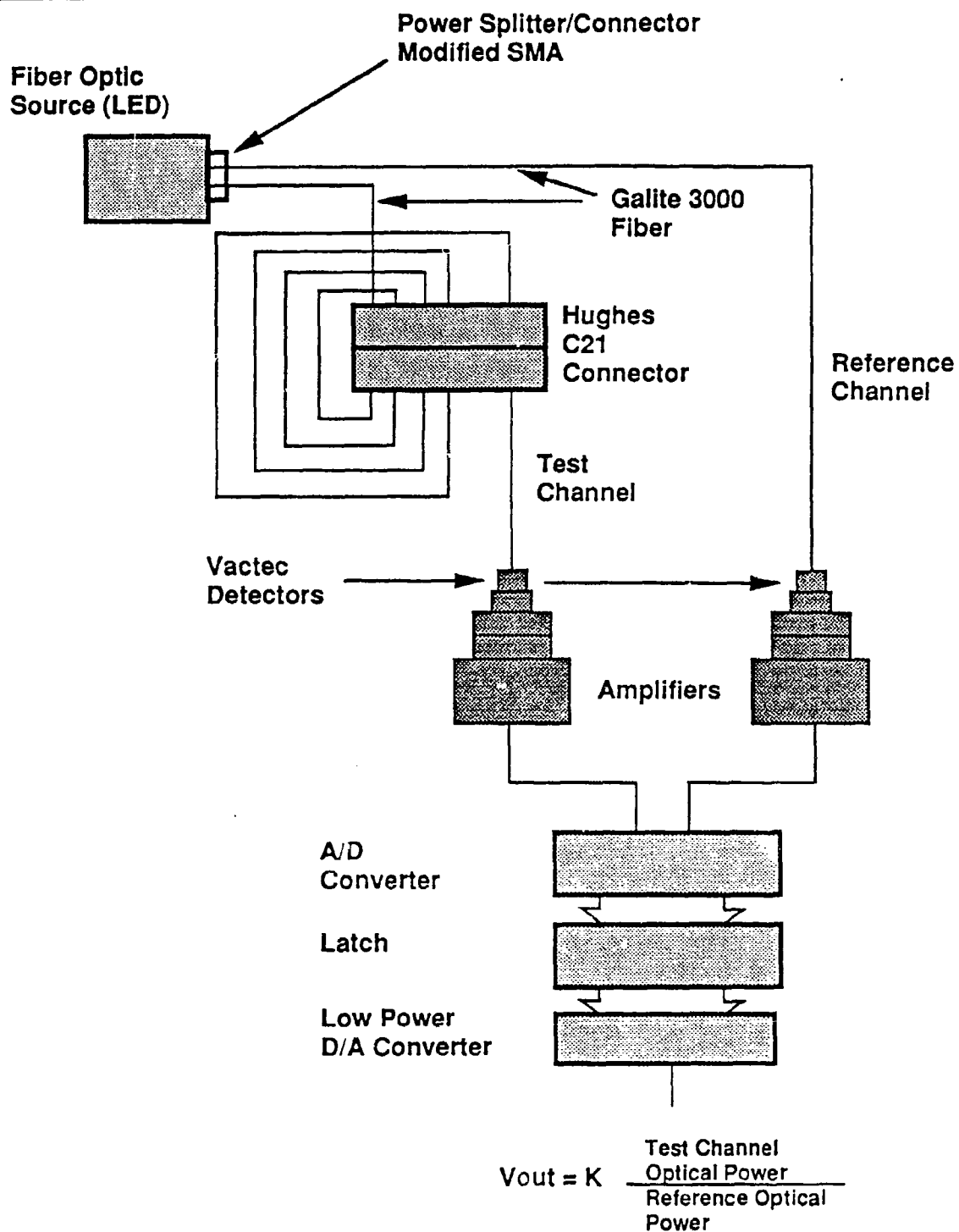


Figure 7-18. Boeing Exp M0003-8 Experiment Block Diagram.

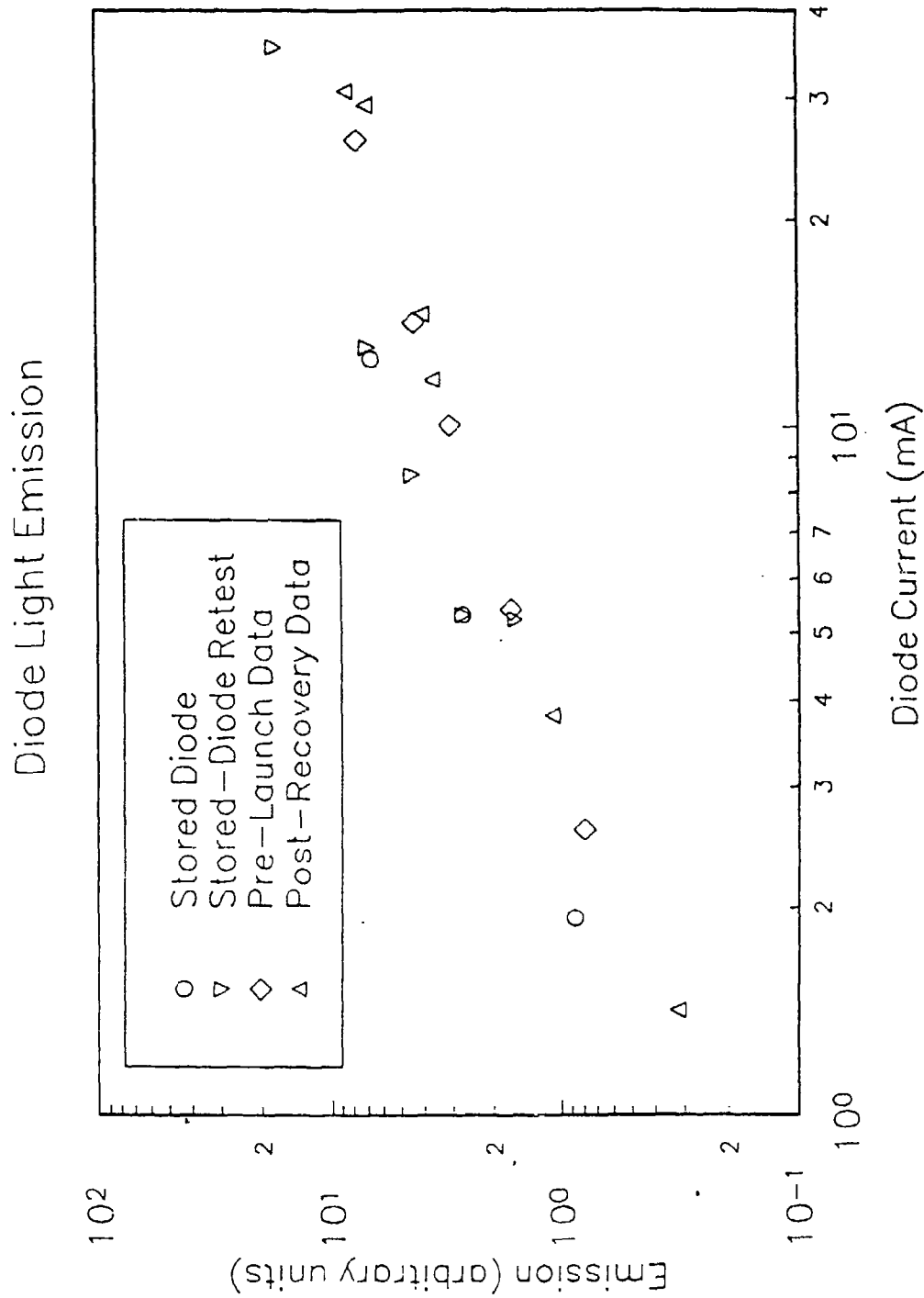


Figure 7-19. Radiation Output vs Forward Current for a GaAsP LED Exposed to the Space Environment and a Stored Diode of the Same Type. The Diodes Reproduce Their Original Characteristics.

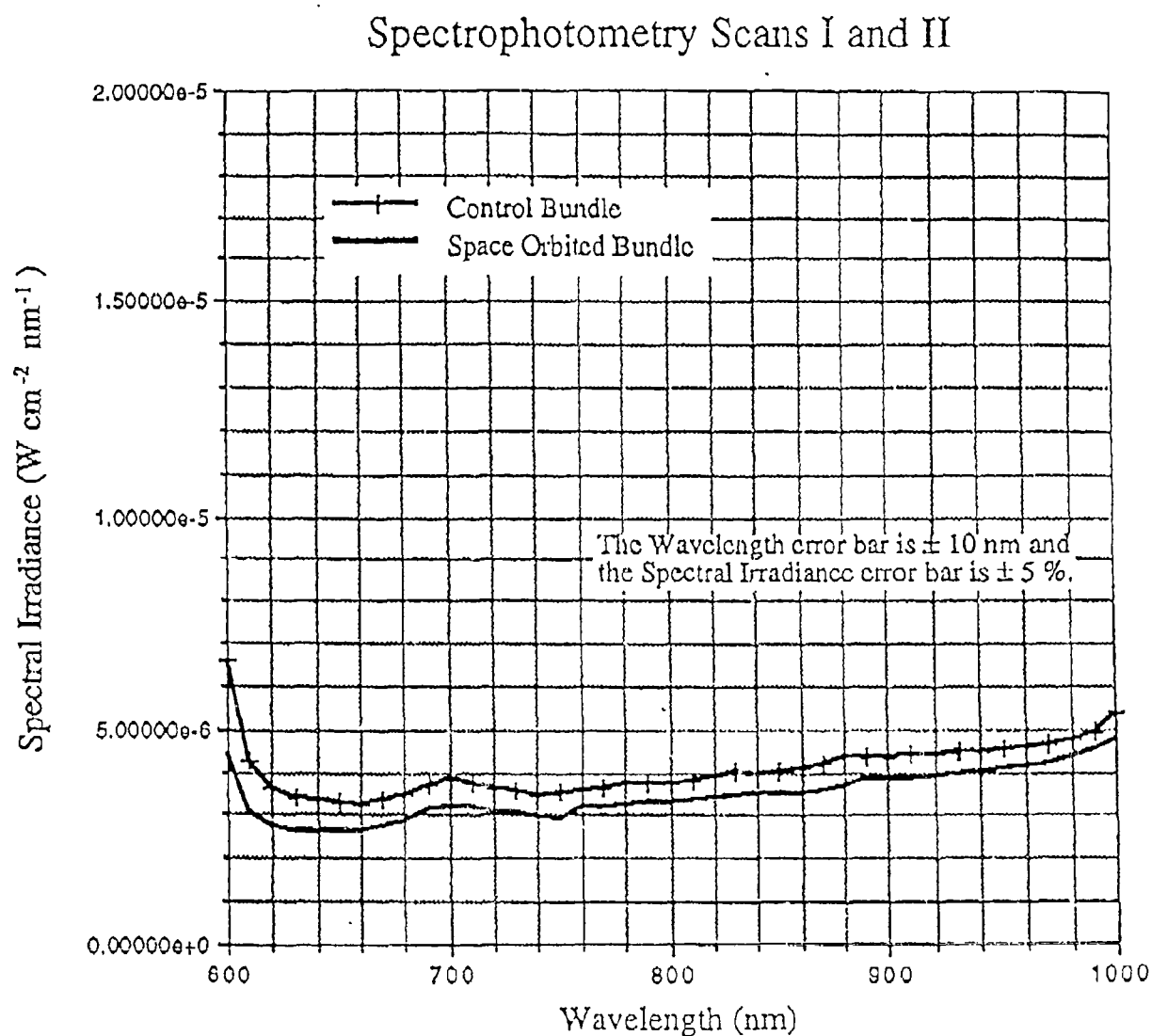


Figure 7-20. The Spectrophotometry Scans I and II have been combined to reveal no significant transmission differences in the comparison of the Control and the Space Orbited FO Bundles.



Table 7-1. Comparison of FO Experiments Orbiting on the LDEF.

Experiment Identification And Responsible Agency	Objective or Title of Experiment	Experiment Orbital Operation	On-Orbit Data Collection (Recorded Parameters and Variables)	Direct Space Exposure of FO Components	Post Orbit Analysis Performed by (Principal Investigator)
M0004 PL-Exp #701 AFMC Phillips Laboratory	Demonstrate active FO systems. Measure Temperature and Radiation Effects	Active	$\alpha$ , T, S/N, BER, V Dosimetry	Cabled Optical Fibers	Phillips Laboratory (E. W. Taylor)
S0109 JPL California Inst. of Tech	Space Exposure of FO Cables	Passive	None	Cabled Optical Fibers	JPL (A. R. Johnston)
S0050 Georgia Tech Research Inst	Exposure of Optical Fibers and Components	Passive	None	None	Georgia Tech Res Inst (M. Blue)
M0006 U.S. Air Force	Space Environment Effects	Passive	None	Cabled non-imaging FO bundle	Phillips Laboratory (E. W. Taylor, S. A. DeWalt)
A0138-7 CERT/ONERA-DERTS	Optical Fibers and Components	Passive	(Possibly Dosimetry)	None	CERT/ONE RA-DERTS (Jacques Bourricau)
M0003-8 Boeing Co	Space Effects on Multipin FO Connectors	Active	T, V	None	Boeing Co (Owen Mulke)

 $\alpha$  = Optical Signal Transmission & Attenuation

T = Temperatures

S/N = Signal-to-Noise Ratio

BER = Burst Error Rates

V = Voltages (Various)

Table 7-2. Abbreviated Thermal Data Measured in Orbit.

Day / Meas #	Therm Max °C	Therm Min °C
6 / 1	Therm 5 / 10	* Avg / -15.0
18 / 3	Therm 4 / 1.9	* Avg / -25.6
60 / 10	Therm 5 / 8.4	* Avg / -27.7
84 / 14	* Avg / 15.3	Therm 1 / 10.5
223 / 41	* Avg / 48.1	Therm 3 / 29.2
247 / 4	Therm 5 / 18.2	* Avg / -10.1
272 / 53	* Avg / 53.5	Therm 3 / 31.7
364 / 76	* Avg / 27.6	Therm 1 / 20.0

\* Note: This is the Average of Thermistors 2, 7, and 8

Table 7-3. Thermistor Location Within Experiment Tray.

Thermistor #	x (cm)	y (cm)	z (cm)	Remarks
1	73.7	14.0	- 6.4	Attached to Transmitters
2	104.1	67.3	- 0.5	Attached to Fiber Plate
3	63.5	63.5	- 6.4	Attached to Circuit Board
4	124.5	10.2	- 6.4	Attached to sidewall
5	35.6	68.6	- 8.9	Attached to bracket inside EPDS cover
6	50.8	76.2	- 14	Attached to base plate (Tray bottom)
7	124.5	95.6	- 0.5	Attached to Fiber Plate
8	104.1	25.4	- 0.5	Attached to Fiber Plate

**Table 7-4. Some Characteristics of Space Exposed Active Optical Fibers,  
Prior to Launch.**

Variable	Link #1	Link #2	Link #3	Link #4
Original Cable Color	Purple	Yellow	Beige	Blue
Cable Type	Loose Tube	Loose tube	Conformal	Conformal
Cable Material	Polyurethane	Tefzel	TBD	Hytrel
Fiber Type	Glass/Glass Semi-Graded	PCS Step Index	PCS Step Index	PCS Step Index
Core/Clad ( $\mu\text{m}/\mu\text{m}$ )	100/140	207/327	207/327	198/358
Numerical (Apertures)	0.30	0.22	0.22	0.33
Bandwidth (3 dB) (MHz - km)	20	25	25	25
Attenuation (dB/km)	6.0 @ 850 nm	5.0 @ 850 nm	5.0 @ 850 nm	9.2 @ 850 nm
Wavelength (nm)	1300	830	830	830
Link Length (m)	45.0	19.7	20.5	48.0

Table 7-5. Interim Analysis of Radiation Doses Experienced by PL Exp #701.

Shielding Depth (g/cm <sup>2</sup> )	Trapped Electrons (Rad)	Trapped Protons (Rad)	GCR*, Other (Rad)	Total Dose
0.01	24,500	515	33	25,000
0.02	12,100	471	33	12,600
0.03	7,320	444	33	7,800
0.04	4,980	425	33	5,440
0.05	3,540	410	33	3,980
0.86	11.9	218	33	263
1.06	3.3	202	33	238
1.25	2.6	193.5	28.4**	224.5 ± 6.0***
2.48	0.1	149.5	37.0**	186.5 ± 5.8***

\* - Values determined from comparison of measurement and calculation

\*\* - Difference between measured and calculated doses

\*\*\* - Measured TLD values

Table 7-6. List of Electro-Optical Components.

PASSIVE COMPONENTS	ACTIVE COMPONENTS	DETECTORS
Six Black Paint Samples	ADP Modulator	Silicon PIN
Neutral Density Filters	Channeltron Array	Silicon PV
Narrow-Band Filters	GaAlAs Laser Diodes	Silicon Gamma-Ray
Laser Mirrors	GaAsP LED	InGaAsP PV
Hot-Mirror Filter	Nd:YAG Rods	InSb PV
Lyman-Alpha Filter	CO <sub>2</sub> Waveguide Laser	PbS
UV Filter 1600 Å	HeNe Laser	PbSe
LiF Window	Holographic Crystal	HgCdTe PV
AlMgF <sub>2</sub>	Laser Flash Lamps	HgCdTe PC
Al <sub>2</sub> O <sub>3</sub> Window		PdSi Arrays
SiO <sub>2</sub> Window		Pyroelectrics
35-mm UV Film		UV PMT
Various Optical Glasses		UV Silicon
Black Polyethylene		

Table 7-7. Electro-Optic Modulator Characteristics.

Measurement	Stored Device (Original)	Stored Device (Remeasured)	Space Exposed Device (Pre- Launch)	Space Exposed Device (Post-Recovery)
Roll-Off Freq (kHz)	20 + 3	25 + 3	17 + 2	18 + 2
Half-Wave Voltage (kV)	240 + 14	250 + 15	227 + 3	225 + 5
Optical Transmission (%)	> 98	> 99	> 98	> 99

Table 7-8. Fiber Optic Bundle Parameters: Known and Observed Incoherent FO Bundle Characterizations.

CABLE	CONTROL BUNDLE	SPACE ORBITED BUNDLE
Material	PVC	PVC
Color	Black	Black
Length	63.5 cm	61.7 cm
Diameter	3.2 mm	3.2 mm
Fiber Quality	1862 +/- 16	1838 +/- 16
Condition, March 1990*	Excellent	Excellent
FIBERS		
Core Material	Flint Glass (Predominantly Silica and Lead	Flint Glass (Predominantly Silica and Lead
Clad Material	Alkaline Resistant Glass (Soda, Lime and Silicate	Alkaline Resistant Glass (Soda, Lime and Silicate
Core Diameter	60 $\mu\text{m}$ +/- 5 $\mu\text{m}$	60 $\mu\text{m}$ +/- 5 $\mu\text{m}$
Clad Diameter	75 $\mu\text{m}$ +/- 5 $\mu\text{m}$	75 $\mu\text{m}$ +/- 5 $\mu\text{m}$
Operational Wavelength**	Visible and Infrared	Visible and Infrared
ATTENUATION		
Cutback Method	2.77 dB / m +/- 0.14 dB / m	2.85 dB / m +/- 0.14 dB / m
Manufacturer	1.20 dB / m +/- 0.10 dB / m	1.20 dB / m +/- 0.10 dB / m

\* - Bundles are in Four Pieces as a result of Cutback Method Measurements

\*\* Tested at 400 nm through 1100 nm, and 1300 nm

Table 7-9. Attenuation Measurements of Control and Space Orbited Bundles.

Hierarchy of Attenuation Measurements					
Measurement Sequence	Measurement Performed	Wavelength ( $\mu\text{m}$ )	Optical Power ( $\mu\text{W}$ )	Control Bundle (dB/m)	Space Orbited Bundle (dB/m)
1	Attenuation	1.3	<1	$\alpha_1 = 5.14$	4.92
2	Attenuation	0.86	<1	$\alpha_2 = 5.97$	5.63
3	Attenuation	1.3	<1	$\alpha_3 = 5.20$	4.72
4	Attenuation	0.86	$\leq 5$	$\alpha_4 = 5.42$	5.28
5	Attenuation	1.3	<1	$\alpha_5 = 5.35$	4.96
Spectrophotometry Scan I (Spectral Irradiance (SI) $\text{W}/\text{cm}^2 \cdot \text{nm}^{-1}$ ) $3.3\text{e-}6 \leq \text{SI} \leq 5.4\text{e-}5$		$0.4 \leq \lambda \leq 0.7$	-----	-----	-----
6	Attenuation	1.3	<1	$\alpha_6 = 5.27$	4.65
7	Attenuation	0.86	<1	$\alpha_7 = 5.80$	5.38
Spectrophotometry Scan II $4.0\text{e-}6 \leq \text{SI} \leq 1.6\text{e-}5$		$0.7 \leq \lambda \leq 1.1$	-----	-----	-----
8	Attenuation	1.3	<1	$\alpha_8 = 5.41$	4.75
9	Attenuation	0.86	<1	$\alpha_9 = 5.66$	5.35





## **APPENDIX A**

### **LDEF EXPERIMENT LOCATIONS, ENVIRONMENTS & MATERIALS**

This appendix organizes the many experiments into a form that allows quick and easy information on the location and their space environment exposure. The plots are based on a map of the LDEF spacecraft, with the skin of the spacecraft unfolded. The panels start with row nine and move back from there. This was done to place the actual RAM direction of the spacecraft on the left side and right side of the chart. In each case, just read straight down the page to get an estimate of the value.

Tables A.1.A and A.1.B - LDEF experiments mapped against the corresponding Cumulative Sun Hours and the Cumulative Atomic Oxygen Fluences. The second chart shows the panels that contain more than two experiments.

Tables A.2.A and A.2.B - LDEF experiments mapped against the corresponding Cumulative Debris and Micrometeoroid Impacts.

Table A.3 - A map of the optical experiments showing what types of optics were found in different experiments. The experiment numbers were used as the simplest way to identify them.

Table A.4 - A map of the optical component types and the materials found in each of the different experiment locations.

Table A.1.A - Map of LDEF Experiments and Environments

	9	10	11	12	1	2	3	4	5	6	7	8
F	A0076	S0001	S0001	S1001	S0001	P0004,P0006	S0001	A0178	S0001	A0038	S0001	M0004
E	S0014	A0178	S0001	A0038	S0001	A0178	A0187,S1002	S0001	S0050,A0044	S1003,M0002	S0001	A0187
D	M0003,M0002	AG054	A0178	A0180,A0023	A0178	S0001,A0189	M0003,M0002	M0003	A0178	S0001,A0701	A0178	M0003
C	A0023,A0201	GRAPPLE	A0178	S0109	GRAPPLE	A0015,A0187	A0023,A0201	S0001	A0178	P0005		
B	S0010,A0134	S1005	S0001	A0201	S0001	S0001	A0138	A0054	A0178	S0001	A0178	S0001,A0068
A	S0069	A0178	A0187	S0001	A0175	A0178	A0187	A0178	S0001	S0001	A0175	A0171

Cumulative Equivalent Sun Hours for Each Tray Row

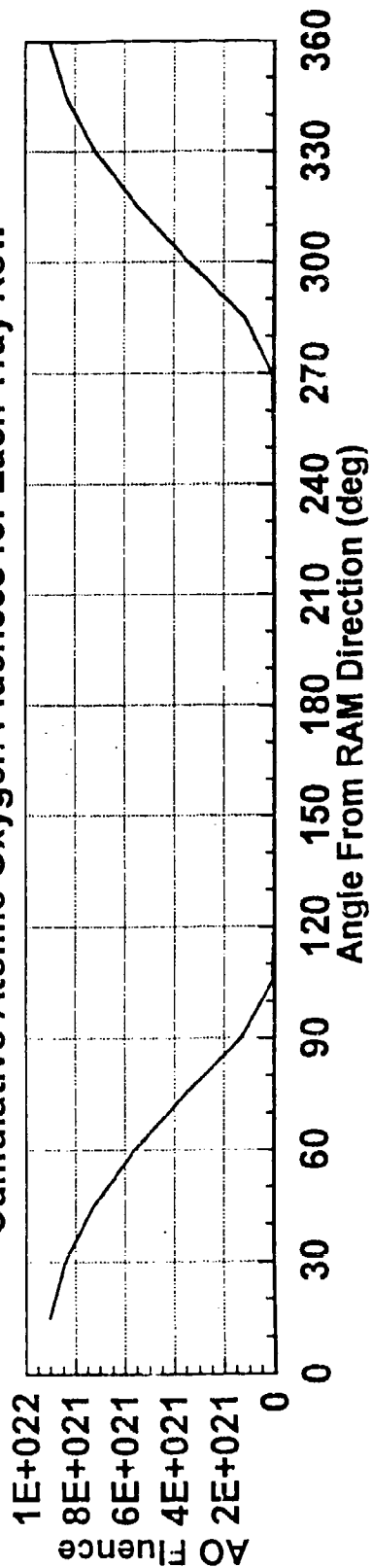
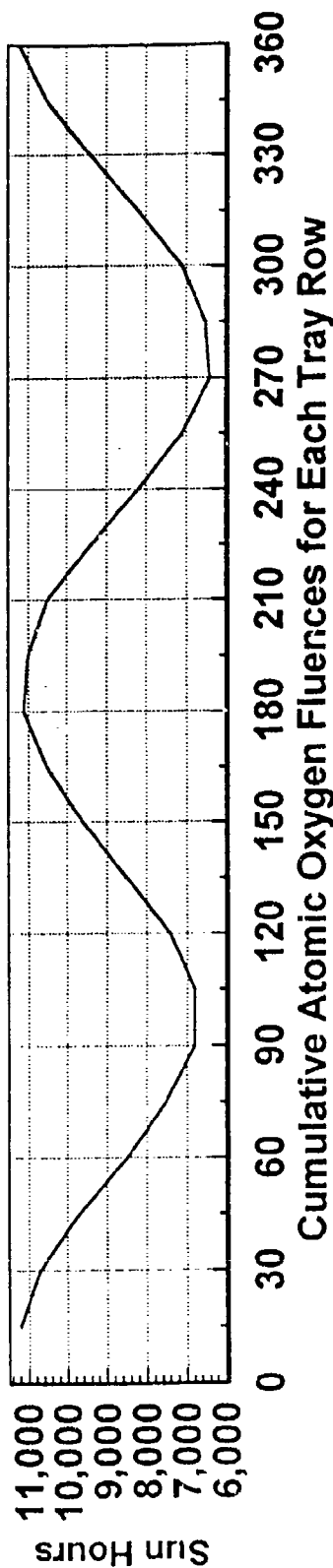
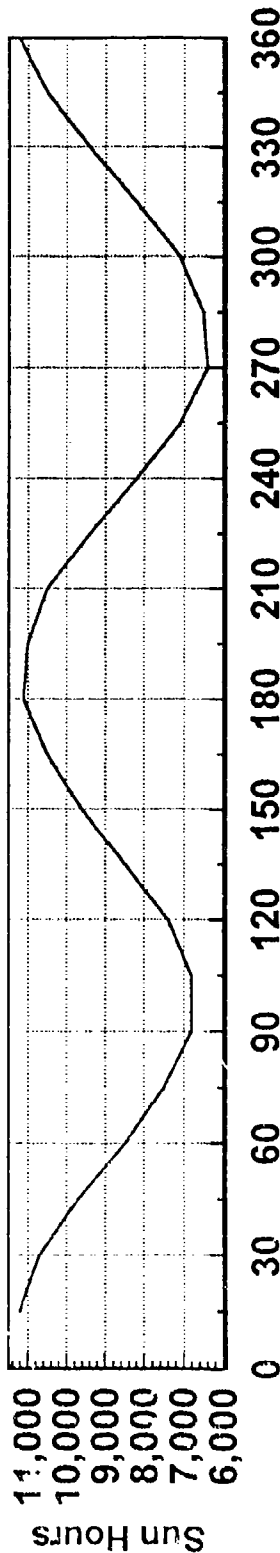


Table A.1.B - Map of LDEF Experiments and Environments

	9	10	11	12	1	2	3	4	5	6	7	8
F												
E									A0135	A0023,S1006		
D												
C									P0005	P0003		
B												
A												

Cumulative Equivalent Sun Hours for Each Tray Row



Cumulative Atomic Oxygen Fluences for Each Tray Row

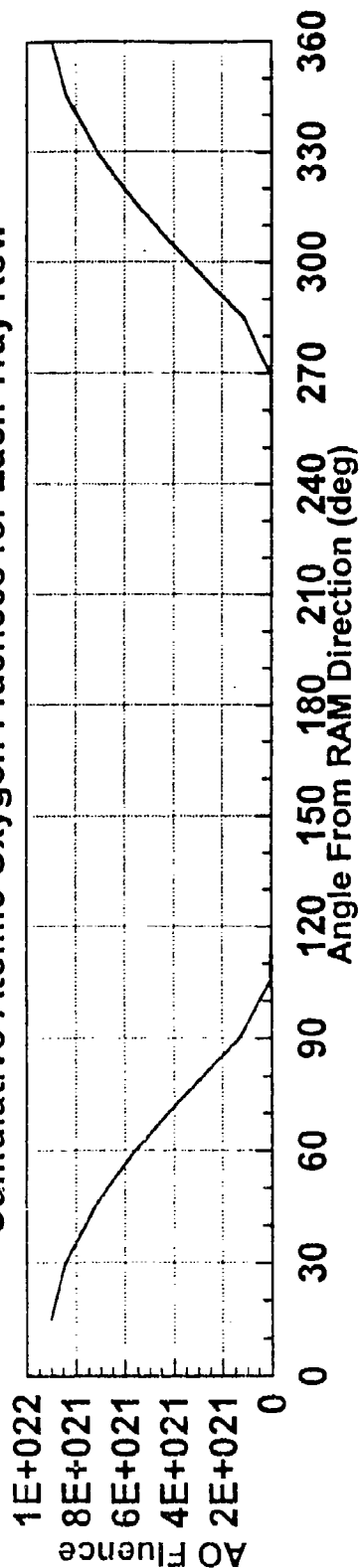


Table A.2.A - Map of LDEF Experiments and Environments

	9	10	11	12	1	2	3	4	5	6	7	8
F	A0076	S0001	S0001	S1001	S0001	P0004/P0006	S0001	A0178	S0001	A0038	S0001	M0004
E	S0014	A0178	S0001	A0038	S0001	A0178	A0187,S1002	S0001	S0050,A0044	S1003,M0002	S0001	A0187
D	M0003,M0002	A0054	A0178	A0180,A0023	A0178	S0001,A0189	M0003,M0002	M0003	A0178	S0001,A0201	A0178	M0003
C	A0023,A0201	GRAPPLE	A0178	S0109	GRAPPLE	A0015,A0187	A0023,A0201	S0001	A0178	A0178	S0001	A0178
B	S0010,A0134	S1005	S0001	A0201	S0001	S0001	A0138	A0054	A0178	S0001	A0178	S0001,A0056
A	S0089	A0178	A0187	S0001	A0175	A0178	A0187	A0187	S0001	S0001	A0175	A0171

### Cumulative Debris & Micrometeoroid Impacts

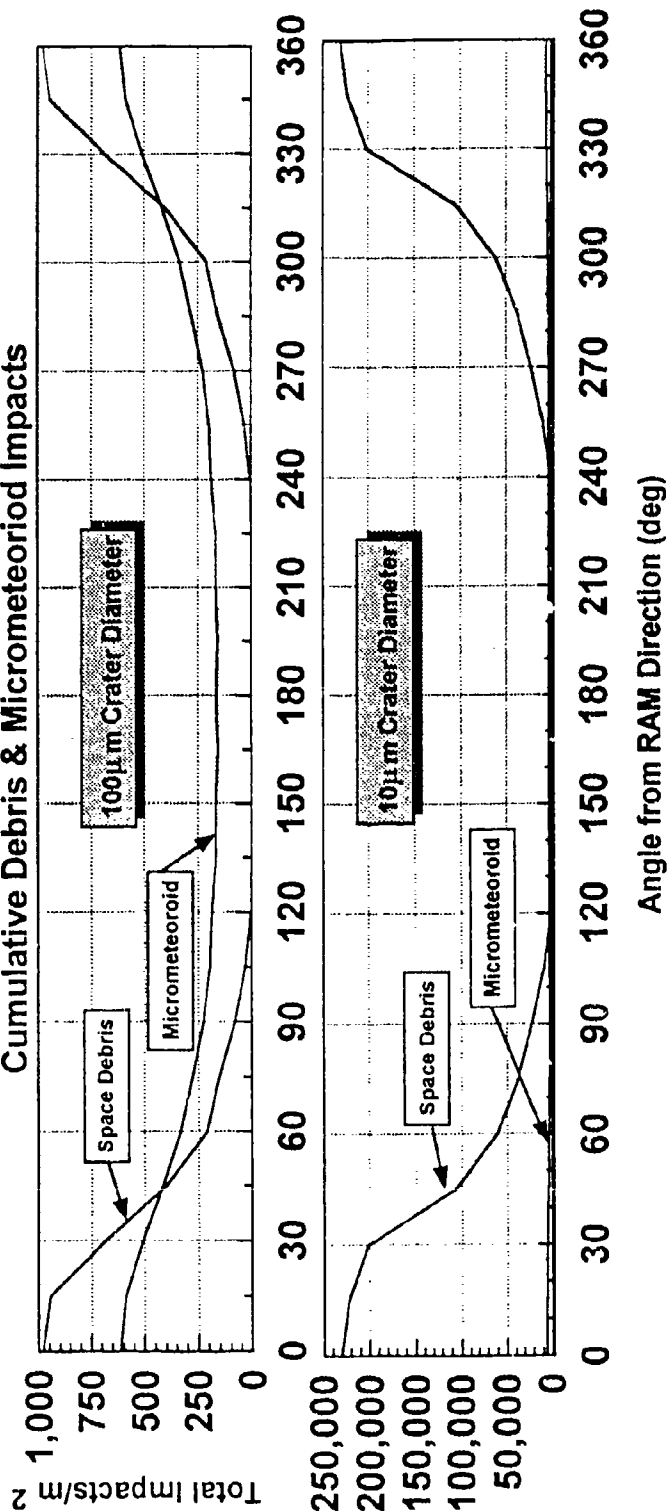


Table A.2.B - Map of LDEF Experiments and Environments

	9	10	11	12	1	2	3	4	5	6	7	8
F												
E									A0135	A0023,S1006		
D						A0172			P0005	P0003		
C	A0034,A0114	GRAPPLE			GRAPPLE	A0187,M0006	A0034,A0114					
B												A0147
A												

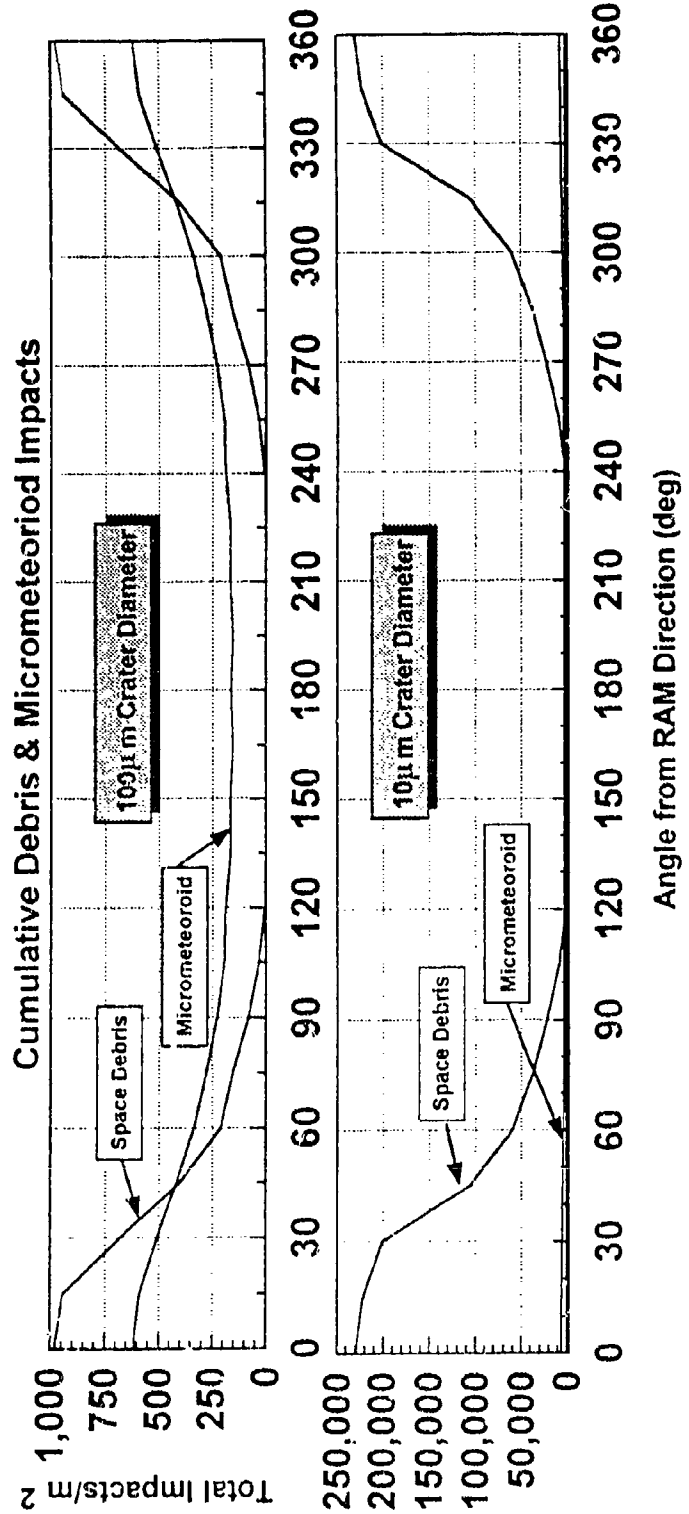


Table A.3 - Map of LDEF Optic Experiments and Optic Types

	9	10	11	12	13	14	15	16	17	18
F										
E	O5				O2,O3,O5		O1,O2,O3,O4	O1		
D	O1,O3,O6	C5		O4	O1,O3,O6	O1,O3,O6				O1,O3,O6
C	C3,O4	GRAPPLE		GRAPPLE	C3,O6	O1				
B	O1,O3				O1,O2,O3,O4	O5				O1,O2
A										O1,O2,O5

O1 = Thin Film Coating (A0138-4,A0138-5,A0034,AC056,A0147,S0050-2,M0003,A0171,M0003-2,S1003,S0010,A0114)

O2 = Optical Filters (A0138-3,A0138-4,S0050,A0056,A0147,S1002,A0171)

O3 = Mirrors (A0138-4,A0138-5,S0050,M0003-7,M0006,S1002,S0010,A0114)

O4 = Optical Windows (S0050,A0034,S0050-1,A0135)

O5 = Solar Cells (S1002,A0171,S0014,S1001,A0054)

O6 = Laser Optics (S0050,M0003,M0006,S0050-3)

Table A.4 - Map of LDEF Optic Experiments and Optic Types

	9	10	11	12	1	2	3	4	5	6	7	8
F												
E	5						O2,O3,O5		O1,O2,O3,O4	O1		
D	O1,O3,O6	O3				O4	O1,O3,O6	O1,O3,O6				O1,O3,O6
C	O1,O3,O4	GRAPPLE			GRAPPLE	O3,O6	O1					
B	O1,O3						O1,O2,O3,O4	O5				O1,O2
A												O1,O2,O5

O1 = Thin Film Coating (Ag,Au,Pt,Nb,Ni,Al,C,Si,Ge,LiF,MgF2,PbTe,ZnSe,ZnS,SiO,PbF2,CdTe,Si2,ZnO,Al2O3)

O2 = Optical Filters (UV Gas Filter, UV Crystal Filter, Metallic Interference Filter, PbTe/ZnSe, Ge/SiO,PbF2,SiO)

O3 = Mirrors (Al, Pt, Au, Ag, Be)

O4 = Optical Windows (SiC2, CaF2, Al2O3, SiO2, BoroSilicate)

O5 = Solar Cells (Silicon Cells 5-Types, GaAs Cells 1 Type)

O6 = Laser Optics (HeNe & CO2 Laser tubes, GaAlAs Diode Laser, Nd:YAG Laser Rod, Flashlamp, Laser Mirrors)





## **APPENDIX B EXPERIMENT DESCRIPTIONS**

This appendix provides a description of each of the optics-related experiments flown on LDEF, listed by experiment number. For each experiment number, the title, experiment LDEF tray locations, principal investigators, and materials flown are listed. This appendix, in conjunction with Appendix A, provides a useful cross-reference in understanding the experimental effects described in Chapter 4.

## Experiment A0034

**TITLE:** Atomic Oxygen Simulated Outgassing Experiment

**TRAY  
LOCATION:** C9, C3

**PRINCIPAL  
INVESTIGATORS:**

Roger C. Linton NASA Marshall Space Flight Center Alabama, 35812	Charles C. Burris Southern University Baton Rouge, LA
Robert L. Scott, Jr. Ciba-Geigy Saint Gabriel, LA	

**OPTICAL  
MATERIALS:**

Coatings on borosilicate or fused silica windows:  
Z-93 whitepaint (ITRI) zinc oxide in potassium silicate  
binder  
A-276 white paint; titanium dioxide pigment in polyurethane  
binder  
S-13G (ITRI); zinc oxide in RTV602 silicone binder  
S-13G/Lo (ITRI); zinc oxide in RTV602 silicone binder,  
improved formulation for outgassing  
Z-306 Chemglaze; black, titanium dioxide and carbon in  
polyurethane binder  
Z-326 Chemglaze;  
YB71 zinc ortho titanate (ZOT) (ITRI)  
anodized aluminum protective cover

## Experiment A0056

**TITLE:** Exposure to Space Radiation of High Performance Infrared Multilayer Filters and Materials

**TRAY LOCATION:** G12, B8,

**PRINCIPAL INVESTIGATORS:** Gary J. Hawkins, John Seeley, Roger Munneman  
The University of Reading, Infrared Multilayer Lab  
Dept. of Cybernetics,  
Reading, Berkshire, RG6 2AY, England

<b>OPTICAL MATERIALS:</b>	<b>UNCOATED CRYSTALS AND MATERIALS</b>	<b>SOFT SUBSTRATE/COATING MATERIALS</b>
	Calcium Fluoride	KRS-5 with 61-layer AS2S3/KRS-5
	Magnesium Fluoride	Krs-6 with 33-layer ZnS/KRS-5 & ZnSe/KRS-5
	Germanium	KRS-5 with 61-layer CdTe/KRS-5 & AS2S3/KRS-5
	Silicon	
	Cadmium Telluride	<b>HARD SUBSTRATE/FILTER COATINGS</b>
	Sapphire	Ge with PbTe/ZnSe
	Y-cut Quartz	Ge with PbTe/ZnS
	Z-cut Quartz	Al <sub>2</sub> O <sub>3</sub> with Ge/SiO <sub>2</sub>
	KRS-5	ZnSe with PbF <sub>2</sub>
	Krs-6	Si with SiO <sub>2</sub>

## Experiment A0138-3

TITLE:	Thin Film Metal Film and Multilayer Experiment
TRAY LOCATION:	B3
PRINCIPAL INVESTIGATORS:	J.P. Delaboudiniere CNRS/LPSP Verrieres le Buisson, France
OPTICAL MATERIALS:	EUV thin films UV gas filters photocathodes UV crystal filters

## Experiment A0138-4

**TITLE:** Vacuum - Deposited Optical Coatings Experiment

**TRAY  
LOCATION:** B3

<b>PRINCIPAL INVESTIGATORS:</b>	Jean Charlier	Irene Alet
	Matra Defense DET/DTO 17, rue Paul Dautier 78140 Velizy Villacoublay FRANCE	CNES/Centre Spatial de Toulouse 18 Avenue Edouard Belin 31055 Toulouse Cedex FRANCE

**OPTICAL  
MATERIALS:**

- Metallic interference filter made in ultrahigh vacuum, wavelength=121.6 nm
- Metallic interference filter made in classical vacuum, wavelength=121.6 nm
- Metallic interference filter, wavelength=130 nm
- Dielectric interference filter, wavelength=500 nm
- Bandpass interference filter, wavelength= 15 um
- Al+MgF<sub>2</sub> metallic mirror on glass substrate measured at 121 nm
- Al+MgF<sub>2</sub> metallic mirror on Kanigen substrate at 121 nm
- Al+LiF metallic mirror on glass substrate at 102 nm
- Al+LiF metallic mirror on Kanigen substrate
- Platinum mirror at 121 nm
- Ag+ThF<sub>3</sub> metallic mirror on glass substrate at 450 nm
- Ag+ThF<sub>3</sub> metallic mirror on Kanigen substrate at 450 nm
- Dielectric mirror at wavelength=250 nm
- Dielectric mirror at wavelength=170 nm
- Metallic selective mirror at wavelength=170 nm
- SiO<sub>2</sub>-TiO<sub>2</sub> dielectric mirrors
- Antireflection coating in 14- to 16-um region
- Antireflection coating in 8- to 13-um region
- Dichromatic separation in visible and infrared region at 10 um

## Experiment A0138-5

**TITLE:** Ruled and Holographic Gratings Experiment

**TRAY  
LOCATION:** B3

<b>PRINCIPAL INVESTIGATORS:</b>	Francis Bonnemason	Renee Alet
	Instruments SA Jobin Yvon Longjumeau, FRANCE	CNES/Centre Spatial de Toulouse 18 Avenue Edouard Belin 31055 Toulouse Cedex, FRANCE

**OPTICAL  
MATERIALS:**

- Replica from ruled grating (glass blank + epoxy photoresist + coating) Type G. Grating characteristic is 1200 G/MM blazed at 250 nm, Al-coated.
- Original master holographic grating (glass blank + sensitive photoresist + coating) Type H. Grating characteristic is 3600 G/MM 50-150 nm spectral range, platinum-coated.
- Ion etched original master grating (glass blank + coating) Type HU. Grating characteristic is 1200 C/MM blazed at 250 nm, Al-coated.
- Control mirrors (glass blank + coating) Type W.

## Experiment A0147

**TITLE:** Passive Exposure of Earth Radiation  
Budget Experiment Components

**TRAY  
LOCATION:** B8, G12, B9

**PRINCIPAL  
INVESTIGATORS:** John. R. Hickey  
The Eppley Laboratory, Inc.  
Newport, RI

Thomas A. Mooney and Ali  
Smajkiewicz  
Barr Associates  
Westford, MA

**OPTICAL  
MATERIALS:** **SOLAR SENSORS**  
[Channel #/filter/spectral band in  
um/thermopile]  
1S fused silica 0.18 to 3.8 N3  
thermopile  
2S fused silica 0.18 to 3.8 N3  
thermopile  
3S None (total rad.) <0.2 to >50 N3  
flat plate  
4S OG-530 glass 0.526 to 2.8 N3  
5S RG-695 glass 0.698 to 2.8 N3  
6S Interference filter 0.395 to 0.510  
N3  
7S Interference filter 0.344 to 0.460  
N3  
8S Interference filter 0.300 to 0.410  
N3  
9S Interference filter 0.285 to 0.365  
K2  
10S Interference filter 0.250 to 0.320  
K2  
10C None (total rad.) <0.2 to >50 HF  
cavity

**EARTH FLUX SENSORS**  
11E None (total rad.) <0.2 to  
>50 N3 flat plate  
12E None (total rad.) <0.2 to  
>50 N# flat plate  
13E Fused silica  
hemispheres 0.2 to 3.8 N3  
14E RG-695 glass  
hemispheres 0.695 to 2.8 N3  
**EPPLEY LAB METAL &  
DIELECTRIC COATING  
MATERIAL**  
Zirconium Oxide  
Zinc Sulfide  
Thorium Fluoride  
Cryolite  
Lead Fluoride  
Lead Chloride



## Experiment A0171

**TITLE:** Solar Array Materials Passive LDEF Experiment

**TRAY  
LOCATION:** A8

**PRINCIPAL  
INVESTIGATORS:** Ann F. Whitaker & Leighton E. Young  
NASA Marshall Space Flight Center  
MSFC, AL

**OPTICAL  
MATERIALS:** This passive experiment contains a total of about 100 materials and material processes which address primarily solar array materials, including solar cells, composites, thin films, paints, metals and other polymers. This database will record results concerning the solar cells only. Seven separate MSFC photovoltaic (solar cells) were flown on this experiment. All test articles underwent substantial atomic oxygen erosion of their polyimide (Kapton) substrate structures with the effect that one module was lost prior to orbiter rendezvous with LDEF; one came loose and drifted away when LDEF was grappled; and one (M3) was attached at only one corner when LDEF was retrieved. The latter was found on the floor of the cargo bay when LDEF was removed.

## Experiment A0172

**TITLE:** Effects of Solar Radiation on Glasses

**TRAY  
LOCATION:** D2, G12

**PRINCIPAL  
INVESTIGATORS:** D. Kinser, R. Weller, M. Mendenhall, D. Wiedlocher  
Vanderbilt University  
Nashville, TN.  
  
R. Nichols, D. Tucker and A. Shitaker  
Marshall Space Flight Center  
MSFC, AK 35812

**OPTICAL  
MATERIALS:** commercial optical fused silica  
low iron soda-lime-silica glass  
pyrex 7740 glass  
vycor 7913 glass  
bk-7 glass  
Zerodur glass ceramic

## Experiment M0003-2

**TITLE:** Laser Optics

**TRAY  
LOCATION:** D3, D4, D8, D9

**PRINCIPAL  
INVESTIGATORS:** Linda De Hainaut  
PL/LTS  
Kirtland AFB, NM

**OPTICAL  
MATERIALS:** Ten sets of six samples each (120 surfaces); each set uniquely exposed; two control sets not flown. Each set contains:  
uncoated fused silica (T22 Supersil-W1, Amersil, Inc., finished at Perkin Elmer)  
MgF2 coated fused silica (coating is M.G.D.A by E.M Chemical Co; 1/2 wavelength at 1.06 um; Perkin Elmer coater)  
bare polished molybdenum (low carbon ARC casted bar stock; Amax Specialty metal)  
molybdenum coated with Cr, Ag & ThF4 (ThF5-Cerac, 99% pure; Ag-Marz Wire, 99.99% pure; Cr-Electronic Space Products, 99.99% pure)  
diamond turned copper (OFHC)  
diamond turned Ni plated Cu (Northrup?)  
Four sets on Leading Edge exposed for: 70 mos., 3 mos., 6 mos. and 9 mos.  
Four sets on Trailing Edge exposed for: 0 mos., 3 mos., 6 mos., and 9 mos.  
Two sets control samples never flown

## Experiment M0003- 4

TITLE:	Advanced Solar Cell and Coverglass Analysis
TRAY LOCATION:	D3, D4, D8, D9
PRINCIPAL INVESTIGATORS:	Terry M. Trumble Aerospace Power Division Aero Propulsion and Power Directorate Wright Patterson AFB, OH
OPTICAL MATERIALS:	The experiment consists of 48 coverglass samples and 12 solar cell strings. Sixteen of the coverglass samples were on the leading edge and 16 on the trailing edge, and 16 on the backside of a tray protected from direct exposure to the Leo environment. An additional 15 samples were used as control samples and were not flown.

## Experiment M0003- 7

TITLE:	Space Environmental Effects on Coated Optics
TRAY LOCATION:	D4, D8, D9
PRINCIPAL INVESTIGATORS:	Terry M. Donovan, J.M. Bennet, R.Z. Dalbey and D.K. Burge Thin Film Physics Section Naval Weapons Center China Lake, CA
OPTICAL MATERIALS:	(Si/Al <sub>2</sub> O <sub>3</sub> ) <sub>3</sub> /Ag/Si (Si/Al <sub>2</sub> O <sub>3</sub> ) <sub>2</sub> /Ag/Mo (ZnS/Al <sub>2</sub> O <sub>3</sub> ) <sub>4</sub> /Ag/Mo (ZnS/ThF <sub>3</sub> ) <sub>5</sub> /Ag/Mo (Al <sub>2</sub> O <sub>3</sub> )/CaF <sub>2</sub>

## Experiment M0003-11

TITLE:	Contamination Monitoring
TRAY LOCATION:	D3, D4, D8, D9
PRINCIPAL INVESTIGATORS:	Eugene Borson The Aerospace Corporation Los Angeles, CA
OPTICAL MATERIALS:	Low Scatter, Black Glass Mirror Aluminized, Fused Silica Mirror, Front Surface Low Scatter, Nickel Mirror Low Scatter, Gold Coated Nickel Mirrors Gold on Copper Mirror KRS-5 & Zinc Selenide Multiple Internal Reflectance Elements Aluminized, Fused Silica Mirror, Second Surface

## Experiment M0003-14

TITLE:	QCM Monitor
TRAY LOCATION:	D3, D9
PRINCIPAL INVESTIGATORS:	W.K. Stuckey, and G. Radhakrishnan Aerospace Corporation  D. Wallace
OPTICAL MATERIALS:	Quartz Crystals Coated with 150 Å of InO <sub>3</sub> /9000 Å (AL+Al <sub>2</sub> O <sub>3</sub> ) Quartz Crystals Coated with 150 Å of ZnS/9000 Å (AL+AL <sub>2</sub> O <sub>3</sub> )

## Experiment S0014

**TITLE:** Advanced Photovoltaic Experiment (APEX): Preliminary Flight Results and Post-Flight Findings

**TRAY  
LOCATION:** E9

**PRINCIPAL  
INVESTIGATORS:** David J. Brinker, John Hickey & The Eppley  
David Scheiman Laboratory, Inc.  
NASA Lewis Research Center Newport, RI  
Cleveland, OH

**OPTICAL  
MATERIALS:** APEX SOLAR CELL TYPES  
Silicon: BSR/BSE, violet, vertical junction, textured,  
5.9 cm PEP, 2 mil thick  
Gallium arsenide: LPE  
Standards: Balloon, rocket, airplane, radiation  
damaged  
Goverglass: fused silica, V- and U-grooved, ceria  
doped microsheet

ABSOLUTE CAVITY RADIOMETER  
DIGITAL ANGLE SUN SENSOR



## Experiment S0050

**TITLE:** Effects of Long Duration Exposure on Active Optical System Components

**TRAY LOCATION:** E5

**PRINCIPAL INVESTIGATORS:** M. Donald Blue  
Georgia Tech. Res. Institute  
Georgia Inst. of Technology  
Atlanta GA

**OPTICAL MATERIALS:**

**PASSIVE COMPONENTS**

Black Paint Samples  
Neutral Density Filters  
Narrow-Band Filters  
Laser Mirrors  
Hot-Mirror Filter  
Lyman-Alpha Filter  
UV Filter 1600Å  
LiF Window  
AlMgF<sub>2</sub> Mirror  
Optical Glasses  
MgF<sub>2</sub> Window  
Al<sub>2</sub>O<sub>3</sub> Window  
35-mm UV Film  
Various Optical Glasses  
Black Polyethylene

**ACTIVE COMPONENTS**

ADP Modulators  
Channeltron Array  
GaAlAs Laser Diodes  
GaAsP LED  
Nd: YAG Rods  
CO<sub>2</sub> Waveguide Laser  
HeNe Laser Holographic Crystals  
Laser Flash Lamps

**DETECTORS**

Silicon PIN  
Silicon PV  
Silicon Gamma-Ray  
InGaAsP PV  
InSb PV  
PbS  
PbSe  
HgCdTe PV  
HgCdTe PC  
PdSi Arrays  
Pyroelectrics  
UV PMT  
UV Silicon

## Experiment S0050-1

TITLE:	Effects of Long Duration Exposure on Optical Systems Components
TRAY LOCATION:	E5
PRINCIPAL INVESTIGATORS:	Gale A. Harvey NASA Langley Research Center Hampton, VA
OPTICAL MATERIALS:	OPTICAL WINDOWS CaF <sub>2</sub> MgF <sub>2</sub> LiF Al <sub>2</sub> O <sub>3</sub> (synthetic Sapphire) SiO <sub>2</sub>

## Experiment S0050-2

<b>TITLE:</b>	Effects of Long Duration Exposure on Optical Substrates and Coatings
<b>TRAY LOCATION:</b>	E5
<b>PRINCIPAL INVESTIGATORS:</b>	John Vallimont and Keith Havey Eastman Kodak Company Rochester, NY
<b>OPTICAL MATERIALS:</b>	Kodak included 12 substrate and coating samples on the LDEF structure. There were 3 fused silica and 3 Ultra Low Expansion (ULE) uncoated glass samples, 2 ULE samples with a high reflectance silver coating, and 2 fused silica samples coated with an antireflectance (AR) coating, and 2 fused silica samples with a solar rejection coating. The samples were 32 mm diameter by 1 mm thick. A set of duplicate control samples was also manufactured and stored in a controlled environment for comparison purposes. ULE glass is described as not tolerant of the radiation environment, and was expected to show some radiation darkening.

## Experiment S0050-2

**TITLE:** Effects of Long Duration Exposure on Optical Substrates and Coatings

**TRAY  
LOCATION:** E5

**PRINCIPAL  
INVESTIGATORS:** John Vallimont and Keith Kavey  
Eastman Kodak Company  
Rochester, NY

**OPTICAL  
MATERIALS:** Kodak included 12 substrate and coating samples on the LDEF structure. There were 3 fused silica and 3 Ultra Low Expansion (ULE) uncoated glass samples, 2 ULE samples with a high reflectance silver coating, and 2 fused silica samples coated with an antireflectance (AR) coating, and 2 fused silica samples with a solar rejection coating. The samples were 32 mm diameter by 1 mm thick. A set of duplicate control samples was also manufactured and stored in a controlled environment for comparison purposes. ULE glass is described as not tolerant of the radiation environment, and was expected to show some radiation darkening.



## APPENDIX C

### LIST OF REFERENCES

#### C.1 REFERENCES FOR CHAPTER 3

1. Kinard, W. H. and Martin, G. D., Long Duration Exposure Facility (LDEF) Space Environments Overview, LDEF--69 Months in Space, First Post-Retrieval Symposium, NASA Conference Publication 3134, Part 1, June 1991.
2. Sawyer, Donald M. and Vette, James I., AP-8 Trapped Proton Environment for Solar Maximum and Solar Minimum, National Science Data Center, Goddard Space Flight Center, NSSDC/WDC-A-R&S 76-06, 1976.
3. Teague, Michael J. and Vette, James I., A Model of the Trapped Electron Population for Solar Minimum, National Science Data Center, Goddard Space Flight Center, NSSDC 74-03, 1974.
4. Vette, James I., The AE-8 Trapped Electron Model Environment, National Science Data Center, Goddard Space Flight Center, NSSDC/WDC-A-R&S 91-24, 1991.
5. Watts, John W., Armstrong, T. W., and Colborn, B. L., Revised Prediction of LDEF Exposure to Trapped Radiation, LDEF Second Post-Retrieval Symposium, NASA Conference Publication 3194, Part 1, 1993.
6. Blake, J. B. and Imamoto S. S., A Measurement of the Radiation Dose to LDEF by Passive Dosimetry, LDEF Second Post-Retrieval Symposium, NASA Conference Publication 3194, Part 1, 1993.
7. Bourrieau, J., LDEF: Dosimetric Measurement Results (AO138-7 Experiment), LDEF Second Post-Retrieval Symposium, NASA Conference Publication 3194, Part 1, 1993.
8. Frank, A. L., Benton, E. V., Armstrong, T. W., and Colborn, B. L., Absorbed Dose Measurements and Predictions on LDEF, LDEF Second Post-Retrieval Symposium, NASA Conference Publication 3194, Part 1, 1993.
9. Space Environment for USAF Space Vehicles, MIL-STD-1809, 15 February 1991.
10. Meteoroid Environment Model, 1969, Near Earth to Lunar Surface, NASA SP-8013, March 1969.
11. Susko, Michael, A Review of Micrometeoroid Flux Measurements and Models for Low Orbital Altitudes of the Space Station, NASA Technical Memorandum 86466, September 1984.

### C.1, References for Chapter 3

---

12. Kessler, D. J., Reynolds, R. C., and Anz-Meador, P. D., Orbital Debris Environment for Spacecraft Designed to Operate in Low Earth Orbit, NASA Technical Memorandum 100471, April 1989.
13. Johnson, N.L., and McKnight, D.S., Artificial Space Debris, Malabar, FL: Orbit Book Company, 1987.
14. Watts, A. et al., Impact Effects on Optics Survivability, POD Associates, 1993.

### C.2 REFERENCES FOR CHAPTER 4

1. Wiedlocher, David E. and Kinser, Donald L., Cratering in Glasses Impacted by Debris of Micrometeorites, Vanderbilt University, LDEF Second Post-Retrieval Symposium, p. 529ff, June 1992.
2. Melosh, H.J., Impact Cratering: A Geological Process, Oxford Monographs on Geology and Geophysics, No. 11, Oxford University Press, New York, 1989.
3. Hörz, F., et al., Dimensionally-Scaled Penetration Experiments to Extract Projectile Sizes From Space-Exposed Surfaces, 1992 Hypervelocity Impact Symposium, Austin, TX, November 1992.
4. Watts, A. et al., Dimensional Scaling for Impact Cratering and Perforation, POD Assoc. (for Lockheed/Houston by NASA JSC), March 16, 1993.
5. DeHainaut, Linda L., Degradation of Optical Components in a Space Environment, Experiment M0003, Subexperiment 2, internal report, Phillips Laboratory, Kirtland Air Force Base, NM, July 23, 1993.
6. Harvey, Gale A., Effects of Long-Duration Exposure on Optical System Components, NASA/Langley Research Center, LDEF First Post-Retrieval Symposium, p. 1327, June 1991.
7. Havey, Keith, Mustico, Arthur; and Vallimont, John, Effects of Long Term Space Environment Exposure on Optical Substrates and Coatings (S0050-2), Eastman Kodak Co., LDEF Second Post-Retrieval Symposium, p. 1389, June 1992.
8. Vallimont, John and Havey, Keith, Effects of Long Term Exposure on Optical Substrates and Coatings (S0050-2), Eastman Kodak Co., LDEF First Post-Retrieval Symposium, p. 1341, June 1991.

## C.2, References for Chapter 4

---

9. DeHainaut, Linda L., Kenemuth, John R., Tidler, Cynthia E., and Seegmiller, David W., Degradation of Optical Components in a Space Environment, LDEF Second Post-Retrieval Symposium, pp. 1361ff, June 1992.
10. Charlier, Jean, Vacuum Deposited Optical Coatings Experiment, LDEF First Post-Retrieval Symposium, p. 1341ff, June 1991.
11. Linton, Roger C., Kamenetzky, Rachel R., and Burris, Charles L., LDEF Experiment A0034: Atomic Oxygen Stimulated Outgassing, NASA MSFC, LDEF First Post-Retrieval Symposium, pp. 763ff, June 1991.
12. Gyetvay, S.R., Coggi, J.M., and Meshishnek, M.J., Aerospace Corporation LDEF M0003 Sample Observation Data Base, 1993.
13. Blue, M. D., LDEF Active Optical System Components Experiment, Georgia Tech Research Institute, LDEF First Post-Retrieval Symposium, pp. 1317ff, June 1991.
14. Blue, M. D., Degradation of Electro-Optical Components Aboard LDEF, Georgia Tech Research Institute, LDEF Second Post-Retrieval Symposium, pp. 1333ff, June 1992.
15. Dursch, H.W., Spear, W.S., Miller, E.A., Bohnhoff-Hlavacek, G.L., and Edelman, J., Analysis of Systems Hardware Flown on LDEF - Results of the Systems Special Investigation Group, NASA Contractor Report 189628, Boeing, April 1992.
16. Hawkins, Gary J., Seeley, John S., and Hunneman, Roger, Exposure to Space Radiation of High Performance Infrared Multilayer Filters & Materials Technology Experiment (A0056), LDEF First Post-Retrieval Symposium, pp. 1477ff, June 1991.
17. Donovan, T.M., Bennett, J.M., Dalbey, R.Z., Burge, D.K., and Gyetvay, S., Space Environmental Effects on Coated Optics, LDEF First Post-Retrieval Symposium, pp. 1361ff, June 1991.
18. Raikar, Ganesh N., Gregory, John C., and Christl, Ligia C., The Interaction of Atomic Oxygen With Copper: An XPS, AES, XRD, Optical Transmission, and Stylus Profilometry Study, LDEF Second Post-Retrieval Symposium, pp. 1169, June 1992.
19. Preuss, L., Evaluation of LDEF Experiment 81002, LDEF First Post-Retrieval Symposium, pp. 1405ff, June 1991.
20. Mason, J.B., Dursch, H., and Edelman, J., Overview of the Systems Special Investigation Group, LDEF Second Post-Retrieval Symposium, pp. 1257ff, June 1992.



21. Stuckey, W.K., Radhakrishnan, G.; and Wallace, D., Post-Flight Analyses of the Crystals from the M0003-14 Quartz Crystal Microbalance Experiment, LDEF Second Post-Retrieval Symposium, pp. 1269ff.
22. George, Pete E. and Hill, Sylvester G., Results from Analysis of Boeing Composite Specimens Flown on LDEF Experiment M0003, LDEF First Post-Retrieval Symposium, pp. 1115ff, June 1991.
23. Bonnemason, Francis, Ruled & Holographic Diffraction Gratings Experiment (A0138-5), LDEF First Post-Retrieval Symposium, pp. 1301ff, June 1991.
24. Mooney, Thomas A., and Smajkiewicz, Ali, Transmittance Measurements of Ultraviolet and Visible Wavelength Filters Flown Aboard LDEF, LDEF First Post-Retrieval Symposium, pp. 1511ff, June 1991.

### C.3 REFERENCES FOR CHAPTER 6

1. Watts, A. J., et al., "Interim Report on the Effects of Space Impacts on Optics".
2. Cour-Palais, B. G., et al., "Meteoroid Environment Model - 1969 (Near Earth to Lunar Surface)", NASA SP-8013, March 1969.
3. Kessler, D. J. and Reynolds, R. C., "Orbital Debris Environment for Spacecraft Designed to Operate in Low Earth Orbit", NASA-TM-100471, September 1, 1988. Also: D.J. Kessler, Orbital Debris Technical Interchange Meeting, Phillips Laboratory presentation, 2-3 April, 1991.
4. Kessler, D. J., presentation at the Phillips Laboratory between Air Force, NASA and Aerospace Corporation, Orbital Debris Technical Interchange Meeting, 2-3 April, 1991.
5. See Reference 4: Data given by D.J. Kessler.
6. Watts, A. J., et al., "Development of Dimensional Scaling for Impact Cratering and Perforations", Lockheed ESC/NASA Johnson Space Center; Contract No. NAS9-17900, P.O. 02N0171219 (March 1993, in press).
7. Zook, H. A., "Flux Versus Direction of Impacts on LDEF by Meteoroids and Orbital Debris", Lunar and Planetary Science XXI, 1990. Also: H.A. Zook and D.J. Kessler private communications 1989 et seq.
8. Erickson data on meteor velocities: provided by H.A. Zook as per Reference 7.

### C.3, References for Chapter 6

---

9. Mirtich, M. J. and Kerslake, W. R., "The Effect of the Near Earth Micrometeoroid Environment on a Mirror Surface after 20 Years in Space", presented at the TMS Meeting, Los Angeles, 19-21 February, 1990. Also: M.J. Mirtich et al, "Effect of Eleven Years in Earth Orbit on a Mirror Surface", *Journal of Spacecraft and Rockets*, vol 27, number 3, May-June, 1990.
10. Coombs, C., Watts, A. J., Wagner, J. and Atkinson, D., "LDEF Data: Comparisons with Existing Models", Lockheed ESC/NASA Johnson Space Center; Contract No. 960-12-171, SC 02N0165768, September 1992.
11. Zolensky, M., Atkinson, D., See, T., Allbrooks, M., Simon, C., Finckenor, M. and Warren, J., "Meteoroid and Orbital Debris Record of the Long Duration Exposure Facility's Frame", *Journal of Spacecraft*, vol 28, number 2, 1991.
12. Kessler, D. J., "Origin of Orbital Debris Impacts on LDEF'S Trailing Surfaces", presented at the 2nd LDEF Symposium, San Diego, California, June 1992.
13. Kessler, D. J., "Collision Probability at Low Altitudes Resulting from Elliptical Orbits", *Adv. Space Res. Vol. 10, No. 3-4*, pp (3)393-(3)396, 1990.
14. Young, R. P., "Low-Scatter Mirror Degradation by Particulate Contamination", *Optical Engineering*, Vol. 15, No. 6, Nov-Dec 1976.
15. Lamb, L. D., "The Scattering of Infrared Light by Small Particles on Substrates", Ph.D. Thesis, Department of Physics, The University of Arizona, October 1991.
16. van de Hulst, H. C., "Light Scattering by Small Particles", Dover Publications, 1957 and 1981.
17. DeHainaut, L. L., Kenemuth, J. R., Tidler, C.E., Seegmiller, D.W., "Degradation of Optical Components in a Space Environment" presented at the 2nd LDEF Symposium, San Diego, California, June 1992.
18. Watts, A. J., et al., "Impact Effects on Optics Survivability", Subcontract No. 29-920005-72, on Prime Contract (SAIC) F29601-91-C0071 (on-going studies).

### C.4 REFERENCES FOR CHAPTER 7

1. E. W. Taylor, "Performance of the First Operable Fiber Optic Systems in Prolonged Space Orbit," *Proc SPIE*, Vol. 1691, pp. 2-16, 1992.

2. E. W. Taylor, et al., "Preliminary Analysis of WL Exp #701. 'Space Environment Effects on Operating Fiber Optic Systems,'" NASA Conf. Pub 3134
3. A. R. Johnston, L. A. Bergman, E. W. Taylor, "Fiber Optic Experiment for the Shuttle Long Duration Exposure Facility," *SPIE*, Vol 296, Aug 82, pp 40-50.
4. E. N. Gilbert, "Capacity of a Burst-noise Channel," *Bell System Technical Journal*, Vol 39, 1960, pp 1253.
5. W. M. Berrios and T. R. Sampir, "Long Duration Exposure Facility, Post-flight Thermal Analysis, Calculated Flight Temperature Data Package, Preliminary," *Proceedings First Post-Retrieval Symposium*, NASA CP-3134, NASA/LDEF Project Office, June 1991.
6. W. M. Berrios and T. R. Sampir, "Long Duration Exposure Facility, Solar Illumination Data Package," *Proceedings First Post-Retrieval Symposium*, NASA CP-3134, NASA/LDEF Project Office, June 1991.
7. E. W. Taylor, "Fiber Optics Space Effects," (presented at FOC 78, Chicago, IL) *Proceedings of Fiber Optics and Communication*, Sep 78, pp 245-7.
8. E. W. Taylor, "Some Recent Fiber Optics Research, Development and Applications Conducted by the Air Force," *Proc. Fiber Optics in the Nuclear Environment, Vol 1 - Applications*, DNA 5308P-1, 30 May 80, pp 209-221.
9. E. W. Taylor, J. M. Emmes, C. E. Barnes, and F. Wiczer "Behavior of Irradiated Plastic Clad Silica Fibers at Low Temperatures," *Photon 80 Conf. Proc. Compte-Rendu*, Paris, FR, Oct 80, pp 110-117.
10. E. W. Taylor, J. M. Emmes, W. R. Ayres, J. D. Wiltse, and J. K. Merritt, "Response of Irradiated Optical Waveguides at Low Temperatures," *SPIE*, Vol 296, Aug 82, pp 40-50.
11. E. W. Taylor, L. J. Myatt, and J. D. Wiltse, "Low Temperature Gamma Irradiation Response of Polymer Coated Optical Waveguides," *Photon 83, SPIE*, Vol 404, Paris, FR, May 1983, pp 55-59.
12. E. V. Benton and W. Heinrich, "Ionizing radiation Exposure of LDEF," USF-TR-77, Aug 1990.
13. D. S. McKnight, R. E. Dueber, and E. W. Taylor, "Space Debris and Micrometeorite Events Experienced by WL Exp #701 in Prolonged Low-Earth Orbit," *J. Geophysical Research, Space Physics*, Vol. 96, No. A6, 1 Jun 91, pp. 9829-9833.

*C.4, References for Chapter 7*

---

14. A. R. Johnston, L. A. Bergman, E. W. Taylor, "Fiber Optic Experiment for the Shuttle Long Duration Exposure Facility," *SPIE*, Vol. 296, Aug 82, pp. 40-50.
15. M. D. Blue, "LDEF Active Optical System Components Experiment," in NASA Conf Pub 3134, Part III, pp. 1317-1326, Jun 2-3, 1991.



## **APPENDIX D**

### **LIST OF ACRONYMS**

<b>AO</b>	Atomic Oxygen
<b>APEX</b>	Advanced Photovoltaic Experiment
<b>AR</b>	Antireflectance
<b>BER</b>	Burst Error Rates
<b>BMDO</b>	Ballistic Missile Defense Organization
<b>BRDF</b>	Bi-directional Reflection Distribution Function
<b>CN</b>	Cumulative Number
<b>DHW</b>	Double Halfwave
<b>DNA</b>	Defense Nuclear Agency
<b>DoD</b>	Department of Defense
<b>DPCA</b>	Data Processor Control Assembly
<b>EO</b>	Electro-optical
<b>EDAX</b>	Energy Dispersive X-ray Analysis
<b>EPDS</b>	Experiment Power & Data System
<b>ESCA</b>	Electron Spectroscopy for Chemical Analysis
<b>EUV</b>	Extreme ultraviolet
<b>FO</b>	Fiber Optics
<b>FTIR</b>	Fourier Transform Infrared
<b>GEO</b>	Geosynchronous Earth Orbit
<b>HRSMI</b>	High Resolution Scatter Mapping Instrument
<b>IF</b>	Interference Filter
<b>IMMA</b>	Ion Microprobe Mass Analyzer
<b>IR</b>	Infrared
<b>KSC</b>	Kennedy Space Center
<b>LDEF</b>	Long Duration Exposure Facility
<b>LEDs</b>	Light Emitting Diodes
<b>LEO</b>	Low Earth Orbit
<b>MEO</b>	Medium Earth Orbit

## *D, List of Acronyms*

---

<b>MIL-STD</b>	Military Standard
<b>MSFC</b>	Marshall Space Flight Center
<b>MTF</b>	Modulation Transfer Function
<b>MTM</b>	Magnetic Tape Memory
<b>NASA</b>	National Aeronautics & Space Administration
<b>NEFD</b>	Noise Equivalent Flux Density
<b>NORAD</b>	North American Aerospace Defense
<b>NRZ</b>	Non-Return-to-Zero
<b>OTDR</b>	Optical Time-Domain Reflectometer
<b>PL</b>	Phillips Laboratory
<b>PNTDs</b>	Plastic Nuclear-Track Detectors
<b>QCM</b>	Quartz Crystal Microbalance
<b>RCVR</b>	Receiver
<b>SEM</b>	Scanning Electron Microscopy
<b>SNR</b>	Signal-to-Noise Ratio
<b>SPENV</b>	Space Environment
<b>SSM</b>	Second Surface Mirror
<b>SSN</b>	Sunspot Number
<b>TC</b>	Thermal Control
<b>THW</b>	Triple Halfwave
<b>TIS</b>	Total Integrated Scatter
<b>TLDs</b>	Thermoluminescent dosimeter
<b>ULE</b>	Ultra Low Expansion
<b>USAF</b>	United States Air Force
<b>UV</b>	Ultraviolet
<b>XPS</b>	X-ray Photoelectron Spectroscopy

## **APPENDIX E**

### **LDEF PHOTOGRAPHS AND DATA REFERENCES**

This appendix contains the photographs, data graphs, and reference citations for data referred to in Chapter 4. For each graphic presented, the literature source for the information, the experiment number on which the sample was flown, and a brief comment on the graphic are presented to allow the reader to correlate this information back to Chapter 4 directly.



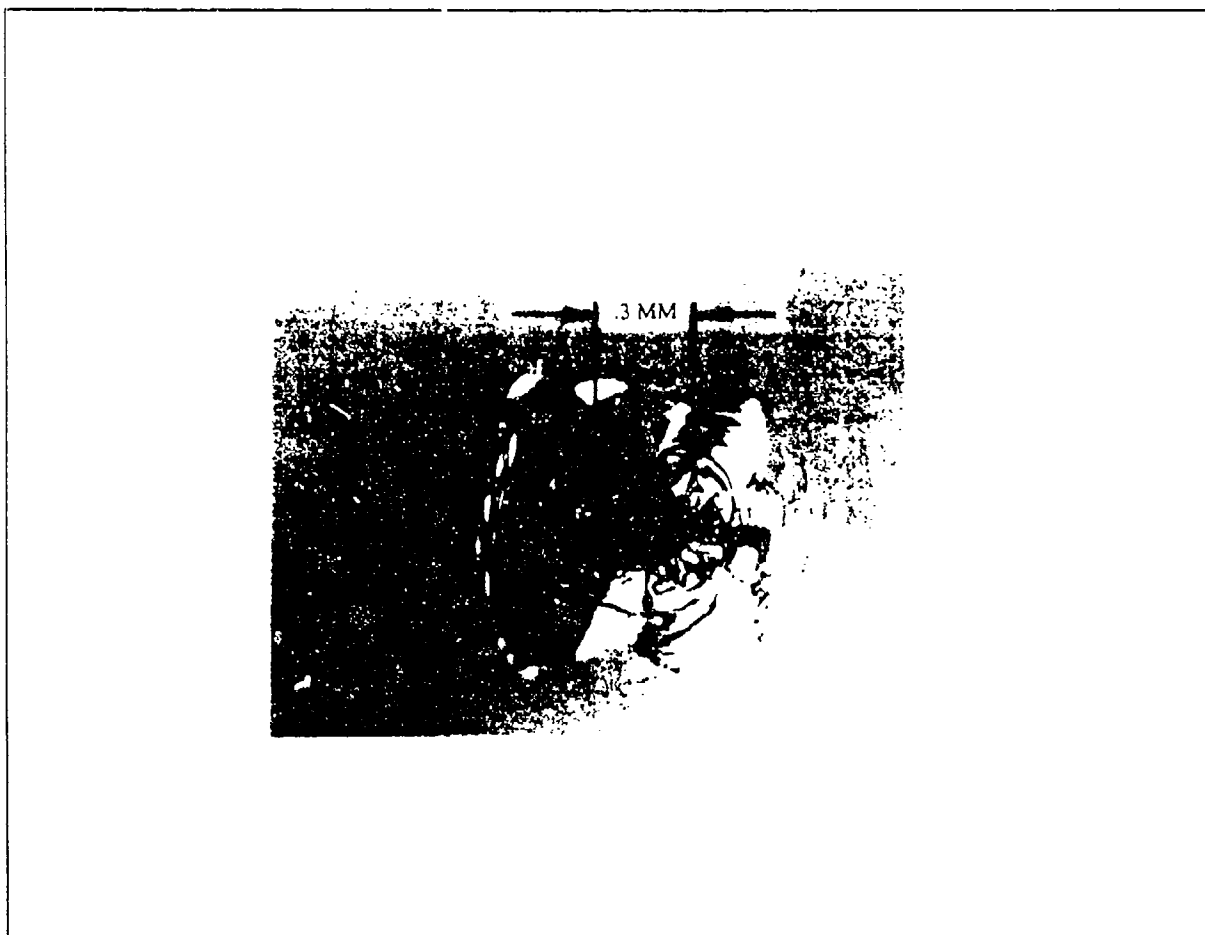


**Figure E.1. Fused Silica Micrometeoroid Impact Crater**

---

<b>REFERENCE:</b>	Havey, Keither, Mustico, Arthur, and Vallimont, John, <u>Effects of Long Term Space Environment Exposure on Optical Substrates and Coatings</u> , LDEF Second Post-Retrieval Symposium, June 1992, p. 1393
<b>EXPERIMENT:</b>	SC150-2
<b>COMMENTS:</b>	Multiple fractures occurred at the impact site.

---

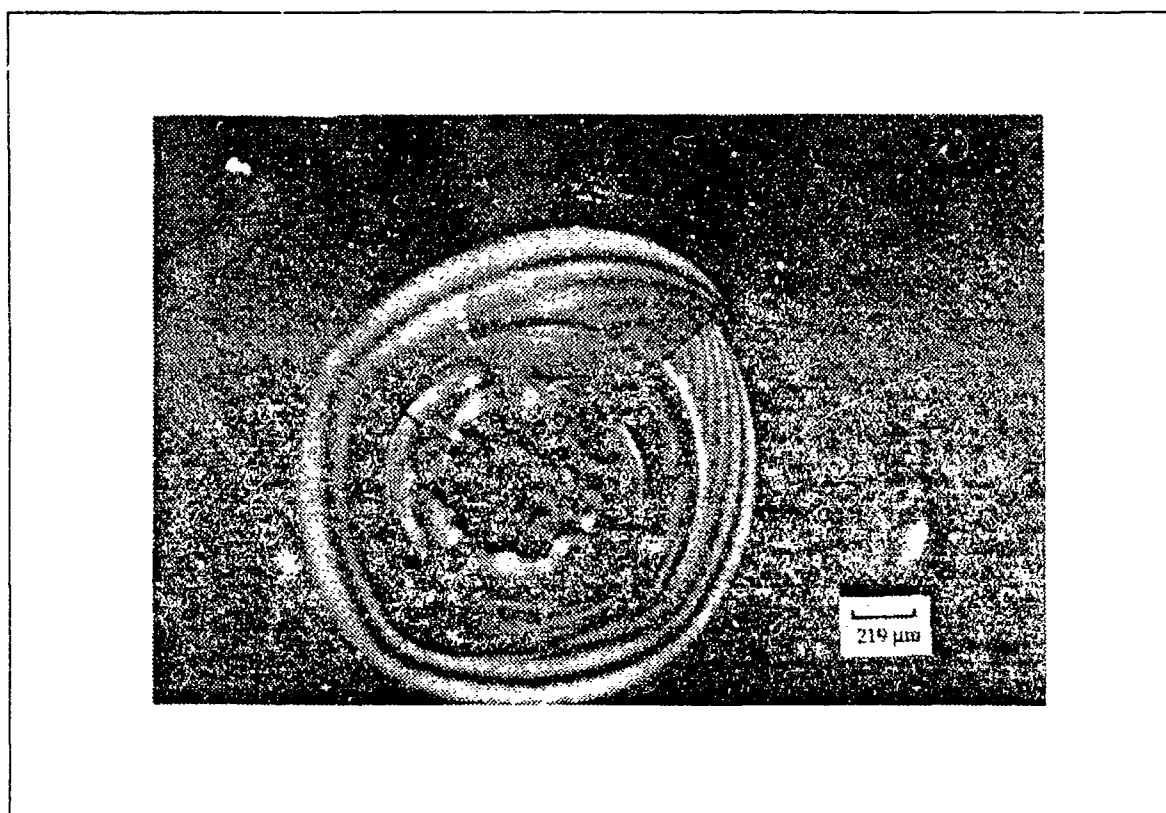


Figure E.2. Impact Effects on 7940 Fused Silica

---

<b>REFERENCE:</b>	Meshishnek, M.J., Gyetvay, S.R., Paschen, K.W., and Coggi, J.M., <u>Long Duration Exposure Facility (LDEF) Experiment M0003 Meteoroid and Debris Survey</u> , LDEF Second Post-Retrieval Symposium, June 1992, p. 395.
<b>EXPERIMENT:</b>	M0003-2
<b>COMMENTS:</b>	Local radial cracking which does not propagate a great distance from impact site.

---



Figure E.3. SEM of Impact on Fused Silica

---

<b>REFERENCE:</b>	Wiedlocher, David E., and Kinser, Donald L., <u>Cratering in Glasses Impacted by Debris or Micrometeorites</u> , LDEF Second Post-Retrieval Symposium, June 1992, p. 537
<b>EXPERIMENT:</b>	A0172
<b>COMMENTS:</b>	Jetting molten glass extends from crater. Fibers 100 μm long extending from impact zone.

---

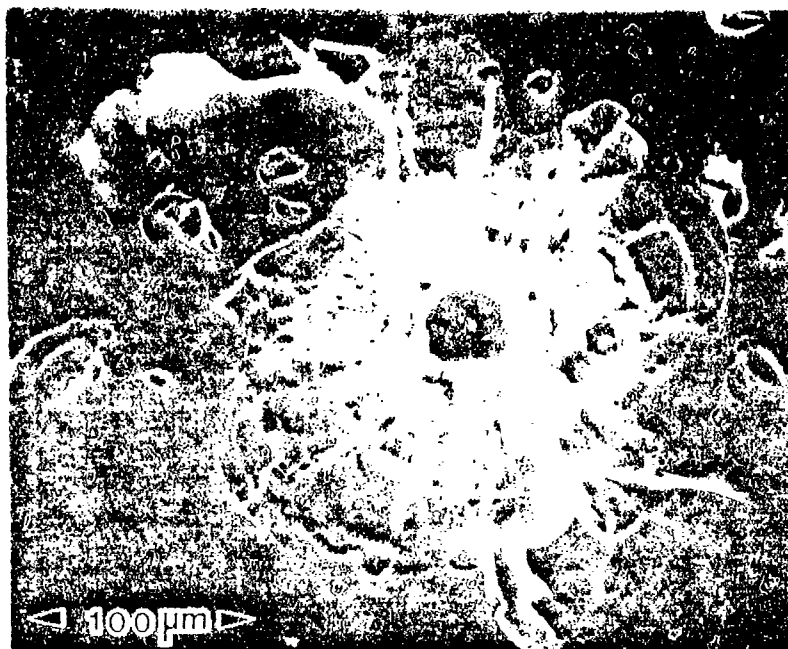


Figure E.4. SEM of Impact on Zerodur

---

REFERENCE:	Wiedlocher, David E., and Kinser, Donald L., <u>Cratering in Glasses Impacted by Debris or Micrometeorites</u> , LDEF Second Post-Retrieval Symposium, June 1992, p. 536
EXPERIMENT:	A0172
COMMENTS:	Central pit is surrounded by a zone of fragmented material with numerous radial cracks. Annular region adjacent to crater missing numerous fragments. Debris from fragmented area captured in melt zone.

---

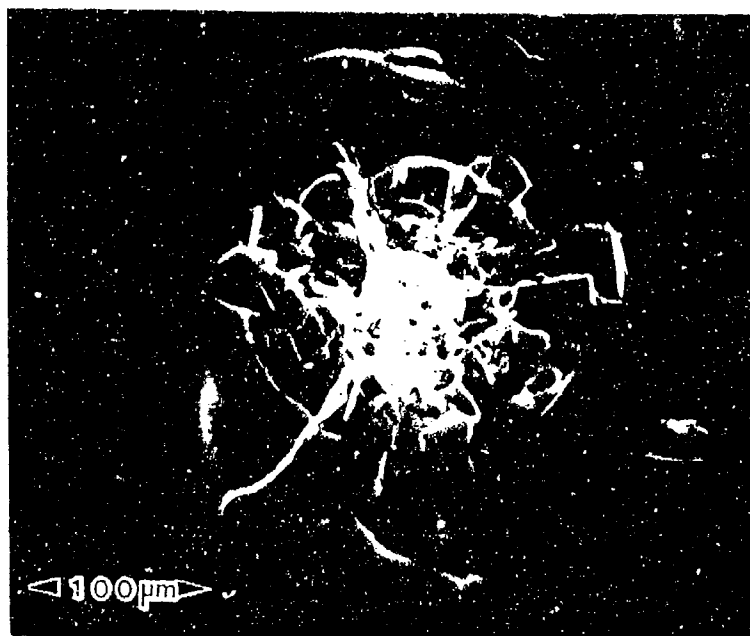


Figure E.5. SEM of Impact on Zerodur

---

REFERENCE:	Wiedlocher, David E., and Kinser, Donald L., <u>Cratering in Glassess Impacted by Debris or Micrometeorites</u> , LDEF Second Post-Retrieval Symposium, June 1992, p.538
EXPERIMENT:	A0172
COMMENTS:	No melting. Fragmentation of the order 0.5 $\mu\text{m}$ . Damage similar to impacts with melt except in central fission zone.

---



Figure E.6. SEM of Impact on Pyrex

---

REFERENCE:	Wiedlocher, David E., and Kinser, Donald L., <u>Cratering in Glasses Impacted by Debris or Micrometeorites</u> , LDEF Second Post-Retrieval Symposium, June 1992, p. 536
EXPERIMENT:	A0172
COMMENTS:	Damage extends five times central pit radius.

---

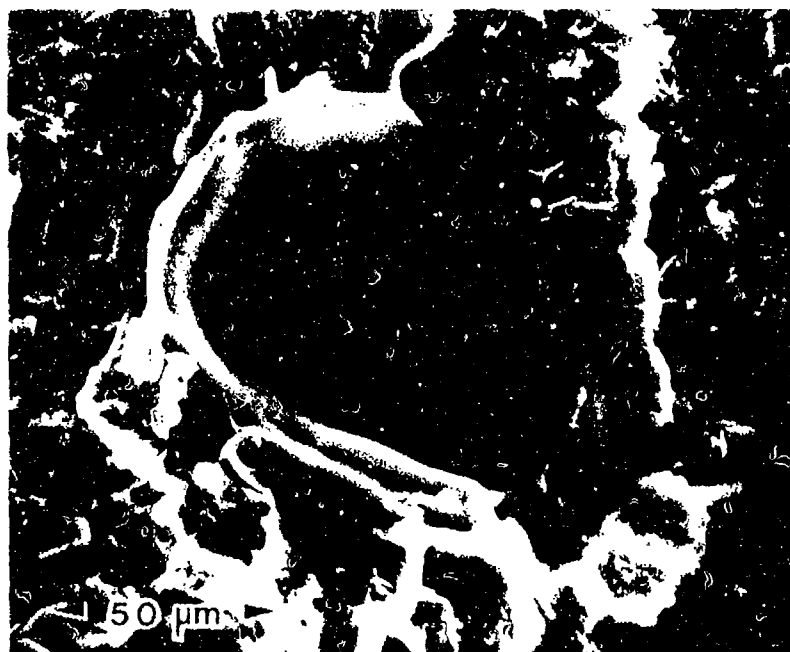


Figure E.7. SEM of Impact on Pyrex

---

REFERENCE:	Wiedlocher, David E., and Kinser, Donald L., <u>Cratering in Glasses Impacted by Debris and Micrometeorites</u> , LDEF Second Post Retrieval Symposium, June 1992, p. 538
EXPERIMENT:	A0172
COMMENTS:	Unsymmetric splash due to oblique impact. Crater is circular.

---

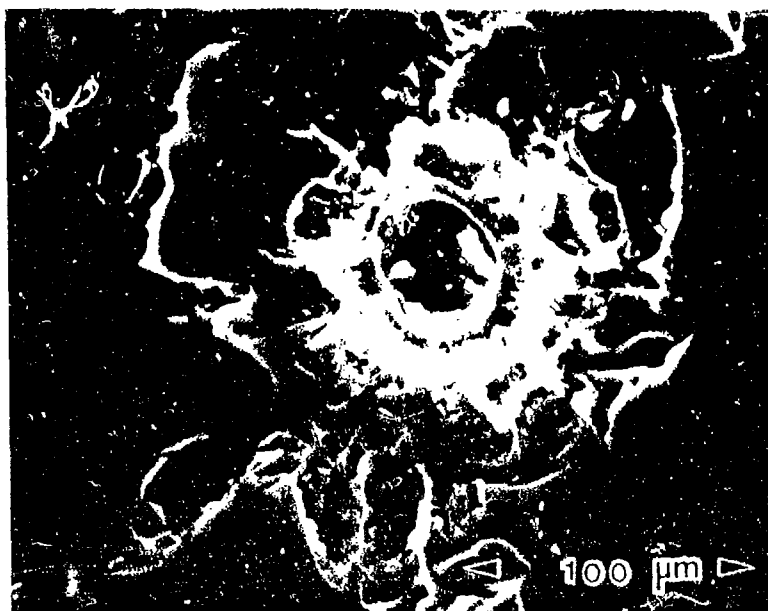


Figure E.8. SEM of Impact on BK-7 Glass

---

REFERENCE:	Wiedlocher, David E., and Kinser, Donald L., <u>Cratering in Glasses Impacted by Debris or Micrometeorites</u> , LDEF Second Post-Retrieval Symposium, June 1992, p.537
EXPERIMENT:	A0172
COMMENTS:	Bubbles escaping the melt region indicate temperature and pressures at impact exceeded those for vaporization.

---



SAMPLE	CENTRAL MELT PIT DIAMETER ( $\mu\text{m}$ )	CRATER DIAMETER ( $\mu\text{m}$ )	SPALL SURFACE DIAMETER ( $\mu\text{m}$ )
BK-7	40	100	200
Fused silica	50	120	250
Soda-Lime-Silica	80	175	475
Pyrex	85	200	400
Zerodur(I)	None Measured	100	275
Zerodur(II)	75	200	400
Zerodur(III)	50	150	300

Figure E.9. Impact Site Damage Size

---

**REFERENCE:** Wiedlocher, David E., and Kinser, Donald L.,  
Cratering in Glasses Impacted by Debris or  
Micrometeorites, LDEF Second Post-Retrieval  
Symposium, June 1992, p.534

**EXPERIMENT:** A0172

**COMMENTS:** Spall surface diameter on the order of factors of 2  
or greater than the crater diameter.

---

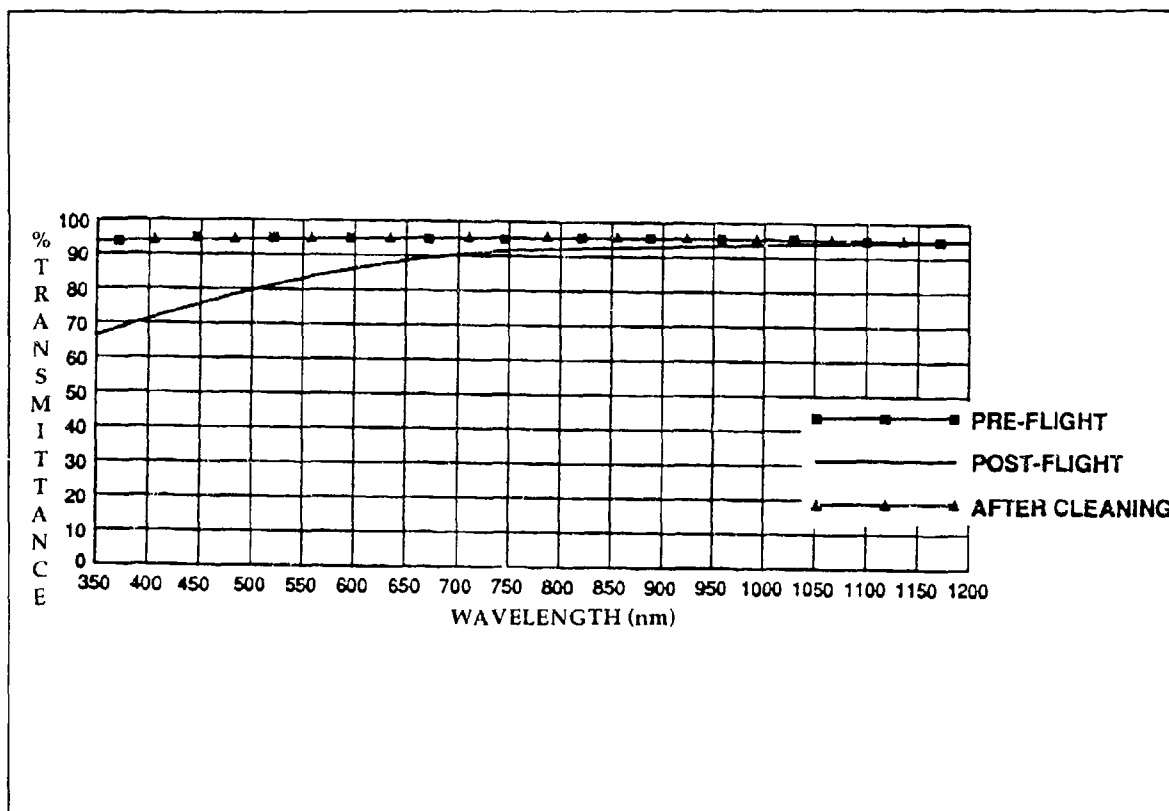


Figure E.10. Spectral Transmission of Uncoated Fused Silica

<b>REFERENCE:</b>	Havey, Keith, Mustico, Arthur, and Vallimont, John, <u>Effects of Long Term Space Environment Exposure on Optical Substrates and coatings (S0050-2)</u> , LDEF Second Post-Retrieval Symposium, June 1992, p.1394
<b>EXPERIMENT:</b>	S0050-2
<b>COMMENTS:</b>	Cleaning returned performance to pre-flight values.

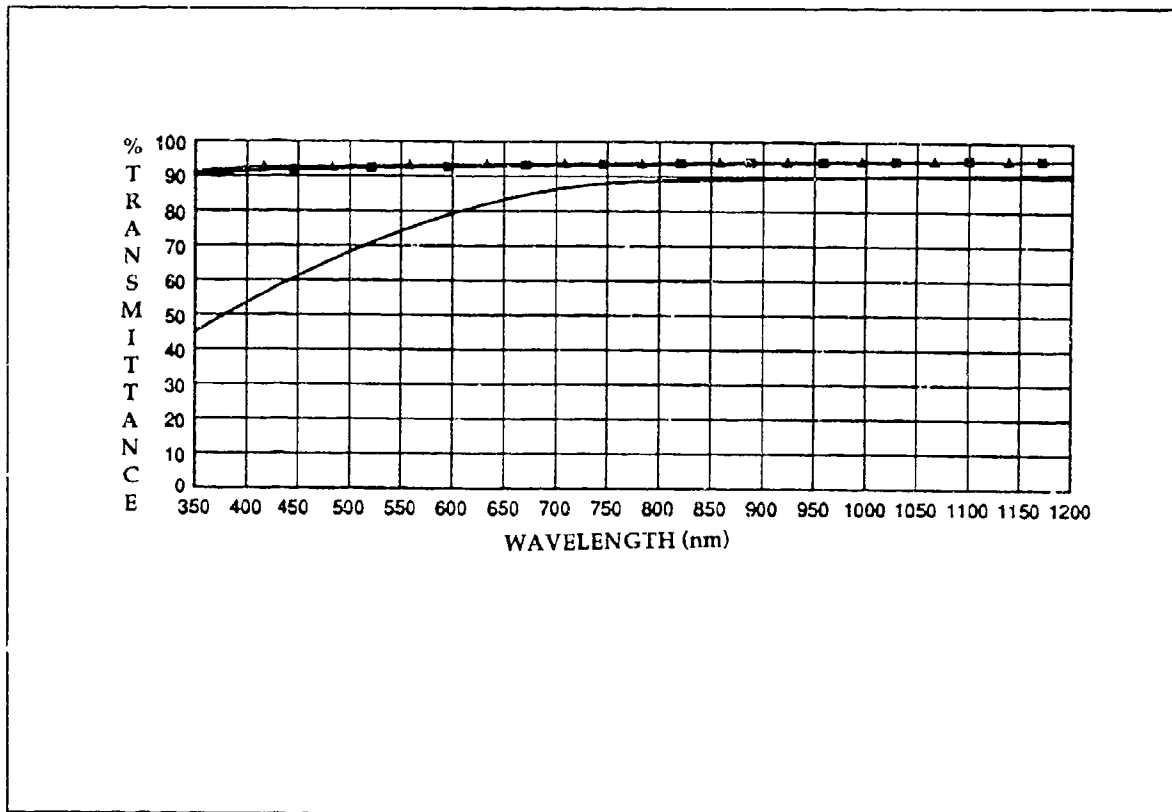


Figure E.11. Spectral Transmission of Uncoated ULE™ Sample

REFERENCE:	Havey, Keith, Mustico, Arthur, and Vallimont, John, <u>Effects of Long Term Space Environment Exposure on Optical Substrates and coatings (S0050-2)</u> , LDEF Second Post-Retrieval Symposium, June 1992, p.1394
EXPERIMENT:	S0050-2
COMMENTS:	Cleaning returned performance to pre-flight values.

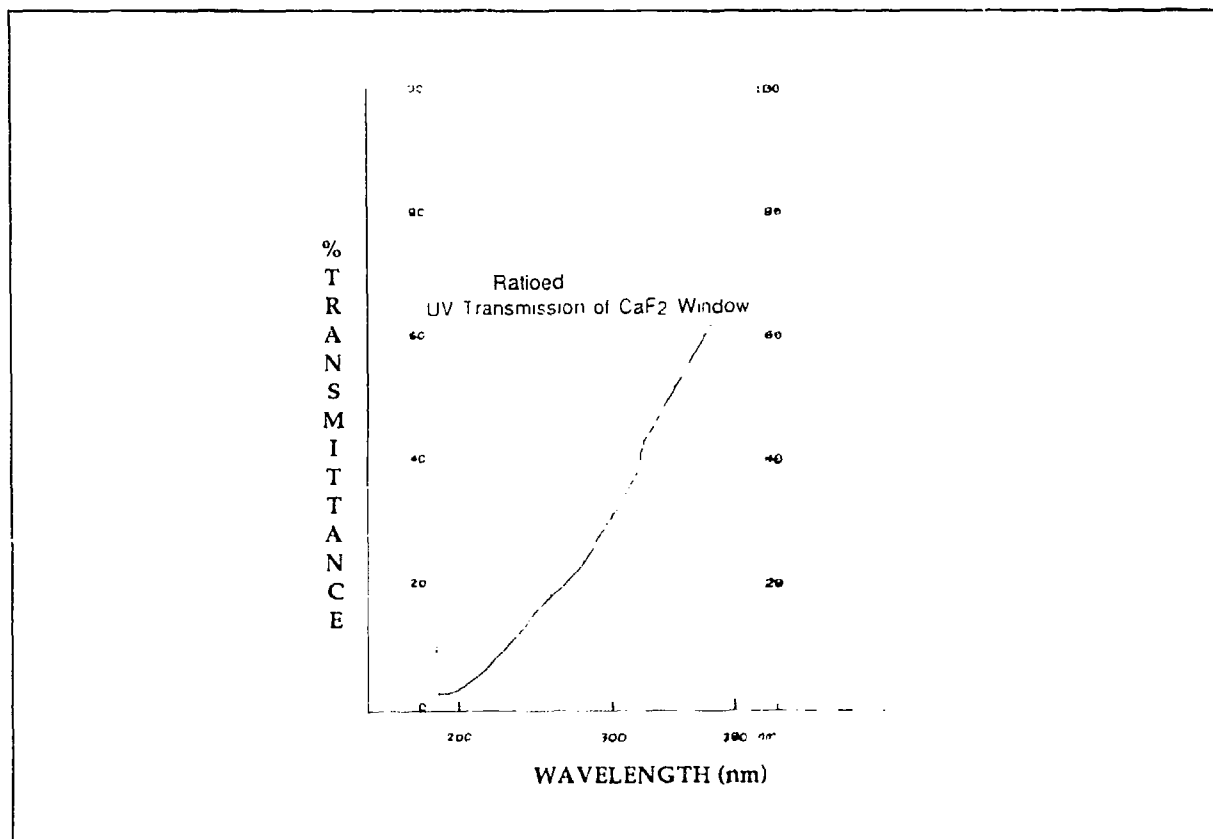


Figure E.12. Ultraviolet Transmission of CaF<sub>2</sub> Window

---

REFERENCE:	Harvey, Gale A., <u>Effects of Long-Duration Exposure on Optical System Components</u> , LDEF First Post-Retrieval Symposium, June 1991, p. 1338
EXPERIMENT:	S0050-1
COMMENTS:	Organic film on both sides. Catastrophic loss in UV transmission. Transmission increases from almost zero at 200 nm to 50 percent at 380 nm.

---

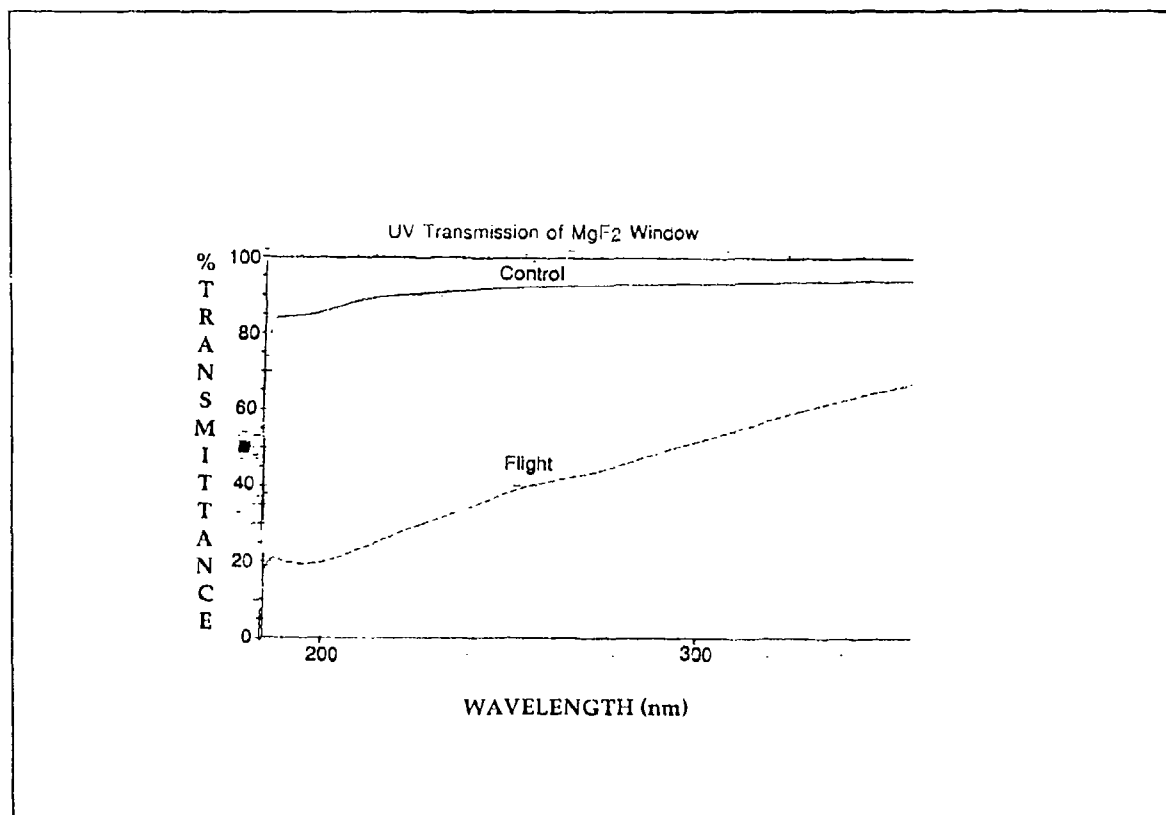


Figure E.13. Ultraviolet Transmission for MgF<sub>2</sub> Window

<b>REFERENCE:</b>	Harvey, Gale A., <u>Effects of Long-Duration Exposure on Optical System Components</u> , LDEF First Post-Retrieval Symposium, June 1991, p.1339
<b>EXPERIMENT:</b>	S0050-1
<b>COMMENTS:</b>	Organic film on front side only. Catastrophic loss in UV transmission.

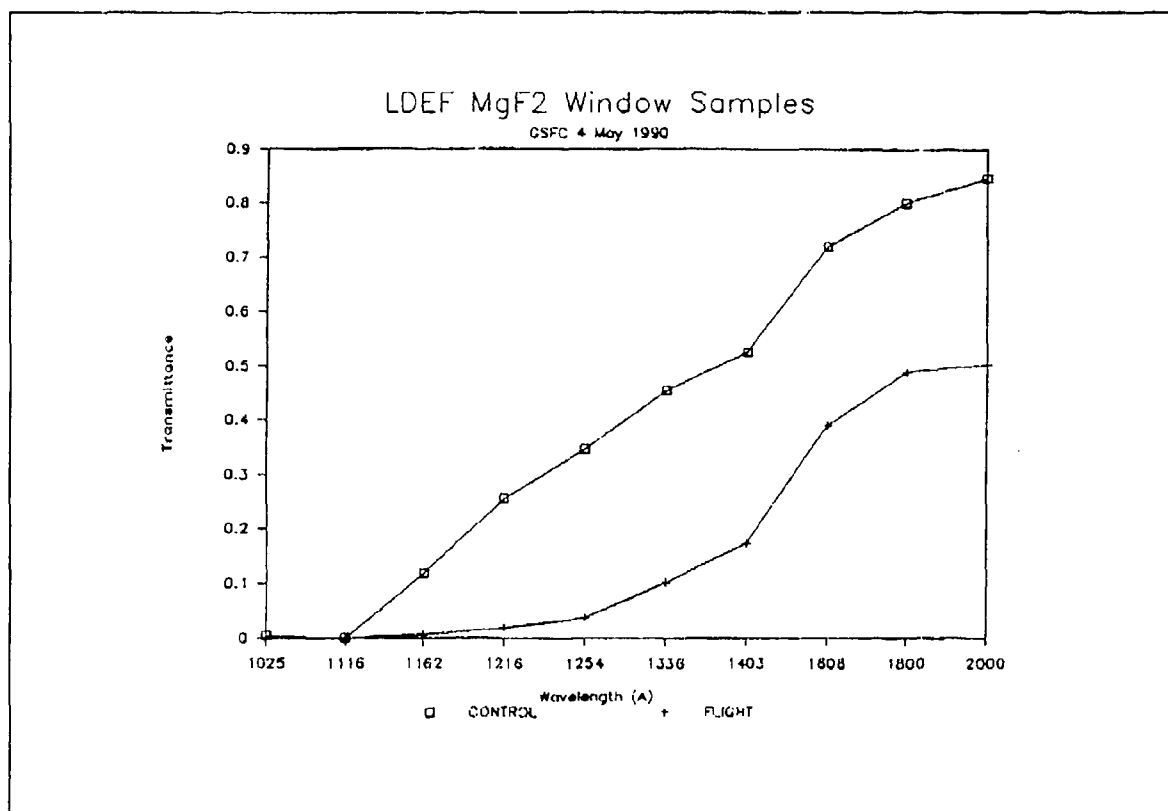


Figure E.14. Vacuum Ultraviolet Transmission for MgF<sub>2</sub> Window

REFERENCE:	Harvey, Gale A., <u>Effects of Long-Duration Exposure on Optical System Components</u> , LDEF First Post-Retrieval Symposium, June 1991, p.1340
EXPERIMENT:	S0050-1
COMMENTS:	Catastrophic loss in UV transmission.

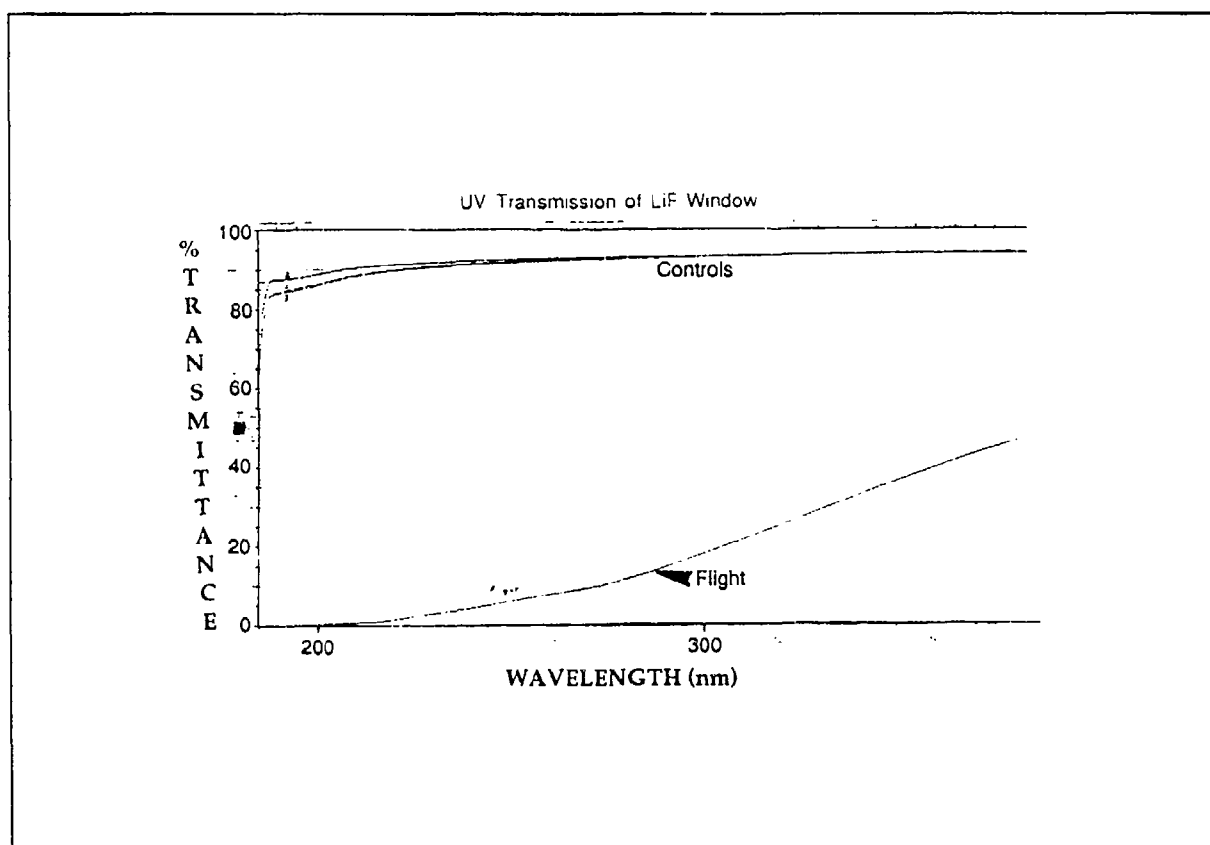


Figure E.15. Ultraviolet Transmission for LiF Window

REFERENCE:	Harvey, Gale A., <u>Effects of Long-Duration Exposure on Optical System Components</u> , LDEF First Post-Retrieval Symposium, June 1991, p. 1339
EXPERIMENT:	S0050-1
COMMENTS:	Organic film on both surfaces. Catastrophic loss in UV.

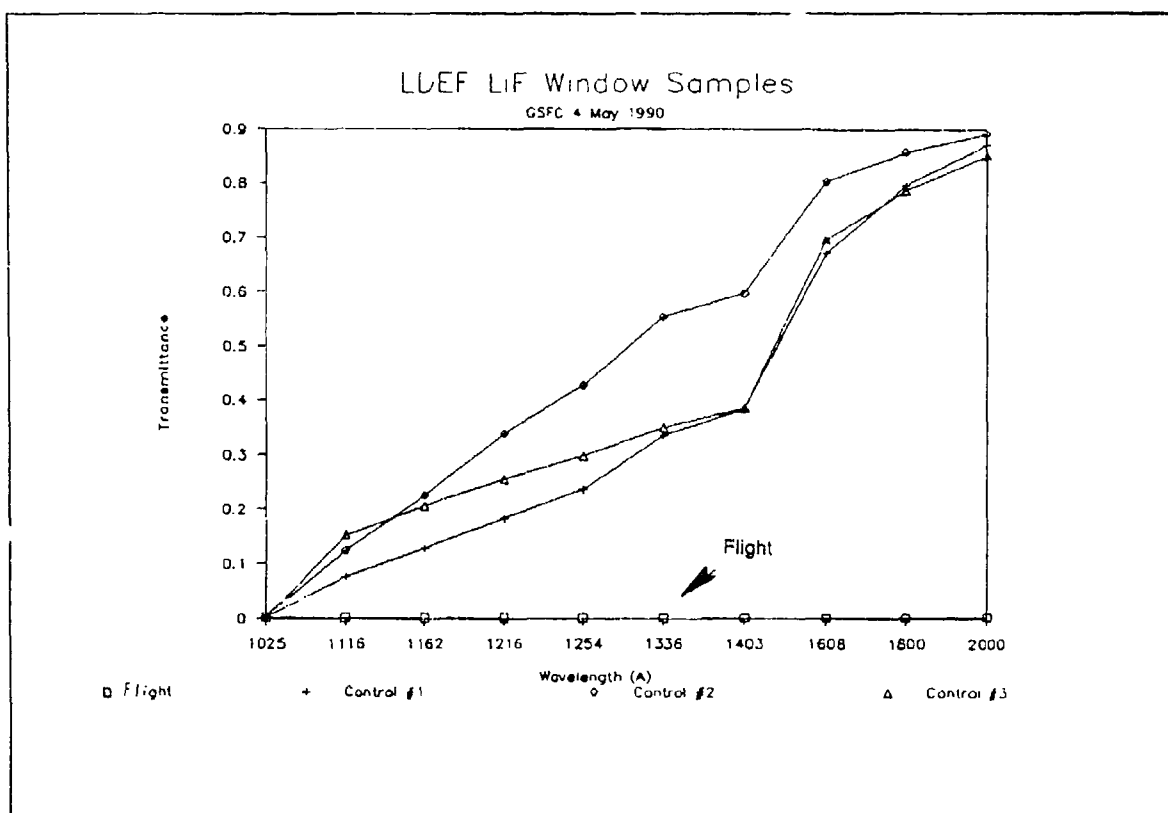


Figure E.16. Vacuum Ultraviolet Transmission for LiF Window

REFERENCE:	Harvey, Gale A., <u>Effects of Long-Duration Exposure on Optical System Components</u> , LDEF First Post-Retrieval Symposium, June 1991, p. 1340
EXPERIMENT:	S0050-1
COMMENTS:	Catastrophic loss in UV.



SAMPLE	PRE- FLIGHT	POST- FLIGHT	AFTER CLEANING	CONTROL SAMPLE
Fused Silica	9.26T	35.3C	2.27T	10.7T
IJLE™	9.51T	38.5C	8.0T	17.1T

T indicates tension stress  
C indicates compression stress

Figure E.17. LDEF Uncoated Refractive Optics Stress Data

<b>REFERENCE:</b>	Harvey, Gale A., <u>Effects of Long-Duration Exposure on Optical System Components</u> , LDEF First Post-Retrieval Symposium, June 1991, p. 1340
<b>EXPERIMENT:</b>	S0050-1
<b>COMMENTS:</b>	Catastrophic loss in UV.

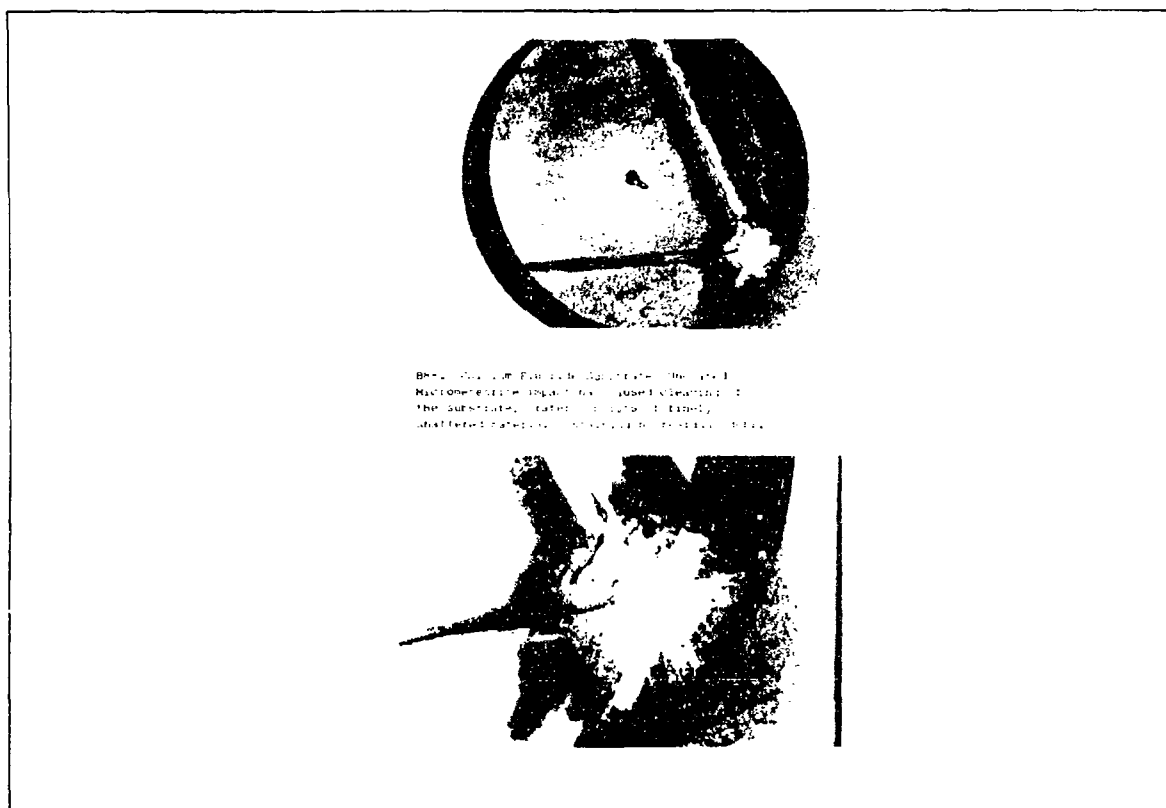


Figure E.18. Micrometeorite Damage on CaF<sub>2</sub>

---

REFERENCE:	Hawkins, Gary J., Seeley, John S., and Hunneman, Roger, <u>Exposure to Space Radiation of High-Performance Infrared Multilayer Filters and Materials Technology Experiment (AO056)</u> , LDEF First Post-Retrieval Symposium, June 1991, p. 1491
EXPERIMENT:	AO056
COMMENTS:	Cleaving of the substrate.

---

SAMPLE	STRENGTH (MPa)	STRENGTH DEVIATION (Mpa)	STRENGTH CONTROL (Mpa)	STRESS DEVIATION (Mpa)	STRESS CONTOUR (% Max)
BK-7 Glass	126	8	124	8	10
Fused Silica	97	4	97	4	38
Soda-Lime- Silica	104	4	100	9	35
Pyrex	105	7	111	4	10
Vycor	101	5	103	4	No Impact
Zerodur (I)	129	8	128	5	30
Zerodur (II)	129	8	128	5	50
Zerodur (III)	129	8	128	5	25

Figure E.19. LDEF Mechanical Strength Data for Uncoated Refractive Optics

<b>REFERENCE:</b>	Wiedlocher, David E., and Kinser, Donald L., <u>Cratering in Glasses Impacted by Debris or Micrometeorites</u> , LDEF Second Post-Retrieval Symposium, June 1992, p. 534
<b>EXPERIMENT:</b>	AO172
<b>COMMENTS:</b>	None.

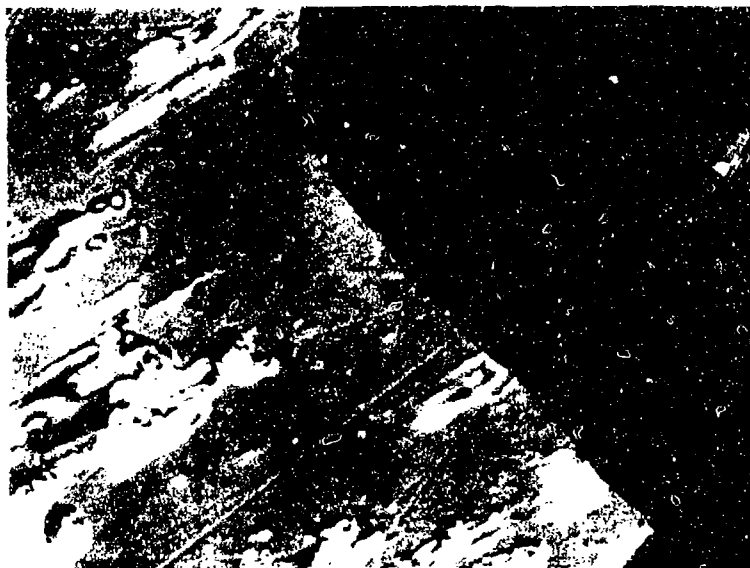


Figure E.20. Film on MgF<sub>2</sub> Window

---

REFERENCE:	Harvey, Gale A., <u>Effects of Long-Duration Exposure on Optical System Components</u> , LDEF First Post-Retrieval Symposium, June 1991, p. 1333
EXPERIMENT:	S0050-1
COMMENTS:	Sharp edges of adhering film indicate that the film is brittle.

---

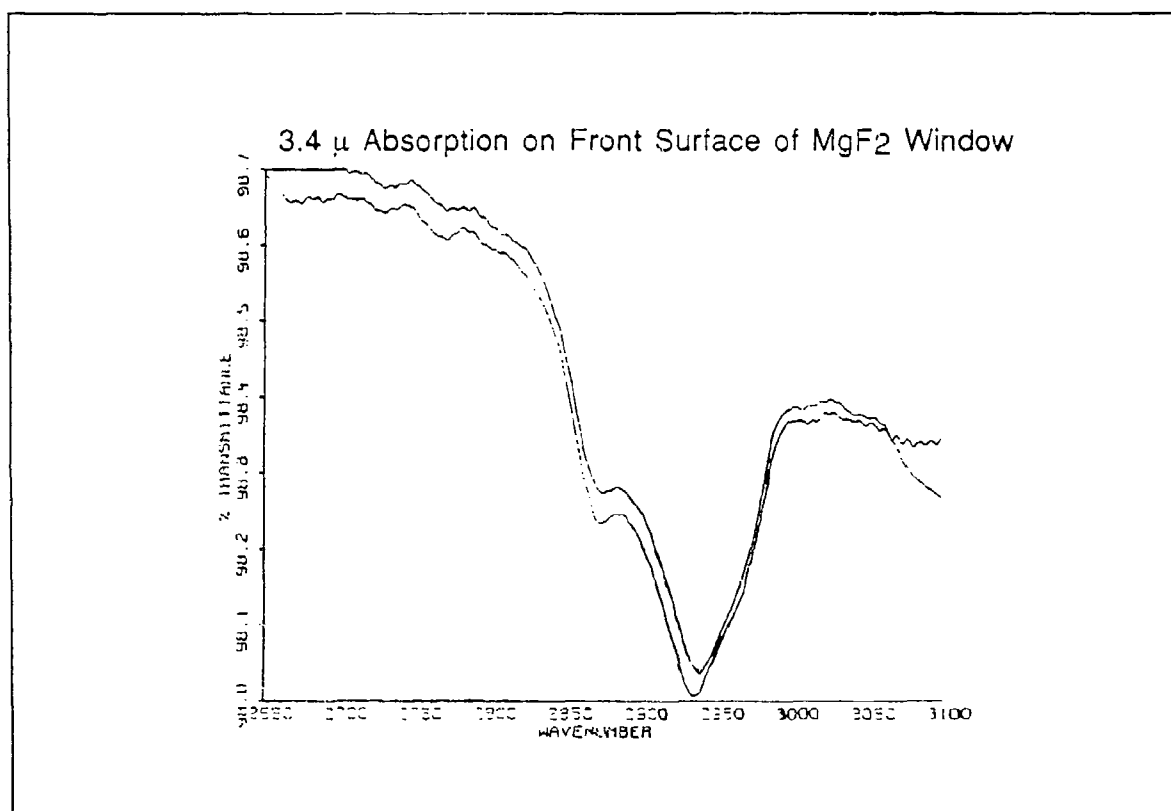


Figure E.21. 3.4 $\mu$  Absorption on Front Surface of MgF<sub>2</sub> Window

---

REFERENCE:	Harvey, Gale A., <u>Effects of Long-Duration Exposure on Optical System Components</u> , LDEF First Post-Retrieval Symposium, June 1991, p. 1336
EXPERIMENT:	S0050-1
COMMENTS:	Slight decrease in transmittance due to contamination on MgF <sub>2</sub> .

---

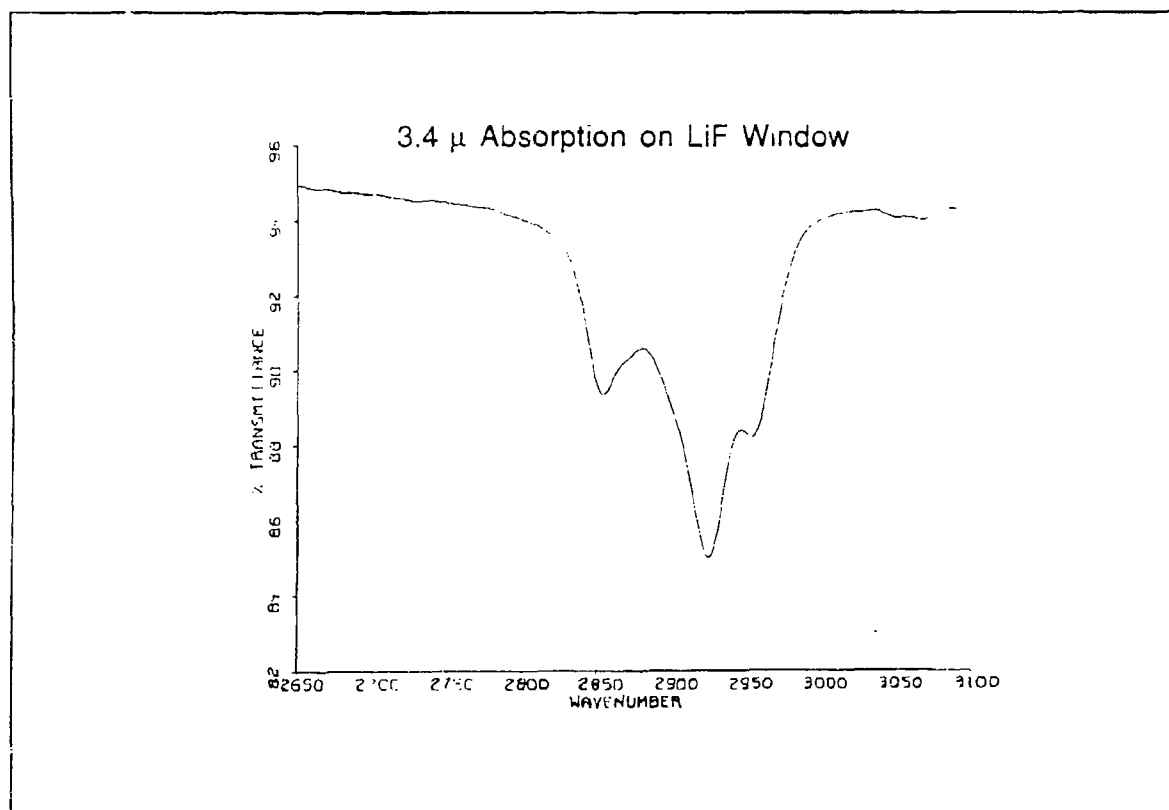


Figure E.22. 3.4 $\mu$  Absorption on Front Surface of LiF Window

---

REFERENCE:	Harvey, Gale A., <u>Effects of Long-Duration Exposure on Optical System Components</u> , LDEF First Post-Retrieval Symposium, June 1991, p. 1336
EXPERIMENT:	S0050-1
COMMENTS:	Almost no decrease in transmittance due to contamination on LiF.

---



Figure E.23. Film on LiF Window

---

REFERENCE:	Harvey, Gale A., <u>Effects of Long-Duration Exposure on Optical System Components</u> , LDEF First Post-Retrieval Symposium, June 1991, p. 1333
EXPERIMENT:	S0050-1
COMMENTS:	Surface film appears sprayed on.

---

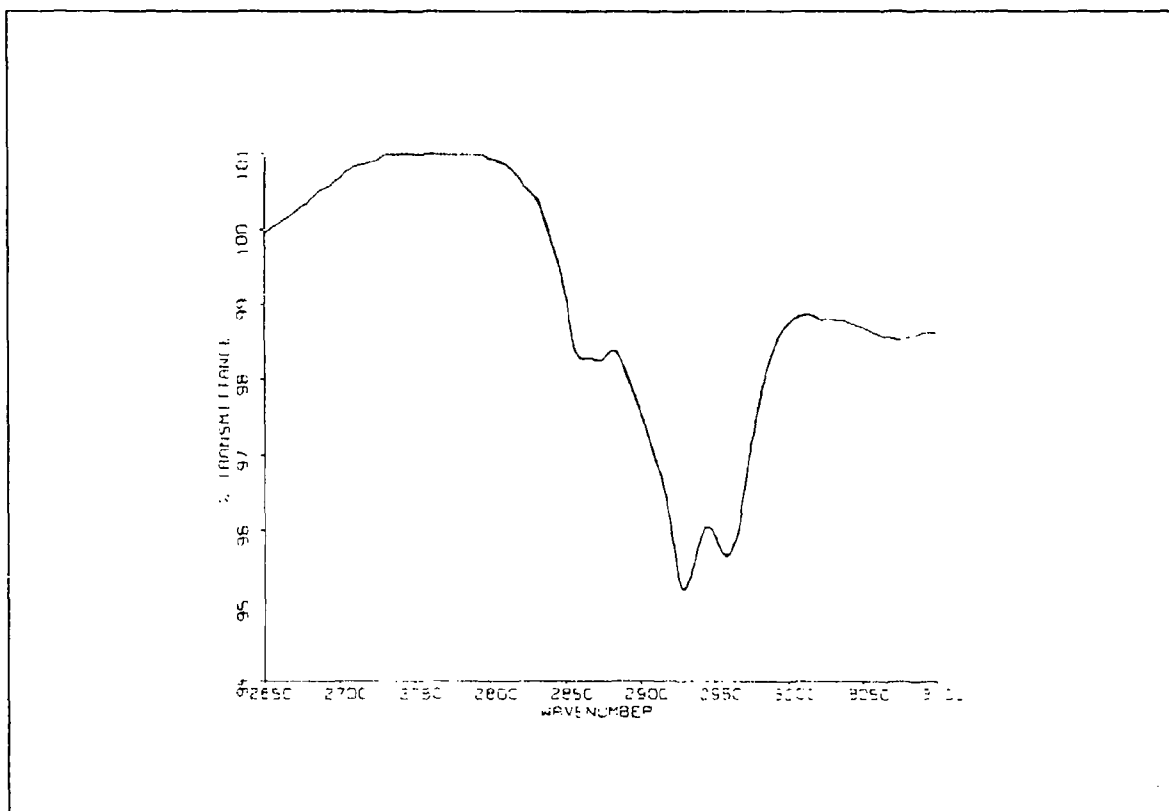


Figure E.24. 3.4 $\mu$  Absorption on Front Surface of Al<sub>2</sub>O<sub>3</sub> Window

REFERENCE:	Harvey, Gale A., <u>Effects of Long-Duration Exposure on Optical System Components</u> , LDEF First Post-Retrieval Symposium, June 1991, p. 1337
EXPERIMENT:	S0050-1
COMMENTS:	Little change in transmittance due to contamination on Al <sub>2</sub> O <sub>3</sub> .



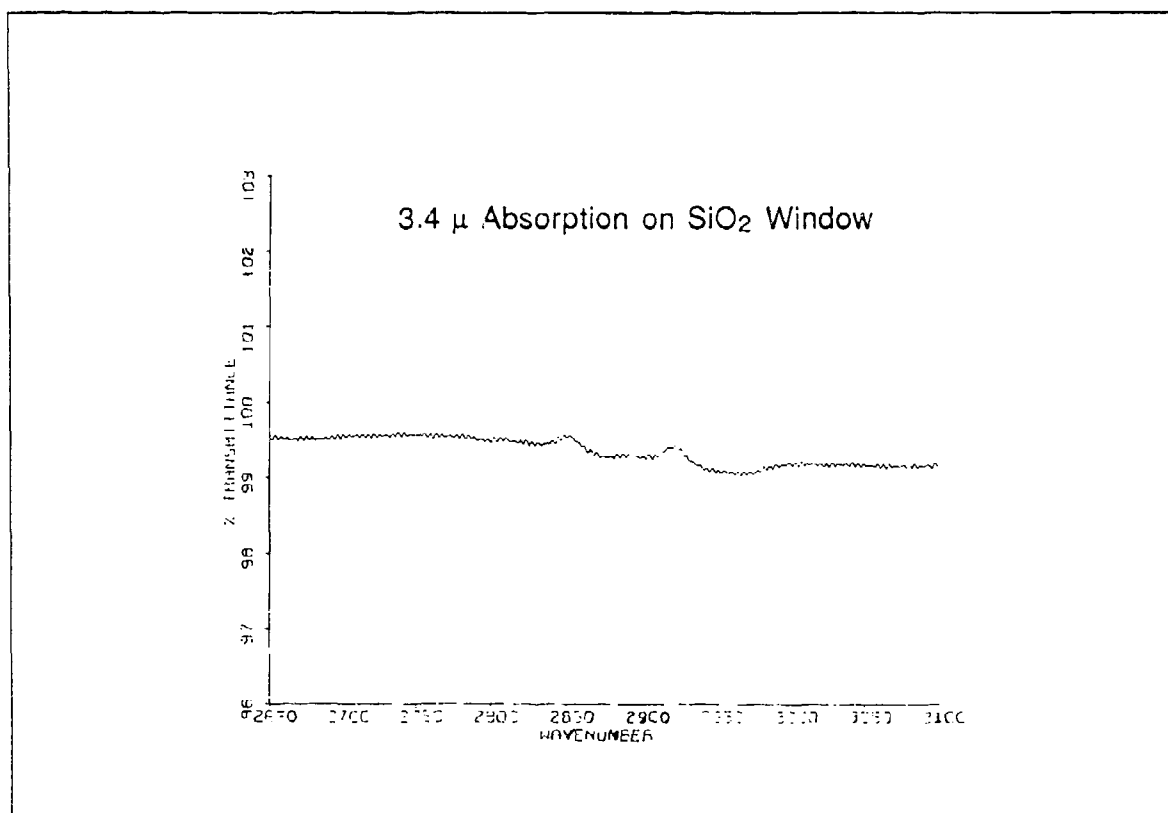


Figure E.25. 3.4 $\mu$  Absorption on SiO<sub>2</sub> Window

---

REFERENCE:	Harvey, Gale A., <u>Effects of Long-Duration Exposure on Optical System Components</u> , LDEF First Post-Retrieval Symposium, June 1991, p. 1338
EXPERIMENT:	S0050-1
COMMENTS:	Little change in transmittance due to contamination on SiO <sub>2</sub> .

---

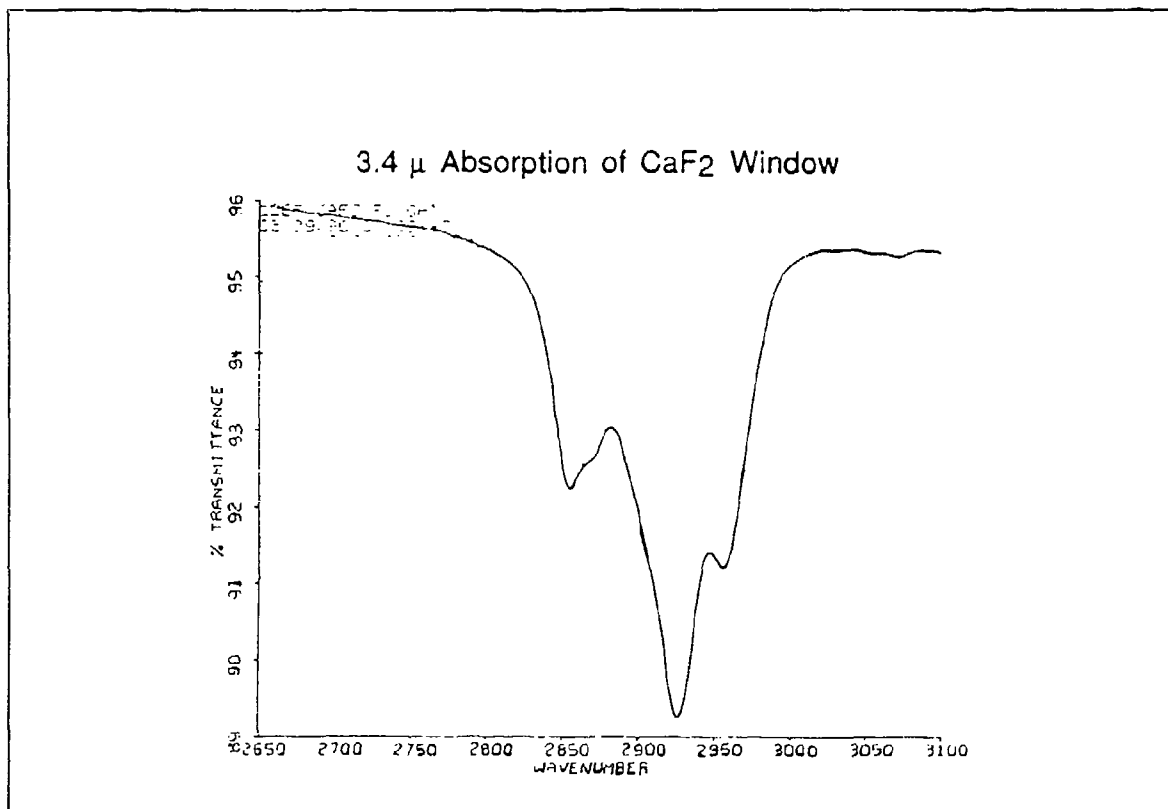
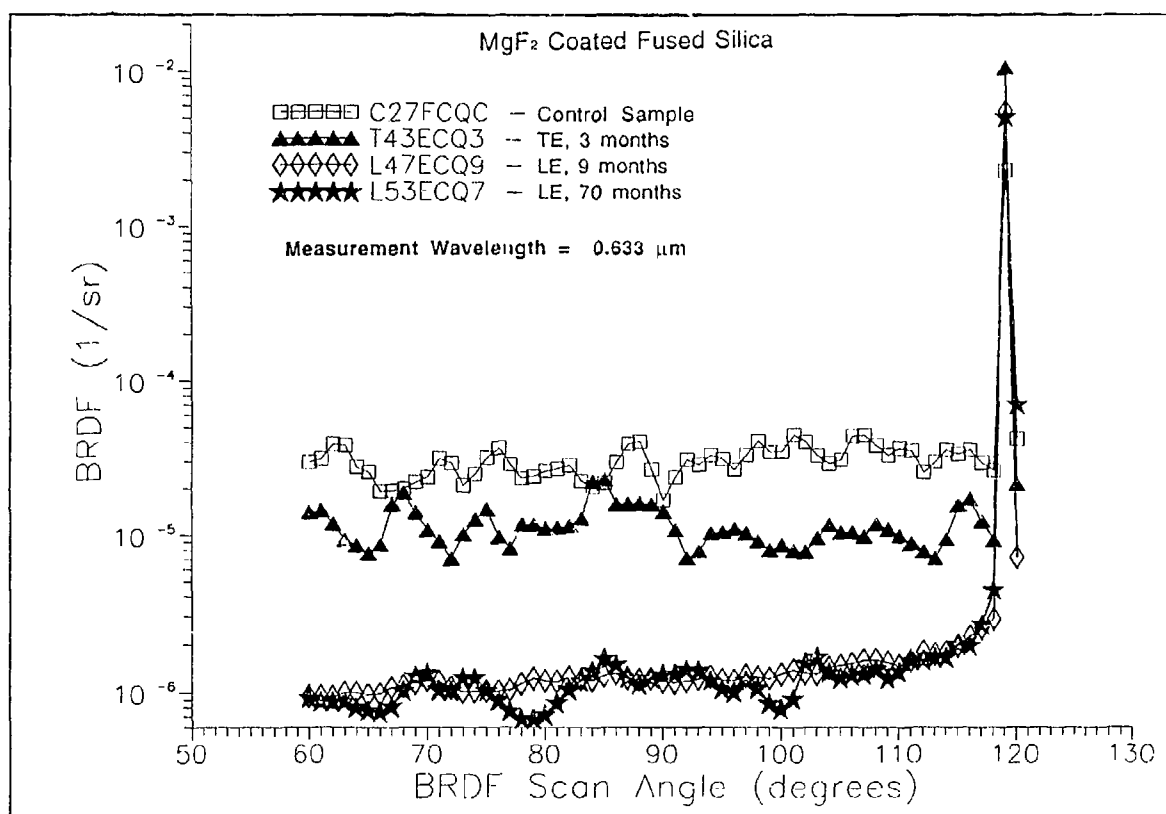


Figure E.26. 3.4 $\mu$  Absorption on Front Surface of CaF<sub>2</sub> Window

---

REFERENCE:	Harvey, Gale A., <u>Effects of Long-Duration Exposure on Optical System Components</u> , LDEF First Post-Retrieval Symposium, June 1991, p. 1335
EXPERIMENT:	S0050-1
COMMENTS:	Little change in transmittance due to contamination on CaF <sub>2</sub> .

---



**Figure E.27. Graph of Scattered Intensity vs. Detector Angle for Four MgF<sub>2</sub>/Fused Silica Samples**

<b>REFERENCE:</b>	DeHainaut, Linda L., Kenemuth, John R., Tidler, Cynthia E., and Seegmiller, David W., <u>Degradation of Optical Components in a Space Environment</u> , LDEF Second Post-Retrieval Symposium, June 1992, p. 1361ff.
<b>EXPERIMENT:</b>	M0003-2
<b>COMMENTS:</b>	Leading edge showed less scatter (coating removal by atomic oxygen).

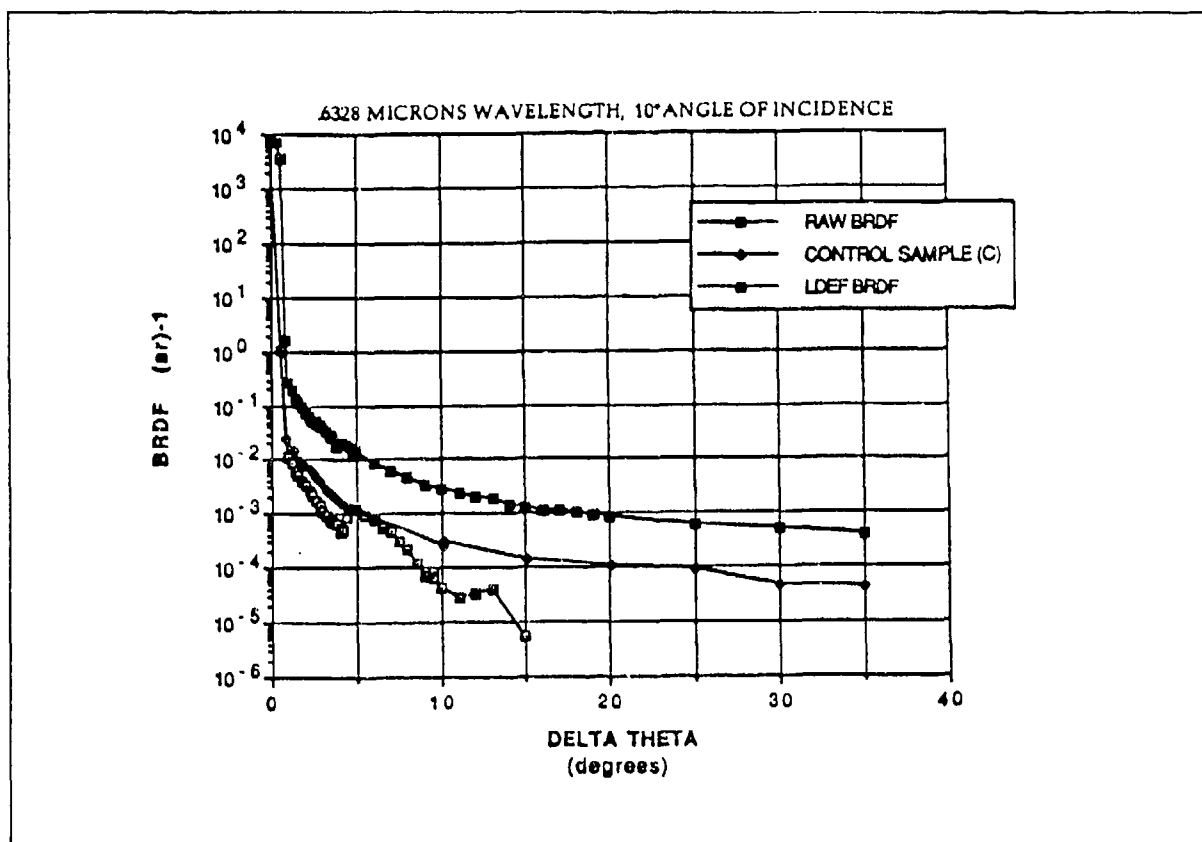


Figure E.28. BRDF Measurement for Silver-Coated Fused ULE™

<b>REFERENCE:</b>	Havey, Keith, Mustico, Arthur, and Vallimont, John, <u>Effects of Long Term Space Environment Exposure on Optical Substrates and Coatings (S0050-2)</u> , LDEF Second Post-Retrieval Symposium, June 1992, p.1396
<b>EXPERIMENT:</b>	S0050-2
<b>COMMENTS:</b>	Increase in scattering.

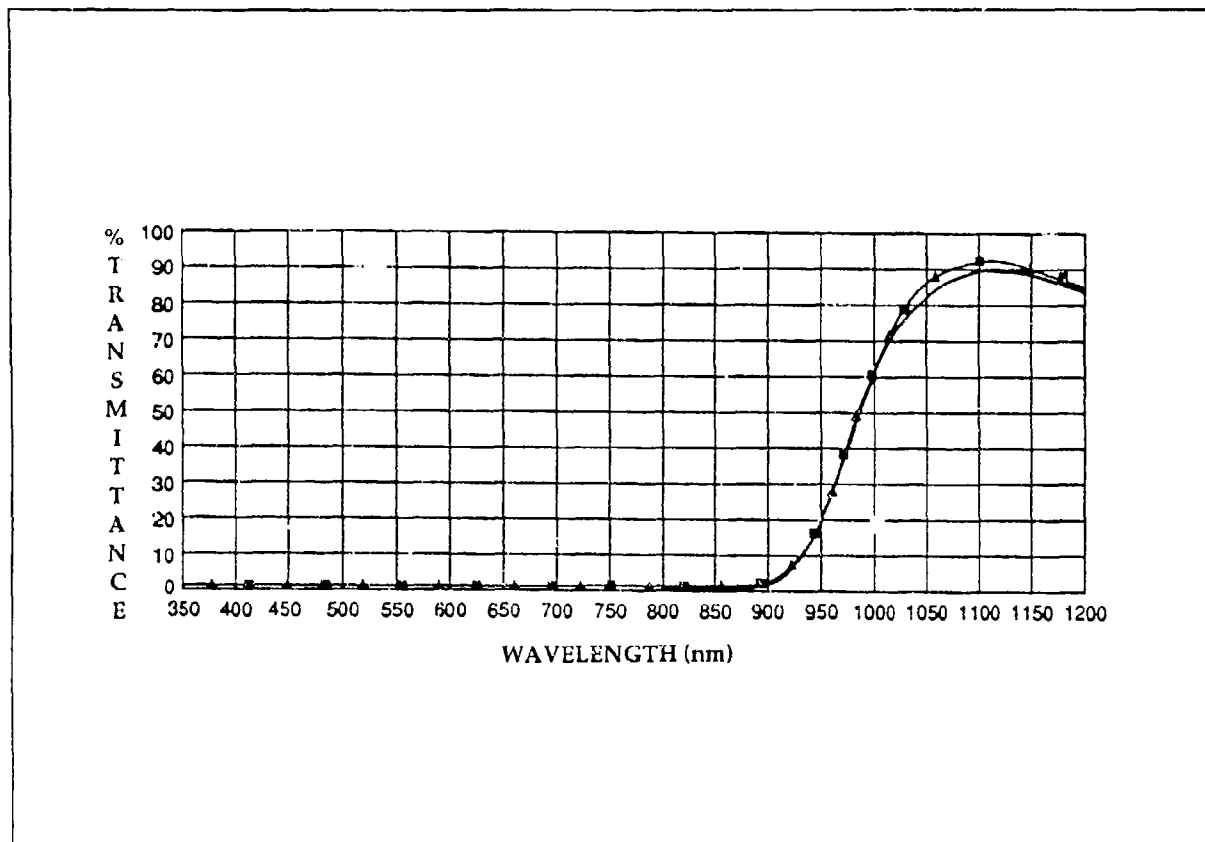


Figure E.29. Transmission for Fused Silica Solar Rejection Coating

---

REFERENCE:	Havey, Keith, Mustico, Arthur, and Vallimont, John, <u>Effects of Long Term Space Environment Exposure on Optical Substrates and Coatings (S0050-2)</u> , LDEF Second Post-Retrieval Symposium, June 1992, p.1395
EXPERIMENT:	S0050-2
COMMENTS:	Cleaning returned performance to pre-flight value.

---

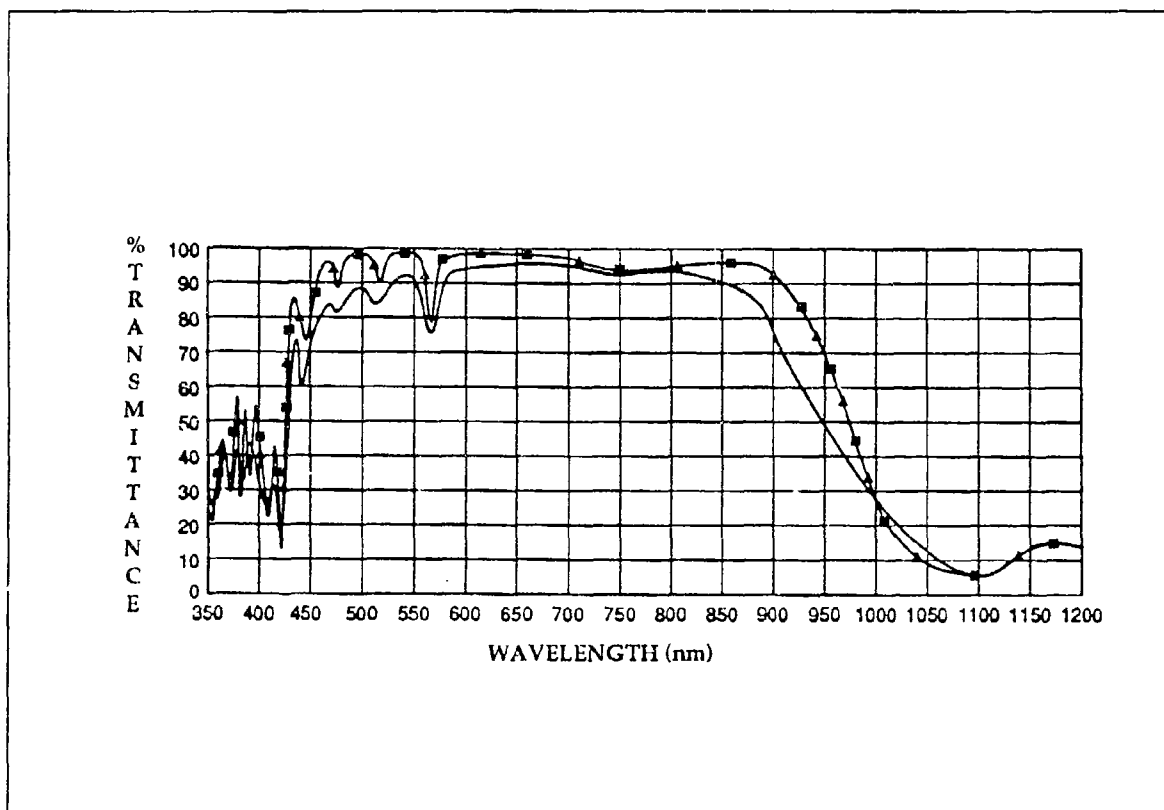


Figure E.30. Reflectance for Fused Silica Solar Rejection Coatings

<b>REFERENCE:</b>	Havey, Keith, Mustico, Arthur, and Vallimont, John, <u>Effects of Long Term Space Environment Exposure on Optical Substrates and Coatings (S0050-2)</u> , LDEF Second Post-Retrieval Symposium, June 1992, p.1395
<b>EXPERIMENT:</b>	S0050-2
<b>COMMENTS:</b>	Cleaning returned performance to pre-flight value.

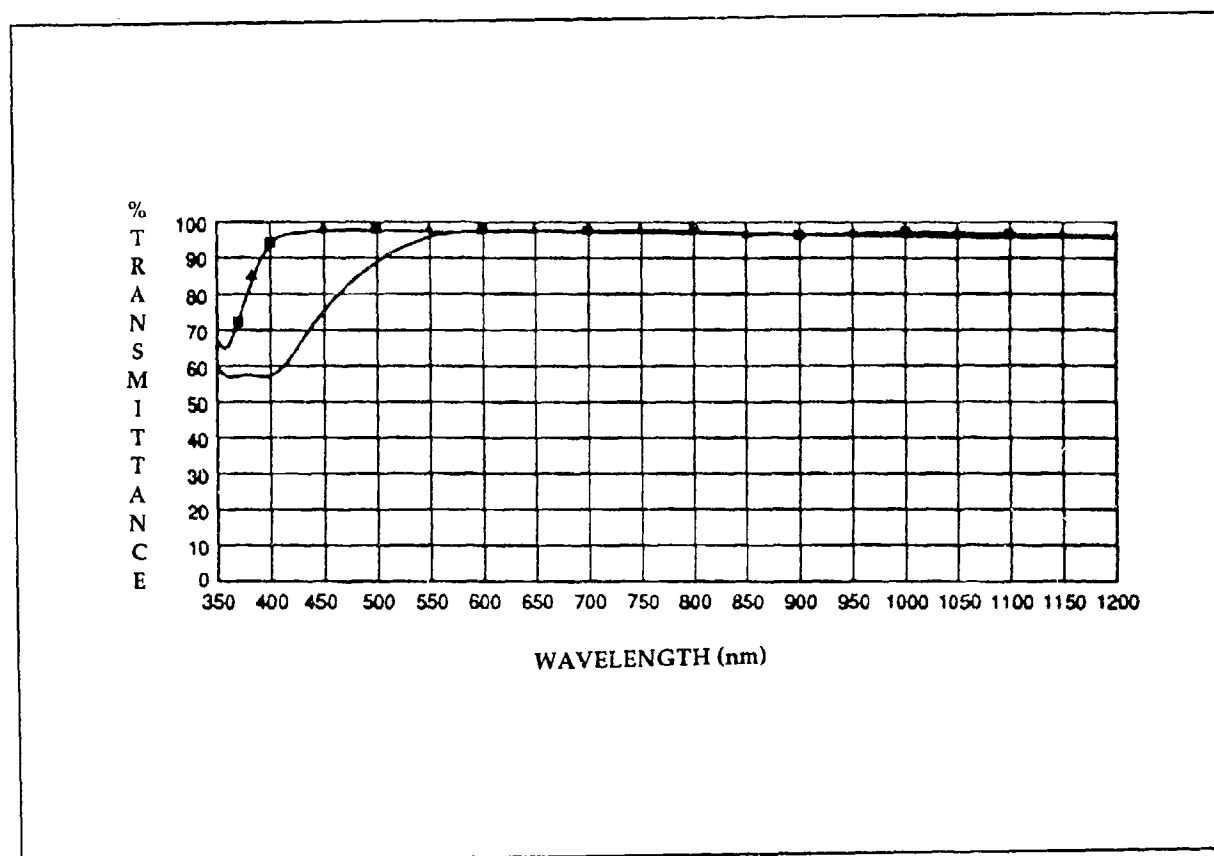


Figure E.31. Reflectance for Silver-Coated ULE™

<b>REFERENCE:</b>	Havey, Keith, Mustico, Arthur, and Vallimont, John, <u>Effects of Long Term Space Environment Exposure on Optical Substrates and Coatings (S0050-2)</u> , LDEF Second Post-Retrieval Symposium, June 1992, p.1394
<b>EXPERIMENT:</b>	S0050-2
<b>COMMENTS:</b>	Cleaning returned performance to pre-flight value.

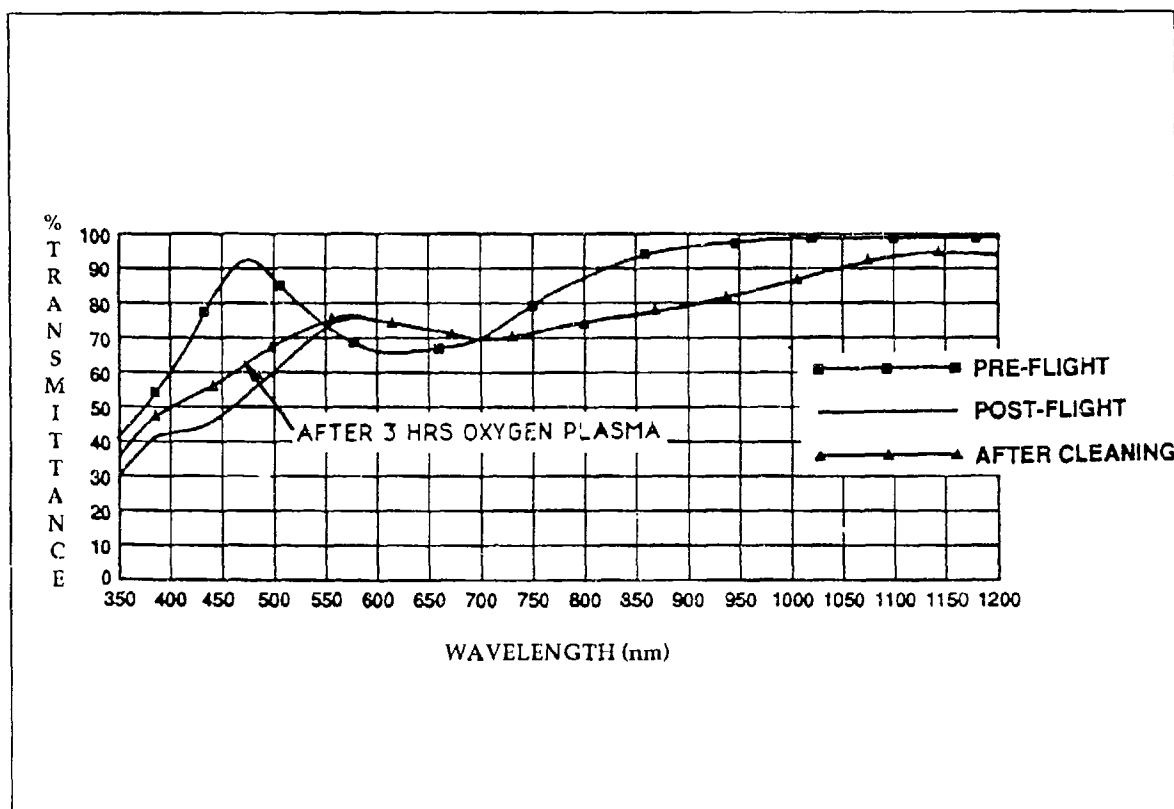


Figure E.32. Transmission for Anti-Reflection-Coated Fused Silica

REFERENCE:	Havey, Keith, Mustico, Arthur, and Vallimont, John, <u>Effects of Long Term Space Environment Exposure on Optical Substrates and Coatings (S0050-2)</u> , LDEF Second Post-Retrieval Symposium, June 1992, p.1393
EXPERIMENT:	S0050-2
COMMENTS:	Normal cleaning methods ineffective. Exposure to atomic oxygen needed to improve performance.



SAMPLE	PRE-FLIGHT	POST-FLIGHT	AFTER CLEANING	CONTROL SAMPLE
Fused Silica/AR	15.6T	16.4T		20.1T
Fused Silica/Ag	676C	553C	569C	557C
Fused Silica/Ag/Uncoated side	210T	185T	160T	150T
ULE™/Ag	14.5T	33.1C	9.0T	15.4T

T indicates tension  
C indicates compression

Figure E.33. LDEF Stress Data Base For Coated Refractive Optics

<b>REFERENCE:</b>	Havey, Keith, Mustico, Arthur, and Vallimont, John, <u>Effects of Long Term Space Environment Exposure on Optical Substrates and Coatings (S0050-2)</u> , LDEF Second Post-Retrieval Symposium, June 1992, p.1392
<b>EXPERIMENT:</b>	S0050-2
<b>COMMENTS:</b>	Contaminants did not introduce appreciable stress.

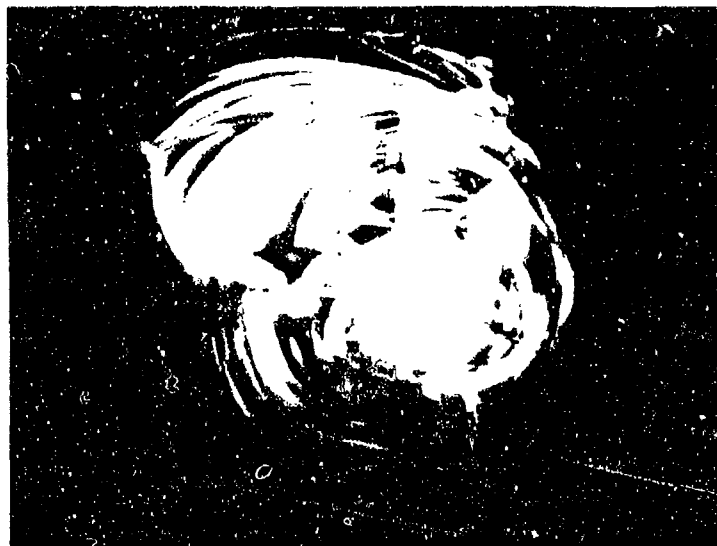


Figure E.34. Impact Effects on Fused Silica

---

REFERENCE:	Donovan, T.M., Bennett, J.M., Dalbey, R.Z., Burge, D.K., and Gyetvay, S., <u>Space Environmental Effects on Coated Optics</u> , LDEF First Post-Retrieval Symposium, June 1991, p. 1370
EXPERIMENT:	M0003-2
COMMENTS:	70-month exposure produced localized chipping and fracture extending many particle diameters.

---

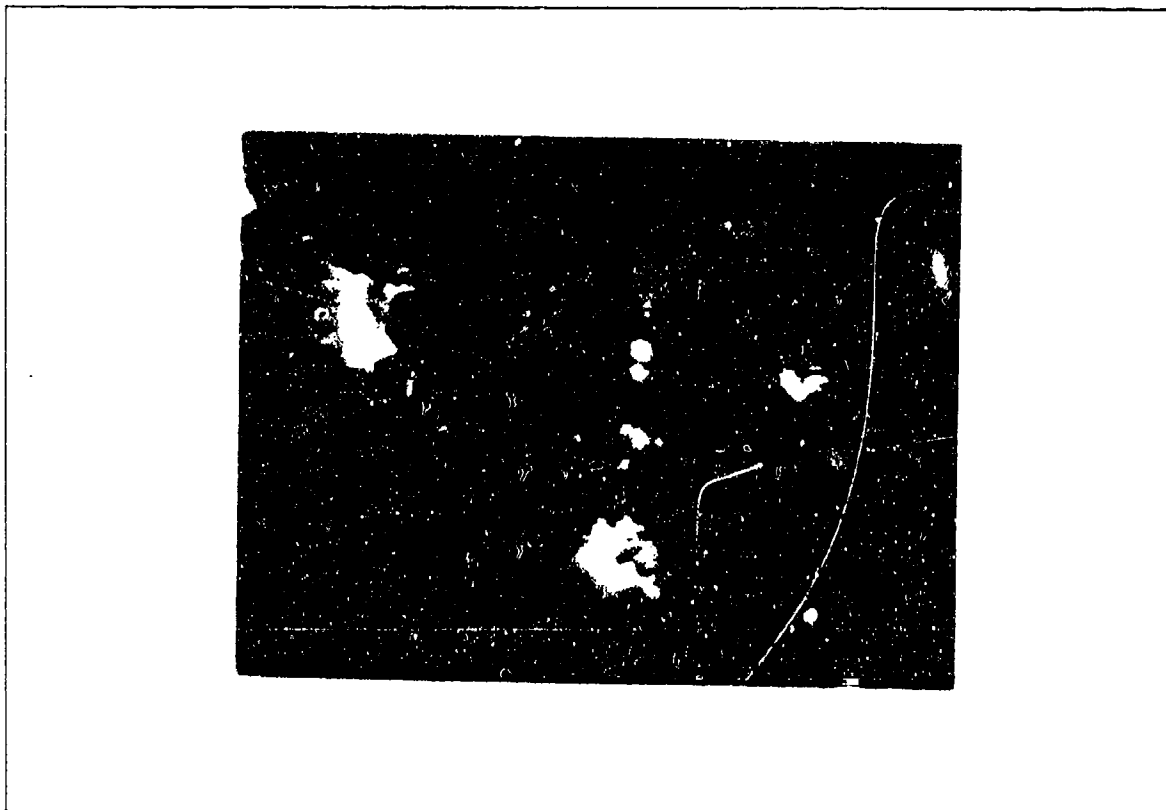


Figure E.35. Fracture Zones on Fused Silica

---

REFERENCE:	Donovan, T.M., Bennett, J.M., Dalbey, R.Z., Burge, D.K., and Gyetvay, S., <u>Space Environmental Effects on Coated Optics</u> , LDEF First Post-Retrieval Symposium, June 1991, p. 1370
EXPERIMENT:	M0003-2
COMMENTS:	70-month exposure produced many impact sites which are potential areas of high scatter and absorption.

---

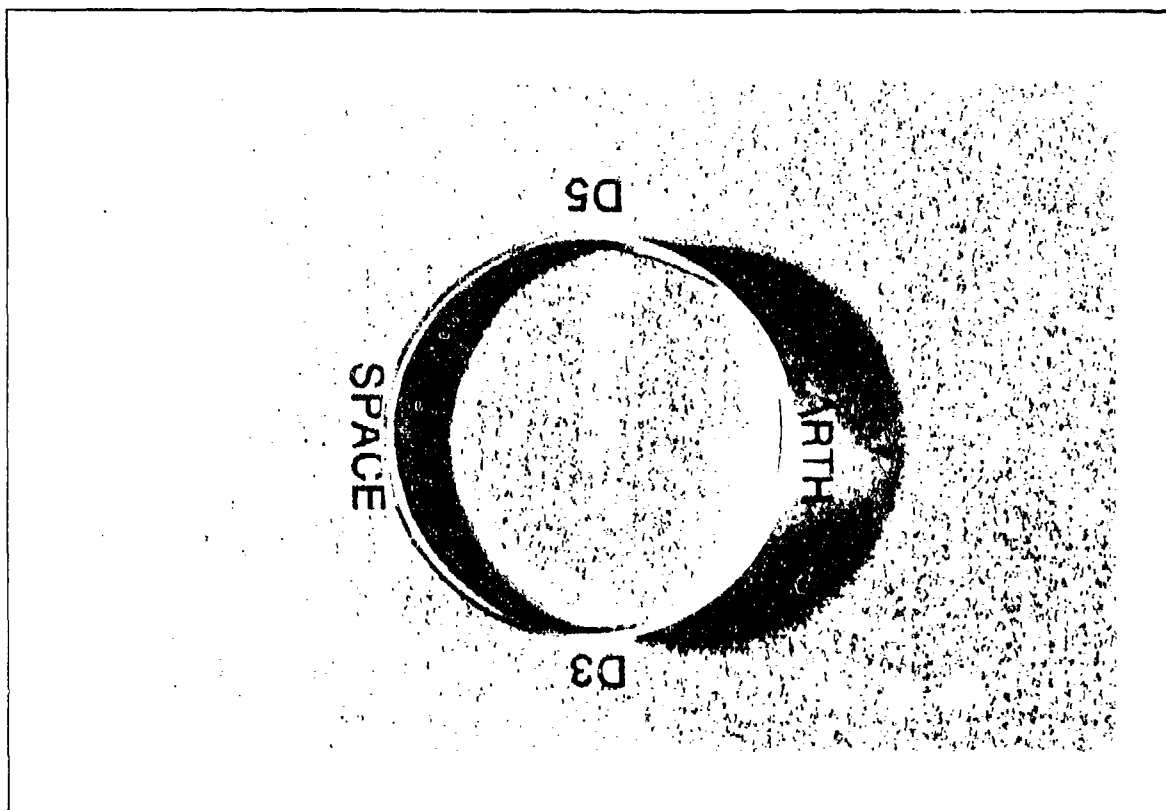


Figure E.36. Macrophotograph of Bare SiO<sub>2</sub> Substrate

---

REFERENCE:	Gyetvay, S., et al., <u>Aerospace Corporation LDEF M0003 Sample Observation Data Base</u> , 1993. Record #1125
EXPERIMENT:	M0003-2
COMMENTS:	No change is discernible except for debris, consisting of metallic film fragments and fibrous matter, on the surface.

---

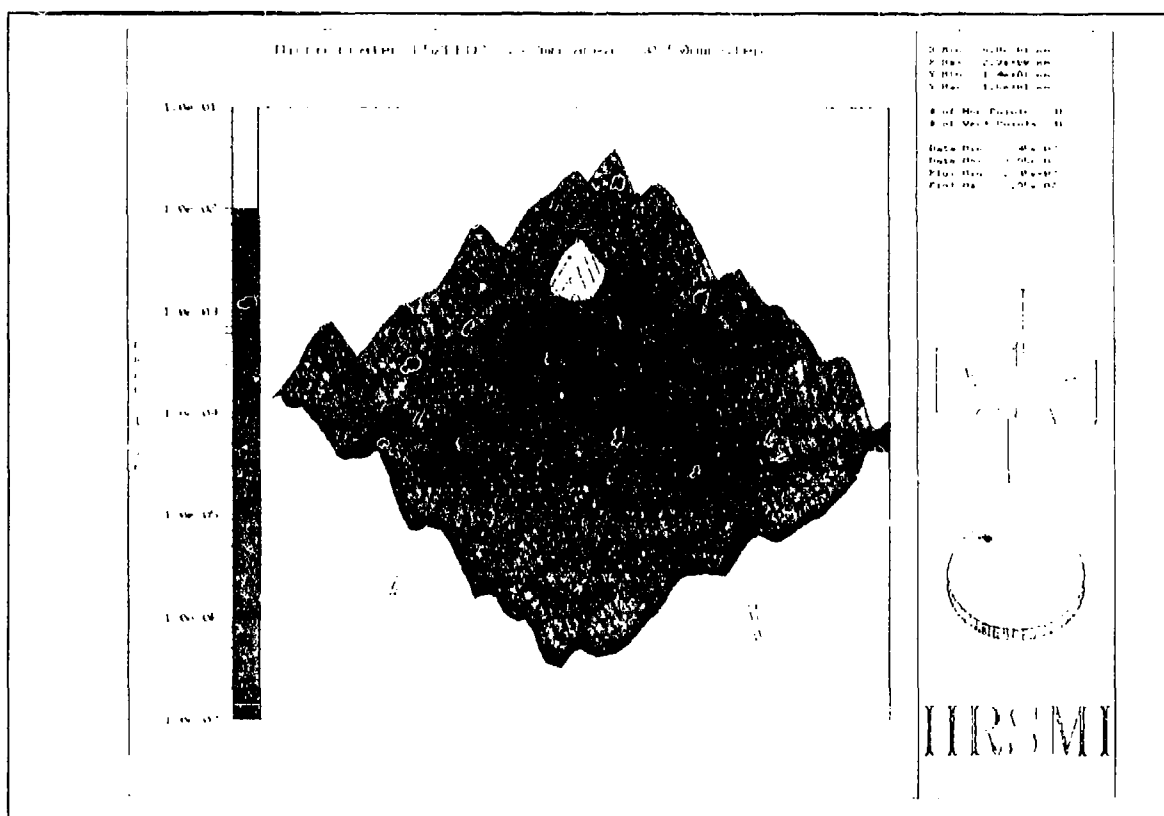


Figure E.37. Scatter Map of Impact Site for Fused Silica

**REFERENCE:** DeHainaut, Linda L., Kenemuth, John R., Tidler, Cynthia E., and Seegmiller, David W., Degradation of Optical Components in a Space Environment, LDEF Second Post-Retrieval Symposium, June 1992, p. 1371

**EXPERIMENT:** M0003-2

**COMMENTS:** 70-month exposure. Scatter intensity from crater is five orders of magnitude that of background. Fracture lines are high scatter sites.

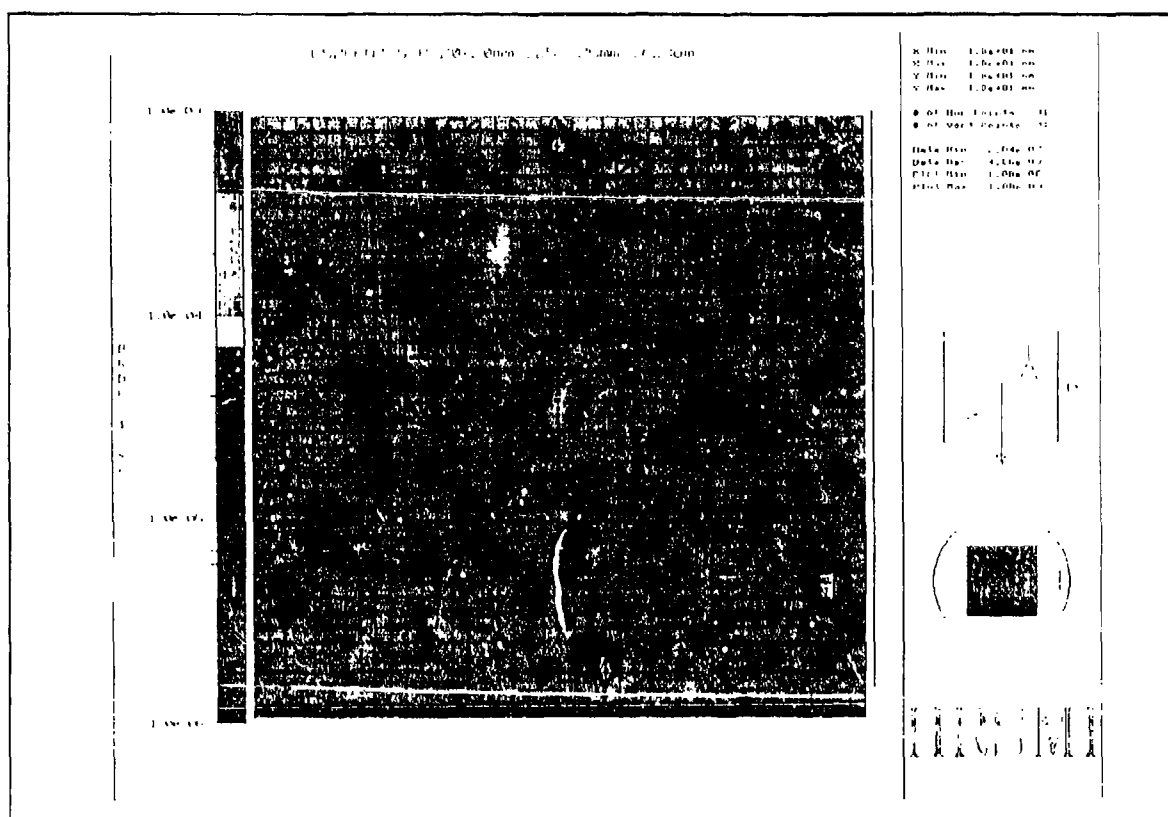


Figure E.38. Fused Silica Scatter Map

**REFERENCE:** DeHainaut, Linda L., Kenemuth, John R., Tidler, Cynthia E., and Seegmiller, David W., Degradation of Optical Components in a Space Environment. LDEF Second Post-Retrieval Symposium, June 1992, p. 1371

**EXPERIMENT:** M0003-2

**COMMENTS:** 70-month exposure. Scatter varies by two orders of magnitude across surface.

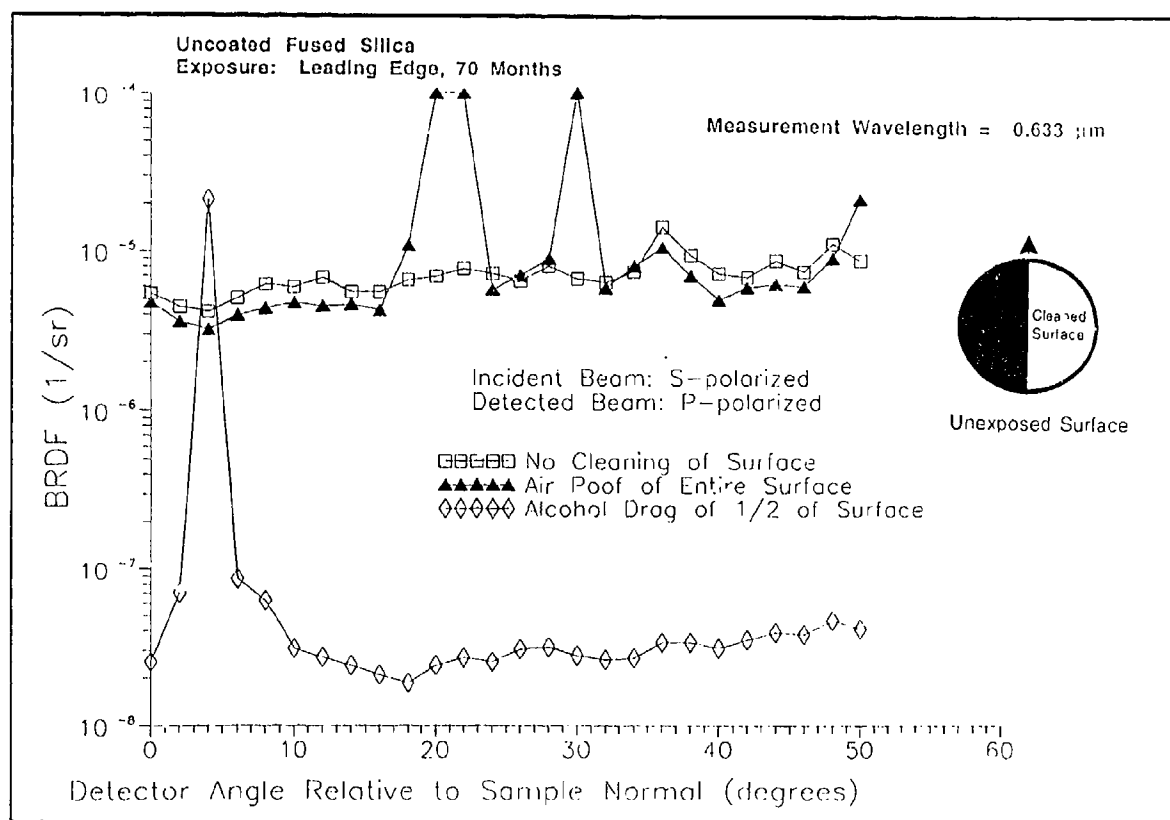


Figure E.39. Effects of Cleaning on Fused Silica Scatter

<b>REFERENCE:</b>	DeHainaut, Linda L., Kenemuth, John R., Tidler, Cynthia E., and Seegmiller, David W., <u>Degradation of Optical Components in a Space Environment</u> , LDEF Second Post-Retrieval Symposium, June 1992, p. 1372
<b>EXPERIMENT:</b>	M0003-2
<b>COMMENTS:</b>	70-month exposure. Cleaning reduced scatter three orders of magnitude.

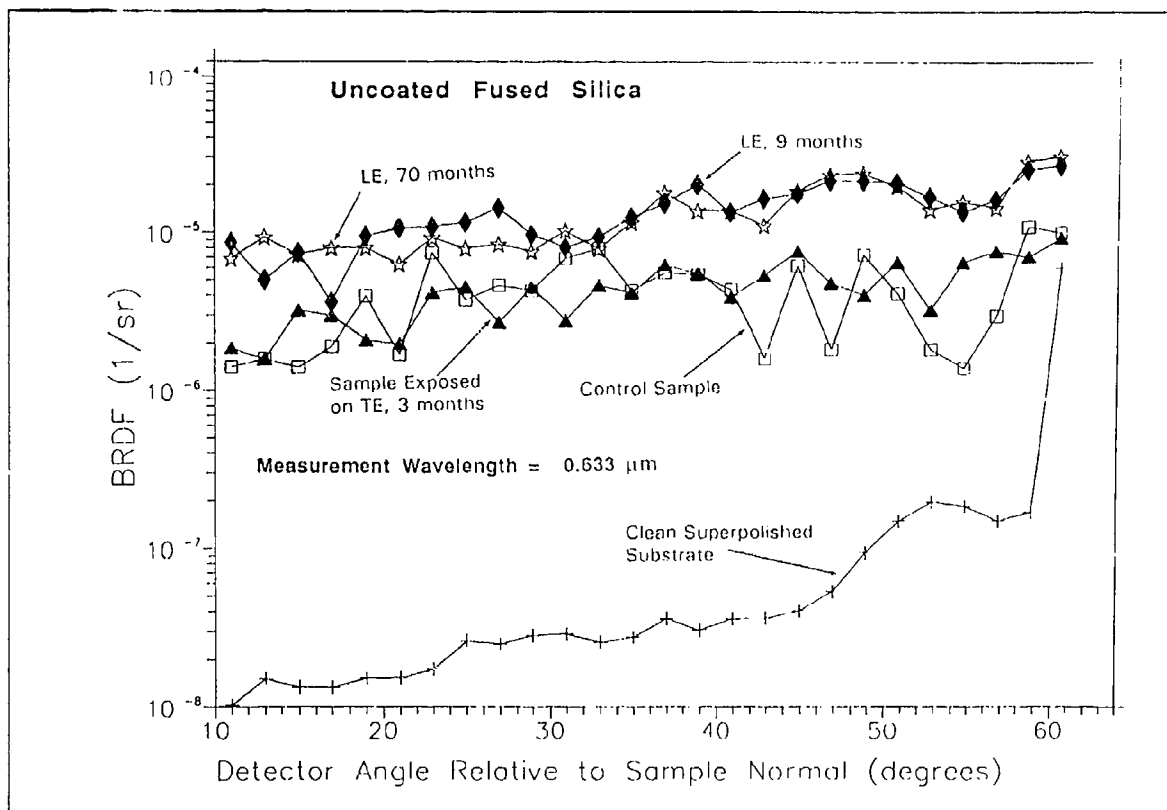


Figure E.40. Exposure Effects on Fused Silica Scatter

<b>REFERENCE:</b>	DeHainaut, Linda L., Kenemuth, John R., Tidler, Cynthia E., and Seegmiller, David W., <u>Degradation of Optical Components in a Space Environment</u> , LDEF Second Post-Retrieval Symposium, June 1992, p. 1372
<b>EXPERIMENT:</b>	M0003-2
<b>COMMENTS:</b>	Leading edge 70-month exposure similar to 9-month exposure.



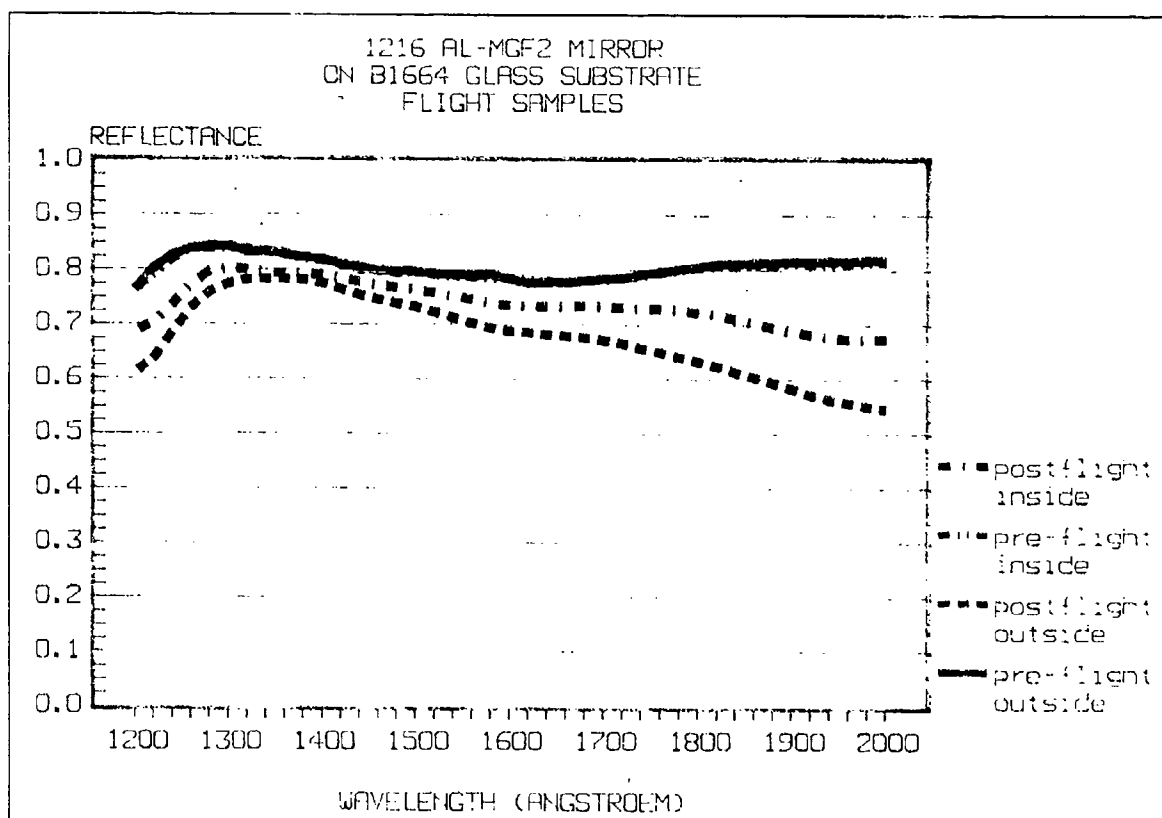


Figure E.41. Reflectance Measurements for Al-Mg<sub>2</sub>/B1664 Glass Mirror

REFERENCE:	Charlier, Jean, <u>Vacuum Deposited Optical Coatings Experiment</u> , LDEF First Post-Retrieval Symposium, June 1991, p. 1354
EXPERIMENT:	A0138-4
COMMENTS:	Outside/inside samples have significantly reduced reflectance over all wavelengths.

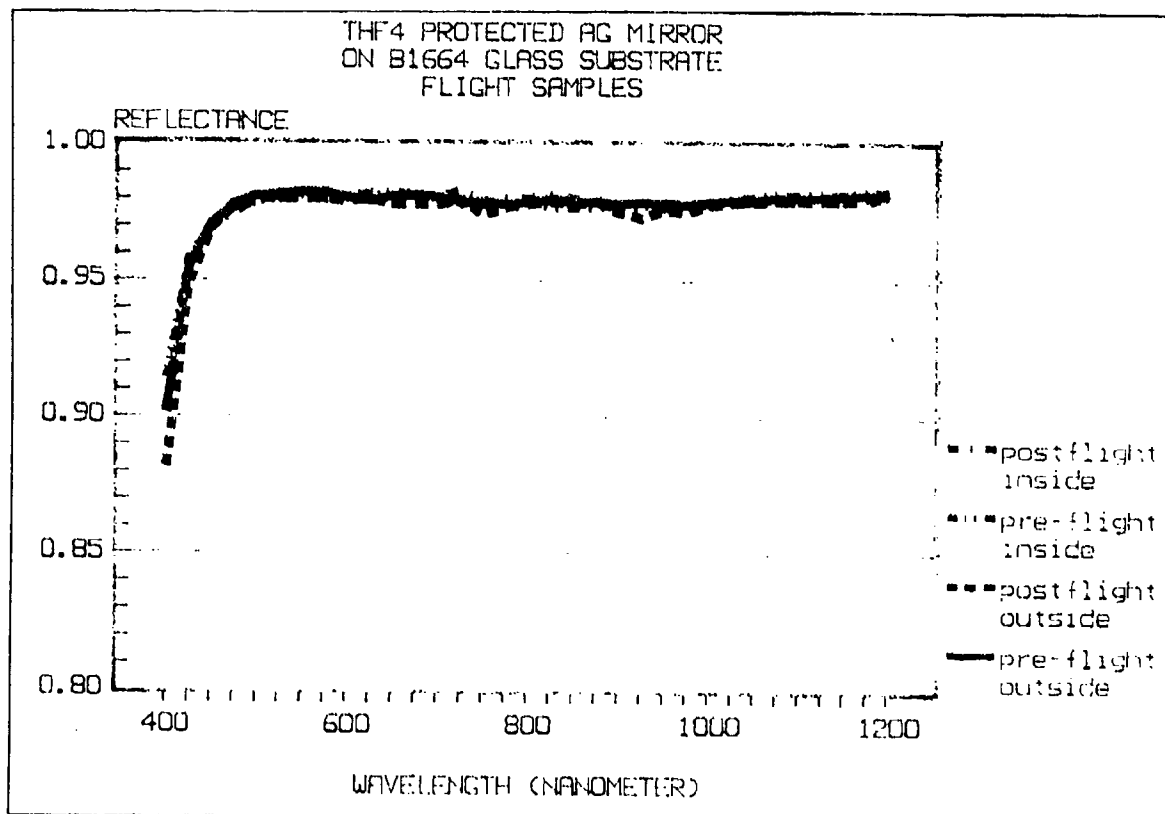


Figure E.42. Reflectance Measurements for ThF<sub>4</sub>-Ag/B1664 Glass Mirror

---

REFERENCE:	Charlier, Jean, <u>Vacuum Deposited Optical Coatings Experiment</u> , LDEF First Post-Retrieval Symposium, June 1991, p. 1354
EXPERIMENT:	A0138-4
COMMENTS:	Outside/inside samples showed little change in reflectance.

---

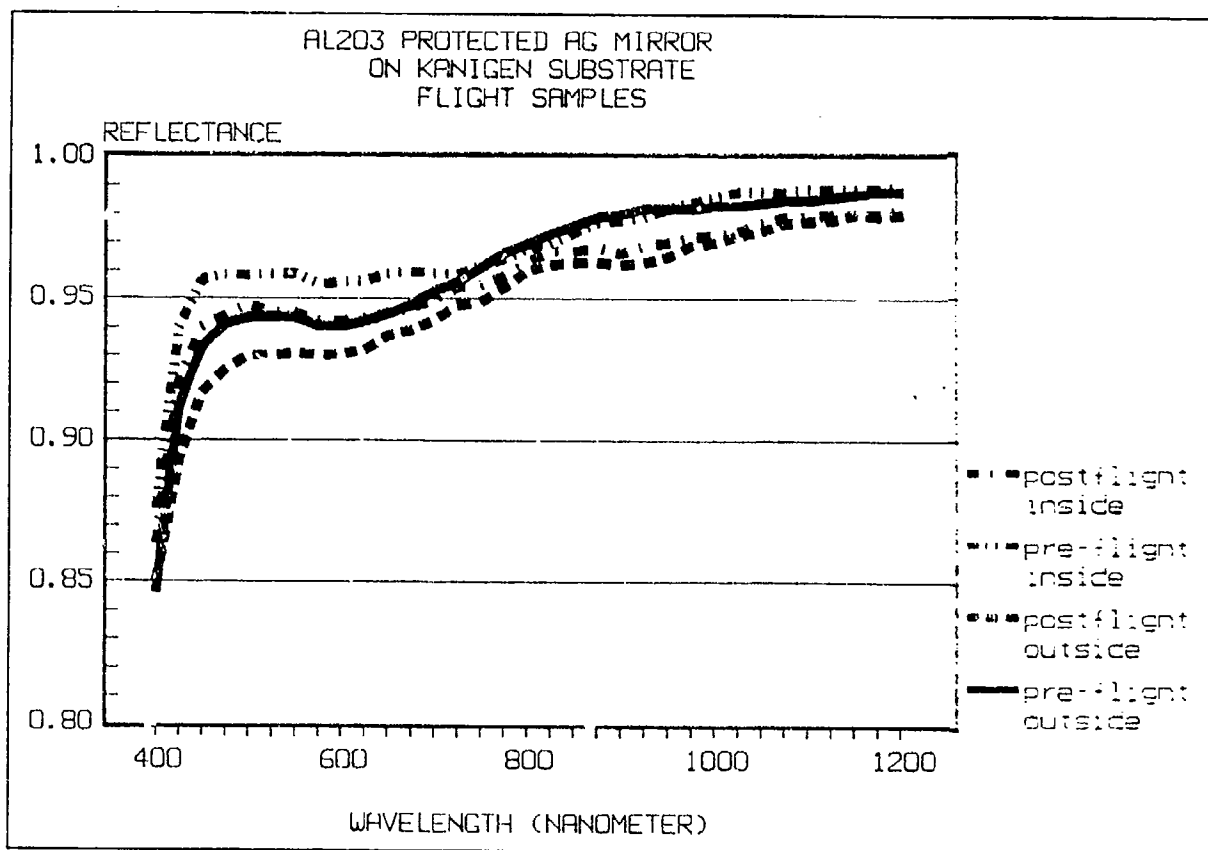


Figure E.43. Reflectance Measurements For  $\text{Al}_2\text{O}_3$ -Ag/Kanigen Mirror

<b>REFERENCE:</b>	Charlier, Jean, <u>Vacuum Deposited Optical Coatings Experiment</u> , LDEF First Post-Retrieval Symposium, June 1991, p. 1358
<b>EXPERIMENT:</b>	A0138-4
<b>COMMENTS:</b>	Outside/inside samples had significantly reduced reflectance except at the blue end.

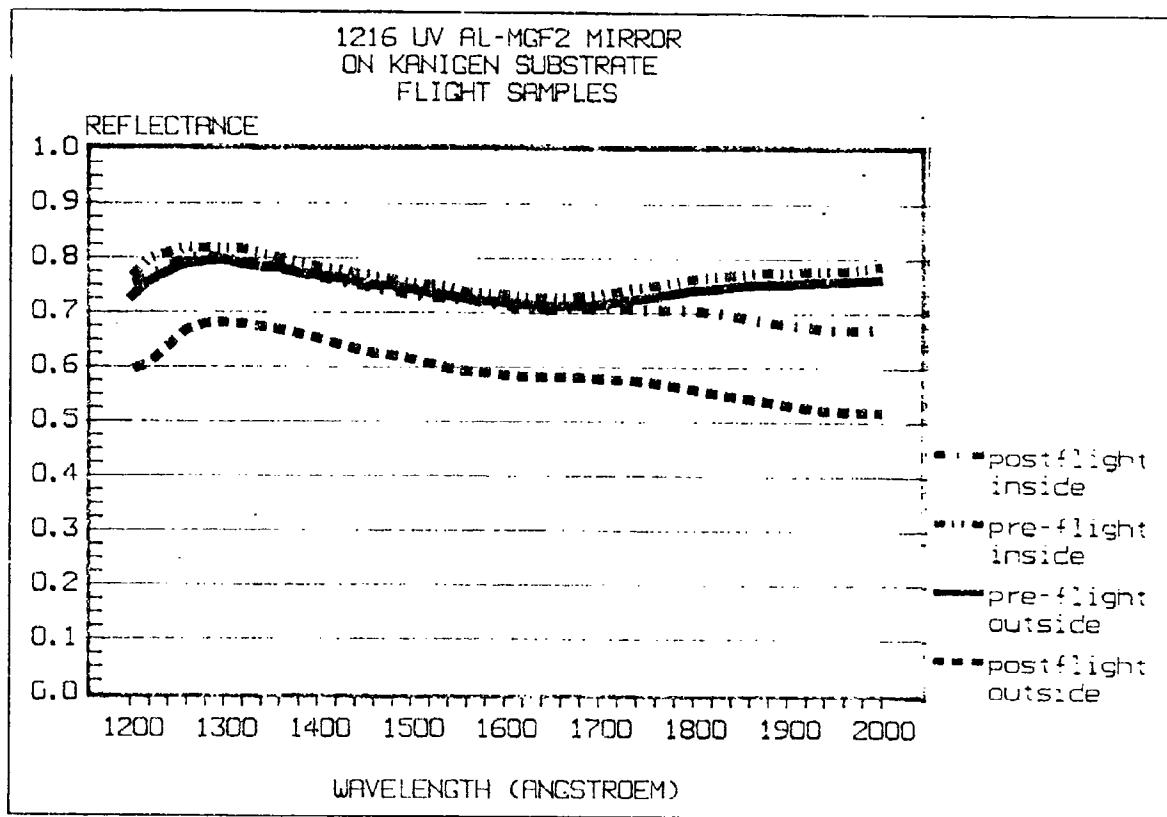


Figure E.44. Reflectance measurements for Al-MgF<sub>2</sub>/Kanigen Mirror

<b>REFERENCE:</b>	Charlier, Jean, <u>Vacuum Deposited Optical Coatings Experiment</u> , LDEF First Post-Retrieval Symposium, June 1991, p. 1355
<b>EXPERIMENT:</b>	A0138-4
<b>COMMENTS:</b>	Inside sample had significant reduction in reflectance at upper end. Outside sample had significant reduction across the entire band.

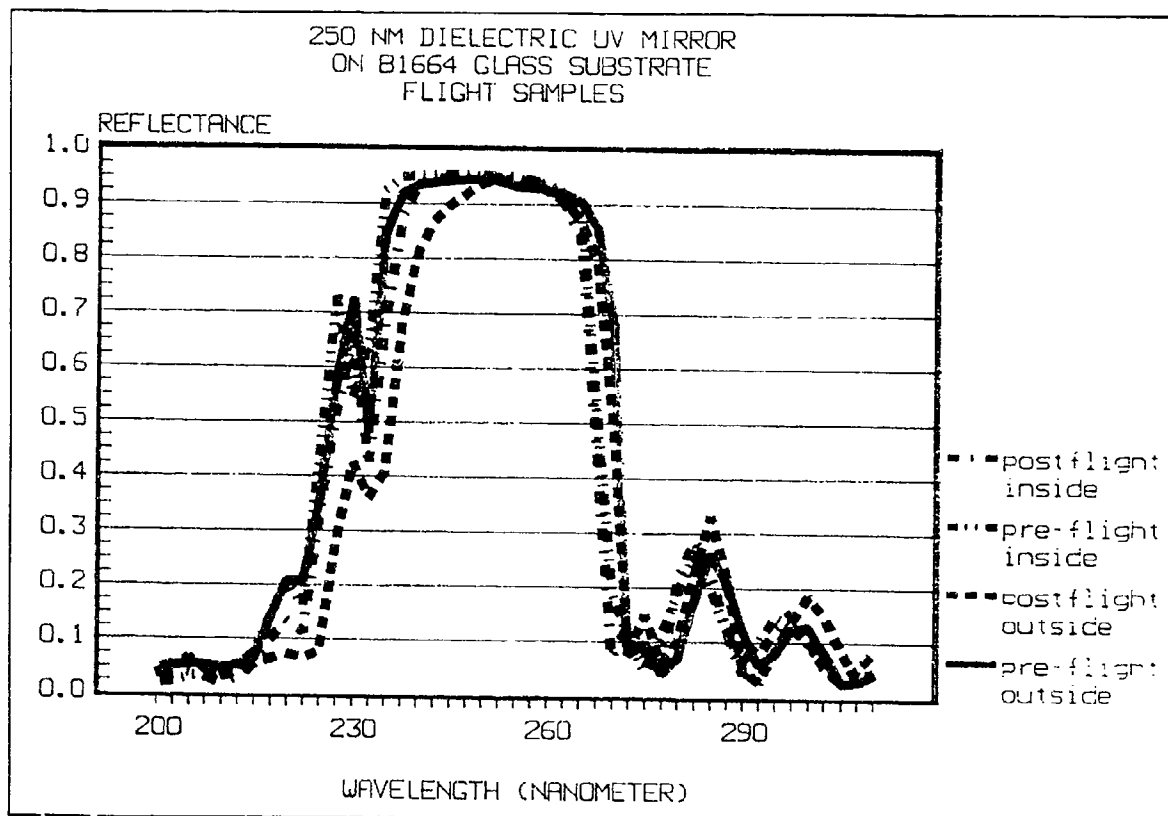


Figure E.45. Reflectance Measurements for 250 nm Dielectric/Glass Mirror

---

REFERENCE:	Charlier, Jean, <u>Vacuum Deposited Optical Coatings Experiment</u> , LDEF First Post-Retrieval Symposium, June 1991, p. 1356
EXPERIMENT:	A0138-4
COMMENTS:	Inside sample showed slight shift in reflectance. Outside sample had a slight shift at the high end.

---

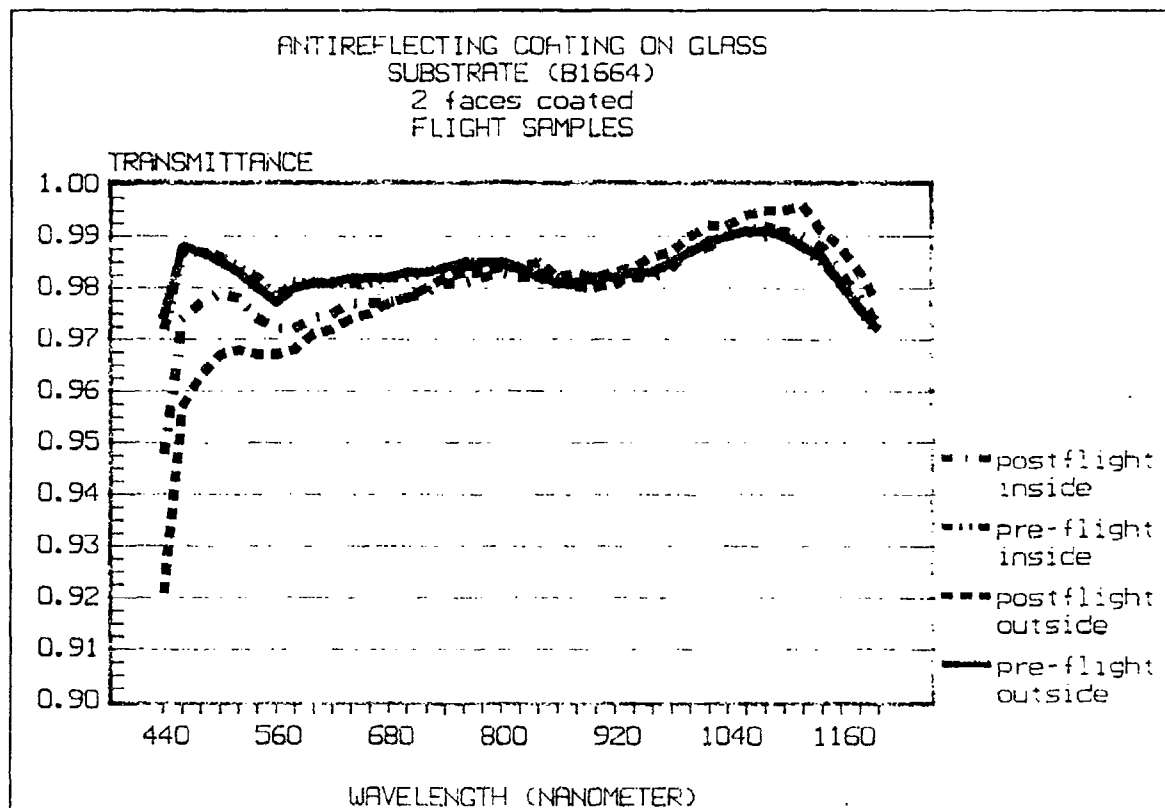


Figure E.46. Transmission measurements for AR on B1664 Glass Mirror

<b>REFERENCE:</b>	Charlier, Jean, <u>Vacuum Deposited Optical Coatings Experiment</u> , LDEF First Post-Retrieval Symposium, June 1991, p. 1360
<b>EXPERIMENT:</b>	A0138-4
<b>COMMENTS:</b>	Inside sample showed a significant reduction in transmittance at the blue end. Outside sample had a significant reduction at the blue end and a slight reduction at the upper end.

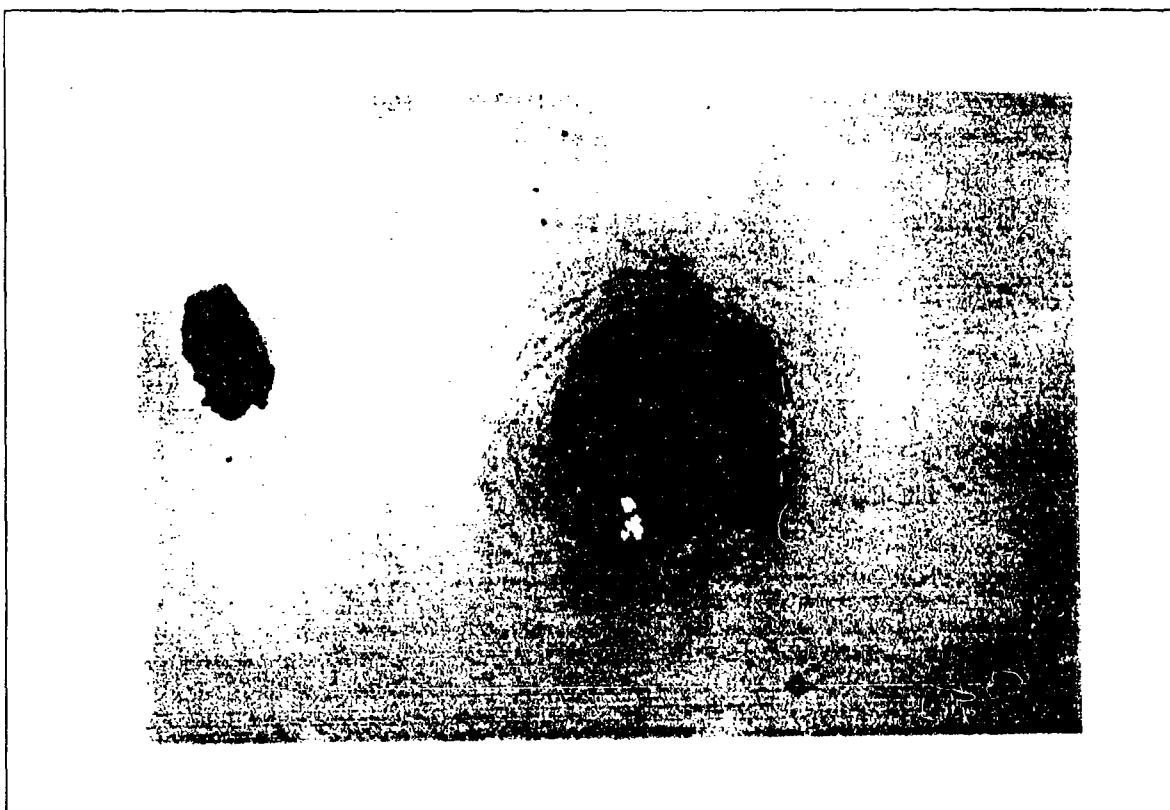


Figure E.47. Impact Damage On  $\text{MgF}_2$  Coated Fused Silica

---

REFERENCE:	DeHainaut, Linda L., Kenemuth, John R., Tidler, Cynthia E., and Seegmiller, David W., <u>Degradation of Optical Components in a Space Environment</u> , LDEF Second Post-Retrieval Symposium, June 1992, p. 1369
EXPERIMENT:	M0003-2
COMMENTS:	Localized damage.

---

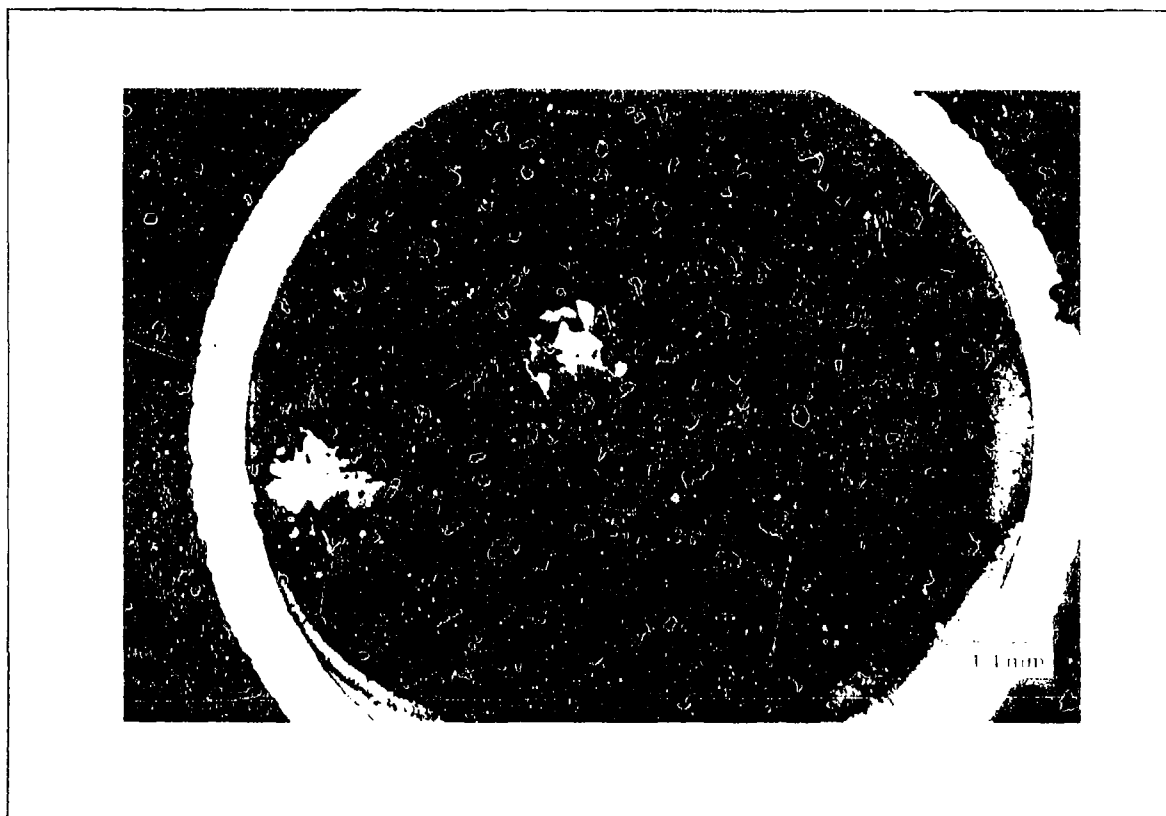


Figure E.48.  $\text{NaF}_2$  Coating on Fused Silica

---

REFERENCE:	M.J. Meshishnek, S.R. Gyetvay, K.W. Pashen, and J.M. Coggi, Long Duration Exposure Facility (LDEF) Experiment M0003 Meteoroid and Debris Survey, LDEF Second Post-Retrieval Symposium, Part 2, June 1 - 5 1992, p. 397
EXPERIMENT:	M0003-7
COMMENTS:	Damage layer has been removed due to UV/atomic oxygen

---



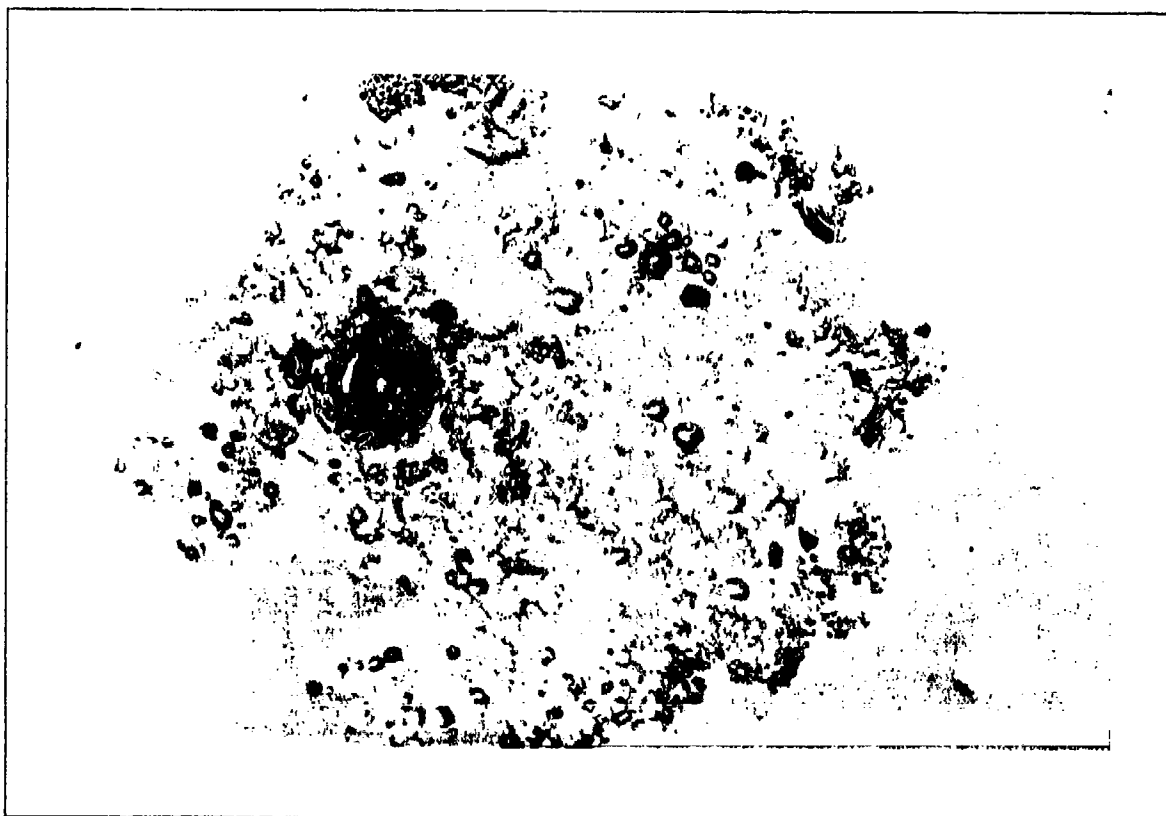


**Figure E.49. Impact Damage on Coated Molybdenum**

---

<b>REFERENCE:</b>	DeHainaut, Linda L., Kenemuth, John R., Tidler, Cynthia E., and Seegmiller, David W., <u>Degradation of Optical Components in a Space Environment</u> , LDEF Second Post-Retrieval Symposium, June 1992, p. 1369
<b>EXPERIMENT:</b>	M0003-2
<b>COMMENTS:</b>	Damage area many times crater size. Coating failure.

---



**Figure E.50. Spiral Cracks and Blisters on  $(\text{Al}_2\text{O}_3/\text{Si})^3/\text{Ag}$  Mirror on Polished Si Substrate**

---

<b>REFERENCE:</b>	Gyetvay, S., et al., <u>Aerospace Corporation LDEF M0003 Sample Observation Data Base</u> , 1993, Record #500
<b>EXPERIMENT:</b>	M0003-7
<b>COMMENTS:</b>	Three small impact craters, surrounded by localized cracking, are evident on exposed coating surface. The coating is cracked in spirals at the perimeter of the exposure area. The coating appears to be blistered in the vicinity of the spiral cracks. Flaking in the cracked region has revealed a corroded and discolored residual surface.

---

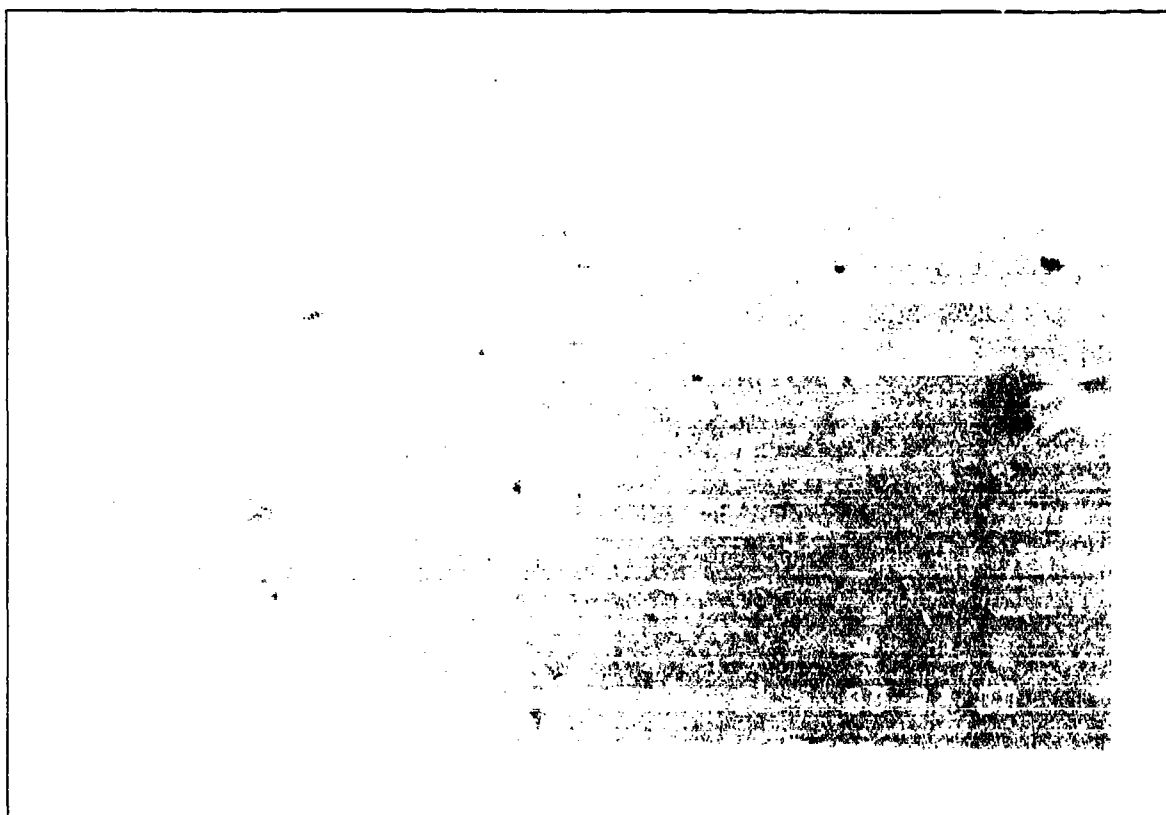


**Figure E.51. Macrophotograph of Crazed and Discolored Al<sub>2</sub>O<sub>3</sub> Coating on SiO<sub>2</sub> Substrate**

---

<b>REFERENCE:</b>	Gyetvay, S., et al., <u>Aerospace Corporation LDEF M0003 Sample Observation Data Base</u> , 1993, Record #635
<b>EXPERIMENT:</b>	M0003-7
<b>COMMENTS:</b>	Fine fractures, which intersect and terminate in defects in the coating, are barely discernible in the exposed surface of the coating. There are some small areas where the coating has flaked away to reveal the smooth surface of the substrate. A small number of individual blisters or bubbles are discernible in the coating. These features vary in size, are randomly distributed, and are globally present on the surface. One possible small impact crater is apparent on the earthward side of the sample. A great deal of extraneous debris is present on the coating surface.

---

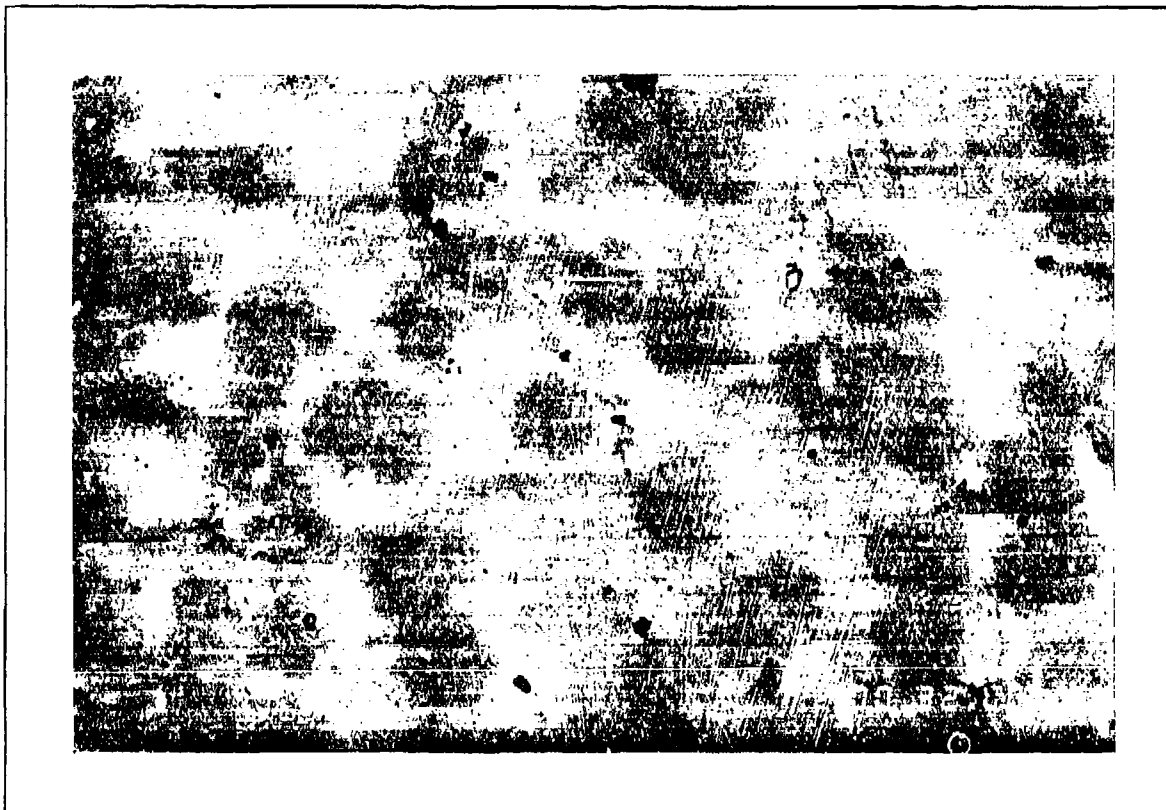


**Figure E.52. Crazed and Discolored  $\text{As}_2\text{Se}_3$  Coating on  $\text{SiO}_2$  Substrate**

---

<b>REFERENCE:</b>	Gyetvay, S., et al., <u>Aerospace Corporation LDEF M0003 Sample Observation Data Base, 1993, Record #639</u>
<b>EXPERIMENT:</b>	M0003-7
<b>COMMENTS:</b>	Coating appears non-uniform in color to the eye. At high magnification, it is apparent that the expose surface is crazed and that the observed variation in color is due to the presence of contiguous green patches in the otherwise pink coating. There are no discernible morphological features associated with the green patches and they do not correspond to the crazed fragments in the coating in any discernible way.

---

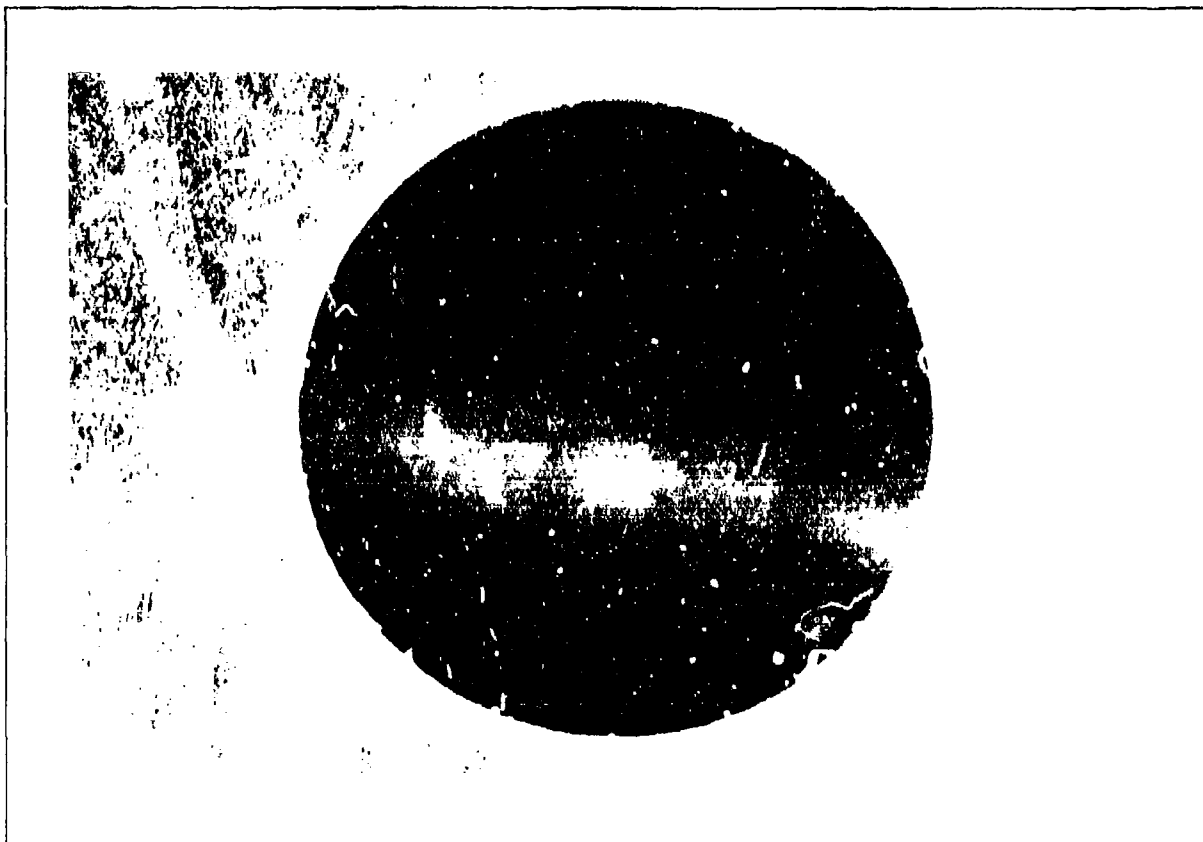


**Figure E.53. Particle-Contaminated Surface of Solar Telescope High Reflective Coating (Electroplated Au on Ni/Al)**

---

<b>REFERENCE:</b>	Gyetvay, S., et al., <u>Aerospace Corporation LDEF M0003 Sample Observation Data Base</u> , 1993, Record #1106.07
<b>EXPERIMENT:</b>	M0003-6
<b>COMMENTS:</b>	Small quantity of debris on surface. No other changes are discernible.

---

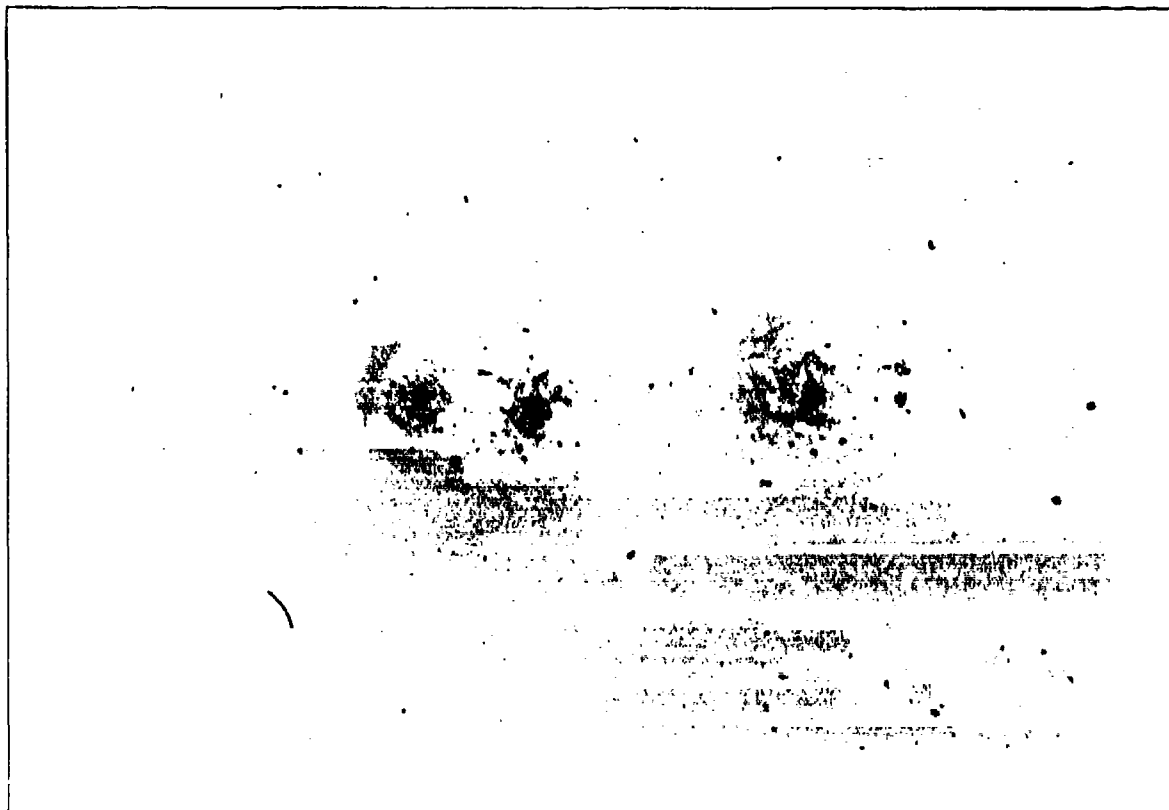


**Figure E.54. Contamination Spots on Surface of Crazed  $\text{MgF}_2$  Coating on  $\text{SiO}_2$  Substrate**

---

<b>REFERENCE:</b>	Gyetvay, S., et al., <u>Aerospace Corporation LDEF M0003 Sample Observation Data Base</u> , 1993, Record #1128
<b>EXPERIMENT:</b>	M0003-2
<b>COMMENTS:</b>	Entire coating is crazed. A great deal of extraneous debris including fibrous matter and metallic film fragments is present on surface. There are three large spots of debris on the spaceward side of the sample where the coating is more extensively crazed. There are blisters around these spots of debris.

---

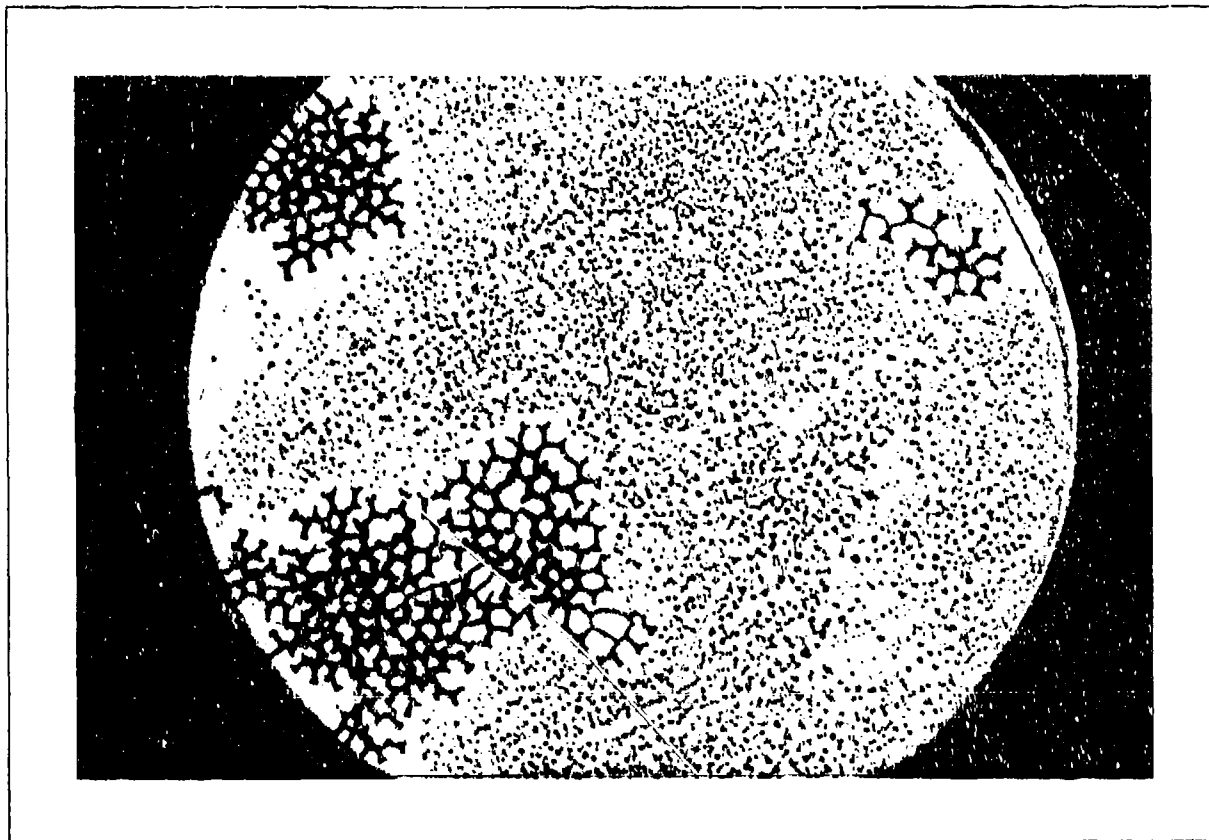


**Figure E.55. Buckled ZnS Coating on SiO<sub>2</sub> Substrate**

---

<b>REFERENCE:</b>	Gyetvay, S., et al., <u>Aerospace Corporation LDEF M0003 Sample Observation Data Base</u> , 1993, Record #640
<b>EXPERIMENT:</b>	M0003-7
<b>COMMENTS:</b>	Coating is buckled in a regular pattern on two large areas of the surface. The entire coating on this sample is blistered. Large blisters, exhibiting many orders of interference fringes, are discernible on the surface of the sample at low magnification. In addition, a high density of very small blisters is apparent throughout the coating at magnifications of 200X and greater. The surface is relatively clean of debris.

---

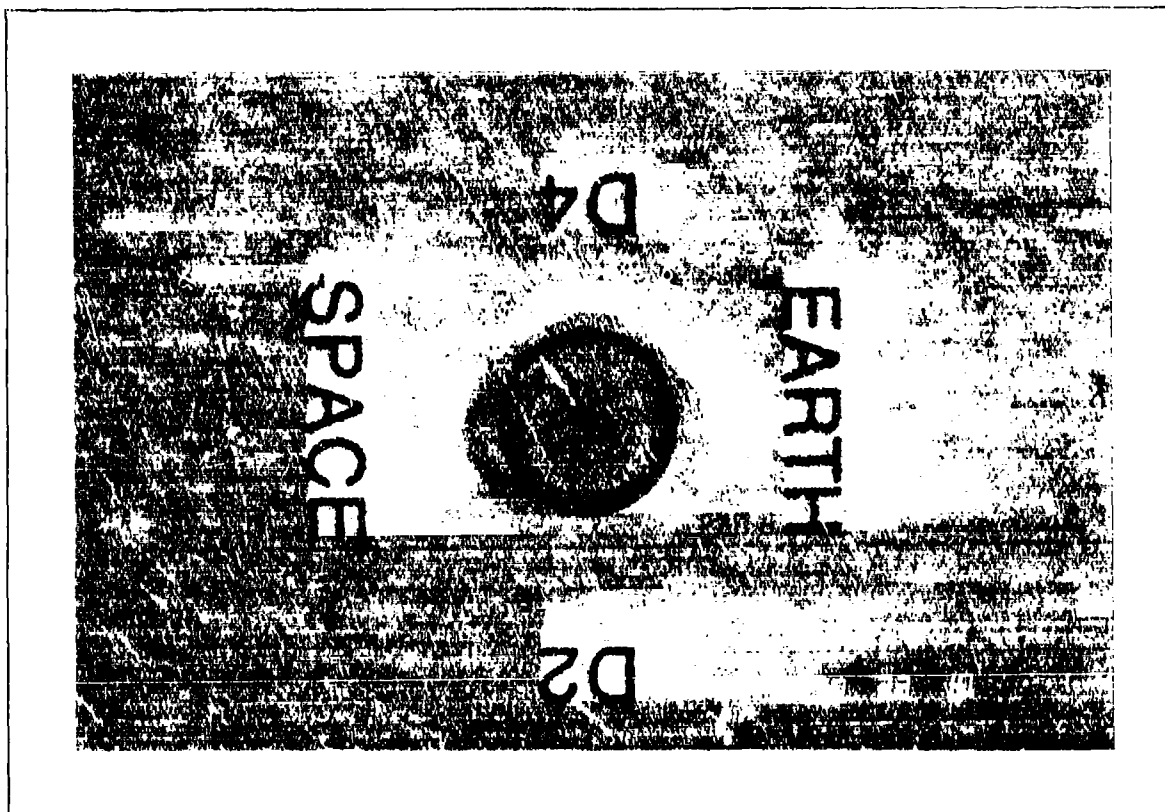


Figure E.56. High Magnification View of Surface of Crazed and Discolored  $\text{Al}_2\text{O}_3$  Coating on  $\text{SiO}_2$  Substrate

---

REFERENCE:	Gyetvay, S., et al., <u>Aerospace Corporation LDEF: M0003 Sample Observation Data Base</u> , 1993, Record #635
EXPERIMENT:	M0003-7
COMMENTS:	Fine fractures, which intersect and terminate in defects in the coating, are barely discernible in the exposed surface of the coating. There are some small areas where the coating has flaked away to reveal the smooth surface of the substrate. A small number of individual blisters or bubbles are discernible in the coating. These features vary in size, are randomly distributed, and are globally present on the surface. One possible small impact crater apparent on the earthward side of the sample. A great deal of extraneous debris is present on the coating surface.

---



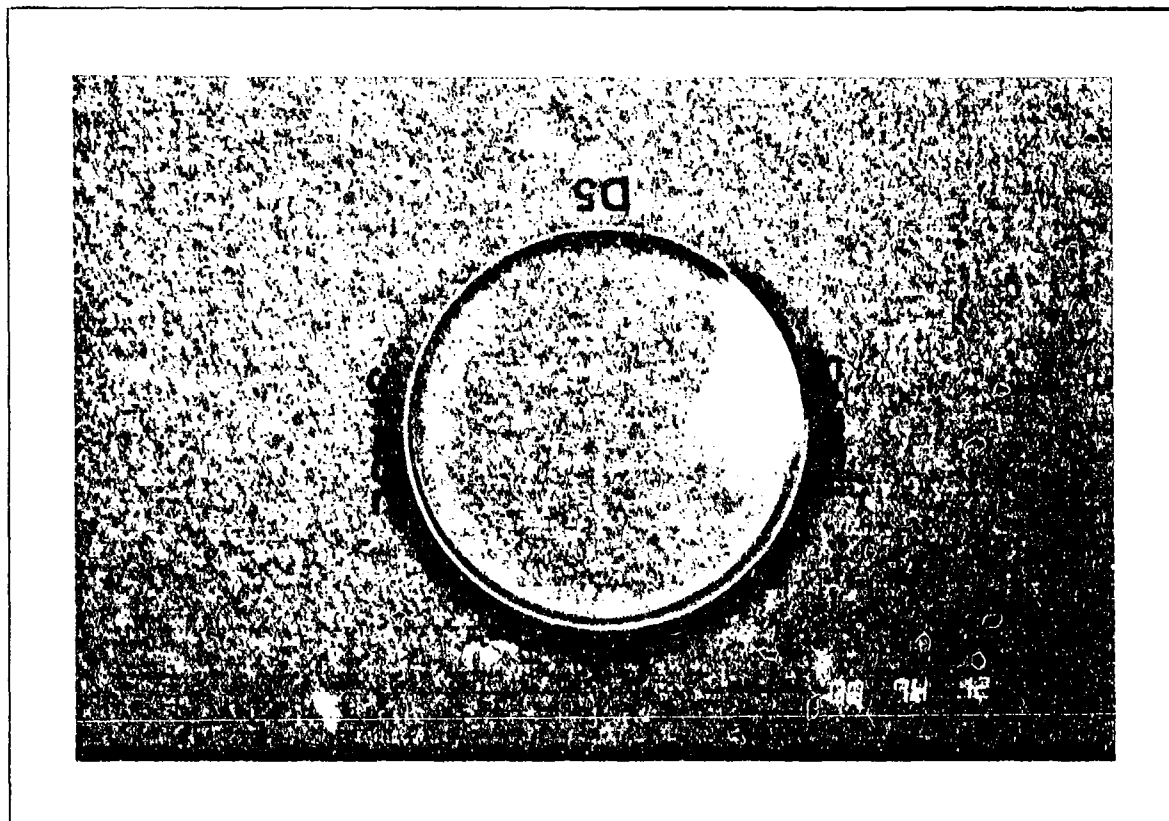
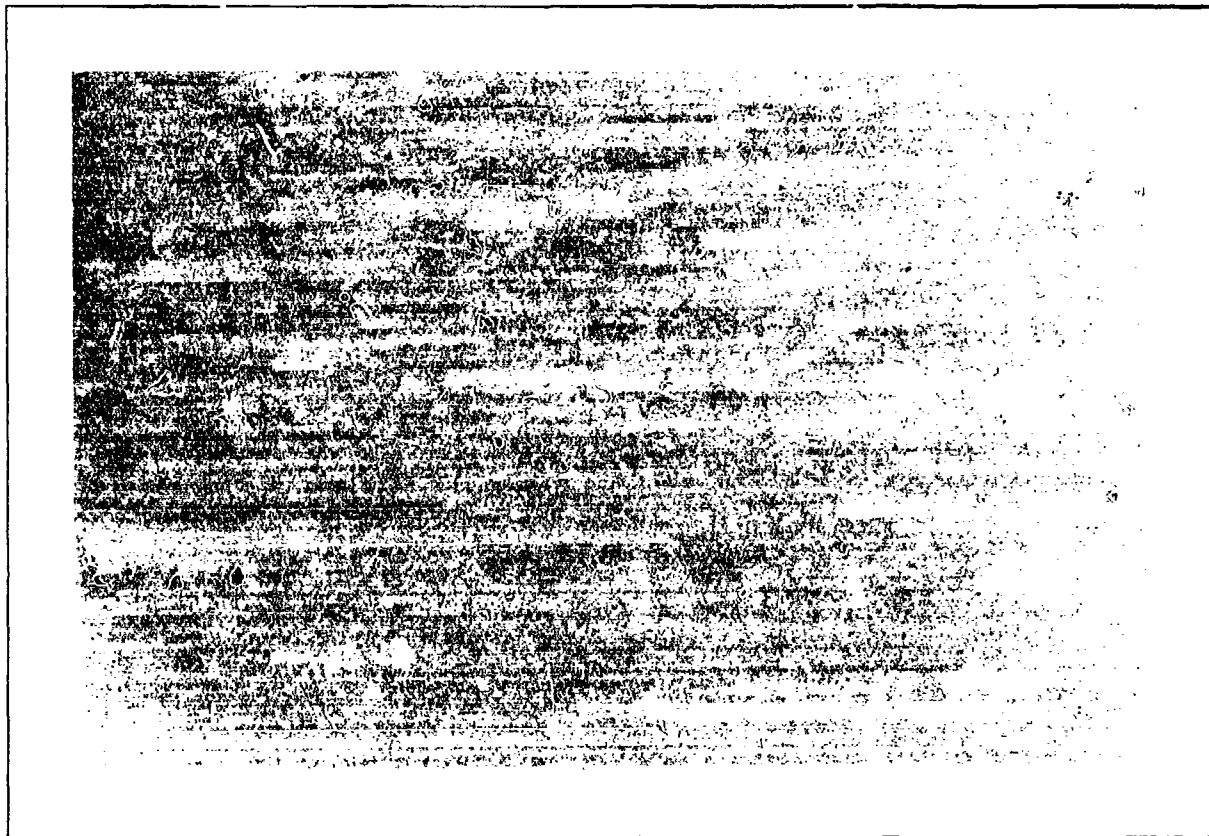


Figure E.57. Surface of Crazed  $\text{MgF}_2$  Coating on  $\text{SiO}_2$  Substrate

---

<b>REFERENCE:</b>	Gyetvay, S., et al., <u>Aerospace Corporation LDEF M0003 Sample Observation Data Base</u> , 1993, Record #1128
<b>EXPERIMENT:</b>	M0003-2
<b>COMMENTS:</b>	Entire coating is crazed. A great deal of extraneous debris including fibrous matter and metallic film fragments is present on surface. There are three large spots of debris on the spaceward side of the sample where the coating is more extensively crazed. There are blisters around these spots of debris.

---



**Figure E.58. Surface of Crazed  $\text{MgF}_2$  Coating on  $\text{SiO}_2$  Substrate**

---

<b>REFERENCE:</b>	Gyetvay, S., et al., <u>Aerospace Corporation LDEF M0003 Sample Observation Data Base</u> , 1993, Record #1128
<b>EXPERIMENT:</b>	M0003-2
<b>COMMENTS:</b>	Entire coating is crazed. A great deal of extraneous debris including fibrous matter and metallic film fragments is present on surface. There are three large spots of debris on the spaceward side of the sample where the coating is more extensively crazed. There are blisters around these spots of debris.

---

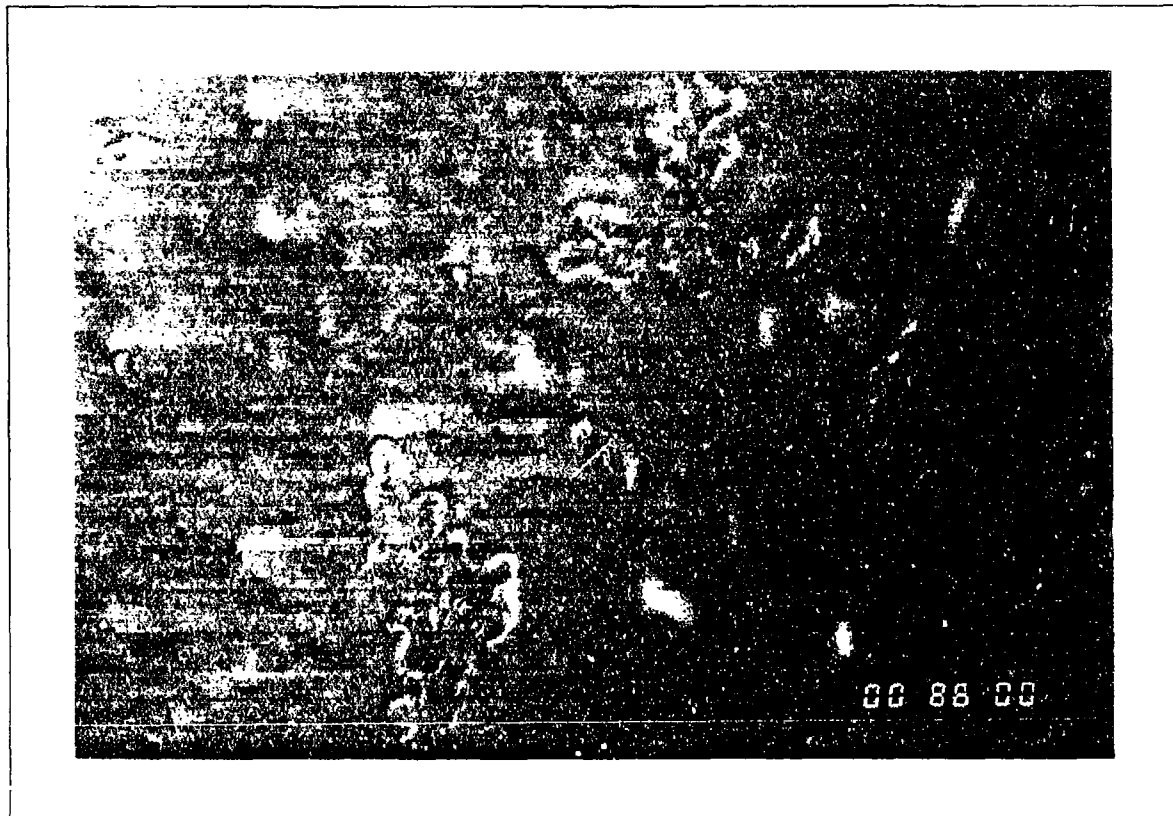


**Figure E.59. High Magnification View of Haze-Producing Dendritic Growth on Surface of  $(\text{Al}_2\text{O}_3/\text{ZnS})/\text{Ag}$  Mirror on Polished Molybdenum Substrate**

---

<b>REFERENCE:</b>	Gyetvay, S., et al., <u>Aerospace Corporation LDEF M0003 Sample Observation Data Base</u> , 1993, Record #566
<b>EXPERIMENT:</b>	M0003-7
<b>COMMENTS:</b>	Coating appears hazy and discolored on exposed surface. Multiple zones of discoloration are apparent. Variation in discoloration is result of varying degrees of dendritic growth. A high density of spots is apparent over the entire coating. Grain boundaries in the substrate are apparent through the coating.

---

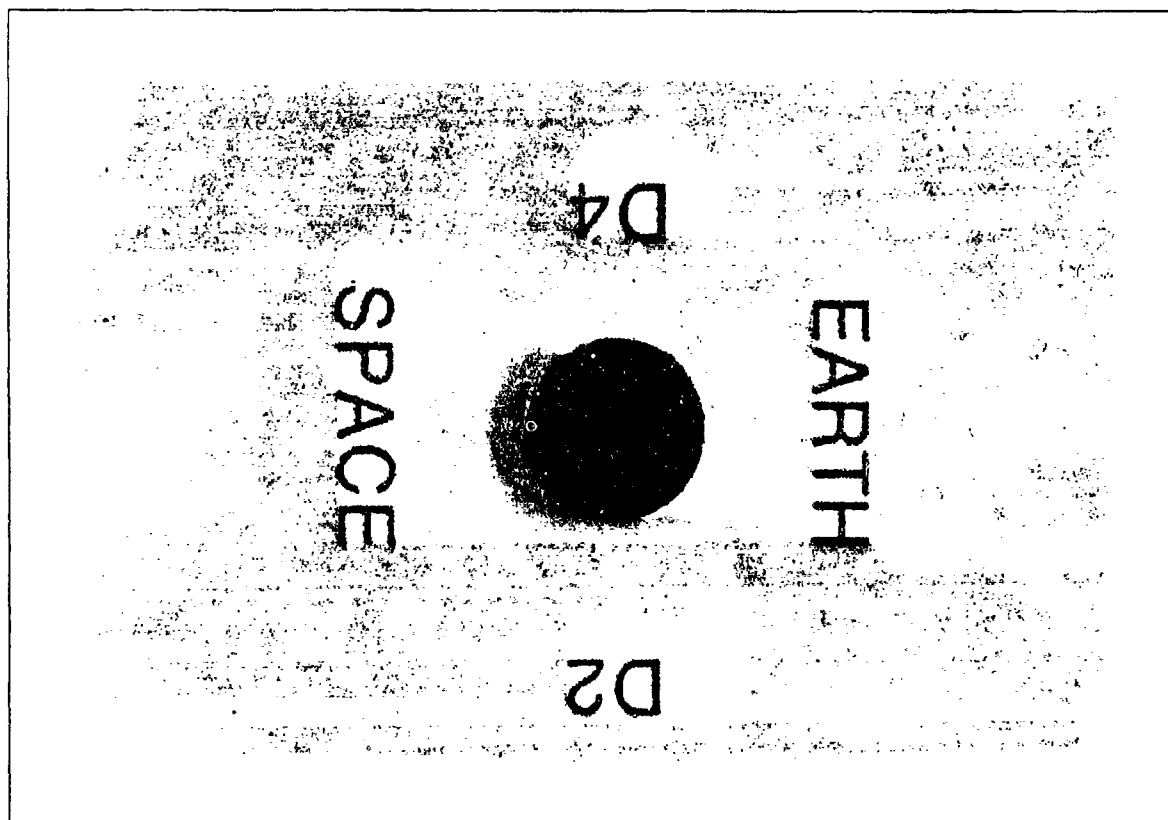


Figure E.60. Macrophotograph of Si Coating on SiO<sub>2</sub> Substrate

---

REFERENCE:	Gyetvay, S., et al., Aerospace Corporation LDEF M0003 Sample Observation Data Base, 1993, Record #636
EXPERIMENT:	M0003-7
COMMENTS:	A great deal of debris is present on the coating surface. Nevertheless, the surface remains highly specular. At least four small circular areas surrounding deposits apparent on surface. These resemble, but are not, impact craters. In these areas, a central deposit of uncertain origin is surrounded by a zone of reacted (discolored) coating.

---

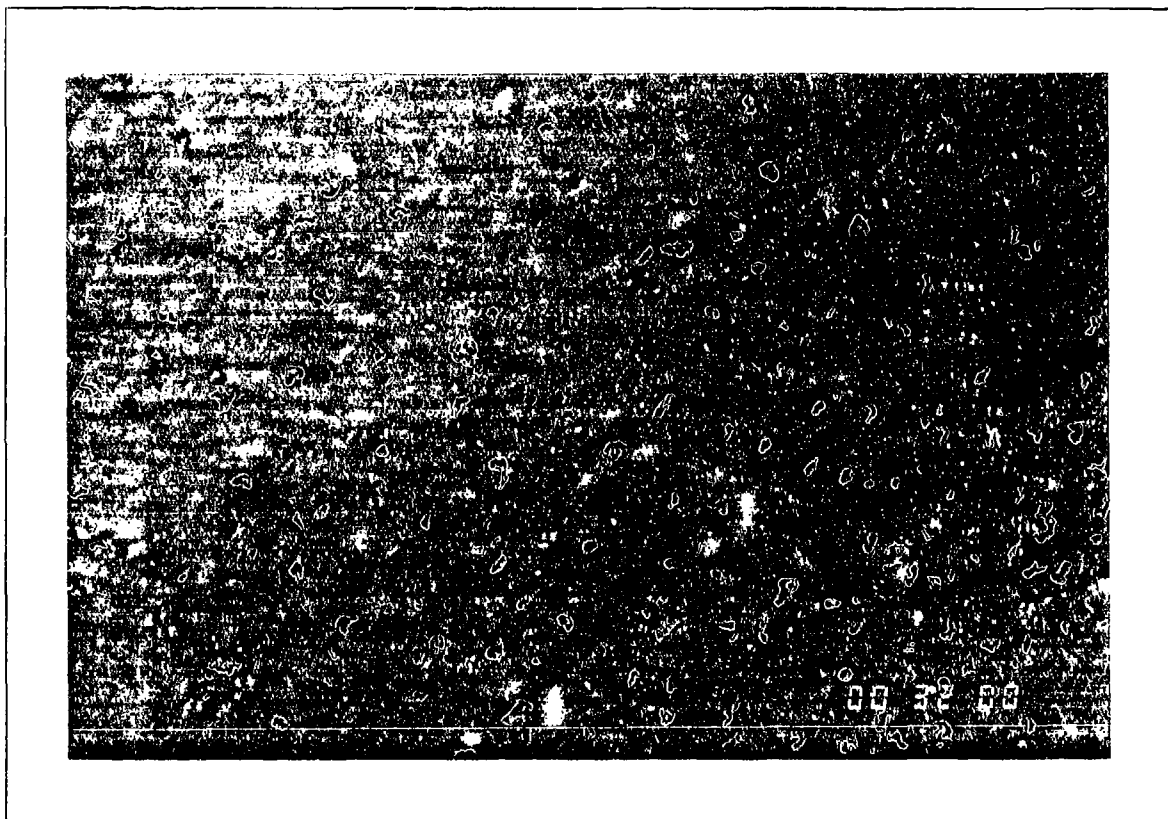


Figure E.61. High Magnification View of  $\text{PbF}_2$  Coating on  $\text{SiO}_2$  Substrate

---

REFERENCE:	Gyetvay, S., et al., <u>Aerospace Corporation LDEF M0003 Sample Observation Data Base</u> , 1993, Record #638
EXPERIMENT:	M0003-7
COMMENTS:	Coating appears dark rust in color. Three or four large gouges or scratches are present in the coating surface. The coating surface is highly textured and replicates a large number of subsurface polishing scratches. Features, which may be bubbles, pinholes, or growth nodules in the coating have formed preferentially along these scratches. Spots of debris, surrounded by reacted material, are present in the surface.

---

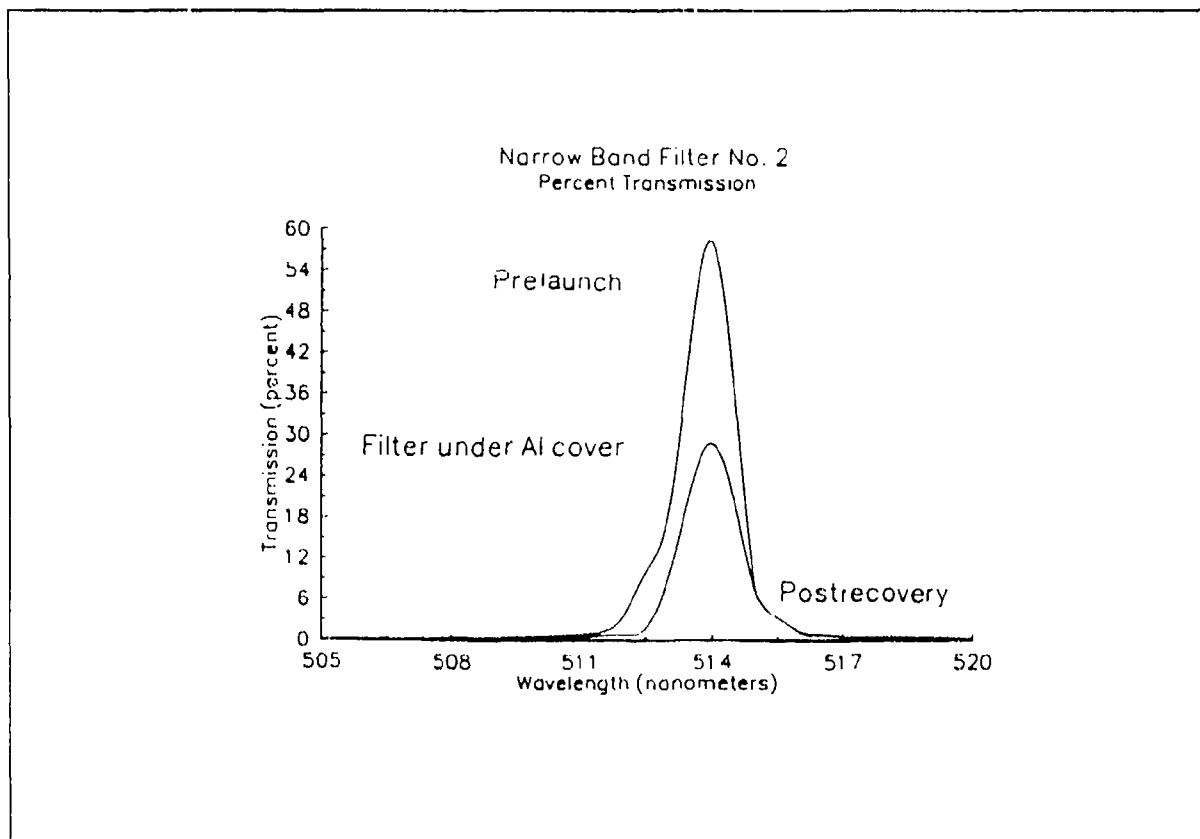
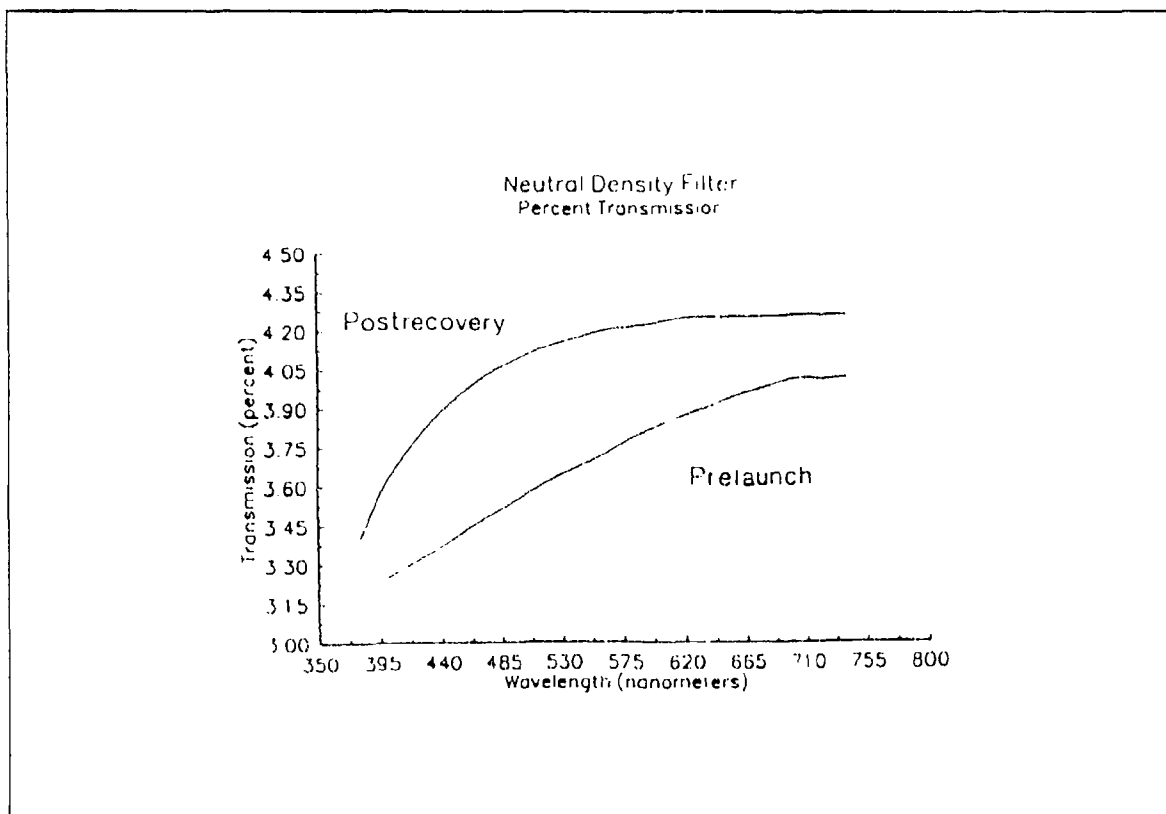


Figure E.62. Pre-Launch and Post-Recovery Transmission of Corion Narrow-Band Filter #2 (Covered)

---

REFERENCE:	M.D. Blue and D.W. Roberts, GTRI, Effects of Space Exposure on Optical Filters, <u>Applied Optics</u> , Vol. 31, No. 25, 1 September 1992, p. 5299
EXPERIMENT:	S0050-2
COMMENTS:	Reduced transmission.

---



**Figure E.63. Pre-Launch and Post-Recovery Transmission of Corion Neutral Density-Band Filter #6 (Covered)**

<b>REFERENCE:</b>	M.D. Blue, GUP1, Investigation of the Effects of LDEF on Active Optical System Components, Final Report
<b>EXPERIMENT:</b>	S0050-2
<b>COMMENTS:</b>	No change in transmission. (This figure is presented by the experimenter for both covered and uncovered neutral density filters. For the covered filter, the transmission was unchanged and its transmission curve overlays the prelaunch curve directly.)

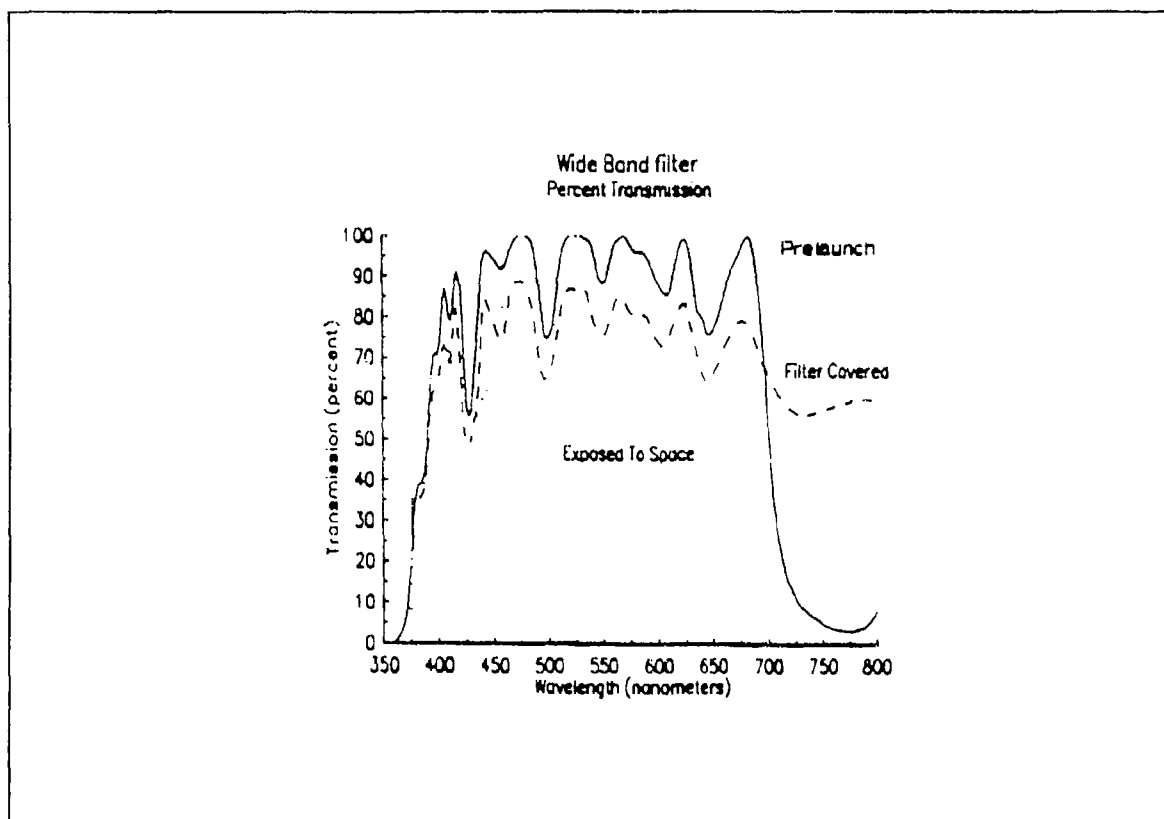


Figure E.64. Pre-Launch and Post-Recovery Transmission of Corion Broadband Filter #9 (Covered)

REFERENCE:	M.D. Blue, GTRI, Investigation of the Effects of LDEF on Active Optical System Components, Final Report
EXPERIMENT:	S0050-2
COMMENTS:	No change in transmission. (This figure is presented by the experimenter for both covered and uncovered IR suppression filters. Filter #9 showed little change in transmission and its transmission curve overlays the prelaunch curve almost directly.)



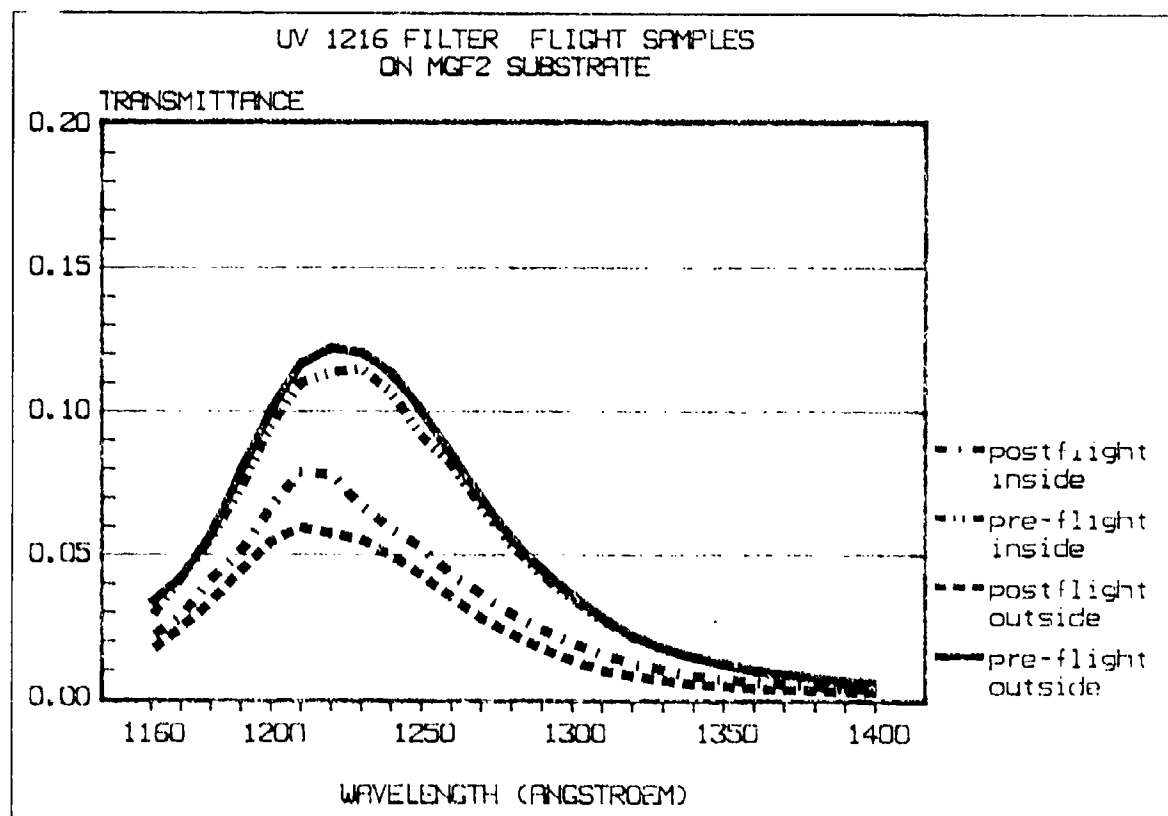


Figure E.65. Pre-Launch and Post-Recovery Transmission of Al/MgF<sub>2</sub> Optical Filter on MgF<sub>2</sub> Substrate (1216 Å) (Covered)

REFERENCE:	Charlier, J., Vacuum Deposited Optical Coatings Experiment, LDEF First Post-Retrieval Symposium, Part 3, p. 1343
EXPERIMENT:	A0138-4
COMMENTS:	Reduced transmittance, shift in center wavelength.

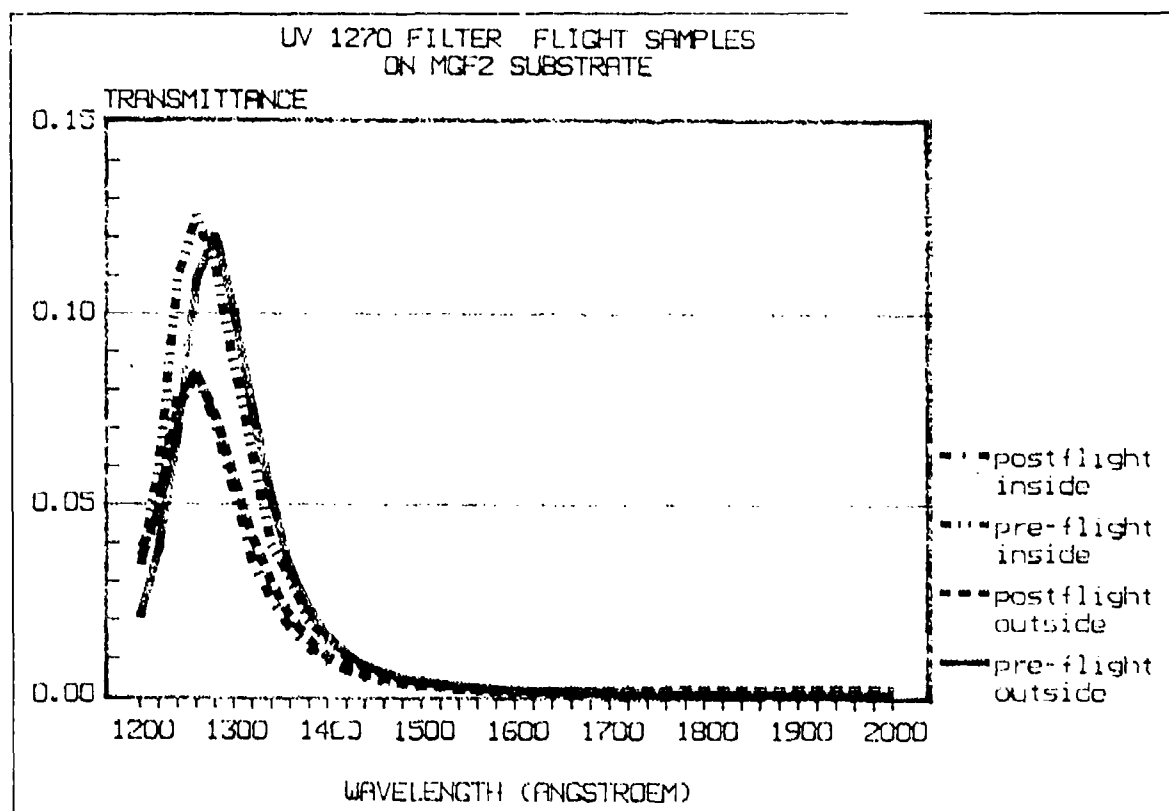


Figure E.66. Pre-Launch and Post-Recovery Transmission of Al/MgF<sub>2</sub> Optical Filter on MgF<sub>2</sub> Substrate (1270 Å) (Covered)

REFERENCE:	Charlier, J., Vacuum Deposited Optical Coatings Experiment, LDEF First Post-Retrieval Symposium, Part 3, p. 1343
EXPERIMENT:	A0138-4
COMMENTS:	Reduced transmittance, shift in center wavelength.

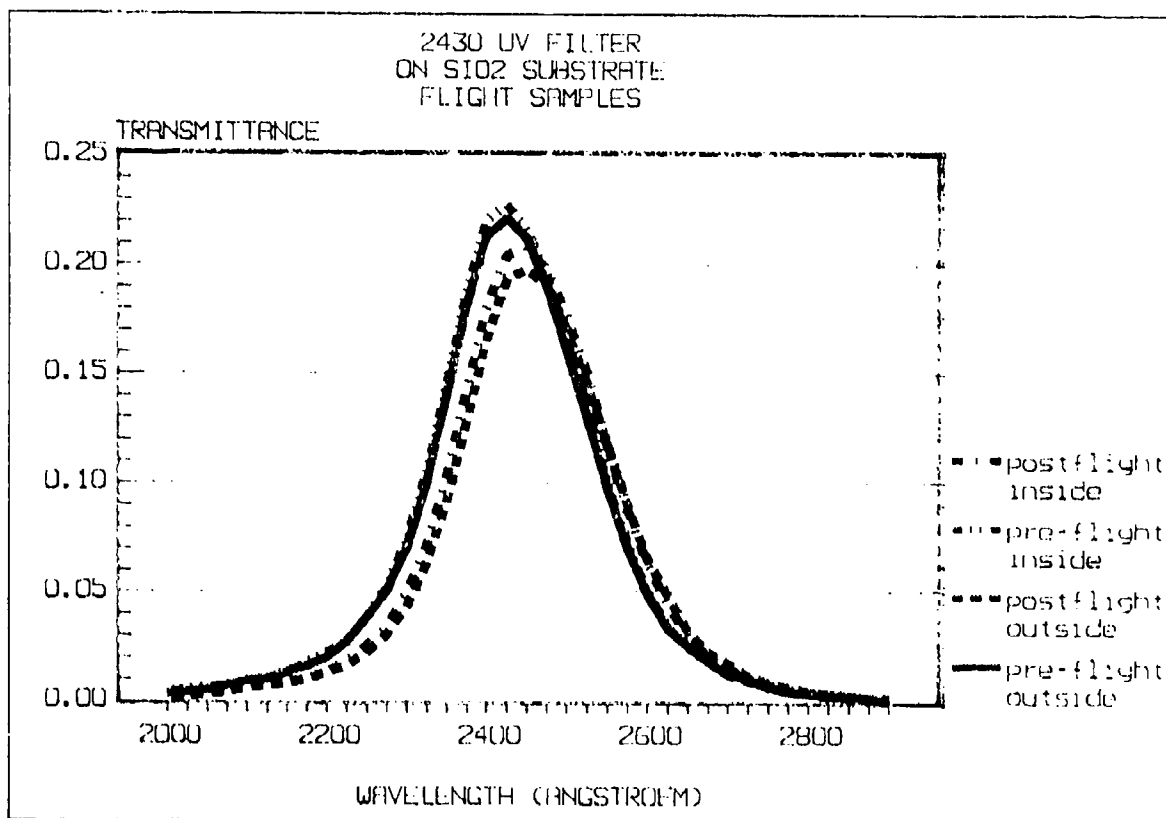


Figure E.67. Pre-Launch and Post-Recovery Transmission of Al/MgF<sub>2</sub> Optical Filter on Quartz Substrate (2430 Å) (Covered)

---

REFERENCE:	Charlier, J., Vacuum Deposited Optical Coatings Experiment, LDEF First Post-Retrieval Symposium, Part 3, p. 1343
EXPERIMENT:	A0138-4
COMMENTS:	Slight reduction in transmittance and shift in center wavelength.

---

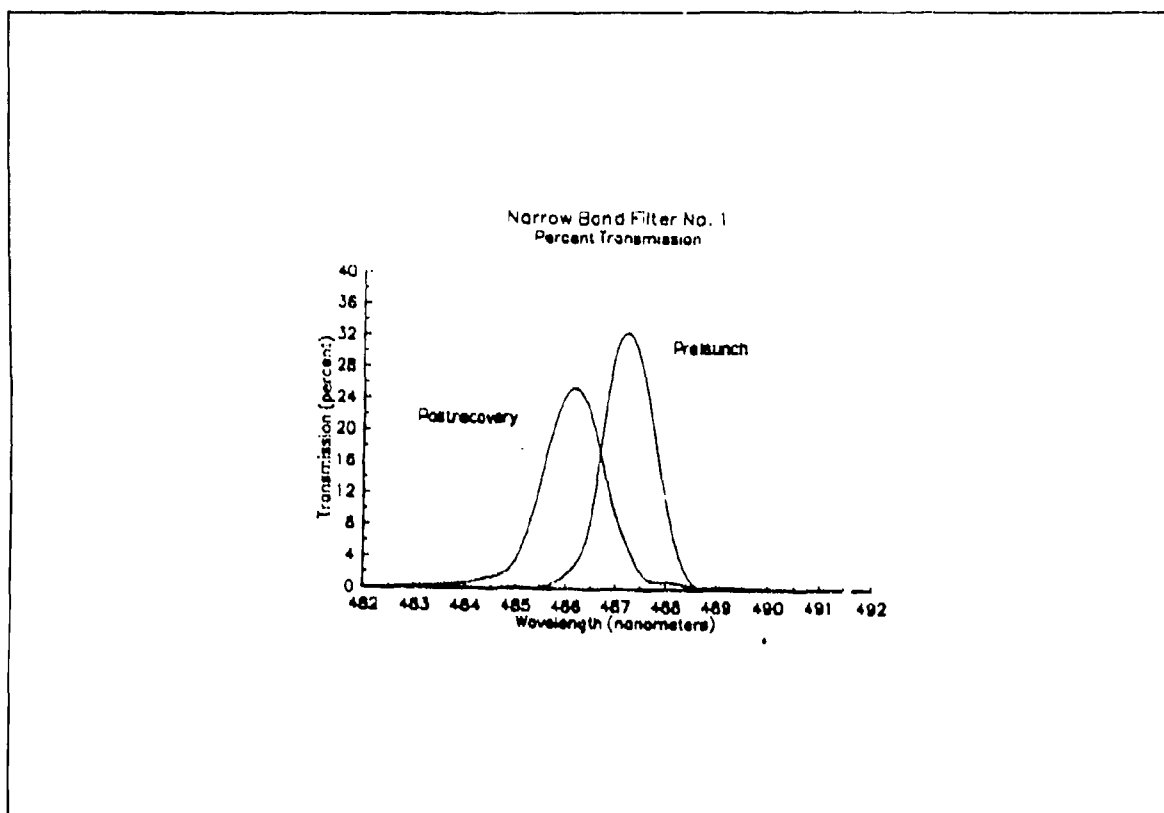


Figure E.68. Pre-Launch and Post-Recovery Transmission of Corion Narrow-Band Filter #1

---

REFERENCE:	M.D. Blue, GTRI, Investigation of the Effects of LDEF on Active Optical System Components, Final Report
EXPERIMENT:	S0050-2
COMMENTS:	Reduced transmission, center frequency shift, broadening of bandwidth.

---

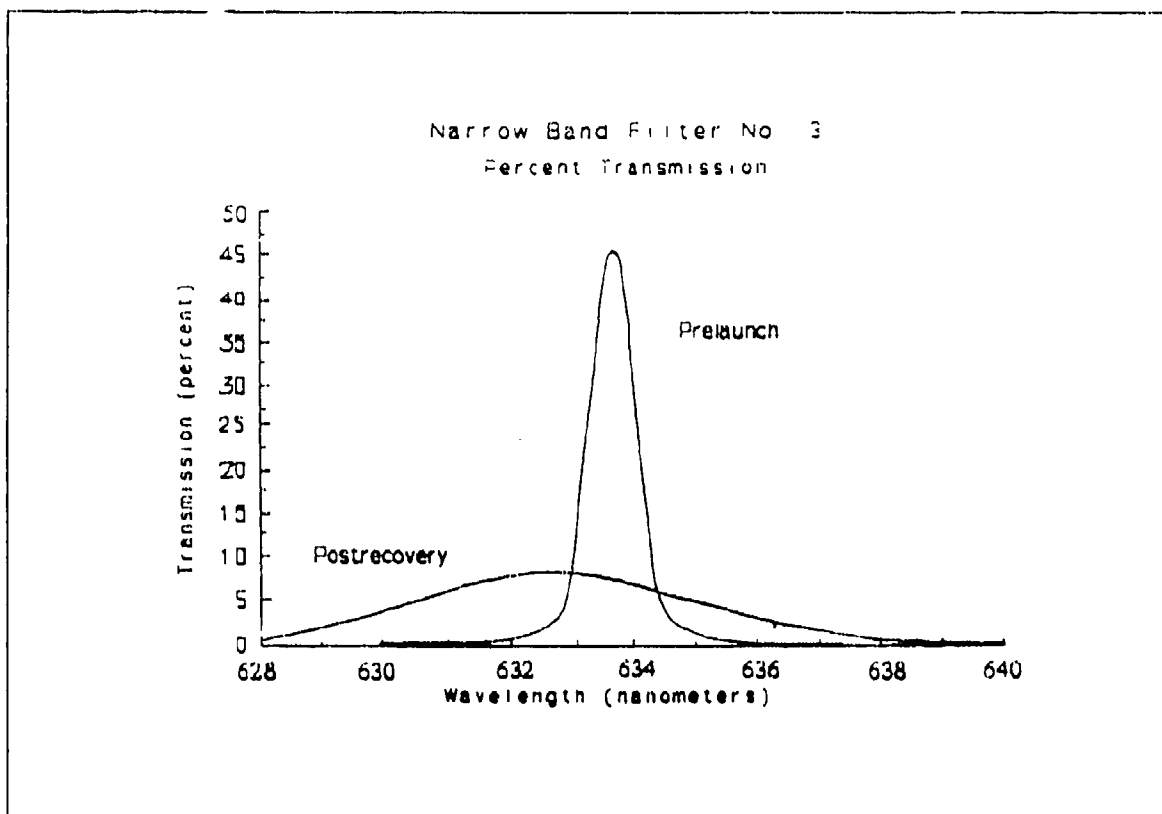


Figure E.69. Pre-Launch and Post-Recovery Transmission of Corion Narrow-Band Filter #3

---

REFERENCE:	M.D. Blue, GTRI, Investigation of the Effects of LDEF on Active Optical System Components, Final Report
EXPERIMENT:	S0050-2
COMMENTS:	Reduced transmission, center frequency shift, broadening of bandwidth.

---

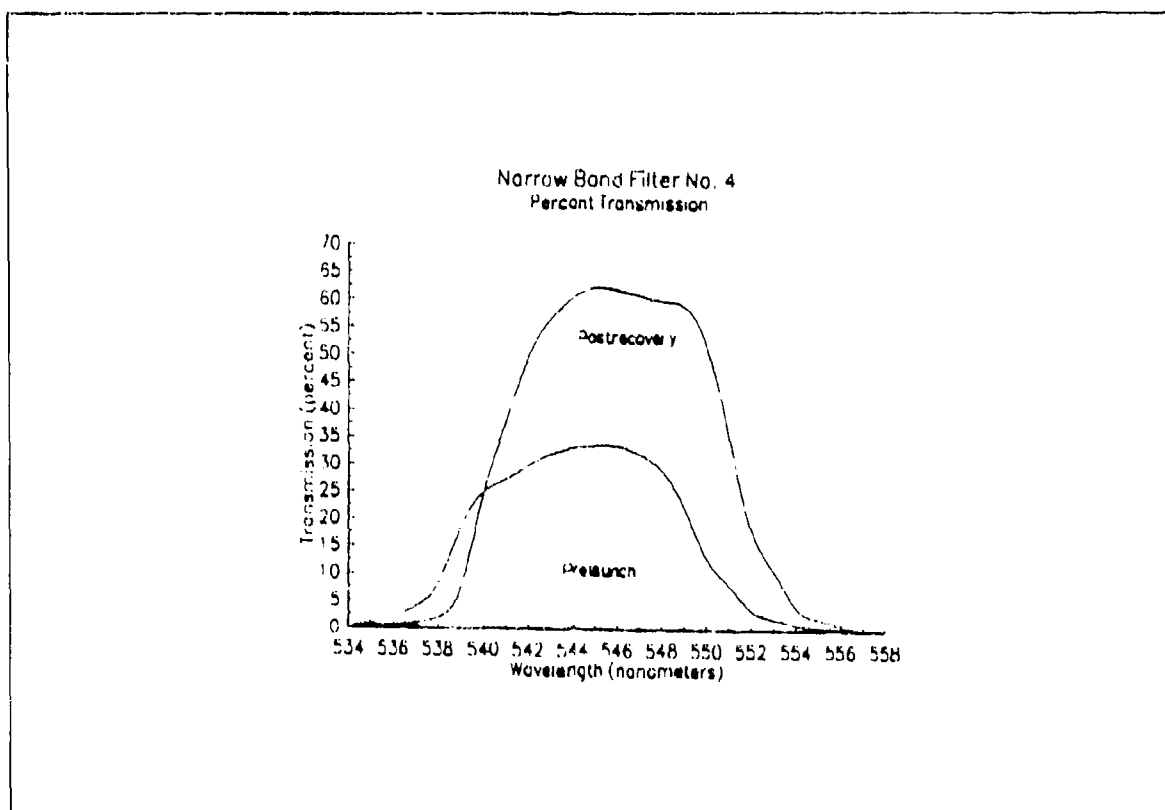
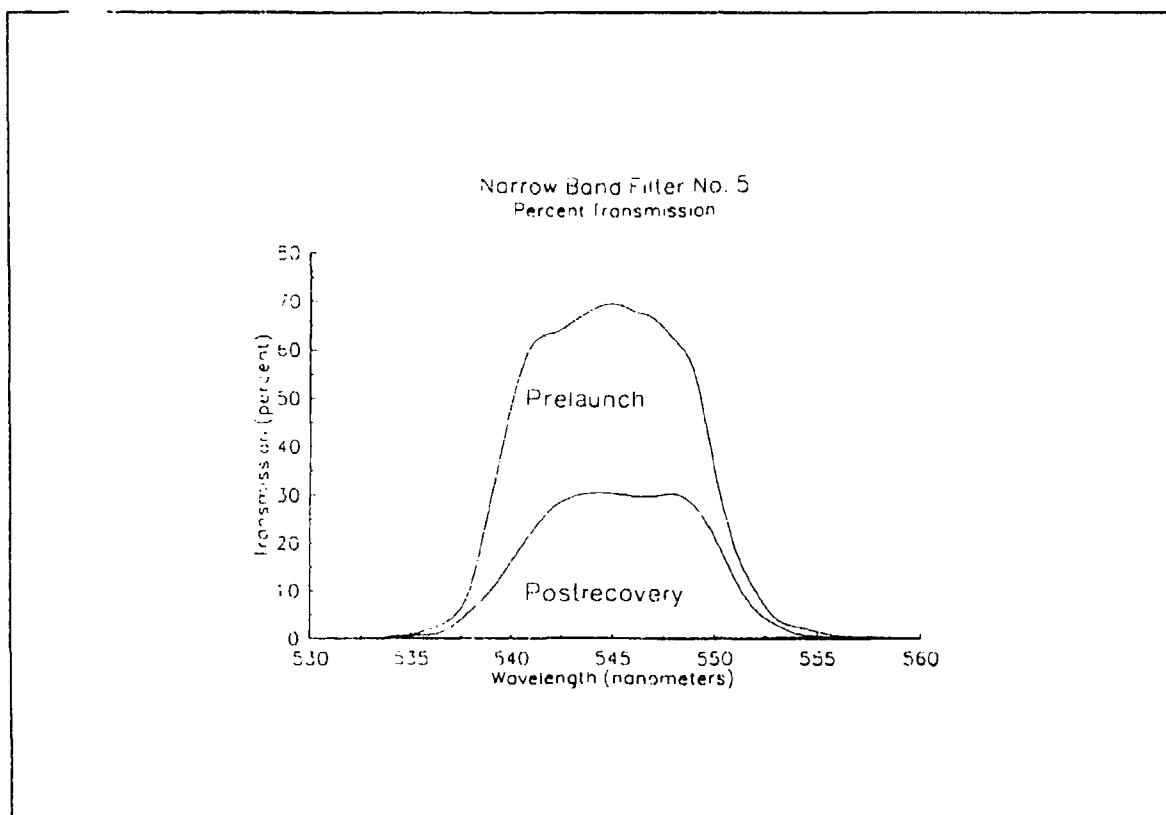


Figure E.70. Pre-Launch and Post-Recovery Transmission of Corion Narrow-Band Filter #4

REFERENCE:	M.D. Blue, GTRI, Investigation of the Effects of LDEF on Active Optical System Components, Final Report
EXPERIMENT:	S0050-2
COMMENTS:	Reduced transmission, center frequency shift, no appreciable broadening of bandwidth.



**Figure E.71. Pre-Launch and Post-Recovery Transmission of Corion Narrow-Band Filter #5**

---

<b>REFERENCE:</b>	M.D. Blue, GTRI, Investigation of the Effects of LDEF on Active Optical System Components, Final Report
<b>EXPERIMENT:</b>	SG050-2
<b>COMMENTS:</b>	Reduced transmission, center frequency shift, no appreciable broadening of bandwidth.

---

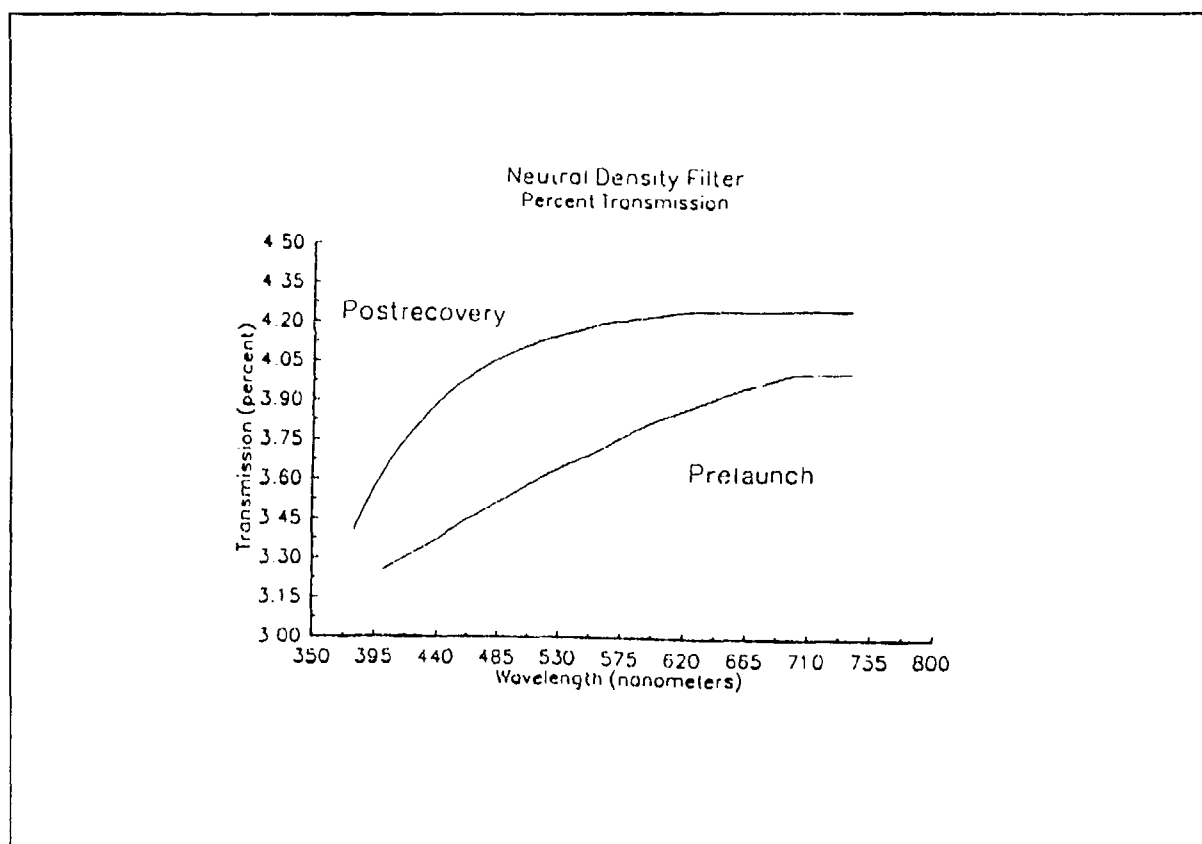


Figure E.72. Pre-Launch and Post-Recovery Transmission of Exposed Corion Neutral Density Filter #6

---

REFERENCE:	M.D. Blue, GTRI, Investigation of the Effects of LDEF on Active Optical System Components, Final Report
EXPERIMENT:	S0050-2
COMMENTS:	Increase in transmittance.

---



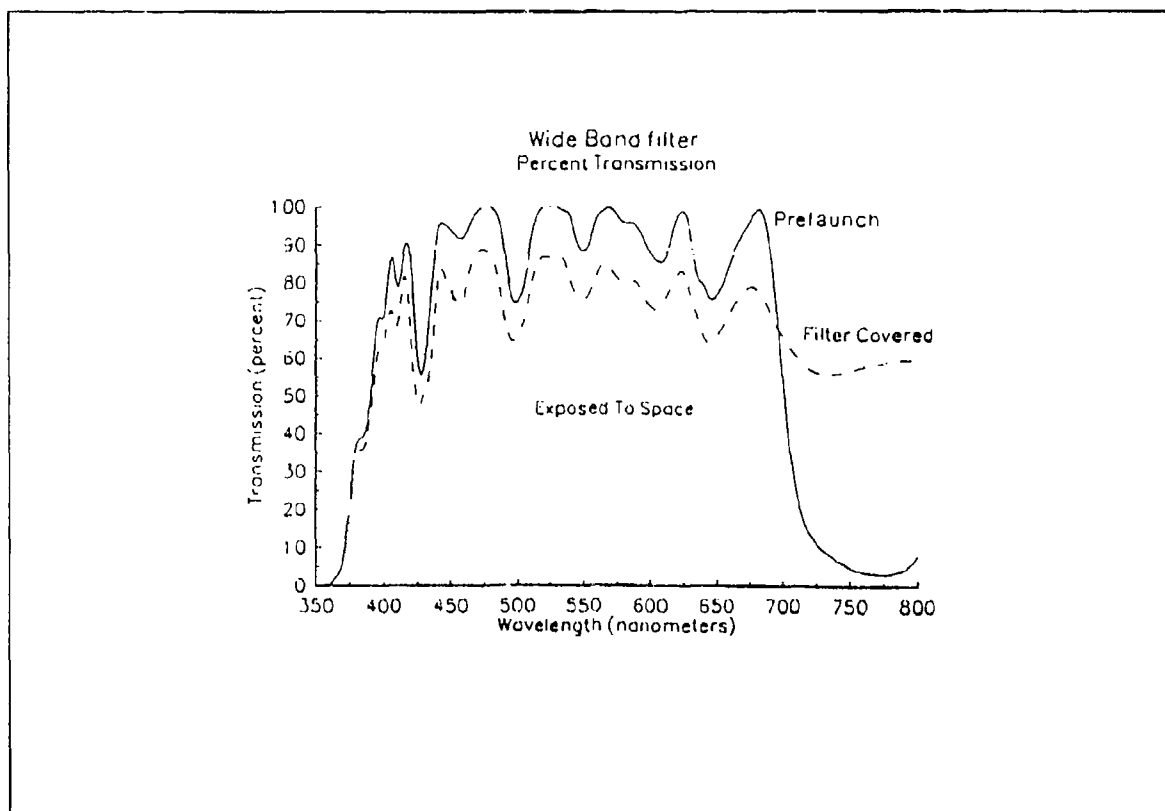


Figure E.73. Pre-Launch and Post-Recovery Transmission of Wide-Band Corion Filters #8 (Exposed) and #9 (Covered)

REFERENCE:	M.D. Blue, GTRI, Investigation of the Effects of LDEF on Active Optical System Components, Final Report
EXPERIMENT:	S0050-2
COMMENTS:	No shift in filter wavelength characteristics. Transmission and long-wave reflectance degraded.

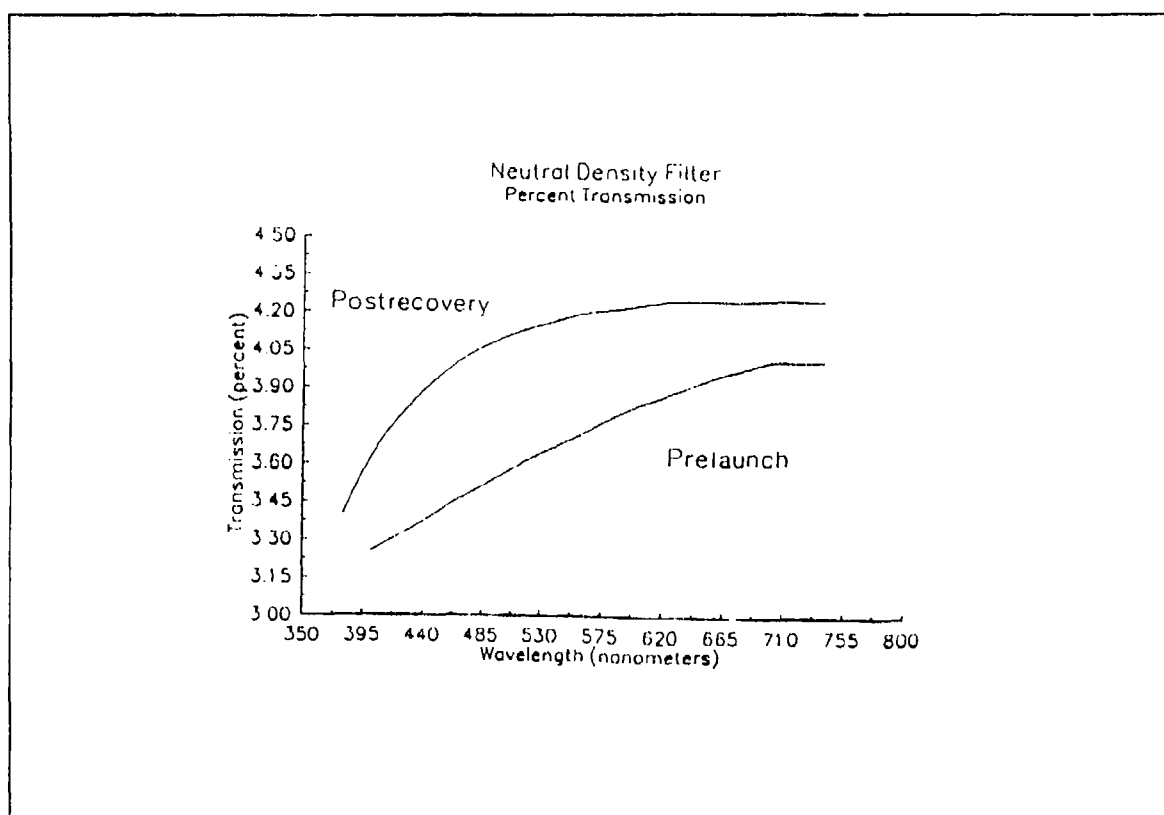


Figure E.72. Pre-Launch and Post-Recovery Transmission of Exposed Corion Neutral Density Filter #6

REFERENCE:	M.D. Blue, GTRI, Investigation of the Effects of LDEF on Active Optical System Components, Final Report
EXPERIMENT:	S0050-2
COMMENTS:	Increase in transmittance.

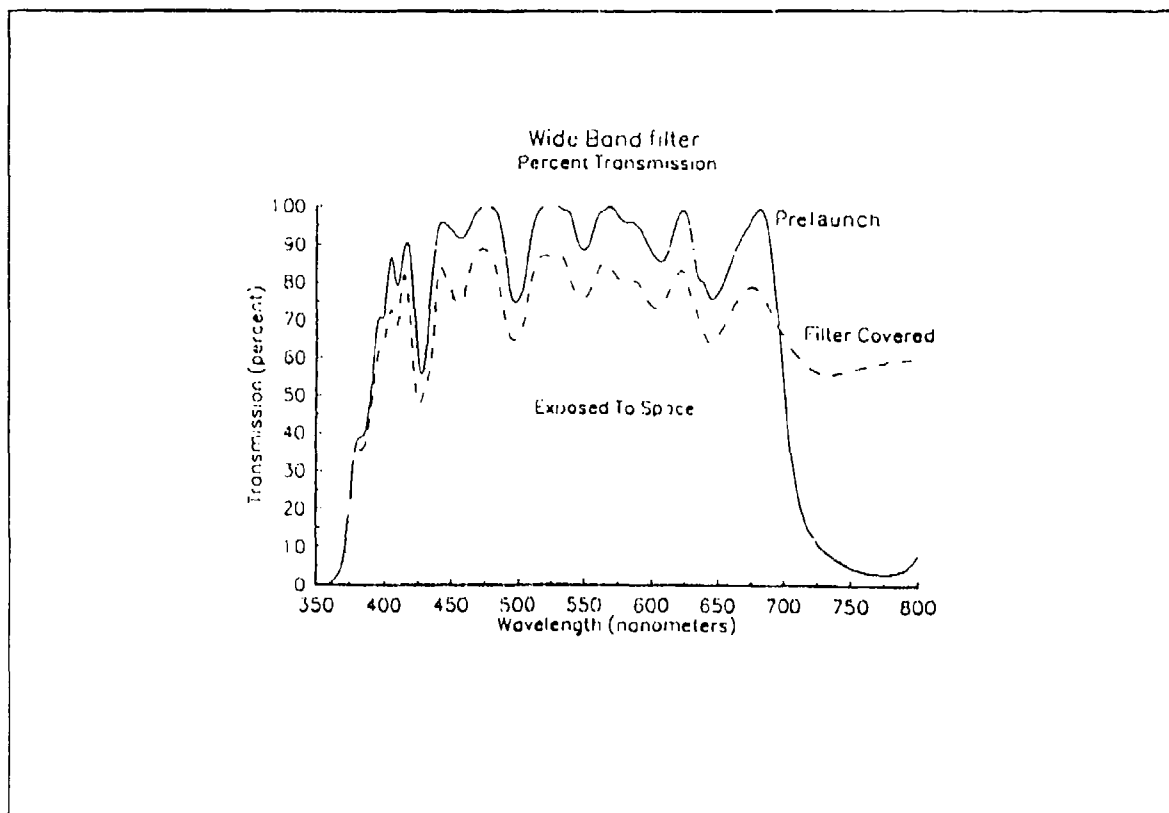


Figure E.73. Pre-Launch and Post-Recovery Transmission of Wide-Band Corion Filters #8 (Exposed) and #9 (Covered)

REFERENCE:	M.D. Blue, GTRI, Investigation of the Effects of LDEF on Active Optical System Components, Final Report
EXPERIMENT:	S0050-2
COMMENTS:	No shift in filter wavelength characteristics. Transmission and long-wave reflectance degraded.

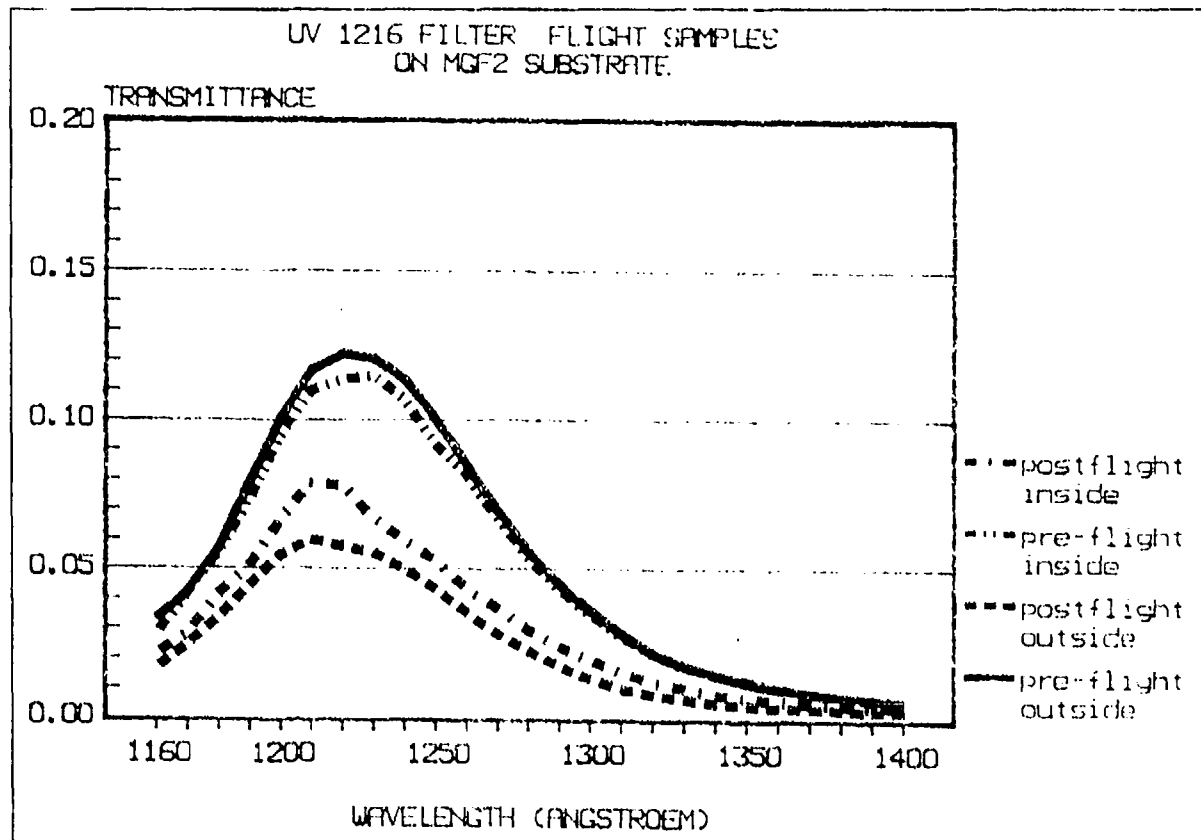


Figure E.74. Pre-Launch and Post-Recovery Transmission of Exposed Al/MgF<sub>2</sub> Optical Filter on MgF<sub>2</sub> Substrate (1216 Å)

REFERENCE:	Charlier, J., Vacuum Deposited Optical Coatings Experiment, LDEF First Post-Retrieval Symposium, Part 3, p. 134
EXPERIMENT:	A0138-4
COMMENTS:	Reduced transmittance, shift in center wavelength.

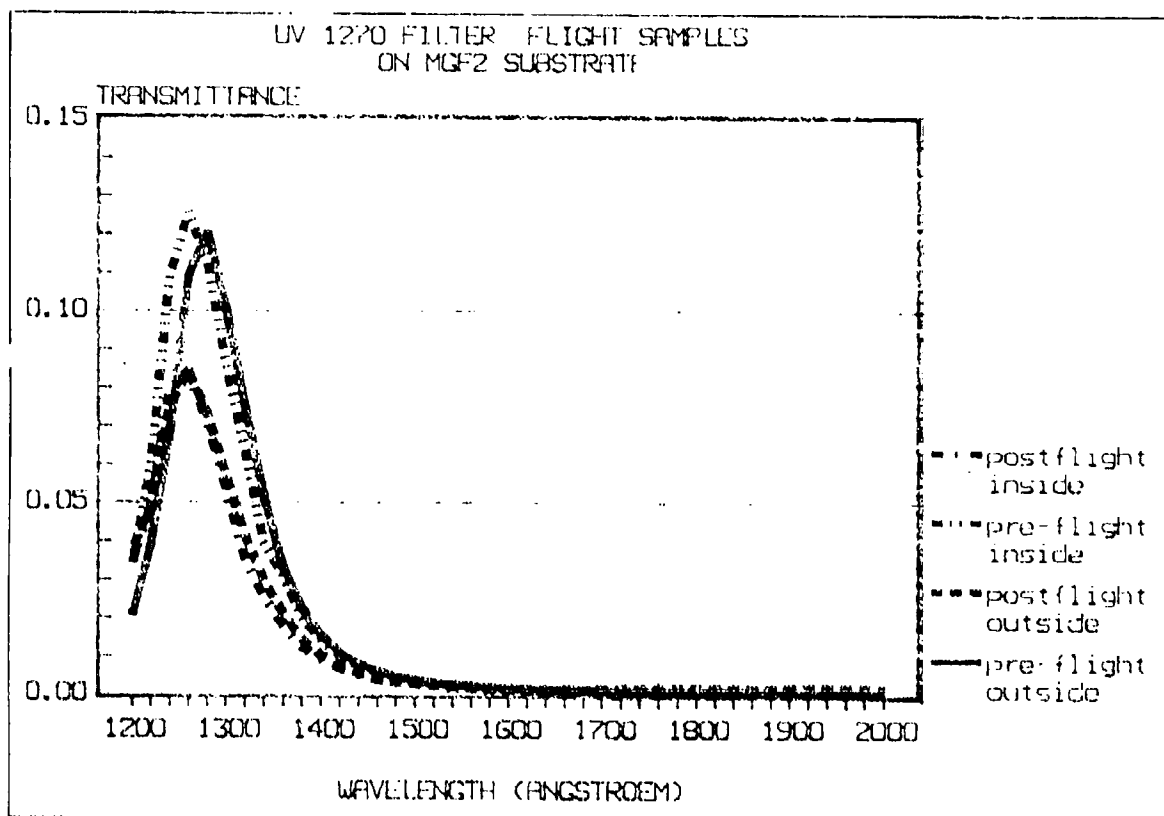


Figure E.75. Pre-Launch and Post-Recovery Transmission of Exposed Al/MgF<sub>2</sub> Optical Filter on MgF<sub>2</sub> Substrate (1270 Å)

REFERENCE:	Charlier, J., Vacuum Deposited Optical Coatings Experiment, LDEF First Post-Retrieval Symposium, Part 3, p. 1343
EXPERIMENT:	A0138-4
COMMENTS:	Reduced transmittance, shift in center wavelength.

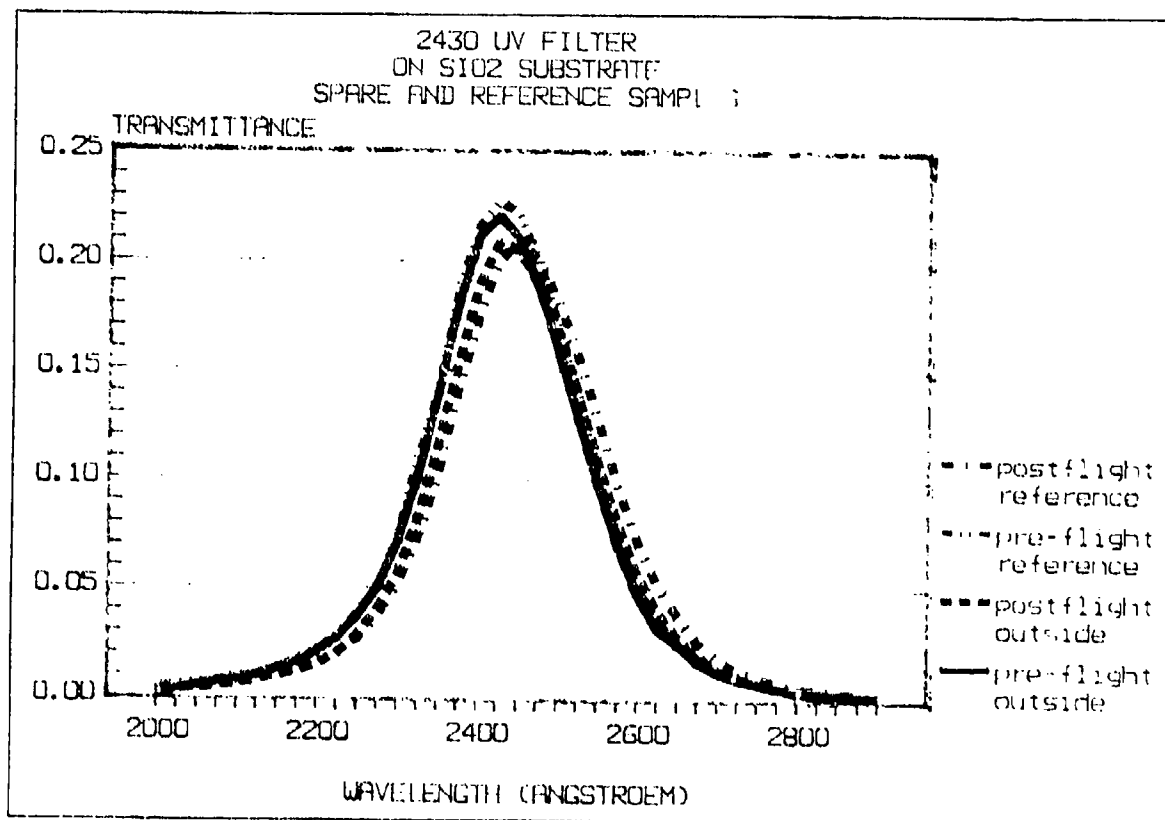


Figure E.76. Pre-Launch and Post-Recovery Transmission of Exposed Al/MgF<sub>2</sub> Optical Filter on Quartz Substrate (2430 Å)

REFERENCE:	Charlier, J., Vacuum Deposited Optical Coatings Experiment, LDEF First Post-Retrieval Symposium, Part 3, p. 1343
EXPERIMENT:	A0138-4
COMMENTS:	Slight reduction in transmittance and shift in center wavelength.

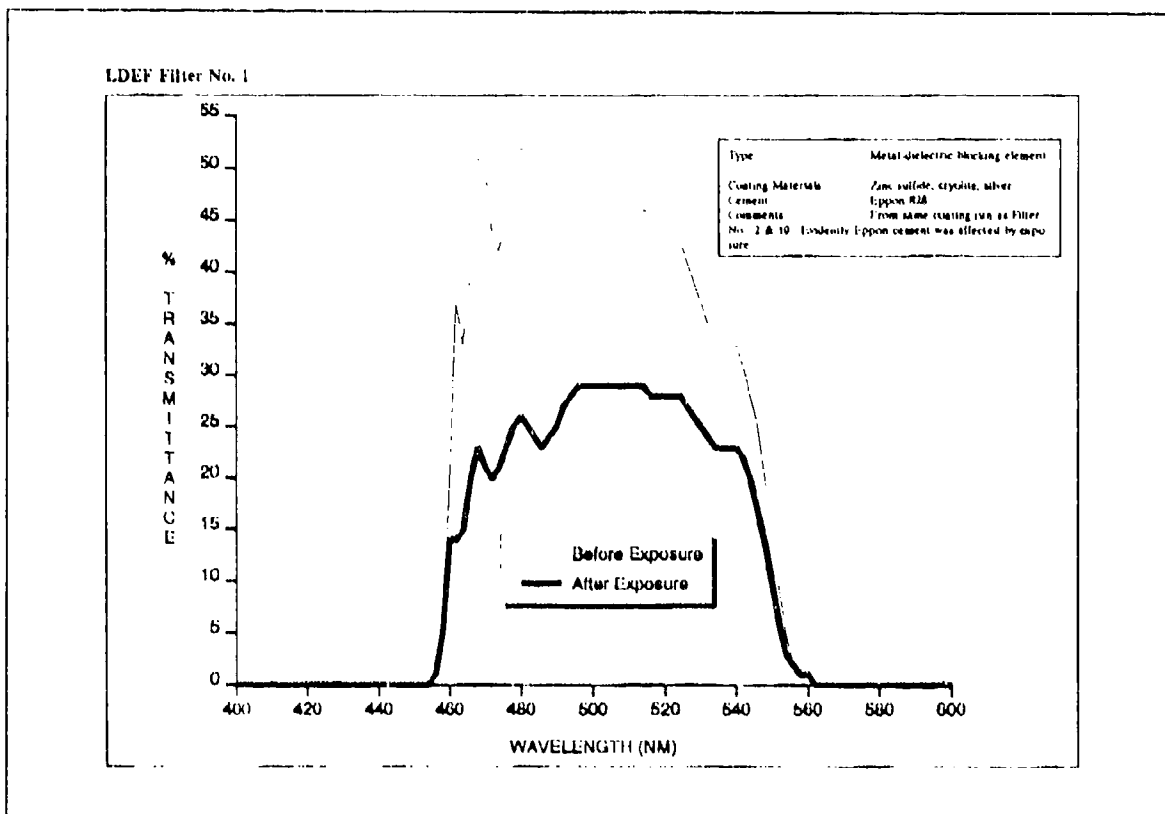


Figure E.77. Pre-Launch and Post-Recovery Transmission of ZnS/Cryolite/Silver on Fused Silica (Cemented With Epon 828)

REFERENCE:	Mooney, T.A., and Smajkiewicz, A., Transmittance Measurements of Ultraviolet and Visible Wavelength Filters Flown Aboard LDEF, LDEF First Post-Retrieval Symposium, Part 3, p. 1511
EXPERIMENT:	AO-147
COMMENTS:	Reduction in transmittance.

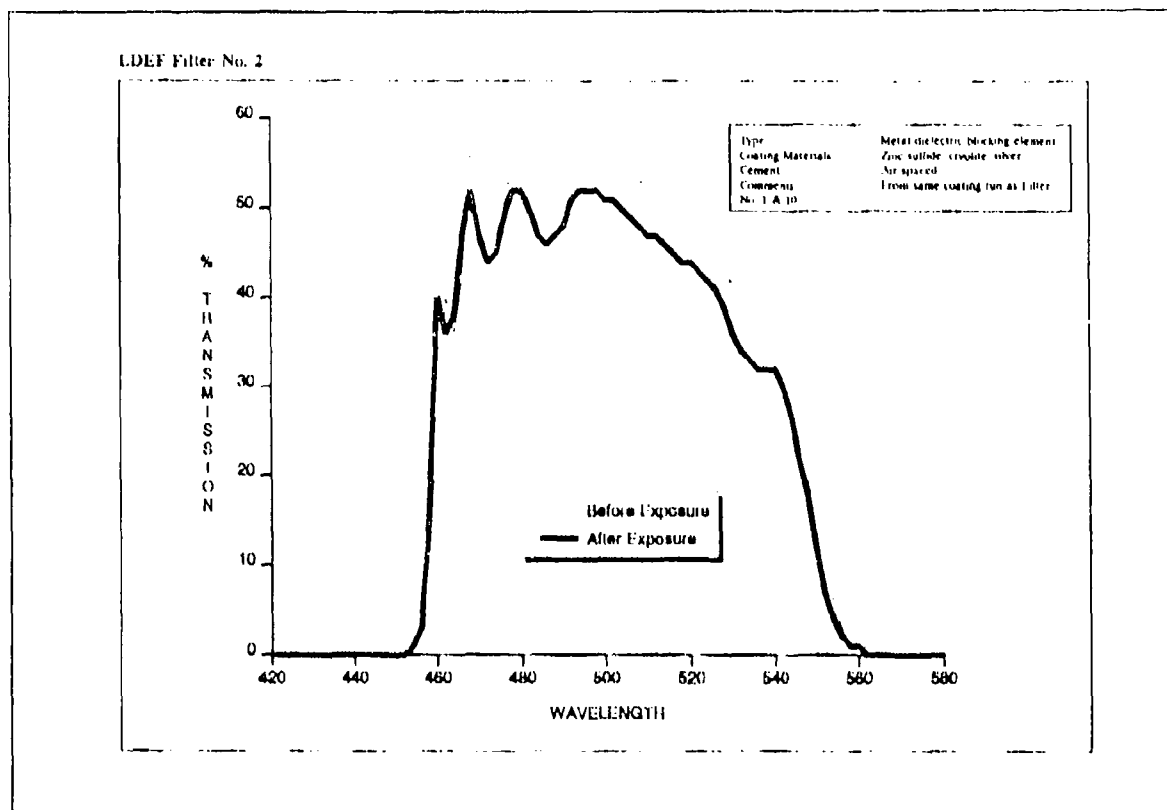


Figure E.78. Pre-Launch and Post-Recovery Transmission of ZnS/Cryolite/Silver on Fused Silica (Air-Spaced, No Cement)

REFERENCE:	Mooney, T.A., and Smajkiewicz, A., Transmittance Measurements of Ultraviolet and Visible Wavelength Filters Flown Aboard LDEF, LDEF First Post-Retrieval Symposium, Part 3, p. 1511
EXPERIMENT:	AO-147
COMMENTS:	Reduction in transmittance and slight shift in center wavelength.



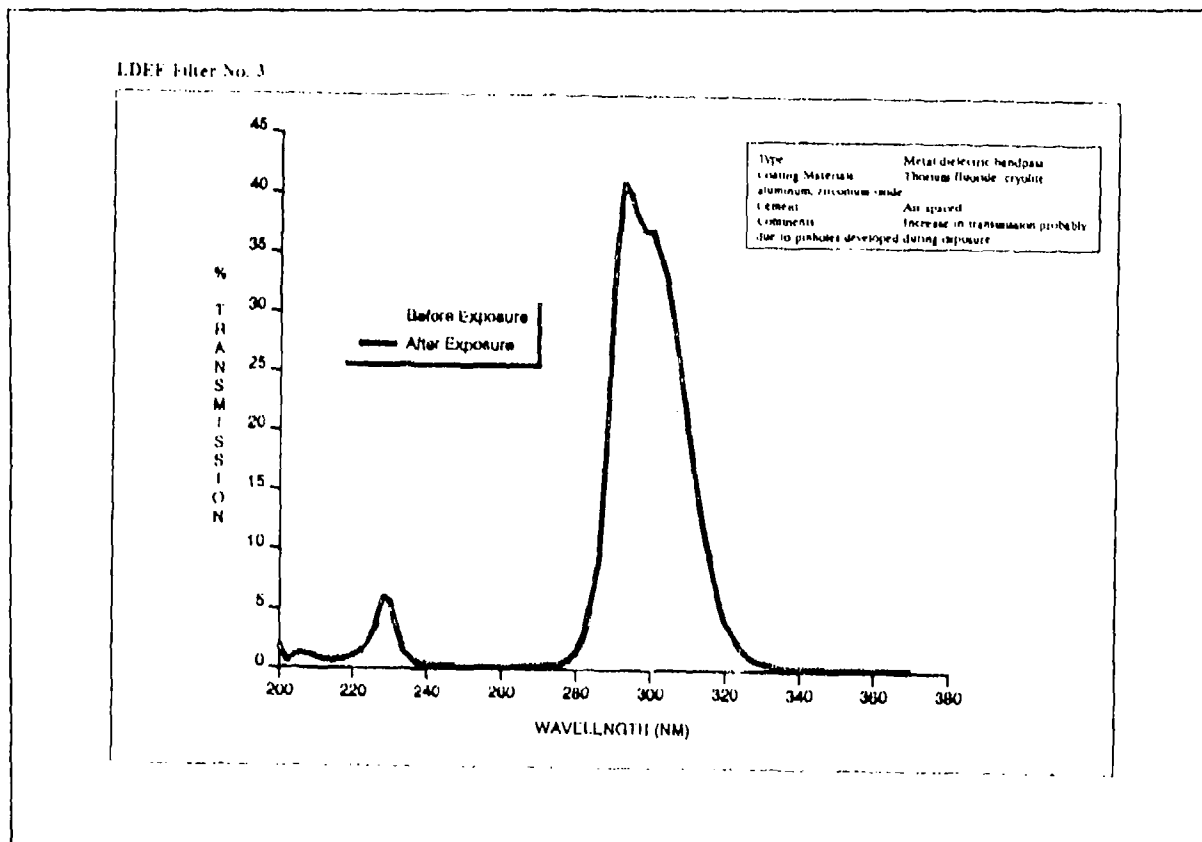


Figure E.79. Pre-Launch and Post-Recovery Transmission of  $\text{ThF}_4/\text{Cryolite}$  on Fused Silica (Air-Spaced, No Cement)

<b>REFERENCE:</b>	Mooney, T.A., and Smajkiewicz, A., Transmittance Measurements of Ultraviolet and Visible Wavelength Filters Flown Aboard LDEF, LDEF First Post-Retrieval Symposium, Part 3, p. 1511
<b>EXPERIMENT:</b>	AO-147
<b>COMMENTS:</b>	Increase in transmittance (due to pinholes in some of the metal-dielectric coatings).

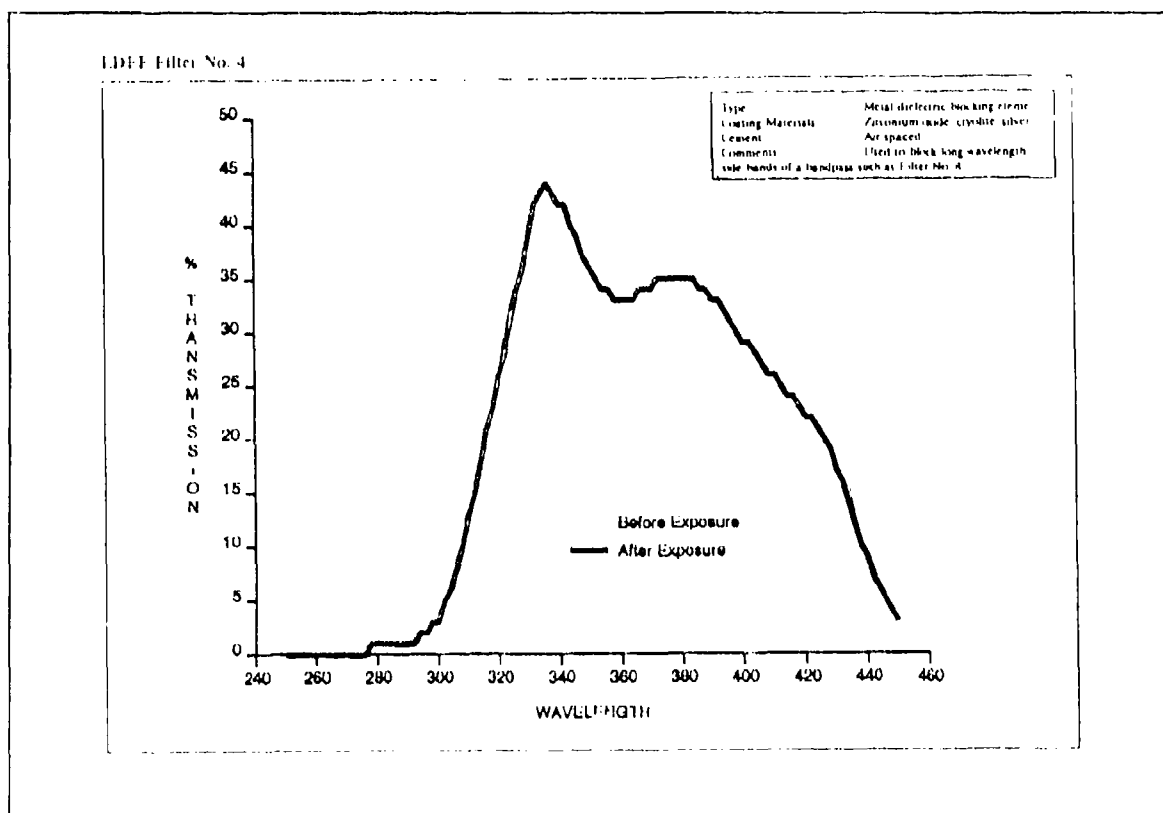


Figure E.80. Pre-Launch and Post-Recovery Transmission of  $ZrO_2$ /Cryolite/Silver on Fused Silica (Air-Spaced, No Cement)

REFERENCE:	Mooney, T.A., and Smajkiewicz, A., Transmittance Measurements of Ultraviolet and Visible Wavelength Filters Flown Aboard LDEF, LDEF First Post-Retrieval Symposium, Part 3, p. 1511
EXPERIMENT:	AO-147
COMMENTS:	Reduced transmittance.

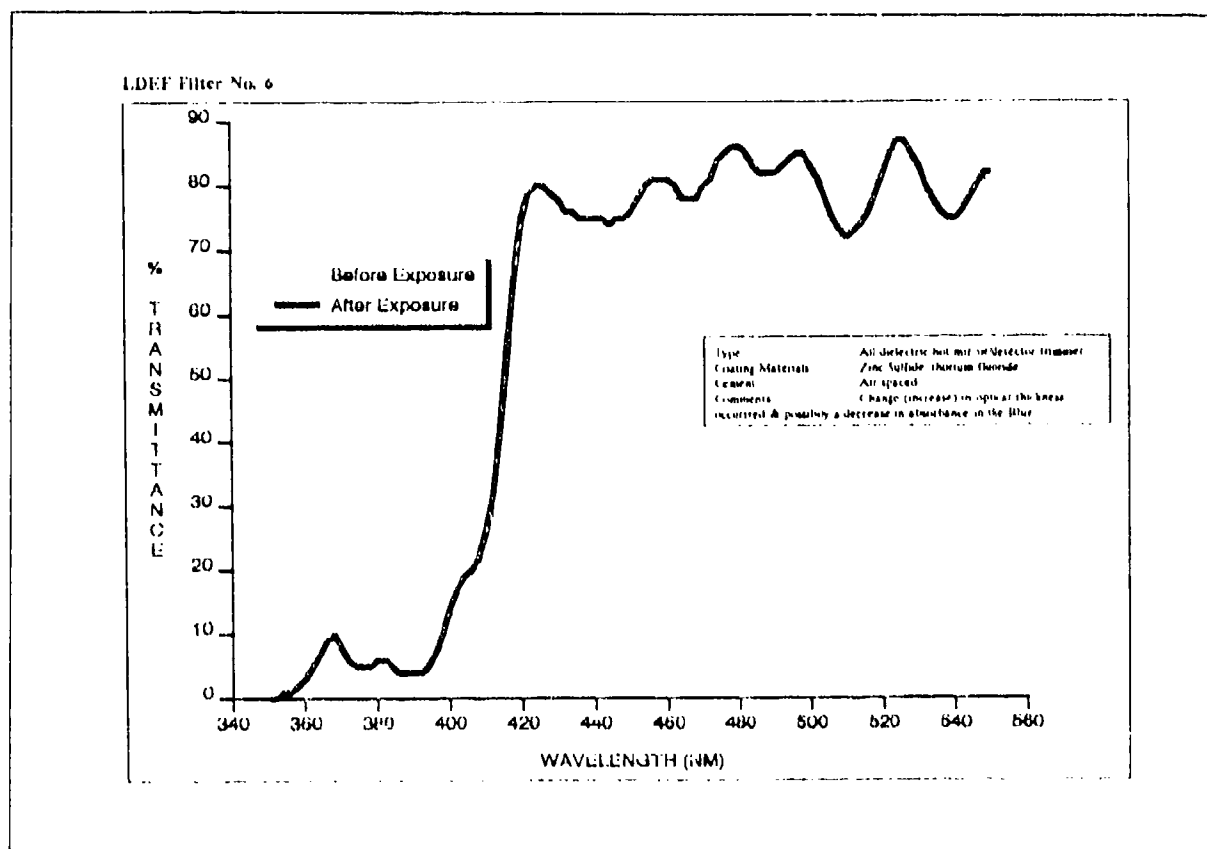


Figure E.81. Pre-Launch and Post-Recovery Transmission of ZnS/TiF<sub>4</sub> on Fused Silica (Air-Spaced, No Cement)

<b>REFERENCE:</b>	Mooney, T.A., and Smajkiewicz, A., Transmittance Measurements of Ultraviolet and Visible Wavelength Filters Flown Aboard LDEF, LDEF First Post-Retrieval Symposium, Part 3, p. 1511
<b>EXPERIMENT:</b>	AO-147
<b>COMMENTS:</b>	Slight decrease in transmittance near center wavelength. Slight increase in transmittance near bluer wavelengths (apparent reduction in extinction coefficient of ZnS).

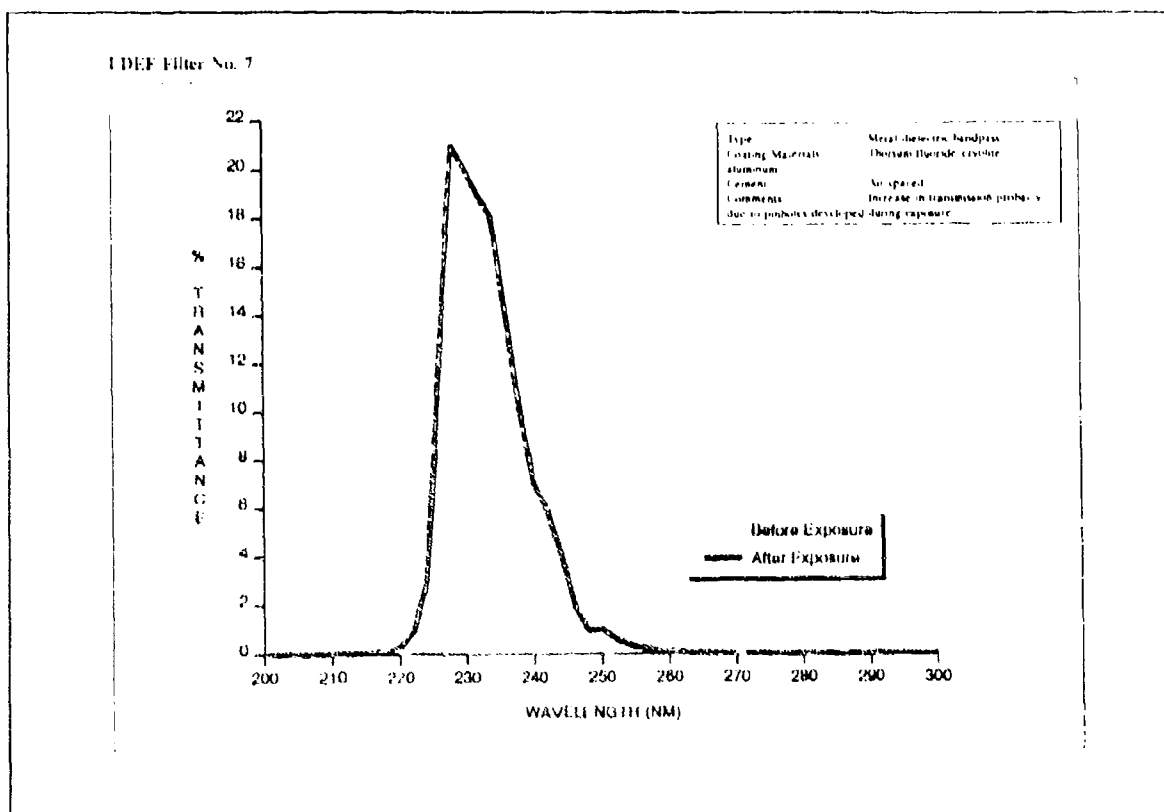


Figure E.82. Pre-Launch and Post-Recovery Transmission of ThF<sub>4</sub>/Cryolite on Fused Silica (Air-Spaced, No Cement)

REFERENCE:	Mooney, T.A., and Smajkiewicz, A., Transmittance Measurements of Ultraviolet and Visible Wavelength Filters Flown Aboard LDEF, LDEF First Post-Retrieval Symposium, Part 3, p. 1511
EXPERIMENT:	AO-147
COMMENTS:	Increase in transmittance (due to pinholes in some of the metal-dielectric coatings).

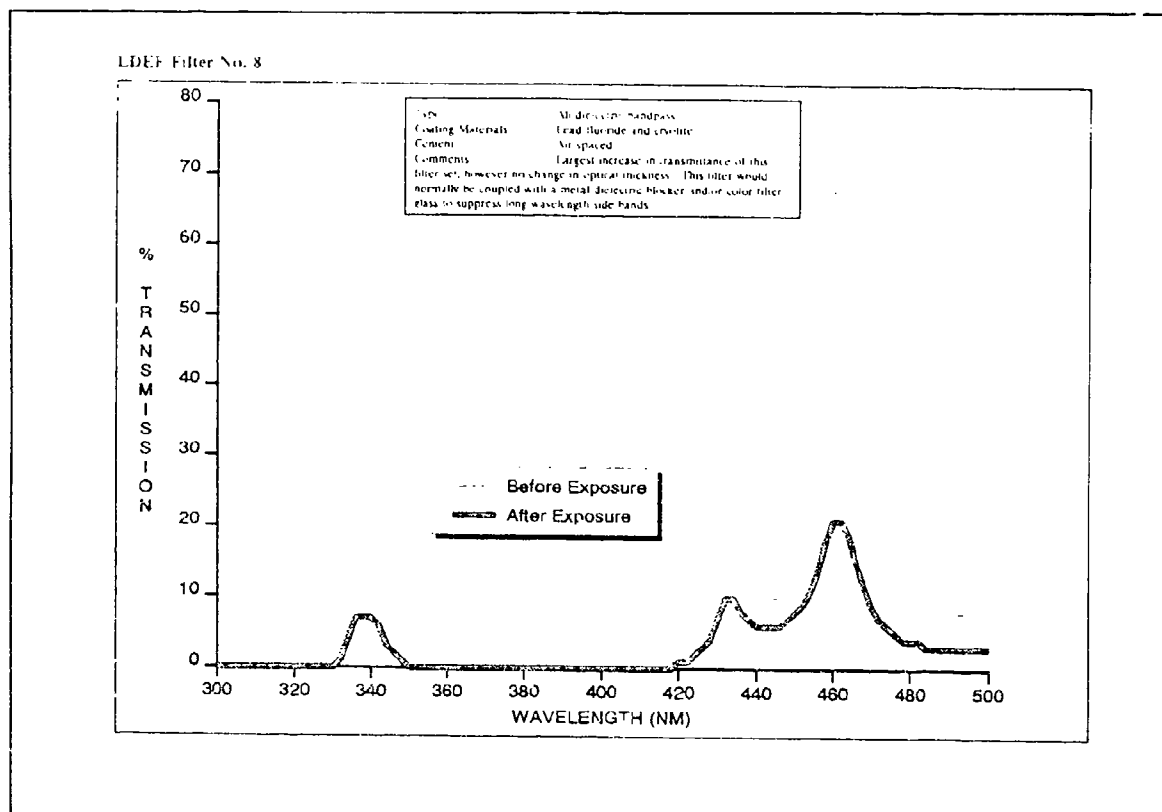


Figure E.83. Pre-Launch and Post-Recovery Transmission of  $\text{PbF}_2/\text{Cryolite}$  on Fused Silica (Air-Spaced, No Cement)

<b>REFERENCE:</b>	Mooney, T.A., and Smajkiewicz, A., Transmittance Measurements of Ultraviolet and Visible Wavelength Filters Flown Aboard LDEF, LDEF First Post-Retrieval Symposium, Part 3, p. 1511
<b>EXPERIMENT:</b>	AO-147
<b>COMMENTS:</b>	Reduced transmittance (due to increased absorption in the lead compound).

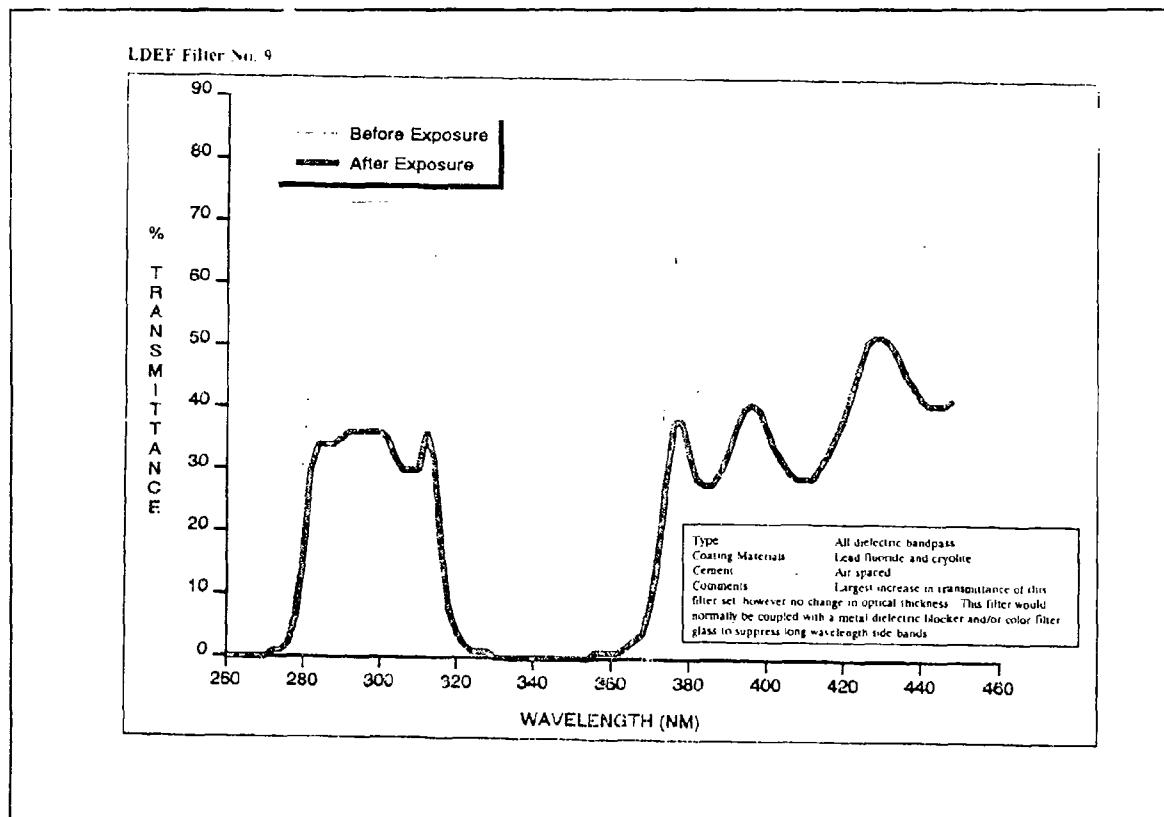


Figure E.84. Pre-Launch and Post-Recovery Transmission of  $PbF_2$ /Cryolite on Fused Silica (Air-Spaced, No Cement)

<b>REFERENCE:</b>	Mooney, T.A., and Smajkiewicz, A., Transmittance Measurements of Ultraviolet and Visible Wavelength Filters Flown Aboard LDEF, LDEF First Post-Retrieval Symposium, Part 3, p. 1511
<b>EXPERIMENT:</b>	AO-147
<b>COMMENTS:</b>	Reduced transmittance (due to increased absorption in the lead compound).

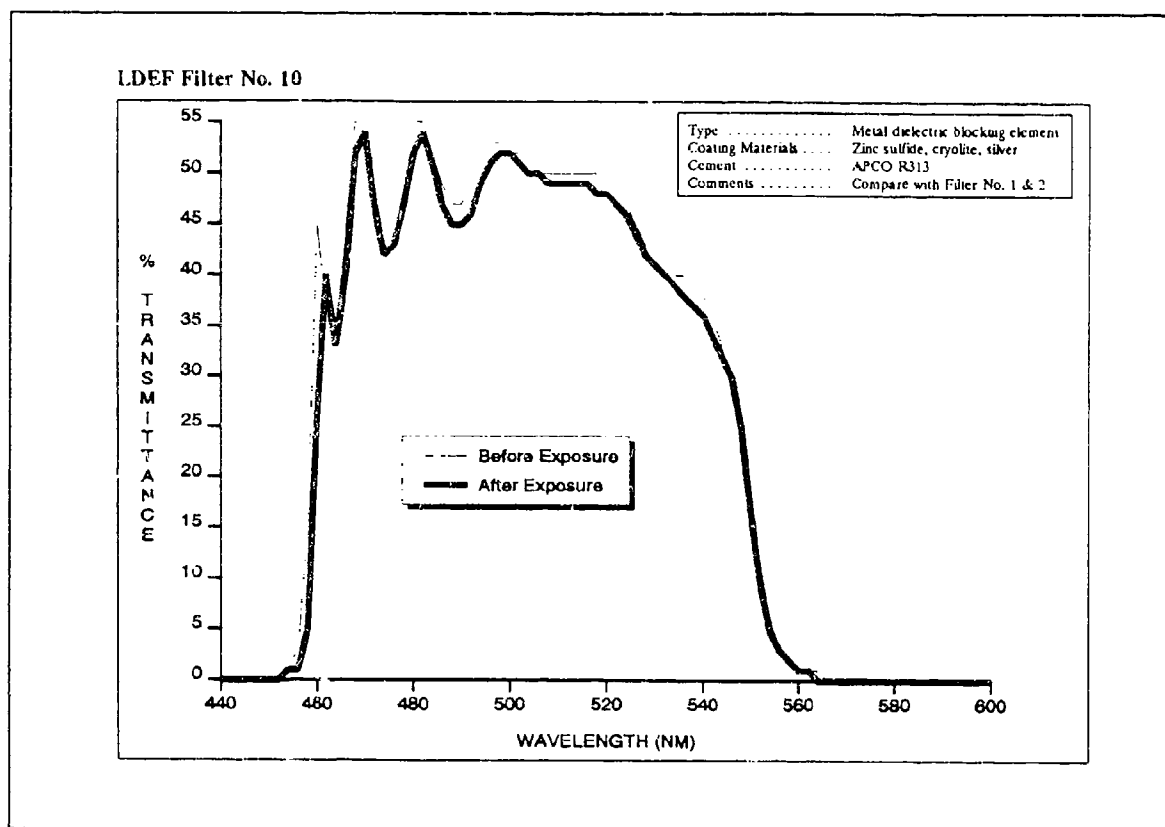


Figure E.85. Pre-Launch and Post-Recovery Transmission of ZnS/Cryolite/Silver on Fused Silica (Cemented With APCO R313)

REFERENCE:	Mooney, T.A., and Smajkiewicz, A., Transmittance Measurements of Ultraviolet and Visible Wavelength Filters Flown Aboard LDEF, LDEF First Post-Retrieval Symposium, Part 3, p. 1511
EXPERIMENT:	AO-147
COMMENTS:	Slight reduction in transmittance.

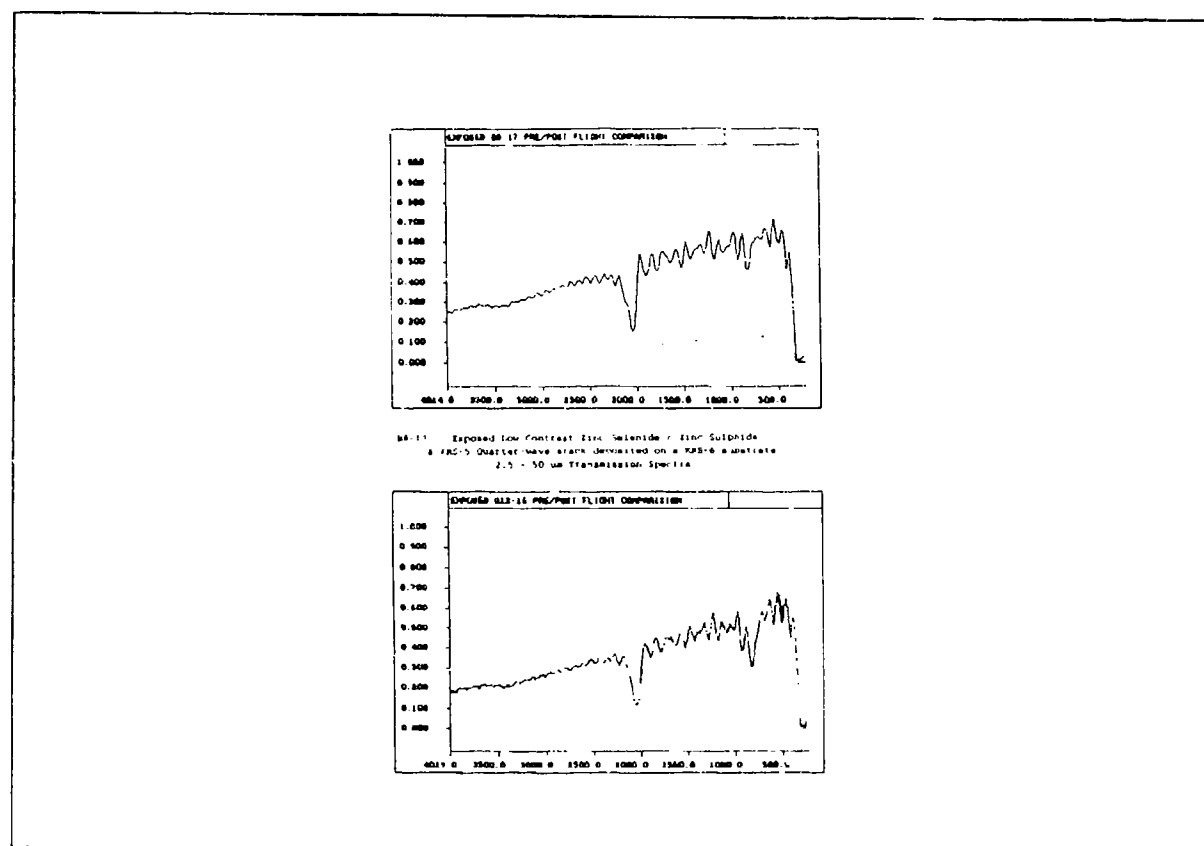
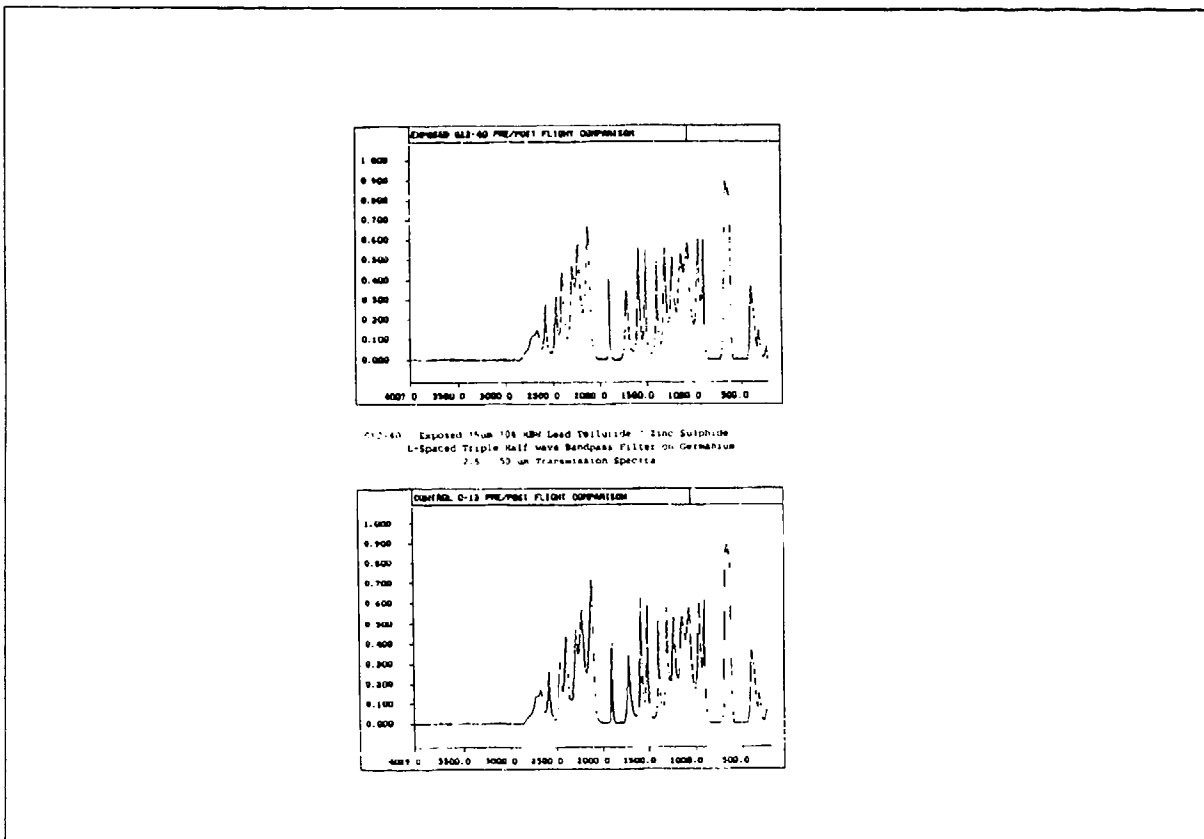


Figure E.86. Pre-Launch and Post-Recovery Transmission of Low Index Ratio Quarter-Wave Blocking ZnSe/ZnS/KRS-5 on KRS-6 Substrate

<b>REFERENCE:</b>	Hawkins, G.J., Seeley, John S., Hunneman, R., Exposure to Space Radiation of High-Performance Infrared Multilayer Filters and Materials Technology Experiment, LDEF First Post-Retrieval Symposium, p. 1477
<b>EXPERIMENT:</b>	A0056
<b>COMMENTS:</b>	Reduced transmission.





**Figure E.87. Pre-Launch and Post-Recovery Transmission of PbTe/ZnS on Ge Substrate  
15 $\mu$ m 10% HBW L-Space THW Band-Pass Filter**

---

<b>REFERENCE:</b>	Hawkins, G.J., Seeley, John S., Hunneman, R., Exposure to Space Radiation of High-Performance Infrared Multilayer Filters and Materials Technology Experiment, LDEF First Post-Retrieval Symposium, p. 1477
<b>EXPERIMENT:</b>	A0056
<b>COMMENTS:</b>	No significant changes in transmission or spectral position.

---

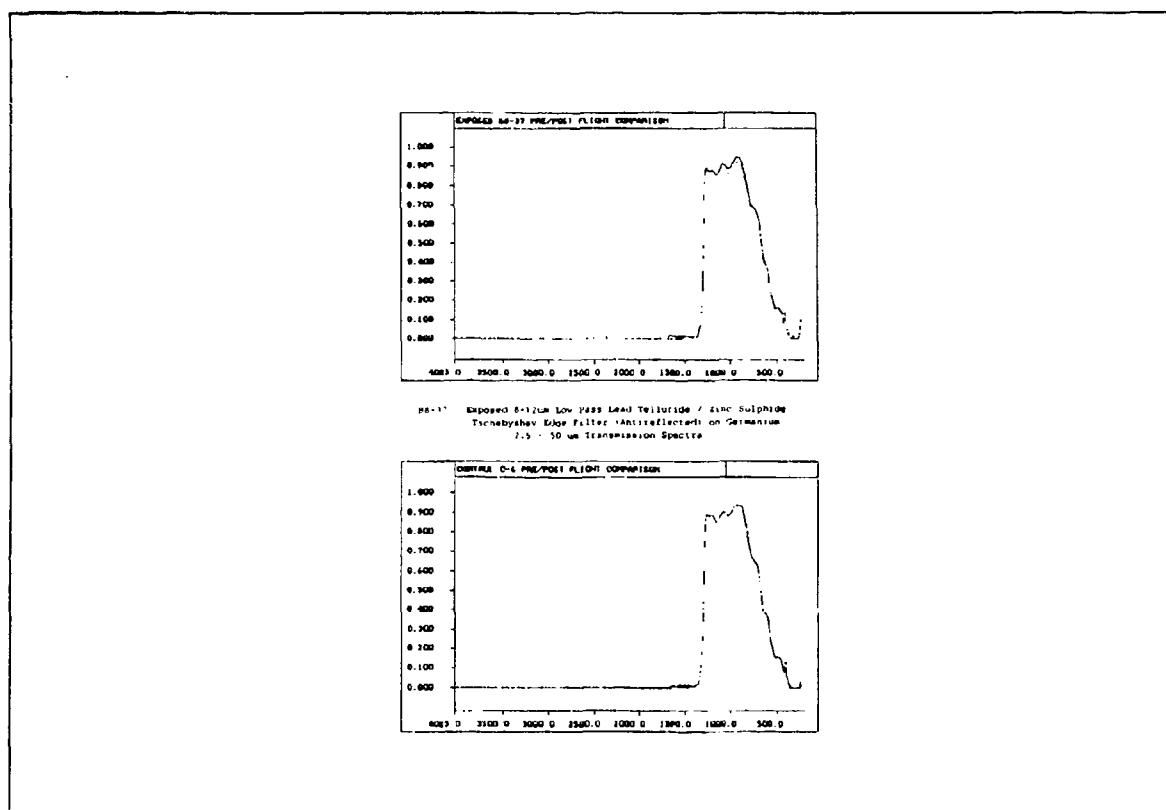


Figure E.88. Pre-Launch and Post-Recovery Transmission of PbTe/ZnS 8-12  $\mu$ m Tschebyshev Edge Band-Pass Filter (Antireflected) on Ge Substrate

<b>REFERENCE:</b>	Hawkins, G.J., Seeley, John S., Hunneman, R., Exposure to Space Radiation of High-Performance Infrared Multilayer Filters and Materials Technology Experiment, LDEF First Post-Retrieval Symposium, p. 1477
<b>EXPERIMENT:</b>	A0056
<b>COMMENTS:</b>	No significant changes in transmission or spectral position.

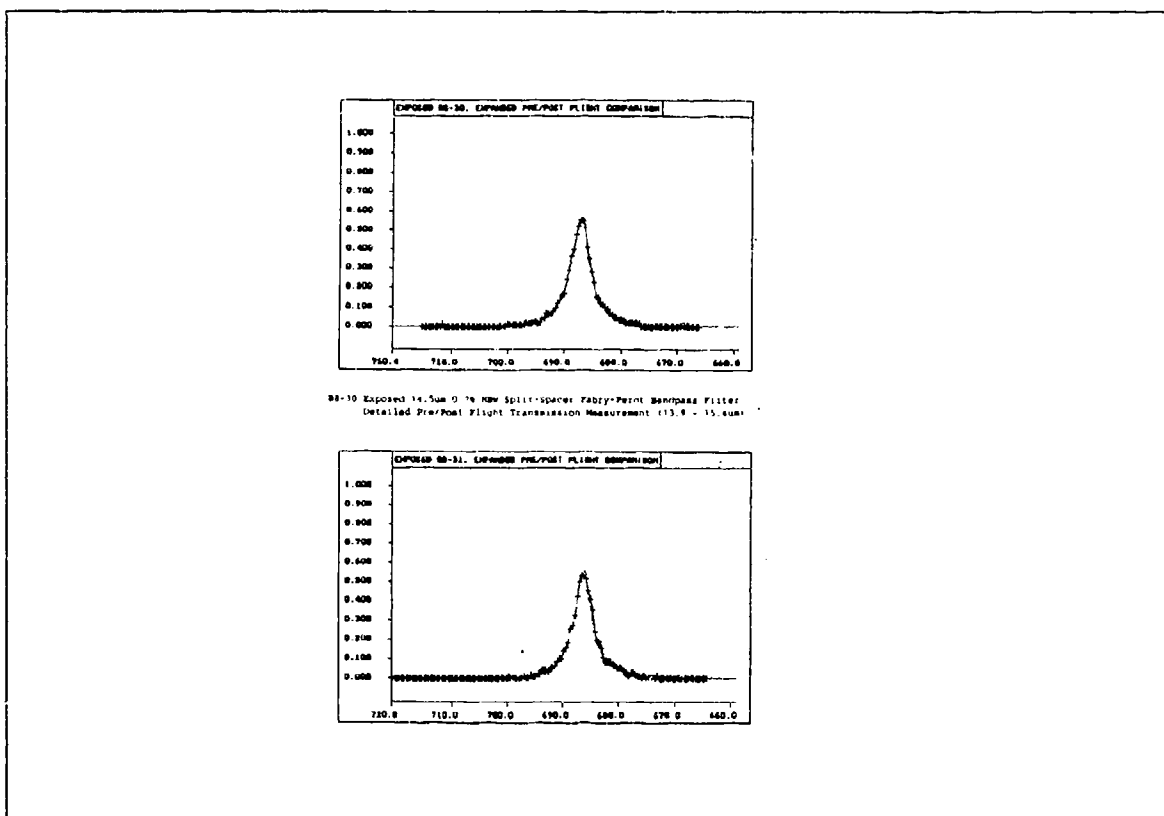


Figure E.89. Pre-Launch and Post-Recovery Transmission of PbTe/ZnS on Ge Substrate  
14.5 $\mu$ m 0.7% HBW Split-Spacer Fabry-Perot Band-Pass Filter

<b>REFERENCE:</b>	Hawkins, GJ Seeley, John S., Hunneman, R., Exposure to Space Radiation of High-Performance Infrared Multilayer Filters and Materials Technology Experiment, LDEF First Post-Retrieval Symposium, p. 1477
<b>EXPERIMENT:</b>	A0056
<b>COMMENTS:</b>	No significant changes in transmission or spectral position.

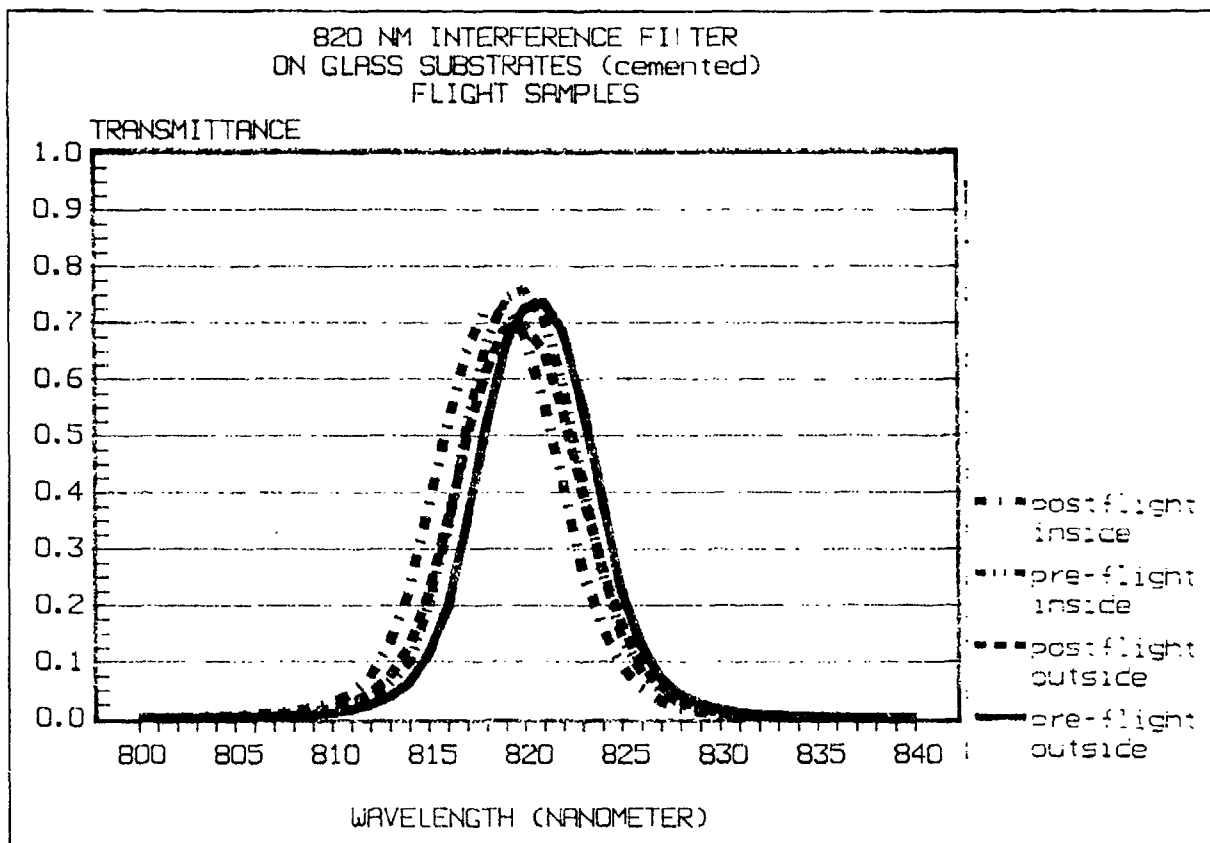


Figure E.90. Pre-Launch and Post-Recovery Transmission of ZnS/Chiolite on BK7G18 and RG780 Glasses (820 nm Interference Filter)

REFERENCE:	Charlier, J., Vacuum Deposited Optical Coatings Experiment, LDEF First Post-Retrieval Symposium, Part 3, p. 1343
EXPERIMENT:	A0138-4
COMMENTS:	Slight reduction in transmission and slight shift of center wavelength to blue.

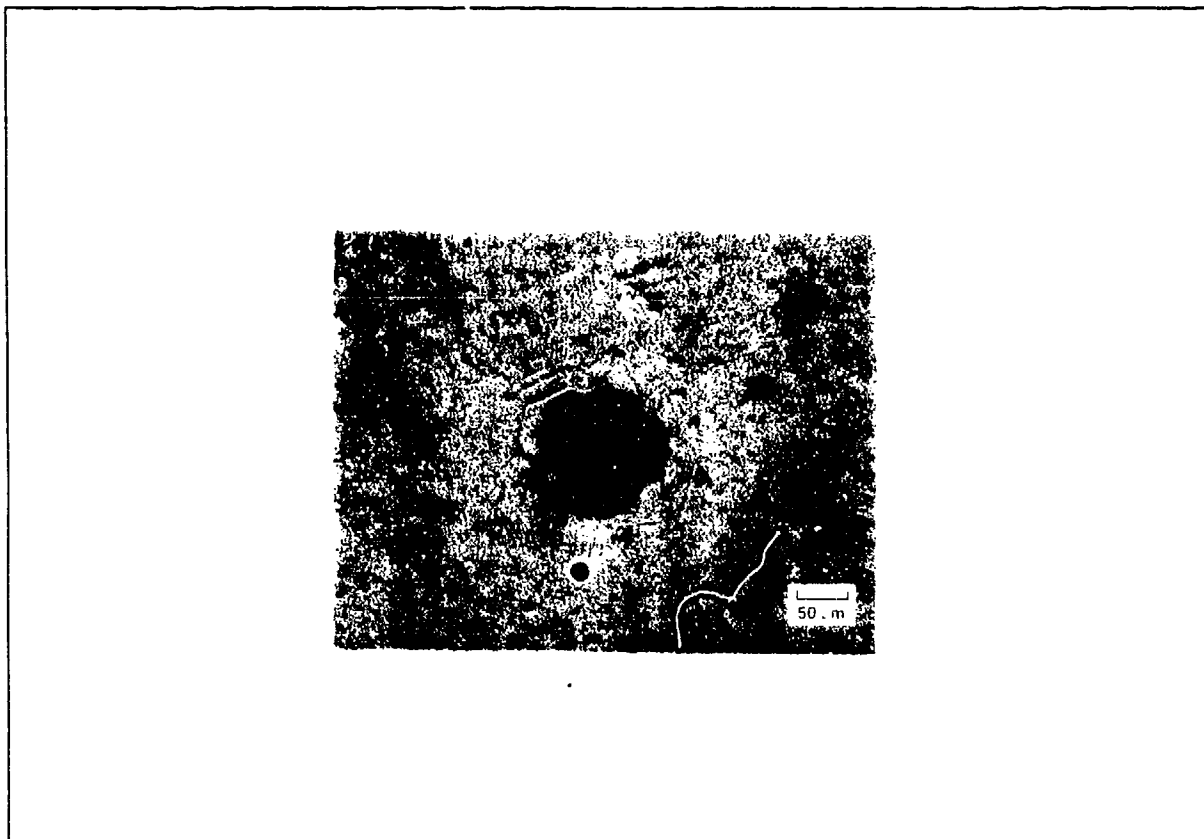


Figure E.91. Impact Effects in Copper Mirrors

---

<b>REFERENCE:</b>	Gyetvay, S., et al., <u>Aerospace Corporation LDEF M0003 Sample Observation Data Base</u> , 1993.
<b>EXPERIMENT:</b>	M0003-2
<b>COMMENTS:</b>	No damage to the substrate beyond area of impact.

---

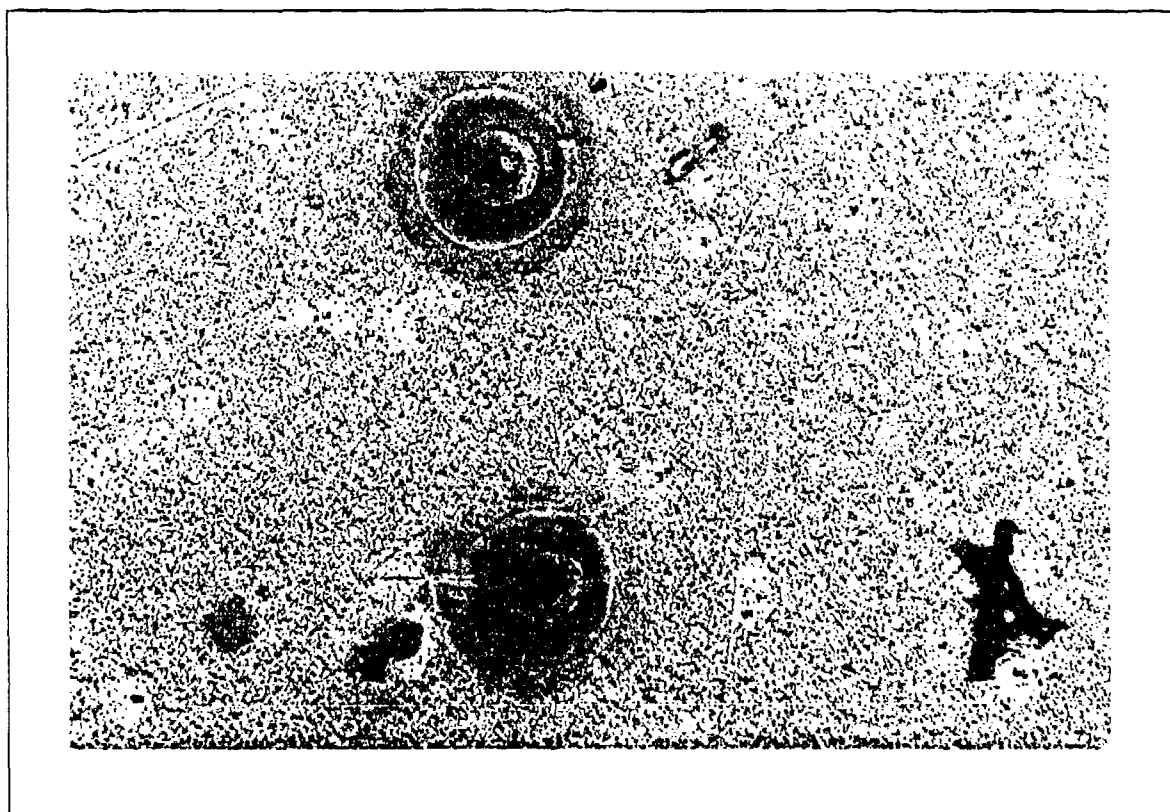
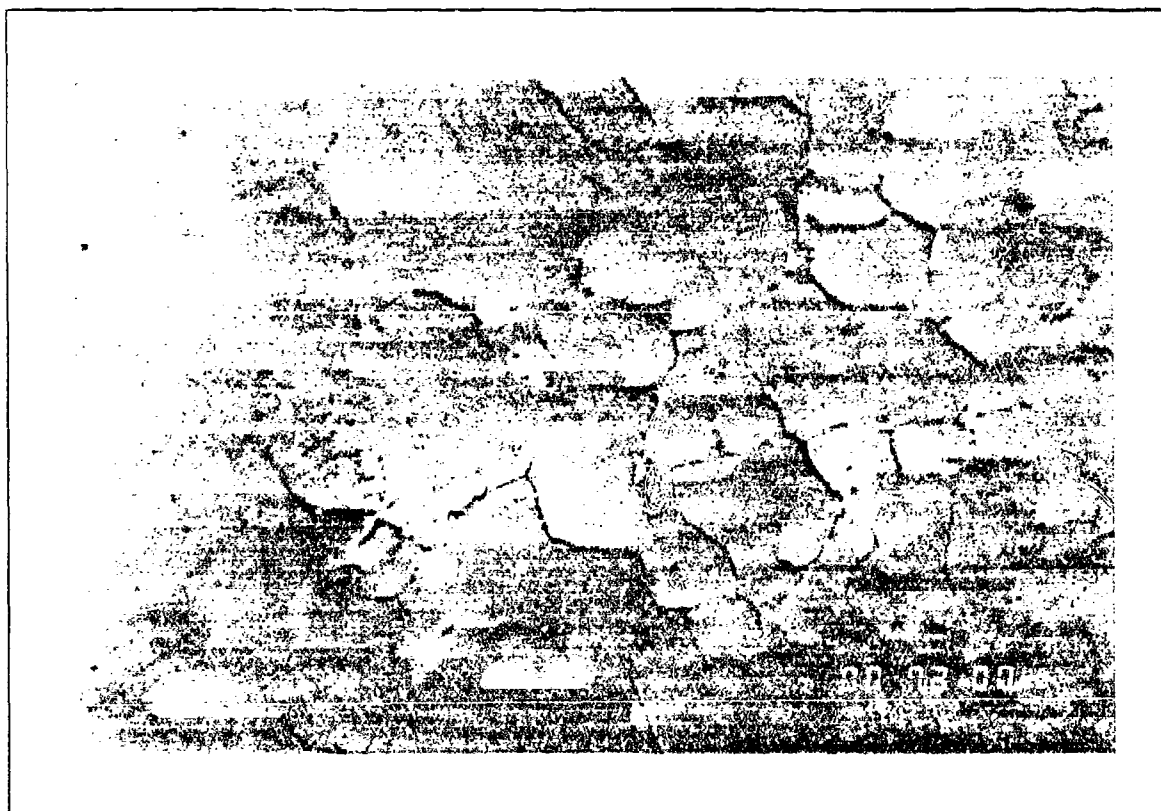


Figure E.92. Hazed And Corroded Surface of Low Scatter Ni Mirror

---

REFERENCE:	Gyetvay, S., et al., <u>Aerospace Corporation LDEF M0003 Sample Observation Data Base</u> , 1993, Record #58
EXPERIMENT:	M0003-11
COMMENTS:	Many spots of corrosion on the surface are surrounded by zones of discolored material.

---



**Figure E.93. Corrosion-Decorated Grain Boundaries in Surface of Diamond-Turned Copper Substrate**

---

<b>REFERENCE:</b>	Gyetvay, S., et al., <u>Aerospace Corporation LDEF M0003 Sample Observation Data Base</u> , 1993, Record #1135
<b>EXPERIMENT:</b>	M0003-2
<b>COMMENTS:</b>	Sample appears hazy when viewed at a glancing angle. There are many spots of corrosion, especially where extraneous matter had contacted the surface. Grain boundaries are apparent in the copper surface; in some areas, these appear decorated with residue. There are two rectangular patches apparent on the surface where something was placed on the surface preflight. The residue from a preflight fingerprint is near the sample center. Discolored residue is present near the perimeter of the sample where TFE tape, used as a liner around the sample, protruded onto the surface.

---

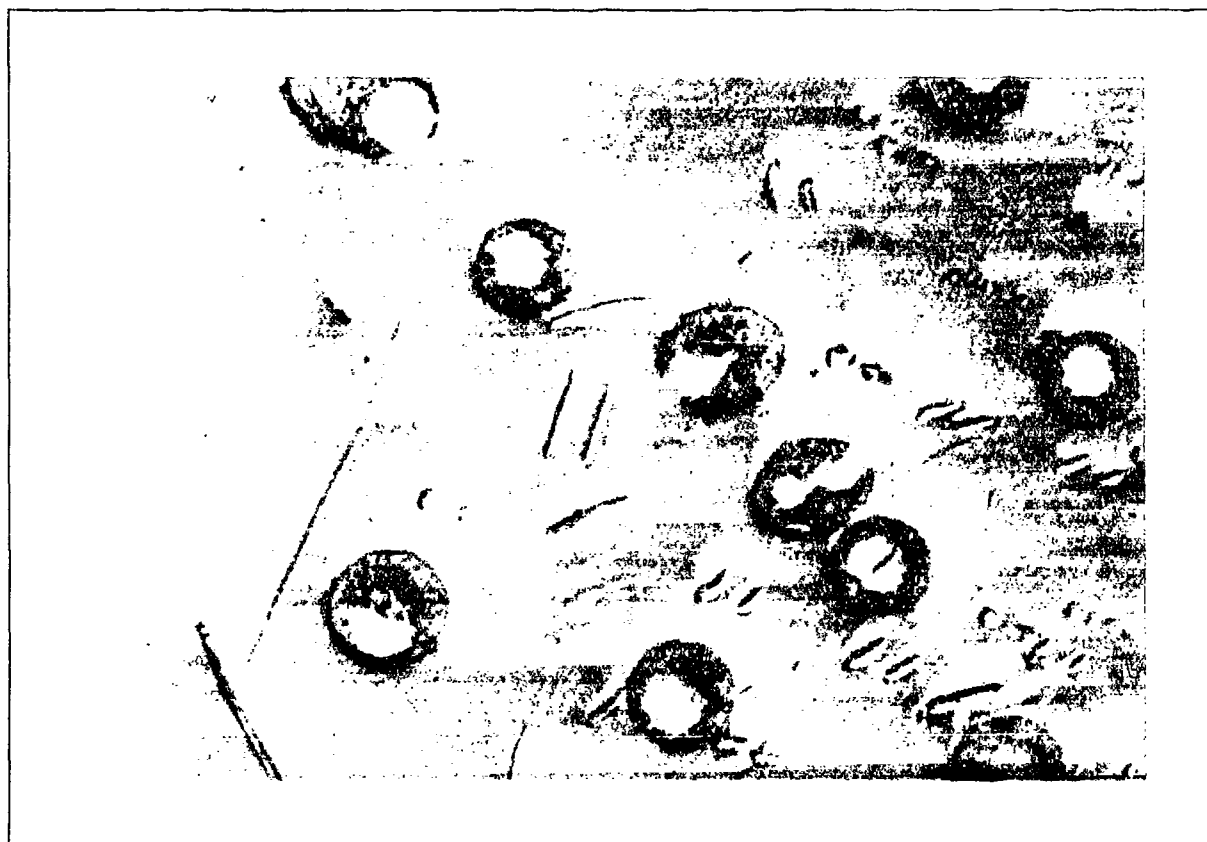


**Figure E.94. High Magnification View of Corrosion Spots on Surface of Diamond Turned Copper Substrate**

---

<b>REFERENCE:</b>	Gyetvay, S., et al., <u>Aerospace Corporation LDEF M0003 Sample Observation Data Base</u> , 1993, Record #1136
<b>EXPERIMENT:</b>	M0003-2
<b>COMMENTS:</b>	Sample appears hazy when viewed at a glancing angle. There is a great deal of extraneous debris on the surface, largely consisting of metallic film flakes. The exposed surface appears darker when viewed at normal incidence, particularly around the perimeter on the spaceward side.

---



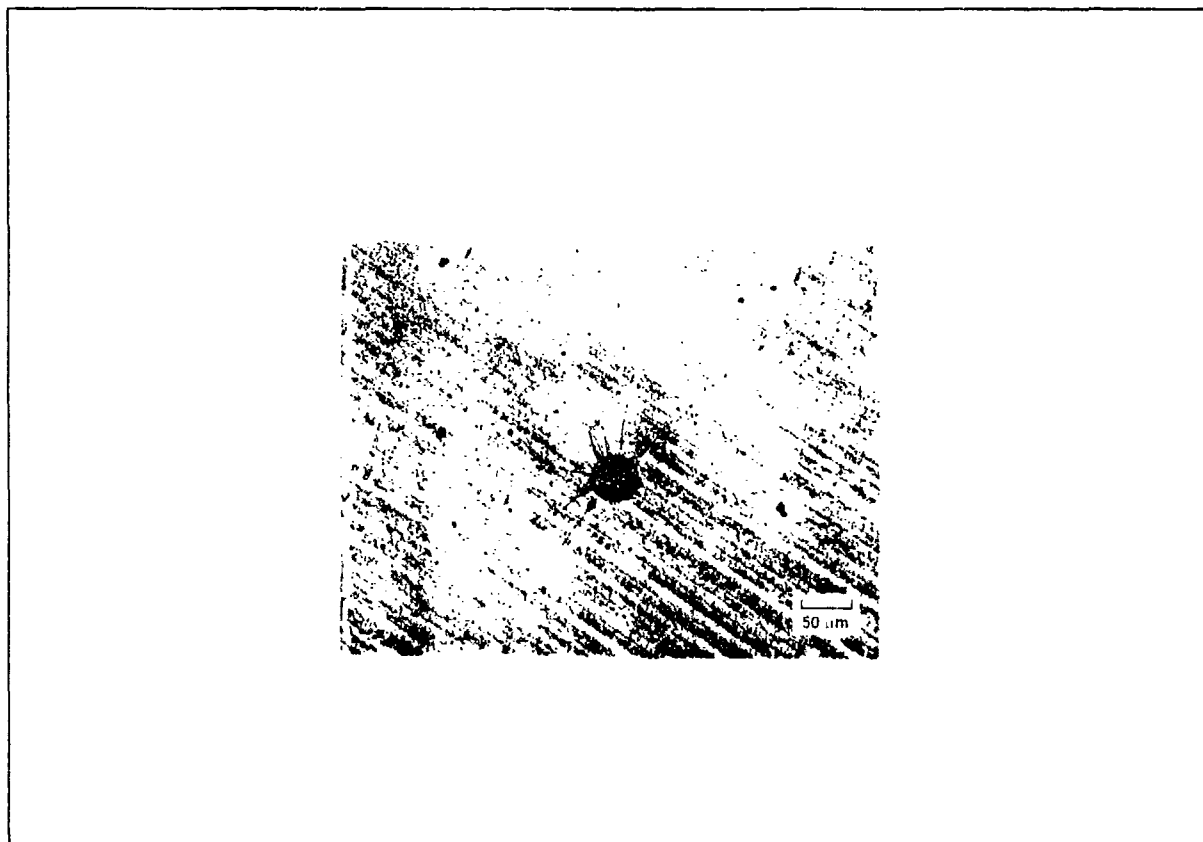


**Figure E.95. Impact Effects in Nickel-Copper Mirrors**

---

<b>REFERENCE:</b>	Gyetvay, S., et al., <u>Aerospace Corporation LDEF M0003 Sample Observation Data Base</u> , 1993.
<b>EXPERIMENT:</b>	M0003-2
<b>COMMENTS:</b>	Splatters of resolidified matter surrounding the craters. Damage is similar to that seen in uncoated copper.

---



**Figure E.96. Effect of a Micrometeoroid on Debris Impact on a Quartz-Silver  
Second Surface Mirror**

---

<b>REFERENCE:</b>	Mason, J.B., Dursch, H., Edelman, J., Overview of the Systems Special Investigation Group Investigation, LDEF Second Post-Retrieval Symposium, p. 1257
<b>EXPERIMENT:</b>	A0038
<b>COMMENTS:</b>	Micrometeoroid impact caused crater with several large conchoidal areas adjacent to impact site.

---

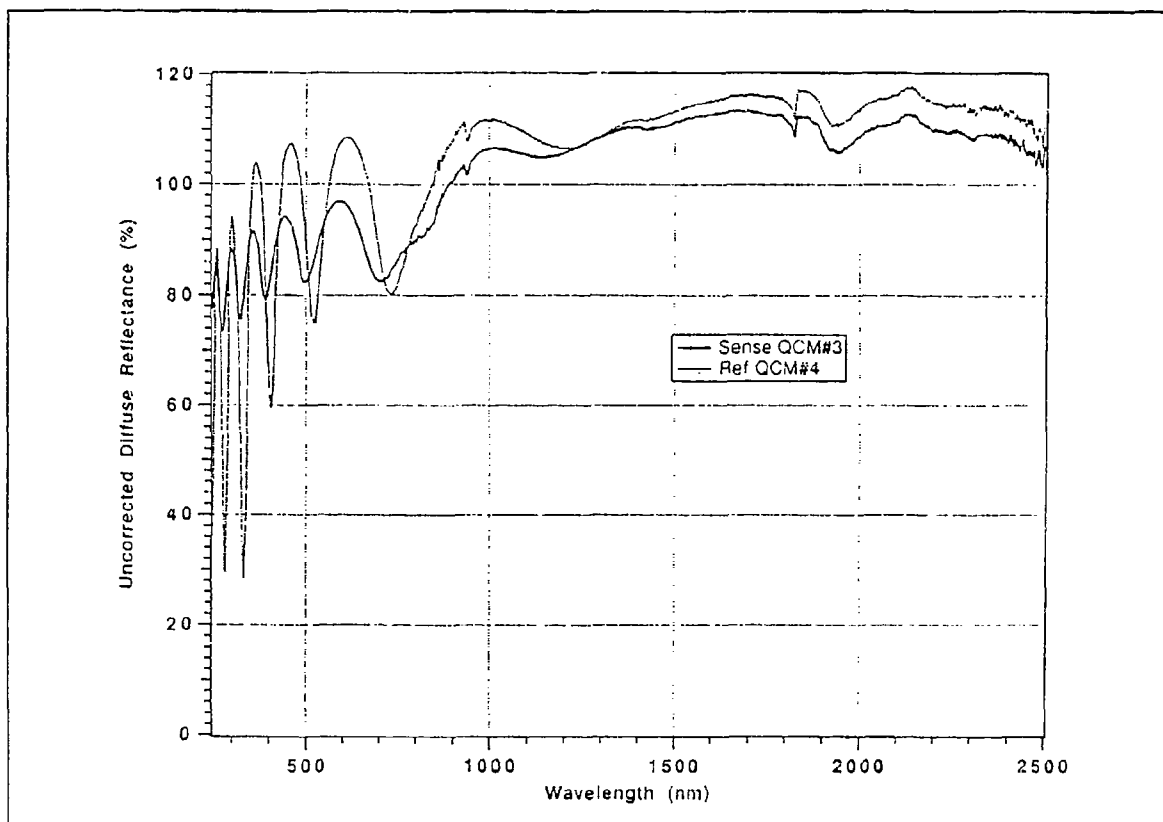


**Figure E.97. Diffuse Reflectance Spectra of  $\text{In}_2\text{O}_3/\text{Al}/\text{Al}_2\text{O}_3$  Coated Quartz Crystal Microbalance, LDEF Leading Edge**

**REFERENCE:** Stuckey, W.K., Radhakrishnan, G., and Wallace, D., Post-Flight Analyses of the Crystals from the M0003-14 Quartz Crystal Microbalance Experiment, LDEF Second Post-Retrieval Symposium, p. 1269

**EXPERIMENT:** M0003-14

**COMMENTS:** For all crystals, there is an increase in average reflectance with increasing wavelength. Positions of the wavelength maxima and minima in the interference patterns are shifted negligibly. Leading edge material (D9, active) showed nearly identical modulation amplitudes.

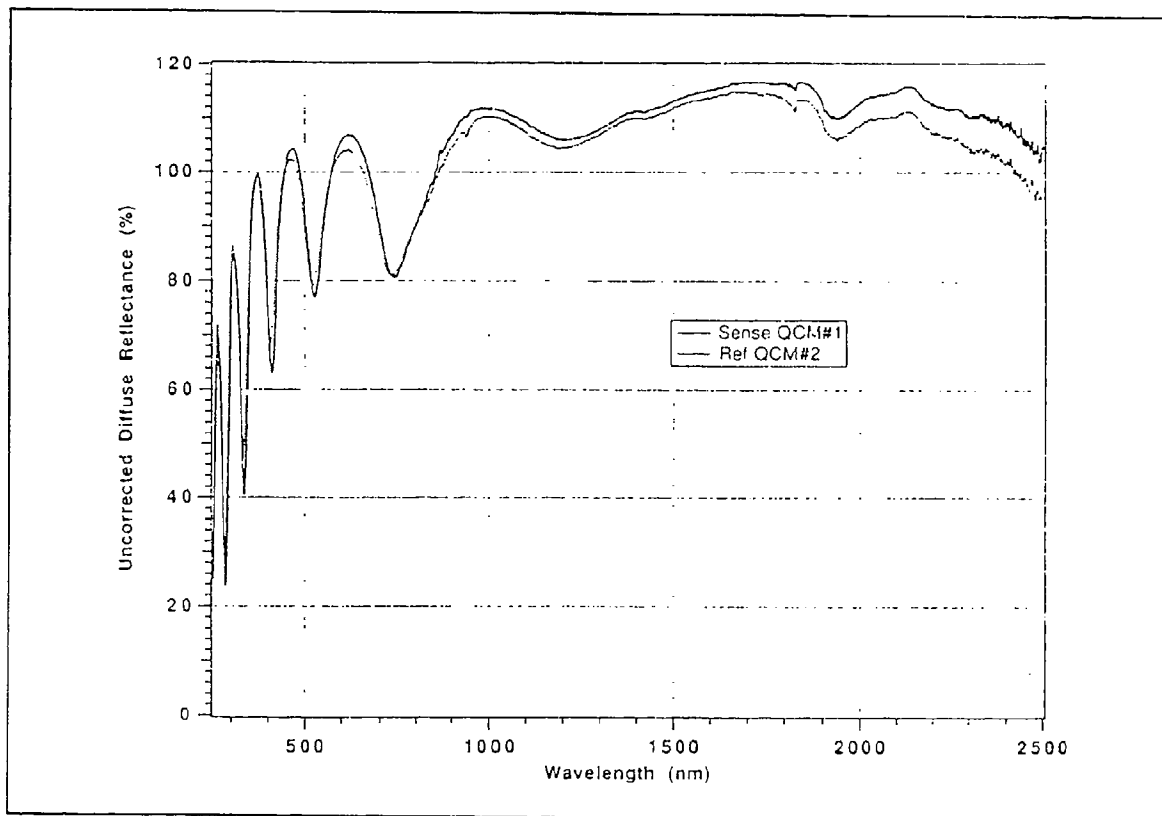


**Figure E.98. Diffuse Reflectance Spectra of  $\text{In}_2\text{O}_3/\text{Al}/\text{Al}_2\text{O}_3$  Coated Quartz Crystal Microbalance, LDEF Trailing Edge**

---

**REFERENCE:** Stuckey, W.K., Radhakrishnan, G., and Wallace, D., Post-Flight Analyses of the Crystals from the M0003-14 Quartz Crystal Microbalance Experiment, LDEF Second Post-Retrieval Symposium, p. 1269

**EXPERIMENT:** M0003-14

**COMMENTS:** For all crystals, there is an increase in average reflectance with increasing wavelength. Positions of the wavelength maxima and minima in the interference patterns are shifted negligibly. Trailing edge material (D3, active) experienced amplitude modulation in uncorrected diffuse reflectance (probably due to thickness interference).

---

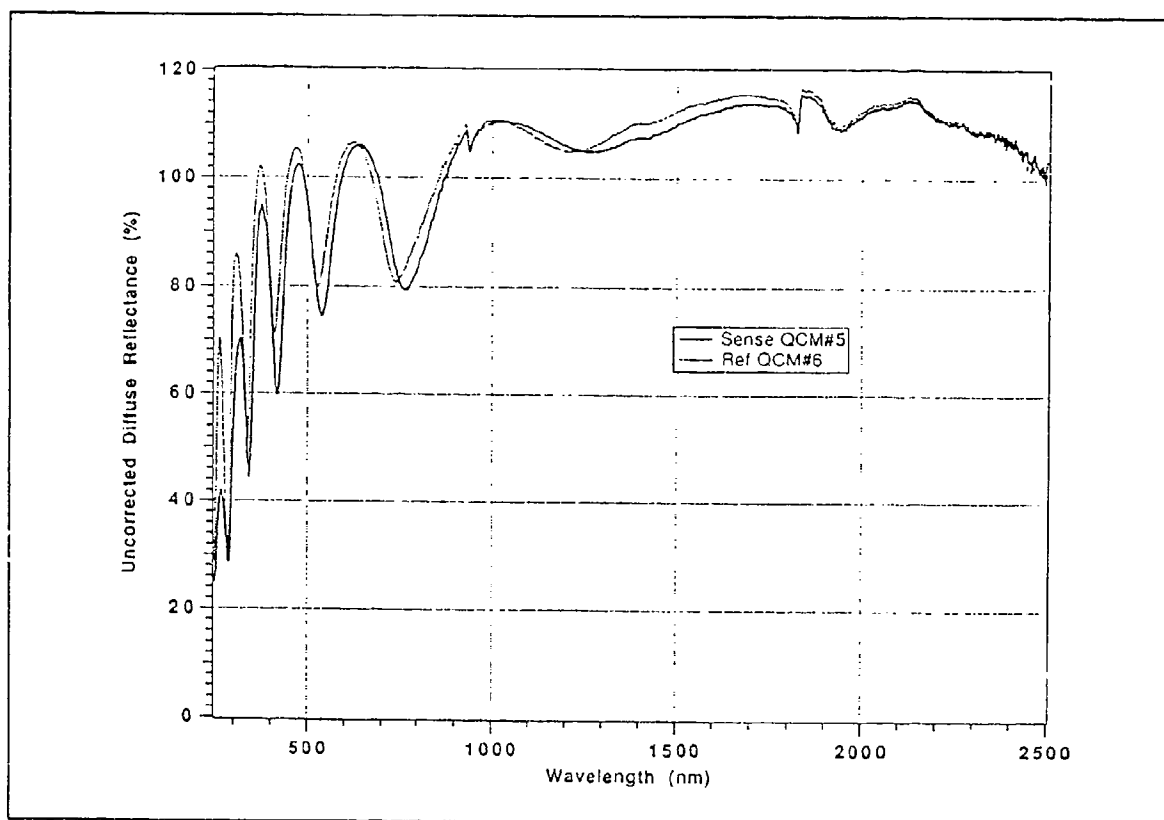


**Figure E.99. Diffuse Reflectance Spectra of ZnS/Al/Al<sub>2</sub>O<sub>3</sub> Coated Quartz Crystal Microbalance, LDEF Leading Edge**

**REFERENCE:**

Stuckey, W.K., Radhakrishnan, G., and Wallace, D., Post-Flight Analyses of the Crystals from the M0003-14 Quartz Crystal Microbalance Experiment, LDEF Second Post-Retrieval Symposium, p. 1269

**EXPERIMENT:**

M0003-14

**COMMENTS:**

For all crystals, there is an increase in average reflectance with increasing wavelength. Positions of the wavelength maxima and minima in the interference patterns are shifted negligibly. Leading edge material (D9, passive) showed significant modulation amplitudes over entire wavelength band.

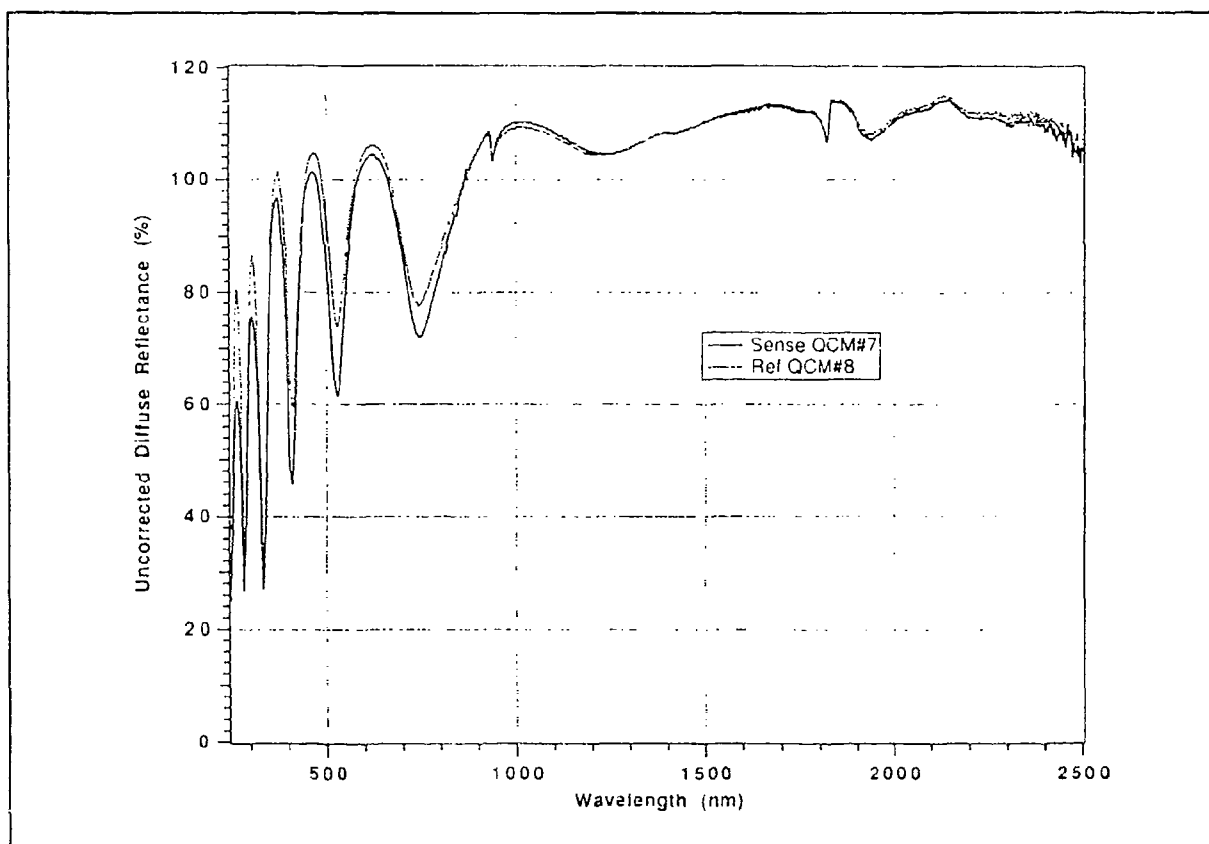


**Figure E.100. Diffuse Reflectance Spectra of ZnS/Al/Al<sub>2</sub>O<sub>3</sub> Coated Quartz Crystal Microbalance, LDEF Trailing Edge**

---

**REFERENCE:**

Stuckey, W.K., Radhakrishnan, G., and Wallace, D., Post-Flight Analyses of the Crystals from the M0003-14 Quartz Crystal Microbalance Experiment, LDEF Second Post-Retrieval Symposium, p. 1269

**EXPERIMENT:**

M0003-14

**COMMENTS:**

For all crystals, there is an increase in average reflectance with increasing wavelength. Positions of the wavelength maxima and minima in the interference patterns are shifted negligibly. Trailing edge material (D3, passive) experienced amplitude modulation in uncorrected diffuse reflectance (probably due to thickness interference).

---

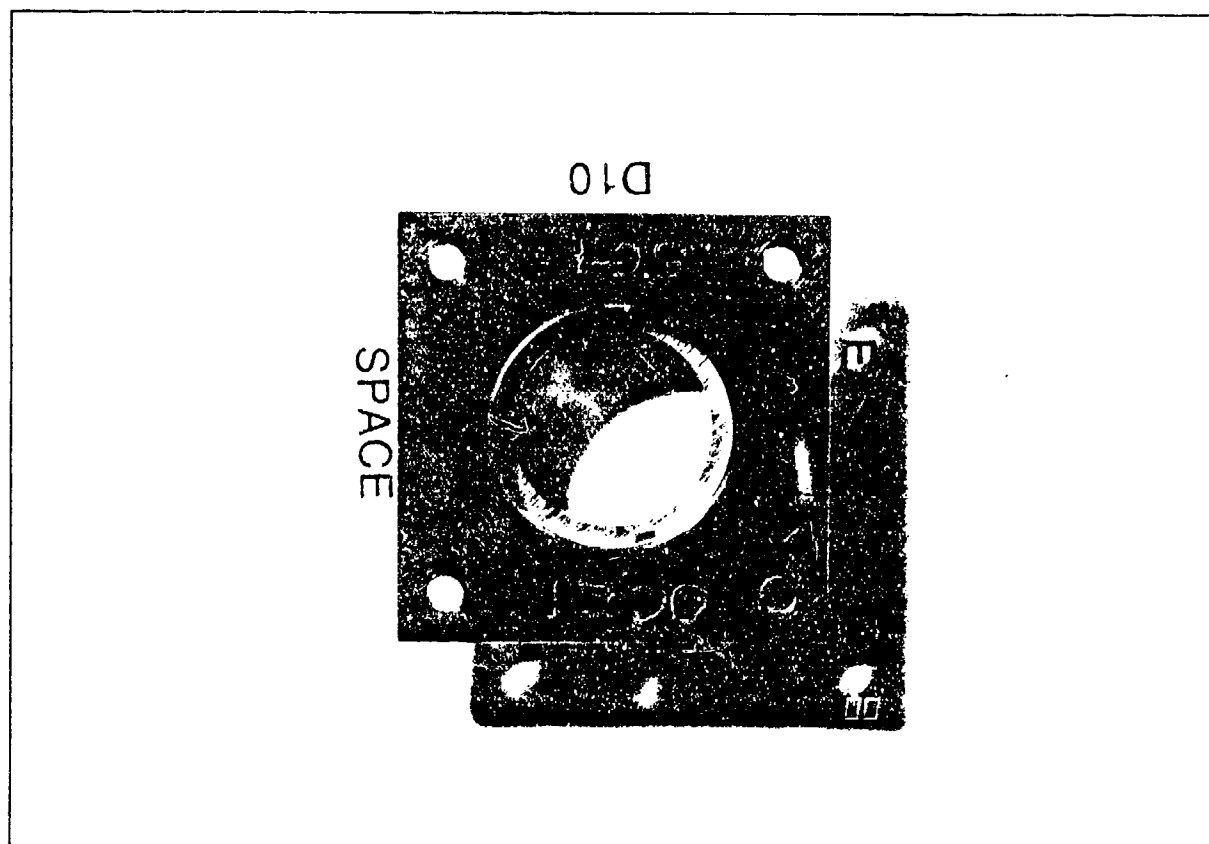


Figure E.101. Microfractured and Contaminated Mark III Coating on 7940 Coverglass

---

REFERENCE:	Gyetvay, S., et al., <u>Aerospace Corporation LDEF M0003 Sample Observation Data Base</u> , 1993, Record #169
EXPERIMENT:	M0003-4
COMMENTS:	Long, fine fractures through the coverglass emanate from impact craters in the surface. Fractures intersect defects in the coating surface. Blisters or droplets of condensate appear on the surface along the fractures. Coating is microfractured and flaking at the perimeter. Some large ruptured and unruptured bubbles appear in the coating. A coating or stain film on the reverse surface of the coverglass appears to have ruptured. The reverse, unexposed surface of the silicon wafer is silver-coated and is corroded and flaking.

---



**Figure E.102. Macrophotograph of Hazed and Contaminated Mark III Coating on 7940 Coverglass**

---

<b>REFERENCE:</b>	Gyetvay, S., et al., <u>Acrospace Corporation LDEF M0003 Sample Observation Data Base</u> , 1993, Record #168
<b>EXPERIMENT:</b>	M0003-4
<b>COMMENTS:</b>	Long, fine fractures through the coverglass emanate from impact craters in the surface. Fractures intersect defects in the coating surface. Blisters or droplets of condensate appear on the surface along the fractures. Coating is microfractured and flaking at the perimeter. Some large ruptured and unruptured bubbles appear in the coating. A coating or stain film on the reverse surface of the coverglass appears to have ruptured. The reverse, unexposed surface of the silicon wafer is silver-coated and is corroded and flaking.

---



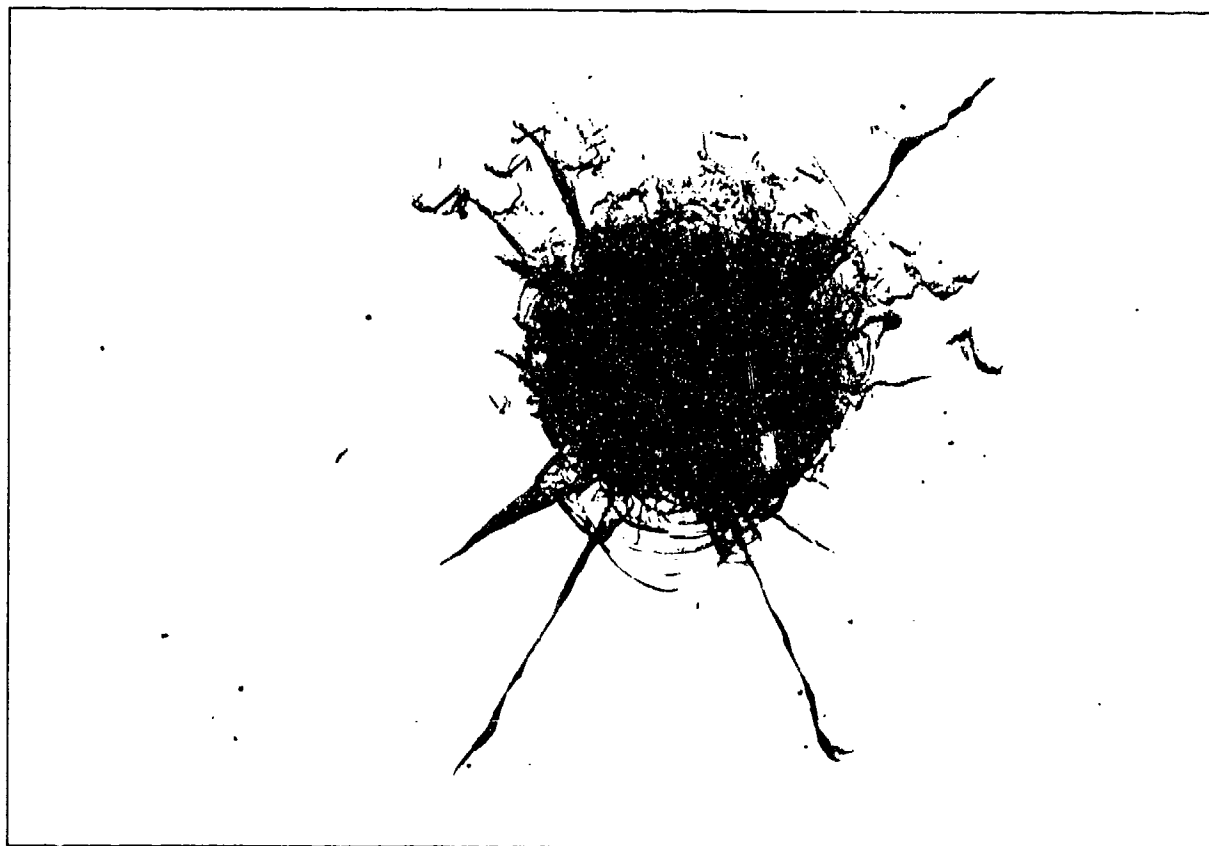


**Figure E.103. Impact Crater, 1.25 mm Diameter, in Surface of Bare 7940 Coverglass**

---

<b>REFERENCE:</b>	Gyetvay, S., et al., <u>Aerospace Corporation LDEF M0003 Sample Observation Data Base</u> , 1993, Record #177
<b>EXPERIMENT:</b>	M0003-4
<b>COMMENTS:</b>	Long fractures through the coverglass emanate from impact craters in the surface.

---

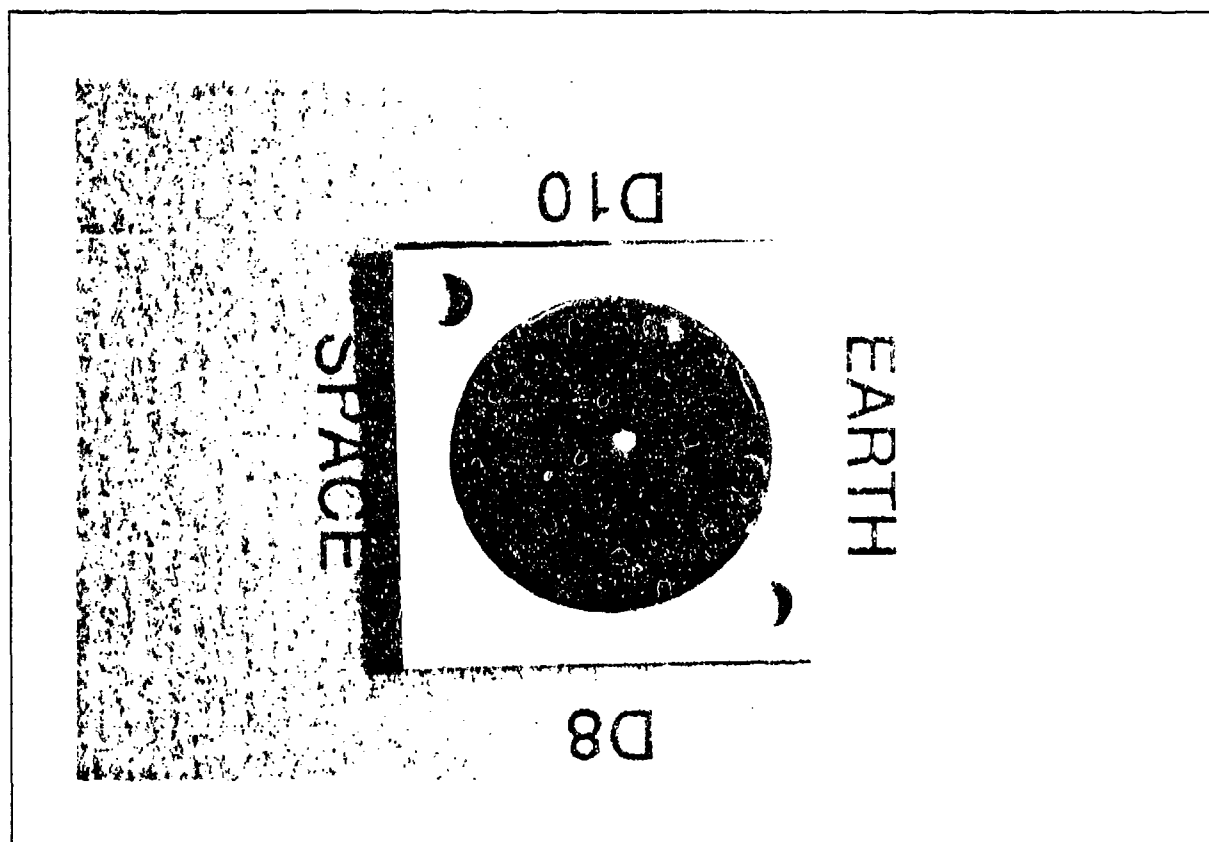


**Figure E.104. Macrophotograph of Hazed and Contaminated 7940 Coverglass with 1.25 mm Diameter Crater Off-Center in Surface**

---

<b>REFERENCE:</b>	Gyetvay, S., et al., <u>Aerospace Corporation LDEF M0003 Sample Observation Data Base</u> , 1993, Record #177
<b>EXPERIMENT:</b>	M0003-4
<b>COMMENTS:</b>	Interference rings are apparent on the surface. There is a large impact crater surrounded by conchoidal fractures and radiating cracks in coverglass. Apparent on D10 side are very minute particles, which appear to be embedded in the surface and have tails of radiating bright spots. The reverse, unexposed surface of the Si wafer is silver-coated and is corroded and flaking.

---



**Figure E.105. Impact Crater, 1.25 mm Diameter, in Surface of Bare 7940 Coverglass**

---

<b>REFERENCE:</b>	Gyetvay, S., et al., <u>Aerospace Corporation LDEF M0003 Sample Observation Data Base</u> , 1993, Record #176
<b>EXPERIMENT:</b>	M0003-4
<b>COMMENTS:</b>	Front surface appears relatively clean, despite erosion of the retainer. Delamination of a coating or film on the reverse surface of the coverglass is apparent. The reverse, unexposed surface of the silicon wafer is silver-coated and is corroded and flaking.

---

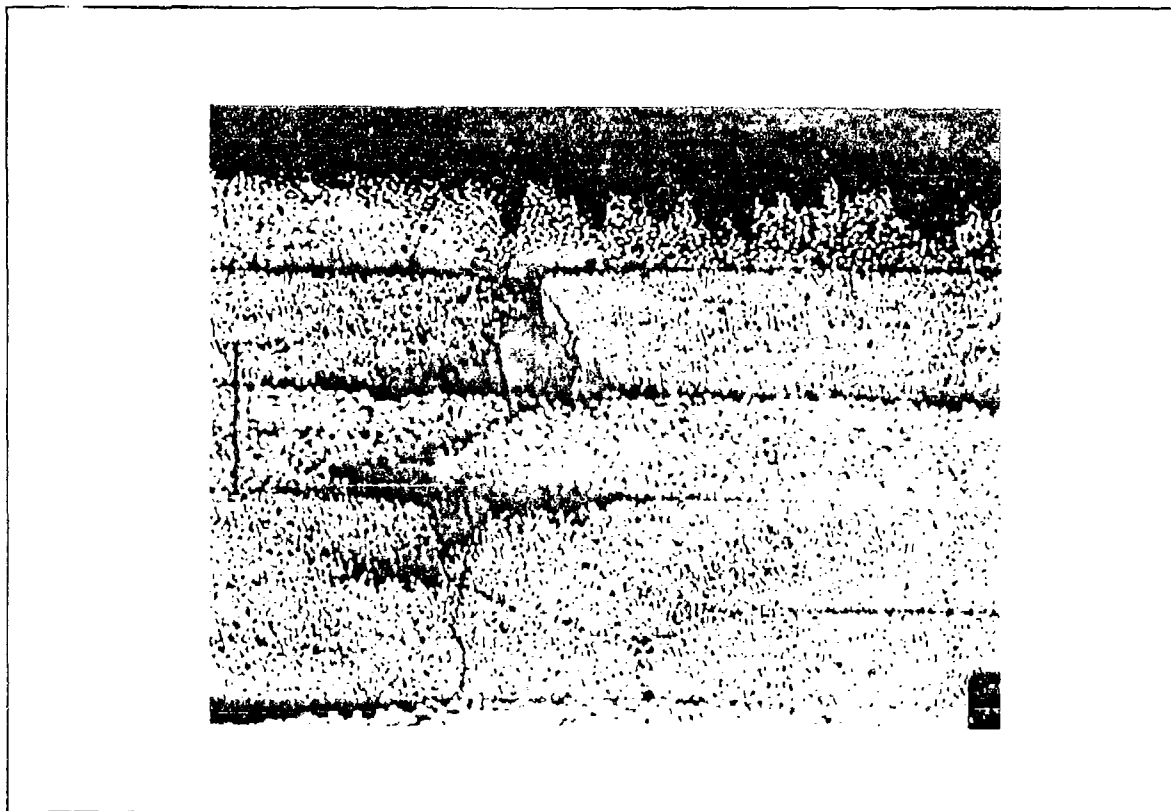


Figure E.106. Microcracked Mark IIID Coating on 7940 Coverglass

---

REFERENCE:	Gyetvay, S., et al., <u>Aerospace Corporation LDEF M0003 Sample Observation Data Base</u> , 1993, Record #168
EXPERIMENT:	M0003-4
COMMENTS:	There are parallel fractures in the coverglass. Faceted features appear on the surface along the microfractures (may be nucleating oxide phases). Dendritic growths are apparent. The reverse, unexposed surface of the silicon wafer is silver-coated and is corroded and flaking.

---



**Figure E.107. P1700 Polysulfone/T300 Leading Edge**

---

<b>REFERENCE:</b>	George, Pete E., and Hill, Sylvester G., <u>Results From Analysis of Boeing Composite Specimens Flown on LDEF Experiment M0003</u> , LDEF First Post-Retrieval Symposium, June 1991, p. 1134
<b>EXPERIMENT:</b>	M0003-8
<b>COMMENTS:</b>	Loss of material due to atomic oxygen exposure.

---

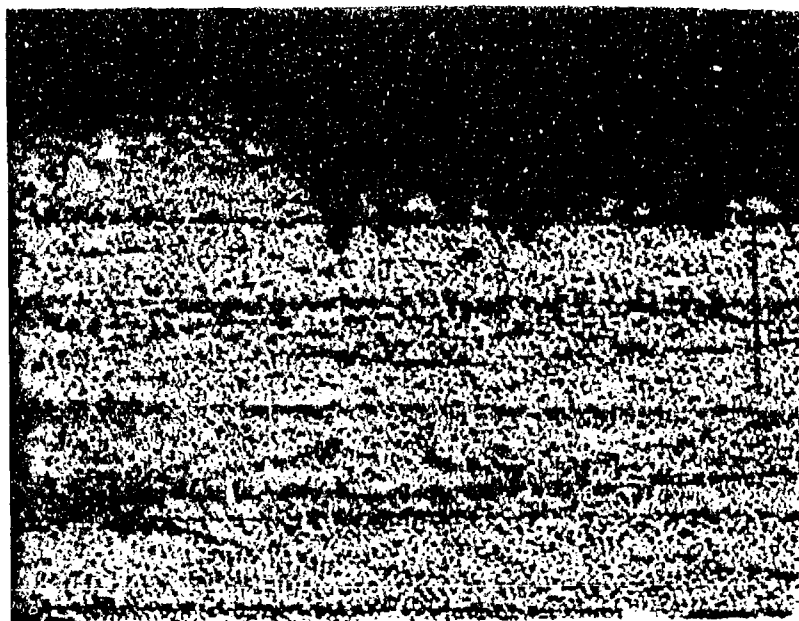
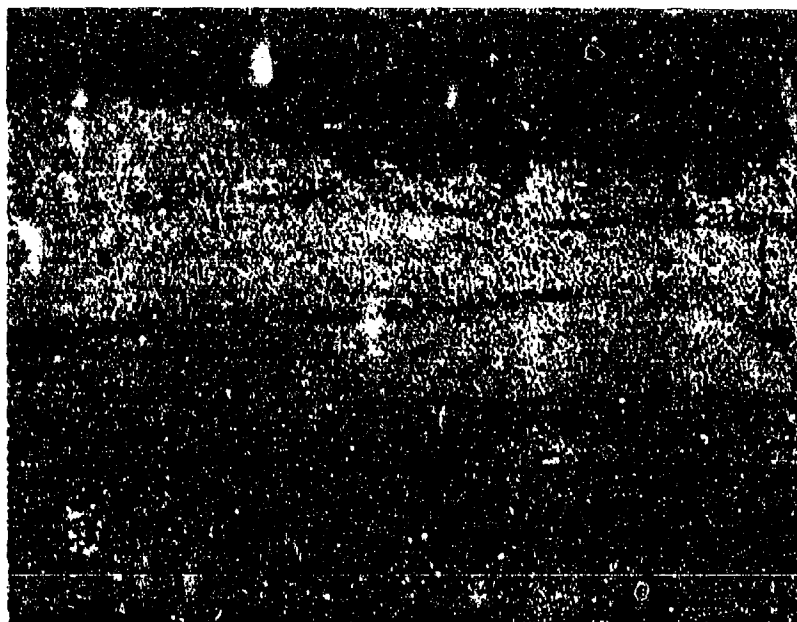


Figure E.108. PMR-15 Polyimide/C6000 Graphite Leading Edge

---

<b>REFERENCE:</b>	George, Pete E., and Hill, Sylvester G., <u>Results From Analysis of Boeing Composite Specimens Flown on LDEF Experiment M0003</u> , LDEF First Post-Retrieval Symposium, June 1991, p. 1135
<b>EXPERIMENT:</b>	M0003-8
<b>COMMENTS:</b>	Loss of material due to atomic oxygen exposure.

---



**Figure E.109. 934 Epoxy/T300 Graphite Leading Edge**

---

<b>REFERENCE:</b>	George, Pete E., and Hill, Sylvester G., <u>Results From Analysis of Boeing Composite Specimens Flown on LDEF Experiment M0003</u> , LDEF First Post-Retrieval Symposium, June 1991, p. 1133
<b>EXPERIMENT:</b>	M0003-8
<b>COMMENTS:</b>	Loss of material due to atomic oxygen exposure.

---

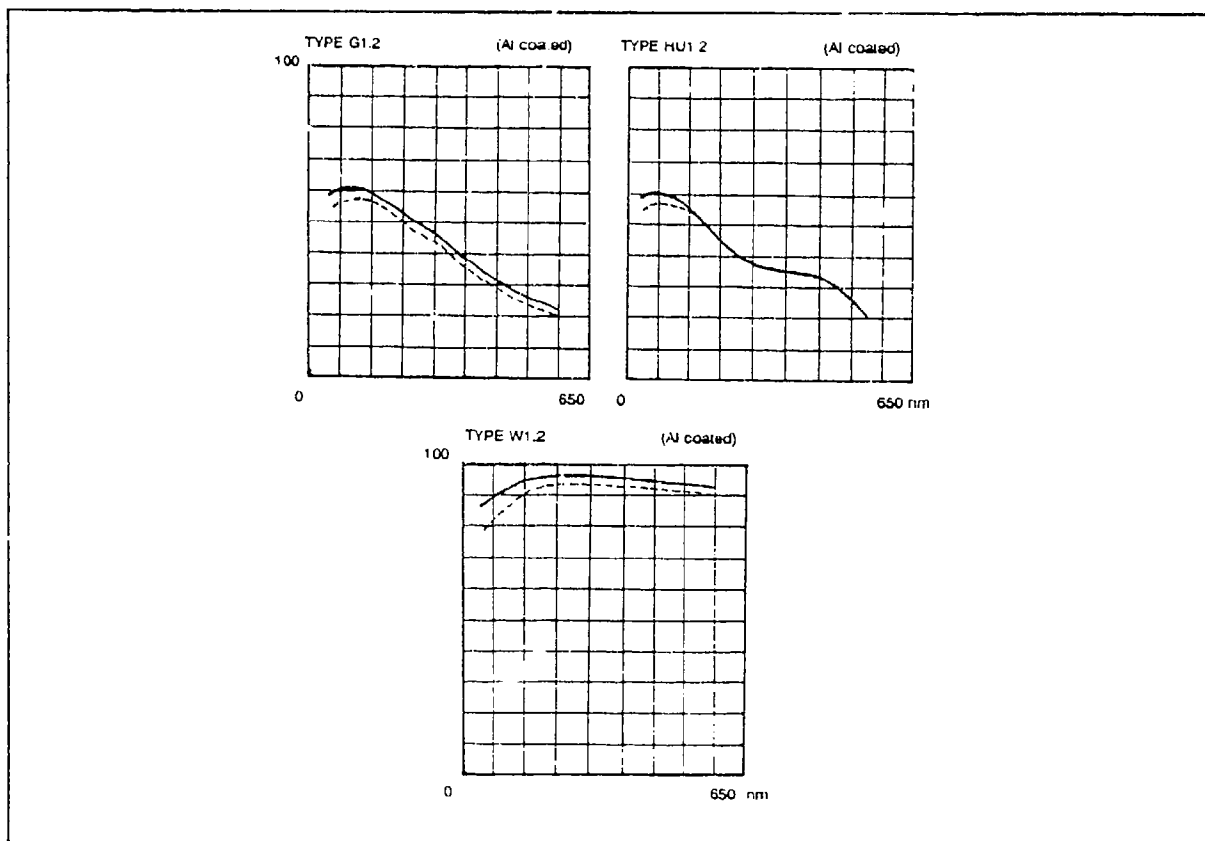


Figure E.110. Al-Coated Efficiency Curves

---

<b>REFERENCE:</b>	Bonnemason, Francis, <u>Ruled and Holographic Diffraction Gratings Experiment (AO138-5)</u> , LDEF First Post-Retrieval Symposium, June 1991, p. 1301
<b>EXPERIMENT:</b>	AO138-5
<b>COMMENTS:</b>	Efficiency loss was less than 10 percent.

---



TYPE H1.2 & W1.2			(Pt coated)		
wavelength (nm)	58.4	74.4	121.6		

reflectivity %	20.0	13.0	20.0	Pre-flight
	18.0	12.0	18.0	Post-flight

O	-1	0.4	2.7	7.7	Pre-flight
R		0.8	2.8	4.9	Post-flight
D %	0	8.7	2.1	3.9	
E		5.8	0.8	4.1	
R	+1	0.9	3.2	8.6	
		1.8	3.4	5.7	
% $\Sigma$		10.0	8.0	20.0	
		8.0	7.0	15.0	

Figure E.111. Pt-Coated Efficiency Data

**REFERENCE:** Bonnemason, Francis, Ruled and Holographic Diffraction Gratings Experiment (AO138-5), LDEF First Post-Retrieval Symposium, June 1991, p. 1301

**EXPERIMENT:** AO138-5

**COMMENTS:** Reflectivity loss was less than 2 percent.

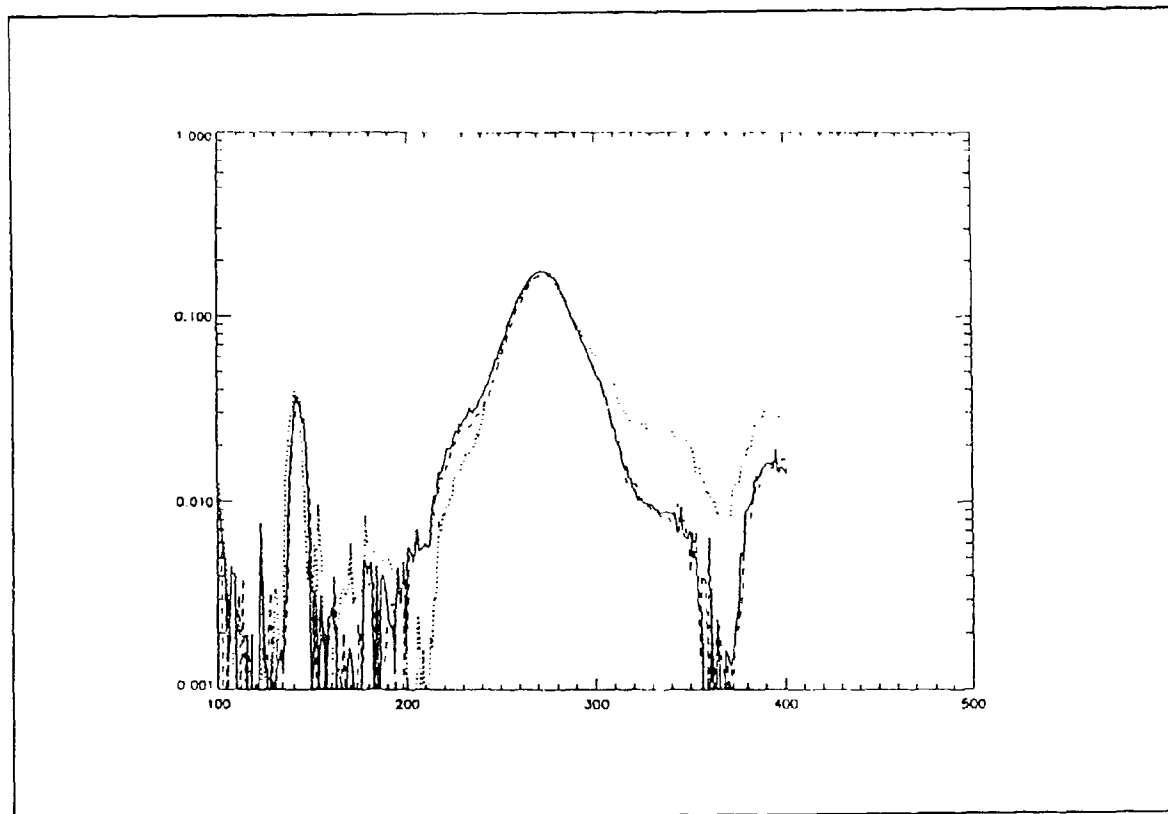


Figure E.112. Si/WRe Reflectivity Measurements

---

REFERENCE:	Delaboudinière, J.P., Carabétian, Ch., and Hochedez, J.F., In <u>Orbit Degradation of EUV Optical Components in the Wavelength Range 10-140 nm (AO138-3)</u> , LDEF Second Post-Retrieval Symposium, June 1992, p. 1356.
EXPERIMENT:	AO138-3
COMMENTS:	Pre- and post-flight measurements are consistent.

---

TABLE IX. - MECHANICAL TEST RESULTS  
(75°F unless otherwise noted)

\* Thermal Cycled Prior To Flight  
\*\* Tested At 350° F

MATERIALS	934 Epoxy/ T300 Graphite(0°)	P1700 P. Epsulfone/ T300 Graphite Fabric (0°/90°)	PMR 15 Polyimide C6000 Graphite (0°/±45,0°/±45°)
TESTS	Strength: Ksi (Modulus) Msi (# Tested)		
PREFLIGHT FLEXURE:	220.5 Ksi 32.4 Msi 5	106.5 Ksi 12.7 Msi 5	111.9 Ksi 17.8 Msi 3
POSTFLIGHT FLEXURE:			
Leading edge unstressed	207.0 Ksi 13.6 Msi 4	97.3 Ksi 7.8 Msi 4	104.6 Ksi 6.3 Msi 4
Leading edge unstressed T.C.*	229.0 Ksi 16.2 Msi 4	N.A.	N.A.
Trailing edge unstressed	238.0 Ksi 17.7 Msi 4	116.0 Ksi 16.4 Msi 4	137.0 Ksi 10.5 Msi 4
Trailing edge unstressed T.C.*	224.9 Ksi 16.1 Msi 4	N.A.	N.A.
Trailing edge prestressed	241.8 Ksi 16.3 Msi 5	118.8 Ksi 8.0 Msi 5	155.1 Ksi 11.4 Msi 5
Trailing edge prestressed (Elevated temperature)	119.7 Ksi 15.6 Msi 5	16.7 Ksi 4.5 Msi 3	81.1 Ksi 6.6 Msi 3
PREFLIGHT TENSION	152.7 Ksi est. 18-20 Msi 3	68.1 Ksi est. 7-9 Msi 3	69.6 Ksi - 3
POSTFLIGHT TENSION:			
Prestressed trailing edge	148.1 Ksi 21.0 Msi 2	66.2 Ksi 7.9 Msi 2	45.4 Ksi 8.0 Msi 2
PREFLIGHT COMPRESSION	113.1 Ksi est. 18-20 Msi 3	81.5 Ksi est. 7-9 Msi 3	64.5 Ksi - 3
POSTFLIGHT COMPRESSION:			
Prestressed trailing edge	106.8 Ksi 8.3 Msi 3	50.4 Ksi 7.2 Msi 2	61.0 Ksi 6.9 Msi 2

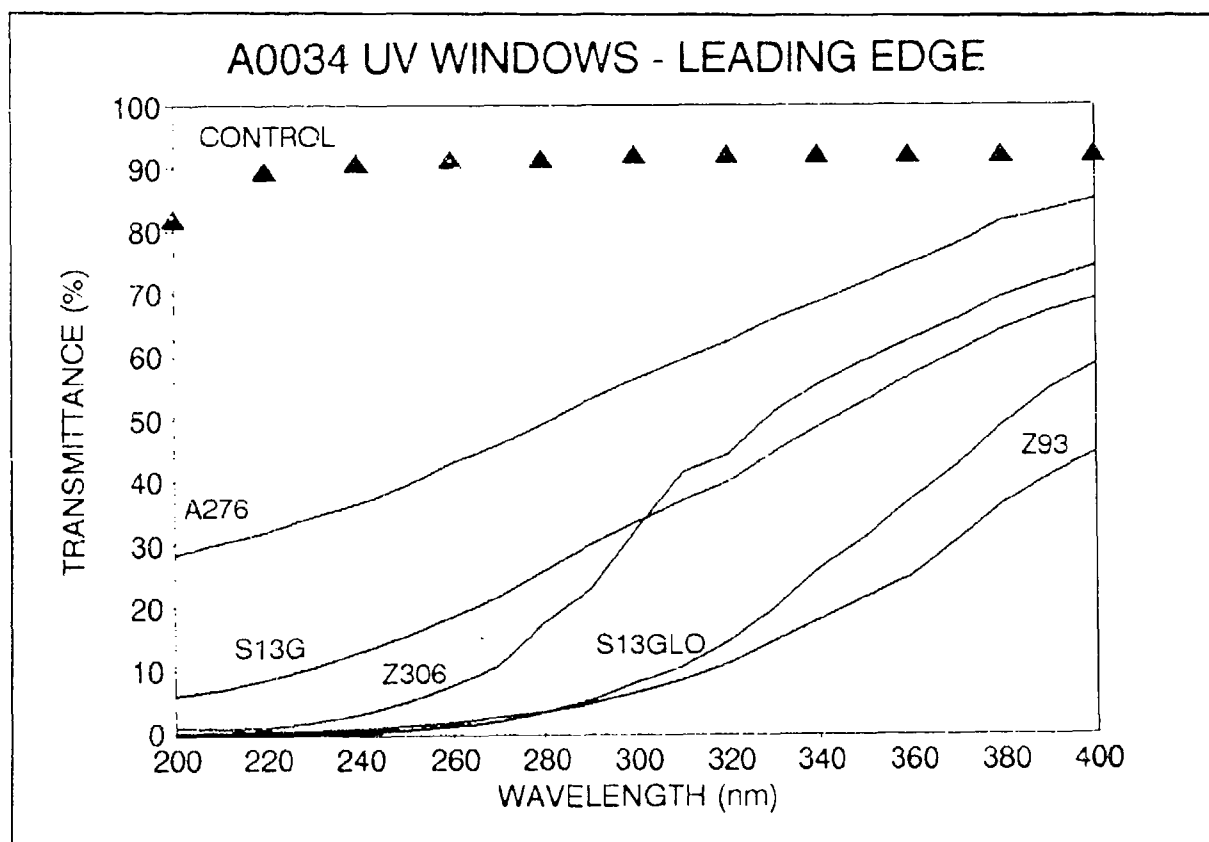
\*\*\* Tested at 600° F

Figure E.113. Composite Materials Mechanical Test Results

**REFERENCE:** George, Pete E., and Hill, Sylvester G., Results From Analysis of Boeing Composite Specimens Flown on LDEF Experiment M0003

**EXPERIMENT:** M0003-8

**COMMENTS:** Pre- and post-flight tensile strengths are similar but below expectations.



**Figure E.114. Thermal Control Generated Transmission Loss: UV Window**

---

<b>REFERENCE:</b>	Linton, Roger C., Kamenetzky, Rachel R., Reynolds, John M., and Burris, Charles L., <u>LDEF Experiment AO034: Atomic Oxygen Stimulated Outgassing</u> , LDEF First Post-Retrieval Symposium, June 1991, p. 779
<b>EXPERIMENT:</b>	AO034
<b>COMMENTS:</b>	Contamination severely degraded transmission.

---

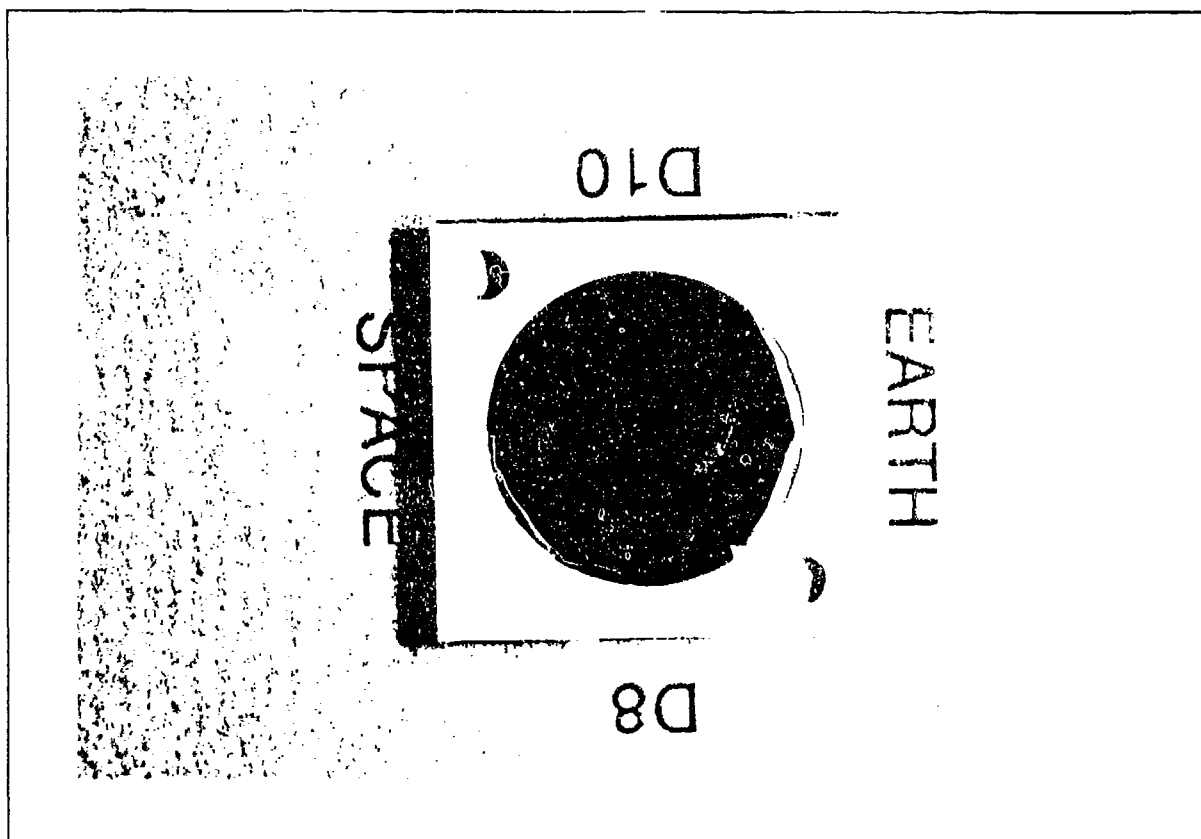
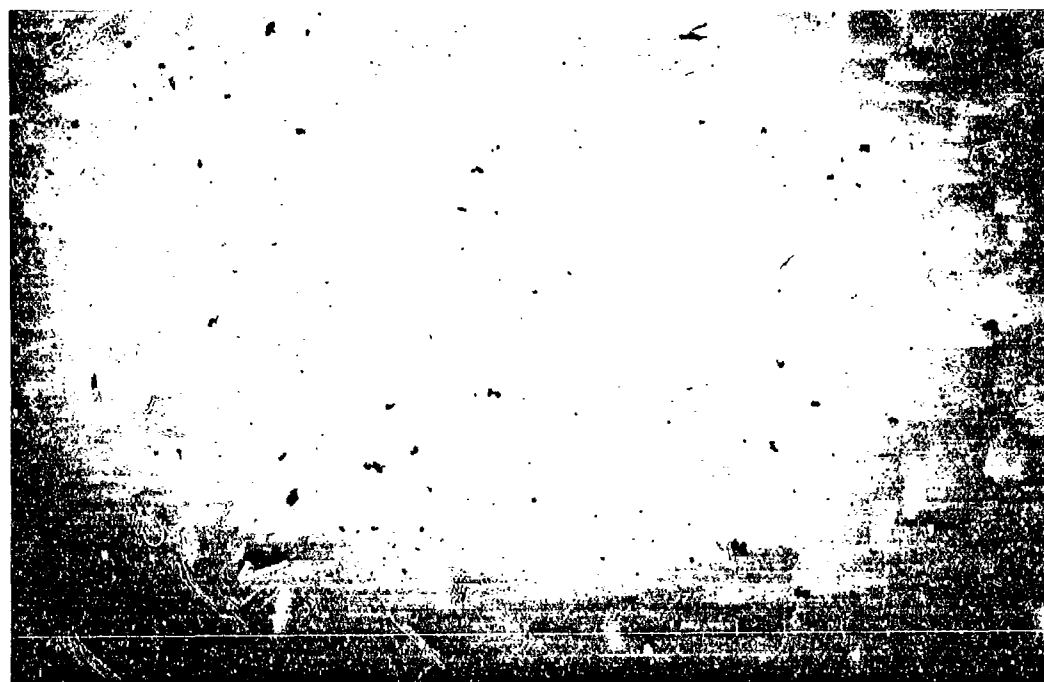


Figure E.115. Hazed and Contaminated Reflective 350 nm Coating on 7940 Fused Silica

<b>REFERENCE:</b>	Gyetvay, S., et al., <u>Aerospace Corporation LDEF M0003 Sample Observation Data Base</u> , 1993, Record #166
<b>EXPERIMENT:</b>	M0003-4
<b>COMMENTS:</b>	Perimeter is hazed. Coating is cracked and flaked.



**Figure E.116. Hazed and Contaminated Reflective 350 nm Coating on Ceria**

---

<b>REFERENCE:</b>	Gyctvay, S., et al., <u>Aerospace Corporation LDEF M0003 Sample Observation Data Base</u> , 1993, Record #166
<b>EXPERIMENT:</b>	M0003-4
<b>COMMENTS:</b>	Perimeter is hazed. Coating is cracked and flaked.

---

